UNIVERSITAT POLITÈCNICA DE VALÈNCIA

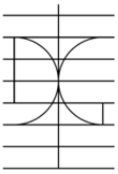

DEPARTMENT OF CONSTRUCTION ENGINEERING AND CIVIL ENGINEERING PROJECTS

Fire response analysis of circular concrete filled tubular columns and the effects of axial and rotational restraints

Thesis submitted in partial fulfilment of the requirements for the degree of Doctor of Philosophy

by

Carmen Ibáñez Usach

Advisors:

Dr. Manuel L. Romero García

Dr. Antonio Hospitaler Pérez

Valencia (Spain), October 2015

Acknowledgements

Firstly, I would like to express my deep gratitude to my supervisors Dr. Manuel L. Romero and Dr. Antonio Hospitaler for their indispensable support and guidance during my doctoral period. Thanks to their confidence, the development and consecution of this thesis have been possible.

I also wish to show my gratitude to my colleagues from Universitat Politècnica de València for the comforting moments which relieved the pressure of this constant work: Ana, Andrés and Toni, thanks for maintaining the same good atmosphere at the office as always. And thanks to the people from the Department of Construction Engineering and Civil Engineering Projects with whom I shared my beginnings: Héctor, Estefanía, Josemi, José Vicente, Juan and Vicente. Special thanks go to Ana Espinós for her wise advice in my first approach to concrete filled tubular columns and in every aspect of my career.

Sincere gratitude goes to my new colleagues from Universitat Jaume I for their constant support even in the distance, especially to David and Roberto who have made easier this hard period.

Another big thank you goes to Dr. Filippou for inviting me to join a leading institution as University of California at Berkeley during part of my doctoral period and for his assistance during my stay there since I had the incredible opportunity of collaborating and attending the master lectures of a referent in the field of nonlinear analysis of structures.

I would like also to thank the encouragement received from all my friends during these years.

Last of all, I would like to give special thanks to my family, in particular to my grandparents, parents and brother for their patience and understanding. This thesis has been possible thanks to you.

Carmen Ibáñez Usach

Valencia, October 2015

Abstract

The combination of different materials to form a single structural member to take profit of their individual good characteristics is a successfully established practice in building industry. In concrete filled tubular columns (CFT) the combined action of steel and concrete results in many positive attributes at ambient temperature: high load-bearing capacity with smaller cross-section size, aesthetics, high stiffness and ductility and reduced construction cost.

In the last decades, the use of CFT columns in building industry, especially in high-rise buildings, has increased not only because of their positive characteristics at room temperature, but also for their inherent high fire resistance. Besides, CFT sections are greatly versatile given that they admit different types of concrete infill such as plain concrete, bar-reinforced concrete or fiber reinforced concrete; and also a wide variety of shapes. Although the more commonly used shapes are circular, and rectangular, new configurations and shapes are continuously appearing together with innovative materials.

The ambient temperature behavior of CFT columns has been deeply studied and, in turn, the investigations dealing with their fire behavior have increased. For its structural analysis, the column can be considered as an isolated member or as a column integrated in a structure interacting with other structural members. The review of the state of the art in the area of CFT columns in fire carried out in the framework of this thesis has pointed out that most works cover the fire response of isolated members and that the existing studies on columns within frames differ in their proposals and conclusions.

In this thesis, the fire response of CFT columns is analyzed by means of a fiber beam element model. First, a realistic cross-sectional thermal model is implemented to be integrated in the thermo-mechanical model developed whose accuracy is validated against experimental results after its calibration. Parametric studies are carried out with the aim of investigating the main factors affecting the problem and developing a simple calculation method based on Eurocode 4 and using the concept of equivalent concrete core cross-section. Finally, given the reduced computational cost of the fiber model, the effects of axial and rotational restraint in the fire response of CFT columns are investigated by integrating the heated CFT column within a frame. A parametric analysis is performed in order to draw conclusions about this interaction and contrast the current code provisions.

The scope of this thesis is limited to circular CFT columns subjected to concentric axial loads.

Resumen

Combinar diferentes materiales en un único elemento estructural para aprovechar las fortalezas individuales de cada uno es una práctica consolidada con éxito en el sector de la construcción. En los pilares tubulares de acero rellenos de hormigón (CFT) la acción conjunta del acero y el hormigón presenta muy buenas cualidades a temperatura ambiente: alta capacidad de carga con secciones pequeñas, buena apariencia, alta rigidez y ductilidad y bajo coste de puesta en obra.

En las últimas décadas, el uso de pilares CFT en el sector de la construcción, especialmente en edificios de gran altura, ha aumentado no solo debido a sus buenas características a temperatura ambiente sino también por su inherente alta resistencia al fuego. Además, las secciones de pilares CFT son muy versátiles ya que admiten diferentes tipos de relleno, como hormigón en masa, con armaduras o reforzado con fibras; y también una amplia variedad de formas. Aunque los perfiles tubulares más usados son los circulares y rectangulares, nuevas configuraciones están continuamente en desarrollo junto con nuevos materiales.

El comportamiento de los pilares CFT a temperatura ambiente ha sido ampliamente estudiado y, a su vez, las investigaciones sobre su comportamiento a fuego han aumentado. Para su análisis estructural, el pilar puede ser considerado como un elemento aislado o como un elemento integrado en una estructura que interactúa con otros elementos estructurales. La revisión del estado del arte en el área de los pilares CFT sometidos a fuego llevado a cabo en el marco de esta tesis ha puesto de manifiesto que la mayoría de los trabajos cubren la respuesta a fuego de elementos aislados y que los estudios existentes sobre pilares en estructuras difieren en sus propuestas y conclusiones.

En esta tesis, la respuesta a fuego de pilares CFT se analiza por medio de un modelo de elementos viga con integración por fibras. En primer lugar, se implementa un modelo térmico realista para ser integrado en el modelo termo-mecánico desarrollado cuya precisión se valida con resultados experimentales después de ser calibrado. Un estudio paramétrico se lleva a cabo con el objeto de estudiar los principales factores que afectan al problema y desarrollar un modelo simplificado de cálculo basado en el Eurocódigo 4 Parte 1-1 y que emplea el concepto de sección equivalente del núcleo de hormigón. Finalmente, dado el reducido coste computacional del modelo de fibras, se investigan los efectos de la restricción axial y rotacional en la respuesta frente al fuego de los pilares CFT integrando la columna expuesta a fuego dentro de una subestructura. Se ejecuta un estudio paramétrico para extraer conclusiones sobre esta interacción y contrastar las prescripciones de la normativa actual.

El alcance de esta tesis queda limitado a pilares CFT sin protección externa, de sección circular y sometidos a carga axial centrada.

Resum

Combinar distints materials en un únic membre estructural per a aprofitar les fortaleses individuals de cada u és una pràctica consolidada amb èxit en el sector de la construcció. En els pilars tubulars d'acer omplerts de formigó (CFT) l'acció conjunta de l'acer i el formigó presenta molt bones qualitats a temperatura ambient: alta capacitat de càrrega amb seccions xicotetes, bona aparença, alta rigidesa i ductilitat i baix cost de posada en obra.

En les últimes dècades, l'ús de pilars CFT en el sector de la construcció, especialment en edificis de gran altura, ha augmentat no sols degut a les seues bones característiques a temperatura ambient, sinó també per la seua inherent alta resistència al foc. A més, les seccions de pilars CFT són molt versàtils, doncs admeten distints tipus de farcit, com formigó en massa, amb armadures o reforçat amb fibres; i també una àmplia varietat de formes. Encara que els perfils tubulars més usats són els circulars i rectangulars, noves configuracions estan contínuament en desenvolupament junt amb nous materials.

El comportament dels pilars CFT a temperatura ambient ha sigut àmpliament estudiat i, al mateix temps, les investigacions sobre el seu comportament a foc han augmentat. Per a la seua anàlisi estructural, el pilar pot ser considerat com un element aïllat o com un element integrat en una estructura que interactua amb altres elements estructurals. La revisió de l'estat de l'art en l'àrea dels pilars CFT sotmesos a foc, duta a terme en el marc d'aquesta tesi, ha posat de manifest que la majoria dels treballs cobreixen la resposta a foc d'elements aïllats, i que els estudis existents sobre pilars en estructures difereixen en les seues propostes i conclusions.

En aquesta tesi, la resposta a foc de pilars CFT s'analitza mitjançant un model d'elements biga amb integració per fibres. En primer lloc, s'implementa un model tèrmic realista per a ser integrat en el model termo-mecànic desenvolupat, i la seua precisió es valida amb resultats experimentals després de ser calibrat. Un estudi paramètric es du a terme amb l'objectiu d'estudiar els principals factors que afecten al problema i desenvolupar un model simplificat de càlcul basat en l'Eurocodi 4, Part 1-1 i que empra el concepte de secció equivalent del nucli de formigó. Finalment, tenint en compte el reduït cost computacional del model de fibres, s'investiguen els efectes de les restriccions axial i rotacional en la resposta a foc dels pilars CFT integrant la columna exposada a foc dins d'una subestructura. Un estudi paramètric s'executa per a obtenir conclusions sobre aquesta interacció i contrastar les prescripcions de la normativa actual.

L'abast d'aquesta tesi queda limitat a pilars CFT sense protecció externa, de secció circular i sotmesos a càrrega axial centrada.

MOTIVATION AND OUTLINE OF THIS THESIS

This thesis continues with the investigations on the fire behavior of concrete filled tubular (CFT) columns initiated within the framework of the research line established by Dr. Hospitaler and Dr. Romero at the Universitat Politècnica de València. Complementary research is carried out by other researchers of the group on aspects such as the behavior of new configurations of CFT columns, the application of new materials in this technology or the study of the connection of CFT columns with other structural members.

Particularly in the area of CFT columns under fire, the response of these composite columns as isolated members has been deeply studied within the group by means of a validated three-dimensional finite element model developed within the framework of the same research line. Thus, the study of the fire response of a CFT column within a frame emerges as the next step to be accomplished to understand the interaction mechanism of the heated CFT columns with other structural members.

Given the nature of three-dimensional finite element models, they are not considered a recommendable tool for performing studies of a whole structure or of a part of it provided that reasonable computing times are desirable. For this purpose, beam models constitute a good alternative due to their inherent lower computational cost. Previously to the initiation of the research line of CFT columns in fire, the room temperature behavior of these composite columns was studied within the group by means of a fiber beam model. Extending this model to the analysis of CFT columns under fire was set as an objective since it could be applied to the study of the fire behavior of CFT columns within frames.

Therefore, with the aim of acquiring new knowledge about the modeling of fiber beam elements and their application to the nonlinear analysis of structures, a stay of the author of this thesis at the University of California at Berkeley (USA) was planned in order to collaborate with Dr. Filippou, a referent on this field who had previously worked with the research group.

Hence, this document starts with an introductory part consisting of Chapters 1, 2 and 3. The initial revision of the theoretical background necessary for the understanding of the fire behavior of CFT columns is covered in Chapter 1. Next, Chapter 2 constitutes the review of the state of the art in this field, covering analytical, numerical and experimental investigations on isolated CFT columns as well as on columns within frames. This part ends with Chapter 3 where the aim and scope of this thesis are established.

Chapters 4 and 5 comprise the part of the dissertation dealing with the development of a thermo-mechanical model.

Chapter 4 presents a detailed description of the thermal model developed for computing the cross-sectional temperatures of circular CFT columns, as well as its validation procedure and an analysis of the thermal response of CFT columns.

Chapter 5 describes with detail the development of a thermo-mechanical numerical model for predicting the fire behavior of axially loaded concrete filled tubular columns together with its validation process and calibration.

In Chapter 6, by means of the validated numerical model, parametric studies are carried out and the data generated are analyzed. As a result, expressions for estimating the cross-sectional temperatures of circular CFT columns are elaborated to complement the development of a new simple calculation method included in the same chapter.

Chapter 7 presents an extensive study of the effects of axial and rotational restraints in the fire behavior of CFT columns in fire. The scheme used for the analysis is described and a parametric analysis is carried out to investigate the main parameters affecting the problem. Besides, the evaluation of the current code provisions is made together with the assessment of the proposed method for the prediction of the fire behavior of CFT columns within frames

Finally, Chapter 8 presents the major conclusions drawn from this thesis and includes some suggestions on future work.

The work presented in this thesis has produced two conference papers and two articles published in international peer-review journals. The details of these publications are the following:

Article 1:

Ibañez C, Romero ML, Hospitaler A. 2013. Fiber beam model for fire response simulation of axially loaded concrete filled tubular columns. *Engineering Structures* 56: 182-193.

Article 2:

Ibañez C, Aguado JV, Romero ML, Espinos A, Hospitaler A. 2015. Fire design method for concrete filled tubular columns based on equivalent concrete core cross-section. *Fire Safety Journal* 78: 10-23.

Conference paper 1:

Ibañez C, Romero ML, Hospitaler A. *Validation of fiber beam model for axially loaded concrete filled tubular columns in fire*. In: 7th European Conference on Steel and Composite Structures (Eurosteel 2014). Naples, Italy (10-09-2014).

Conference paper 2:

Ibañez C, Romero M.L., Hospitaler A., Pascual A. *Fiber beam model for axially loaded concrete filled tubular columns fire simulation*. In: 8th International Conference on Structures in Fire. Shanghai, China (11-06-14).

TABLE OF CONTENTS

CHAPTER 1. INTRODUCTION....1
1.1.Background....2
1.1.1. Advantages of CFT columns....5
1.1.2. Practical applications....8
1.1.3. Construction considerations....15
1.2.Fire behavior of CFT columns....17
1.2.1. Fire dynamics analysis....22
1.2.2. Heat transfer analysis....26
1.2.3. Structural analysis....29
CHAPTER 2. STATE OF THE ART....31
2.1.General....32
2.2.Thermal models....34
2.3.Isolated member models....35
2.3.1. Analytical models....35
2.3.2. Numerical models....36
2.4.Global structural models....43
2.4.1. Global models for steel columns....43
2.4.2. Global models for CFT columns....46
2.5.Experimental programs....48
2.5.1. Experimental programs on isolated CFT columns....49
2.5.2. Experimental programs on structural continuity....55
2.6.Simple calculation models....58
CHAPTER 3. AIM AND SCOPE OF THIS THESIS....65
3.1.Aim of this thesis....66
3.1.1. Specific objectives....67
3.2.Scope and limitations of this thesis....68

CHAPTER 4. DEVELOPMENT OF THE THERMAL MODEL 69
4.1.Introduction 70
4.2.Unprotected concrete filled tubular columns 71
4.2.1. Discretization of the section 71
4.2.2. Cross-sectional temperatures 73
4.2.3. Content of moisture in the concrete core 76
4.3.Protected concrete filled tubular columns 77
4.3.1. Discretization of the section 77
4.3.2. Cross-sectional temperatures 79
4.3.3. Content of moisture in the concrete core 80
4.4.Validation of the thermal model 81
4.4.1. Experimental tests for validation 81
4.4.1.1. Unprotected CFT columns 81
4.4.1.2. Protected CFT columns 83
4.4.2. Thermal properties at high temperatures 84
4.4.3. Thermal analysis parameters 85
4.4.4. Thermal response 86
4.4.4.1. Unprotected CFT columns 86
4.4.4.2. Protected CFT columns 91
4.4.5. Effect of gap conductance on the thermal response 95
4.5.Assessment of the steel tube temperature 97
4.5.1. Effect of the concrete infill on protection thickness 98
4.5.2. Effect of the concrete infill on heating rate 100
CHAPTER 5. DEVELOPMENT OF THE THERMO-MECHANICAL MODEL 103
5.1.Characteristics of the thermo-mechanical model 104
5.1.1. Introduction 104
5.1.2. FedeasLab toolbox 105

5.1.3. Description of the model 105
5.1.4. Description of the fiber beam element 108
5.1.4.1. Outline of beam theory 108
5.1.4.2. Co-rotational formulation 110
5.1.4.3. Distributed plasticity 111
5.1.4.4. Mixed formulation 112
5.1.4.5. Formulation with section integration 114
5.1.4.6. Finite element technology 117
5.1.5. Material properties at high temperatures 117
5.1.5.1. Thermal properties 117
5.1.5.2. Mechanical properties 117
5.1.6. Analysis procedure 118
5.2. Calibration of the thermo-mechanical model 119
5.2.1. Number of elements per column 120
5.2.2. Number of integration points per element 122
5.2.3. Discretization of the section 124
5.2.4. Initial geometric imperfection of the column 127
5.2.5. Stiffness of the transversal and longitudinal links 127
5.2.6. Mechanical model for normal strength concrete 129
5.3. Validation of the model 131
5.3.1. Experimental tests for validation 131
5.3.1.1. Own tests 131
5.3.1.2. Tests from the literature 132
5.3.2. Three-dimensional model for validation 134
5.3.3. Mechanical response 135
CHAPTER 6. DEVELOPMENT OF A SIMPLE CALCULATION MODEL 149
6.1. Review of current simple calculation methods in Eurocode 4 150

6.2.CEN-Horizontal Group Fire guidelines..... 153

6.3.Development of expressions for the cross-sectional temperature field of CFT columns.…..154

6.3.1. Parametric analysis 154

6.3.2. Equations for the cross-sectional temperature field 155

6.4.Development of a simple calculation model 160

6.4.1. Equivalent concrete core cross-section 160

6.4.2. Buckling correction factor 164

6.4.3. Parametric analysis 165

6.4.4. Comparison of the proposed method with experiments..... 170

6.4.5. Design example..... 171

6.5.Summary of the proposed calculation method 173

CHAPTER 7. STRUCTURAL CONTINUITY ANALYSIS 175

7.1.Introduction 176

7.2.Description of the subframe model 177

7.3.Consideration of the fire effective length in Eurocode 4..... 178

7.4.Fire behavior of CFT columns within frames 180

7.4.1. Parametric analysis 180

7.4.2. Analysis of results..... 182

7.4.3. Influence of the parameters studied 192

7.4.3.1. Influence of the load level..... 192

7.4.3.2. Influence of the stiffness ratio..... 194

7.4.4. Evaluation of the effective length 197

7.5.Analysis of current Eurocode 4 guidelines..... 200

7.5.1. Comparison with effective length considerations in Eurocode 4..... 201

7.5.2. Comparison with effective length considerations in UK National Annex to Eurocode 4..... 203

7.6.Assessment of the proposed method 206
7.6.1. Proposed method predictions with 0.5L 206
7.6.2. Proposed method predictions with 0.7L 209
7.6.3. Proposed method predictions with β =β(T) 212
7.6.4. Proposal for the effective length in fire 215
CHAPTER 8. CONCLUSIONS 221
8.1.General conclusions 222
8.2.Specific conclusions 222
8.3.Future work 227
REFERENCES 229
ANNEX I. PARAMETRIC ANALYSIS ON STRUCTURAL CONTIINUITY
ANNEX II. MATERIAL CONSTITUTIVE MODELLING

LIST OF FIGURES

Figure 1.1. Axial compressive behavior of stub columns (Han et al. 2014). 2

Figure 1.2. Possible shapes of CFT cross-sections. 3

Figure 1.3. General configurations of CFT cross-sections. 4

Figure 1.4. Failure modes of hollow steel tube, concrete and CFT stub columns 6

(Han et al. 2014) 6

Figure 1.5. Fire resistance enhancement achieved by filling steel hollow section columns with concrete (Adapted from Zhao et al. 2010). 7

Figure 1.6. High-rise buildings with CFT columns. 10

Figure 1.7. Office buildings with CFT columns. 11

Figure 1.8. Residential buildings with CFT columns. 12

Figure 1.9. Public buildings with CFT columns. 13

Figure 1.10. Car parks with CFT columns. 14

Figure 1.11. Schematic view of concrete placement systems (Han et al. 2014): 17

Figure 1.12. Effect of using different types of concrete infill on the fire resistance of CFT columns (Kodur 1999, 2007). 18

Figure 1.13. Typical behavior of a CFT column subjected to elevated temperatures. 19

Figure 1.14. Different stages in the evolution of a fire 23

Figure 1.15. Different types of fire curves. 24

Figure 4.1. Unprotected CFT column. Discretization of the section for thermal analysis. 72

Figure 4.2. Detail: Gap conductance at steel-concrete boundary. 73

Figure 4.3. Protected CFT column. Discretization of the section for thermal analysis. 77

Figure 4.4. Detail: Protection layer and gap conductance for a protected CFT column. 78

Figure 4.5. Comparison between measured and thermal model predicted temperatures for specimens with different type of aggregate. 87

Figure 4.6. Comparison between measured and thermal model predicted temperatures for specimens with different type of concrete infill. 88

Figure 4.7. Comparison of temperatures at failure: model vs. test. 89

Figure 4.8. Protected columns. Comparison between measured and predicted steel tube temperatures. 93

Figure 4.9. Typical failure of spray protection after fire tests (Han et al. 2003a). 94

Figure 4.10. Comparison of measured and calculated temperatures with different steel-concrete boundary model: gap conductance versus perfect contact. 96

Figure 5.6. Comparison of measured and predicted axial displacement with different numbers of elements per column. 121

Figure 5.7. Comparison of measured and predicted axial displacement with different numbers of integration points per element. 123

Figure 5.8. Cross-sectional discretization. 124

Figure 5.9. Comparison of measured and predicted axial displacement with different cross-sectional discretization patterns. 125

Figure 5.11. Comparison of measured and predicted axial displacement with different concrete models. 130

Figure 5.12. Components and finite element mesh of the three-dimensional model by Espinos et al. (2010). 135

Figure 5.13. Comparison of measured and predicted axial displacement, own tests (Romero et al. 2011). 137

Figure 5.14. Comparison of measured and predicted axial displacement, tests from literature (Lie & Chabot, Kim et al. 2005). 139

Figure 5.17. Comparison of numerical simulations with experimental data. 145

Figure 5.18. Comparison of numerical results: fiber model vs. 3D model. 146

Figure 6.1. Temperature profile of a longitudinal section of a CFT column. 156

Figure 6.2. Comparison of the predicted temperatures given by the equations proposed and the values generated in the thermal parametric analysis. 158

Figure 6.3. Temperature at failure: equation prediction versus test temperatures. 159

Figure 6.4. Comparison of test temperatures with temperatures calculated by thermal model and proposed equations for one of the specimens analyzed (C-09). 159

Figure 6.5. Cross-section schemes for CFT columns used for calculation. 162

Figure 6.6. Comparison of predicted and numerical values of the radius of the equivalent concrete core cross-section. 164

Figure 6.7. Relative error. Comparison between the results of the calculation proposal and the numerical simulations. 168

Figure 6.8. Frequency histogram for the prediction error obtained with the proposed design method. 168

Figure 6.9. Comparison between the proposed method and numerical simulations. 169

Figure 6.10. Comparison between predicted loads and tests loads. 170

Figure 7.1. Scheme used by Bailey (2000) 177

Figure 7.2. Subframe scheme used in the analysis 178

Figure 7.3. Structural behaviour of columns in braced frames (CEN 2005c). 179

Figure 7.4. Effective length of columns in fire situation according to BS NA EN1994-1-2 (Hicks & Newman 2002). 180

Figure 7.5. Typical behaviour of a CFT column within a frame 182

Figure 7.6. Detection of outliers in a boxplot. 183

Figure 7.8. Fire response of specimen C193-5-1351-0.3 μ=0.3 α=0.5. 186

Figure 7.9. Fire response of specimen C193-5-9010-2 μ=0.3 α=0.5. 188

Figure 7.10. Fire response of specimen C273-16-8402-2 μ=0.3 α=0.5. 191

Figure 7.11. Influence of the load level on the axial displacement. 192

Figure 7.12. Influence of the load level on the restraining forces. 193

Figure 7.13. Influence of the stiffness ratio on the axial displacement. 195

Figure 7.14. Influence of the stiffness ratio on the restraining forces 196

Figure 7.18. All cases. Comparison of predictions given by EC4 method with 0.5L with fiber model results 202

Figure 7.19. Relative error. Comparison between predictions given by EC4 with 0.5L and fiber model simulations. 203

Figure 7.21. All cases. Comparison between the EC4+UK NA with 0.7L and numerical simulations 205

Figure 7.22. Relative error. Comparison between the results of the general method of EC4+UKNA with 0.7L and the numerical simulations. 206

Figure 7.24. All cases. Comparison between the proposed method with 0.5L and numerical simulations. 208

Figure 7.25. Relative error. Comparison between the results of the proposed method with 0.5L and the numerical simulations.....209

Figure 7.27. All cases. Comparison between the proposed method with 0.7L and numerical simulations. 211

Figure 7.28. Relative error. Comparison between the results of the proposed method with 0.7L and the numerical simulations.....211

Figure 7.29. Distribution coefficients in Wood method for an intermediate column. 212

Figure 7.30. All cases. Comparison between the proposed method with $\beta=\beta(T)$ and numerical simulations. 213

Figure 7.32. Relative error. Comparison between the results of the proposed method with $\beta=\beta(T)$ and the numerical simulations. 215

Figure 7.33. Relative error. Comparison between the results of the proposed method with the recommended effective lengths and the numerical simulations. 216

Figure 7.34. Comparison between the proposed method and numerical simulations. 217

Figure 7.35. Relative error for all the columns studied with respect to numerical simulations. 218

Figure 7.36. Frequency histogram for the prediction error of the proposed method. 218

Figure 7.37. Comparison of the numerical simulation with the predictions given by the methods studied.....219

LIST OF TABLES

Table 1.1. High-rise buildings with CFT columns built in the last years 9

Table 1.2. Formulation of nominal fire curves included in EN 1991-1-2 (CEN 2002) 25

Table 4.1. List of unprotected CFT columns for thermal model validation, own tests (Romero et al. 2011, Moliner et al. 2013) 82

Table 4.2. List of unprotected CFT columns for thermal model validation, tests by other authors (Lie & Chabot 1992) 83

Table 4.3. List of protected CFT columns for thermal model validation (Han et al. 2003a) .. 84

Table 4.4. Temperature at failure for unprotected CFT columns, own tests (Romero et al. 2011, Moliner et al. 2013) 90

Table 4.5. Temperature at failure for unprotected CFT columns, tests by other authors (Lie & Chabot 1992) 91

Table 4.6. Temperature at failure for protected CFT columns (Han et al. 2003a) 94

Table 4.7. Time at 500ºC for different type of columns and protection thickness 100

Table 5.1. Calibration of the number of elements per element 120

Table 5.2. Calibration of the number of integration points 122

Table 5.3. Calibration of the cross-sectional discretization pattern 126

Table 5.4. List of CFT columns analysed, own tests (Romero et al. 2011) 132

Table 5.5. List of CFT columns analysed from the literature 133

Table 5.6. Predicted an measured FRR and maximum axial displacement, own tests (Romero et al. 2011) 143

Table 5.7. Predicted an measured FRR and maximum axial displacement, tests from literature 144

Table 6.1. Adopted values for the parameters of the thermal parametric analysis. 155

Table 6.2. Adopted values for the parameters studied in the parametric analysis. 165

Table 7.1. Summary of the cases included in the parametric analysis 180

NOTATION

Latin upper case letters

$A_{a,\theta}$	Cross-sectional area of the steel profile at the temperature θ
$A_{c,\theta}$	Cross-sectional area of the concrete at the temperature θ
A_m/V	Section factor
D	Outer diameter of a circular section
$E_{a,\theta}$	Modulus of elasticity of steel at the temperature θ
$E_{c,\theta}$	Tangent modulus of concrete at the temperature θ
$E_{c,sec,\theta}$	Secant modulus of concrete at the temperature θ
$(EI)_{fi,eff}$	Effective flexural stiffness in the fire situation
$I_{a,\theta}$	Second moment of area of the steel profile at the temperature θ
$I_{c,\theta}$	Second moment of area of the concrete at the temperature θ
L	Length of the column
N	Applied axial load
$N_{fi,cr}$	Elastic critical load in the fire situation
$N_{fi,pl,Rd}$	Design cross-sectional plastic resistance to axial compression in fire
$N_{fi,Rd}$	Design axial buckling load of the column in the fire situation
N_{Rd}	Resistance of the column in axial compression at room temperature
N_u	Ultimate resistance of the column at room temperature
P	Perimeter of the section
Q	Internal heat generation rate per unit of volume
R	Standard fire resistance

Latin lower case letters

c_i	Specific heat
e	Loading eccentricity
f_c	Compressive cylinder strength of concrete at room temperature (test date)
f_{ck}	Characteristic compressive cylinder strength of concrete at 28 days
$f_{ck,cube}$	Characteristic compressive cube strength of concrete at 28 days
$f_{ck,t}$	Characteristic tensile strength of concrete
f_s	Yield strength of reinforcing steel at room temperature

f_y	Yield strength of structural steel at room temperature
h_j	Thermal gap conductance
$\dot{h}_{net}$	Net heat flux
$k_{i,\theta}$	Reduction factor for a material property at elevated temperature
ℓ_θ	Buckling length of the column in the fire situation
q	Heat flux vector per unit surface
t	Thickness of the steel tube

Greek upper case letters

$(\Delta l/l)_i$	Thermal elongation
Φ	Configuration factor

Greek lower case letters

α	Imperfection factor for the buckling curves/ Stiffness ratio
α_c	Coefficient of heat transfer by convection
α_i	Thermal expansion coefficient
β	Buckling coefficient/ Effective length ratio
χ	Member slenderness reduction factor ($\chi = N_{fi,Rd} / N_{fi,pl,Rd}$)
δ_{max}	Maximum axial displacement
ε	Strain
ε_f	Emissivity of the fire
ε_m	Emissivity of the exposed surface
$\gamma_{M,fi}$	Partial factor for a material property in the fire situation
$\varphi_{i,\theta}$	Reduction coefficient to make allowance for the effect of thermal stresses
μ	Axial load level ($\mu = N/N_{Rd}$) / Friction coefficient
λ_i	Thermal conductivity
$\overline{\lambda}$	Relative slenderness of the column at room temperature
$\overline{\lambda}_\theta$	Relative slenderness of the column in the fire situation
θ	Temperature
ρ_i	Density
ξ	Relative error

Abbreviations

(cal)	Concrete with calcareous aggregates
CFD	Computational fluid dynamics
CFDT	Concrete filled double tube
CFST	Concrete filled steel tube
CFT	Concrete filled tube
CHS	Circular hollow section
EC1	Eurocode 1 Part 1.2 (EN 1991-1-2)
EC2	Eurocode 2 Part 1.2 (EN 1992-1-2)
EC3	Eurocode 3 Part 1.2 (EN 1993-1-2)
EC4	Eurocode 4 Part 1.2 (EN 1994-1-2)
EHS	Elliptical hollow section
FC	Fiber reinforced concrete
FEA	Finite element analysis
FEM	Finite element modelling
F-F	Fixed-fixed supporting conditions
FRR	Fire resistance rating
HSC	High strength concrete
NF	French National Annex to Eurocode 4 Part 1.2
NS	Numerical simulation
NSC	Normal strength concrete
PC	Plain concrete
P-P	Pinned-pinned supporting conditions
RC	Bar-reinforced concrete
RHS	Rectangular hollow section
SHS	Square hollow section / Steel hollow section
SI	Strength index
(sil)	Concrete with siliceous aggregates

1. INTRODUCTION

This chapter introduces the structural technology of concrete filled steel tubular columns and their fire resistance characteristics. The benefits of using these composite columns as well as some of their applications are described. The three problems which constitute the whole fire analysis of a CFT column are explained: the fire dynamics, the thermal and the structural analysis.

1.1. BACKGROUND

Combining different materials in a single structural member to take advantage of the good qualities that they both have separately has always been a recognized strategy in building industry. Concrete filled steel tubular columns (CFT) are a type of composite columns in which the combined action of steel and concrete leads to an exceptional structural behavior. In this case, the compressive strength of the element increases due to the passive confinement that the steel tube generates on the concrete core. Simultaneously, the local buckling of the steel tube is improved due to the support of the concrete core which prevents it from suffering this phenomenon inwards.

Structural hollow sections (SHS) are the most efficient steel sections in resisting compression loads. Generating a new composite section by filling the hollow tube with concrete allows not only retaining all the advantageous features of the empty section but also developing new excellent properties. This fact reveals the synergy existing when these two elements work in conjunction. Figure 1.1 shows the behavior of a steel tubular column, a reinforced concrete (RC) stub column and a concrete filled steel tubular stub column without reinforcing bars. As it can be observed, the summation of the steel tube and the RC columns ultimate strength is less than that achieved by the CFT column (Han et al. 2014).

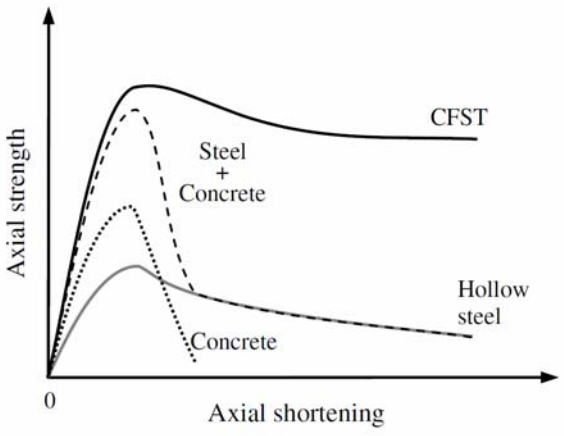

Figure 1.1. Axial compressive behavior of stub columns (Han et al. 2014).

Concrete filled tubular (CFT) columns have many positive attributes at ambient temperature for building industry: high load-bearing capacity with smaller cross-section size, attractive appearance, high stiffness and ductility, high seismic resistance and reduced construction cost and time since no formwork is necessary.

In recent years, the use of concrete filled tubular columns in construction industry, especially in high-rise buildings, has increased not only because of these positive characteristics at room temperature, but also for their inherent high fire resistance. The joined action of the steel tube and the concrete core leads to an excellent fire resistance behavior: the concrete core retards the heating of the steel tube, while, at the same time, the steel tube protects the concrete core from direct fire exposure, thus delaying the integrity loss of the concrete, which, furthermore, degrades slower than steel under fire (Twilt et al. 1996).

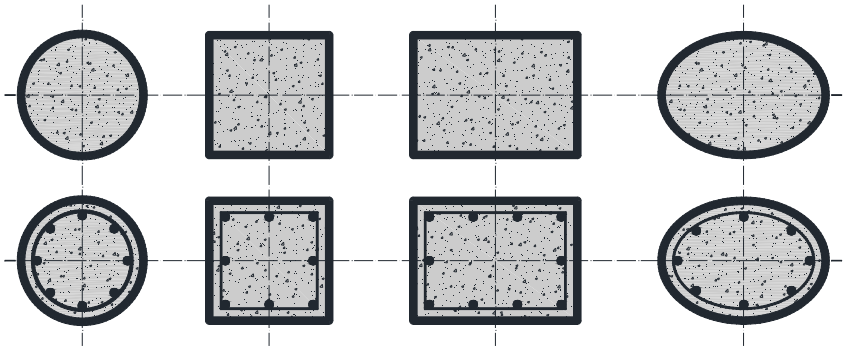

Figure 1.2. Possible shapes of CFT cross-sections.

Among the most commonly used shapes of CFT columns, it can be found circular and rectangular cross-sections (Figure 1.2) although new shapes, such as elliptical profiles, are appearing. A wide variety of concrete infills can be used such as plain concrete, bar-reinforced concrete or fiber reinforced concrete. As mentioned above, the combination of these elements permits the design of columns with reduced cross-section. However, when free spaces and higher net usable surfaces are desirable, the cross-section of the CFT column can be even smaller if high strength materials are employed, solution which is hugely applied by high-rise buildings designers.

Apart from the shapes shown in Figure 1.2, a whole concrete-filled steel tube family has been developed concurrently with the increment in the use of this type of

composite section and the interest of engineers and architects in incorporating these elements in their designs. Some of these variants are included in Figure 1.3.

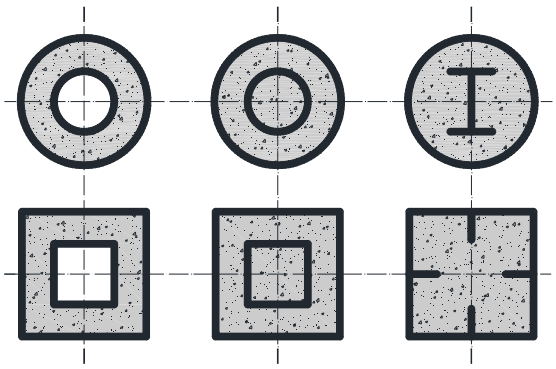

Figure 1.3. General configurations of CFT cross-sections.

Concrete filled double-skin tube or double-tube (CFDT) sections consist of an inner and an outer tube with concrete filling the cavity between them. In the case of double-tube cross-sections, the inner tube is also filled with concrete. This shape presents a high bending stiffness and higher fire resistance than the regular CFT columns due to the protection provided by the concrete to the inner steel tube (Han et al. 2014).

Structural steel reinforced CFT columns are usually employed in order to improve the resistance of the column without changing the original column shape. Finally, stiffened CFT columns, formed by welding longitudinal or transverse stiffeners on the steel tube, are a good option to avoid local buckling when it arises as a critical issue in high strength steel tubes.

The response of a structural element under a fire is full of uncertainties given the numerous phenomena implicated. The presence of external fire protection, the evolution of the temperatures in the element and the consequent degradation of the materials (very different in the case of steel and concrete in CFT columns), convert the fire behavior into a very nonlinear problem to solve and the fire resistance rating (FRR) into a very hard data to estimate.

Many have been the researchers involved in the study of the fire performance of concrete CFT columns giving as a result several models. Although existing analytical models are able to give an approximate prediction of the FRR, the overall fire response of the column cannot be reproduced. Three-dimensional numerical

models, sectional numerical models and numerical models based on fiber beam-column elements permit reproducing the whole fire behavior since they can take into account more variables. Nevertheless, in favor of simplicity and rapidity, sometimes some of these factors are neglected, what makes the solution lose realism.

The fire behavior of isolated CFT columns is being deeply studied but it has been proved that the fire behavior of a column within a complete building or within a frame is very different since its interaction with other structural members changes its boundary conditions. Studies related to this task have been carried out with the aim of analyzing the effective length of the column to be considered in the fire situation. However, there is still a lack of solid proposals and agreement in their conclusions.

Knowledge derived from the proposed models could be integrated into the current design codes in the form of proposals or simple calculation models to facilitate the task of designing with CFT columns and prevent practitioners from desisting in their intention of using these composite columns and turning into typical structural elements.

In the case of the European codes, structural designers and architects may find tedious their methods for checking the fire resistance, since they involved different stages such as the calculation of the sectional temperature field. Due to these drawbacks and other limitations, numerous opportunities of employing CFT columns are lost. Furthermore, in places where CFT columns are used, no full advantage of their inherent fire resistance is taken since the applied external protection could have been reduced or even suppressed (Kodur 2007).

This thesis focuses on circular concrete filled tubular columns, whose fire behavior as an isolated column as well as a part of a structure will be studied. This research is made with the aim of obtaining useful conclusions and give practical proposals to facilitate and promote the employment of CFT columns in the daily practice of structural engineers and architects.

1.1.1. Advantages of CFT columns

As cited previously, the use of concrete filled tubular hollow sections provides a series of benefits which make this technology very attractive for designers and structural engineers (Twilt et al. 1996, Zhao et al. 2010, Han et al. 2014). The incorporation of CFT columns to new designs has experienced an ascending trend in the last decades due mainly to the following advantages of these composite elements over other classical structural members.

Economic advantages

- This technology provides a high efficiency in the construction process since the steel tube can support significant construction loads prior to the pumping of concrete.
- Supplementary formwork for concrete pouring is not needed. The steel tube acts simultaneously as formwork and as external reinforcement for the concrete core. Besides, casting equipment used in normal concrete structures can be employed and not extra machinery is needed.
- As a result of the advanced assembly techniques currently used in structural engineering, problems with connections rarely appear. This facilitates and permits prefabrication on plant and a quick and dry assembly on site.
- The hardening of concrete does not block the construction process. The time for assembly and erection is short without any delay which implies minimum waiting times and reduced costs.

Structural advantages

- Passive confinement is provided by the steel tube to the concrete core, increasing its load-bearing capacity. In addition, inward local buckling of the steel tube is improved due to the support of the concrete core (Figure 1.4).

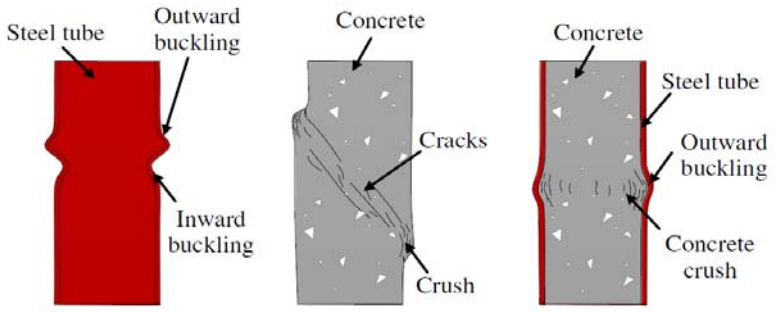

Figure 1.4. Failure modes of hollow steel tube, concrete and CFT stub columns (Han et al. 2014)

- CFT columns have higher seismic resistance than unfilled steel hollow section columns due to their higher ductility and energy absorption during earthquakes.
- The tubular steel profile has higher rigidity and load-bearing capacity due to the influence of the concrete infill. Therefore, even aesthetic slender columns can sustain higher loads without the need of increasing the external dimensions. In order to intensify this effect, reinforcing bars can be used.

Architectural advantages

- Thanks to the reduced dimensions of the column cross-section for a certain design load, the net functional floor area increases.
- Owing to the reduction in the external surface area of the columns, painting and corrosion protection coating costs decrease. The visible steel allows a wide variety of architectural designs with different surface finishings.

Fire resistance advantages

- The fire resistance of the tubular steel column increases due to the influence of the concrete infill. Concrete filled tubular columns can achieve an elevated fire resistance time without the need of fire external protection by using the appropriate amount of reinforcement (Figure 1.5).

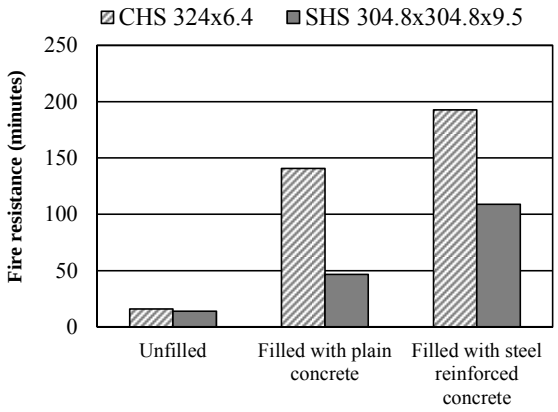

Figure 1.5. Fire resistance enhancement achieved by filling steel hollow section columns with concrete (Adapted from Zhao et al. 2010).

Since this works deals exclusively with the study of the fire behavior of circular CFT columns, this last point is the one that acquires more relevance. In

Figure 1.1 it was shown how the compressive strength of the composite column augmented by filling the steel tube with concrete. In Figure 1.5 it can be observed how not only the room temperature resistance increases, also there is a clear enhancement in the fire resistances times, which improve with the use of reinforcement.

1.1.2. Practical applications

The advantages of using CFT columns were early recognized worldwide but the lack of knowledge among designers and engineers about the structural behavior of these columns jointly with the limited variety of commercially available shapes created reticence on the use of these composite sections.

Therefore, although the first documented patent regarding concrete filled circular hollow sections dates from 1898, it was not until the middle of the 20th century that the use of this technology took relevance after several researches in this field started to bear fruit (Hicks & Newman 2002).

Thus, during the last decades, the incorporation of CFT sections to structural designs has increased becoming an indispensable compressive element in the construction of high-rise buildings and bridges and appearing more and more in other type of structures such as industrial buildings, electricity transmitting poles, subways or office blocks (Zhao et al. 2010, Han et al. 2014).

Some early applications of CFT can be found in Japan, where a great number of buildings were built between 1993 and 2004 mainly due to the construction efficiency of this technology as reported by Ikeda & Ohmiya (2009). Other examples of these buildings are the Mitsui Soko Hakozaki Building in Tokio (1989) a 19-story building with square CFT columns with external fire protection; and the Nakanoshima Intes Building in Osaka (1992) a building with 22 stories employing square and circular CFT columns (Twilt et al. 1996).

High-rise buildings

CFT columns have always found a high demand in the construction of high-rise buildings where great net usable surfaces are desirable. It is also in this field where high strength materials (steel and concrete) are being gradually introduced in the configuration of CFT columns since their use allows achieving higher load-bearing capacity with smaller cross-section size (Liew et al. 2014).

Some examples can be found in Europe dating from the late 90s. The Millennium Tower in Wien (Austria, 1999) is a 55-story building where CFT

columns were employed jointly with other elements. In Düsseldorf (Germany, 1999), the City Gate, a building composed of two 16-story towers connected by a 3-story attic to a portal was built using CFT columns of different diameters.

The SEG Plaza in Shenzhen (2000) is the tallest completed building in China using CFT columns. It has a total height of 361 m with 76 stories and circular CFT columns with diameters between 900and 1600 m were used. Two and a half stories were built per week, which makes it an example of the construction efficiency of these composite columns (Zhao et al. 2010).

Table 1.1 contains the most recent notable examples of high-rise buildings where the CFT columns technology is applied. The Taipei 101 building is a 508 m tower made of structural steel. It has a square plant with eight bar-reinforced concrete filled tubular super-columns distributed on its sides. Their dimensions at the base are 2400m x 3000m (Poon et al. 2002)

Another example is the Wuhan International Securities Building, which uses CFT columns of square and rectangular sections, reaching 249.2 m high (Zhao et al. 2010).

Table 1.1. High-rise buildings with CFT columns built in the last years

Project	***Country***	***Year Completed***
Taipei 101	Taiwan	2004
Wuhan International Securities Building	China	2008
Otemachi Tower	Japan	2014
Abeno Harukas	Japan	2014
Goldin 117 Tower	China	2016 (under construction)
Wilshire Grand Tower	USA	2017 (under construction)
Greenland's Suzhou Center	China	2018 (under construction)

In Tokyo it is located the Otemachi tower (Figure 1.6a), a high-rise building which reaches 199.7 m (38 stories above ground and 6 stories underground). The special features of the architectural planning of this building are that at the first floor a large space is provided for a forest developed on artificial ground and the concourse of the metro in the underground. To avoid causing obstructions on these spaces, square ultra-high strength CFT columns were developed to be placed specially in this areas. These columns have a reduced cross-section compared to the one obtained for CFT columns with normal strength materials designed under these situation, which proves the efficiency of this technology (Matsumoto et al. 2014).

Abeno Harukas is Japan's tallest skyscraper (Figure 1.6b). It was completed in 2014 in Osaka and is 300 m high, rising 60 stories above ground and 5 underground. This tower is a vertical city which incorporates diverse functions: a terminal station, stores, an art museum, offices, a hotel and more. Since the construction space was limited, CFT columns with high strength materials were used to minimize columns cross-section (Liew et al. 2014, Hirakawa et al. 2014).

The Tianjin Goldin Tower reaches an architectural height of 597 m being the building with the highest structural roof under construction in China (completion planned in 2016). It will hold offices and a hotel. Among all the technical issues, resisting seism and wind were the main objectives due to its slenderness (height to width ratio is 9.5). The tower has a square plan in whose corners are located six-sided polygonal CFT mega-columns formed by several inter-connected internal plates originating separable chambers (Liu et al. 2012, Han et al. 2014).

a) Otemachi Tower (Tokyo, Japan)

b) Abeno Harukas (Osaka , Japan)

Figure 1.6. High-rise buildings with CFT columns.

The Wilshire Grand Tower is a high-rise building under construction in Los Angeles which construction is planned to be completed in 2017. It will become the tallest building in the West Coast of the USA reaching 335 m (73 stories above ground and 5 stories underground) and will hold offices and a hotel. The perimeter building columns are steel sections filled with structural concrete.

The high-rise building whose construction started most recently is the Greenland's Suzhou center in Wujiang (China). It is a 358 m high tower mainly characterized by having a hollowed portion on the building core in the upper levels. It was projected to have perimeter moment resisting frames consisting of steel beams and circular CFT columns to facilitate the continual variation of the tower geometry. Its construction started in 2014 and its completion is planned in 2018 (Wimer et al. 2012).

Office buildings

Regarding office buildings using CFT columns it is worthy to mention the Fleet Place House in London (UK, 2000) an eight-story building where circular CFT columns of 323.9 mm external diameter were employed (Hicks and Newman 2002).

The multi-story Arcelor Mittal Steel Center in Liege (Belgium, 2008) is an innovative office building designed to provide an example of sustainable development (Figure 1.7a). The use of unprotected circular bar-reinforced CFT columns permitted to achieve the required fire resistance leading to a considerable reduction in fire protection materials. This construction technology enabled extensive prefabrication and a rapid built what reduced the environmental impact (AM 2008).

a) A. M.Steel Center (Liege, Belgium)

b) Obayashi TRI (Tokyo, Japan)

Figure 1.7. Office buildings with CFT columns.

In 2006, the Palestra building was finally completed in London (UK). Composite columns were used due to their structural efficiency and constructability. In this case, double-tube circular CFT columns (outer tube diameter 508 mm, inner tube diameter 273 mm) able to achieve the required 120 min of fire resistance without external fire protection were employed (SCI 2008).

A more recent example is the Obayashi Technical Research Institute (Figure 1.7b)., a multi-story building built in 2010 in Tokyo (Japan) to hold the different spread facilities and offices of the Obayashi Corporation. In order to achieve an open and flexible space, the main structural frame is arranged on one side and the columns supporting the free space are circular CFT columns made of ultra-high strength concrete and steel (Ishikawa et al. 2010, Liew et al. 2014).

Residential buildings

A good example from the early 2000s is the Montevetro apartment block in London (UK, 2000) where CFT columns of circular shape and different sections were used on its facade, Figure 1.8a.

a) Montevetro apartments (London, UK)

b) Student residence (Toulouse, France)

Figure 1.8. Residential buildings with CFT columns.

Another apartment building with CFT columns in its design is the Montevideo Residential Tower, built on the Wilhelmina pier in Rotterdam (Netherlands, 2005). The tower was projected with a hybrid structure where its

lower section is constructed with CFT columns. These columns are visible elements of the structure and are treated with an intumescent coating to achieve the required 90 minutes of resistance to fire (AM 2005).

Another example worthy to mention is the renovation of the two students residences located on the ENA (Ecole Nationales de l'Aviation Civile) in Toulouse (France, 2010). The silhouette of the two buildings was completely redesigned and modernized. As shown in Figure 1.8b, external metallic corridors were installed to give access to the renovated studios and to fulfil the requirements of fire safety. The columns of the corridors are circular CFT columns fabricated with galvanized steel and with a diameter of 160 mm, which enhances the elevation of the building (AM 2010).

Public buildings

The Museum of Flight at King County Airport in Seattle (USA) is an example of building where bar-reinforced CFT columns were used for supporting the roof of the exhibit hall, thus permitting the required fire resistance without the need of sprayed fire protection for the sake of aesthetics (Figure 1.9a). The inclusion of CFT columns came as a consequence of the extension and renovation carried out in 1994 in which the objective was allowing the entrance of natural light in the museum but assuring high free space (Kodur & MacKinnon 2000).

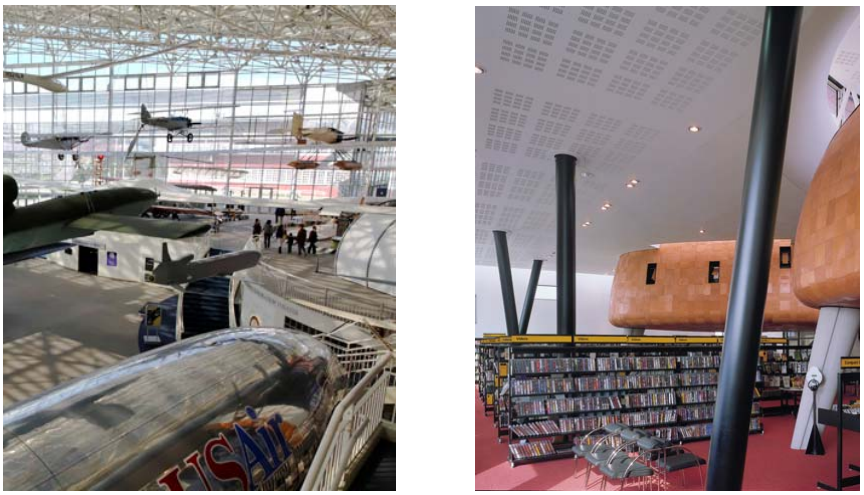

a) Museum of Flight (Seattle, USA) b) Peckham Library (London, UK)

Figure 1.9. Public buildings with CFT columns.

Another application can be found in the St. Thomas Elementary School in Ontario (Canada), where circular CFT columns with different concrete strengths were employed in the design to ensure the required one hour fire resistance rating despite the slenderness of the members (Kodur & MacKinnon 2000).

An example from 2000 is the Peckham Library in London (UK) which includes in its structure circular CFT columns working to support its front and arranged forming angles at its facade as it is shown in Figure 1.9b.

Car parks

In 2004, the extension of the car park of the Carrefour Hypermarket Aix in Les Milles (France) was completed (Figure 1.10a). It is an exposed metal structure with circular CFT columns of reduced cross-section which increase the useful area for maneuvering and parking. The easy constructability of these composite columns permitted that the work did not interfere with the regular business activity. (AM 2004).

a) Car park (Les Milles, France) b) Flinders Link Car Park (Adelaide, Australia)

Figure 1.10. Car parks with CFT columns.

The Flinders Link Car Park, Figure 1.10b, is a 700-space nine-story car park sited in Adelaide (Australia) completed in 2006. The fire engineering assessment demonstrated that the 400x300x12.5mm concrete filled rectangular hollow section

(RHS) and the 300x300x10mm concrete filled square hollow section (SHS) columns employed in the car park provided 60 minutes of fire resistance. These columns also support the two top floors of the adjacent office building that extends over the car park. Due to the simplicity of fabrication, the first construction stages were completed satisfying the tight construction schedule. (OSS 2007)

Bridges

In the case of their application to bridges, steel hollow sections filled with concrete can be found in various types of bridges, such as cable stayed bridges, suspension bridges and truss bridges. CFT members can work as piers, bridge towers and arches, and even as a part of the bridge deck system (Han et al. 2014). In China, a big amount of bridges have been built using this technology as reported by several authors like Zhao et al. (2010) and Han et al. (2014).

The main benefit of using CFT sections is the significant reduction of the construction cost due to the fact that, during the stage of erection, the hollow tube serves as the formwork for casting the concrete. In addition, given the inherent stability of the tubular structure, the aid of a temporary bridging is not necessary in most cases.

1.1.3. Construction considerations

One of the main concerns of structural engineers is to ensure the composite action between the steel tube and the concrete core. The fact of filling a steel hollow section with concrete does not make active the benefits that this structural solution presents both at room and elevated temperatures.

Regarding the concrete quality, this must satisfy the required load bearing capacity of the concrete core in fire situation but, in general, there are no special requirements for the type of cement or aggregates except for the maximum size of the coarse aggregate whose election should take into consideration the geometrical properties of the steel hollow tube (Twilt et al. 1996).

Due to the impossibility of carrying out a visual inspection of the concrete after filling, the high quality of the construction process must be guaranteed to ensure that the concrete fills the steel section completely. It is recommended for the concrete to have sufficient workability to ensure correct compaction and appropriate cohesiveness to reduce the probability of segregation and bleeding (Hicks & Newman 2002).

In case of setting reinforcing bars, they must be fixed by the use of stirrups and spacers. In this case, it is not necessary to design stirrups for shear forces because of the high shear force resistance of the hollow section under fire (Twilt et al. 1996). Normally, the use of bar-reinforced infill is not recommended for HSS columns smaller than 200 mm due to the practical difficulties in the location of the bars and in reaching the proper consolidation of the concrete. In those cases, a good alternative is opting by the fiber reinforced CFT columns (Kodur 2007).

An adequate concreting practice should be particularly maintained in order to ensure sufficient fire performance. The frame of steel hollow tubes and beams can be formed prior to the placement of the concrete mix or, instead, concrete filling can be done prior to assembly. Usually, the former option is chosen only for single story constructions due to the weight restrictions of a completely filled column. In the case of multi-story continuous columns, a complete erection of the empty structure is possible and also desirable (Twilt et al. 1996).

In order to place the concrete into the empty assembled steel hollow tubes, several ways can be found. Two typical concrete pouring techniques are shown in Figure 1.11: pump filling and gravity filling. The inner surface of the steel tube must be clean, free from water and oil but any extra treatment is required. In addition, it is worthy to mention that regardless the filling system used, special care in joint detailing and executions is need to ensure that the concrete mix flows freely. (Twilt et al. 1996, Han et al. 2014).

In the pump filling method, the concrete is pumped from the bottom of the column for which a pumping hole is usually opened at the base of the column. The concrete pumping can be extended to several floors according to the construction progress and the characteristics of the pumping machine (Han et al. 2014).

If concrete is placed from the top of the column by gravity, the depth of the fresh concrete is frequently made in stages and it should be vibrated after being placed to ensure the inexistence of voids in the columns. In the case that a peripheral concrete pipe is used it is desirable that it is located below the surface of the fresh concrete to guarantee a proper compactness.

Small drain holes are required to provide venting to the steel shell to allow any steam to escape during the fire situation. When the water content in the concrete is heated, steam is produced and it makes the steel tube be under a level of pressure that must be reduced by using the holes. Such holes must be provided in pairs for each story length at each floor level. (Twilt et al. 1996, Hicks & Newman 2002, Han et al. 2014). According to EN 1994-1-4 Section 5.3.2 (CEN 2005c) the maximum

recommended diameter for the holes is 20 mm and the spacing between them should not exceed 5m.

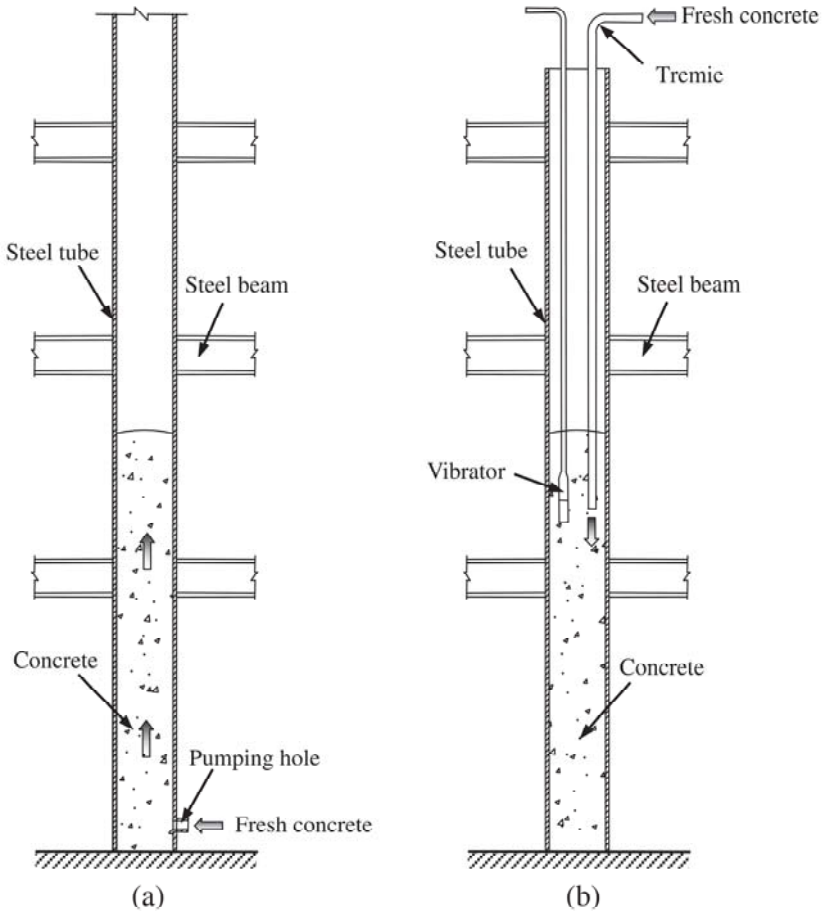

Figure 1.11. Schematic view of concrete placement systems (Han et al. 2014):
(a) pump filling and (b) gravity filling.

1.2. FIRE BEHAVIOR OF CFT COLUMNS

The fire resistance rating of unprotected hollow steel tubular columns is normally found to be about 20-30 minutes, Figure 1.5. For CFT columns, the filling of concrete can significantly increase the fire resistance since heat is absorbed by the concrete core and this delays the steel tube heating. In addition, the concrete core

has an important mechanical contribution preventing the steel tube from local buckling and also helping to bear the applied load (Han et al. 2014). This combined action provides the CFT columns an inherent high fire resistance which permits to reduce the amount of external passive fire protection to be applied or, in some cases, makes it not necessary.

The increment in the FRR can be magnified with the use of internal reinforcement. The fire resistance reached by bar-reinforced concrete (RC) filled tubular columns is higher than that achieved by steel tube columns filled with fiber reinforced concrete (FC), which, at the same time, is higher than the FRR shown by plain concrete filled hollow steel section columns (Kodur 2007).

Figure 1.12 illustrates the comparison of the FRR achieved by the three types of concrete filling for three columns with different dimensions and shapes. As it can be observed, the FRR reached can have a difference of more than 120 minutes between columns depending on their size, section and type of filling.

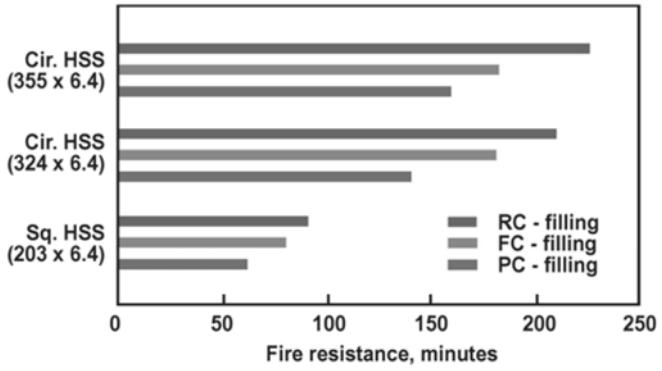

Figure 1.12. Effect of using different types of concrete infill on the fire resistance of CFT columns (Kodur 1999, 2007).

Although filling the hollow steel section column with plain concrete (PC) without any type of steel reinforcement offers the most economical combination from the perspective of fire behavior, in some cases, especially with large column dimensions, PC filled columns fail at a relatively low applied loads during fire exposure. Excessive local stresses in the concrete core due to the loss of compressive strength with temperature and also the early cracking originated by the strength reduction in the steel tube exposed to fire can be the sources of this premature failure (Kodur and Lie 1996, Kodur 2007).

The existence of steel bars in a reinforced concrete CFT column not only improves the load bearing capacity of the concrete core but also prevents concrete from crack propagation and sudden strength loss. Nevertheless, it implies the additional cost of steel bars and their installation in the CFT column (Lie and Kodur 1996, Kodur 2007).

The use of fiber reinforced CFT columns increases the load bearing capacity of the column to a certain degree and provides better fire behavior than plain concrete infill. In this case, the supplement in the cost comes only from the steel fibers (Kodur 2007).

The fire response of CFT columns can be subdivided into four clearly identified stages. Figure 1.13 displays the general fire behavior of a CFT column expressed as the evolution of the column axial displacement along time. At first phase of a fire, the steel tube expands faster than the concrete core due to its higher thermal conductivity and its direct exposure to fire and, as a result, the axial displacement rate of both components is decoupled. Owing to this fact, the axial load ratio of the steel tube progressively increases, up to a point where the whole applied load is supported uniquely by the steel tube (stage 1).

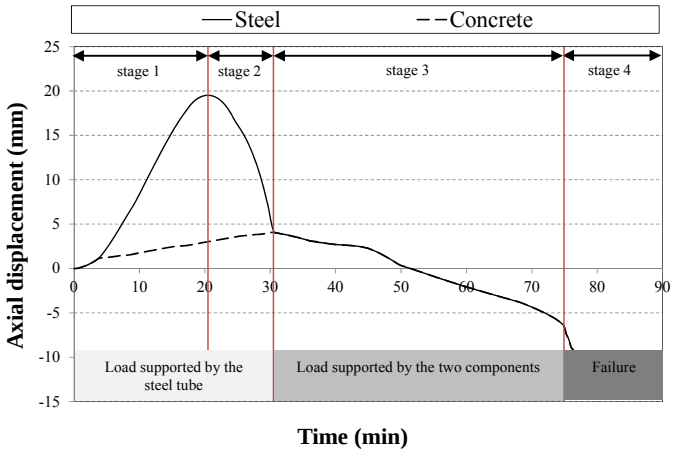

Figure 1.13. Typical behavior of a CFT column subjected to elevated temperatures.

When the steel tube reaches its critical temperature and the local yielding of the steel section occurs (stage 2), the steel tube starts to shorten, allowing the loading plate to contact back the concrete core. At this point, the axial force ratio undergoes an inversion since the load sustained by the steel tube is gradually

transferred to the concrete core as the column shortens (stage 3). In previous stages, the steel tube has lost its load-bearing capacity and now the concrete core is the element showing more resistance. The ultimate failure occurs when the concrete core completely loses its strength and stiffness after a significant period of time during which its mechanical properties are completely degraded (stage 4).

The combination of two materials with different thermal conductivity such as steel and concrete in the same member generates pronounced sectional temperature differentials which are the responsible of the fire performance described above.

This thermal behavior clearly differs from that shown by steel hollow sections where the temperature profile at a given fire exposure time can be practically considered uniform through the section and, as a consequence, also the loss of strength can be also supposed identical along the thickness tube.

However, in a CFT column, given the nonlinear temperature field in the cross-section the different components lose their original properties in a stepped manner. Although the steel tube is the element which more rapidly loses its room temperature strength because of its direct exposure to fire, due to the sink effect of the concrete core on delaying the steel tube heating, the decreasing velocity is less than that exhibited for the corresponding hollow tube.

By contrast, the concrete core, characterized by a low thermal conductivity, retains a higher percentage of its ambient temperature strength during a longer lapse of time, especially its most inner region.

Obviously, the strength reduction of a component during a fire depends on its position within the composite cross-section (Twilt et al. 1996). Therefore, in the case of steel bar reinforced CFT columns, reinforcing bars loss their initial strength at a slow rate. Even though they are usually located at the peripheral area of the concrete core, they are yet protected by a certain thickness of concrete.

This strength loss process reveals that the performance of CFT columns at room temperature is far from their fire behavior. At ambient temperature, the steel tube is the governing component of the composite section because of its higher strength and relative position. Nevertheless, at elevated temperatures it losses its original strength very fast and the concrete core bears part of the load since it is less affected by fire.

During a fire, not only the room temperature strength of the materials decreases, also the stiffness does. Therefore, the reduction of the load bearing capacity of the column is accompanied by an increment in the element

deformability. It implies that slenderness will be a parameter to consider in the study of CFT columns in fire.

In addition, the effect of structural continuity in the FRR of a CFT column within a frame is an aspect to be taken into account. When a CFT column is affected by a fire but not the surrounding beams and columns, the increment of the relative stiffness between the heated column and the enclosing frame modifies the boundary conditions of the column, affecting its effective length and, thus, its fire resistance rating.

From the great number of reported investigations and parametric studies, the most important parameters influencing the fire behavior of CFT columns can be identified. These are:

- Steel strength
- Concrete strength
- Type of concrete infill (plain, bar-reinforced or fiber reinforced)
- Type of aggregate (calcareous or siliceous)
- Outer diameter or width of the column
- Load of the column
- Eccentricity of the load
- Column slenderness
- Effective length of the column

Fire resistance is defined by EN 1991-1-2 (CEN 2002) as the ability of a structure, a part of a structure or a member to fulfil its required functions (load bearing function and/or separating function) for a specified exposure period of time, usually measured in minutes.

Hence, the main objective when carrying out the whole structural fire behavior analysis of a structural member is to determine the length of time that it will be able to resist collapse when it is exposed to a fire. This aim can have other interpretations, such as determining the time interval in achieving a certain strength reduction; or obtaining the time to achieve a given temperature; or calculating the strength for a specific time, although all of them have the same finality.

Studying the structural behavior of a member is a complicated process since it involves many variables such as fire growth and duration, temperature distribution

in structural members, interaction between structural members, changes in material properties and the effect of loads.

Therefore, in order to compute the fire resistance time of a structural member and give an accurate treatment to all these variables, it is necessary to address three problems of different nature: a fire dynamics analysis, a thermal analysis and a structural analysis. The adoption of a fire dynamics model allows the determination of the heating regime affecting the member; by means of the heat transfer model the element temperatures evolution is computed; and the structural model permits the calculation of forces and stresses to evaluate when the collapse occurs.

The next sections deal with the description of the basis of each of these problems which need to be solved to obtain the fire resistance of a CFT column.

1.2.1. Fire dynamics analysis

The response of a structural member depends on the nature of the fire which can vary substantially from fire to fire and, besides, is function of the gas temperature, which can fluctuate throughout the fire compartment considered. The key feature of the fire relevant to the structural element is the temperature-time curve imposed by the fire to its surface which is characterized mainly by the rate of temperature increase, the maximum temperature level, the duration of the fire and the cooling regime.

The evolution of compartment fires is often treated in terms of growth stages as shown in Figure 1.14. Although not every fire follow this idealized evolution, it is useful for study purposes. All fires start with an ignition stage followed by a growth stage which finally results in a flashover. This phenomenon implies the transition from a growing fire to a fully developed fire accompanied by sudden changes in the compartment atmosphere since all combustible substances in the compartment are involved in fire. During the time lapse when the fully developed fire is taking place, the rate of heat release reaches its maximum. As the fuel becomes consumed the heat release ratio declines leading to the decay stage.

Hence, the first step when the fire resistance of a member is evaluated is to adopt a fire dynamics model to simulate the actual fire in a realistic but conservative manner. According to their level of realism and complexity, three different categories can be found when modeling fire dynamics: advanced fire models, parametric fire curves and nominal fire curves.

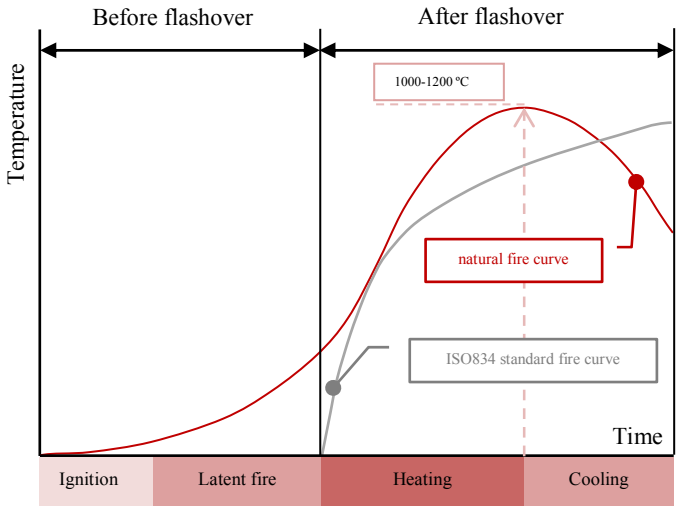

Figure 1.14. Different stages in the evolution of a fire

Eurocode 1 Part 1.2 (CEN 2002) in its Section 3.2 classifies advanced fire models and parametric fire curves as two sub-categories of natural fire models. Advanced fire models constitute the most accurate manner to simulate authentic fires. The adoption of these models involves solving the equations of the conservation of energy and mass for each zone or element. They are mainly used for research purposes. Among them it can be found the two-zone and the computational fluid dynamics (CFD) models. While two-zone models assume a constant temperature in the smoke layer, CFD models take into account a spatial temperature.

Conversely, a natural fire model can be simulated in a more simplified manner by parametric fire curves. These curves assume a uniform temperature distribution in the fire compartment and have limited field of application since they consider specific physical parameters regarding the fire load, the openings characteristics and the enclosure thermal properties. Parametric fire curves usually display both growing and cooling branches which make them not practical for testing structural elements since simulating the descending part may be difficult to control by furnace systems. On the contrary, these set of curves are very useful for design and they give an improved prediction compared to that offered by nominal fire curves. Nevertheless, their application requires the election of the proper material constitutive equations which include the modeling during the cooling situation.

Nominal curves are idealized simplified fires represented by a temperature-time relation. Precisely, they are denominated this manner because they have no dependence neither on the fire load density nor the compartment boundary conditions. These curves were initially developed for fire resistance furnace tests for the assessment and classification of structural members and materials. Although the fire resistance time determined by means of these tests does not represent the real time that the structural element can resist until collapse, it serves as a standard pattern to compare the effectiveness of different structural solutions. Figure 1.15 displays the different types of fire curves.

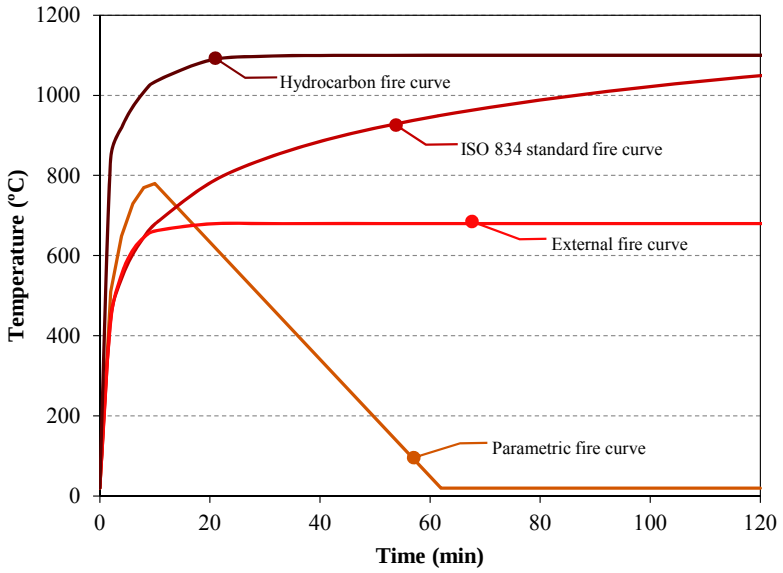

Figure 1.15. Different types of fire curves.

The best known and most widely used is the standard ISO 834 fire curve (ISO 1980) which represents a fully developed fire and assumes that the temperature in a fire compartment is uniform and that it increases indefinitely according to a logarithmic relationship with time, thus not having descending branch. Despite its limitations, this nominal standard fire curve has been incorporated into a wide number of design codes as a basis for their prescriptive methods and, by force, the most usual performance based design (PBD) approaches have been also developed based on the results and observations from standard fire tests.

EN 1991-1-2 (CEN 2002) in its Section 3.2 includes the standard ISO 834 fire curve jointly with other internationally adopted temperature-time curves employed to assess the fire resistance of structural members, all of them shown in Table 1.2.

Table 1.2. Formulation of nominal fire curves included in EN 1991-1-2 (CEN 2002)

Standard fire curve	***Formulation***	
Standard temperature-time curve (ISO 834)	$\theta_g = 20 + 345 \cdot \log_{10}(8 \cdot t + 1)$ where: -θ_g is the gas temperature in the fire compartment [ºC] -t is the time [min] -convection coefficient $\alpha_c = 25$ W/m^{2}K	(1.1)
External fire curve	$\theta_g = 660 \cdot (1 - 0.687 \cdot e^{-0.32 \cdot t} - 0.313 \cdot e^{-3.8 \cdot t}) + 20$ where: -θ_g is the gas temperature near the member [ºC] -t is the time [min] -convection coefficient $\alpha_c = 25$ W/m^{2}K	(1.2)
Hydrocarbon fire curve	$\theta_g = 1080 \cdot (1 - 0.325 \cdot e^{-0.167 \cdot t} - 0.675 \cdot e^{-2.5 \cdot t}) + 20$ where: -θ_g is the gas temperature near the member [ºC] -t is the time [min] -convection coefficient $\alpha_c = 50$ W/m^{2}K	(1.3)

While the standard fire curve represents a typical building fire based upon a cellulosic fire, the hydrocarbon fire curve represents fuel fires with an initial rapid temperature rise which can be originated in offshores and petrochemical industries.

The external fire curve is meant to be used for the evaluation of a fire affecting the outer surface of separating outside walls (i.e. facades). These members may result affected by the plume of smoke and flames going through the facade openings coming from an adjacent compartment or from a cubicle situated below the external member.

1.2.2. Heat transfer analysis

The main objective of this stage is to study the transfer of heat from the fire to the structural member. As a result, the variation along time of the temperature distribution in the member is determined.

In order to accomplish with this analysis it is necessary to know the compartment temperature-time evolution regardless of whether it comes from the response described by a standard fire curve or from the data generated by a natural fire. Besides, the fire regime can have the form either of a continuous function or a discrete pairs of temperature-time points provided that they define with enough accuracy the progression of the heating source.

Two parts can be clearly differenced in the study of the heat transfer process of a structural member. The first part deals with the transfer of heat through the border from the heat source into the exposed surface of the member which is normally considered as boundary conditions with the combination of convection and radiation; the second part is about the heat transfer within the structural member governed by the heat conduction mechanism.

Governing equation

The heat transfer by conduction within the member is described by the Fourier differential equation:

$$q = -\lambda \nabla \theta \tag{1.4}$$

where q is the heat flux vector per unit surface, λ is the thermal conductivity tensor and θ is the temperature.

This phenomenon occurs due to the difference of temperature between two points of the member and the thermal energy is transferred through the solid or fluid between them but no matter moving is observed since it takes place at atomic levels. Integrating the law of conservation of energy into the Fourier equation results in:

$$\rho c \frac{\partial \theta}{\partial t} = -\nabla \cdot q + Q \tag{1.5}$$

where ρ is the density, c the specific heat, t the time and Q the internal heat generation rate per unit of volume.

The specific heat of the material can be dependent of temperature, which introduces a non-linearity in this equation. Replacing equation (1.4) in equation (1.5) results in:

$$\rho c \frac{\partial \theta}{\partial t} = \nabla \cdot (\lambda \nabla \theta) + Q \tag{1.6}$$

which constitutes the heat transfer conduction equation to be solved subjected to an adequate initial state and boundary conditions.

Boundary conditions

First of all, the initial condition must be defined which implies specifying the temperature at which the element is submitted at the initial time.

Next, the boundary conditions of the element have to be established. The type of boundary condition applied to the fire exposed surface of the structural member is denominated Neumann boundary condition. It defines the normal derivative of the temperature as follows:

$$\lambda \frac{\partial \theta_m}{\partial n} = \dot{h}_{net} \tag{1.7}$$

where n is the normal to the surface and $\dot{h}_{net}$ the net heat flux per unit surface.

The definition of the boundary conditions may adopt several forms depending on the heat source affecting the element. In the case of a structural member subjected to fire, EN 1991-1-2 (CEN 2002) includes in its Section 3 the thermal actions to be considered at the surface of a fire exposed member which are given by the net heat flux $\dot{h}_{net}$ produced by convection ($\dot{h}_{net,c}$) and radiation ($\dot{h}_{net,r}$).

$$\dot{h}_{net} = \dot{h}_{net,c} + \dot{h}_{net,r} \ \ (\mathrm{W/m^2}) \tag{1.8}$$

Except for the initial stages of the fire, radiation is the heat transfer mechanism governing the process. It does not require any medium for transferring the heat since it takes place by means of electromagnetic radiation waves which propagate through the vacuum.

The net radiative heat flux per unit area is defined by the next equation:

$$\dot{h}_{net,r} = \Phi \cdot \varepsilon_m \cdot \varepsilon_f \cdot \sigma \cdot \left[(\theta_r + 273)^4 - (\theta_m + 273)^4 \right] \ (\mathrm{W/m^2}) \tag{1.9}$$

where:

- Φ is the configuration factor
- ε_m is the surface emissivity of the member
- ε_f is the emissivity of the fire
- σ is the Stephan-Boltzmann constant, equal to 5.67×10^{-8} $\mathrm{W/m^2K^4}$
- θ_r is the effective radiation temperature of the fire environment [ºC]
- θ_m is the surface temperature of the member [ºC]

As observed, a configuration factor is included in the formulation which allows keeping the emissivity of the surface and the fire constant while varying radiative heat flux levels. According to EN 1991-1-2 (CEN 2002) Section 3, a conservative option is taking $\Phi=1$ but a more realistic value can be obtained by the method in its Annex G to account for the so called position and shadow effects.

The fire emissivity is generally taken as ε_f = 1.0. For the rest of emissivity values and according to EN 1991-1-2, Section 3, ε_m = 0.8 may be chosen unless a specific value is included in the material related fire parts of the same European code. In fact, EN 1994-1-2 in its Section 2 recommends a value of ε_m = 0.7 for the coefficient of steel and concrete related to the member surface.

Convection is the other heat transfer mechanism acting simultaneously with radiation. In this case, the thermal energy transfer takes place due to the motion of a fluid and, thus, mass transfer is observed.

The net convective heat flux component should be determined by:

$$\dot{h}_{net,c} = \alpha_c \cdot (\theta_g - \theta_m) \ (\mathrm{W/m^2}) \tag{1.10}$$

where:

- α_c is the coefficient of heat transfer by convection [$\mathrm{W/m^2K}$]
- θ_g is the gas temperature in the vicinity of the fire exposed member [ºC]
- θ_m is the surface temperature of the member [ºC]

For the coefficient of heat transfer by convection α_c, EN 1991-1-2 in its Section 3 recommends different values in function of the nominal fire curve chosen which can be consulted in Table 1.2 of this document. These coefficients are not an intrinsic characteristic of the surrounding fluid, but they are parameters obtained through a series of experiments taking into consideration several variables such as the geometry of the exposed surface of the structural element, the fluid properties or the origin of the fluid movement and its velocity.

Jointly with equation (1.6), equation (1.11) is also non-linear, in this case, as a consequence of the radiative boundary condition which implies the consideration of a non-linear term of the temperature. All the nonlinearities associated to the problem justify the habitual use of numerical methods to solve this type of heat transfer analysis.

Resolution of the heat transfer problem

With regard to the process of solving the heat transfer problem, it is worthy to mention that, generally, the calculation of the thermal response of a structural member can be decoupled from the computation of the structural response provided that the geometry of the structure does not have substantial changes during the period considered.

In order to solve the heat transfer problem and obtain the evolution of the temperature field with time, numerical modelling software is often used. Models developed with generic finite element analysis programs such as ABAQUS or with other programs more specialized in structures in fire like SAFIR can be employed.

Addressing the resolution of the differential heat transfer equation with an analytical approach can become a complicated and tedious work. Only for those cases where the heat transfer problem can be reduced to a sectional problem, analytical models are a reasonable option.

1.2.3. Structural analysis

In order to obtain the fire resistance rating of a member, the last step is to carry out the pertinent structural analysis. This step takes as a starting point the previously determined field of temperatures for the period of fire exposure considered. At every time step of the calculation process, the material temperature dependent constitutive equations are updated to account for the actual strains and stresses of the element. Finally, the FRR will be determined as the instant of time when the member collapse under a certain applied load.

In the field of CFT columns, several three-dimensional models, sectional models and also analytical models have been developed in the last decades with the aim of simulating the fire behavior of this type of composite columns.

In the next chapter, an extensive review of the state of the art which covers analytical, numerical and experimental investigations on isolated CFT columns as well as on columns within frames will be accomplished with the aim of acquiring the specific knowledge for dealing with the analysis of concrete filled tubular columns in fire and focusing the efforts in the study of the actual problem.

2.

STATE OF THE ART

In this chapter, a revision of the current situation of the investigations dealing with the fire behavior of concrete filled tubular columns is presented. A review of the existing thermo-mechanical models for this type of composite columns is included, both for isolated columns and columns within structures. A description of the experimental programs carried out so far and also a revision of the published calculation proposals are part of the content of this chapter.

2.1. GENERAL

With regard to the study of structural elements in fire, researchers focused their works on various topics depending on their nature. Therefore, the combination of contributions from the different research fields supposes advances in the knowledge of the fire performance of CFT columns.

The behavior of materials at high temperatures, the resolution of the thermal problem or the determination of the structural state both for single columns and for columns within frames are the main areas where researchers have focused their efforts.

Eurocode 4 Part 1.2 (CEN 2005c), the reference code in Europe for the fire behavior of composite members, includes the option of employing advanced calculation models to obtain more accurate and realistic simulations for the fire behavior of CFT columns. According to this code, separated calculation models can be considered: a thermal model for the determination of the thermal response and a mechanical response model for the study of strains and stresses.

Regarding the thermal model, the temperature dependent thermal properties of materials, the effects of non-uniform heating and the influence of moisture content should be considered. Concerning the mechanical response, Eurocode 4 Part 1.2 suggests taking into account the combined effects of mechanical actions, geometrical imperfections and thermal actions; and the temperature dependent mechanical properties of the materials. It is also recommended their validation against relevant tests in terms of deformations, temperature and FRR.

In order to model properly all these phenomena and take into account these characteristics, several works and studies have been carried out during decades.

Many research works dealing with the behavior of steel and concrete at high temperatures have been developed. Given the complex response of concrete, numerous efforts have been concentrated in the investigation of its behavior under fire conditions and thus, several models have been proposed (Anderberg & Thelandersson 1976, Schneider 1986, 1988, Diederichs 1987, Terro 1998). An extensive revision of the most relevant models can be found in the work published by Li & Purkiss (2005) who, in addition, made their own contribution by means of a new proposal; and in the publication of Youssef & Moftah (2007).

In the ambit of constitutive equations for steel and concrete applied to CFT columns, it must be highlighted the work developed by Lie (1994) who proposed

models for steel and concrete at elevated temperatures. The assessment of the influence in concrete of the lateral confinement has been always an issue in perpetual study and thus, Han (2001) determined experimentally the constitutive expressions for concrete in CFT columns under fire considering this effect. In the same line, Youssef & Moftah (2007) presented analytical proposals to model confined concrete at high temperatures.

In the matter of the thermal analysis, which constitutes the step prior to conducting the mechanical analysis, several proposals for solving the heat transfer problem of CFT columns have been published in literature, where one of the forefathers was Lie (1984) with his finite differences proposal based on the previous work from Dusinberre (1961).

Nevertheless, nowadays designers have at their disposal a wide range of finite element programs to solve both the nonlinear thermal analysis and the mechanical problem.

With respect to the platforms exclusively built for the fire analysis of structural members, one of the earliest and most widely used is FIRES-T3 (Iding et al. 1977), developed at the University of California at Berkeley (USA). The packages TASEF (Sterner & Wickström 1990), created at Lund Institute of Technology (Sweden), and SAFIR (Franssen 2003), produced at Liège University (Belgium), are also two interesting options.

General purpose programs constitute an excellent alternative to simulate the whole fire response of CFT columns through the corresponding thermo-mechanical problem. Good examples of these are ABAQUS, ANSYS or DIANA, amongst others.

An attempt to model the fire behavior of CFT columns with neural networks was presented by Al-Khaleefi et al. (2002) who, after completing an experimental campaign, developed a model of these characteristics. However, a great number of tests results are needed to carry out a proper training of the neural network to achieve acceptable accuracy levels.

Although the common practice so far has been implementing thermo-mechanical models, an approach with more complexity are thermo-hygro-mechanical models which take into account the movement of water vapor in the material due to the increment of temperature and some authors have worked on developing models to account for this phenomenon in porous materials such as concrete (Gawin 1999, 2003, Bianco et al. 2003, Benes & Stefan 2015).

In the next sections, the numerous research works that can be found in literature referring CFT columns in fire are reviewed. The state of the art of analytical and numerical models dealing with both thermal and mechanical analysis is revised. Two categories must be distinguished: isolated member models and global structural models. The most relevant experimental programs conducted on CFT columns at elevated temperatures, as well as the main simplified proposals for fire design found in literature are hereafter described.

2.2. THERMAL MODELS

Thermal analysis is the first step to carry out when the whole response of a CFT column is analyzed. In the reviewed literature, most of the studies considered realistic features regarding the heat transfer process, but these works focused on models to study the global fire behavior of CFT columns. Usually, computing the temperature distribution of the column is just an implicit step within the entire calculation and it is not presented in detail as a specific procedure.

Therefore, with regard to studies dealing exclusively and explicitly with the thermal analysis of CFT columns, just few publications can be located.

The first publication found which presents a model for the resolution of the thermal problem is the work carried out by Lie (1984) who employed finite differences to develop a model for circular CFT columns and also an analytical model to account for the mechanical response of the column. Hence, Lie (1984) developed a theoretical formulation for circular CFT columns based on the general methodology proposed by Dusinberre (1961). The details of this model can be found in several publications (Lie 1984, Lie & Chabot 1990, Lie 1994) and it is based on a layered discretization of the section. This formulation was later extended to rectangular CFT columns subdividing the section in rectangular elements (Lie & Irwin 1995). In this model, perfect contact was assumed at steel-concrete interface in the fire situation, which later has been proved to be unrealistic.

A numerical method using the Green's function approach was developed by Wang & Tan (2006) to solve the heat transfer problem in CFT columns permitting the calculation of the cross-sectional field of temperatures and the heat flux at the steel-concrete boundaries of the composite element. However, the concrete and steel properties were considered temperature independent, perfect contact between materials was assumed and also the presence of moisture in the concrete was neglected.

As a consequence of the conservative assumptions usually made, the theoretical models proposed may lose accuracy and realism in their predictions. With respect to the modelling of the steel–concrete interface of these composite columns, the simplistic assumption of perfect contact was traditionally adopted. Just the research carried out by Ghojel (2004) dealt with the determination of the value of the thermal conductance at the steel-concrete boundary. This author studied the heat transfer through the steel-concrete interface of circular steel tubes filled with plain concrete for both loaded and unloaded conditions. Finally, an equation where the thermal conductance is function of the steel tube temperature was presented.

Although some realistic features were not considered, these works presented solid formulations to obtain the temperature distribution at the cross-section of CFT columns. In spite of this, since no straightforward equations were provided, designers may find tedious and time-consuming implementing them in the daily practice.

In addition, it is worthy to mention that these formulations focused only in the thermal analysis of unprotected members and were not extended to protected CFT columns.

2.3. ISOLATED MEMBER MODELS

2.3.1. Analytical models

As mentioned above, the first published theoretical research about fire behavior of CFT columns belongs to Lie (1984) who jointly with the equations for the cross-sectional temperatures computation developed a mathematical proposal to calculate the mechanical response. Thus, given a certain curvature at column mid-height, the axial strain is used as the iteration variable to satisfy equilibrium between the applied and resisting moment. With this procedure, the force-mid-height deflection relation is determined step by step during fire exposure in order to arrive at the maximum column load carrying capacity. The model was validated against experimental results of circular (Lie 1984, Lie & Chabot 1990, Lie 1994) and square (Lie & Irwin 1995) CFT columns under fire. Specific formulations for the constitutive laws of steel and concrete at elevated temperatures were used. Lie pointed out the discrepancy between measured data and analytical axial deformation values as a result of the thermal expansion and creep that cannot be completely accounted for in this type of model.

Han (2001) presented a structural model to predict the fire resistance of CFT by means of an analytical procedure. Thermal dependent constitutive equations for steel and concrete were employed, taking into account the confinement effect in the concrete stress-strain relationships. Hence the model accounted for the physical and geometrical non-linearities existing in the fire behavior of CFT columns. Tests of square and circular CFT columns were used in validation. This theoretical model was used to provide information about the necessary fire protection measures for the CFT columns in the SEG Plaza in Shenzen, the highest high-rise building finished in China which includes CFT columns in its design.

A new approach came from Tan & Tang (2004) who extended the Rankine method to predict the fire behavior of plain and reinforced CFT columns in the form of the plastic squash load and the elastic buckling capacity at room temperature. Based on the same approach, Hu et al. (2015) recently proposed a modified Rankine method considering the shear bond effect between the two failure modes. The conventional Rankine approach uniquely considered a linear interaction between the two failure modes and ignored their coupling interaction which results in a lower limit prediction in comparison with measured failure loads. Model results were validated against test data from different programs and also compared to the EN 1994-1-2 predictions.

Also for circular and square CFT columns, Yin et al. (2006) developed an analytical nonlinear model. The first step of the model deals with the calculation of the temperatures by solving the corresponding heat transfer equations. Next, a mechanical analysis to obtain strain and stresses at elevated temperatures is presented, where the compression failure mode was exclusively considered, assuming no bending and straight columns at failure. In this case, for the concrete core the constitutive expressions by Li & Purkiss (2005) for normal strength concrete were applied; for the steel, strain-stress equations proposed by Lie (1994) were employed. For comparison purposes, the square and circular columns studied were selected to have the same cross-section areas for both steel tube and concrete core, concluding that columns with circular shape presented a slightly higher fire resistance.

2.3.2. Numerical models

With regard to numerical models for the fire simulation of isolated CFT columns, fiber models, sectional models and three-dimensional models can be found in literature. The trend followed by numerous authors is developing sectional and three-dimensional models capable of reproducing the remarkably nonlinear behavior

of these members at high temperatures. Nevertheless, fiber models are the most efficient in terms of computational cost although sometimes some assumptions are made for the sake of simplicity.

Three-dimensional models

Zha (2003) presented a finite element three-dimensional model for circular CFT columns. Two programs were employed to carry out the thermal and mechanical analysis: FIRES-T3 (Iding et al. 1977) for computing the cross-sectional temperature field and DYNA3D, a three-dimensional nonlinear finite element code developed by the author. Once the temperature field was computed, a time-dependent thermal-stress analysis was executed using eight-node solid elements. Material models for elevated temperatures were employed: the model proposed by Schneider (1988) for the concrete core and the equations presented by Witteveen et al. (1977) for the steel tube. Since circular columns where considered, modelling a quarter of the section was enough due to symmetry. A specific value of 2L/1000 was adopted for the initial imperfection of the composite column. In this work, no comparison with experimental data for calibration was included and only the fire resistance times obtained were compared to those given by the pertinent codes.

A three-dimensional model was developed by Ding & Wang (2008) using the commercial finite element software ANSYS. The model covered the study of circular and square CFT columns in fire. The analysis procedure was a sequentially coupled thermal –stress analysis. First, a model with 2-D solid thermal elements was used to solve the transient heat transfer problem. Once the temperature distribution was obtained, the nodal temperatures were introduced as an input to a mechanical model consisting of eight-node 3-D solid elements. Material properties at elevated temperatures were defined according to EN 1994-1-2 (CEN 2005c). The authors considered some significant aspects sometimes ignored for the sake of simplicity. These aspects were the concrete moisture content, the gap thermal resistance at the steel-concrete interface and the relative slip between the two components represented in this case by a surface to surface contact. The model was able to produce satisfactory predictions from the point of view of the fire resistance rating.

In the same line, Hong & Varma (2009) proposed another three-dimensional model for CFT columns in fire using the finite elements analysis package ABAQUS. Square steel tubular columns filled with plain and bar-reinforced concrete were studied. In this model, the fire dynamics analysis was considered as a prior step to the sequentially coupled thermal-stress analysis which transformed the model in a

three-step procedure. Instead of adopting a nominal fire curve or experimental temperature-time points as the thermal load, a fire dynamics analysis was carried out by means of the software FDS (Fire Dynamics Simulator), developed by researchers from the NIST Building and Fire Research Laboratory. As a result, a temperature-time curve was obtained to be the input of the thermal analysis model. For the heat transfer and stress analysis, eight-node solid elements were used to model the concrete core and four-node shell elements for the steel tube. For the specimens with reinforcing bars, two-node truss elements were used for the longitudinal elements. After evaluating the response of several materials mechanical models, Lie & Irwin (1995) for concrete and Poh (2001) for steel were adopted. However, these authors modeled the steel-concrete interface as perfect contact, assuming that no heat loss exists at this boundary.

In the last years, other type of materials applied to this type of composite columns has been investigated. The fire response of high strength self-consolidating CFT stub columns of square section was studied by Lu et al. (2009) who presented a finite element model developed by using the commercial program ABAQUS accompanied of an experimental program. Linear four-node shell elements were employed for the steel hollow section whereas for the concrete core linear three-dimensional eight-node solid elements were used. Again, a sequentially coupled thermal-stress analysis procedure was proposed. For high strength concrete, the thermal properties presented by Kodur (2007) were used except for the thermal expansion coefficient for which the model from Lie (1994) was adopted for both concrete and steel. The mechanical models implemented were the uniaxial stress-strain model at elevated temperatures from Lie (1994) for the steel tube; and the compressive uniaxial stress-strain relation proposed by Han et al. (2003b) with a concrete damaged plasticity model for the core. This model was intended to analyze the failure mechanism of these composite columns in fire and to investigate aspects like the concrete fracture energy, the steel-concrete contact, the load distribution between components or the local buckling of the steel tube.

Song et al. (2010) developed a realistic finite element three-dimensional model in ABAQUS to simulate a set of experiments of concrete filled steel tubular stub columns under various thermal and mechanical loading conditions. This investigation was planned following the same scheme than the previous research carried out by Yang et al. (2008a) and the model developed was then used to study all the stages during a fire: ambient, heating, cooling and post-fire, using the corresponding stress-strain relationships for each stage. In this three-dimensional model also a sequentially coupled thermal-stress analysis was implemented and

four-node shell elements and eight-node brick elements were used for steel and concrete respectively. In order to model the interaction between the two surfaces at the steel-concrete interface, a contact pressure model in the normal direction and a Coulomb friction model in the tangential direction were adopted.

Espinos et al. (2010) presented an advanced three-dimensional model taking into account some of the aspects neglected by other researchers which introduced more realism to the model. The model focused on the fire behavior of unprotected CFT columns of circular shape. ABAQUS was again the package employed to simulate the sequentially coupled thermal-stress analysis. Once the temperature field was obtained the nodal temperatures were the input of the mechanical analysis in form of predefined field. The model was meshed with three-dimensional eight-node solid elements for both the steel tube and the concrete core, and two-node truss elements for the reinforcing bars. The steel mechanical model from EN 1993-1-2 (CEN 2005b) and the concrete mechanical model developed by Lie (1994) were adopted. The model was validated against experimental results and a sensitivity analysis was carried out. The thermal conductance at steel-concrete interface, the relative longitudinal displacement occurring between the two components, the initial imperfection and the moisture content in the concrete were some of the realistic considerations included. Thus, not only the model was able to produce accurate results of the FRR but also the whole response of the columns along time was well captured.

Given the trend of using new shapes and configurations for CFT columns jointly with special materials new works and studies have emerged.

With the aim of putting some light in the performance of elliptical CFT columns, the same authors proposed also a model for simulating their room and elevated temperature behavior. The model proposed by Espinos et al. (2011) was built on the previous work carried out by the authors on circular CFT columns. A room temperature model for elliptical CFT stub columns was validated against test data and subsequently extended to evaluate their fire response. Provided that no experimental data at high temperatures was available, the same material properties and parameters of the consolidated model for circular CFT columns (Espinos et al. 2010) were adopted. Eight-node elements were used to mesh the member with the ABAQUS package and a sequentially coupled thermal-stress analysis was employed. Besides, a parametric study and a comparative study were carried out to assess the effect of main parameters variations and the effectiveness of the section shape when compared to circular CFT columns, concluding that under certain

concentric loads and only for stub columns circular members showed a better fire comportment.

In the same line of new configurations, Lu et al. (2011) developed a model for double-skin CFT columns with circular and square hollow section for both inner and outer tubes. ABAQUS package was employed to develop a sequentially coupled thermal-stress analysis. Interaction was considered to be a very important factor in the fire behavior of these columns. For the concrete the model proposed by Han et al. (2003) was used and for steel Lie's model (1994) was adopted. Once the model was validated, a parametric analysis was executed to study aspects like the capacity of inner and steel tubes, the fire protection or the sectional dimensions. Some design recommendations were given.

Wang &Young (2013) investigated the effects of using high strength steel in CFT columns. A three-dimensional numerical model was developed using ABAQUS and calibrated against tests results of CFT columns with normal strength concrete given the lack of experimental data regarding this material. A two-step analysis was modeled: first, a thermal model was executed and next a nonlinear structural analysis was completed. A parametric study was carried out to evaluate the influence of high strength steel with yield strength of 690 MPa on CFT columns. The fire resistance of the members with high strength steel showed a significant improvement with respect to the CFT columns whose steel tubes had yield strength of 275 MPa, but it did not occur when specimens under the same load level were compared.

Tondini et al (2013) also investigated the characteristics of high strength steel at elevated temperatures. A three-dimensional finite element model was developed in the SAFIR platform to represent numerically the fire behavior of some circular hollow sections tubes and concrete filled circular tubes that had been previously tested by the authors. The main purpose was to check the applicability of the reduction factors recommended by EN 1993-1-2 (CEN 2005b) and there were evidences of an overestimation of the fire resistance. However, given the limited number of experiments used in validation these conclusions were not as solid as desirable.

Recently, it has been the study of the post-fire behavior which has taken part of the current outlook of CFT columns investigations.

Thus, Yang et al. (2015) developed a three-dimensional model in ABAQUS to simulate the post-fire behavior of slender bar-reinforced CFT columns. A sequentially coupled thermal –stress model was implemented. It was validated

against experimental data from tests carried out by the authors within the same study. The heating phase following the nominal standard fire curve and the cooling phase were included in the analysis. Once the model was calibrated, a parametric study was executed to identify the influence of key parameters on the post-fire behavior. The residual capacities were observed to be sensitive to heating time, cross-sectional dimension, slenderness ratio, material strength, steel tube to concrete area ratio and reinforcement ratio, whereas the buckling reduction factor was found to depend mainly on the slenderness ratio, the heating time and the cross-sectional dimension. Finally, a simplified design method was proposed for predicting the load-bearing capacity after exposure to standard fires.

Yao & Hu (2015) studied the cooling behavior and the residual strength of CFT columns subjected to fire. The authors presented a three-dimensional model developed in ABAQUS which covered all the stages of the complete fire. The analysis was sequentially coupled; first a thermal analysis was carried out and then the temperature filed was introduced as a predefined field for the structural analysis. Heating conditions were varied, employing both nominal and natural fire curves. The model was validated against numerous experiments and a parametric study was developed. It was observed that the residual strength of CFT columns after natural fire exposure is generally affected by the fire duration time, cross-sectional dimension and slenderness ratio.

Sectional models

Schaumann et al. (2009) developed a sectional numerical model to predict the fire behavior of high strength CFT columns with different type of reinforcement. The program BoFIRE, developed by the authors, was used to implement the model and four-node isoparametric elements were used. It was able to reproduce the thermal and structural behavior of steel and composite structures at elevated temperatures with the appropriate temperature dependent material properties and considering the actual temperature distribution. The analysis was carried out by means of an incremental procedure where thermal and structural responses were coupled at every step. Although the finite differences method used for the cross-sectional thermal analysis reproduced the temperature field with great accuracy, the whole model was not able to represent local effects such as the contact mechanism that occurs under fire and, consequently, the mechanical response obtained was a little away from the actual one.

Fiber models

Renaud et al. (2003) developed an advanced numerical model using beam-column elements with an updated lagrangian formulation to simulate the fire behavior of steel-concrete columns taking into account the interaction between the hollow steel section and the concrete core. The thermal and the mechanical behavior of the columns were assumed to be uncoupled. The authors modeled a CFT column combining in a parallel way the next elements: one beam-column element for the steel hollow section with two nodes and three degrees of freedom at each node; a second element of the same characteristics representing the concrete core; and a third element acting as a longitudinal shear link between them along the whole length. Each element had its corresponding fiber discretized section. A uniform temperature was assumed over the entire column length and the cross-section thermal analysis was carried out by a finite differences method. Thermal and mechanical material properties from EN 1994-1-2 (CEN 2005c) were used. Although slip between the two components was taken into consideration, the gap phenomenon between steel and concrete was neglected. The authors found that when the whole response was analyzed from the point of view of the axial displacement along time, the column elongation was overestimated at the end of the test, even when slip between steel and concrete was considered. However, the model proved to give a good estimation of the fire resistance time.

Chung et al. (2008) developed a simplified fiber model for square CFT columns under concentric loads which after was extended to eccentric loads (Chung et al. 2009). The discretization of the section was based on square elements. The thermal analysis, carried out by means of finite differences, was decoupled from the mechanical analysis. Material thermal and mechanical properties from Eurocode 4 (CEN 2005c) were employed. The numerical model was simplified due to some assumptions made by the authors such as ignoring the local buckling of the steel tube, not modelling the steel-concrete interaction or neglecting the initial imperfection of the column.

Yang et al. (2008a) developed NFEACFST, a finite element model for CFT columns which considers the column length sub-divided into two-node finite elements. Circular and square columns were modeled with the composite cross-section discretized in small blocks. In this work, the model not only covered the heating phase in a fire but also the rest of stages: initial state at room temperature, cooling and post-fire loading to fire. Again, some simplifications were considered such as neglecting the steel tube local buckling or ignoring the relative slip existing between the steel tube and the concrete core at elevated temperatures.

Along these lines, Jeffers & Sotelino (2009) presented a three-node fiber heat transfer element accounting for transverse and longitudinal temperature variation in a structural member for modeling the three-dimensional response of structures in fire. However, the authors did not focus on developing a model for the fire behavior of CFT columns but rather they developed a heat transfer element which could be used in a multitude of elements and more complex structures. The effort was made on solving the heat transfer problem and making the element compatible with any beam-column element so that once the finite element was implemented in commercial software such as ABAQUS, a sequentially coupled thermal-mechanical analysis could be run using elements available in the software.

2.4. GLOBAL STRUCTURAL MODELS

The behavior of a column in a complete building is different from that of an isolated column and this is even more noticeable when its fire behavior is analyzed. It is very important to take into consideration the structural continuity in the fire behavior of a composite column, since its interaction with other structural members in a frame changes not only its boundary conditions, but also the loading conditions.

Therefore, researchers detected the necessity of studying this combined behavior to be able to predict and evaluate the fire resistance of a column.

Currently, Eurocode 3 Part 1.2 (CEN 2005b) and Eurocode 4 Part 1.2 (CEN 2005c) take into consideration the influence of the structural continuity in the design assumptions for composite columns. An effective length of 0.5L is recommended in the case of a composite column continuous at both ends (intermediate story), whereas for a column continuous at one end only (top story), a value of 0.7L is suggested (e.g. L is the system length).

In this section a detailed revision of the state of the art on global structural models for CFT columns subjected to fire is presented. The main models which can be found currently in the literature will be reviewed.

2.4.1. Global models for steel columns

In contrast to the case of CFT columns, the fire behavior of steel columns with structural continuity has been studied in depth by means of numerous numerical programs and many examples of it can be found in the literature. Before analyzing the situation of global structural models in the field of CFT columns, the

most relevant studies dealing with steel columns within frames will be presented to shed some light on the knowledge of the structural continuity effects.

Wang et al. (1995) early detected the necessity of understanding the structural behavior of steel frames during a fire. The authors developed their own program for structural analysis of frames at high temperatures where uniquely the column was subjected to fire and the rest of the frame remained at ambient temperature. The authors noticed the important dependency of its bearing capacity on its slenderness, which, in turn, was dependent on its end restraints. Moreover, the variation of the column relative stiffness to the adjacent members of a frame due to the different rates of reduction of stiffness in the various frame members was detected. A parametric study was carried out and according to the authors, the effect of fire on end column conditions was proved and thus, the support conditions of a column could be considered as built-in.

Along these lines, Wang (1997a) went deep and performed a parametric study to evaluate the effects of structural continuity on the fire resistance of steel columns in frames. Two aspects were studied: the beneficial contribution related to the enhancement of the rotational restraint of the column; and the detrimental effect of the restrained thermal expansion which increases the column compressive load. It was found that these two effects canceled each other in columns used in practice. In this work, again the most dangerous scenario was adopted where only the column was heated. For intermediate stories, Wang considered that a value of 0.6L for the effective length was the most accurate instead of 0.5L as recommended in Eurocode 3. However, since the effect of axial restraint was not considered in this proposal, the limiting temperature was still overestimated. In order to compensate this, the author recommended increasing a 20% the fire protection thickness calculated under cold condition (effective length and axial load at ambient temperature).

Gomes et al. (2007) proposed a reduced analytical model for the stability analysis of steel frames. In this case, the study combined the location of the column subjected to fire (intermediate or top story) and the fire protection of the beams at the top of the columns (cold or heated). The assessment of the results pointed out the high sensitivity of the fire resistance to the columns slenderness. According to the authors, recommendations of Eurocode 3 Part 1.2 produced unsafe predictions particularly for intermediate columns. The authors also proposed a linear solution which fits well with analytical results produced by their model.

Shepherd & Burgess (2011) developed a simplified finite element model of an axially restrained column using the Vulcan program which incorporated

geometric nonlinearities and used EN 1993-1-2 material properties. Axial restraint was modeled by means of a spring element at the same end where the load was applied. Besides, this model was able to reproduce the post-buckling behavior of the columns. A detailed theoretical explanation about the fire performance of steel columns within frames was included to set the values of the parameters for the numerical analysis. The authors investigated the effects of varying the slenderness and load ratio of the specimens. Some design recommendations for steel-framed columns were proposed. The need of designing steel frames for robustness to ensure that a new equilibrium state is reached after sudden buckling was also pointed out by the authors.

Correia et al. (2013) developed a three-dimensional model in ABAQUS to reproduce the fire behavior of a steel column with restrained thermal elongation. The model adopted the temperature dependent properties of EN 1993-1-2 (CEN 2005b). A coupled temperature-displacement analysis was employed where thermal and mechanical responses were performed together at the same time. The model was validated against tests of columns within a frame so in the numerical model this frame was reproduced. Once validation was completed, a parametric study was carried out. The authors found that the detrimental effect of the restraint to thermal elongation was cancelled by the beneficial effect of the rotational restrain provided by the structure. An analytical formulation for the assessment of the fire performance of steel columns taking into account building restrictions was presented in the same work.

Couto et al. (2013) developed a model with beam elements implemented in the software CLoad which was able to calculate accurately the evolution of the critical load of frames in the fire situation. In this model, some simplifications were done such as neglecting the axial deformation of the elements. The results of the buckling analysis executed by CLoad were validated against other results at normal and high temperatures. Once the model was validated for multi-story buildings in fire situation, a parametric analysis was conducted. Both braced and unbraced frames were studied and different column support conditions were also considered. The number of stories and bays also varied. The authors concluded that the fire effective lengths obtained by simulation tended towards the values suggested by EN 1993-1-2 (CEN 2005b) for braced framed. For unbraced frames, this code does not include any suggested value and thus a proposal was made for these cases.

As it can be observed, for steel columns within a frame researchers has not reached an agreement about the appropriate value of the effective length in fire although some of them seem to agree with the recommendations from EN 1993-1-2

(CEN 2005b). However, the conclusions from all the works coincided in the importance on taking into account the effects of the surrounding frame on the fire behavior of the column.

2.4.2. Global models for CFT columns

For concrete filled tubular columns, most of the published works focus on the study of CFT columns in fire but as isolated columns with explicitly well-defined boundary conditions which do not change during the fire exposure time. Nevertheless, some relevant global structural models dealing with the study of CFT columns in fire within a frame can be found in the literature.

Wang (1999) presented a global model to evaluate the effects of structural continuity on the fire resistance of CFT columns. A FEA computer program was developed by the author to simulate the structural response of composite frames at high temperatures. A finite element analysis was executed for obtaining cross-sectional temperatures and the mechanical response in fire. For the thermal analysis, two-node fiber elements were used, with each element representing a circular slice of the cross-section. Thermal properties of the materials and stress-strain relationships from EN 1994-1-2 (CEN 2005c) were used and the thermal resistance at the steel-concrete interface was neglected, since the cross-section was treated as a continuous medium.

In the same work (Wang, 1999), a series of numerical studies were carried out. According to Wang, at the fire limit state, the structural continuity should provide built-in conditions and should reduce bending moments to a negligible level since the bending stiffness at elevated temperatures is very low. In the case of steel columns, the stiffness reduces uniformly but it is not the case of CFT columns. In these composite columns, the temperature distribution in the composite cross-section is non-uniform, which may cause a different behavior. However, after evaluating the results of the numerical simulations, Wang concluded that Eurocode 4 Part 1.2 (CEN 2005c) recommendations for the effective length of CFT columns within a frame could be applicable since produced accurate results.

In these lines, Bailey (2000) also presented a global structural model for the study of the effective length of square CFT columns in fire. A finite element model for simulating square CFT columns at room and high temperatures was programmed to be incorporated to a pre-existent computer model. One-dimensional two-node finite elements with 7 degrees of freedom at each node were employed and the cross-section was subdivided into a number of square or rectangular segments. The

temperature dependent material constitutive models from EN 1994-1-2 (CEN 2005c) were adopted and the concrete tensile strength was update at each step and calculated as the 10% of the reduced compressive strength. As a first step, the two-dimensional thermal computer package TFIRE was employed to obtain the temperature distribution through the cross-section. Local buckling could not be directly reproduced since fiber elements were employed. Therefore, a specific local buckling element was employed in the model.

According to Bailey, the results from the numerical analyses showed that, for columns continuous at both ends, a value of effective length ratio of 0.55 could be assumed, provided local buckling did not occur. However, reported tests on isolated square CFT columns showed local buckling typically occurs due to the differential expansion through the cross-section. As the column is heated, the steel tube expands at a greater rate than the concrete core due to higher temperatures. The concrete core also shows different rates of expansion due to the thermal gradient existing through the cross-section. This differential expansion makes the concrete core inner part go into tension, while the outer steel tube is supporting the whole load. It is in this situation when the steel tube is more likely to show local buckling.

As pointed out by Bailey, ignoring the effects of local buckling in those cases will result in assuming a non-conservative effective length of the column in fire situation. Therefore, considering the effects of local buckling, the author recommended the next effective length design values for concrete filled tubular columns at fire limit state: for columns continuous at both ends 0.75L; for columns continuous at one end 0.8L (continuous at their base); and for columns with pin foundation 1.0L.

Since fiber models (one-dimensional) are the most efficient from the computational point of view, it was the option chosen for the two structural models presented before where part of a structure is modeled. Although it implies the assumption of some simplifications, in occasions the improvement in the response given by more realistic models does not compensate the increase of computational cost associated.

On the other hand, Yu et al. (2010) developed a three-dimensional model in ABAQUS for circular CFT columns. To maximize the efficiency of the numerical procedure with acceptable loss of accuracy some simplifications such as neglecting the slip and separation between the steel tube and the concrete core were adopted. This model served to integrate the CFT column in a frame where the rest of elements which were not exposed to fire were modelled with beam elements to

reduce the computational time. Only three different configurations of frames were adopted in the study varying the number of stories and the location of the heated column. Among the conclusions extracted the authors highlighted two aspects that could be considered in fire design: the FRR of the column within a frame improved and, due to the redistribution of internal forces, the bending moment in the heated column was significantly reduced.

In the same way Han et al. (2012) employed the commercial program ABAQUS to develop a three-dimensional model. A particular planar composite frame consisting of two circular CFT columns and a RC beam with slab was modeled as a replica of the generic frames previously tested in an experimental program of the same research line. A sequentially coupled thermal-stress analysis was adopted. The model was validated against the recorded test data. A parametric analysis was then carried out to study the effect of beam-column linear rotation restraint ration and load level. However, since the model assumed the heating of all the elements of the frame, the variation of the relative stiffness of the column with respect to the adjacent members and its effects on the column effective length could not be investigated.

2.5. EXPERIMENTAL PROGRAMS

With regard to experimental programs for the fire behavior of CFT columns, several campaigns can be found in literature. Between the years 1917 and 1919 an extensive program of fire tests in columns was developed by AFMFIC, the Associated Factory Mutual Fire Insurance Companies (AFMFIC 1917). In this campaign different types of columns used in the interior of buildings were tested, amongst them also CFT columns, with the aim of determining the ultimate resistance against fire to propose some requirements regarding the design and protection application. The columns were loaded and exposed to fire a certain period of time. Not only the fire resistance was assessed, also the impact resistance and the sudden cooling effects were included in the study.

It was not until the 80s that fire testing programs dealing exclusively with fire performance of CFT columns appeared. Plain and bar-reinforced concrete were the infills which first were investigated combined with the traditional circular and square cross-section shapes, and always subjected to concentric loads. Once the behavior of this type of configurations was understood in an acceptable level, tests under eccentric loads were carried out to complement the previous one.

With the advances in innovative materials and new cross-section shapes, researchers reformulated the design of test programs to include them in their studies. Thus, tests using steel fiber reinforced concrete or high strength concrete as infill for CFT columns were conducted. More recently, a new variety of materials such as self-consolidating concrete or ultra-high strength are being included in experimental campaigns in combination with novel forms and configuration such as elliptical hollow steel section or concrete filled double-skin steel tubular columns.

In addition, a new branch addressing the post-fire behavior of CFT columns is also gaining interest among researchers.

Special mention deserves the scarce number of fire tests to study the effect of structural continuity on the fire response of CFT columns conducted in the last years.

2.5.1. Experimental programs on isolated CFT columns

The first time that the behavior of CFT columns under fire was experimentally investigated was between the years 1974 and 1982 by means of a research line sponsored by CIDECT (Comité International pour le Développement et l'Etude de la Construction Tubulaire) with the conduction of several experimental campaigns (COMETUBE 1976, Grandjean et al. 1980, Kordina & Klingsch 1983).

In the CIDECT research project 15A (COMETUBE 1976) 75 tests on protected and unprotected CFT columns of square cross-section (just one circular CFT columns was included) were carried out. Amongst them 6 columns were tested as hollow steel tubular columns, 19 with bar-reinforced concrete as infill and the remaining 50 columns were filled with ordinary concrete. All the columns were 3600 mm long but the external dimensions varied from 140 to 225 mm. The experiments were performed at Maizières-les-Metz and Champs-sur-Marne (France)

The effect of eccentricity was the new aspect to study introduced in the CIDECT research project 15 B (Grandjean et al. 1980). In this campaign, circular and square CFT columns combining three types of infill (plain, bar-reinforced and steel-fiber reinforced concrete) were tested. A total of 86 tests were carried out in the framework of this program. In this case, the sectional dimensions of the square columns varied from 140 to 350 mm and up to 406.3 mm in the case of the external diameter of the circular specimens. The length of the columns was 3600 mm

The report of the CIDECT research project 15 C (Kordina & Klingsch 1983) included the results of a series of 74 fire tests of different types of composite columns. In this case, the typologies tested were: CFT columns, hot rolled open

section columns embedded fully in concrete and cold formed C type section columns filled up with concrete and conventional solid steel columns. Five contrast fire tests were additionally conducted in different European laboratories. With regard to the CFT columns studied, they had principally square section and were filled with bar-reinforced concrete. A total of 26 specimens with lengths ranging from 3700 to 5700 mm were tested at elevated temperatures in the facilities from Brunswick University (Germany).

In 1991, an experimental campaign was performed in Borehamwood (UK) dealing with the fire resistance of circular CFT columns (Wainman & Toner 1992). Three different diameters were considered, ranging from 244.5 mm to 355.6 mm. All the columns were filled with plain concrete and had an exposed length of 3100 mm.

The CIDECT research project 15P (Hass et al. 2000) consisted of a series of fire tests on CFT columns with high strength concrete (HSC) infill carried out in Brunswick (Germany). Although only one full-size fire test was conducted to study the type of failure of this type of columns, the other five small scale tests were served to investigate some effects of the use of high strength concrete at elevated temperatures.

In 2004, an experimental program was carried out in the framework of the new CIDECT research project 15R (Renaud & Kruppa 2004) in order to investigate the fire response of eccentrically loaded concrete filled tubular columns. In total four columns were tested, two of them of circular shape and the other two of square section. All columns had bar-reinforced normal strength concrete as infill and a total length of 3450 mm, although only 3100 mm were exposed to fire. The eccentricities applied were 0.75 and 1.5 times the cross- sectional dimension. The results of this experimental program also constituted the benchmark for the validation of the simplified calculation method for eccentrically loaded columns developed within the CIDECT project 15Q (Renaud et al. 2004).

It is worthy to mention the consecutive experimental campaigns regarding CFT columns in fire (Lie & Chabot 1992, Chabot & Lie 1992, Kodur & Lie 1995) which were carried out by the researchers from the Institute for Research in Construction at the NRCC (National Research Council of Canada) between the years 1982 and 1994. CFT columns of circular and square sections combining three types of infill: plain, bar-reinforced and steel-fiber reinforced concrete were included in the programs. The cross-sectional dimension of the columns varied from 141.3 to 406.4 mm and the steel tube thicknesses ranged from 4.78 mm to 12.70 mm. All the

columns were 3810 mm long and were generally tested under fixed end conditions and subjected to concentric axial load. The percentage of reinforcement included in the bar-reinforced specimens was approximately a 2.3%, while the percentage of steel fibers in the concrete mix for the steel-fiber reinforced columns was 1.76% by mass.

It was again in the NRCC where a series of experiments addressing specifically the fire behavior of CFT columns with high strength concrete were conducted (Kodur & Latour 2005). In this program, six circular CFT columns with diameters ranging from 219.1 to 406.4 mm and two square CFT columns of 203.2 mm width were included. Again, the length of the column specimens was 3810 mm Reinforcing bars or steel fibers were used as reinforcement in some of the specimens to complement and improve the fire comportment of high strength concrete.

In the early 2000s, the group headed by professor Han in China took notoriety in the field of fire tests conducted on CFT columns due to the successive campaigns carried out (Han & Huo 2003, Han et al. 2003 a, b, Han & Lin 2004, Han et al. 2005). The investigations performed by this group were focused on obtaining results regarding the residual strength of CFT columns by means of tests conducted in Tianjin (China). Both circular and square shape columns under monotonic or cyclic load after exposure to a standard fire were studied. Results are available on stub columns of 400 mm length and D/t ratio equal to 27.7 after 90 minutes of fire exposure.

The fire response of slender CFT columns was also assessed by the University of Fuzhou group (Han et al. 2003a). In this program, a series of protected an unprotected CFT columns were tested under loads applied with various levels of eccentricity (0-0.6 mm). The specimens had circular shape with external diameters varying from 150 to 478mm and steel tube thicknesses ranging from 4.6 to 8 mm. The 13 columns studied were 3810 mm long.

The research group from the University of Seoul (Korea) (Kim et al. 2005, Park et al. 2007, 2008) carried out tests on square CFT columns under both concentric and eccentric axial loads. Seven specimens of 300×9 and 350×9 mm section and 3500 mm long were tested in a first research (Kim et al. 2005). They were subjected to concentric load and different effective heating lengths. Tests in another 12 square CFT columns of 300×9mm section (Park et al. 2008) completed the study. These specimens were tested under concentric load and filled with normal strength concrete.

In 2009, a series of fire tests on high strength self-consolidating concrete filled steel tubular stub columns were carried out by Lu et al. (2009). Six columns of square section with varying cross-section size, load case (concentric or eccentric load) and load level were tested. The cylinder compressive strength of concrete at 28 days was 90 MPa. All the specimens, which were 760 mm long, were tested in the Civil Engineering Laboratory at Monash University (Clayton, Australia).

In the last five years, the research group led by professor Romero from Universitat Politècnica de València (Spain) has carried out several experimental campaigns (Romero et al. 2011, Moliner et al. 2013, Espinos et al. 2014, Espinos et al. 2015a, b, Romero et al. 2015). Through these programs the fire behavior of CFT columns of different cross-section shapes and configurations, diverse type of infill and reinforcement and various load levels and eccentricities have been addressed. All the fire tests conducted by the group were tested in Valencia (Spain), in the facilities of AIDICO (Asociación de Investigación de las Industrias de la Construcción – Instituto Tecnológico de la Construcción). On the other hand, the several room temperature tests conducted by the group were carried out at the Universitat Jaume I in Castellón (Spain).

As a first stage, Romero et al. (2011) presented the results of an experimental program on slender axially loaded CFT columns subjected to fire. The aim of the testing program was to study the effects of three main parameters on the fire behavior of these composite columns: concrete strength, type of concrete infill (plain, bar-reinforced and steel fiber reinforced) and load level. In total, sixteen fire tests were performed on axially loaded columns combining mixtures of normal (NSC) and high strength concrete (HSC). All the specimens had a length of 3180 mm and a circular cross-section of 159×6 mm.

As a continuation of this experimental program conducted by the group headed by professor Romero, a series of tests focused on the application of eccentric loads in fire was performed (Moliner et al. 2013). The new campaign was designed to assess the fire response of eccentrically loaded slender circular CFT columns with normal and high strength concrete. The specimen's length and cross-sectional dimensions were the same as in the previous campaign for comparison purposes. The main objective of this work was to study the influence of eccentricity in combination with the type of concrete infill and load level. In this case, a total of 24 fire tests were carried out.

With the experience gained through the previous experimental programs, the research group from Universitat Politècnica de València (Spain) decided to

undertake a novel experimental campaign on concrete filled elliptical hollow section (EHS) columns. Until that moment, no published works on elliptical CFT columns fire tests could be found in literature. First, an experimental program on slender EHS columns filled with concrete was carried out (Espinos et al. 2014). A total of 12 specimens were tested, six of them at room temperature and the other six at elevated temperatures. The tests parameters were the load eccentricity and type of infill (plain concrete or bar-reinforced concrete). The columns tested at room temperature were 2135 mm long whereas the length of the fire tested specimens was 3180 mm. Cold formed elliptical steel hollow sections with external dimensions 220x110 mm and a wall thickness of 12 mm were studied.

In order to complete this research line, Espinos et al. (2015a) conducted an experimental campaign on CFT columns of elliptical and rectangular shape under fire conditions. Two different cross-sectional dimensions were used for the rectangular columns, 2510x150 mm and 350x150mm, both with a wall thickness of 10 mm. The section size of the elliptical columns analyzed was 320x160 mm with a wall thickness of 12.5 mm. A total of 12 rectangular columns and 6 elliptical columns were tested. All the columns were 3180 mm long. The effect of load eccentricity, percentage of reinforcement (considering both major and minor axis) and cross-section shape on the fire response of these columns was studied.

Afterward, Espinos et al. (2015b) conducted a series of fire tests on circular and square slender CFT columns under large eccentricities. A total of 12 specimens were tested: 6 with circular cross-section and other 6 with square cross-section shape. Two cross-sections sizes were tested for each shape: for circular columns, 193.7x8 mm and 273x10 mm sections were tested; for square columns, 150x8 mm and 220x10 mm sections were used. The eccentricities applied were 0, 0.5 and 0.75 times the cross- sectional dimension. All the specimens were bar-reinforced and had a length of 3180 mm. The influence of cross-section shape, load eccentricity and percentage of reinforcement were studied focusing on the effect of large eccentricities on very slender columns.

More recently, Romero et al. (2015) got involved in the study of an innovative cross-sectional configuration of CFT columns. Thus, an experimental campaign dealing with the study of both ambient and elevated temperatures behavior of six double-tube concrete filled steel tubular columns with different combination of outer and inner steel tube thicknesses was conducted. First, the room behavior was addressed and, after, the experiments under fire conditions were carried out with the aim of comparing the behavior between these two situations. The influence on the fire resistance of filling the inner tube with concrete was

assessed. Besides, the effect of different combinations of concrete strengths was investigated. The length of the columns tested at ambient temperature was 3315 mm while the fire tested specimens were 3180 mm long.

Following the line of investigating the applicability of new materials to CFT columns in fire, Han et al. (2013) carried out a series of tests using stainless steel and self-consolidating concrete. Five full-scale tests on square and circular CFT columns subjected to axial compression were tested. The steel tube was made of austenitic stainless steel and the infill was self-consolidating concrete. Load level and sectional type and dimensions were the main parameters studied in this program. The total height of the CFT columns was 3600 mm, being exposed to fire the central 3000 mm. The tests were performed in Tianjin Fire Research Institute (China).

During the past few decades, the main trend has been the study of the performance of CFT columns subjected to uniform fires. However, the knowledge of the behavior of columns exposed to three sides, which in practice is a common scenario, is very limited. Thus, Yang et al. (2013b) carried out an experimental study to investigate the effects of non-uniform exposure on square CFT columns. Six columns were tested to failure to observe the effects of the number of exposed sides, load ratio and load eccentricity. The specimens had dimensions of 300x300 mm and a total length of 3810 mm. Four of them had three sides exposed to fire and the rest just on side. This experimental campaign was right after extended to rectangular CFT columns (Yang et al. 2013a). In this case, just three full-scale tests were conducted: one column with one side heated and two columns with three sides exposed to fire. The columns were 200x300 mm and had the same length than the specimens of the previous program. The nine experiments were conducted at Suzhou University of Science and technology (China).

In the field of the post-fire behavior of CFT columns some experimental results can be found in literature. Tao et al. (2011) carried out a series of push-out tests on 64 columns previously exposed to the ISO 834 fire curve for a determined period of time (90 or 180 minutes). The aim of these tests was to extract some conclusions about the post-fire bond between the steel tube and concrete core in CFT columns. For comparison purposes, 12 more tests on unheated specimens were conducted. The tests results indicated the relevant influence of the fire exposure. Concrete filled tubular columns of both shapes, square and circular, were studied and circular specimens showed much higher bond than square ones.

In the same line, Rush et al. (2015) presented the results of an experimental program of post-fire residual compression tests on protected and unprotected CFT columns. In total 25 columns were tested: 19 specimens were tested after being subjected to a fire and the remaining 6 were tested without prior heating and used as control specimens. CFT columns of both square (7) and circular (18) cross-section shape were employed. The experimental campaign aimed to assess the effect on the post-fire residual capacity of the cross-section shape, the steel tube wall thickness, the heating curve and the fire protection applied.

2.5.2. Experimental programs on structural continuity

With regard to experimental investigations dealing with the study of the effects of structural continuity on the fire behavior of CFT columns few works can be found.

Steel columns

In the field of steel frames subjected to fire this effect has been studied in depth as proved by the publications of several authors. However, it is an issue which is still addressed in experimental programs since there is no consensus about the requirements and recommendations that should be taken into account in design.

Ali & Connor (2001) presented an experimental campaign to investigate the structural performance of steel columns in fire. In this program, 10 columns were vertically tested, and all the specimens were half scale with a length of 1800 mm. Tests were carried out at Fire Research Center, University of Ulster (UK). The columns were both axially and rotationally restrained. The authors presented a method for evaluating the effective length of fixed ends columns under fire by using the geometrical data of the deformed column after test and locating the contra-flexure points. The distance between these two points represented the effective length of the column. Those specimens with high rotational restraint presented an average value of effective length of 0.56L, whereas those columns tested under a low rotational restraint showed an effective length of 0.61L. Comparison with the Eurocode 3 Part 1.2 (CEN 2005b), 0.5L, indicated that in those cases it was non-conservative.

In 2003, Wang & Davies (2003a) from the Structures and Fire Research Group at the University of Manchester (UK) noticed the complexity of the fire behavior of a steel column in a complete structure due to the interactions with the other members. This leads to changes in the column loads and boundary conditions affecting the resistance of the column. Therefore, an experimental program was

designed to evaluate the fire behavior of a column as a part of a realistic frame structure. The assembly consisted of a column and two beams connected to the web of the column at one of its ends. The experiments were conducted at the Fire Testing Laboratory of the same university. Although the experimental campaign was focused on determining the changes in bending moments of the column specimens under different levels of initial loading conditions, it was detected that the buckling length of the column under fire was different from that at ambient temperature due to changes in the relative bending stiffness of the column to the surrounding structure. The effective length of the columns was shorter than the length obtained when both ends are pinned.

Tan et al. (2007) from the Nanyang Technological University (Singapore) also developed an experimental investigation to determine the failure time of unprotected steel columns subjected to various axial restraint ratios to analyze the thermal restraint effects due to the cooler parts of a steel structure. The specimens, with a length of 1740 mm, were tested horizontally. However, during the heating process, a monotonically increasing heating condition was followed instead of the standard fire curve.

In the same line, Li et al. (2010) carried out two tests in real–size steel columns that were 3000 mm long, with the aim of calibrating a finite element model and performing a parametric study to propose a simple approach for buckling temperatures of restrained columns. In this case, the columns were axially and rotationally restrained and the restraint stiffness was varied by changing the cross-section of the restraining beam. Columns were also tested horizontally. It was observed that columns with higher axial restraint stiffness had a lower buckling temperature. After buckling, it was detected that a new equilibrium state was achieved so the column was able to bear the load until failure was reached.

In 2012, Correia & Rodrigues (2012) designed and built a new experimental system to perform a series of fire tests on steel columns subjected to axial and rotational restraint. The objective of these tests was to assess the influence of the rotational restraint combined with the axial restrain. The parameters studied were the slenderness, the load ratio and the axial stiffness of the surrounding structure. The experimental system was constructed in the Laboratory of Testing Materials and Structures of the University of Coimbra (Portugal).

CFT columns

Returning to the experimental programs dealing with the effects of structural continuity in CFT columns, the next works need to be mentioned.

One of the first works was carried out by Kimura et al. (1990) in the Takenaka Technical Research Laboratory. The effects of surrounding structure in the fire behavior of square CFT columns was studied by means of a test in which the column was subjected to axial load and bending moment transferred from the adjacent beams. Some interesting conclusions were extracted. As temperature increased, the bending moment that was transferred by the beams decreased with the loss of strength and rigidity of the steel section of the column, which indicated that the axial load ratio is the crucial loading parameter at fire limit state.

The Structures and Fire Research Group from the University of Manchester (UK) also got involved in the study of CFT columns within frames. In order to go a step forward in the knowledge of this problem, Wang & Davies (2003b) carried out an experimental study of the behavior of concrete filled tubular column assemblies using extended end plate connections. The authors were familiar with this type of studies after the execution of a similar campaign on steel columns (Wang & Davies 2003a). In this work, two series of specimens, characterized for having different thicknesses of the steel tube, were tested. The most significant conclusion of this study was the effect of the possible local buckling of the steel tube on the effective length of a concrete filled tubular column within a frame. The behavior detected for the two series was different. For those cases in which no local buckling of the steel tube was observed, recommendation of Eurocode 4 Part 1.2 (CEN 2005c) may be used. Nevertheless, in the case of tests with thinner tubes, local buckling was observed and, thus, design calculations showed that these recommendations may not be safe.

Han et al. (2010), who had experience in modeling and testing the fire behavior of isolated CFT columns, got involved in the study of the fire response of CFT columns within frames. Six fire tests on reinforced concrete beam to CFT columns planar frames were carried out. The tests were conducted at the Key Laboratory of Civil Engineering Safety and Durability of China. The columns of four of the frames had circular cross-section and the remaining two were square CFT columns. The parameters evaluated were the axial load level in the columns, the load level in the beams and the linear rotational restraint ratio between beams and column. In this case, all the elements of the frame were subjected to the heating

regime of the standard curve. Therefore, the influence of the unheated surrounding members on the fire response of the CFT columns was not addressed.

More recently, Pires et al. (2012) presented the results of an extensive experimental program where 40 concrete filled circular hollow columns with different type of infill were tested. The specimens were subjected to thermal elongation restraint. In this study, several parameters where investigated, such as the slenderness of the column, its load level, the stiffness of the surrounding structure, the percentage of steel reinforcement and the degree of concrete infill inside the column. The tests were conducted at the facilities of the Laboratory of Testing Materials and Structures of the University of Coimbra (Portugal). Although the main failure mode of the columns observed was global buckling, in several cases, local buckling also occurred. The authors noticed that local buckling occurred more often in the specimens with high load ratio, in those cases where the stiffness of the surrounding structure was lower, in the columns with higher external diameter and in hollow or partially encased concrete filled specimens.

Considering all, it can be concluded that it is necessary to determine realistic and appropriate values for the effective length of concrete filled tubular columns within a frame in fire situation, in order to establish whether the Eurocode 4 Part 1.2 recommendations are applicable or, on the contrary, may lead to non-conservative predictions.

2.6. SIMPLE CALCULATION MODELS

In order to facilitate the use of CFT columns in structural design, it is necessary to provide simple calculation models which facilitates the determination of the member resistance both the room and fire resistance. The employment of this type of composite columns in actual constructions has increased in the last decades precisely due to their inherent fire behavior and it has revealed the necessity of relying on a consistent simple calculation model for fire design.

With the background of the successive experimental campaigns sponsored, the CIDECT (Twilt et al. 1996) developed a design guide for the fire response of CFT columns. This document included a dissertation about the critical aspects of CFT columns in fire and covered the most common cross-section shapes and sizes and also gave calculation rules in function of the type of infill, geometric characteristic or loading conditions.

Following the lines of the CIDECT guide, in 2002 the Corus Tubes guide (Hicks & Newman 2002) was published in order to update the knowledge about the fire response of these composite columns in fire and provide design recommendations for structural designers.

As expected, most of the simple calculation proposals published in literature were presented by the main research groups which have investigated in depth, experimentally and numerically, the behavior of CFT columns under fire. Some of them have been already included in the respective national code to provide a reliable calculation tool to practitioners.

A clear example of this process can be seen in the proposal incorporated to the Chinese Code DBJI3-51 (2003). It consists of a set of expressions to compute both the strength index of CFT columns without external protection in fire and also the thickness of external fire protection to apply in order to achieve a given FRR. These equations were provided by Han et al. (2003a, b) after conducting an extensive series of fire tests on square and circular CFT columns and investigating the effect of the main parameters. The group led by professor Han also proposed an expression for the residual strength as the final step of experimental works (Han & Huo 2003, Han & Lin 2004).

In Japan and Korea, designers opt for different approaches. While in Japan the reference has been the manual for the design of CFT columns presented by the Association of New Urban Housing Technology (ANUHT 2004, Harada 2004), in Korea took relevance an empirical expression proposed by Park et al. (2007, 2008) for CFT columns of square shape which was obtained after an statistics analysis taking as a basis the main variables of the problem.

However, the most common fire resistance approaches for the design of CFT columns are the ones currently recommended in North America and Europe, as stated Rush et al. (2012) in a recent work where a careful review of the structural performance of CFT columns in fire was presented. It is also worthy to mention the previous revision of the current calculation proposals carried out by Zhao et al. (2010).

In North America, the American Society of Civil Engineers (ASCE 1999) incorporated the design equation proposed by Kodur and collaborators (Kodur 1999, Kodur & MacKinnon 2000, Kodur 2007). With the knowledge acquired after having performed the extensive experimental campaigns at NRCC, a calculation proposal for the fire design of CFT columns was presented. The applicability of the formula includes square and circular CFT columns with any kind of infill (plain, bar-

reinforced or fiber reinforced concrete) of both normal and high strength. The expression was also integrated in the AISC Steel Design Guide 19 (Ruddy et al. 2003) and in the ACI 216 (ACI 2007). In Canada it was integrated in its respective code, the National Building Code of Canada (NRCC 2005).

In turn, the Eurocode 4 Part 1.2 (CEN 2005c) is the reference code in Europe for the fire design of composite structures including CFT columns. Due to proximity, the content of this code will be described with detail hereafter. In this document, three approaches are considered with different levels of accuracy and difficulty: tabulated data, simple calculation models and advanced calculation models.

The former is indicated for the study of the fire response of a sub-structure or a complete structure and, especially, for those cases regarding isolated members where simplistic models cannot be used. They are based on fundamental physical behavior and provide a good approximation of the actual structural behavior under fire conditions. In the daily practice they are not used in common designs since they are time consuming and sometimes require special knowledge of calculation programs. Therefore, they are usually relegated to analysis and research and only employed in design for special structures.

Tabulated data is the most immediate and simplest option for fire design contemplated by EN 1994-1-2 (CEN 2005c) For classical cross-section shapes, this option gives through tables the minimum cross-sectional dimensions as well as the minimum reinforcement ratio and axial distance of reinforcing bars which are needed to achieve certain FRR under an specific applied load level. Although the own code informs about the conservatism of this method, some authors have noted that its predictions can be excessively save (Rush et al. 2012).

With regard to the simple calculation model included in Eurocode 4 Part 1.2, which is the part concerning this section, a complete procedure can be found in its Clause 4.3.5.1. A general method for the calculation of the design value in the fire situation of the resistance under axial compression of composite columns, including CFT columns, is provided. First, the cross-sectional temperature field needs to be obtained and after discretizing the cross-section in elements, the design fire resistance is computed considering the contribution of all the components in the cross-section of the column. Eurocode 4 Part 1.2 uniquely gives some principles for the thermal analysis. Different methods can be used to determine the temperatures in the cross-section such as finite element analysis or one-dimensional heat transfer analysis. While the calculation of the axial buckling load is straightforward, the

determination of the cross-sectional temperature field can result a tedious procedure to be implemented in the daily practice.

In fact, Wang et al. (2000) developed a simple method for designers in which is not necessary to obtain explicitly the cross-sectional temperature distribution. This method evaluates the load bearing capacity of circular CFT columns in fire based on two values: the squash load and the rigidity. This proposal was intended to be a very simple method for designers and thus it is not necessary to obtain explicitly the cross-sectional temperature distribution. The authors carried out a parametric study based on the general approach of Eurocode 4 Part 1.2 (CEN 2005c) to check the accuracy of their proposal. The information needed for its implementation is given through tables and can be used by linear interpolation.

In addition, the Annex H of the Eurocode 4 Part 1.2 (CEN 2005c) presents a simple calculation model specifically developed for concrete filled tubular columns. It is based on a prior method proposed for CFT columns at ambient temperature (Guiaux & Janss 1970). Renaud et al. (2004), in the framework of CIDECT project 15Q developed a numerical investigation and pointed out the theoretical shortcomings of the method. Also the basis of this proposal were questioned and it was proved its inaccuracy given the very unsafe results which were produced for columns with common levels of slenderness (Wang & Orton 2008, Aribert et al. 2008). These actions led to the inclusion of a correction in Annex H to point out that the applicability of the method was restricted to CFT columns with a value of relative slenderness equal or less than 0.5.

Due to these results and provided that the specific method for CFT columns was tedious to apply in spite of its assumed simplicity, the trend followed by most researchers (Wang 1997b, 2000, Wang & Orton 2008, Aribert et al. 2008, Ribeiro et al. 2008, Leskela 2009) was to study the general approach of Eurocode 4 Part 1.2 described in its Clause 4.3.5.1. In order to take a further step on this issue, some works were carried out to investigate the applicability of this general method specifically to CFT columns. Hence, the National Annex to EN 1994-1-2 developed in France (AFNOR 2007) considered the work and conclusions extracted by the CTICM group regarding fire design of CFT columns, another clear example of how finally research can help to promote the use of CFT in structural designs.

Along this line, Espinos et al. (2012) proposed a simple calculation model for evaluating the fire resistance of unreinforced axially loaded CFT columns based on the general approach from EN 1994-1-2 Clause 4.3.5.1 (CEN 2005c). In this method, the traditional calculation of the non-uniform cross-sectional temperature

field is substituted by a given set of equations to compute the steel tube temperature and the equivalent concrete core temperature for a given FRR and as a function of the geometrical characteristics of the column. Regarding the mechanical model, Espinos et al. (2012) proposed appropriated flexural stiffness reduction coefficients for the calculation of the effective flexural stiffness in fire situation as a result of an extensive parametric study and its subsequent statistical analysis. The method was validated against tests results and proved to give predictions with reasonable accuracy, generally on the safe side. This simple model extends the limitations of applicability of the general approach from Clause 4.3.5.1 to more slender columns. As a continuation of this work, the simple calculation model was extended to bar-reinforced columns of circular and elliptical cross-section taking into account the reinforcement ratio (Espinos et al. 2013) and, although the expressions provided for circular specimens proved to be valid for elliptical shape cross-sections, adjusted expressions were especially obtained for this innovative section.

Although it was not a full procedure for obtaining the bearing capacity of CFT column under fire, the work developed by Dai & Lam (2012) must be highlighted. The authors studied the shape effect on the fire behavior of axially loaded CFT stub tubular columns and proposed a simplified method to calculate the maximum axial compressive capacity of CFT columns according to the general method for composite columns from Eurocode 4 Part 1.2 (CEN 2005c). The approach presented by Dai & Lam (2012) to solve the thermal problem considered an average temperature for the concrete core obtained as a percentage of the maximum temperature of the steel tube. The equation varied in function of the cross-section shape considered. In this study, elliptical, circular, square and rectangular concrete filled tubular columns were included.

In 2014, Yu et al. (2014) also published a fire design proposal using the average temperature approach. In this case, two average temperatures were considered: one for the steel tube and another for the concrete core. These were calculated by equations developed by the authors after the corresponding regression analysis and considering the cross-sectional dimensions. Then, a design method based on the room temperature method from Eurocode 4 Part 1-1 (CEN 2004b) was presented. The average temperature approach is also applied to an own previous expression for the bearing capacity at ambient temperature developed by the authors. The proposal covered circular and polygonal sections and, according to the authors, showed acceptable accuracy in its predictions.

More recently and in the field of double-tube CFT columns, Imani et al. (2015) presented a simplified analytical procedure for the calculation of the fire

resistance of concrete filled double-tube steel tubular columns subjected to any heating curve. The method combined an analytical solution to the heat transfer analysis and the calculation of the axial load capacity using the temperature dependent properties from EN 1994-1-2. The authors made a simplistic assumption since they considered that the outer steel tube temperature was equal to that of the heating curve. The axial load capacity calculation procedure proposed was similar to the simple model for CFT columns included in Annex H of EN 1994-1-2, although a simplified step by step procedure was presented. The method was only verified against one experiment and, as pointed out by the authors, more research is necessary to properly check the accuracy of the proposal.

Once the review of the current outlook of the research works dealing with the study of concrete filled tubular columns has been completed, the main and specific objectives of this work can be established taking into account the areas of knowledge where the necessity of more studies was detected. Mainly, these are the investigation of the fire behavior of CFT columns within frames and the effects of axial and rotational restraints in their fire resistance time.

3.

AIM AND SCOPE OF THIS THESIS

This chapter describes the general aim of this thesis, as well as the specific objectives which are settled throughout this research work for its accomplishment. The scope and limitations of this research are also presented.

3.1. AIM OF THIS THESIS

The general aim of this thesis is to study the fire response of circular axially loaded concrete filled tubular columns and the effects of the axial and rotational restraints arising when they are assembled to other structural elements within a frame. First, in order to investigate the thermal response of CFT columns a cross-sectional thermal model will be elaborated taking into account realistic considerations. This model will be validated against tests data for both unprotected and protected specimens. Next, a fiber beam thermo-mechanical model will be developed integrating the thermal model previously proposed. The predictions obtained by this model will be contrasted with results from experimental programs and once the validation process has been concluded, the model will be employed to analyze in depth the fire response of the columns and the main parameters affecting their behavior.

In particular, the validated thermal model will be used to carry out a thermal parametric analysis in order to develop a set of expressions for computing the cross-sectional temperature distribution of CFT columns which, in the future, will be useful for the design of this type of composite members.

On the other hand, the design guidelines included in Eurocode 4 for the design of composite columns and specifically for CFT columns will be reviewed. Parametric studies will be performed in order to propose a simple calculation method which could support designers in the calculation process of CFT columns under fire condition.

As it has been previously exposed, the structural behavior of a column within a frame differs from that observed in isolated columns and this phenomenon is more noticeable in fire situation. Given the reduced computational cost of models based on fiber beam elements, the numerical model developed will be used to simulate the fire response of a CFT column integrated into a structure. A parametric analysis will be performed with the aim of examining the effects of axial and rotational restraints in the behavior of these composite columns at elevated temperatures. The study of the generated data will permit the evaluation of the influence of the different parameters involved and the proposal of some design recommendations with regard to CFT columns within frames.

3.1.1. Specific objectives

In order to accomplish the general aim of this thesis, the specific objectives presented below must be previously achieved:

- Initial review of the current outlook of concrete filled tubular columns in the construction sector and summary of their main applications as well as the new configurations and materials recently incorporated to this field.
- Analysis of the governing principles and basis of the fire dynamics, heat transfer and structural analysis problems involved in the study of the fire response of a structural member. Subsequent review of the models of the materials employed in this composite section for its analysis at elevated temperature.
- Specific revision of the models available in the literature for the fire behavior of CFT columns as isolated members as well as members within frames. Corresponding review of the main experimental investigations dealing with CFT columns in fire and the most relevant simple model proposals published in literature.
- Development of a finite differences model for the determination of the cross-sectional temperature field of unprotected and protected CFT columns.
- Validation of the thermal model by contrasting the model predictions with test data from own experiments and from other campaigns available in literature.
- Elaboration of a fiber beam thermo-mechanical model for the fire response of CFT columns which includes realistic considerations in order to obtain not only an accurate prediction of the fire resistance time but also a precise reproduction of the whole fire response along time.
- Calibration of the fiber beam model to set the values of the diverse variables involved in the definition of the numerical model.
- Validation of the thermo-mechanical model against experimental data extracted from own fire tests as well as from tests conducted by other researchers.
- Performance of parametric analysis in order to study the manner in which they affect the fire behavior of the column. The range of values assigned to these parameters in the analysis will cover those usually employed in practice.

- Development of a set of expressions for computing the temperature distribution on the cross-section of CFT columns which will be a useful tool in the initial steps of the design procedure.
- Development of a simple calculation method which complements the existing procedures and could be useful to practitioners when designing CFT columns at the fire limit state.
- Elaboration of a subframe model for examining the effects of axial and rotational restraints on CFT columns under fire.
- Conduction of parametric studies for CFT columns within frames which comprise a wide range of values for the parameters implicated and which permit to extract conclusions on their influences.
- Comparison of the data generated in the analysis with the provisions given in the Eurocode 4 for columns within frames in fire situation and with the predictions obtained by the proposed simple model.

3.2. SCOPE AND LIMITATIONS OF THIS THESIS

The scope of this thesis is restricted to concrete filled tubular columns of circular cross-sectional shape. Although the thermal model is developed for both unprotected and protected CFT members, the subsequent numerical structural model focuses only on unprotected columns. Thus, the modeling and study of the structural behavior of protected columns will be left out for future work. The numerical model is valid for columns of any type of infill: plain, bar-reinforced and steel fiber reinforced concrete of both normal and high strength.

With regard to the simple calculation model, it uniquely covers columns with normal strength plain concrete. It is proposed for further work its extension to other type of concrete infill.

The field of application of this work is limited to members which are subjected to concentric loads. Some specimens tested under eccentric loads were used exclusively for the validation of the thermal model. The expansion of the model to eccentrically loaded columns is thought to be part of the forthcoming work.

With respect to the study of the influence of the axial and rotational restraints on the fire behavior of CFT columns, it has been focused mainly on columns placed at an intermediate floor within a frame. The analysis of the effects on columns located at top floors will be addressed in future work.

4. DEVELOPMENT OF THE THERMAL MODEL

This chapter presents the thermal model developed for reproducing the thermal response of unprotected and externally protected concrete filled tubular columns. The thermal model is valid for CFT columns of any type of infill: plain, bar-reinforced or steel fiber reinforced concrete, of normal or high strength. The basis of the model is presented and the equations describing the model are developed. Next, the thermal model is validated against experimental data from tests reported in the literature and from own tests. Finally, an assessment of the steel tube temperature is done under different assumptions to contribute to the understanding of the effects of concrete infill and external fire protection on CFT columns.

4.1. INTRODUCTION

The heat transfer analysis is the first step to execute when the whole response of a CFT column is studied. Generally, with independency of the method selected for the analysis (analytical models, numerical models or simplified methods), the evolution during time of the element temperature needs to be evaluated.

For instance, if the guidelines of European code EN 1994-1-2 (CEN 2005c) are followed in the design of a CFT column, prior to apply either the general method for composite columns included in its Clause 4.3.5.1 or the specific simple model for CFT columns proposed in its Annex H, the cross-sectional temperature field have to be obtained taking into account the temperature dependent thermal properties of the materials. However, the code does not provide any information about the thermal model to be employed and, just in the case of Annex H, indicates that the temperature distribution can be computed neglecting the thermal resistance at steel-concrete interface for the sake of simplicity.

In spite of the existing necessity of having practical thermal models available for structural designers to be applied in these cases, a review of the current outlook in the field of circular CFT columns brings to light that the number of works treating uniquely the development of thermal models for concrete filled tubular columns is scarce. In addition, frequently not all the parameters and nonlinearities involved in this process are included in the models for simplicity.

The use of general purpose or specific commercial packages can result tedious and non-affordable in the daily practice. In general, these are more appropriate for research purposes and when numerical models are implemented in these platforms, usually the thermal analysis is just a mere step integrated in the whole analysis.

In this section, a practical thermal model for circular CFT column where the heat transfer problem is solved by means of the finite differences method is developed. The heat transfer model involves two steps: the calculation of the temperatures given by the fire curve to which the column is exposed and the determination of the column cross-sectional temperatures.

The model formulation is based on the finite differences method with an explicit scheme and follows the line proposed by Dusinberre (1961). Previously, Lie (1994) had already taken as a basis the same approach to solve the heat transfer

problem for circular CFT columns but ignoring the gap conductance that appears between the steel tube and the concrete core which clearly reduces the thermal response accuracy.

The proposed model aims to improve the answer of the initial approach (Dusimberre 1961) by considering not only the effects of the gap conductance at steel-concrete interface but also all the detected nonlinearities involved in the heat transfer process to obtain a response as realistic as possible.

The heat transfer model proposed is valid for a wide range of concrete infill: plain, bar-reinforced and steel fiber reinforced concrete of both normal and high strength and their predictions are contrasted against experimental results to prove its validity.

In order to go a step forward, the thermal model, which initially was developed for unprotected CFT columns, is extended also to protected members, thus covering an existing gap in the research field of these composite columns.

This thermal analysis procedure was implemented in Matlab and it represents the first step of a thermo-mechanical fiber beam model developed for simulating the fire response of circular CFT columns which will be presented in the next chapter.

4.2. UNPROTECTED CONCRETE FILLED TUBULAR COLUMNS

4.2.1. Discretization of the section

The nomenclature used by Lie (1994) is maintained in this work in order to make easier any comparison between both formulations. Due to axisymmetric conditions, the heat transfer problem becomes unidirectional what simplifies the discretization of the section as well as the calculation process.

The discretization of the composite section for thermal analysis is shown in Figure 4.1. For each material, the division is made in equal increments of the radius. The number of subdivisions in the steel tube is $(M_1 - 1)$ and $(M_2 - M_1 + 1)$ in the concrete core. The temperature is calculated for the target points which are placed at the layer boundaries as it can be observed in Figure 4.2. These calculation points are represented by P_m.

The main improvement with respect to the method presented by Lie (1994) lies in the consideration of the existence of a gap conductance at the steel-concrete interface with the aim of obtaining a realistic thermal response.

Gap conductance is a phenomenon arising at the interface between two materials due to the loss of contact in almost the totality of the facing surfaces. When two solid materials remain in contact in a small number of points, the generated gaps can contain water steam characterized by a considerably lower thermal conductivity than the other solid materials. In a CFT column, due to the different thermal expansion coefficients, the clearance between the two contacting surfaces will increase as they progressively separate from each other during a fire.

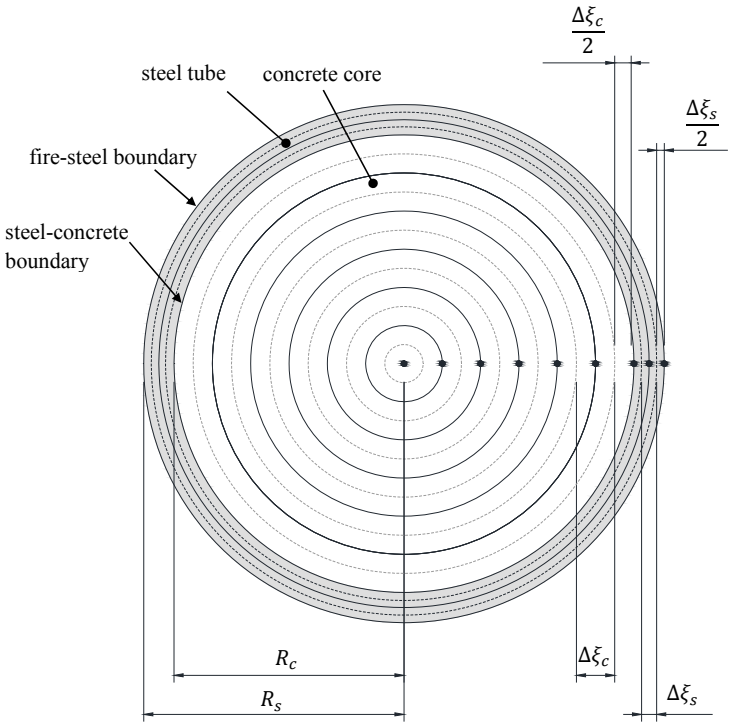

Figure 4.1. Unprotected CFT column. Discretization of the section for thermal analysis.

In order to represent this event, the node physically placed at the steel-concrete boundary is theoretically split into two nodes: one node belongs to the steel tube inner surface and the second node is located at the concrete core outer surface, Figure 4.2. Thus, it is possible to consider the steel-concrete gap as a new layer of thickness zero characterized by a thermal conductance that reproduces the sudden drop of temperatures from the steel tube to the concrete core.

The thickness of all the layers in the steel tube is $\Delta\xi_s$, except for the first layer and the layer at the steel-concrete boundary which are ½ $\Delta\xi_s$ thick. The same occurs in the concrete core, while all the inner layers have a thickness of $\Delta\xi_c$, the layer at steel-concrete interface and the layer at the center of the column are ½ $\Delta\xi_c$.

For deriving the next equations, an arc of 1 radian is used and the depth in the axial direction is taken as unity as pointed out by Dusinberre (1961).

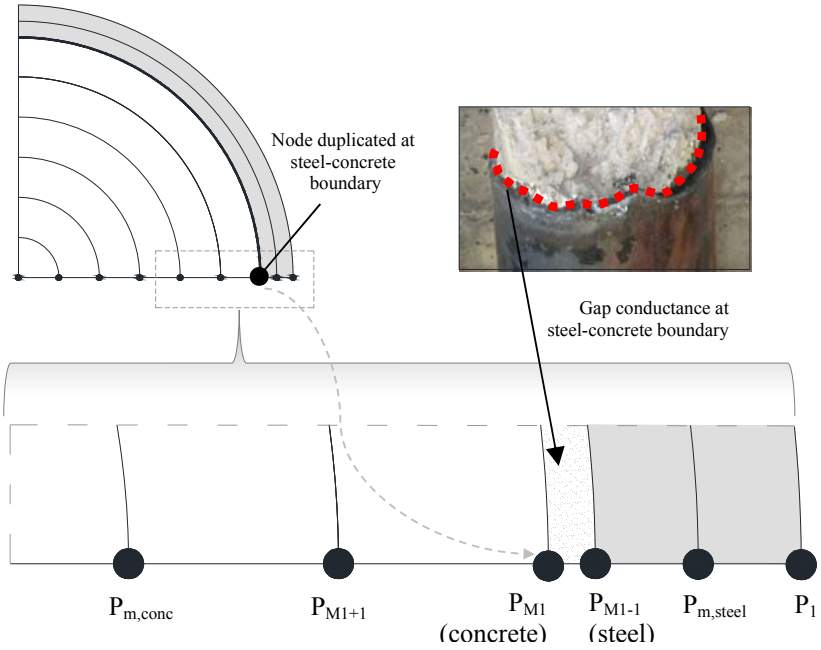

Figure 4.2. Detail: Gap conductance at steel-concrete boundary.

4.2.2. Cross-sectional temperatures

In this work, the whole length of the column is supposed to be uniformly exposed to a fire. Just for description purposes, it is assumed that the fire evolution follows the standard fire curve ISO 834 (ISO 1980, CEN 2002). Note that this curve can be replaced by the heating curve characterizing an actual fire or by another standard fire curve when it is necessary.

The fire curve ISO 834 is represented by the next expression:

$$T_f^j = 20 + 345\log(8\tau + 1) \tag{4.1}$$

where τ is the time in minutes and T_f^j is the fire temperature, in ºC, at time τ = jΔτ.

For a CFT column, at time τ = (j+1)Δτ, the temperature at the different points of the section can be calculated as follows:

Equations for fire-steel boundary *(m = 1)*

$$T_1^{j+1} = T_1^j + \frac{2\Delta\tau R_s}{\rho_s^j c_{ps}^j \left(R_s - \frac{\Delta\xi_s}{4}\right)\Delta\xi_s}\left\{\sigma\varepsilon_f\varepsilon_p\left[\left(T_f^j + 273\right)^4 - \left(T_1^j + 273\right)^4\right] + \right.$$
$$\left. + h\left(T_f^j - T_1^j\right)\right\} - \frac{\Delta\tau\left(R_s - \frac{\Delta\xi_s}{2}\right)}{\rho_s c_{ps}^j \left(R_s - \frac{\Delta\xi_s}{4}\right)\Delta\xi_s^{\,2}}\left[\left(k_s\right)_1^j + \left(k_s\right)_2^j\right]\left(T_1^j - T_2^j\right) \tag{4.2}$$

where T_1^{j+1} is the temperature at the surface of the steel tube at time $\tau = (j+1)\Delta\tau$; R_s is the external CFT column radius; $\Delta\xi_s$ is the thickness of steel tube layers; ρ_s, c_{ps} and k_s are the density, specific heat and conductivity of steel; ε_f is the emissivity of the fire; ε_p is the emissivity of the exposed surface (steel tube); σ is the Stephan-Boltzmann constant; and h is the coefficient of convective heat transfer.

Equations for inside steel tube *(1 < m < M_1 - 1)*

To obtain the temperature at the inner layers of the steel tube the expression to be used is the next:

$$T_m^{j+1} = T_m^j + \frac{\Delta\tau}{2\rho_s^j c_{ps}^j\left[R_s - (m-1)\Delta\xi_s\right]\Delta\xi_s^{\,2}}\left\{\left[R_s - \left(m - \frac{3}{2}\right)\Delta\xi_s\right]\cdot\right.$$
$$\left.\cdot\left[\left(k_s\right)_{m-1}^j + \left(k_s\right)_m^j\right]\left(T_{m-1}^j - T_m^j\right) - \left[R_s - \left(m - \frac{1}{2}\right)\Delta\xi_s\right]\left[\left(k_s\right)_m^j + \left(k_s\right)_{m+1}^j\right]\left(T_m^j - T_{m+1}^j\right)\right\} \tag{4.3}$$

where T_m^{j+1} is the temperature at point *m* inside the steel at time $\tau = (j+1)\Delta\tau$.

Equations for steel-concrete boundary: Steel tube inner surface *(m = M_1 - 1)*

As explained above, the contact between the steel tube and the concrete core is represented in a realistic way by modeling the gap conductance at the steel-concrete interface. The temperature at the steel tube inner surface at time $\tau = (j+1)\Delta\tau$ is given by:

$$T_{M_1-1}^{j+1} = T_{M_1-1}^{j} + \frac{\Delta\tau}{\rho_s^j c_{ps}^j \left[R_s - \left(M_1 - \frac{9}{4}\right)\Delta\xi_s\right]\Delta\xi_s^{\,2}} \left\{\left[R_s - \left(M_1 - \frac{5}{2}\right)\Delta\xi_s\right]\cdot \right.$$
$$\left. \cdot \left[(k_s)_{M_1-2}^j + (k_s)_{M_1-1}^j\right]\left(T_{M_1-2}^j - T_{M_1-1}^j\right) - 2h_{gap}R_c\Delta\xi_s\left(T_{M_1-1}^j - T_{M_1}^j\right)\right\} \quad (4.4)$$

where h_{gap} is the thermal gap conductance at steel-concrete interface. It is defined as the conductance of the separation layer appearing between the two components.

Equations for steel-concrete boundary: Concrete core outer surface *($m = M_1$)*

On the other hand, the temperature at the surface of concrete core in the steel-concrete boundary at time $\tau = (j+1)\Delta\tau$ is given by:

$$T_{M_1}^{j+1} = T_{M_1}^{j} + \frac{\Delta\tau}{\left[\rho_c^j c_{pc}^j + \rho_w^j c_{pw}^j \phi_{M_1}^j\right]\left[R_c - \frac{\Delta\xi_c}{4}\right]\Delta\xi_c^{\,2}} \left\{2h_{gap}R_c\Delta\xi_c\left(T_{M_1-1}^j - T_{M_1}^j\right) - \right.$$
$$\left. - \left(R_c - \frac{\Delta\xi_c}{2}\right)\left[(k_c)_{M_1}^j + (k_c)_{M_1+1}^j\right]\left(T_{M_1}^j - T_{M_1+1}^j\right)\right\} \quad (4.5)$$

where ρ_c, c_{pc} and k_c are the density, specific heat and conductivity of concrete; $\Delta\xi_c$ is the thickness of concrete core layers; ρ_w and c_{pw} are the density and specific heat of water; ϕ is the concrete moisture content; and R_c is the concrete core radius.

Equations for inside concrete core *($M_1 + 1 \le m < M_2$)*

For the interior points of the concrete core, except for the point located at the center of the concrete core cross-section, the temperature at time $\tau = (j+1)\Delta\tau$ can be determined by the next equation:

$$T_m^{j+1} = T_m^j + \frac{\Delta\tau}{2\left[\rho_c^j c_{pc}^j + \rho_w^j c_{pw}^j \phi_m^j\right]\left[R_c - (m - M_1)\Delta\xi_c\right]\Delta\xi_c^{\,2}} \cdot$$
$$\cdot \left\{\left[R_c - \left(m - M_1 - \frac{1}{2}\right)\Delta\xi_c\right]\left[(k_c)_{m-1}^j + (k_c)_m^j\right]\left(T_{m-1}^j - T_m^j\right) - \right.$$
$$\left. - \left[R_c - \left(m - M_1 + \frac{1}{2}\right)\Delta\xi_c\right]\left[(k_c)_m^j + (k_c)_{m+1}^j\right]\left(T_m^j - T_{m+1}^j\right)\right\} \quad (4.6)$$

Equations for the center of concrete core *(m = M2)*

The temperature at the center of the concrete core at time $\tau = (j+1)\Delta\tau$ is given by:

$$T_{M_2}^{j+1} = T_{M_2}^{j} + \frac{2\Delta\tau}{\rho_c^j c_{pc}^j \Delta\xi_c^{\,2}}\left[\left(k_c\right)_{M_2-1}^{j} + \left(k_c\right)_{M_2}^{j}\right]\left(T_{M_2-1}^{j} - T_{M_2}^{j}\right) \tag{4.7}$$

4.2.3. Content of moisture in the concrete core

The effect of moisture on the concrete is taken into account by assuming that the initial volume of moisture in the concrete starts to evaporate when the temperature reaches 100ºC. During the evaporation all the heat provided is consumed in this process so that the temperature does not increase until the water has evaporated completely.

The initial content of moisture expressed in volume and the volume of moisture evaporated during a period of time $\Delta\tau$ is given by:

Steel-concrete boundary: Concrete core outer surface *($m = M_1$)*

For the external layer of the concrete core, the expressions are:

$$V_{M_1} = 2\pi\left[R_c - \frac{\Delta\xi_c}{4}\right]\frac{\Delta\xi_c}{2}\phi_{M_1} = \pi\left[R_c - \frac{\Delta\xi_c}{4}\right]\Delta\xi_c\phi_{M_1} \tag{4.8}$$

$$\begin{aligned}\Delta V_{M_1}^{j} = {} & \pi\frac{\pi\Delta\tau}{\rho_w\lambda_w\Delta\xi_c}\left\{2\lambda R_c\,\Delta\xi_c\left(T_{M_1-1}^{j} - T_{M_1}^{j}\right) - \right. \\ & \left. - \left(R_c - \frac{\Delta\xi_c}{2}\right)\left[\left(k_c\right)_{M_1}^{j} + \left(k_c\right)_{M_1+1}^{j}\right]\left(T_{M_1}^{j} - T_{M_1+1}^{j}\right)\right\}\end{aligned} \tag{4.9}$$

Inside concrete core ***($M_1+1 \le m < M_2$)***

In the case of the inner regions of the concrete core, except for the point representing the central area, the equations are:

$$V_m = 2\pi\left[R_c - \left(m - M_1\right)\Delta\xi_c\right]\Delta\xi_c\phi_m \tag{4.10}$$

$$\begin{aligned}\Delta V_m^{j} = {} & \frac{\pi\Delta\tau}{\rho_w\lambda_w\Delta\xi_c}\left\{\left[R_c - \left(m - M_1 - \frac{1}{2}\right)\Delta\xi_c\right]\left[\left(k_c\right)_{m-1}^{j} + \left(k_c\right)_{m}^{j}\right]\left(T_{m-1}^{j} - T_m^{j}\right) - \right. \\ & \left. - \left[R_c - \left(m - M_1 + \frac{1}{2}\right)\Delta\xi_c\right]\left[\left(k_c\right)_{m}^{j} + \left(k_c\right)_{m+1}^{j}\right]\left(T_m^{j} - T_{m+1}^{j}\right)\right\}\end{aligned} \tag{4.11}$$

Center of concrete core *($m = M_2$)*

Finally, for the concrete core central region, the next expressions are used:

$$V_{M_2} = 2\pi \frac{\Delta\xi_c^{\,2}}{8}\phi_{M_2} = \pi \frac{\Delta\xi_c^{\,2}}{4}\phi_{M_2} \tag{4.12}$$

$$\Delta V_{M_2}^{j} = \frac{\pi\Delta\tau}{2\rho_w\lambda_w}\left[(k_c)_{M_2-1}^{j} + (k_c)_{M_2}^{j}\right]\left(T_{M_2-1}^{j} - T_{M_2}^{j}\right) \tag{4.13}$$

4.3. PROTECTED CONCRETE FILLED TUBULAR COLUMNS

4.3.1. Discretization of the section

Jointly with the consideration of the gap conductance existing at the steel-concrete interface, another important feature which incorporates this thermal model is its extension to externally protected concrete filled tubular columns (Figure 4.3).

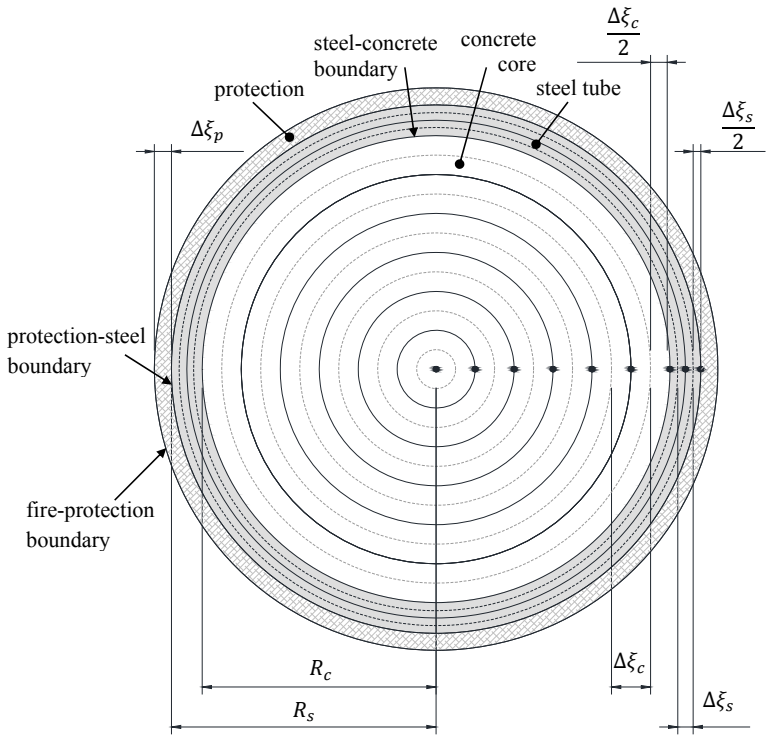

Figure 4.3. Protected CFT column. Discretization of the section for thermal analysis.

Given that the variation of the thickness of the protection layer is not considered in this model, the expressions here presented are valid to simulate the behavior of fire protected CFT specimens in which the protection layer thickness remains constant during the fire exposure time, such as spray protection.

In this case, the protection material applied is represented by one layer in the discretization scheme as showed in Figure 4.3. For these equations, the same reference is taken for the calculation points, i.e., M_2 represents the total number of calculation points and M_1 identifies the point located at the outer surface of the concrete core. Therefore, the number of layers employed to discretize the steel tube is $(M_1 - 2)$ and $(M_2 - M_1 + 3)$ are the layers in the concrete core. Again, the temperature target points are located at the boundary of the defined layers and represented by P_m.

The thickness of the protection layer is $\Delta\xi_p$. The thickness of all the layers in the steel tube is $\Delta\xi_s$, except for the layers at the protection-steel and steel-concrete boundaries which are ½ $\Delta\xi_s$ thick. The same occurs in the concrete core, while all the inner layers have a thickness of $\Delta\xi_c$, the layer at steel-concrete interface and the layer at the center of the column are ½ $\Delta\xi_c$.

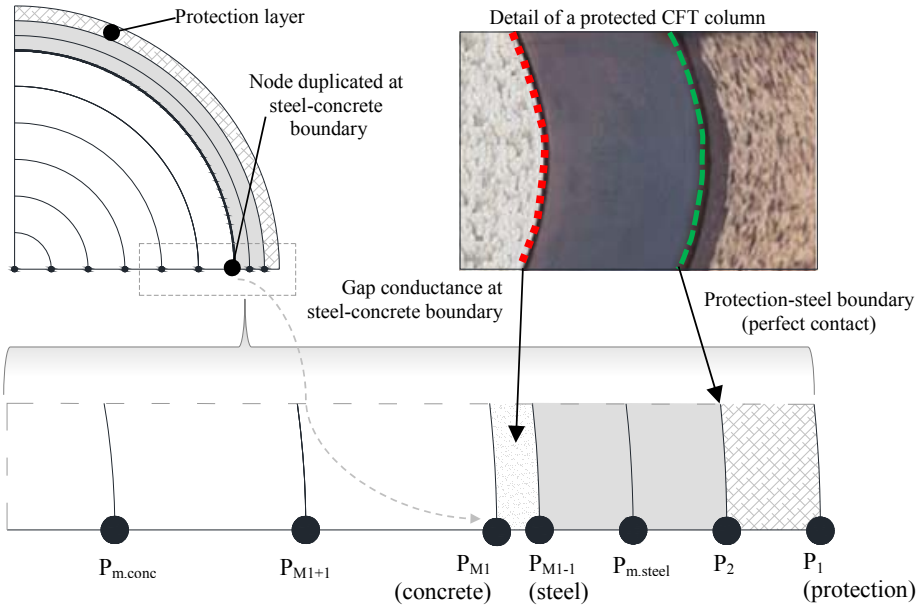

Figure 4.4. Detail: Protection layer and gap conductance for a protected CFT column.

The contact between the protection material and the steel tube is assumed as perfect when modelling the interfaces of the cross-section. In Figure 4.4 a detail of a protected CFT column is shown jointly with the specification of the temperature calculation points through the cross-section and the definition of the boundaries existing between the different components.

4.3.2. Cross-sectional temperatures

The assumption of homogeneous fire exposure for all the column length is maintained also in this case.

For a protected CFT column, at time $\tau = (j+1)\Delta\tau$, the temperature at the different points of the section can be calculated using the expressions:

Equations for fire-protection boundary *(m = 1)*

The expression to obtain the temperature at the surface of the protection layer T_1^{j+1}, at time $\tau = (j+1)\Delta\tau$ is:

$$T_1^{j+1} = T_1^j + \frac{2\Delta\tau\left(R_s + \Delta\xi_p\right)}{\rho_p^j c_{pp}^j \left(R_s + \frac{3}{4}\Delta\xi_p\right)\Delta\xi_p}\left\{\sigma\varepsilon_f\varepsilon_p\left[\left(T_f^j + 273\right)^4 - \left(T_1^j + 273\right)^4\right] + h\left(T_f^j - T_1^j\right)\right\} - \frac{\Delta\tau\left(R_s + \frac{\Delta\xi_p}{2}\right)}{\rho_p^j c_{pp}^j \left(R_s + \frac{3}{4}\Delta\xi_p\right)\Delta\xi_p^{\,2}}\left[\left(k_p\right)_1^j + \left(k_p\right)_2^j\right]\left(T_1^j - T_2^j\right) \quad (4.14)$$

where R_s is the external CFT column radius; $\Delta\xi_p$ is the protection layer thickness; ρ_p, c_{pp} and k_p are the density, specific heat and conductivity of the fire protection material; ε_f is the emissivity of the fire; ε_p is the emissivity of the exposed surface (protection layer); σ is the Stephan-Boltzmann constant; and h is the coefficient of convective heat transfer.

Equations for protection-steel boundary *(m = 2)*

As exposed above, perfect contact is assumed at the protection-steel boundary. Therefore, the temperature at the inner part of the protection layer is the same that at the outer part of the steel tube. The temperature at the protection-steel boundary at time $\tau = (j+1)\Delta\tau$ is given by the equation:

$$T_2^{j+1} = T_2^j + \frac{\Delta\tau}{\rho_p^j c_{pp}^j \left(R_s + \frac{\Delta\xi_p}{4}\right)\frac{\Delta\xi_p}{2} + \rho_s^j c_{ps}^j \left(R_s - \frac{\Delta\xi_s}{4}\right)\frac{\Delta\xi_s}{2}} \cdot$$

$$\cdot \left\{ \frac{R_s + \frac{\Delta\xi_p}{2}}{2\Delta\xi_p}\left[\left(k_p\right)_1^j + \left(k_p\right)_2^j\right]\left(T_1^j - T_2^j\right) - \frac{R_s - \frac{\Delta\xi_s}{2}}{2\Delta\xi_s}\left[\left(k_s\right)_2^j + \left(k_s\right)_3^j\right]\left(T_2^j - T_3^j\right) \right\} \quad (4.15)$$

where ρ_s, c_{ps} and k_s are the density, specific heat and conductivity of steel; and $\Delta\xi_s$ is the thickness of steel tube layers.

Equations for inside steel tube ***(3 ≤ m < M₁ - 2)***

When the temperature at the inner layers of the steel tube is going to be obtained, the expression to be used is the next:

$$T_m^{j+1} = T_m^j + \frac{\Delta\tau}{2\rho_s^j c_{ps}^j \left[R_s - (m-1)\Delta\xi_s\right]\Delta\xi_s^{\,2}} \left\{ \left[R_s - \left(m - \frac{3}{2}\right)\Delta\xi_s \right] \cdot \right.$$

$$\left. \cdot \left[\left(k_s\right)_{m-1}^j + \left(k_s\right)_m^j\right]\left(T_{m-1}^j - T_m^j\right) - \left[R_s - \left(m - \frac{1}{2}\right)\Delta\xi_s \right]\left[\left(k_s\right)_m^j + \left(k_s\right)_{m+1}^j\right]\left(T_m^j - T_{m+1}^j\right) \right\} \quad (4.16)$$

where T_m^{j+1} is the temperature at point m inside the steel at time $\tau = (j+1)\Delta\tau$.

Note that for the rest of the regions:

- Steel-concrete boundary: Steel tube inner surface *(m = M₁ - 1)*
- Steel-concrete boundary: Concrete core outer surface *(m = M₁)*
- Inside concrete core *(M₁ +1 ≤ m < M₂)*
- Center of concrete core *(m = M₂)*

equations 4.4 to 4.7 given for unprotected CFT columns are equally applicable for protected CFT columns since the subscripts referring to these regions are not affected by the consideration of the external fire protection layer.

4.3.3. Content of moisture in the concrete core

Given that the consideration of the extra layer representing the external fire protection affects uniquely to the numeration of the steel and protection layer

calculation points, the equations presented in section 4.2.3 are equally valid to be applied for protected CFT columns.

4.4. VALIDATION OF THE THERMAL MODEL

4.4.1. Experimental tests for validation

4.4.1.1. Unprotected CFT columns

In order to validate the thermal model for its application to unprotected CFT columns, the data from two experimental campaigns were used.

On the one hand, results from own tests reported in literature were employed (Romero et al. 2011, Moliner et al. 2013). In this case, all the CFT columns were tested at AIDICO (Instituto Tecnológico de la Construcción) in Valencia, Spain.

The analyzed specimens comprised columns filled with normal and high strength concrete of different type infill: plain, bar-reinforced and steel fiber reinforced concrete. The aggregates were calcareous for the 38 columns analyzed. These specimens were heated following the standard ISO-834 curve (ISO 1980, CEN 2002). The main characteristics of these columns are listed in Table 4.1.

On the other hand, data from tests performed by Lie & Chabot (1992) were also used so that the validation process was not limited to comparison with own experimental results. The thermal response of 23 columns specimens tested at the National Research Council of Canada (NRCC) was simulated.

These columns were filled with normal strength concrete, with both siliceous and calcareous aggregates. For those specimens containing siliceous aggregates, a moisture content value of 3% in concrete weight was employed, since they seem to retain less humidity than concrete with calcareous aggregates, for which a value of 10% was applied. In these tests, the standard fire curve followed was the ASTM-E119 (ASTM 1990). In Table 4.2 the main parameters which describe the characteristics of these specimens are shown.

For those specimens filled with normal strength concrete, the comparison was extended to the results obtained by the validated three-dimensional model developed by Espinos et al. (2010) using the general purpose package ABAQUS.

Table 4.1. List of unprotected CFT columns for thermal model validation, own tests (Romero et al. 2011, Moliner et al. 2013)

	Column No.	*D* (mm)	*t* (mm)	Moisture content (%)	*FRR* (min)
Romero et al. 2011	C159-6-3-30-0-20	159	6	1.80	42
	C159-6-3-30-0-40	159	6	2.30	25
	C159-6-3-30-0-60	159	6	2.00	14
	C159-6-3-80-0-20	159	6	2.85	37
	C159-6-3-80-0-40	159	6	2.00	11
	RC159-6-3-30-0-20	159	6	-[(1)]	43
	RC159-6-3-30-0-40	159	6	-[(1)]	30
	RC159-6-3-30-0-60	159	6	4.00	13
	RC159-6-3-80-0-20	159	6	1.00	64
	RC159-6-3-80-0-40	159	6	0.80	18
	FC159-6-3-30-0-20	159	6	6.49	36
	FC159-6-3-30-0-40	159	6	3.21	22
	FC159-6-3-80-0-20	159	6	-[(2)]	35
	FC159-6-3-80-0-40	159	6	0.81	15
Moliner et al. 2013	C159-6-3-30-20-20	159	6	2.86	33
	C159-6-3-30-20-40	159	6	6.00	17
	C159-6-3-30-50-20	159	6	3.41	31
	C159-6-3-30-50-40	159	6	3.32	24
	C159-6-3-90-20-20	159	6	1.00	35
	C159-6-3-90-20-40	159	6	2.26	13
	C159-6-3-90-50-20	159	6	2.63	31
	C159-6-3-90-50-40	159	6	0.99	17
	RC159-6-3-30-20-20	159	6	4.30	49
	RC159-6-3-30-20-40	159	6	5.43	25
	RC159-6-3-30-50-20	159	6	6.41	40
	RC159-6-3-30-50-40	159	6	6.59	21
	RC159-6-3-90-20-20	159	6	1.07	49
	RC159-6-3-90-20-40	159	6	2.00	25
	RC159-6-3-90-50-20	159	6	1.46	41
	RC159-6-3-90-50-40	159	6	0.57	17
	FC159-6-3-30-20-20	159	6	5.61	32
	FC159-6-3-30-20-40	159	6	5.77	18
	FC159-6-3-30-50-20	159	6	6.23	31
	FC159-6-3-30-50-40	159	6	6.19	25
	FC159-6-3-90-20-20	159	6	1.11	24
	FC159-6-3-90-20-40	159	6	1.37	14
	FC159-6-3-90-50-20	159	6	3.15	30
	FC159-6-3-90-50-40	159	6	3.21	16

[(1)] Moisture content data not available. A value of 4.00% was assumed.
[(2)] Moisture content data not available. A value of 1.00% was assumed.

In this table, the columns can be identified as follows: NXXX-T-L-FF-EE-AA, where N is the type of concrete (C stands for plain concrete, RC for reinforced concrete and FC for fiber reinforced concrete), XXX is the diameter of the column,

T the steel tube wall thickness, L the length of the column in meters, FF the nominal concrete strength in MPa, EE the load eccentricity and AA the axial load level.

Table 4.2. List of unprotected CFT columns for thermal model validation, tests by other authors (Lie & Chabot 1992)

Column No.	*D* (mm)	*t* (mm)	Type of aggregate	Type of concrete	FRR (min)
C-02	141.3	6.55	Siliceous	NSC	55
C-04	141.3	6.55	Siliceous	NSC	57
C-05	168.3	4.78	Siliceous	NSC	76
C-06	168.3	4.78	Siliceous	NSC	60
C-08	168.3	4.78	Siliceous	NSC	56
C-09	168.3	6.35	Siliceous	NSC	81
C-11	219.1	4.78	Siliceous	NSC	80
C-13	219.1	4.78	Siliceous	NSC	102
C-15	219.1	8.18	Siliceous	NSC	73
C-17	219.1	8.18	Siliceous	NSC	82
C-20	273.1	5.56	Siliceous	NSC	112
C-21	273.1	5.56	Siliceous	NSC	133
C-22	273.1	5.56	Siliceous	NSC	70
C-23	273.1	12.70	Siliceous	NSC	143
C-31	141.3	6.55	Calcareous	NSC	82
C-32	141.3	6.55	Calcareous	NSC	64
C-34	219.1	4.78	Calcareous	NSC	111
C-35	219.1	4.78	Calcareous	NSC	108
C-37	219.1	8.18	Calcareous	NSC	102
C-40	273.1	6.35	Calcareous	NSC	106
C-41	273.1	6.35	Calcareous	HSC	76
C-42	273.1	6.35	Calcareous	HSC	90
C-44	273.1	6.35	Calcareous	NSC	178

4.4.1.2. Protected CFT columns

For spray protected CFT column specimens, predictions given by the model were contrasted with the results from the experimental campaign conducted by Han et al. (2003a). It is worthy to mention that, among the literature reviewed at the time of elaboration of this thesis, the number of experimental programs involving protected circular CFT columns was limited.

Hence, the thermal model was validated by comparing its predictions with experimental data from Han et al. (2003a) who only reported the evolution of the

temperature at the steel tube surface. The specimens used in validation were filled with both normal and high strength plain concrete. Since no specific data for the actual concrete moisture content was provided, a value of 10% was assumed for normal strength concrete (calcareous coarse aggregates).

For those specimens filled with high strength concrete, with significantly less water content, a value of 1% was adopted. The thickness of the spray protection layer applied to the columns varied from 15 to 25 mm. The experimental program was carried out in the Tianjin Fire Research Institute and the fire curve followed in the heating process was the standard ISO-834 curve (ISO 1980, CEN 2002). The description of these columns is collected in Table 4.3.

Table 4.3. List of protected CFT columns for thermal model validation (Han et al. 2003a)

Column No.	D (mm)	t (mm)	d_p (mm)	Type of aggregate	Type of concrete	FRR (min)
C1-3	478	8	15	Calcareous	NSC	196
C2-3	219	5	15	Calcareous	NSC	132
C2-4	219	5	25	Calcareous	NSC	175
C3-4	219	4.6	15	Calcareous	HSC	120

4.4.2. Thermal properties at high temperatures

The thermal model takes into account the variation with temperature of the thermal properties of the materials.

Concrete

The thermal properties for concrete at elevated temperatures from EN 1992-1-2 (CEN 2004a) were adopted. For the thermal conductivity of concrete, the upper limit was adopted.

EN 1992-1-2 does not provide specific expressions for the thermal properties of high strength concrete and assumes that HSC has the same thermal properties as NSC. In this model, the specific expressions for the thermal properties of high strength concrete proposed by Kodur & Sultan (2003) were implemented.

Steel fiber reinforced concrete

When modeling the specimens filled with steel fiber reinforced concrete of normal strength, the thermal properties at high temperatures developed by Lie & Kodur were used (Lie & Kodur 1995b, Kodur & Lie 1996).

On the other hand, for those specimens with high strength steel fiber reinforced concrete as infill, the relationships for thermal properties at high temperatures presented by Kodur & Sultan (2003) were adopted.

Steel

For structural steel, the temperature dependent thermal properties recommended in EN 1993-1-2 (CEN 2005b) were implemented. According to EN 1994-1-2 (CEN 2005c), for reinforcing steel the thermal properties are the same as those employed for structural steel.

Spray protection

The fire protection spray applied to the cases analyzed is a heat-insulating material based on vermiculite for which the consulted literature (Surorov & Skunkhin 2002, Wang et al. 2013) provided values that ranged from 0.09 to 0.18 W/mK varying with temperature, although the existing data for high temperature properties is scarce. Thus, a value of 0.16 W/mK was adopted in this case since it proved to be the one that, on average, produced the most accurate response.

For the density and the specific heat of the protection material, the values of 400 ± 20 kg/m^3 and 1047 J/kgK were taken (Han et al. 2003a).

4.4.3. Thermal analysis parameters

The main parameters of the heat transfer problem and the adopted values, according to EN 1991-1-2 (CEN 2002), were the next:

- Coefficient of convective heat transfer at the exposed surface: $h = 25$ W/m^2 K
- Configuration factor for radiation at the exposed surface: $\Phi = 1$
- Stephan-Boltzmann constant: $\sigma = 5.67 \cdot 10^{-8}$ W/m^2 K^4
- Emissivity of the exposed surface (steel): $\varepsilon_s = 0.7$
- Emissivity of the exposed surface (protection): $\varepsilon_p = 0.7$
- Emissivity of the fire: $\varepsilon_f = 1$
- Initial temperature: $T_0 = 20$ºC

In this case, a constant value of 200 W/m^{2}K was employed for the gap conductance at the steel-concrete interface. The adoption of this constant value has been suggested by authors like Espinos et al. (2010) and Ding & Wang (2008) after employing it in their respective works for representing the gap conductance.

In this model, radiation at steel-concrete interface was not explicitly considered. The three-dimensional numerical model developed by Espinos et al. (2010) for CFT columns in fire took into account the gap radiation by assuming an emissivity value of 0.7 for both materials. However, comparison of the temperature predictions obtained with the model here presented with those given by the 3D model showed an excellent agreement and confirmed the absence of significant differences in their predictions. These comparisons will be presented in the section dedicated to the development and validation of the thermo-mechanical model. Thus, for simplicity it is assumed that, in this practical situation, the radiation across the gap can be neglected.

Depending on the case analyzed, the exposed surface of the CFT column is heated following the corresponding standard fire curve (ISO 834 or ASTM-E119) or the furnace temperature-time curve if it was reported and the deviation was very pronounced.

With regard to the discretization of the section in the thermal analysis, for each specimen, the number of layers was established so that for the hollow steel section the layer was not more than 10 mm thick which implied to considered one or two layers. In the case of the concrete core, the number of layers was varied to obtain a size close to 20 mm which is recommended for thermal analysis and typical size used in other models (Espinos et al. 2010).

4.4.4. Thermal response

4.4.4.1. Unprotected CFT columns

The temperature evolution registered by the thermocouples placed at different points of the cross-section was compared with the predicted temperatures at these locations. Data results reported in literature include not only the evolution of the steel tube surface temperature (point T1) but also the temperature registered by the thermocouples located at the inner points of the concrete core (points T2 and T3). The calculated temperatures along the cross-section showed a good agreement with the tests results, for both specimens with calcareous and siliceous aggregates as can be observed in Figure 4.5.

For those specimens with normal strength plain concrete, the comparison with the three-dimensional model by Espinos et al. (2010) showed that using a finite differences model to simulate the cross-sectional temperatures does not imply a loss of accuracy with respect to the predictions obtained by the three-dimensional model which, due to its nature allows achieving more realistic predictions.

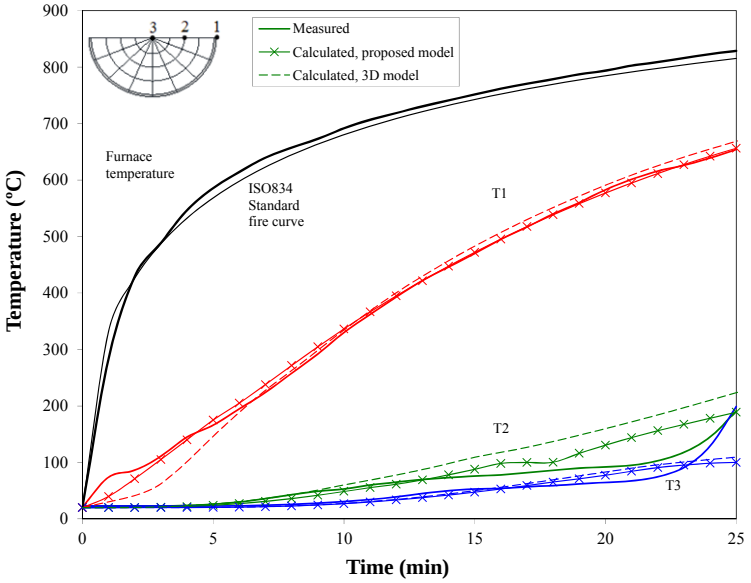

(a) Column C159-6-3-30-0-40, calcareous aggregates

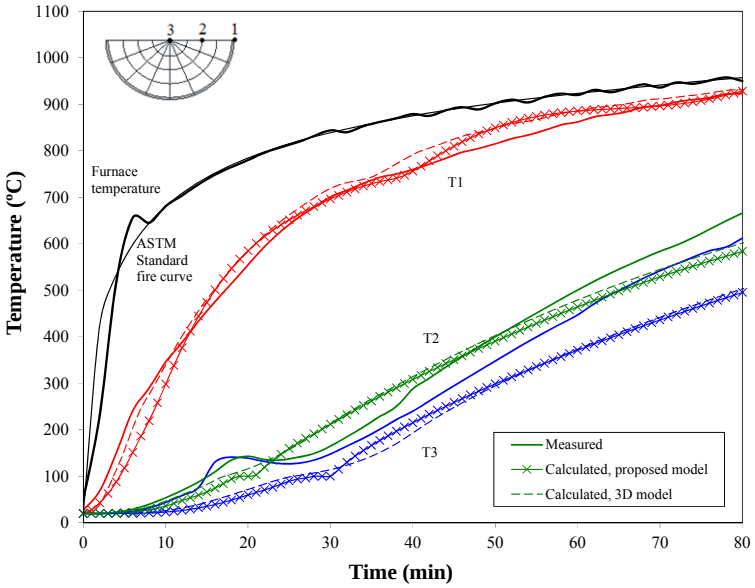

(b) Column C-09, siliceous aggregates

Figure 4.5. Comparison between measured and thermal model predicted temperatures for specimens with different type of aggregate.

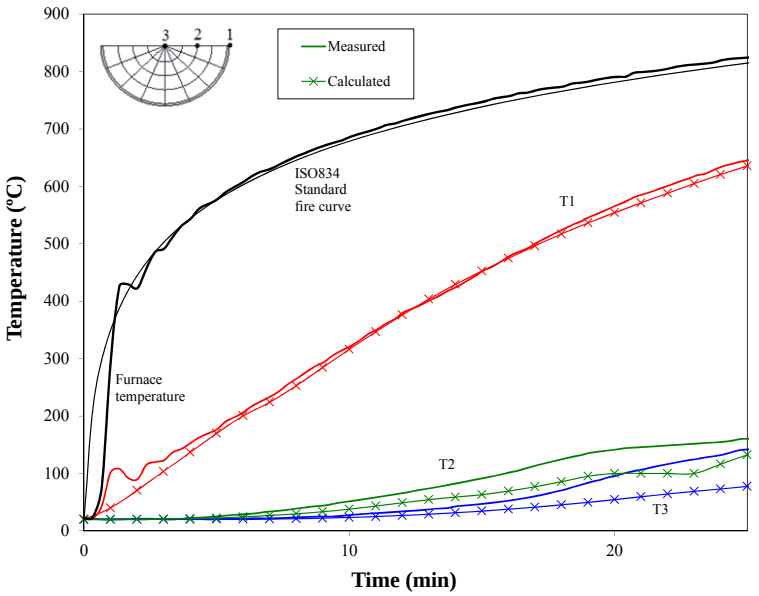

(a) Column FC159-6-3-30-50-40, steel fiber reinforced concrete

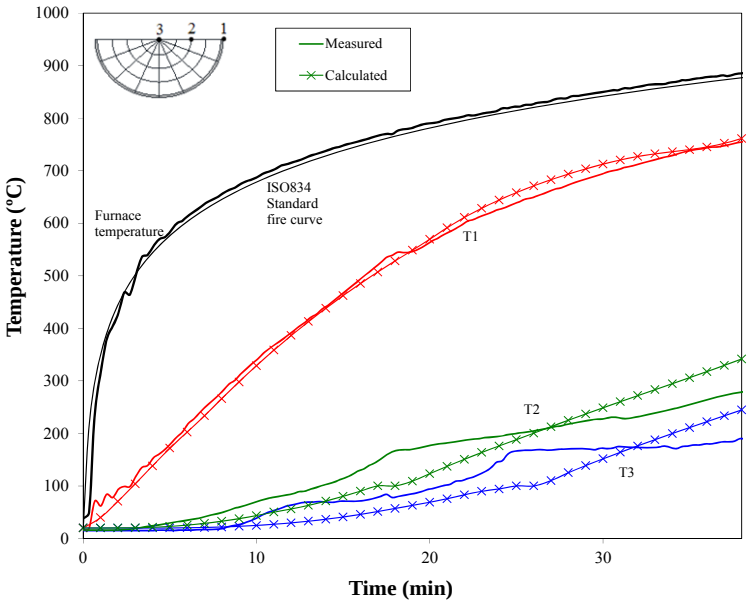

(b) Column C159-6-3-80-20, high strength concrete

Figure 4.6. Comparison between measured and thermal model predicted temperatures for specimens with different type of concrete infill.

With regard to the type of infill, the thermal model proved to give accurate predictions during the fire exposure time independently of the type of concrete or reinforcement used and their strength. As an example, Figure 4.6 depicts the comparison of temperature evolution made for two of the specimens filled with different type of concrete.

Nevertheless, it is worthy to mention that a little deviation between actual and calculated temperatures exists around temperatures of 100ºC. This discrepancy can be explained by the way in which the moisture consumption is modeled. As described above, in this model the variation of moisture content through time is modeled as a straightforward procedure, so that when the temperature of a concrete area reaches 100ºC, all the heat applied is employed in evaporating the water and while this process is taking place, the temperature is not increased.

Another parameter of validation employed was the temperature at time of failure. The contrast was made between the measured steel tube surface temperature at failure and the one given by the thermal model at that time. These pairs of values as well as the corresponding error are included in Table 4.4 and Table 4.5 for columns from own tests and for columns from programs reported in the literature respectively. As it can be checked in Figure 4.7, the agreement between test data and model temperatures for all the unprotected specimens analyzed is remarkably good with a mean error value of 1.00 and a standard deviation of 0.06.

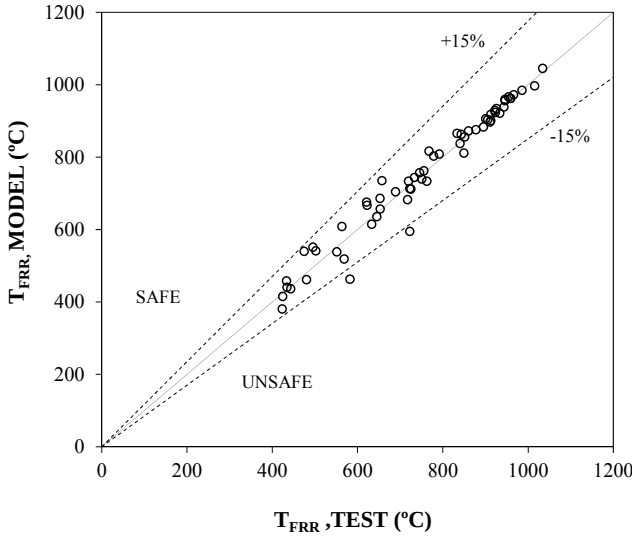

Figure 4.7. Comparison of temperatures at failure: model vs. test.

Table 4.4. Temperature at failure for unprotected CFT columns, own tests (Romero et al. 2011, Moliner et al. 2013)

	Column No	***FRR*** **(min)**	$T_{FRR_{TEST}}$ **(ºC)**	$T_{FRR_{MODEL}}$ **(ºC)**	$\frac{T_{FRR_{TEST}}}{T_{FRR_{MODEL}}}$
Romero et al. 2011	C159-6-3-30-0-20	42	850	810	1.05
	C159-6-3-30-0-40	25	654	656	1.00
	C159-6-3-30-0-60	14	583	462	1.26
	C159-6-3-80-0-20	37	756	761	0.99
	C159-6-3-80-0-40	11	424	380	1.12
	RC159-6-3-30-0-20	43	768	816	0.94
	RC159-6-3-30-0-40	30	726	711	1.02
	RC159-6-3-30-0-60	13	444	436	1.02
	RC159-6-3-80-0-20	64	913	900	1.01
	RC159-6-3-80-0-40	18	496	551	0.90
	FC159-6-3-30-0-20	36	751	739	1.02
	FC159-6-3-30-0-40	22	723	594	1.22
	FC159-6-3-80-0-20	35	763	733	1.04
	FC159-6-3-80-0-40	15	481	461	1.04
Moliner et al. 2013	C159-6-3-30-20-20	33	734	743	0.99
	C159-6-3-30-20-40	17	552	538	1.03
	C159-6-3-30-50-20	31	658	735	0.90
	C159-6-3-30-50-40	24	623	667	0.93
	C159-6-3-90-20-20	35	746	754	0.99
	C159-6-3-90-20-40	13	435	438	0.99
	C159-6-3-90-50-20	31	720	733	0.98
	C159-6-3-90-50-40	17	475	539	0.88
	RC159-6-3-30-20-20	49	834	865	0.96
	RC159-6-3-30-20-40	25	622	675	0.92
	RC159-6-3-30-50-20	40	792	814	0.97
	RC159-6-3-30-50-40	21	634	623	1.02
	RC159-6-3-90-20-20	49	841	835	1.01
	RC159-6-3-90-20-40	25	718	675	1.06
	RC159-6-3-90-50-20	41	779	802	0.97
	RC159-6-3-90-50-40	17	503	541	0.93
	FC159-6-3-30-20-20	32	723	713	1.01
	FC159-6-3-30-20-40	18	569	518	1.10
	FC159-6-3-30-50-20	31	690	710	0.97
	FC159-6-3-30-50-40	25	646	644	1.00
	FC159-6-3-90-20-20	24	564	599	0.94
	FC159-6-3-90-20-40	14	425	407	1.04
	FC159-6-3-90-50-20	30	653	685	0.95
	FC159-6-3-90-50-40	16	434	458	0.95
				Mean	1.00
				Standard deviation	0.01

Table 4.5. Temperature at failure for unprotected CFT columns, tests by other authors (Lie & Chabot 1992)

Column No.	*FRR* (min)	$T_{FRR_{TEST}}$ (ºC)	$T_{FRR_{MODEL}}$ (ºC)	$\frac{T_{FRR_{TEST}}}{T_{FRR_{MODEL}}}$
C-02	55	852	855	1.00
C-04	57	844	862	0.98
C-05	76	913	917	1.00
C-06	60	878	875	1.00
C-08	56	896	882	1.02
C-09	81	923	928	0.99
C-11	80	924	923	1.00
C-13	102	960	961	1.00
C-15	73	906	903	1.00
C-17	82	934	921	1.01
C-20	112	959	961	1.00
C-21	133	986	984	1.00
C-22	70	861	871	0.99
C-23	143	1016	996	1.02
C-31	82	944	937	1.01
C-32	64	911	896	1.02
C-34	111	967	971	1.00
C-35	108	955	965	0.99
C-37	102	947	955	0.99
C-40	106	946	959	0.99
C-41	76	901	905	1.00
C-42	90	926	933	0.99
C-44	178	1035	1045	0.99
		Mean		1.00
		Standard deviation		0.08

The calculated mean and standard deviation error values are reasonably good for both groups of columns and no relevant differences exist between their results, which show the same value for the mean error (1.00) and small values of the standard deviation. The stability of the statistics parameters in both cases proves the consistency of the thermal model for predicting the temperature at failure with independency of the type of infill for unprotected CFT columns.

4.4.4.2. Protected CFT columns

In the case of protected CFT columns, the data reported by Han et al. (2003a) only referred to the temperature measured at the steel tube surface (point T1). The comparison between measured and calculated values for the protected specimens is shown in Figure 4.8. It can be noted that the evolution of the predicted temperatures follows the same trend that the test data for all the cases.

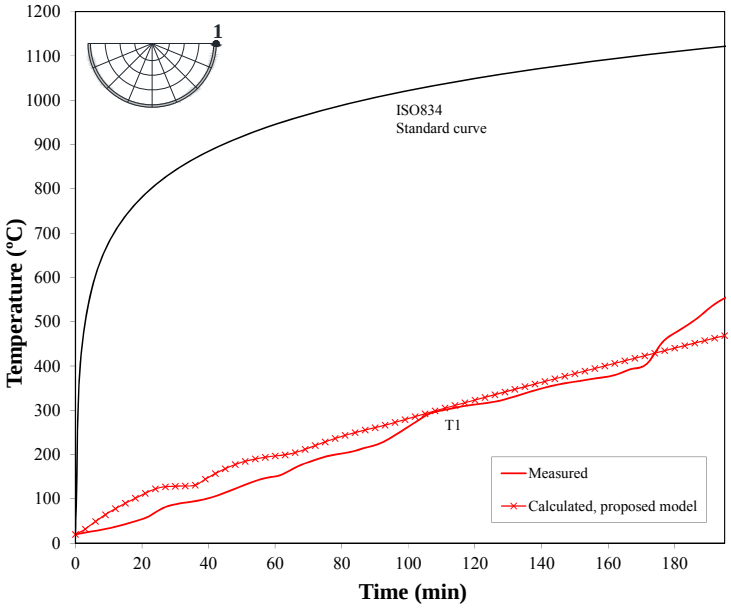

(a) Column C1-3

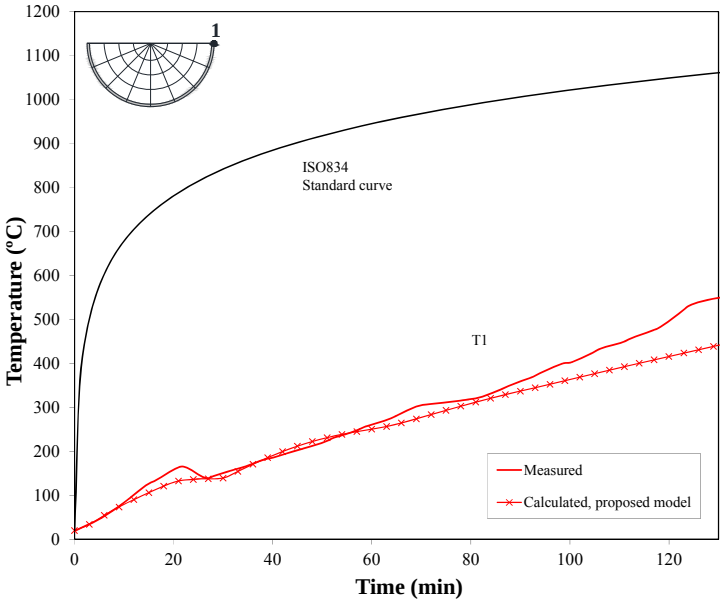

(b) Column C2-3

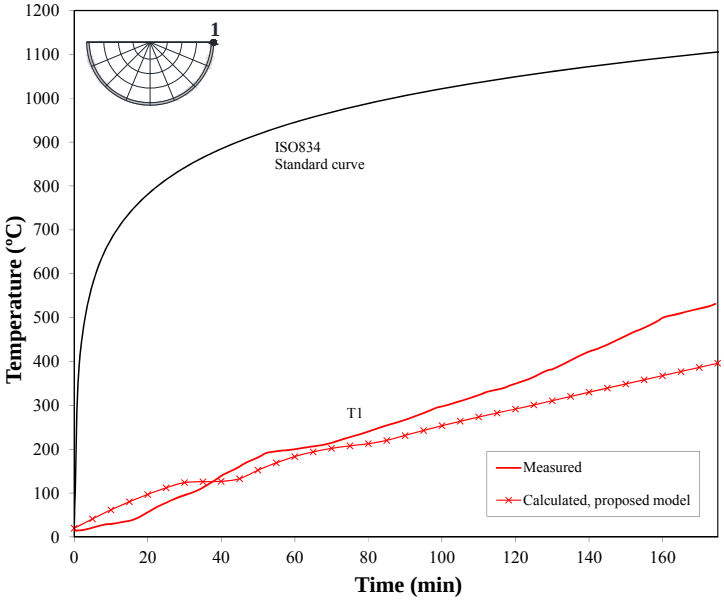

(c) Column C2-4

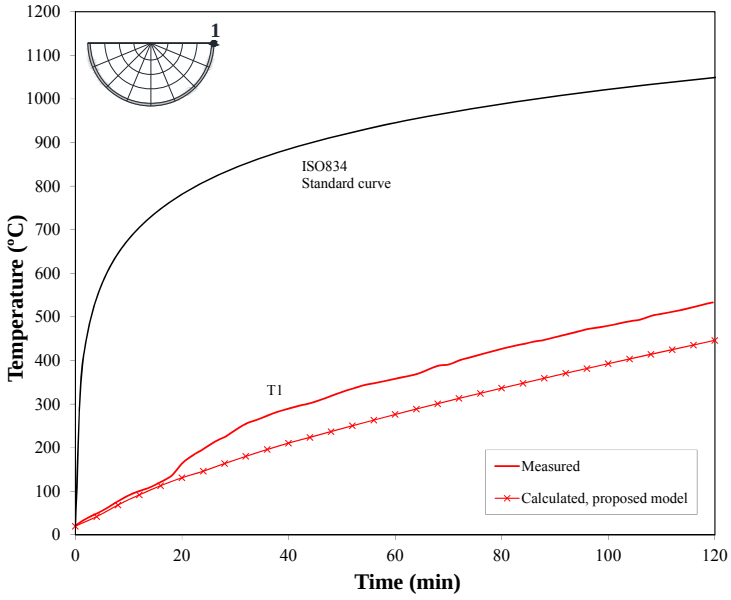

(d) Column C3-4

Figure 4.8. Protected columns. Comparison between measured and predicted steel tube temperatures.

Following the same procedure adopted for unprotected specimens, the temperature at time of failure was used as a parameter of comparison. For protected columns the obtained results and the ones registered in the tests are shown in Table 4.6. In this case, an error average of 1.26 is obtained, higher than for the case of unprotected columns.

Table 4.6. Temperature at failure for protected CFT columns (Han et al. 2003a)

Column No.	***d*** **(mm)**	***FRR*** **(min)**	$T_{FRR_{Test}}$ **(ºC)**	$T_{FRR_{Num}}$ **(ºC)**	$\xi_{T_{FRR}=\frac{T_{FRR_{Test}}}{T_{FRR_{Num}}}}$
C1-3	15	196	564	462	1.22
C2-3	15	132	555	451	1.23
C2-4	25	175	534	390	1.37
C3-4	15	120	537	446	1.20
				Mean	1.26
				Standard deviation	0.08

Thus, although the temperature evolution during the fire exposure generally fits the experimental data for the specimens analyzed, it can be seen in Figure 4.8 that at the end of the tests predicted temperatures deviate from measured temperature which experiment a rapid grow.

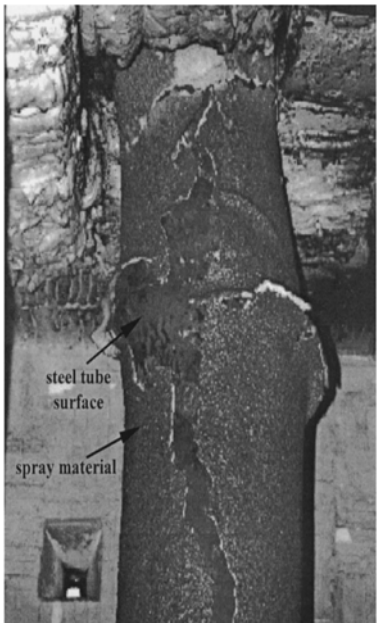

Figure 4.9. Typical failure of spray protection after fire tests (Han et al. 2003a).

This discrepancy between temperatures at failure may be due to the behavior of the protection material at the end of the fire test. The layer of insulation material starts to crumble and fall to pieces, leaving some areas of the steel tube to the direct fire exposure which makes the steel tube reach local higher temperatures. As an example, in Figure 4.9 the state after the fire test for one of the specimens analyzed is shown. This was reported by Han et al. (2003a) as the typical failure mode of the spray protection in a CFT column and it can be appreciated how the insulation material is fractured and disintegrated in some areas leaving the steel tube external surface directly exposed to fire.

4.4.5. Effect of gap conductance on the thermal response

As described above, with the aim to obtain a more realistic cross-sectional thermal response, the developed thermal model takes into consideration the existence of a gap conductance at the steel-concrete boundary generated due to the different thermal expansion coefficients of both materials. For two of the specimens analyzed, Figure 4.10 shows the comparison of the test temperatures against results obtained when perfect contact between steel and concrete is assumed and when the existence of the gap conductance is considered.

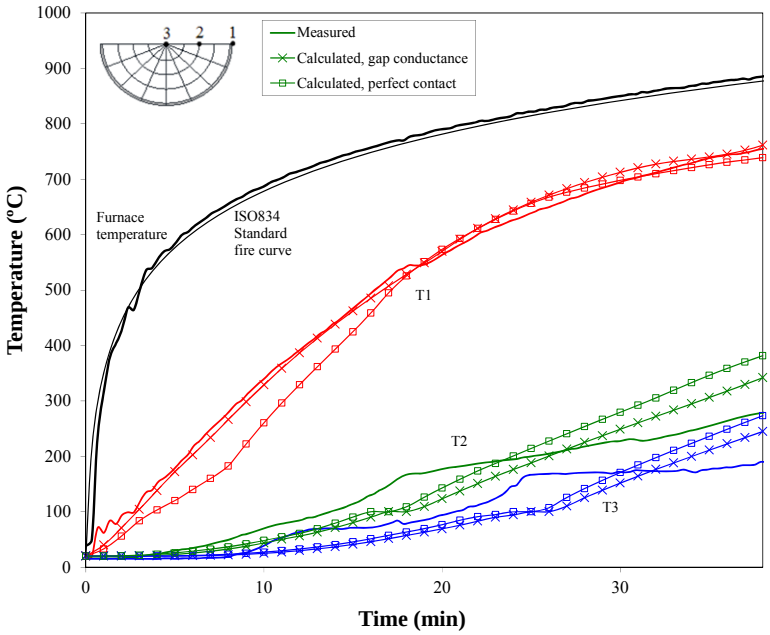

(a) Column C-159-6-3-80-0-20

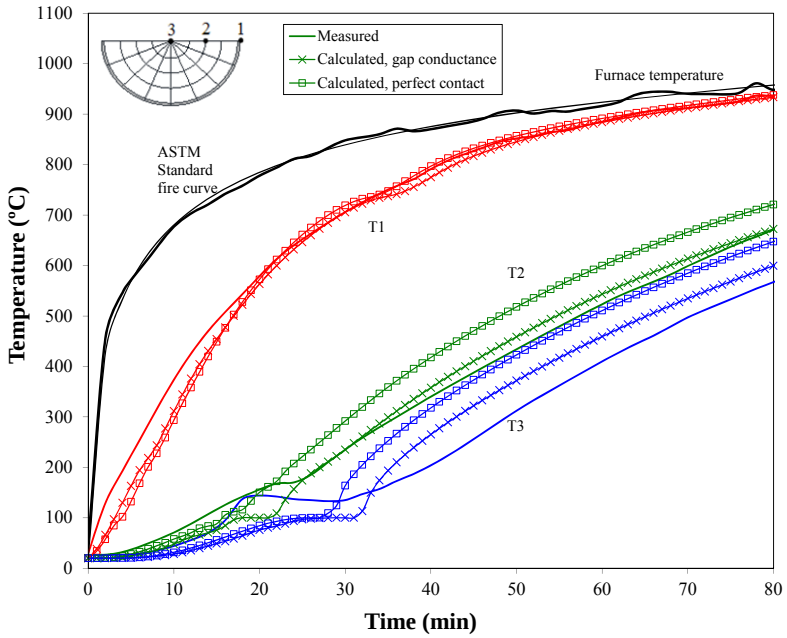

(b) Column C-31

Figure 4.10. Comparison of measured and calculated temperatures with different steel-concrete boundary model: gap conductance versus perfect contact.

For the temperatures measured in the steel tube, the response given under the assumption of perfect contact lays below the test temperatures during the most of the time. This behavior is due to the fact that no resistance opposes to the heat flow when crossing the steel-concrete boundary. The easier the heat flows through the section, the lower the temperatures achieved by the steel tube and the higher the temperatures in the concrete core. The effect on the steel tube temperatures is clearly visible in Figure 4.10a for column C159-6-3-80-0-20, especially during the first part of the fire exposure.

On the contrary, the influence of the type of steel-concrete boundary on concrete core temperatures is more pronounced when the time of fire exposure is prolonged and the stationary regime has been achieved. Thus, in Figure 4.10b, for column C-31 which has a FRR of 80 min, it can be observed how the temperature evolution for the inner points of concrete when contact perfect is assumed is overestimated due to the lack of resistance found by the heat flow at the steel-concrete interface.

4.5. ASSESSMENT OF THE STEEL TUBE TEMPERATURE

As pointed out in previous sections, the combined action of steel tube and concrete core in CFT columns makes this type of columns very suitable for fire situations and supposes a great enhancement respect to the use of hollow steel tube columns. The study of the notable effects of filling a hollow steel section with concrete will contribute to shed some light in measuring up to which extent the concrete infill improves the steel tube fire behavior.

Therefore, an assessment of the steel tube temperature development under fire situation was carried out for different types of columns. The objective was to compare the steel tube temperature under different situations, for unprotected and protected columns formed by HSS or CFT sections, and its effects on the protection layer thickness and the heating rate.

For comparison purposes, circular HSS columns with the same diameter as the previously studied CFT columns are analyzed with the aim of contrasting the evolution of the steel tube temperatures in both cases. In the case of HSS, the steel tube temperature is calculated by means of the expressions proposed in EN 1993-1-2 (CEN 2005b) for unprotected and for protected specimens.

According to Clause 4.2.5.1 of EN 1993-1-2, to obtain the equivalent uniform temperature distribution in the cross-section of an unprotected steel member, the increase of temperature $\Delta\theta_{a,t}$ during a time interval Δt should be determined from:

$$\Delta\theta_{a,t} = k_{sh}\frac{A_m/V}{c_a\rho_a}\dot{h}_{net}\,\Delta t \tag{4.17}$$

where k_{sh} is a correction factor for the shadow effect (taken as 1 to be conservative), A_m/V is the section factor for unprotected steel members; A_m is the surface area of the member per unit length; V is the volume of the member per unit length [m³/m]; c_a is the specific heat of steel; Δt is the time interval; ρ_a is the unit mass of steel; and $\dot{h}_{net}$ is the design value of the net heat flux per unit area calculated according to EN 1991-1-2 (CEN 2002) and already defined in equation 1.8 of the section 1.2.2 of this work .

On the other hand, for protected steel members, Clause 4.2.5.2 of EN 1993-1-2 establishes that, in order to compute the uniform temperature distribution in a cross-section, the temperature increase $\Delta\theta_{a,t}$ of the member during a time interval Δt should be obtained from the next expressions:

$$\Delta\theta_{a,t} = \frac{\lambda_p A_p/V}{d_p c_a \rho_a} \cdot \frac{(\theta_{g,t} - \theta_{a,t})}{(1+\phi/3)} \cdot \Delta t - (e^{\phi/10} - 1)\Delta\theta_{g,t} \quad (4.18)$$

$$\phi = \frac{c_p \rho_p}{c_a \rho_a} d_p A_p/V \quad (4.19)$$

where A_p/V is the section factor for steel members insulated by fire protection material; A_p is the area of fire protection material per unit length of the member; V is the volume of the member per unit length; c_p is the temperature independent specific heat of the fire protection material; d_p is the thickness of the fire protection material; $\theta_{g,t}$ is the ambient gas temperature at time t; $\Delta\theta_{g,t}$ is the increase of the ambient gas temperature during the time interval Δt; λ_p is the thermal conductivity of the fire protection system; and ρ_p is the unit mass of the fire protection material.

However, the desirable direct comparison with temperature results for CFT columns computed by expressions included in the pertinent code cannot be accomplished since, as pointed out at the beginning of this chapter, the Eurocode 4 Part 1.2 (CEN 2005c) for composite structures in fire does not provide any practical expression for that purpose. Therefore, for protected and unprotected CFT columns, the validated proposed thermal model is used to calculate the steel tube temperatures along time.

4.5.1. Effect of the concrete infill on protection thickness

The steel tube temperature evolution has been obtained for different types of columns taking as a basis the dimensions of the sections of the protected columns studied (Han et al. 2003a). Thus, for each section, the configurations studied have been the next: unprotected hollow steel section (HSS) and concrete filled tubular section, and protected HSS and CFT section with different protection layer thicknesses. Figure 4.11 shows, for two of the geometries analyzed, the steel tube temperature obtained for the all the configurations mentioned before.

Unprotected and protected CFT columns show lower temperatures in all the cases when are compared to their respective hollow steel sections. However, the beneficial effect of concrete infill is much more noticeable in protected profiles. Although the concrete core acts as a heat sink and takes heat from the steel tube, in the case of unprotected specimens the heating rate of the profile is so high that this effect is greatly reduced. On the contrary, for protected columns with the outer spray

acting as a barrier to the heat transfer, the profile heating is delayed which emphasizes and prolongs the action of the concrete core acting as a heat sink.

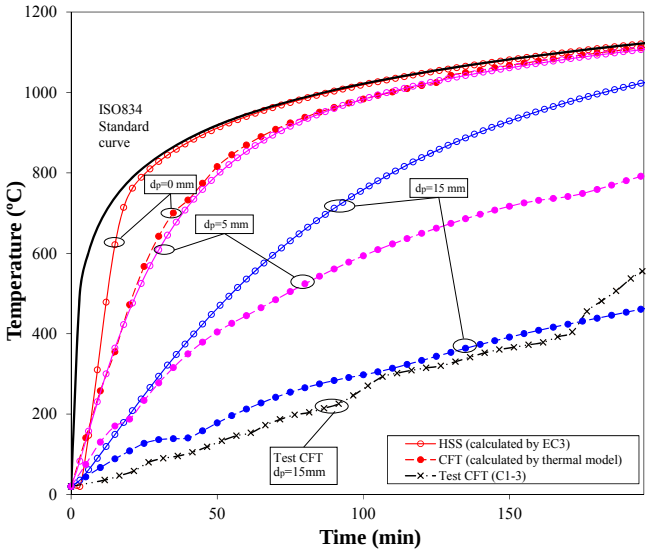

(a) Section C478x8 (Test column C1-3)

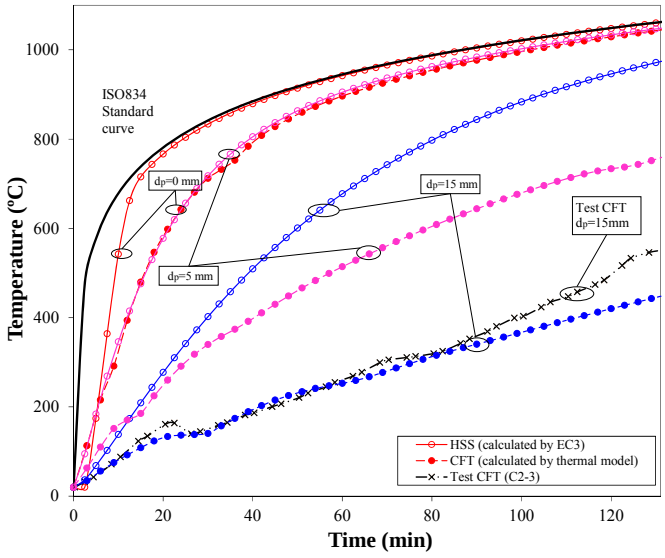

(b) Section C219x5 (Test column C2-3)

Figure 4.11. Steel tube temperatures for HSS and CFT sections

4.5.2. Effect of the concrete infill on heating rate

The fire resistance evaluation of a member can also be carried out in the temperature domain by means of the critical temperature. For fire resistant design of steel structures, EN 1993-1-2 (CEN 2005b) gives a critical temperature-load ratio relationship. In the fire situation, the load ratio or load level μ is defined as the relation between the applied load in fire design and the load carrying capacity at room temperature. Therefore, the critical temperature in a steel member is achieved when the applied load in fire situation equals the load capacity at room temperature.

The load ratio of all the specimens tested by Han et al. (2003a) had a value of 0.77. Again, for analysis purposes, the corresponding HSS of these columns were considered in order to calculate their corresponding critical temperature by applying the next formula proposed in EN 1993-1-2 (CEN 2005b)

$$\theta_{a,cr} = 39.19 \cdot ln\left[\frac{1}{0.9674 \cdot {\mu_0}^{3.833}} - 1\right] + 482 \qquad (4.20)$$

For a load level of 0.77 the value obtained for the critical temperature of the hollow steel tubes was 500ºC.

Table 4.7 resumes the times at which this temperature is reached in unprotected profiles and in protected HSS and CFT columns with two different values of protection thickness. As it was already established, CFT specimens reach higher fire exposure times than HSS columns for the same protection thickness. Only the results of the three specimens with different dimensions and the same initial protection thickness were compared.

Table 4.7. Time at 500ºC for different type of columns and protection thickness

Protection thickness		**d_p = 0 mm**	**d_p = 5 mm**		**d_p = 15 mm**	
Section	**Type**	**t (min)**	**t (min)**	$t_{d_p 5}/t_{d_p 0}$	**t (min)**	$t_{d_p 15}/t_{d_p 0}$
C478x6	HSS	12.45	22.47	1.80	54.97	4.42
	CFT	21.35	73.89	3.46	221.78	10.39
C219x5	HSS	9.41	16.11	1.71	39.07	4.15
	CFT	15.84	57.2	3.61	152.13	9.60
C219x4.6	HSS	8.7	15.58	1.79	37.24	4.28
	CFT	15.29	54	3.53	137.51	8.99

When a thickness protection layer of 5 mm was applied, the $t_{500ºC}$ of the HSS profiles was about 1.7 times higher than the one of the bare HSS profiles. However, in the case of the CFT sections with a protection layer of 5 mm, this increment was

twice the increment of the respective HSS, being about 3.5 times the one registered for the unprotected CFT sections.

The same trend was observed for the case in which the protection layer was 15 mm thick. In this case, while the $t_{500ºC}$ obtained for the protected HSS with respect to the corresponding bare sections was about 4.2 higher, the protection layer was much more effective for CFT sections for which the time registered at 500ºC was up to 10 times higher than the $t_{500ºC}$ for the respective unprotected CFT sections.

These relationships can be also observed in Figure 4.12. It can be seen the significant increment of the $t_{500ºC}$ for CFT specimens for the same variation of protection thickness. Besides, this effect is even more noticeable when bigger diameters are employed and the $t_{500ºC}$ of a CFT can become 4 times the $t_{500ºC}$ of the corresponding HSS (case of d_p=15 mm).

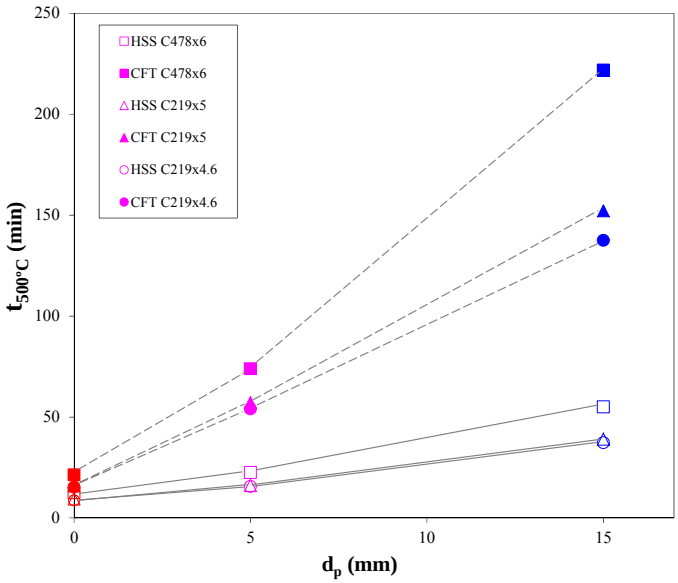

Figure 4.12. Steel tube temperatures for HSS and CFT sections Effect of protection thickness on HSS columns versus CFT columns.

These results definitely corroborate the renowned characteristic associated with CFT columns regarding the enhanced and more effective action of external fire protection when applied to these composite columns.

Since the combined action of steel and concrete in a CFT column produces benefits in its thermal response due to the concrete core acting as a heat sink and

delaying the steel tube heating, it is possible to reduce the fire protection thickness compared to the respective hollow steel section. Therefore, it is crucial to have a thermal model able to reproduce faithfully the thermal behavior of protected CFT columns.

In summary, in this chapter a cross-sectional thermal model for the temperature prediction of unprotected and protected concrete filled tubular columns has been elaborated. Since it has been satisfactorily validated, in the next chapter, this model will be taken into account in the development of a thermo-mechanical model for axially loaded circular concrete filled tubular columns without external fire protection.

5.

DEVELOPMENT OF THE THERMO-MECHANICAL MODEL

This chapter includes a detailed description of the fiber beam model developed in this thesis. The principal features of the model are described and the calibration study executed on the relevant parameters to characterize the thermo-mechanical model is presented. The numerical model is validated against own fire tests, as well as against experimental results found in literature. Predictions produced by a three-dimensional model for CFT columns in fire are also employed to contrast the fiber beam model results.

5.1. CHARACTERISTICS OF THE THERMO-MECHANICAL MODEL

5.1.1. Introduction

As seen in the first chapters, researchers have employed different types of finite elements to implement numerical models to simulate the fire behavior of concrete filled tubular columns. Although it is true that models using three-dimensional elements permit to reproduce more realistic responses due to their nature, their computational cost is high. Models based on fiber beam elements have proved to be an excellent alternative to three-dimensional models since, despite of their simplicity, they can be designed to simulate the whole fire response of concrete filled tubular columns with a reduced computing time given their minimal storage and processing requirements.

Despite several fiber beam-column models have been developed trying to analyze the fire behavior of CFT columns, it cannot be found in the literature any fiber finite element model that gives accurate fire resistance times and also reproduces with precision the overall response of a CFT column under a fire.

In this thesis, a fiber beam element model is presented in order to study the actual fire behavior of axially loaded circular CFT columns, so that not only the fire resistance time is obtained with accuracy but also the model leads to a realistic response evolution path during the fire. This model takes into account some realistic considerations that other researchers have not considered such as the influence of the steel-concrete gap or the complete slip between the steel tube and the concrete core. The former is achieved by considering the components of the column as two parallel elements joined at their nodes.

The main objective of the model here described is representing the fire behavior of axially loaded circular CFT columns with a wide range of concrete infill types: plain, bar-reinforced and steel fiber reinforced concrete of both normal and high strength.

The fiber finite element model developed for simulating the fire response of axially loaded circular concrete filled tubular columns takes as a basis the FedeasLab platform (Filippou & Constantinides 2004), a Matlab toolbox for the nonlinear analysis of structures, where the thermal load was included in order to simulate the thermo-mechanical response of circular CFT columns in fire.

5.1.2. FedeasLab toolbox

The FedeasLab platform is a Matlab toolbox whose development originally started in 1998 by professor Filippou at the University of California at Berkeley. It is a versatile tool suitable for linear and nonlinear, static and dynamic structural analysis which has the advantage to provide a general framework for physical parameterization of finite element models. The program supports path-dependent static and transient response under multiple force and displacement patterns.

The most characteristic property of FedeasLab is its modular structure which separates the different levels found in structural analysis: structure level, element level, section level and fiber or materials levels. The toolbox is formed by several functions arranged in different categories and, subsequently, divided in separated directories. These basic functions operate on five fundamental data structures regarding the model definition, the loading, the element properties, the structural response state and the solution strategy parameters.

Matlab adopts an interpreted language, a programming language version in which implementations are not compiled and translated into a low-level code prior to their execution. Due to that fact, a fiber beam finite element model implemented in this program will run more slowly and less efficiently than those in compiled languages but, still, they present a lower computational cost than three-dimensional finite element models developed for the same purpose.

In addition, this code is easier to manage which makes FedeasLab an appropriate tool for prototyping new elements and materials and for developing innovative solution strategies. It is particularly adequate for educational purposes and for the analysis of small structures.

Portolés et al. (2011) had previously chosen this package to develop a numerical model for slender CFT columns at room temperature using elements available in this platform demonstrating enough accuracy. In this work, the thermal load was included in the toolbox and, more specifically, a thermal analysis model for CFT columns of circular section was implemented along with a mechanical model considering the temperature.

5.1.3. Description of the model

The fire response of CFT columns expressed as the evolution of the column axial displacement along time was presented in the introduction section. As it can be observed in Figure 5.1, four stages can be clearly identified. Due to its direct exposure to fire and its thermal expansion coefficient, at the first stage of the fire,

the steel tube expands faster than the concrete core and it results in the uncoupling of the axial displacement of both components. In practice, this phenomenon, combined with the existence of a gap at the steel-concrete interface (included in the presented thermal model), causes the loss of contact of the concrete core with the loading plate. During this period, the whole applied load is supported by the steel tube alone (stage 1). When the steel tube reaches its critical temperature and the local yielding of the steel section occurs (stage 2), the steel tube starts to shorten, and the loading plate contacts back the concrete core so that the applied load is supported by the two components (stage 3), but now the concrete core is the element showing more resistance. The ultimate failure occurs when the concrete core completely loses its strength and stiffness after a significant period of time during which its mechanical properties are completely degraded (stage 4).

Stage 1. The steel tube expands faster. The concrete core separates from the loading plate. The steel tube supports the whole applied load.

Stage 2. The steel tube achieves its critical temperature and local yielding occurs. The loading plate contacts back the concrete core.

Stage 3. The load is supported by the two components.

Stage 4. Ultimate failure: concrete core mechanical properties are completely degraded.

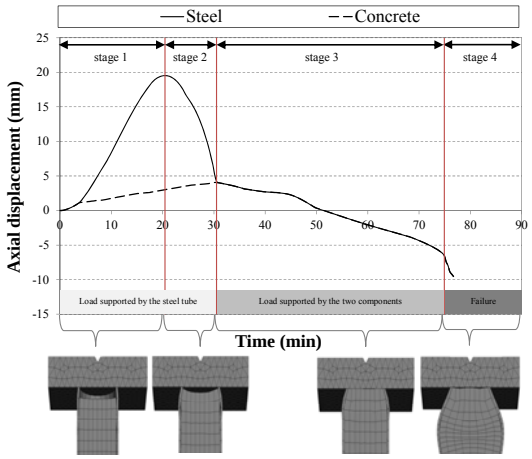

Figure 5.1. Stages on typical behavior of a CFT in fire.

Therefore, in order to reproduce accurately the overall response of CFT columns under fire it is totally necessary to simulate the existing relative sliding and separation between the steel tube and the concrete core and also their evolution along time since this interaction mechanism is the main responsible of the bearing capacity and response of this type of composite columns under fire.

Thus, the basis of the developed model lies in the clear differentiation of phases discussed above and represented schematically in Figure 5.2. In the model, a complete circular CFT column is formed by assembling in parallel two simple columns: a circular steel hollow section column and a circular concrete column. It

consisted of three parts: the concrete core, the steel tube and the link elements, which connect the former two.

In this case, the main parameters of the model are the column length (L), the external diameter (D), the steel tube thickness (t), the boundary conditions, the axial load level (μ) and the thermal and mechanical material properties.

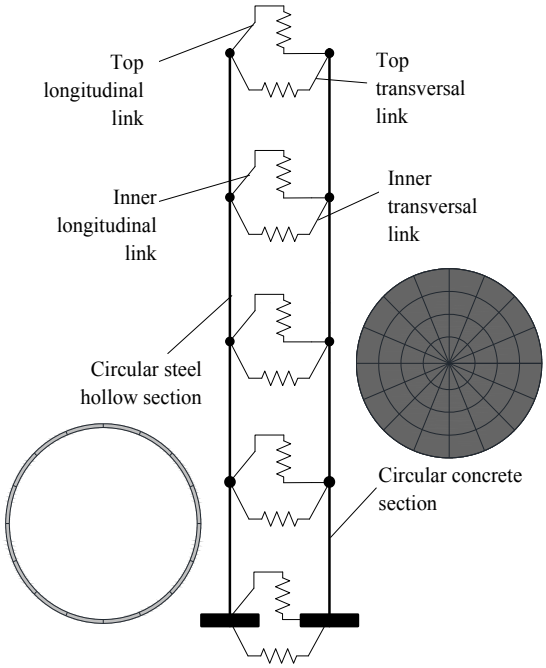

Figure 5.2. Parallel model scheme.

These columns are modeled with fiber beam finite elements connected at their nodes by link elements both longitudinally and transversely as shown in Figure 5.2. Details about the finite beam element employed will be given in the corresponding section.

Transversal link elements adopt a high stiffness in order to assure that the two simple columns have the same deformed shape. However, the longitudinal link elements work in a different way. The link connecting the top nodes of both simple columns (top longitudinal link) is designed to show an elevated rigidity under compression. In contrast, when the longitudinal link is in tension its stiffness is practically zero. By means of this comportment it is sought to imitate the behavior

of the whole composite column. When the load is applied, the link element is under compression and the steel hollow section column transfers part of the load to the column representing the concrete core. Once the model is loaded and fire has started, the steel tube expands longitudinally faster than the concrete core, so that the link acting in this direction is in tension and is not able to transmit any load to the concrete column.

On the other hand, the longitudinal link elements tying the rest of pairing nodes (inner longitudinal links) reproduce the friction that may arise between the steel tube and the concrete core.

In comparison with the fiber finite element model presented by Renaud et al. (2003), there is a difference in the way the links are conceived. In the model here described, links are point single degree of freedom elements located just at the nodes, knotting the steel tube and the concrete core columns. In contrast, in the model by Renaud et al. (2003) links are beam columns elements, with a fiber discretized section, acting as a shear links between the steel tube and the concrete core along the whole length of the element.

5.1.4. Description of the fiber beam element

The fiber beam element employed to model the two simple columns has a co-rotational formulation with distributed plasticity and a mixed interpolation iterative scheme (Taylor et al. 2003).

5.1.4.1. Outline of beam theory

When a structural member has one of its dimensions much larger than the other two, such as a usual column in a building, its structural analysis can be simplified using beam models (Figure 5.3). The axis of the structural member is defined along its longer dimension and the cross-section is assumed to be normal to this axis.

In general, a beam model is a one-dimensional model which aims to replace the governing equations of the actual three-dimensional member into a set of equations in terms of just one elemental variable which is the member axis.

The governing equations of beam theory as in continuum mechanics are composed of kinematics, equilibrium and constitutive equations. The kinematics deal with a continuous displacement field and a continuous strain field which satisfy certain strain-displacement relation at any material point of the member; the equilibrium equations ensure the conservation of linear and angular momenta; and

the constitutive equations, which are usually derived from energetic principles, describe the behavior of the material. Therefore, modelling a structural member with a beam model implies the replacement of the three-dimensional components by their one-dimensional equivalents.

The derivation of the beam model involves the adoption of several kinematics assumptions which permits the transformation of the three-dimensional displacements and strain field in terms of the one-dimensional beam displacements and strain field. Those assumptions regarding the extension and bending are known as Euler-Bernoulli assumptions and are the next:

1. Cross-sections of the beam do not deform in a significant manner under the application of transverse or axial loads and can be assumed as rigid. Any material point in the plane of the cross-section uniquely has associated two rigid body translations.
2. During deformation, the cross-section of the beam is assumed to remain planar and normal to the deformed axis of the beam.

Experimental observations have shown that for slender structural members subjected to extension and bending deformations and consisting of solid cross-sections of isotropic materials, these assumptions are reasonable.

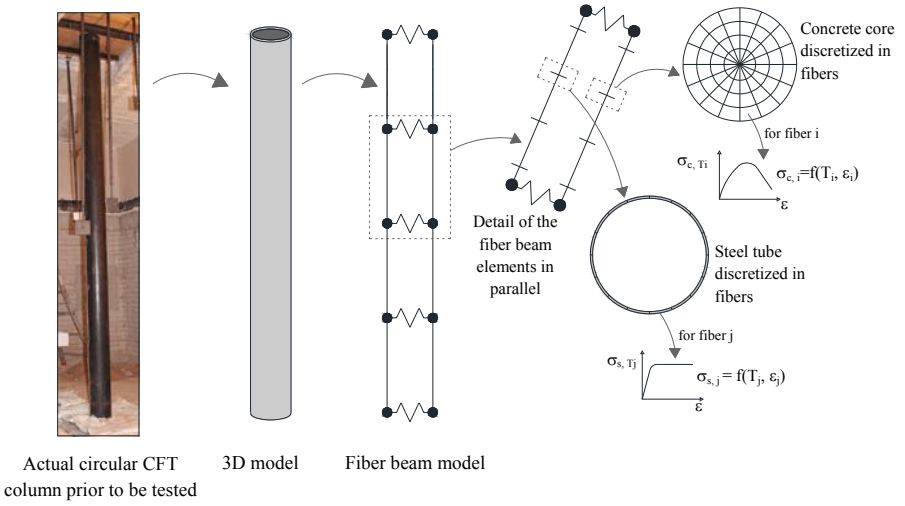

Figure 5.3. Modeling of a CFT column.

5.1.4.2. Co-rotational formulation

The simulation of the failure of structural members is a highly nonlinear problem involving large displacements, rotations and inelastic material behavior. When finite element models are used to reproduce these situations, several calculation problems may arise which do not permit the completion of the simulation.

Although the development of beam elements for the simulation of structures up to failure has experienced many advances, these elements still show some weaknesses. Usually, accuracy problems arise in the simulation of large displacements along the length of the element and in the description of the material nonlinearities.

In order to improve the modeling of nonlinear materials, fiber beam elements constitute an excellent option. In the same way, to gain precision when considering large displacements, co-rotational formulation can be employed.

The co-rotational approach (Crisfield 1991) is commonly used in finite element formulations for the analysis of structures due to its ability to separate the nonlinear geometric response of a beam element from its nonlinear material response.

The main objective of co-rotational formulation is to perform a nonlinear analysis of a structure and determine the global displacement behavior as well as the stress and strain which cause local deformations. For a small region of a body with its corresponding local coordinate system attached to it, the rigid body rotations and translations can be considered as negligible with respect to this local system (co-rotational frame) and only deformational modes (strain producing deformations in the material) remain (Yaw et al. 2008). Therefore, the material response is defined in a reference frame that rotates and translates with the element, Figure 5.4.

Several advantages are associated with co-rotational formulation. The element displacements can be described with a lower number of degrees of freedom which shortens the calculation procedure. Besides, given that the deformational modes are relatively small, some simplifications can be adopted in strain determination. It is not required the employment of a finite strain formulation or alternative stress definitions to consider the geometric nonlinearities due to large displacements and rotations (Yaw et al. 2008, Denavit & Hajjar 2010).

Regarding the co-rotational frame, when the material response is determined, the assumption of small deformations is valid since the structural member can be

subdivided into smaller elements if needed. Thus, nonlinear constitutive equations take the same form as in the case of small deformations theory which simplifies the integration of such equations. Besides, existing beam finite element models developed under the small deformations theory can be employed to simulate the material nonlinearities, especially elements with distributed plasticity as it will see in the next section.

For the co-rotational formulation, the next parts are fundamental: the relationship between global and local variables to transform the element displacement and forces; the elimination of the rigid body modes from the element displacement field with the consequent determination of the angle of rotation of the co-rotational reference system; and the equilibrium relationship between the forces in the co-rotating frame of reference and the forces in the local coordinate system by means of the corresponding variationally consistent tangent stiffness matrix (Filippou & Fenves 2004).

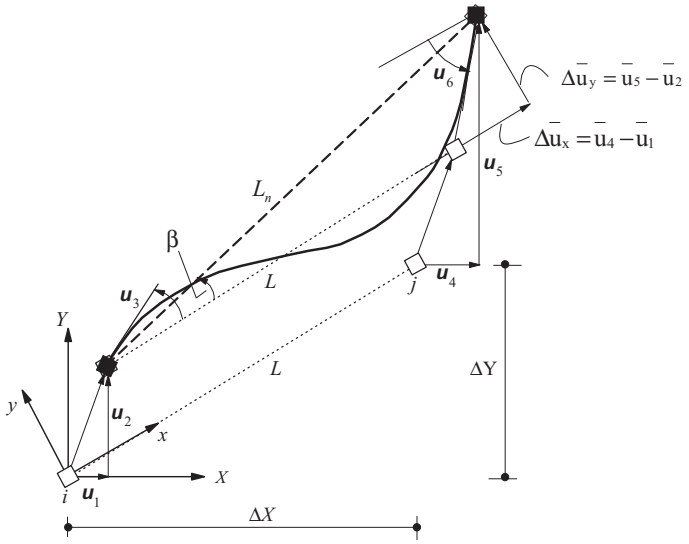

Figure 5.4. Fiber beam element (Filippou 2011).

5.1.4.3. Distributed plasticity

According to how the plasticity of the element is modelled along its length, two categories can be found. Distributed plasticity elements where plasticity can take place anywhere along the length element, and concentrated plasticity elements in which the formation of plastic hinges is limited to the end of the element.

Concentrated plasticity elements are appropriate for beam elements used to model structural members under strong lateral forces since it is in those cases when the plastic hinges are expected to occur at the ends of the element (Hajjar & Gourley 1997).

On the contrary, plasticity occurring at any point along the member length can be reproduced if elements with distributed plasticity are employed (Hajjar et al. 1998a, 1998b, Varma el al 2002, Denavit & Hajjar 2010). The number of integration points where the inelasticity is monitored is determined in function of the numerical integration method used.

As expected, models with distributed plasticity present a higher computational cost since the element length is no longer assumed to be elastic and inelasticity is computed at several points of the length. However, they are more accurate than concentrated plasticity models and due to their generality distributed plasticity becomes an attractive option for researchers to model highly nonlinear structural problems.

Commonly, the formulation employed to model distributed plasticity is the fiber element approach. The two-dimensional cross-section is subdivided into fibers and a uniaxial material model is assigned to each fiber to monitor its stress-strain behavior explicitly during the loading history. It is worthy to note that computational cost can decrease by regulating the density of the section discretization.

The use of the fiber approach becomes crucial when a composite structural member such as CFT column is modeled since it has not homogeneous cross-section. In this case, stress-strain relationships are needed for three different materials -concrete, structural steel and reinforcing steel (for bar-reinforced columns)- in order to represent with precision the cross-sectional response taking into account the different properties of the materials.

5.1.4.4. Mixed formulation

Depending on the variables that are taken as primary unknowns, beam elements can be classified into displacement-based, force-based and mixed elements.

Nodal displacements are the primary unknowns in displacement-based elements. In this case, element deformations are computed by means of interpolation functions and therefore element internal forces are obtained from the assumed displacement field so that equilibrium is satisfy in the variational sense but not in a strict way (Denavit & Hajjar 2010).

This type of formulation is easy to implement and to extend to geometric nonlinear behavior. Nevertheless, it presents a drawback for those cases in which the structural member experiences plastic hinges and the curvature distribution along the element is nonlinear since the interpolation functions typically used are uniquely able to model linear curvature distributions.

Thus, in order to capture the actual field of deformation by means of displacement-based elements, each structural member needs to be discretized into several elements. This refined discretization leads to an elevated number of degrees of freedom in the whole numerical model which increments the computational cost. Another option is the use of displacement interpolation functions of higher order but this requires the posterior condensation of various internal degrees of freedom during the element state determination and the refined mesh discretization is still necessary to assure enough level of precision (Taylor et al. 2003).

Due to the difficulties found with displacement formulation, researchers resorted to force-based elements which have element forces as primary unknowns. With this formulation, force interpolation functions are employed to compute the stress resultants along the length of the element so the element equilibrium is exactly satisfy. On the other hand, compatibility of deformations within the element is satisfied only from the variational point of view (Denavit & Hajjar 2010).

Force-based formulations are computationally less efficient than displacement-based elements and involve laborious procedures. The main problem appears in the element state determination phase. Commonly, this phase comprises the determination of the stiffness matrix and the element resisting forces for given displacements. However, in a force-based element the stiffness matrix is determined by means of the inversion of the flexibility matrix and the calculation of the element resisting forces is not simple (Spacone et al. 1996).

In traditional displacement formulations, the element resisting forces are computed directly through the weighted integral of the section. In a force-based element, the section deformations can be determined from the section forces but the difficulty emerges in the calculation of the element resisting forces. This is due to the fact that the constitutive relationships of the section are rigorously satisfy which leads to deformations of the sections that are not possible to associate with the element resisting forces (Spacone et al. 1996).

The problem exposed above is especially significant for those cases that involve a strong interaction between element displacements and internal forces, like in the case of a slender column under axial load, which indicates that this

formulation may not be the most appropriate for simulating the highly nonlinear behavior of circular CFT columns in fire.

Mixed formulation considers both element resisting forces and nodal displacements as primary unknowns and employs independent interpolation functions along the length of the element for both element deformations and stress resultants. The selection of the order and continuity of the force and interpolation functions is very important in the mixed formulation since inadequate functions may produce meaningless results (Zienkiewicz & Taylor 1989). In this formulation, the equilibrium equations are displacement dependent and the state determination employs a solution algorithm based on residual deformations instead of residual forces at the section and element level (Spacone et al. 1996).

Although the procedure of state determination for mixed formulation is more complicated than those for displacement and force formulations, it offers more accurate simulations of nonlinear curvatures along the length of the element and also presents the ability to incorporate directly geometric nonlinearities (Denavit & Hajjar 2010).

One of the first attempts to develop a consistent mixed formulation for nonlinear beam finite elements was carried out by Spacone et al. (1996) and later several works have proposed generalized formulations to mixed methods and have corroborated the consistency of this numerical implementation (Ayoub & Filippou 2000, Taylor et al. 2003, Pi et al. 2006, Mazzoni et al. 2009).

Researchers were motivated because of the fact that beam elements which enforce equilibrium rather than compatibility along the length of the element were proved to give more precise predictions of the nonlinear behavior of structural members. In particular, this is significant for elements which suffer a loss of strength and stiffness under loading conditions (Spacone et al. 1996).

In the context of CFT columns in fire, this aspect is especially critical due to the degradation of material properties at high temperatures. Therefore, in order to assure an accurate modeling of both geometric and material nonlinearities, the element employed to constitute the thermo-mechanical model here developed adopts a mixed formulation scheme taking as a reference the formulation presented by Taylor et al. (2003).

5.1.4.5. Formulation with section integration

As exposed above, the beam element employed in the developed model has distributed plasticity and a co-rotational formulation to account for large

displacements. The integration of local constitutive equations is executed on each cross-section. At the local level, where the displacements are assumed to vary linearly over the cross-section according to beam theory, the displacement field in two dimensions is:

$$u_1(x,y) = u(x) - yw_{,x} \tag{5.1}$$

$$u_2(x,y) = w(x) \tag{5.2}$$

where $(\cdot)_{,x}$ denotes differentiation with respect to x.

Considering that:

$$\varepsilon(x) = \frac{\partial u}{\partial x} \tag{5.3}$$

$$\kappa(x) = \frac{\partial^2 w}{\partial x^2} \tag{5.4}$$

the field of displacements leads to the next expression for the axial strain:

$$\varepsilon_1(x,y) = \varepsilon(x) - y\kappa(x) \tag{5.5}$$

If uniquely the effects of stress σ_1 are considered, the resultant of the axial force and the bending moment are, respectively:

$$N(\varepsilon_1, T) = \int_A \sigma_1(\varepsilon, T)dA \tag{5.6}$$

$$M(\varepsilon_1, T) = -\int_A y\sigma_1(\varepsilon, T)dA \tag{5.7}$$

The conditions to satisfy the equilibrium in both the axial and transverse directions are, respectively:

$$\frac{\partial N}{\partial x} + b_x = 0 \tag{5.8}$$

$$\frac{\partial^2 M}{\partial x^2} + b_y = 0 \tag{5.9}$$

where b_x and b_y are the loadings per unit length of the beam in x and y directions.

Note that $\sigma_1 = f(\varepsilon_1, T)$ and for its evaluation it is required to turn to the corresponding materials constitutive equations.

Variational formulation

This approach is based on the Hu-Washizu variational principle to permit ineslastic material behavior. For an elastic material with stress σ_1 and strain ε_1, the standard definition of the Hu-Washizu principle can be written as:

$$\prod_{hw}(\sigma_1,\varepsilon_1,\vec{u}) = \int_{\Omega} W(\varepsilon_1)d\Omega + \int_{\Omega}\sigma_1\left[\frac{\partial u_1}{\partial x_1} - \varepsilon_1\right]d\Omega - \prod_{ext} \tag{5.10}$$

where $W(\varepsilon_1)$ is the stored energy function from which stresses are computed as

$$\sigma_1 = \frac{\partial W}{\partial \varepsilon_1} \tag{5.11}$$

and $\prod_{ext}$ is the potential for the body and boundary loading.

In order to take into account the nonlinearities due to plasticity and temperature effects, $\sigma_1(\varepsilon_1)$ is replaced by $\hat{\sigma}_1(\varepsilon_1,T)$ which represents a stress computed from any constitutive model.

Finite element approximation

The selection of interpolation functions is very important. In order to ensure numerical stability in mixed formulation problems the LBB condition and the mixed patch test count condition (Taylor et al. 2003) have to be satisfied. As a rule, it has to be ensured that the number of terms taken for each variable satisfy consistency and stability conditions. In this case, it has to be satisfied:

$$n_\varepsilon \geq n_N \geq 1 \tag{5.12}$$

$$n_\kappa \geq n_M \geq 2 \tag{5.13}$$

where n_N and n_M are, respectively, the number of unknown element parameters in N and M; and n_ε and n_κ are the number of unknown element parameters in ε and κ, respectively.

For each variable are commonly taken as approximations continuous polynomials within each element. With regard to the strains approximations, it is worthy to mention that several advantages arise whether discontinuous functions are adopted.

5.1.4.6. Finite element technology

In particular, regarding the beam finite element employed some aspects must be noted:

- The element has three degrees of freedom per node.
- For the elements, Gauss-Lobatto shape functions are adopted, since they are more efficient generally.
- The iterative solution strategy is Newton–Raphson. Load is imposed in several steps on the structure and for each step the linearized system of equations of the current state is solved for the unknown increments of the primary variables. Once the current state is updated and the new increments of the primary variables under the residuals are determined, the iteration process continues until convergence is achieved to a specified tolerance after which the algorithm advances to a new load step.
- As explained before, LBB condition is satisfied to couple forces and displacements.
- A compromise has been adopted between the computational cost and the number of integration points per element as it will see in the corresponding section.

5.1.5. Material properties at high temperatures

In the model developed the temperature dependent thermal and mechanical properties are taken into account.

5.1.5.1. Thermal properties

The thermal properties adopted for each material were described in detail in Chapter 4, section 4.4.2.

5.1.5.2. Mechanical properties

Concrete

For normal strength concrete, the constitutive model developed by Lie (1994) was used. Espinos et al. (2010) proved that this model was the one that showed the most realistic response when modeling the infill of CFT columns.

In case of high strength concrete, the model presented by Kodur et al. (2004) was employed to represent its mechanical behavior.

Since during most of the time of analysis the column is subjected mainly to compression, the tensile strength is ignored. This statement was proved by Portolés et al. (2011) showing accurate results.

With regard to the thermal expansion coefficient, the value recommended by Hong & Varma (2009) was employed: $\alpha_c = 6x10^{-6}$ ºC^{-1} for both normal and high strength concrete.

Steel fiber reinforced concrete

When modeling the specimens filled with steel fiber reinforced normal strength concrete, the mechanical relationships at high temperatures developed by Lie & Kodur were used (Lie & Kodur 1995b, Kodur & Lie 1996).

For specimens filled with high strength concrete reinforced with steel fibers, the mechanical model proposed by Kodur et al. (2004) was applied. Also in these cases the value suggested by Hong & Varma (2009) for the thermal expansion coefficient was applied: $\alpha_c = 6x10^{-6}$ ºC^{-1}.

Steel

For structural steel, the temperature dependent mechanical properties recommended in EN 1993-1-2 (CEN 2005b) were implemented.

For reinforcing steel, according to EN 1994-1-2 (CEN 2005c), the mechanical model employed was the same as for structural steel, but with the reduction factors recommended in EN 1992-1-2 (CEN 2004a).

5.1.6. Analysis procedure

For analyzing the fire response of CFT columns, a thermo-mechanical analysis has to be carried out. Traditionally, there are two approaches to solve this combined problem. The first one is to perform a fully coupled thermal–stress analysis, where the gap conductance existing in the steel-concrete interface is assumed to be a function of the distance between the two components.

Due to the different thermal expansion coefficients the two components start to separate and, as a consequence, the gap resistance increases. In this case, the thermal and mechanical problems influence each other significantly, what makes necessary to compute simultaneously the stress and temperature fields, turning the problem into a highly nonlinear process. Therefore, this approach is very time consuming and many convergence problems arise when it is executed.

However, if the thermal resistance at the steel-concrete interface is assumed to be independent of the gap clearance, it is possible to run a sequentially coupled thermal-stress analysis. In this approach, used by several authors (Renaud et al. 2003, Ding & Wang 2008, Hong & Varma 2009, Lu et al. 2009, Espinos et al. 2010), the stress field is dependent on the temperature field but no inverse dependency exists and, as a result, it is less computationally costly.

Therefore, in this work, a simple sequentially coupled thermal-stress analysis was performed, as shown schematically in Figure 5.5. Two analysis steps can be differenced: a thermal analysis and a mechanical analysis. First, a thermal analysis is carried out to compute the temperature field of the columns and subsequently, a mechanical problem is solved to obtain the structural response.

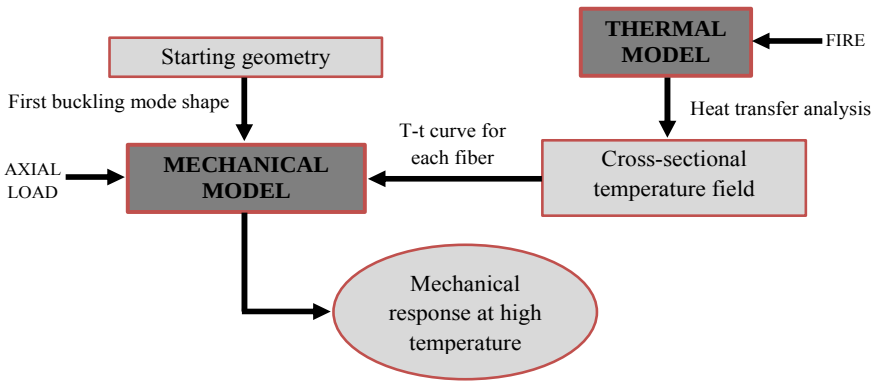

Figure 5.5. Scheme of the analysis procedure.

After performing this research and in view of the results obtained, it can be concluded that is not necessary to execute a fully coupled thermal-stress analysis since running a sequentially coupled thermal-stress analysis has given accurate results, as it will be discussed in the corresponding section.

5.2. CALIBRATION OF THE THERMO-MECHANICAL MODEL

In order to establish the value of some of the decisive parameters of the fiber beam model, the calibration of the model is carried out. The parameters included are the number of elements per column, the number of integration points per element, the cross-sectional discretization pattern (total number of fibers), the initial geometric imperfection of the column and the stiffness of the links.

For this purpose, two columns specimens of those used for the validation of the model are employed. They present similar characteristics regarding the material properties and similar buckling length but different D/t ratio in order to be able to extent the conclusions extracted to specimens with high and low steel contribution. In this case, the two columns are coded as C159-6-3-30-0-20 and C-13 and their properties are summarized in Table 5.4 and Table 5.5. It is worthy to mention that the calibration of the cross-sectional mesh density has been determined by using the column CAL1 instead of C-13 since the former has a larger diameter and the influence of the section size is critical in this case.

5.2.1. Number of elements per column

Given that the model is going to be validated for axially loaded CFT columns, the member will experiment simple bending and the maximum values of the bending moment and deflection will occur at the mid-length section.

Therefore, it is crucial to capture the response at this section and in order to accomplish with this task the columns will have an even number of elements.

The number of fiber beam elements per column was determined after a study where the computational time was registered for several simulations varying this parameter. Portolés et al. (2011), in their model for CFT columns at room temperature employed 4 elements per column obtaining accurate predictions of the room temperature behavior. Thus, given that the fire situation makes the problem more nonlinear, the starting point of this study is taken as 4 elements so that in the rest of configurations studied, the number of element increases. The results for the two different columns are shown as example in Table 5.1 and the whole response registered in terms of axial displacement-time is depicted in Figure 5.6.

Table 5.1. Calibration of the number of elements per element

Column No.	**Number of elements**	**Computing time (s)**	**FRR (min)**	$\xi_{FRR} = \frac{FRR_{Test}}{FRR_{MODEL}}$
C159-6-3-30-0-20	4	280.3	40	1.05
	6	411.84	39	1.08
	8	504.17	39	1.08
C-13	4	652.61	99	1.03
	6	827.75	91	1.12
	8	1177.3	95	1.07

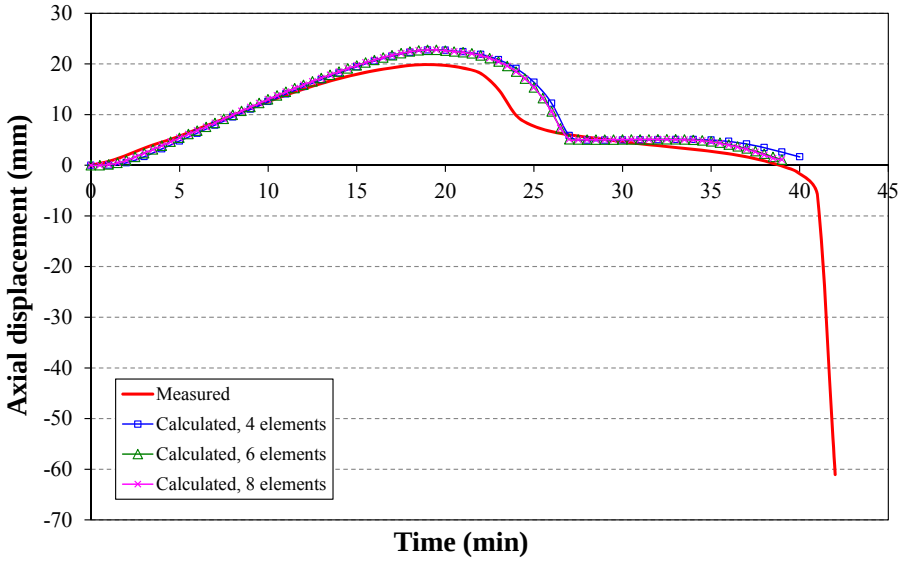

(a) Column C159-6-3-30-0-20

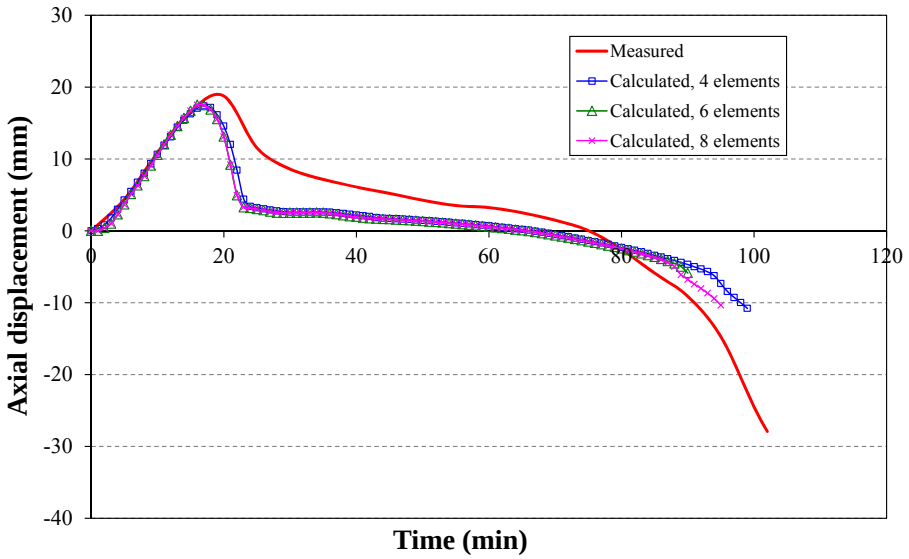

(b) Column C-13

Figure 5.6. Comparison of measured and predicted axial displacement with different numbers of elements per column.

As it can be observed in the results obtained, an increment in the number of elements may lead to a more flexible comportment of the column and lower FRR are achieved. This is more significant for those cases where the concrete core is acting during a long period of time, as in the case of the column shown in Figure 5.6, and the ductile failure of the concrete is accelerated by this increment of flexibility. Regarding the axial displacement-time response, differences were not observed.

In general, it has been detected that increasing the number of elements do not produce a significant improvement in the precision of the responses. In fact, the type of element employed has distributed plasticity along its length which already confers accuracy in the simulation of nonlinear responses and makes no necessary the utilization of a denser mesh of finite elements.

Finally, in the view of the results a compromise is achieved by employing 4 fiber beam elements per column.

5.2.2. Number of integration points per element

In order to determine the number of integration points to be placed along the length of the element, the same procedure followed in the previous section was carried out, in this case to study the influence of the number of integration points in the precision of the model response and in the computing time.

As a reference, it is worthy to mention that the model proposed by Portolés et al. (2011) for this type of columns at room temperature takes 4 integration points per element according to the recommendations by Filippou & Fenves (2004). However, since the action of the temperature increases the nonlinearity of the problem, it is recommended to check if the adoption of this value is appropriate. The results for two of the columns analyzed are shown in Table 5.2 and Figure 5.7.

Table 5.2. Calibration of the number of integration points

Column No.	**Number of integration points**	**Computing time (s)**	**FRR (min)**	$\xi_{FRR} = \frac{FRR_{Test}}{FRR_{MODEL}}$
C159-6-3-30-0-20	2	158.6	37	1.14
	4	280.3	40	1.05
	6	393.49	40	1.05
	8	515.22	40	1.05
C-13	2	309.94	80	1.28
	4	652.61	99	1.03
	6	897.15	99	1.03
	8	1166.62	99	1.03

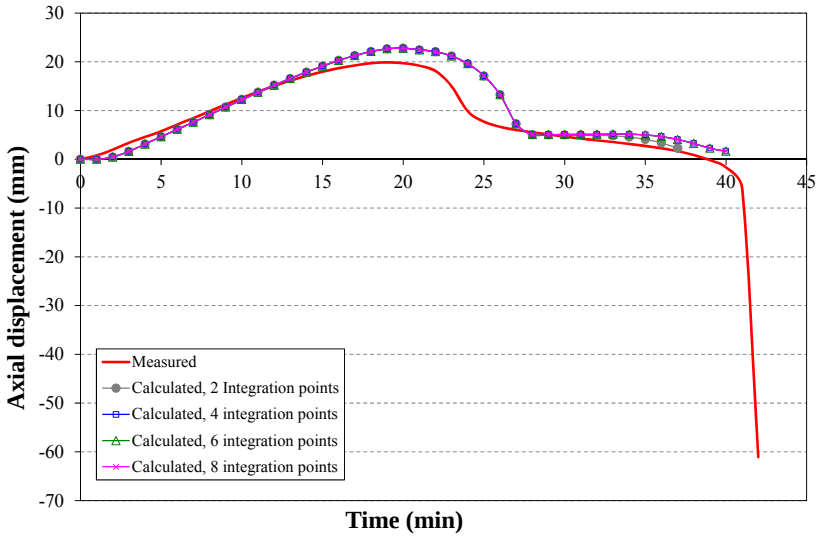

(a) Column C159-6-3-30-0-20

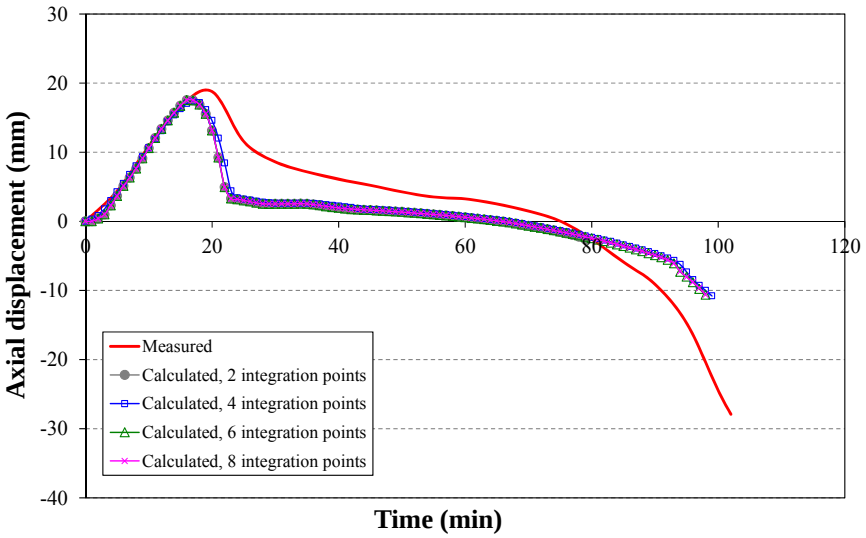

(b) Column C-13

Figure 5.7. Comparison of measured and predicted axial displacement with different numbers of integration points per element.

As it can be observed, for 4 integration points or more, the response does not suffer any change neither in terms of FRR nor in terms of axial displacement-time.

Nevertheless, the increment in the number of integration points results in an increment of the time of calculation required.

Therefore, the number of integration points selected for the fiber beam element is 4, corroborating the conclusions and results of other researchers (Portolés et al. 2011, Filippou & Fenves 2004).

5.2.3. Discretization of the section

During the process of analysis carried out with fiber beam elements models, the numerical integration of the section is executed in numerous occasions which constitute a considerable fraction of the total computing time.

Therefore, it becomes really important to establish a cross-sectional discretization pattern in order to assure convergence and enough accuracy in the model predictions jointly with a reasonable computing time.

The composite section is discretized following the same scheme that Portolés et al. (2011) adopted in their proposed model for circular concrete filled tubular columns eccentrically loaded at room temperature. The discretization pattern divides the section into a regular array of fibers in both radial and circumferential directions as can be seen in Figure 5.8.

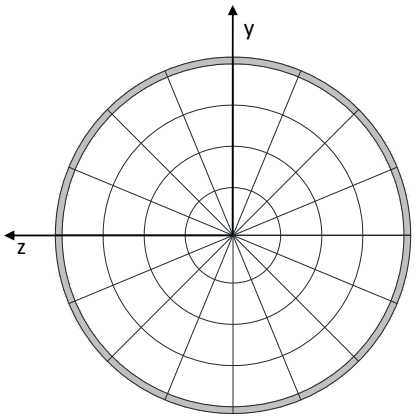

Figure 5.8. Cross-sectional discretization.

A study for the calibration of the cross-sectional mesh density was carried out. In Table 5.3 and in Figure 5.9, the results obtained for two of the specimens are shown. In this case, two columns with similar characteristics but with different

external diameter have been selected since the section size is the determining parameter in the discretization.

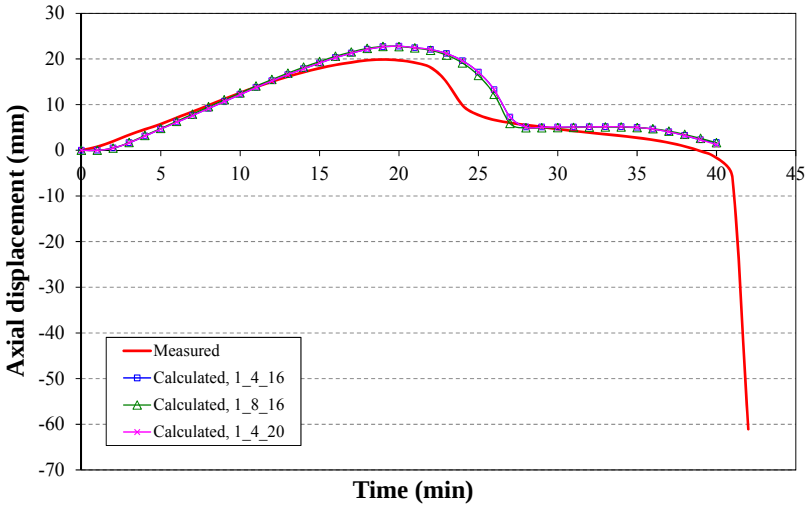

(a) Column C159-6-3-30-0-20

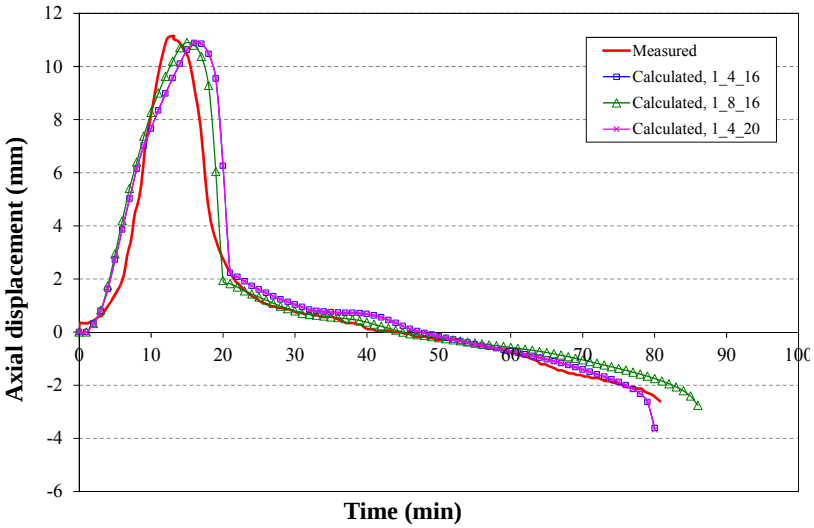

(b) Column CAL1

Figure 5.9. Comparison of measured and predicted axial displacement with different cross-sectional discretization patterns.

Table 5.3. Calibration of the cross-sectional discretization pattern

Column No.	Discretization pattern	Computing time (s)	FRR (min)	$\xi_{FRR} = \frac{FRR_{Test}}{FRR_{MODEL}}$
C159-6-3-30-0-20	1-4-16	280.31	40	1.05
	1-8-16	475.72	40	1.05
	2-4-16	312.27	39	1.08
	2-8-16	507.43	40	1.05
	1-4-20	347.24	40	1.05
	1-8-20	348.78	40	1.05
	1-4-24	391.12	40	1.05
CAL1	1-4-16	462.13	80	1.00
	1-8-16	825.23	86	0.93
	2-4-16	514.82	80	1.00
	2-8-16	883.12	87	0.92
	1-4-20	547.16	80	1.00
	1-8-20	1058.2	90	0.89
	1-4-48	2259.76	90	0.89

In this table, the pattern is coded as A-B-C, where A and B are the number of fibers in the radial direction for the steel tube and the concrete core respectively, and C is the number of fibers in the circumferential direction.

Several patterns were studied and it was seen for the specimen C159-6-3-30-0-20 that no improvement was achieved with a denser mesh. With regard to the second specimen, CAL1, which presented higher diameter and more contribution of the concrete core, it was observed that a denser mesh results in unsafe results predicting FRR higher than the one registered in the test. This can be due to the fact that an increment of the number of fibers leads to a more ductile failure which distorts the prediction and results in a unrealistic FRR.

In Figure 5.9 the evolution of the axial displacement along time is presented for the two columns and, for clarity, only for three of the patterns studied. It can be observed that both columns show different behavior and that the extension of the stage in which the concrete core supports the total applied load is larger for the column with higher diameter. It is worthy to mention that the selection of the discretization pattern does not have significant influence in the evolution of the axial displacement, except for the last minutes of the simulation.

After the calibration of the mesh, the configuration that showed accurate predictions with the lowest computational cost was selected. It is worthy to note that the computing times registered are very low for all the cases if they are compared to the times required for three-dimensional models to execute an analysis of the same characteristics.

Finally, the set of values adopted for the discretization of the section were the next:

- In the radial direction:
  - For the hollow steel section: 1 fiber.
  - For the concrete core the number of fibers was varied to obtain a size of the cell close to 20 mm, since it was the approximate size which showed better accuracy-computing time relation. Besides, it is the typical size used in other models (Espinos et al. 2010) and the minimum size recommended for thermal analysis.
- In the circumferential direction: 16 fibers.

5.2.4. Initial geometric imperfection of the column

In practice, columns are not perfectly straight, but they show a geometric imperfection due to its own manufacturing process. This lack of accuracy is taken into account in the proposed model simulated as the first buckling mode shape of a pinned-pinned column which exhibits a sinusoidal shape.

$$y(x) = e_{imp} \cdot \sin\left(\frac{x}{L}\pi\right) \tag{5.14}$$

The value adopted for the out-of-straightness of the column was L/1000, as it has proved to give accurate results in other models existing in literature (Espinós et al. 2010) and it is the value normally employed by the majority of researchers of this field.

5.2.5. Stiffness of the transversal and longitudinal links

- Transversal links: $k_t = 1{\cdot}10^{15}\ kN/m$
- Top longitudinal link:
  - Tension: $k_{l,top,tens} = 0\,kN/m$
  - Compression: $k_{l,top,comp} = 1{\cdot}10^{15}\ kN/m$
- Inner longitudinal links : $k_{l,inner} = 0 - 10\,kN/m$

In the case of the stiffness value of the inner longitudinal links, a sensitivity analysis was carried out to investigate its effect on the whole fire behavior of the columns.

As described above, during a fire the steel tube expands faster than the concrete core leading to a sliding phenomenon between both components whose longitudinal interaction is modeled by means of such links.

Figure 5.10 shows the sensitivity analysis performed for one of the columns varying the rigidity value given to the inner longitudinal links. As expected, when a very high value is adopted ($1x10^{15}$ kN/m), the behavior obtained differs noticeably from the registered during the test. On the contrary, the simulated behavior practically matches with the one measured when zero stiffness is assumed which leads to assume a frictionless relative displacement between both components. This also corroborates the assumed fact that when a CFT column is exposed to a fire full slip exists between the steel tube and the concrete core during the most of the fire exposure time.

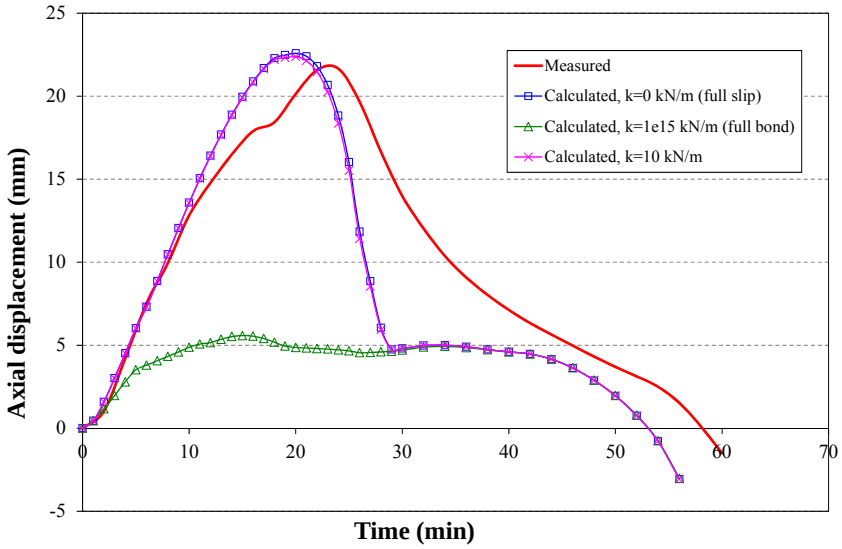

Figure 5.10. Comparison of measured and predicted axial displacement with different slip conditions. Column C-06.

Espinos et al. (2010) came to the same conclusion when analyzed the influence of different friction models in the overall fire response given by the 3D numerical model developed by the authors.

Nevertheless, if the slight friction that may exist when the slip process between the two components initiates is considered, a value ranging from 0 to 10

kN/m may be adopted. These values were also studied and no difference was obtained in the whole fire response.

With regard to the FRR obtained for the different options, it is worthy to mention that it is not influenced by the stiffness value assigned to the inner longitudinal links in contrast to what occurred with the overall axial displacement-time response. This was also stated by Renaud et al. (2003) who studied the sliding phenomenon between the two components of a CFT column in fire.

5.2.6. Mechanical model for normal strength concrete

The constitutive equations employed for the different materials involved in the analysis have been presented in section 5.1.5.

In the case of concrete, particularly for high strength concrete and steel fiber reinforced concrete, EN 1992-1-2 (CEN 2004a) does not provide explicit models for these type of materials. In those cases, specific relationships proposed by different researchers have been employed producing good results as it will be see in the next section.

However, for normal strength concrete, EN 1992-1-2 (CEN 2004a) includes a specific model for high temperatures whose application is necessary to analyze.

For this purpose, the fire response of two of the specimens used for validation was simulated employing two different normal strength concrete models: the expressions by Eurocode 2 Part 1.2 and the constitutive relationships proposed by Lie (1994).

Figure 5.11 shows the predictions obtained for the two selected column specimens in terms of axial displacement along time. The constitutive equations used to model the concrete core determine the duration of the stage in which the concrete core controls the fire behavior (stage 3 in Figure 5.1) and also the ultimate failure of the column.

When comparing the response given by these models, it can be seen that the model proposed by Lie is the one that produces the most accurate prediction and that the model from EN 1992-1-2 (CEN 2004a) gives conservative results.

Therefore, the stress-strain relationships presented by Lie were finally the ones adopted in the thermo-mechanical model for the simulation of normal strength circular CFT columns. The accuracy of this model in predicting the fire behavior of CFT column is corroborated by other researchers (Espinos et al. 2010) who used this model in their simulations.

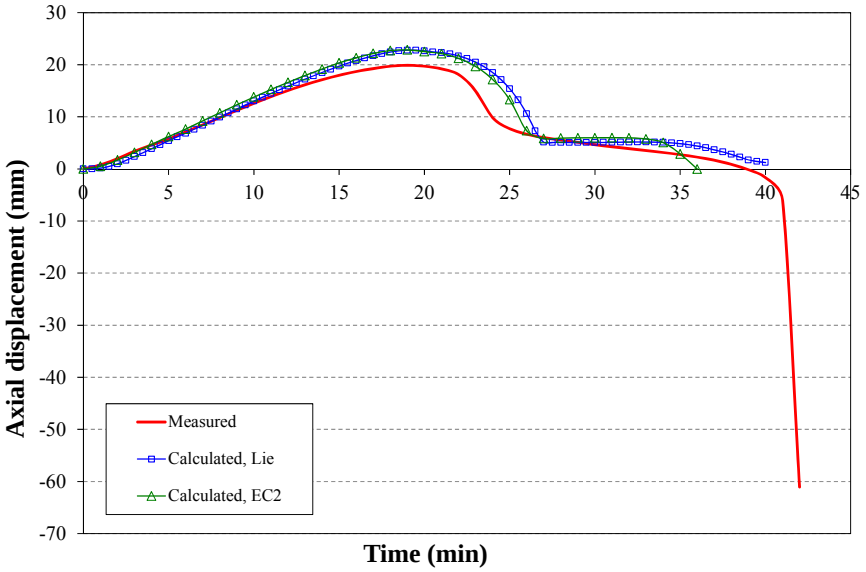

(a) Column C159-6-3-30-0-20

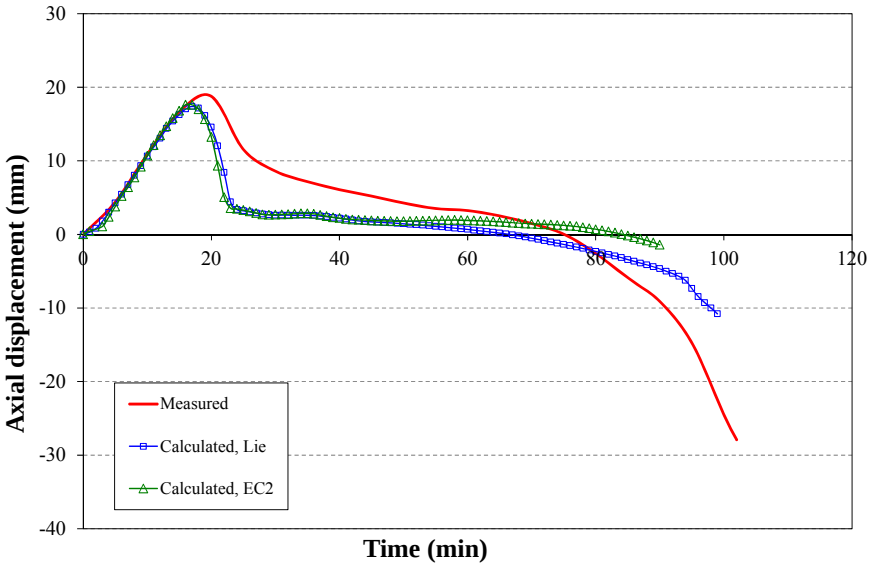

(b) Column C-13

Figure 5.11. Comparison of measured and predicted axial displacement with different concrete models.

5.3. VALIDATION OF THE MODEL

5.3.1. Experimental tests for validation

The fiber beam model presented was validated by comparing the computed results with experimental test data of circular axially loaded CFT columns. Comparisons were made with fire tests carried out by the authors (Romero et al. 2011) and also with results from experimental programs by other researchers available in the literature (Lie & Chabot 1992, Kim et al. 2005).

5.3.1.1. Own tests

The fiber beam model was validated against experimental data from tests carried out by the research group at which the author of this work belongs and that were performed simultaneously with the development of this thesis. In this case, 14 column specimens from this experimental program were analyzed. All the columns were tested at AIDICO (Instituto Tecnológico de la Construcción) in Valencia, Spain. The total length of the columns was 3180 mm, although only 3000 mm were exposed to direct heating. The values of concrete nominal strength varied from 30 MPa to 80 MPa.

With regard to the characteristics of the infill of the columns, three different types of infill were employed: plain, bar-reinforced and steel fiber reinforced concrete. Independently of the type of concrete, the aggregates were calcareous in all the cases. In bar-reinforced concrete columns, the reinforcement was composed by four longitudinal bars of 12 mm of diameter. Detailed information about this experimental campaign can be found in Romero et al (2011). A summary of the more relevant characteristics of these columns is shown in Table 5.4.

According to EN 1991-1-2 (CEN 2002), the fire curve followed for the heating of the specimens was the standard ISO 834 curve (ISO 1980).

In this program, all the specimens tested were subjected to concentric load and the load level defined as the ratio between the applied load and the resistance of the column at room temperature varied from 0.2 to 0.6.

For all the specimens, the end conditions during the test were the same: fixed at the bottom end and pinned at the top end.

Table 5.4. List of CFT columns analysed, own tests (Romero et al. 2011)

Column No.	D (mm)	t (mm)	f_y (N/mm^2)	f_c (N/mm^2)	End Cond.	D/t	λ	N (kN)	μ	FRR (min)
C159-6-3-30-0-20	159	6	337.8	35.75	F-P	26.5	0.58	198	0.2	42
C159-6-3-30-0-40	159	6	337.8	28.55	F-P	26.5	0.58	396	0.4	25
C159-6-3-30-0-60	159	6	337.8	34.05	F-P	26.5	0.58	594	0.6	14
C159-6-3-80-0-20	159	6	341.4	71.14	F-P	26.5	0.71	335	0.2	37
C159-6-3-80-0-40	159	6	341.4	69	F-P	26.5	0.71	670	0.4	11
RC159-6-3-30-0-20	159	6	337.8	23.9	F-P	26.5	0.62	229	0.2	43
RC159-6-3-30-0-40	159	6	337.8	30	F-P	26.5	0.62	458	0.4	30
RC159-6-3-30-0-60	159	6	337.8	33.7	F-P	26.5	0.62	687	0.6	13
RC159-6-3-80-0-20	159	6	337.8	69.03	F-P	26.5	0.74	343	0.2	64
RC159-6-3-80-0-40	159	6	337.8	77	F-P	26.5	0.73	720	0.4	18
FC159-6-3-30-0-20	159	6	337.8	28.3	F-P	26.5	0.58	198	0.2	36
FC159-6-3-30-0-40	159	6	334.4	26.7	F-P	26.5	0.58	396	0.4	22
FC159-6-3-80-0-20	159	6	337.8	93.62	F-P	26.5	0.70	335	0.2	35
FC159-6-3-80-0-40	159	6	334.4	90.16	F-P	26.5	0.70	670	0.4	15

5.3.1.2. Tests from the literature

In order to not limiting the validation of the fiber beam model to the cases tested by the authors, experimental results from other researchers reported in the literature were used.

Most of the specimens used in validation were tested at the National Research Council of Canada (NRCC). The 23 columns analyzed were 3810 mm long, but only the central 3048 mm were directly exposed to fire. The values of concrete nominal strength varied from 30 MPa to 50 MPa. Regarding the concrete infill, these columns were filled with both siliceous and calcareous aggregate concrete. For those specimens containing siliceous aggregates a moisture content value of 3% in concrete weight was employed, since they seem to retain less humidity than concrete with calcareous aggregates, for which a value of 10% was applied. The work reported by Lie & Chabot (1992) comprises all the detail about this experimental program. In Table 5.5, the main characteristics of the studied columns are listed.

Table 5.5. List of CFT columns analysed from the literature

	Column No.	D (mm)	t (mm)	f_y (N/mm^2)	f_c (N/mm^2)	End Cond.	D/t	λ	N (kN)	μ	FRR (min)
Lie & Chabot (1992)	C-02	141.3	6.55	350	33.1	F-F	21.6	0.57	110	0.12	55
	C-04	141.3	6.55	350	31.0	F-F	21.6	0.57	131	0.14	57
	C-05	168.3	4.78	350	32.7	F-F	35.2	0.49	150	0.16	76
	C-06	168.3	4.78	350	32.7	P-P	35.2	0.69	150	0.19	60
	C-08	168.3	4.78	350	35.5	F-F	35.2	0.50	218	0.23	56
	C-09	168.3	6.35	350	35.4	F-F	26.5	0.49	150	0.13	81
	C-11	219.1	4.78	350	31.0	F-F	45.8	0.38	492	0.35	80
	C-13	219.1	4.78	350	32.3	F-F	45.8	0.38	384	0.27	102
	C-15	219.1	8.18	350	31.9	P-P	26.8	0.52	525	0.28	73
	C-17	219.1	8.18	350	31.7	F-F	26.8	0.37	525	0.26	82
	C-20	273.1	5.56	350	28.6	F-F	49.1	0.30	574	0.26	112
	C-21	273.1	5.56	350	29.0	F-F	49.1	0.30	525	0.23	133
	C-22	273.1	5.56	350	27.2	F-F	49.1	0.30	1000	0.45	70
	C-23	273.1	12.70	350	27.4	F-F	21.5	0.29	525	0.13	143
	C-31	141.3	6.55	300	30.2	F-F	21.6	0.54	80	0.09	82
	C-32	141.3	6.55	300	34.8	F-F	21.6	0.55	143	0.17	64
	C-34	219.1	4.78	300	35.4	F-F	45.8	0.38	500	0.36	111
	C-35	219.1	4.78	300	42.7	F-F	45.8	0.39	560	0.36	108
	C-37	219.1	8.18	350	28.7	F-F	26.8	0.36	560	0.25	102
	C-40	273.1	6.35	350	46.5	F-F	43	0.33	1050	0.37	106
	C-41	273.1	6.35	350	50.7	F-F	43	0.34	1050	0.37	76
	C-42	273.1	6.35	350	55.4	F-F	43	0.34	1050	0.35	90
	C-44	273.1	6.35	350	38.7	F-F	43	0.32	715	0.27	178
Kim et al. (2005)	CAL1	318.5	7	304	27.5	P-P	45.5	0.45	940.8	0.55	80
	CAL2	318.5	7	304	27.5	P-P	45.5	0.45	774.2	0.45	150
	CBL1	406.4	9	311	27.5	P-P	45.2	0.35	1675.8	0.6	80
	CBL2	406.4	9	311	27.5	P-P	45.2	0.35	1254.4	0.45	120

In this table, P-P=pinned-pinned and F-F=fixed-fixed.

For all the columns tested in this program, the standard fire curve followed was the ASTM-E119 (ASTM 1990). All of them were subjected to concentric load and tested fixed at both ends, except for two of them, tested as pinned-pinned.

In addition, four column specimens from Kim et al. (2005) were also simulated. All the specimens had a length of 3500 mm although the actual effective heating length varied from one specimen to another. The columns analyzed were filled with plain concrete with a design compressive concrete strength of 23.5 MPa, silica-based sand and a moisture content of 6.6%, as reported in the work published by Kim et al. (2005). In this case, all the CFT columns simulated presented pinned-pinned end conditions and were tested under concentric loads. During the test, the KSF 2257 standard fire curve (similar to ASTM-E119) was applied. Again, a summary of the most important data describing these specimens can be found in Table 5.5.

It is worthy to note that when the consideration of the part of the column that is not exposed to fire has a significant influence on the fire behavior of the CFT columns, 6 elements instead of 4 are used to model the column. The two extra elements added correspond to the top and base partial lengths which are not exposed to any heating curve. This is especially important in the NRCC specimens where 762 mm remain out from the fire action and in the columns from Kim et al. (2005) where the unexposed length varies from 300 to 1000 mm.

5.3.2. Three-dimensional model for validation

The fiber model was validated by comparing the numerical results with the experimental data from the tests presented in the previous section.

In addition to these comparisons, the results of a nonlinear finite element three-dimensional model developed by Espinos et al. (2010) were also used to contrast the fire response obtained by the presented fiber model for some of the specimens studied since they were also employed for the validation of this three-dimensional model which was developed using a general purpose nonlinear finite element package, ABAQUS (2010).

The model consisted of three parts: the concrete core and the steel tube, meshed both with three-dimensional eight-node solid elements; and the loading device, modeled as a perfectly elastic part. The procedure followed in this 3D model was also a sequentially coupled thermal-stress analysis. The components and mesh of the model are shown in Figure 5.12. More details about the development and validation of this model can be found in Espinos et al. (2010).

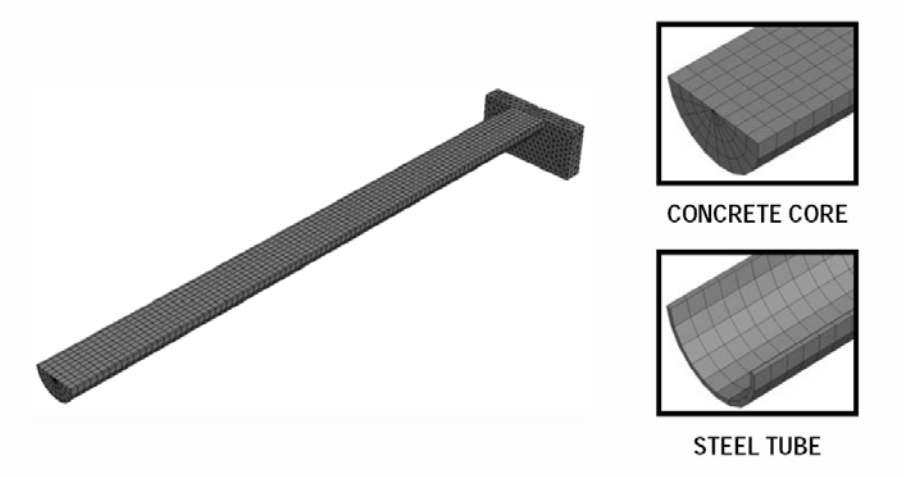

Figure 5.12. Components and finite element mesh of the three-dimensional model by Espinos et al. (2010).

5.3.3. Mechanical response

The mechanical behavior of all the columns studied was recorded in terms of axial displacement-time as shown schematically in Figure 5.1 and in the comparisons included in the calibration section. For each specimen listed in Table 5.4 and in Table 5.5, the axial displacement at the top of the column recorded during the test was compared to the calculated values given by the fiber beam model here presented. For some of the specimens analyzed, the fiber beam model predictions were also compared to the results of the three-dimensional model presented by Espinos et al (2010).

Figure 5.13 presents the comparison made for three of the specimens studied which belong to the testing program carried out by the authors (Romero et al. 2011). These specimens are a representation of the three types of infill studied in this program. Thus, it can be observed that for any type of infill: plain concrete in Figure 5.13a, reinforced concrete in Figure 5.13b and steel fiber reinforced concrete in Figure 5.13c; and for any value of concrete strength (normal or high strength), there is a good agreement between the experimental and calculated values.

Nevertheless, it is important mentioning that in those cases with reinforced concrete infill, the fiber model reproduces perfectly the behavior during the first stages of the fire exposure but, at the last phase, when the behavior of the columns is

dominated by the concrete core, the curve does not match completely the experimental response.

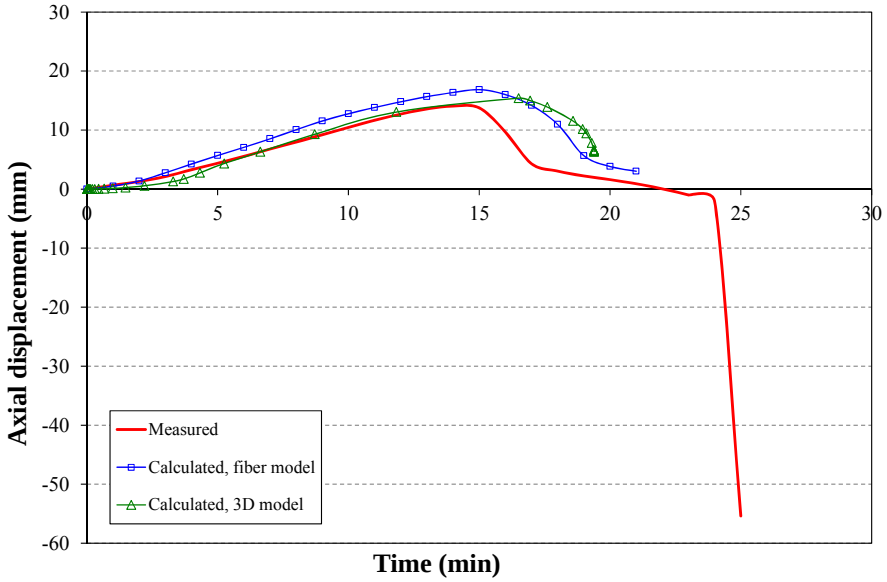

(a) Column C159-6-3-30-0-40

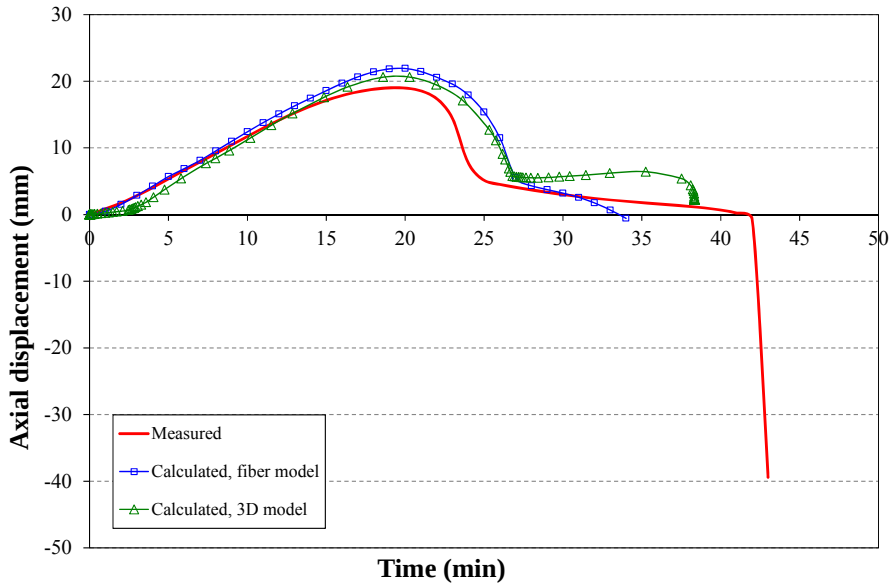

(b) Column RC159-6-3-30-0-20

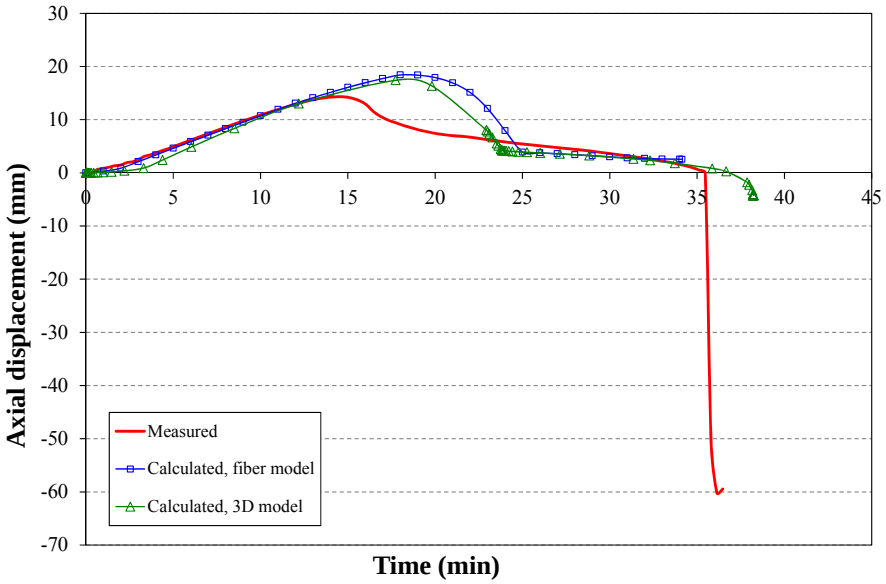

(c) FC159-6-80-0-20

Figure 5.13. Comparison of measured and predicted axial displacement, own tests (Romero et al. 2011).

In the case of the columns tested by other authors (Lie & Chabot 1992, Kim et al. 2005), the same comparison was carried out.

In Figure 5.14 four examples of the specimens analyzed are shown. After comparison it was found that the overall response predicted by the fiber beam model reproduced with high precision the real behavior shown by these columns in the tests.

With regard to the comparison with the three-dimensional model, a great agreement between the calculated results of both models was observed. This fact reveals that the fiber beam model is able to provide satisfactory predictions for the fire behavior of CFT columns with a considerable lower computational cost.

Regarding the columns reported as pinned-pinned in the work by Lie & Chabot (1992), Espinos et al. (2010) studied their response under different end conditions and detected that the pinned-fixed configuration was the one that best fitted the real behavior and the deformed shape after the fire test. Thus, following this practice, these columns (C-06 and C-15) were finally modeled as pinned-fixed and the accuracy of the results obtained corroborated the observation made by Espinos et al. (2010). An example of this is depicted in Figure 5.14c.

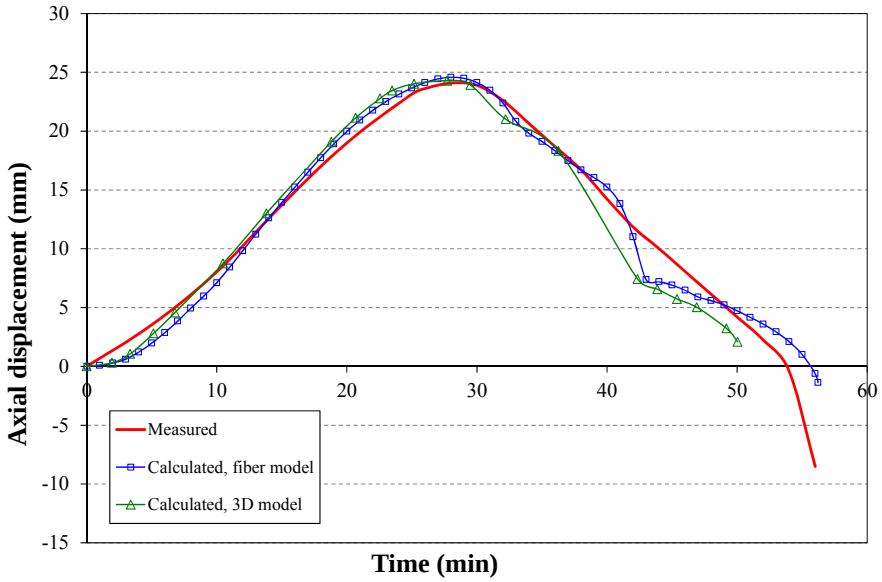

(a) Column C-04

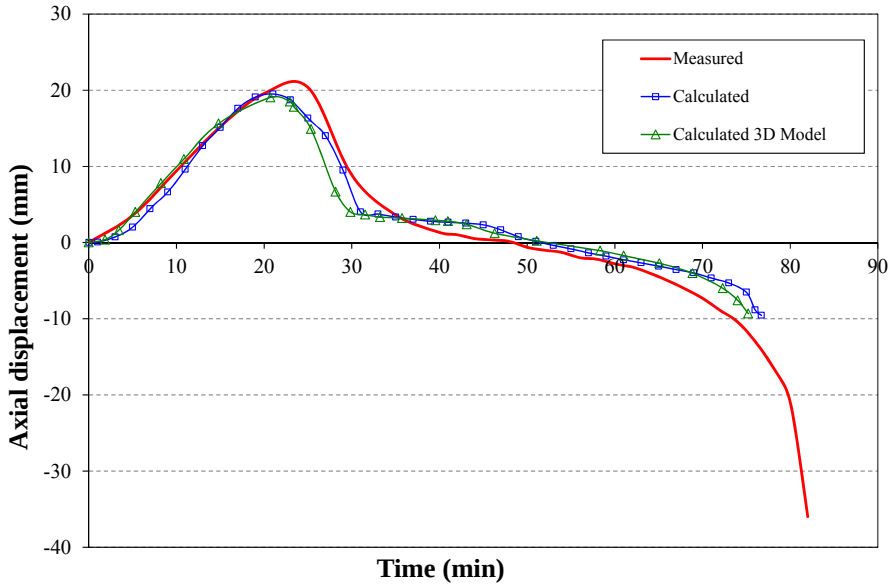

(b) Column C-17

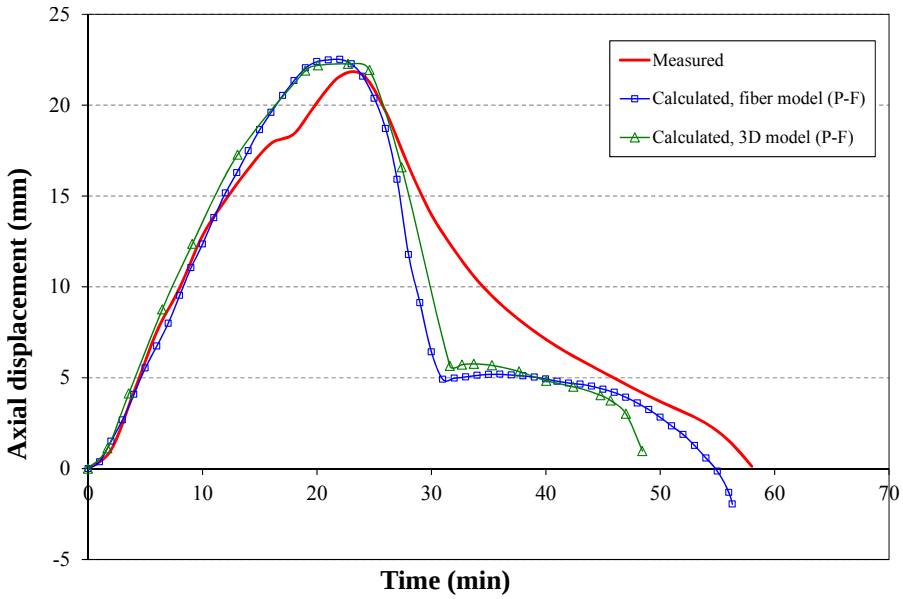

(c) C-06

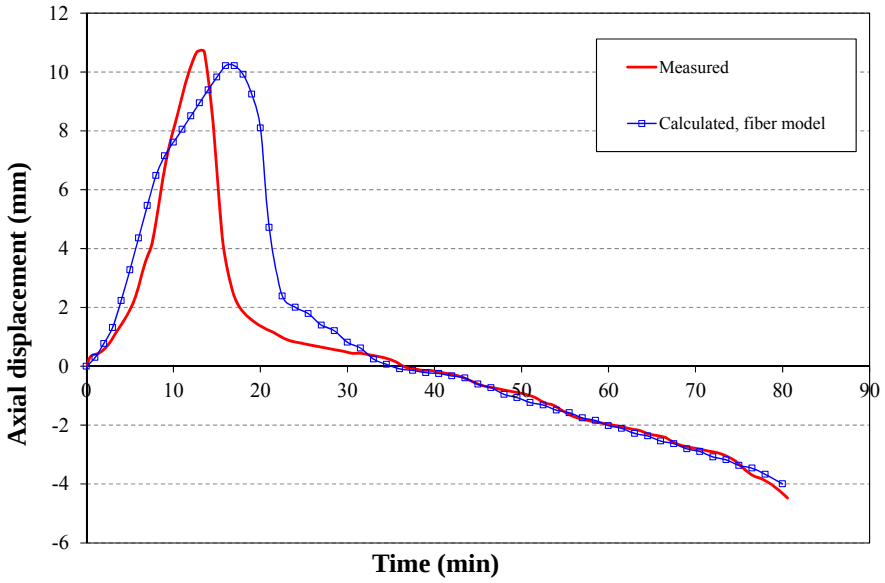

(d) CBL1

Figure 5.14. Comparison of measured and predicted axial displacement, tests from literature (Lie & Chabot, Kim et al. 2005).

The presented fiber beam model has the capability to capture the whole response of a CFT under fire which can be clearly observed in Figure 5.15 where both the evolution of the axial displacement along time and the axial force ratio history are plotted. For each of these variables, the behavior of the steel tube and the concrete core is graphed separately.

With respect to the evolution of the axial force ratio along time, it can be observed that during the first stages of the fire exposure, the steel tube and the concrete core work independently and during this period it is solely the steel tube which is supporting the total applied load. The concrete core remains unloaded until the steel tube losses its integrity which leads to a state where the two components start to support the load jointly.

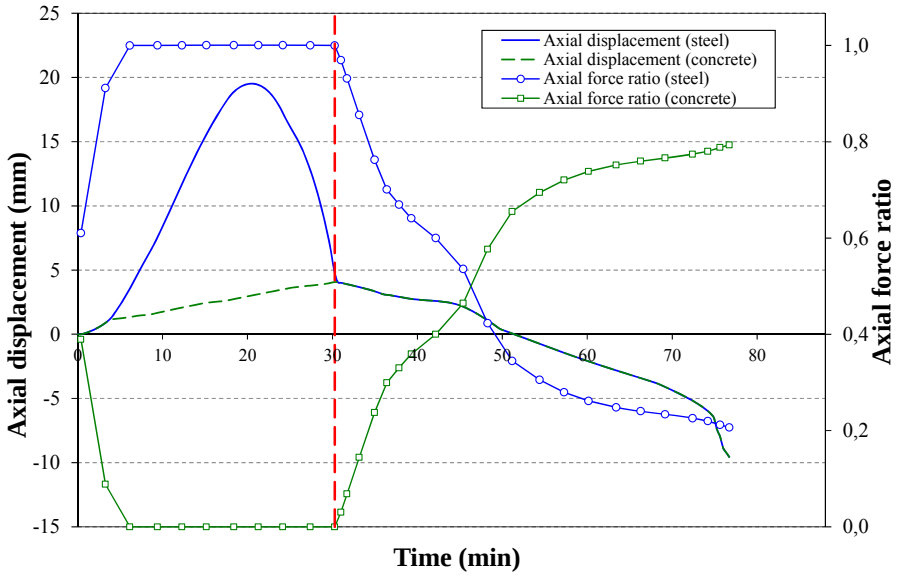

Figure 5.15. Axial displacement and axial force ratio vs. time, column C-17.

The described behavior is in concordance with what is detected if attention is paid to the axial displacement-time history of both components, plotted in the same figure. It is noted how the steel tube expands much more rapidly than the concrete core which is also expanding but at a lower rate. The steel tube is directly exposed to fire and protects the concrete core from heating. This fact, jointly with the different thermal expansion coefficients of both materials, are the responsible of the slip

appearing between the two components, which generate the described load distribution.

The axial displacement path of both components becomes one when the steel tube reaches its critical temperature and local yielding occurs. At this point, the steel tube is not able to carry the whole load by itself and shortens, reaching the level of the expanded concrete core. From this point forward (marked in Figure 5.15 with a dashed red line), an inversion in the axial force ratio takes place which results in the concrete core being the component controlling the behavior of the column.

Finally, the column fails when the resistance and stiffness of the concrete are completely degraded. Due to the lower conductivity of concrete, the degradation process tends to be slow but the extension of these last stages will depend on the section geometry, load level and load conditions.

The occurrence and distinction of the typical stages in the fire response of a CFT column in fire was detected in specimens with a moderate load level (μ=0.2) like the specimen C-17 shown in Figure 5.15 which presents load level of 0.26. However, a different failure mechanism can be observed for those specimens with elevated load levels.

In Figure 5.16 the fire response in terms of axial displacement along time, as well as the axial load ratio are plotted for column C159-6-3-30-0-60, a specimen submitted to a load which represents the 60% of its resistance at ambient temperature. Although the length of this specimen is slightly lower than the length of specimen C-17 represented in Figure 5.15, it can be clearly seen how the maximum axial displacement achieve is much lower than in the previous case. The considerable compression generated by the axial load applied mitigates the thermal expansion of the steel tube. Thus, although slip still appears between the steel tube and the concrete core, the relative displacement is not significant, unlike the result obtained for specimens with moderate load level.

During most of the time it is the steel tube the component supporting the total applied load and that the reversal of the axial force ratio does not take place, as can be noticed in Figure 5.16. Under a high load level, both pieces (steel tube and concrete core), are supporting a load relatively close to the value of their maximum resistance at ambient temperature. The degradation of the material due to high temperatures and the second order effects lead to the considerably fast achievement of the maximum capacity of the column. The concrete core can barely sustain the load that the steel tube tries to transfer after reaching its critical temperature.

Therefore, last stages of the typical behavior identified in Figure 5.1 are condensate in a very short branch resulting in a rather sudden failure of the column.

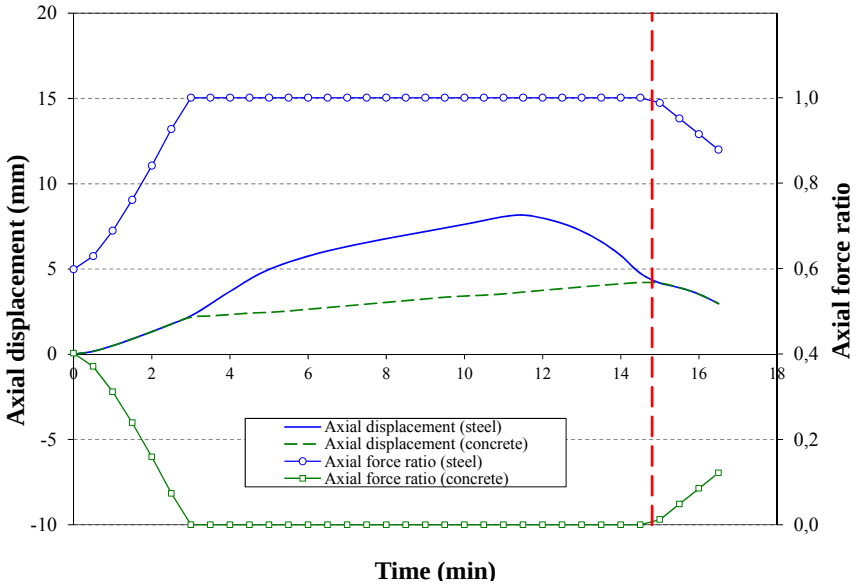

Figure 5.16. Axial displacement and axial force ratio vs. time, column C159-6-3-30-0-60.

After analyzing the overall response of the columns, the fire resistance rating and the maximum axial displacement were extracted from the different curves and listed with the experimental data in Table 5.6 and Table 5.7 for specimens from own tests and from tests found in literature, respectively.

For the totality of the columns analyzed, comparison between measured and calculated values of the fire resistance rating and maximum axial displacement are made in Figure 5.17. As it can be observed most of the numerical values lie in the region of the 15% error, in both FRR and maximum axial displacement analysis.

Nevertheless, in the case of FRR, it is necessary to mention that those specimens which lie in the unsafe side correspond to columns that having high diameters, present higher D/t ratio and lower slenderness (λ= 0.3-0.34). In these specimens the concrete and its highly nonlinear behavior have an important role in the last part of the column fire response, as exposed when the typical behavior of a CFT column was described

In addition, specimens C-40, C-41 and C-42 from NRCC (Lie & Chabot 1992) do not fail due to overall buckling but they do due to compression. The participation of the concrete in this mode of failure and the likely existence of brittle cracking in concrete may explain the deviation of the numerical results from the test data since the concrete material model used may not be able to capture this phenomenon.

Table 5.6. Predicted an measured FRR and maximum axial displacement, own tests (Romero et al. 2011)

Column No.	FRR (min)		$\frac{FRR_{TEST}}{FRR_{MODEL}}$	δ_{max} (mm)		$\frac{\delta_{max,TEST}}{\delta_{max,MODEL}}$
	Test	Simulation		Test	Simulation	
C159-6-3-30-0-20	42	40	1.05	19.89	22.8	0.87
C159-6-3-30-0-40	25	21	1.19	14.06	16.87	0.83
C159-6-3-30-0-60	14	17	0.82	9.37	8.2	1.14
C159-6-3-80-0-20	37	29	1.28	15.95	18.52	0.86
C159-6-3-80-0-40	11	18	0.61	5.33	4.2	1.27
RC159-6-3-30-0-20	43	34	1.26	18.99	21.94	0.87
RC159-6-3-30-0-40	30	22	1.36	12.47	14.12	0.88
RC159-6-3-30-0-60	13	16	0.81	5.58	3.79	1.47
RC159-6-3-80-0-20	64	34	1.88	15.48	18.2	0.85
RC159-6-3-80-0-40	18	18	1.00	4.21	3.27	1.29
FC159-6-3-30-0-20	36	34	1.06	20.45	22.9	0.89
FC159-6-3-30-0-40	22	21	1.05	15.45	16.84	0.92
FC159-6-3-80-0-20	35	34	1.03	14.30	18.43	0.78
FC159-6-3-80-0-40	15	20	0.75	7.25	3.39	2.14
		Mean	**1.08**		**Mean**	**1.08**
		Standard deviation	**0.31**		**Standard deviation**	**0.37**

There are also some cases with very low FRR that also lie in the unsafe side, but in these situations the existing deviation can be associated with the fact that in the early stage of the heating process, the effect of the concrete moisture content is more remarkable and a slight deviation on its experimentally measured value supposes a high divergence between the calculated FRR and the value registered in the test.

Table 5.7. Predicted an measured FRR and maximum axial displacement, tests from literature

	Column No.	FRR (min)		$\frac{FRR_{TEST}}{FRR_{MODEL}}$	δ_{max} (mm)		$\frac{\delta_{max,TEST}}{\delta_{max,MODEL}}$
		Test	**Simulation**		**Test**	**Simulation**	
Lie & Chabot (1992)	C-02	55	54	1.02	24.57	25.63	0.96
	C-04	57	56	1.02	24.09	24.58	0.98
	C-05	76	78	0.97	22.77	22.56	1.01
	C-06	60	56	1.07	21.66	22.54	0.96
	C-08	56	60	0.93	20.48	20.2	1.01
	C-09	81	79	1.03	25.77	24.61	1.05
	C-11	80	80	1.00	18.13	14.21	1.28
	C-13	102	99	1.03	18.77	17.39	1.08
	C-15	73	49	1.49	19.52	19.48	1.00
	C-17	82	76	1.08	20.36	19.52	1.04
	C-20	112	141	0.79	19.44	17.11	1.14
	C-21	133	155	0.86	20.25	17.97	1.13
	C-22	70	83	0.84	5.51	6.93	0.80
	C-23	143	136	1.05	26.09	23.99	1.09
	C-31	82	69	1.19	30.53	26.63	1.15
	C-32	64	53	1.21	28.50	22.94	1.24
	C-34	111	96	1.16	20.09	13.73	1.46
	C-37	102	69	1.48	20.20	18.7	1.08
	C-44	178	151	1.18	20.36	15.79	1.29
	C-35	108	100	1.08	15.59	11.22	1.39
	C-40	106	131	0.81	15.22	8.19	1.86
	C-41	76	102	0.75	16.05	8.08	1.99
	C-42	90	107	0.84	14.16	8.05	1.76
Kim et al. (2005)	CAL1	80	79	1.01	11.14	10.88	1.02
	CAL2	150	121	1.24	12.15	12.35	0.98
	CBL1	80	80	1.00	10.68	10.22	1.05
	CBL2	120	130	0.92	14.94	16.46	0.91
			Mean	**1.04**		**Mean**	**1.17**
		Standard deviation		**0.18**	**Standard deviation**		**0.29**

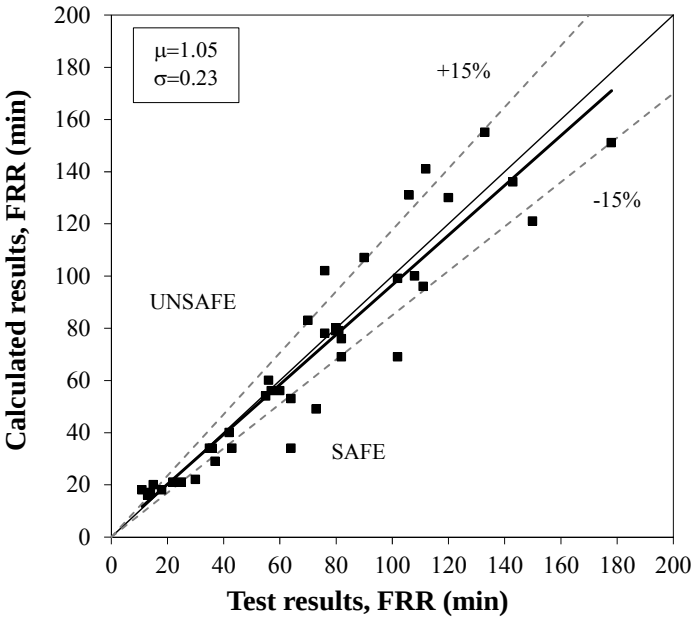

(a) Fire resistant rating

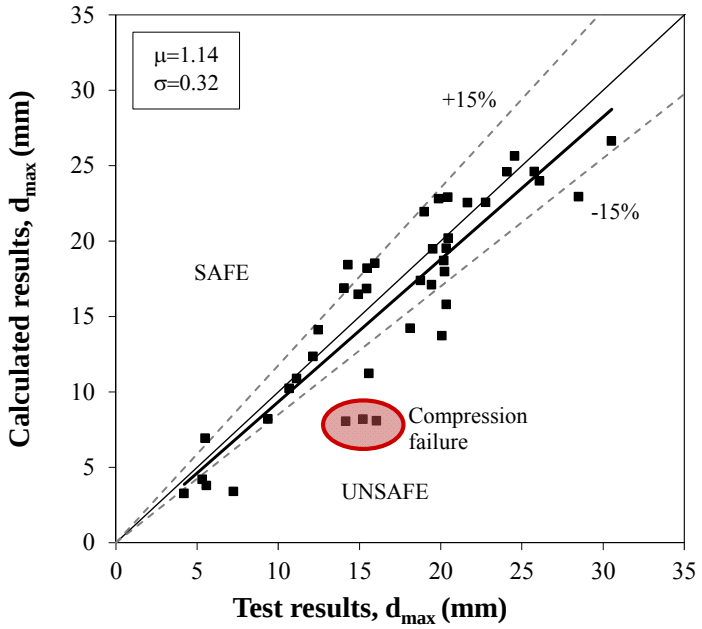

(b) Maximum axial displacement

Figure 5.17. Comparison of numerical simulations with experimental data.

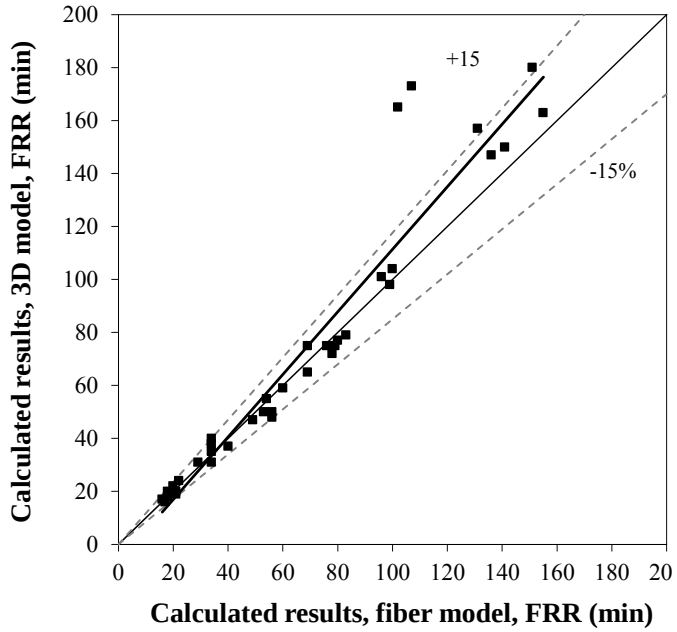

(c) Fire resistant rating

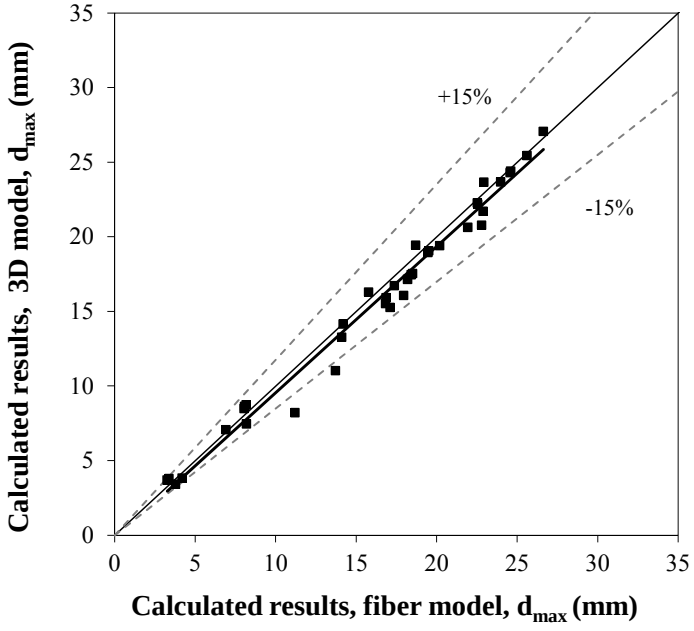

(d) Maximum axial displacement

Figure 5.18. Comparison of numerical results: fiber model vs. 3D model.

Similarly, comparison between numerical results from the fiber model and three-dimensional model is shown in Figure 5.18. In the case of maximum axial displacement, Figure 5.18b, it can be observed that an excellent agreement between the calculated values given by both methods exists.

However, when comparing the FRR results, Figure 5.18a, there are some specimens for which the calculated values do not match. These specimens lie out of the 15% area and correspond to columns C-40, C-41 and C-42. As commented previously, in these cases, the prediction given by the fiber model was not as good as desirable but it resulted to be more accurate than the one produced by the three-dimensional model used in comparisons which predicts values of FRR much higher than the actual ones. This can be due to the fact that Espinos et al. (2010) developed the model focused on specimens filled with normal strength concrete and high strength concrete filled tubular columns were out of the range of application of the model.

In this chapter, the development of a fiber beam model has been covered. The basis of the model has been explained and the calibration of the model has been accomplished. The numerical model was validated against tests from several sources showing good accuracy in the prediction of the fire response of CFT columns. Therefore, the model can be employed as a tool for developing extensive analysis in order to investigate in depth the fire behavior of this type of composite columns and draw well-founded conclusions.

6. DEVELOPMENT OF A SIMPLE CALCULATION MODEL

Given that both the thermal and the mechanical model have demonstrated their accuracy in reproducing the temperature evolution and the structural response of axially loaded concrete filled tubular columns in fire with very low computational cost, they can be employed to develop simplified calculation methods. In this chapter, firstly a set of expressions for the calculation of the cross-sectional temperature field which complements the application of the current design code methods is proposed. Next, it is presented the development of a simple calculation model based on the equivalent concrete core cross-section at room temperature which could support designers in the calculation process of CFT columns.

6.1. REVIEW OF CURRENT SIMPLE CALCULATION METHODS IN EUROCODE 4

Eurocode 4 Part 1.2 (CEN 2005c) is the reference code in Europe for the calculation of composite structures including CFT columns. As exposed in chapter 2, three approaches are considered in this code: tabulated data, simple calculation models and advanced calculation models.

Regarding to the simple calculation models included in Eurocode 4 Part 1.2, two options are presented, a general method for composite columns proposed in its Clause 4.3.5.1 and a specific simplified calculation method included in Annex H, which is only of an informative character. A brief review of both procedures is presented in the next sections.

6.1.1. General method for composite columns in Clause 4.3.5.1

In Clause 4.3.5.1 of Eurocode 4 Part 1.2, a general method for the calculation of the design value in the fire situation of the resistance under axial compression of composite columns, including CFT columns, is provided. In this method, first the cross-sectional temperature field has to be computed and after discretizing the cross-section in elements, the design fire resistance is computed considering the contribution of all the components of the cross-section of the column.

For composite columns under axial compression in fire situation, the design value of the resistance ($N_{fi,Rd}$) is obtained by:

$$N_{fi,Rd} = \chi N_{fi,pl,Rd} \tag{6.1}$$

where $N_{fi,pl,Rd}$ is the design value of the cross-sectional plastic resistance to axial compression in fire and χ is the reduction coefficient for buckling curve "c" given in Clause 6.3.1.2 of EN 1993-1-1 (CEN 2005a) and that is function of the relative slenderness at elevated temperature.

The design value of the cross-sectional plastic resistance in fire is computed by considering the contribution of all the components of the composite section by:

$$N_{fi,pl,Rd} = \sum_j (A_{a,\theta} f_{ay,\theta}) / \gamma_{M,fi,a} + \sum_k (A_{s,\theta} f_{sy,\theta}) / \gamma_{M,fi,s} + \\ + \sum_m (A_{c,\theta} f_{c,\theta}) / \gamma_{M,fi,c} \tag{6.2}$$

where $\gamma_{M,fi,i}$ are the partial factors for the materials in the fire situation and $A_{i,\theta}$ is the area of each element of the cross-section submitted to a certain temperature θ. Note that subscripts "*a*", "*s*" and "*c*" refer to the steel profile, reinforcing bars and concrete core, respectively.

Under the same premise, the effective flexural stiffness of the column is also calculated considering the influence of the different components at high temperatures:

$$(EI)_{fi,eff} = \sum_j (\varphi_{a,\theta} E_{a,\theta} I_{a,\theta}) + \sum_k (\varphi_{s,\theta} E_{s,\theta} I_{s,\theta}) + \sum_m (\varphi_{c,\theta} E_{c,\sec,\theta} I_{c,\theta}) \quad (6.3)$$

where $I_{i,\theta}$ is the second moment of area of each element of the cross-section at a certain temperature θ, $\varphi_{i,\theta}$ is a reduction coefficient depending on the effect of thermal stresses and $E_{c,sec,\theta}$ is the secant modulus of concrete at the temperature θ.

The inclusion of the flexural stiffness reduction coefficients obeys to the necessity of accounting for the effect of the self-equilibrated thermal stresses caused by the non-uniform temperature distribution within the composite cross-section and the unequal thermal expansion of steel and concrete (Lennon et al. 2007) but their values have not been established yet. Few works can be found in the literature dedicated to define appropriate values for these coefficients for CFT columns. One relevant work was the study conducted by the CTICM group (Renaud et al. 2004, Aribert et al. 2008) dealing with this issue. In fact, the National Annex to EN 1994-1-2 developed in France (AFNOR 2007) considered the work and conclusions extracted by the CTICM group regarding fire design of CFT columns. Given that currently no predefined values exist, it is common in practice to take them equal to unity (Lennon et al. 2007). The problem was also covered in the research carried out by Espinos et al. (2012) where, in the framework of the development of a simple method for CFT columns, proposed a definition for these reduction coefficients based on the geometric characteristics of the column.

The next step after computing the effective flexural stiffness is obtaining the Euler buckling load in the fire situation:

$$N_{fi,cr} = \pi^2 (EI)_{fi,eff} / \ell_\theta^2 \quad (6.4)$$

where ℓ_θ is the effective length of the column at temperature θ.

The relative slenderness of the column at elevated temperatures is given by:

$$\overline{\lambda}_{\theta} = \sqrt{N_{fi,pl,R} / N_{fi,cr}} \tag{6.5}$$

where $N_{fi,pl,R}$ is the value of $N_{fi,pl,Rd}$ when the material factors are taken as 1.0. In order to enter to the buckling curve "c" and determine the reduction coefficient χ, this value of the relative slenderness is used.

6.1.2. Simple calculation model in Annex H

Annex H of the same document (CEN 2005c), which is of an informative character, presents a simple calculation model specifically developed for concrete filled tubular columns. It is based on a prior method proposed for CFT columns at ambient temperature (Guiaux & Janss 1970) which was generalized for its use at elevated temperature.

In this method, the design axial buckling load can be obtained from the following equilibrium equation:

$$N_{fi,Rd}(\varepsilon) = N_{fi,cr}(\varepsilon) = N_{fi,pl,Rd}(\varepsilon) \tag{6.6}$$

where $N_{fi,Rd}(\varepsilon)$ is the design value of the fire resistance of the column in axial compression, $N_{fi,cr}(\varepsilon)$ is the Euler buckling load of the column in the fire situation and $N_{fi,pl,Rd}(\varepsilon)$ is the design value of the plastic resistance to axial compression of the cross-section at high temperature. An incremental procedure is needed to found the stress distribution which fulfills the equilibrium at a certain axial strain. Taking into account the premise that the axial strain of all the components of the cross-section is the same, the calculation procedure involves increasing the strain in steps until $N_{fi,cr}(\varepsilon)$ and $N_{fi,pl,Rd}(\varepsilon)$ are equal. For each strain level, the variation with the temperature of the stress and tangent modulus of each material is considered.

When using this method, a contradictory situation may arise where the fire resistance of short columns is found smaller than that of the longer columns, or even negative equilibrium values of the load can be obtained. In fact, at elevated temperatures, the application of the method can lead to equilibrium strains which are in the softening regime for some concrete layers where the tangent stiffness of concrete becomes negative.

Renaud et al. (2004) in the framework of CIDECT project 15Q developed a numerical investigation and pointed out the theoretical shortcomings of the method. Also the basis of this proposal was questioned and it was proved its inaccuracy given the very unsafe results which are produced for columns with common levels

of slenderness (Wang & Orton 2008, Aribert et al. 2008). It was found out that Annex H produces fire buckling loads which lay on the unsafe side when the relative slenderness of the column at room temperature exceeds 0.4 (Aribert et al. 2008). These actions led to the inclusion of a correction in Annex H to point out that the applicability of the method is restricted to CFT columns with a value of relative slenderness equal or less than 0.5.

This observation was also corroborated by Espinos et al. (2012) after the study of the applicability of the calculation methods of Eurocode 1994 Part 1.2 (CEN 2005c) to axially loaded CFT columns. They found that method from Annex H can lead to buckling loads which result unsafe for slender columns.

Therefore, the method in Annex H can only be applied to columns with buckling lengths in the fire situation $\ell_\theta \leq 4.5$ m, diameter of cross-section 140 mm $\leq D \leq$ 400 mm, concrete grades C20/25 – C40/50 and standard fire resistance $R \leq$ 120 min.

As a consequence of these results and provided that the specific method for CFT columns was tedious to apply in spite of its assumed simplicity, the trend followed by most researchers (Wang 1997b, 2000, Wang & Orton 2008, Aribert et al. 2008, Ribeiro et al. 2008, Leskela 2009) has been to resort to the general approach of Eurocode 4 Part 1.2, but as it has been exposed just few researchers have taken a further step to investigate the applicability of this general method specifically to CFT columns (Wang 1997, Renaud et al. 2004, Aribert et al. 2008).

6.2. CEN-HORIZONTAL GROUP FIRE GUIDELINES

In order to evaluate the accuracy of the proposed equations, the approach for the assessment of the accuracy of simplified methods proposed by CEN-Horizontal Group Fire (CEN 1999b) was employed. The mentioned assessment method set the next criteria to check the acceptability of a simplified method:

- Calculation results shall not be on the unsafe side by more than the 15% of the reference value.
- A maximum of 20% of the individual calculation results shall be on the unsafe side.
- The mean value of all percentage differences shall be on the safe side.

Therefore, in the process of adjustment of the equations for the cross-sectional temperatures presented hereafter, the above guidelines will be considered

so that the calculated values accomplish with these criteria when they are compared to the numerical predictions given by the developed thermal model through the parametric analysis.

In this line, for the development of the expressions for the simple calculation method these guidelines will be applied in order to assure that the predicted values of the buckling fire resistance fulfil the requirements of the document (CEN 1999b) when they are contrasted to the numerical results given by the fiber beam model.

6.3. DEVELOPMENT OF EXPRESSIONS FOR THE CROSS-SECTIONAL TEMPERATURE FIELD OF CFT COLUMNS

The application of the two described calculation methods included in Eurocode 1994 Part 1.2 (CEN 2005c) obligatorily involves the prior definition of the cross-sectional temperature field. Different methods can be used to determine the temperatures in the cross-section such as finite element analysis or one-dimensional heat transfer analysis.

In the case of the general method of Clause 4.3.5.1, once the thermal analysis has been accomplished, the calculation of the axial buckling load is straightforward, but the determination of the cross-sectional temperature field can result a tedious procedure to be implemented in the daily practice. Besides, Eurocode 4 Part 1.2 uniquely gives some principles for the thermal analysis but no indications to the designers are given for computing the temperatures in this composite section. Therefore, it is clear the necessity of having an available method for obtaining the temperatures in the cross-section.

Along this section, a set of equations for the cross-sectional temperature determination of circular CFT columns is proposed using the validated thermal model presented in Chapter 4.

6.3.1. Parametric analysis

An extensive thermal parametric analysis based on the cross-sections employed by Espinos et al. (2012) was carried out in order to generate enough data to obtain an accurate formulation by means of a nonlinear regression analysis. This parametric analysis covered section external diameters ranging from 139 to 508 mm combined with the minimum and maximum commercially available values of steel tube thicknesses for each case. The geometry of the analyzed composite sections can be found in Table 6.1.

Table 6.1. Adopted values for the parameters of the thermal parametric analysis.

Parameters studied	*D* *(mm)*	*t* *(mm)*	*R* *(min)*
Adopted values	139.7	3.2; 12.5	30; 60; 90; 120
	193.7	5; 16	
	273	5; 16	
	323.9	6.3; 16	
	406.4	8; 16	
	508	10; 16	

For each specimen, the analysis lasted 180 min so all the standard fire classes were covered (form R30 to R120) and data of the cross-sectional temperature distribution was registered every minute. The concrete core of the CFT columns included in the thermal parametric analysis was considered to be normal strength concrete with a moisture content of 3% for all the cases.

6.3.2. Equations for the cross-sectional temperature field

The set of practical equations here presented was obtained following the well-known procedure developed by Wickström (1986) who provided a simple method for estimating the temperature distribution in fire exposed concrete members which was constructed following a typical structure based on multiplying factors. In contrast to this research, Wickström (1986) did not consider either the temperature dependent thermal properties of the materials or the concrete moisture content.

The equations proposed for the temperature distribution in the steel tube and in the concrete core of a circular CFT column cross-section had the following shape:

$$\theta_a = \theta_{room} + \Delta\theta_a = \theta_{room} + \theta_f \cdot \eta_s \cdot \eta_a \prec \theta_{room} \quad (6.7)$$

$$\theta_c = \theta_{room} + \Delta\theta_c = \theta_{room} + \Delta\theta_a \cdot \eta_c = \theta_{room} + \theta_f \cdot \eta_s \cdot \eta_a \cdot \eta_c \prec \theta_{room} \quad (6.8)$$

where θ_a is the steel tube temperature; θ_{room} accounts for room temperature (20ºC in this case); $\Delta\theta_a$ is the steel tube temperature rise; θ_f represents the fire temperature rise; η_s is the factor accounting for the temperature drop at the boundary layer; η_a considers the temperature variation in the steel tube; and η_c is the ratio between the temperature rise of a concrete core inner point $\Delta\theta_c$ and the steel tube temperature rise $\Delta\theta_a$. These terms can be identified in Figure 6.1 where the temperature profile at a certain time is plotted in a longitudinal cut of a CFT column.

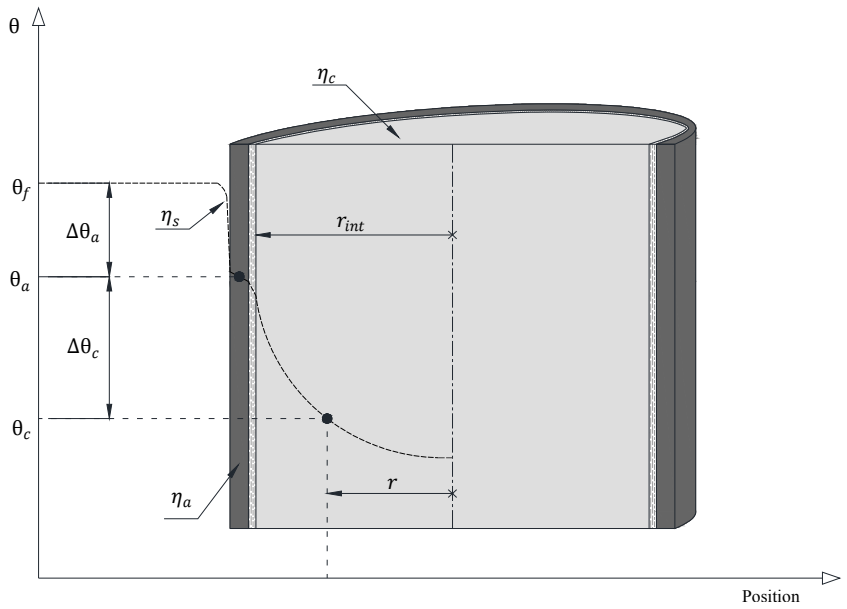

Figure 6.1. Temperature profile of a longitudinal section of a CFT column.

In order to define every term of the proposed expressions, a multiple nonlinear regression analysis was carried out with the data generated in the parametric analysis. Finally, the proposed equations were established as follows:

$$\theta_f = 345log(8R + 1) \tag{6.9}$$

$$\eta_s = 1 - 3.38R^{-0.18} \tag{6.10}$$

$$\eta_a = 1 - [0.155R^{0.58} + t^{-0.1}] \tag{6.11}$$

$$\eta_c = 1 - \left[0.073ln\left(\frac{r_{int}}{r_{int} - r}\right) + 0.63 \cdot \frac{(r_{int} - r)^{0.23}}{R^{0.03}} - 100\ \frac{(r_{int} - r)^{0.41}}{{r_{int}}^{1.79}} - 0.318R^{0.21}\right] \tag{6.12}$$

where R is the fire exposure time in minutes; t is the steel tube wall thickness in mm; r_{int} is the concrete core radius in mm; r is the radius in mm which indicates the position in the concrete core where the temperature is calculated .

For the steel tube, a lumped capacitance model was adopted so that the variation of the temperature through the thickness of the steel tube wall is negligible.

In Figure 6.2, the prediction given by the proposed equations for the steel tube and inner points of the concrete core at different fire exposure times are compared to the values generated through the parametric analysis by means of the developed thermal model. In Figure 6.2a and b , it can be observed that the point cloud lays mainly in the inner part of the deviation boundaries fixed at ±15% according to the CEN-Horizontal Group Fire (CEN 1999b). Besides, both graphs show some points that exceed the boundaries, but always placed on the safe side. The number of unsafe cases has been controlled as well as the characteristics of the mean. The linear regression equation and its coefficient of determination R^2 for the temperature prediction can be found in the graphs of Figure 6.2. In the case of the steel tube temperature prediction, the error mean value was 1.01 with a standard deviation of 0.09. Regarding the concrete core temperatures, the mean value of the error was 1.18 with a standard deviation value of 0.28.

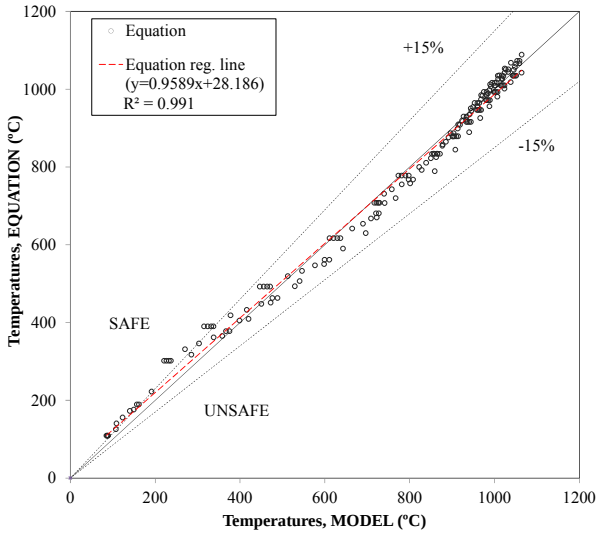

(a) Steel tube temperatures

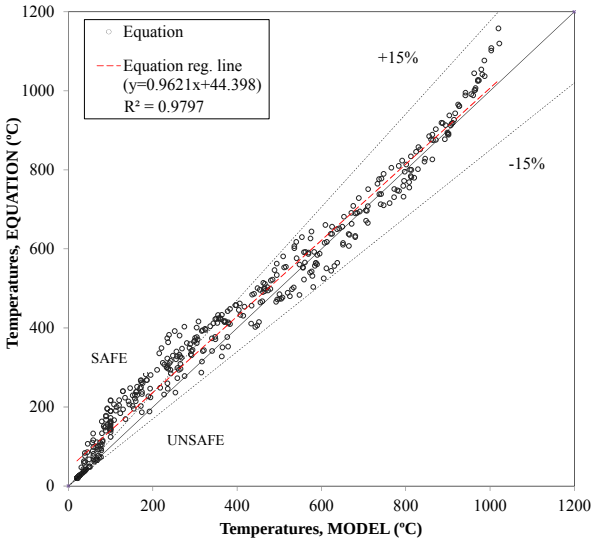

(b) Concrete core temperatures

Figure 6.2. Comparison of the predicted temperatures given by the equations proposed and the values generated in the thermal parametric analysis.

In addition, to complement the information analyzed before, another significant parameter was studied. Thus, the temperature at failure given by the proposed equation was compared with the available test data as is shown in Figure 6.3. The agreement existing is remarkably good as observed in the graph where in most of the cases the predictions are safe and always lying in between the limits.

The whole thermal response along time given by the proposed equations jointly with the experimental data and the temperatures calculated by the finite differences thermal model are shown in Figure 6.4 for comparison.

It can be noted that the curves given by the equations tend to overestimate the temperatures which will result in a faster degradation of the material and lower fire resistance times. This tendency obeys to the conservative rules suggested by CEN-Horizontal Group Fire (CEN 1999b) being more noticeable in the concrete core since it is in the component where the temperature field has a non-uniform temperature distribution. Despite of this aspect, the set of formula is able to predict the evolution of the temperatures along time for both the steel tube and the concrete core with reasonable accuracy.

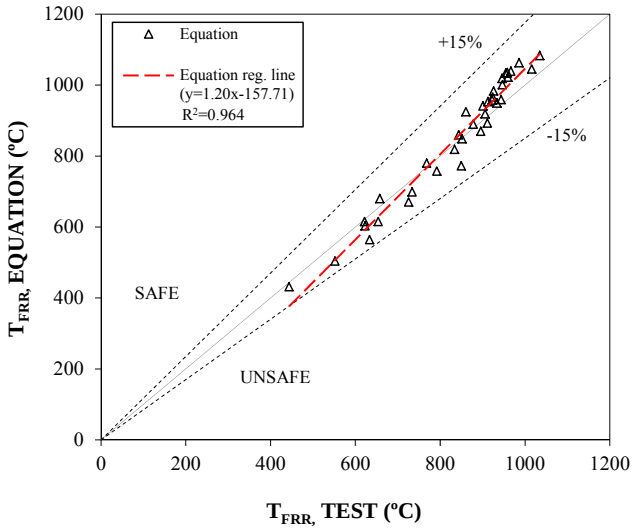

Figure 6.3. Temperature at failure: equation prediction versus test temperatures.

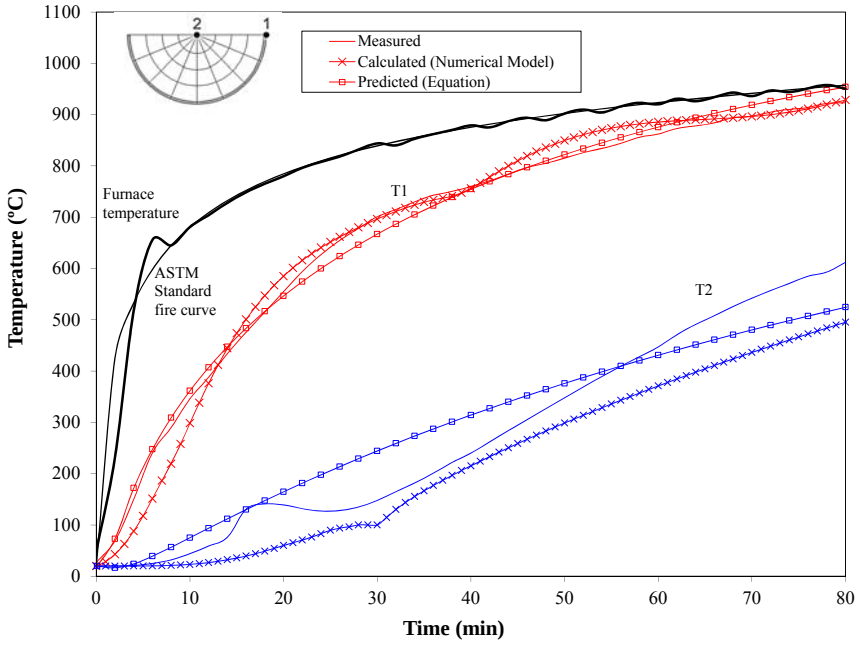

Figure 6.4. Comparison of test temperatures with temperatures calculated by thermal model and proposed equations for one of the specimens analyzed (C-09).

6.4. DEVELOPMENT OF A SIMPLE CALCULATION MODEL

The equations provided in the previous section could be very useful to obtain the cross-sectional thermal distribution when the fire design methods available in EN 1994-1-2 (CEN 2005c) are employed. Besides, taking as a starting point the proposed thermal expressions does not produce loss of accuracy since the effect of the realistic considerations such as the gap conductance at steel-concrete interface, the concrete moisture content of concrete and the temperature dependent thermal properties of the materials are implicitly taken into account.

Nowadays, the common practice consists of discretizing the concrete core in concentric layers as shown in Figure 6.5b and the temperature of each one is computed by means of specific software or by numerical modelling, which can result time-consuming. However, in the daily practice it is not usually required to obtain a detailed definition of the cross-sectional temperature field since the thermal analysis is a mere phase to obtain the fire resistance of the column.

Working in this line, it was considered the possibility of taking a step forward to develop a design method for CFT columns in fire where the cross-sectional temperature field is not explicitly defined. Thus, through this section, an alternative simple calculation model is developed on the basis of the Eurocode 4 Part 1-1 (CEN 2004b) using the concept of equivalent concrete core cross-section at room temperature. Due to this fact, the method becomes simpler and faster since the cross-sectional temperature field does not need to be completely calculated and only the temperature history of the steel tube is computed. The basis of the proposed method and the steps followed for its elaboration are described hereafter.

6.4.1. Equivalent concrete core cross-section

The equivalent concrete core cross-section of a circular CFT column for a given fire exposure time is a concrete core cross-section at room temperature whose contribution to the fire resistance of a CFT column is equivalent to the influence of the original concrete core cross-section subjected to the corresponding temperature field.

The calculation method presented hereafter follows the general rules of the simplified method of Clause 6.7.3 of EN 1994-1-1 (CEN 2004b) for the design of composite columns at room temperature. The external tube maintains its initial dimension and is made of a material representing the actual degraded steel for the given fire exposure time. However, the concrete core is represented by the equivalent concrete core cross-section with room temperature mechanical properties.

This procedure is conceptually similar to the simple method proposed in Annex B.1 of EN 1992-1-2 (CEN 2004a) for reinforced concrete members exposed to fire. In this approach, the cross-section size suffers a general reduction with respect to the fire damaged area at the concrete surface. This method, generally known as "500ºC isotherm method", comprises the no contribution to the load bearing capacity of the member of that external area of concrete whose temperature is higher than 500ºC. On the contrary, the inner area of concrete with temperatures lower than 500ºC is assumed to retain its original mechanical properties.

In the case of CFT columns cross-sections, due to the combination of different steel tube thicknesses jointly with different column external diameters, it cannot be found a unique isotherm which determines the concrete core area contributing to the load bearing capacity. Therefore, this area will be determined by means of the radius of the equivalent concrete core cross-section which will be obviously dependent on the geometrical characteristics of the composite section and the fire exposure time. It is obtained through the procedure exposed below.

In the method proposed, the plastic resistance to axial compression of the section in the fire situation is calculated as follows:

$$N_{fi,pl,Rd} = A_a \cdot f_{a,\theta} + A_{c,eq} \cdot f_c \tag{6.13}$$

and the effective flexural stiffness is obtained:

$$(EI)_{fi,eff} = E_{a,\theta} \cdot I_a + K_e \cdot E_c \cdot I_{c,eq} \tag{6.14}$$

where A_a and I_a are the area and second moment of area respectively of the steel tube cross-section; $f_{a,\theta}$ is the steel strength at the temperature θ; $E_{a,\theta}$ is the modulus of elasticity of steel at the temperature θ; $A_{c,eq}$ and $I_{c,eq}$ are the equivalent area and equivalent second moment of area correspondingly of the concrete core cross-section; f_c is the concrete strength at room temperature; K_e is a correction factor that should be taken as 0.6; and E_c is the secant modulus of concrete at room temperature. In Figure 6.5a it is shown the cross-section calculation scheme considered in the developed method, where the striped area indicates the equivalent concrete core cross-section defined by its radius $r_{c,eq}$.

In this approach, the confinement in the composite section is not considered and therefore, the increase of concrete compressive strength caused by this phenomenon is neglected.

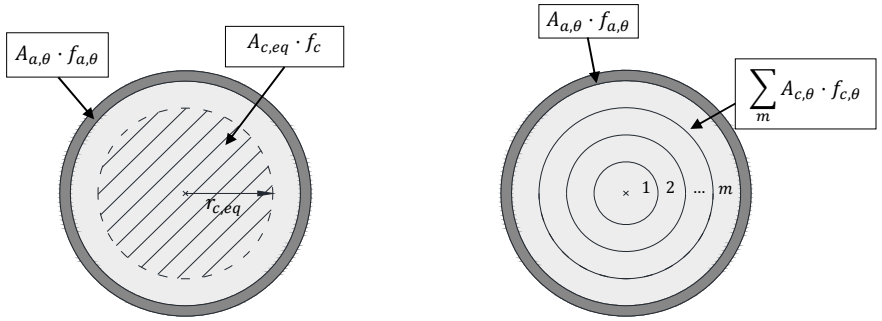

(a) Equivalent cross-section adopted by the proposed method.

(b) Layer discretization of the cross-section according to EN 1994-1-2.

Figure 6.5. Cross-section schemes for CFT columns used for calculation.

On the other hand, according to EN 1994-1-2 (CEN 2005c), in order to analyze the fire resistance of a CFT column, each element of the composite section is divided into several layers as was exposed above. Assuming that for the steel tube just one layer is considered, the cross-section scheme used for calculation purposes is the one presented in Figure 6.5b. Therefore, the plastic resistance in fire for the composite section is equal to:

$$N_{fi,pl,Rd} = A_{a,\theta} \cdot f_{a,\theta} + \sum_m A_{c,\theta} \cdot f_{c,\theta} \tag{6.15}$$

and the effective flexural stiffness is calculated as follows:

$$(EI)_{fi,eff} = E_{a,\theta} \cdot I_{a,\theta} + \sum_m E_{c,\theta} \cdot I_{c,\theta} \tag{6.16}$$

where for the steel tube, $A_{a,\theta}$ and $I_{a,\theta}$ account for the area and second moment of area of one layer at temperature θ. For the concrete core, $A_{c,\theta}$ is the area and $I_{c,\theta}$ represents the second moment of area at temperature θ of one layer.

Therefore, the radius of the equivalent concrete core cross-section at room temperature can be obtained following two different methods:

a) Plastic resistance method

Since the term referring the steel tube remains equal, the equivalent area of concrete core which produces the same plastic resistance than the original composite section submitted to fire is given by:

$$\sum_m A_{c,\theta} \cdot f_{c,\theta} = A_{c,eq} \cdot f_c \tag{6.17}$$

from where $r_{c,eq,A}$ is obtained.

b) Effective flexural stiffness method

Once more, given that the part corresponding to the steel tube does not vary, the second moment of area which produces the same flexural stiffness is:

$$\sum_m E_{c,\theta} \cdot I_{c,\theta} = K_e \cdot E_c \cdot I_{c,eq} \tag{6.18}$$

and from this equation, $r_{c,eq,EI}$ is directly calculated.

In each case, the equivalent concrete core radius will be given by $r_{c.eq} = \min\{r_{c.eq.A}, r_{c,eq,EI}\}$ since it will be the most restrictive value.

Since in the development of the proposed method, the calculation approaches for composite columns at room temperature and under fire of Eurocode 4 Part 1-1 (CEN 2004b) and the Eurocode 4 Part 1.2 (CEN 2005c) are employed, the mechanical properties adopted for the materials are those recommended in this code. For the concrete, both the mechanical properties at room temperature and at elevated temperature given in the European code (CEN 2004a, CEN 2004b) are adopted depending on the calculation that is being accomplished. In the case of structural steel, the mechanical model for high temperatures given in EN 1993-1-2 (CEN 2005b) is used.

The previous equations were applied to the cross-sections considered for the parametric study and, for each section, $r_{c,eq}$ was obtained. In most cases, it was the plastic resistance approach the one producing the most restrictive values but particularly for the two smallest diameters, the flexural stiffness method gave smaller values of $r_{c,eq}$.

Note that once the equivalent concrete core cross-section at room temperature is calculated with the predicted $r_{c,eq}$, all the related geometrical and mechanical characteristics change as a consequence, including the relative slenderness of the column used for the calculation of the reduction coefficient for buckling.

Once this step was completed, a nonlinear regression analysis was done to evaluate the influence of the different parameters to take into account. Thus, the next expression, that gives the $r_{c,eq}$ as a function of the section geometry and the fire exposure time R, was obtained:

$$r_{c,eq} = r_{int} + 23\left(\frac{A}{V}\right)^{-0.01} - 10R^{0.45} \not< 0 \tag{6.19}$$

In Figure 6.6, the comparison between the values of the equivalent concrete core cross-section radius calculated by the model and the ones given by the expression proposed is shown. As it can be observed, the predictions obtained by the expression have a high accuracy, with a safe mean error of 1.09 (σ=0.22). In this case, the error is calculated by:

$$\xi_r = 1 - \frac{r_{c,eq\ EQUATION} - r_{c,eq\ MODEL}}{r_{c,eq\ MODEL}} \tag{6.20}$$

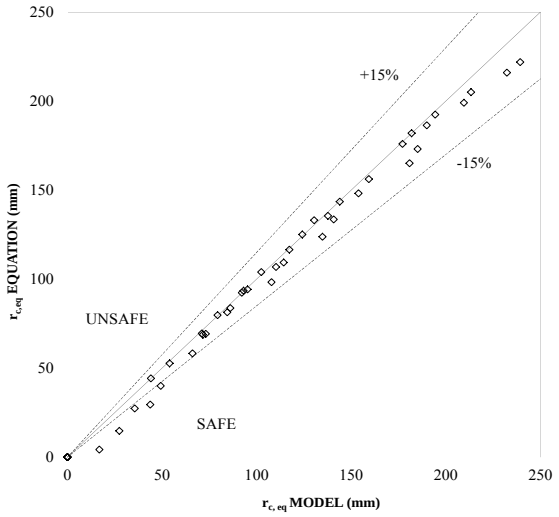

Figure 6.6. Comparison of predicted and numerical values of the radius of the equivalent concrete core cross-section.

6.4.2. Buckling correction factor

Once the equivalent concrete core cross-section is calculated, the next steps are executed. The relative slenderness $\bar{\lambda}$ at high temperatures is given by:

$$\bar{\lambda}_\theta = \sqrt{\frac{N_{fi,pl,R}}{N_{cr}}} \tag{6.21}$$

where N_{cr} is the elastic critical normal force calculated as follows:

$$N_{cr} = \frac{\pi^2 (EI)_{fi,eff}}{l_\theta^2} \tag{6.22}$$

In the calculation model here proposed, the value of the fire resistance of a CFT column in axial compression is calculated as follows:

$$N_{fi,Rd} = \eta_{buckling} \cdot \chi \cdot N_{fi,pl,Rd} \tag{6.23}$$

where χ is the reduction coefficient for the relevant buckling mode given in EN 1994-1-1 (CEN 2004b), which in this case corresponds to buckling curve "a"; and $\eta_{buckling}$ is the buckling correction factor to account for the influence of second orders effects at high temperatures. As it can be observed, the simple method proposed employs the buckling curve "a" for calculation. The development of a new buckling curve is not considered in the method, just the adoption of such a correction factor.

6.4.3. Parametric analysis

A thermo-mechanical analysis was executed based on the cross-sections used previously to carry out the parametric studies in the thermal field. The parametric analysis was performed through the fiber beam model presented in this work to generate numerical data of the buckling fire resistance of CFT columns with the aim of defining the shape of the buckling correction factor.

Again, following the basis of the parametric analysis performed by Espinos et al (2012) by means of their three-dimensional model, the maximum slenderness analyzed for each cross-section was selected so that the associated buckling length of the columns did not exceed 10 m as can be observed in Table 6.2. The same pattern was adopted in this case to facilitate possible further comparison between the precision of both models. The relative slenderness of the columns at room temperature were calculated according to EN 1994-1-1 Clause 6.7.3.3 (CEN 2004b)

Table 6.2. Adopted values for the parameters studied in the parametric analysis.

Parameters studied	***D* (mm)**	***t* (mm)**	$\bar{\lambda}$	***R* (min)**
Adopted values	139.7	3.2; 12.5	0.3; 0.5; 1; 1.5; 2	30; 60; 90; 120
	193.7	5; 16	0.3; 0.5; 1; 1.5; 2	
	273	5; 16	0.3; 0.5; 1; 1.5	
	323.9	6.3; 16	0.3; 0.5; 1	
	406.4	8; 16	0.3; 0.5; 1	
	508	10; 16	0.3; 0.5	

All the specimens were assumed to have a compressive strength of 30 MPa for the concrete and a yield strength of 355 MPa for the steel. Once more, analysis results were obtained for the four standard fire resistance classes (R30, R60, R90 and R120) for the 176 cases studied. Thus, in Table 6.2, the parameters studied and the values considered which set the limits of applicability of the simple method proposed can be found.

In the thermo-mechanical parametric analysis, the procedure to obtain the fire buckling resistance of each column was the next. First, each one of the specimens was analyzed under different load levels to obtain the corresponding FRR. These applied loads were defined as a percentage of the room temperature buckling axial resistance, ranging from 0 to 90% to cover a wide range of FRR values.

Once the $N_{fi,Rd}$-FRR curve is obtained for each column, the fire buckling resistance, $N_{fi,Rd,}$ at R30, R60, R90 and R120 minutes is calculated by linear interpolation. Finally, for each one of the cases analyzed, the buckling correction factor was calculated by:

$$\eta_{buckling} = \frac{N_{fi,Rd,MODEL}}{\chi \cdot N_{fi,pl,Rd,PREDICTED}} \tag{6.24}$$

The buckling correction factor values were obtained for all the specimens and based on the entire sample, a statistical study was implemented. The possibility of assigning a single value to the buckling correction factor was rejected since the analysis showed that the data was strongly dependent on the different geometrical variables (l_θ*/D, A/V, D/t*) whose role is considerably important in this problem. Therefore, an expression which is function of the different variables was proposed. The equation is composed by the product of three partial coefficients:

$$\eta_{buckling} = \eta_{l_\theta/D} \cdot \eta_{A/V} \cdot \eta_{D/t} \tag{6.25}$$

Once the intensity of the effect that each variable has on the buckling correction factor was studied by means of a correlation analysis, a multiple nonlinear regression analysis was carried out. The shape proposed for each of the terms multiplying was:

$$\eta_{l_\theta/D} = [a + b \cdot (l_\theta/D)^c] \tag{6.26}$$

$$\eta_{A/V} = [d + e \cdot (A/V)^f] \tag{6.27}$$

$$\eta_{D/t} = \left[g + h \cdot (D/t)^i\right] \tag{6.28}$$

When the influence of the relative slenderness at room temperature on the buckling correction factor was studied, it was detected the convenience of developing two different buckling correction factors: one for the specimens with $\overline{\lambda}\leq 0.5$ and another one for the cases with $\overline{\lambda}>0.5$.

For cases with $\overline{\lambda}\leq 0.5$ (stub columns):

$$\eta_{l_\theta/D} = [-4.16 + 4.208 \cdot (l_\theta/D)^{-0.003}] \tag{6.29}$$

$$\eta_{A/V} = [0.13 + 9.8 \cdot (A/V)^{1.6}] \tag{6.30}$$

$$\eta_{D/t} = [266 + 0.26 \cdot (D/t)^{1.5}] \tag{6.31}$$

For cases with $\lambda>0.5$ (slender columns):

$$\eta_{l_\theta/D} = [0.72 + 0.008 \cdot (l_\theta/D)^{1.322}] \tag{6.32}$$

$$\eta_{A/V} = [0.67 + 7.4 \cdot (A/V)^{1.81}] \tag{6.33}$$

$$\eta_{D/t} = [0.52 + 0.11 \cdot (D/t)^{-0.03}] \tag{6.34}$$

Finally, the equations presented above are applied to all the cases covered in the parametric analysis in order to obtain the values of the buckling resistance in fire situation. For each specimen, the predicted value was compared to the numerical value and the error was computed using the next expression:

$$\xi_{N,fi} = 1 - \frac{N_{fi,Rd,PREDICTED} - N_{fi,Rd,MODEL}}{N_{fi,Rd,MODEL}} \tag{6.35}$$

Proceeding in the same way as in the definition of the expression for the cross-sectional thermal distribution, in order to check the accuracy of the simple method proposed, the criteria of the assessment proposal made by CEN-Horizontal Group Fire (CEN 1999b) were again adopted.

In Figure 6.7, the error is plotted for the different values of relative slenderness at room temperature. According to CEN-Horizontal Group Fire (CEN 1999b), it can be observed that the simplified method produces values whose deviations with respect to the model predictions are concentrated between the 15% limits. Besides, the mean value of the error is equal to 1.07 which lies on the safe side and the calculated standard deviation is 0.16.

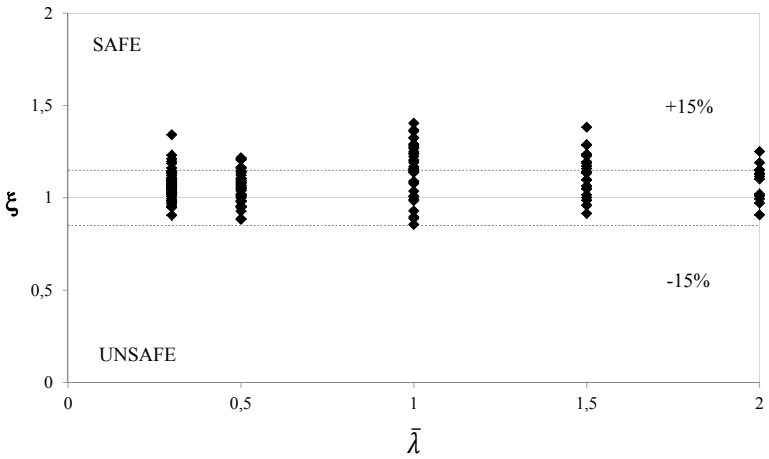

Figure 6.7. Relative error. Comparison between the results of the calculation proposal and the numerical simulations.

The frequency histogram presented in Figure 6.8 shows that the calculated errors follow the shape of a normal distribution. The calculated mean is located in the safe side where also the most frequent values can be found agreeing the criteria proposed by CEN-Horizontal Group Fire (CEN 1999b).

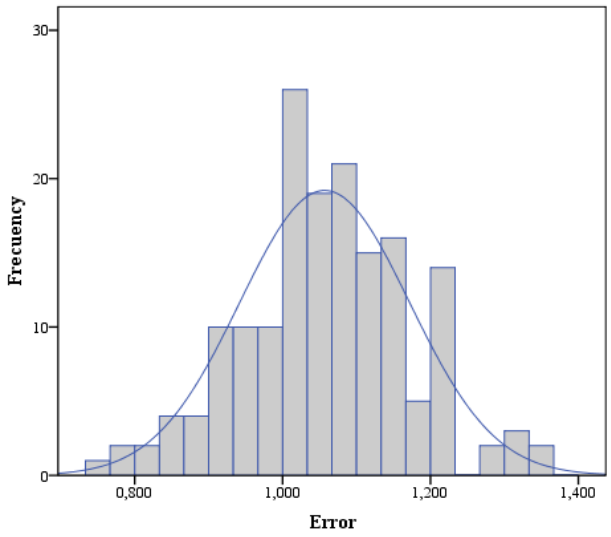

Figure 6.8. Frequency histogram for the prediction error obtained with the proposed design method.

In Figure 6.9, predicted and numerical values of $N_{fi,Rd}$ are compared. Due to the wide range of fire buckling resistances two graphs are provided.

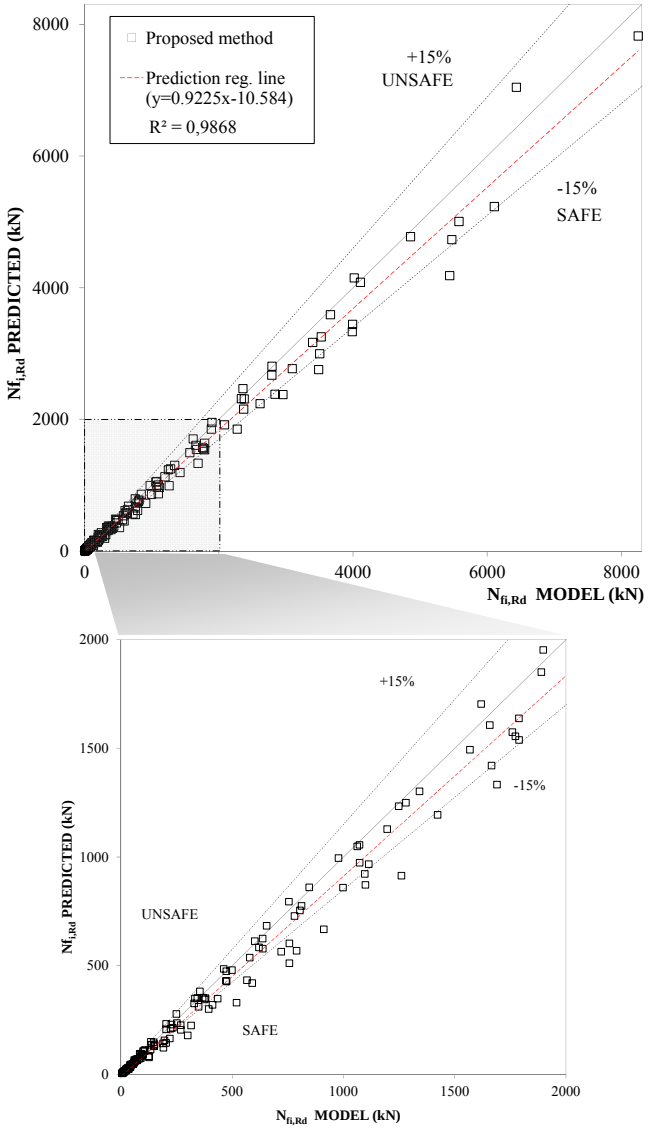

Figure 6.9. Comparison between the proposed method and numerical simulations.

This representation complements the information provided by Figure 6.7 and Figure 6.8 since it allows the observation of the regression line and its coefficient of

determination R^2 as recommended by CEN-Horizontal Group Fire (CEN 1999b) when simple models are proposed.

6.4.4. Comparison of the proposed method with experiments

Predictions given by the proposed method were compared to experimental data from actual fire tests. The calculation procedure here presented is valid for circular CFT columns filled with unreinforced normal strength concrete and under axial load. Therefore, only data from experimental programs that obey these conditions were contrasted.

For this purpose, both the results from tests carried out by the research group to which the author of this thesis belongs (Romero et al. 2011) and data from tests found in the literature (Lie & Chabot 1992) were used. A description of these tests can be found in Table 5.4 and Table 5.5.

The comparison in terms of axial buckling load is presented in Figure 6.10 where it can be observed that the accuracy of the proposed method is satisfactory and that its predictions are generally conservative.

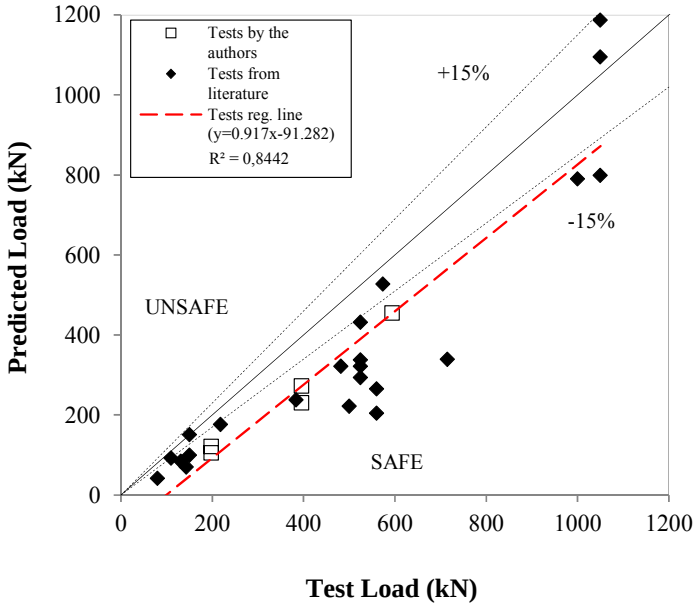

Figure 6.10. Comparison between predicted loads and tests loads.

6.4.5. Design example

In this section, a case of a CFT column fire design is included to exemplify the use of the fire design method presented.

The unprotected CFT column used in this example is 3400 mm long, has an external diameter of 193.7 mm and a wall steel tube thickness of 16 mm. The compressive strength of the concrete core is 30 MPa and for steel, a yield strength of 355 MPa is considered.

In this example, the axial buckling load in the fire situation for a column placed in an intermediate floor for a fire exposure time of 30 minutes (R30) is asked to be determined.

First, the geometric parameters are calculated:

$$l_\theta = L_{ei} = 0.5 \cdot L = 0.5x3400 = 1700\ mm$$

EN 1994-1-2 establishes that the buckling length in fire of a column in an intermediate story is L_{ei} defined as 0.5 times the original length.

$$A/V = 4/D = 4/193.7 = 0.02065\ mm^{-1}$$

$$D/t = 193.7/16 = 12.11$$

$$l_\theta/D = 1700/193.7 = 8.77$$

Next, the steel tube temperature is computed:

$$\theta_a = \theta_{room} + \theta_f \cdot \eta_s \cdot \eta_a = 20 + 345log(8\ x\ 30 + 1)\ x\ (1 - 3.38\ x\ 30^{-0.18})x$$

$$x\ (1 - 0.155\ x\ 30^{0.58} - 16^{-0.1}) = 616.76\ ºC$$

And also the $r_{c,eq}$:

$$r_{c,eq} = 80.85 + 23x0.02065^{-0.01} - 10x30^{0.45} = 58.55\ mm$$

For a steel tube temperature of 616.76 ºC, the reduction factors for the yield strength $k_{y,\theta}$ and the modulus of elasticity $k_{E,\theta}$ of the steel are taken from table 3.2 of EN-1994-1-2 (CEN 2005c) by linear interpolation:

$$k_{E,616.76} = 0.2798 \qquad k_{y,616.76} = 0.4297$$

Once this is done, the cross-sectional plastic resistance and the effective flexural stiffness can be calculated.

$$N_{fi,pl,Rd} = A_a \cdot f_{a,\theta} + A_{c,eq} \cdot f_c$$

$$= 8932.2\ mm^2 x 0.4297 x 355\ MPa + \ 10769.7\ mm^2 x 30\ MPa$$

$$= 1685640.1N = 1685.64\ kN$$

$$(EI)_{fi,eff} = E_{a,\theta} \cdot I_a + K_e \cdot E_c \cdot I_{c,eq}$$

$$= 0.2798\ x\ 210000\ x\ 35542569.5\ +\ 0.6\ x\ 32836.6\ x\ 9231981.14$$

$$=\ 2.2703 x 10^{12}\ N \cdot mm^2$$

Next, the Euler buckling load and the relative slenderness of the equivalent column can be calculated:

$$N_{cr} = \pi^2 (EI)_{fi,eff} / L^2 = \pi^2 x 2.2703 x 10^{12}\ / 1700^2 = 7753274.35\ N = 7753.27\ kN$$

$$\bar{\lambda}_\theta = \sqrt{N_{fi,pl,R} / N_{cr}} = \sqrt{1685.64\ / 7753.27} = 0.466$$

According to EN 1994-1-1, the reduction coefficient χ obtained from buckling curve "a" for the given relative slenderness is 0.934.

Finally, the buckling correction factor should be obtained. In this case, for this column (with an initial room temperature relative slenderness of 0.74), the partial terms are given by:

$$\eta_{buckling} = \eta_{L/D} \cdot \eta_{A/V} \cdot \eta_{D/t} =$$

$$= (0.72 + 0.008\ x\ 8.77^{1.322})\ x\ (0.67 + 7.4\ x\ 0.02065^{1.81})\ x\ (0.52$$

$$+ 0.11\ x\ 12.11^{-0.03}) = 0.3625$$

Therefore, the fire resistance to the column to axial compression for a fire exposure time of R30 is:

$$N_{fi,Rd} = \chi \cdot \eta_{buckling} \cdot N_{fi,pl,Rd} = 0.934\ x\ 0.3625\ x\ 1685.64\ = 570.48\ kN$$

6.5. SUMMARY OF THE PROPOSED CALCULATION METHOD

A simple calculation method for the fire design of circular CFT columns under concentric axial loads is presented. The calculation procedure employs the concept of equivalent concrete core cross-section at room temperature and takes as a reference the general rules of Eurocode 4 Part 1.1 (CEN 2004b). Expressions for obtaining the radius of the equivalent concrete core and for the calculation of a buckling correction factor are included in the new proposal. An overview of the proposed method is given next:

1. Determine the effective length of the column l_θ, the section factor A/V and the D/t ratio.
2. Calculate the steel tube temperature θ_a and the radius of the equivalent concrete core cross-section $r_{c,eq}$.

$$\theta_a = \theta_{room} + \Delta\theta_a = \theta_{room} + \theta_f \cdot \eta_s \cdot \eta_a \preccurlyeq \theta_{room}$$

$$r_{c,eq} = r_{int} + 23\left(\frac{A}{V}\right)^{-0.01} - 10R^{0.45} \preccurlyeq 0$$

3. Obtain the cross-sectional plastic resistance and the effective flexural stiffness using the temperature dependent steel mechanical properties from EN 1993-1-2 (CEN 2005b).

$$N_{fi,pl,Rd} = A_a \cdot f_{a,\theta} + A_{c,eq} \cdot f_c$$

$$(EI)_{fi,eff} = E_{a,\theta} \cdot I_a + K_e \cdot E_c \cdot I_{c,eq}$$

4. Compute the Euler buckling load and the relative slenderness in fire.
5. Calculate the buckling reduction coefficient from buckling curve "a" as it is indicated in EN 1994-1-1 (CEN 2004b).
6. Calculate the buckling correction factor.

$$\eta_{buckling} = \eta_{l_\theta/D} \cdot \eta_{A/V} \cdot \eta_{D/t}$$

7. Obtain the axial buckling load in the fire situation.

$$N_{fi,Rd} = \eta_{buckling} \cdot \chi \cdot N_{fi,pl,Rd}$$

7.

STRUCTURAL CONTINUITY ANALYSIS

Given the considerably lower computational cost of the fiber beam model proposed, it becomes an excellent tool to study the fire response of CFT columns within frames and the effects of axial and rotational restraints. This chapter presents the details of a parametric analysis carried out to evaluate the effects of structural continuity on the fire response of circular CFT columns. A description of the main recommendations given by the current codes and a comparison between their results and the predictions obtained by the model is included.

7.1. INTRODUCTION

Although the theoretical basis of the fire response of CFT columns is maintained when the column is analyzed as a part of a frame instead of isolated, the interaction of the member with the rest of the structure changes not only its boundary conditions but also its loading conditions. The fire action intensifies the effects of structural continuity in comparison with those at room temperature since the degradation of the column properties at high temperature increases the stiffness ratio existing between the column and the parts of the structure which remain unheated.

In several works dealing with the fire response of columns within frames, the importance of column stability to building safety has been pointed out since it can lead to a sudden failure and can initiate progressive collapse (Wang 1997a, Shepherd & Burgess 2011). The more dangerous scenario in this case is that where the columns are not affected by the fire in the same way and present different heating rates or when the fire action is confined to a part of the frame. Therefore, it is crucial to ensure that buildings are designed for robustness so that the rest of the structural elements constitute alternative load bearing routes when the sudden buckling failure of a columns occurs.

The main aspects of the effects of structural continuity on the fire behavior of a column within a frame can be grouped into two opposite groups. On the one hand, the action of the surrounding structure in the heated column has a positive effect coming from the increment in the rotational restraint to the column resulting in a reduction of its effective length and the consequent improvement of its load bearing capacity. Besides, when the CFT columns mechanical properties are highly degraded, new redistribution paths appear and part of the applied load is gradually transferred to the adjacent beams thus increasing the fire resistance time of the column. On the other hand, the negative effect of the axial restraint to the thermal elongation of the column which induces restraining forces to the member and thus increases the load that the column is supporting.

The mechanical analysis of a frame involving a concrete filled tubular column in fire would require an elevated computational cost given the multitude of elements implicated and the nonlinearities associated to the analysis of the fire response of a CFT column in fire. However, the proposed fiber model presents a substantially lower computing time which makes it a suitable analysis tool to carry out this type of studies with a reduced computational cost.

7.2. DESCRIPTION OF THE SUBFRAME MODEL

As a first reference, the scheme employed by Bailey (2000) to study the effective length of square concrete filled tubular columns was considered. This scheme consisted of three continuous columns where the intermediate one was the heated member as shown in Figure 7.1. The ends of the columns have the transversal movement restricted but they can elongate freely.

As exposed, this model is useful to study the buckling length of the heated column in fire situation but not for the study of the restraining forces arising when the longitudinal thermal expansion of the columns is limited. Nevertheless, since the effect of the restraining forces generated by the adjacent beams of the structures was an aspect of interest to be studied, the subframe model finally adopted was the one showed in Figure 7.2.

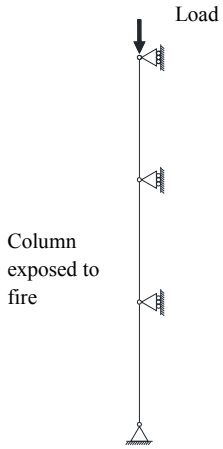

Figure 7.1. Scheme used by Bailey (2000)

In this case, uniquely the structural continuity of an intermediate column is going to be analyzed. The subframe is formed by three continuous circular CFT columns which are connected to their corresponding beams at their ends. The intermediate column is the member subjected to fire while the rest of the structural members remain cold. As explained before, this corresponds to one of the potentiality most severe situations where the fire action is just affecting to a part of the frame. Note that if the subframe consisted of more spans and all the columns were heated following the same fire curve, the detrimental effect of the restriction to

the thermal elongation could not be studied and the observed resultant effect would be always positive.

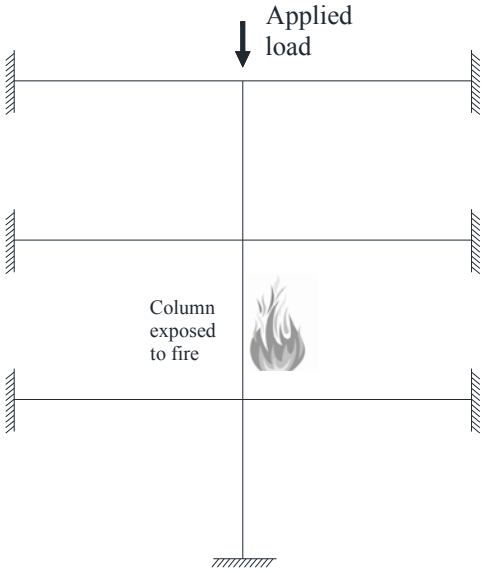

Figure 7.2. Subframe scheme used in the analysis.

As it can be observed, the frame employed for the study is a non-sway frame where the external ends of the frames which are not connected to any column are modeled as fixed since this configuration provides the highest level of restriction to the column. The axial load is concentrically applied to the top of the assembly.

In the case of the columns, these are modelled according to the validated model presented in this thesis. The adjacent beams are modelled by means of beam elements with linear elastic material in order to simplify and accelerate the calculation procedure.

7.3. CONSIDERATION OF THE FIRE EFFECTIVE LENGTH IN EUROCODE 4

With regard to composite columns in buildings, Eurocode 4 Part 1.2 (CEN 2005c) takes into consideration the influence of the structural continuity in the design assumptions by means of a reduction in the effective length of the columns in fire. Thus, according to Figure 7.3 an effective length of 0.5L is recommended in the case of a composite column placed in an intermediate story (continuous at both

ends), whereas for a column continuous at one end only (top story), a value of 0.7L is suggested (e.g. L is the system length).

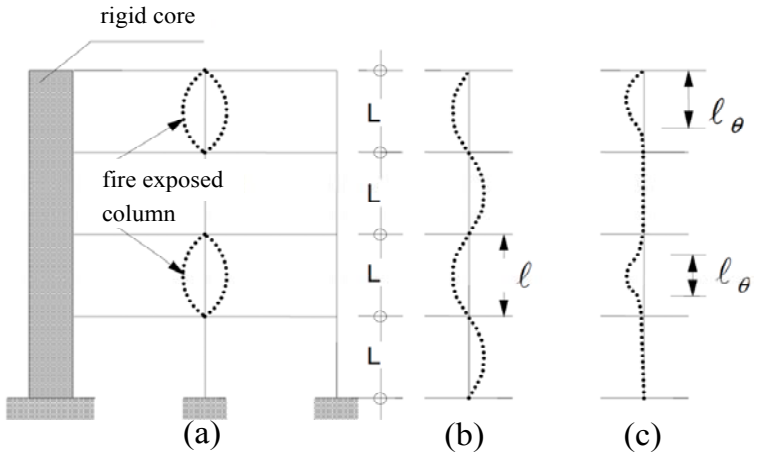

(a) section through the building
(b) deformation mode at room temperature
(c) deformation mode at elevated temperature

Figure 7.3. Structural behaviour of columns in braced frames (CEN 2005c).

For steel frames, the same recommendations are given in Eurocode 3 Part 1.2 (CEN 2005b) so that no specific recommendations are proposed for the case of concrete filled tubular columns.

However, the adoption of these assumptions in the design of CFT columns has been an issue of discussion for researchers in the last decade. In the case of steel columns within frames, the profile of the column exposed to fire heats uniformly and rapidly so that the column stiffness reduces in the same way. For steel columns, the consideration of the column ends as fixed can be acceptable since the ratio between the fire exposed column stiffness and the unheated surrounding structure is considerably low. However, in concrete filled tubular columns the cross-sectional temperature field is clearly non-uniform which together with the relative sliding appearing between the steel tube and the concrete core can lead to a very different behavior and, for this type of column, the guidelines of Eurocode 4 Part 1.2 can lead to unsafe results.

In fact, following these lines, in the UK National Annex to Eurocode 4 Part 1.2 (BS NA EN 1994-1-2), the factors of 0.5 and 0.7 have been conservatively increased to 0.7 and 0.85 respectively (Hicks & Newman 2002).

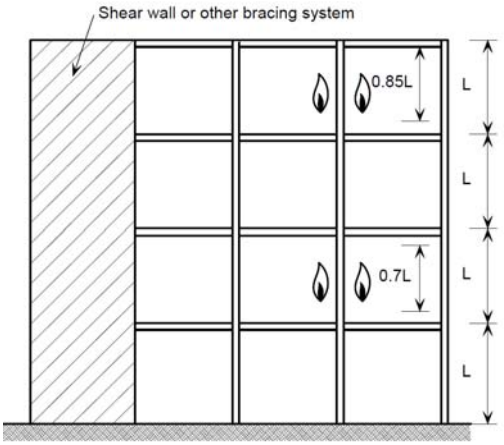

Figure 7.4. Effective length of columns in fire situation according to BS NA EN1994-1-2 (Hicks & Newman 2002).

7.4. FIRE BEHAVIOR OF CFT COLUMNS WITHIN FRAMES

7.4.1. Parametric analysis

A parametric analysis was carried out taking as a basis the subframe presented above and using the numerical model described in previous sections to simulate the fire behavior of the CFT column exposed to fire. In this case, the parameters affecting the fire resistance included in the study were the outer diameter of the column (D), the thickness of the steel tube (t), the relative slenderness of the column at room temperature ($\overline{\lambda}$), the applied load level (μ) and the stiffness ratio between the stiffness of the adjacent beams and the exposed column at room temperature (α). A summary of the cases analyzed is shown in Table 7.1.

Table 7.1. Summary of the cases included in the parametric analysis

Parameters studied	***D*** **(mm)**	***t*** **(mm)**	$\overline{\lambda}$	μ	α
Adopted values	139.7	3.2	0.3; 0.5; 1; 1.5; 2	0.3; 0.5; 0.7	0.1; 0.5; 1; 2
	193.7	5			
	273	5; 16			
	323.9	6.3			
	508	16			

Note that in comparison with the parametric analysis performed in the previous section for the development of the simple calculation model, the number of outer diameter-steel tube thickness combinations has been reduced in order to account for the inclusion of a new parameter regarding the rigidity of the surrounding frame which adopts four different values (α). As listed above, this parameter is the initial stiffness ratio between the adjacent beams and the column studied. It is designated by α and calculated as follows:

$$\alpha = K_{beam} / K_{column} \tag{7.1}$$

where $K = EI / L$ for the corresponding member. This parameter is just a reference of the level of rigidity of the surrounding beams with respect to the initial state of the column. As shown in Table 7.1, the values of 0.1, 0.5, 1 and 2 have been selected for this parameter, ranging from the configuration on which the column stiffness is 10 times that of the beams to the case in which the beams are two times more rigid than the column.

In all the cases analyzed, the beams presented a length of 5000 mm, which is a span value commonly found in practice. The beams were modeled with a double T profile of 300 mm of height (with the European normalized denomination of IPE300). The variation of the stiffness of the beams was obtained by incrementing linearly the value of the modulus of elasticity E. As a starting point, the beams were assumed to be of steel with a value of E=210000 N/mm^2 but in any case this is just a reference since this value was multiplied for the corresponding factor to obtain the desired α in each case.

Following the line established in the parametric study developed in the previous chapter for the development of the simple method, in this case the material properties employed were the same. For the steel tube the thermal and mechanical properties of Eurocode 3 Part 1.2 were assumed (CEN 2005b) and for the concrete core the expressions proposed by Eurocode 2 Part 1.2 were used (CEN 2004a). For all the columns the yield strength assumed for the steel tube was 355 MPa and a nominal compressive strength of 30 MPa was assigned to the concrete core. This is done with the aim of having the same reference point when comparing whit code guidelines and with the simple method proposed.

As seen in Table 7.1, three levels of applied load were evaluated: 0.3, 0.5 and 0.7. Although the level of 0.7 can be less usual in the daily practice than the other two, it has been included in order to cover a wider range. In all the cases the load will be axially applied since the numerical model developed is restricted to this type

of loads. However, it cannot be considered as a limitation of this study since previous theoretical analysis of this issue (Wang 1999) have proved that at the fire limit state both slender and short columns may be assumed to resist only axial loads given the rapid reductions in the column flexural bending stiffness.

Therefore, for each combination of stiffness ratio value and applied load level, the fire response of the different columns was simulated. In total, 360 cases were executed.

7.4.2. Analysis of results

From the analysis performed, different types of results were employed to draw conclusions. On the one hand, the evolution along time of the fire response of the columns in terms of axial displacement, axial force ratio and restraining forces are obtained. The latter is defined as the relation between the absolute load of the column and the initial applied load (P / P_0) as can be observed in Figure 7.5.

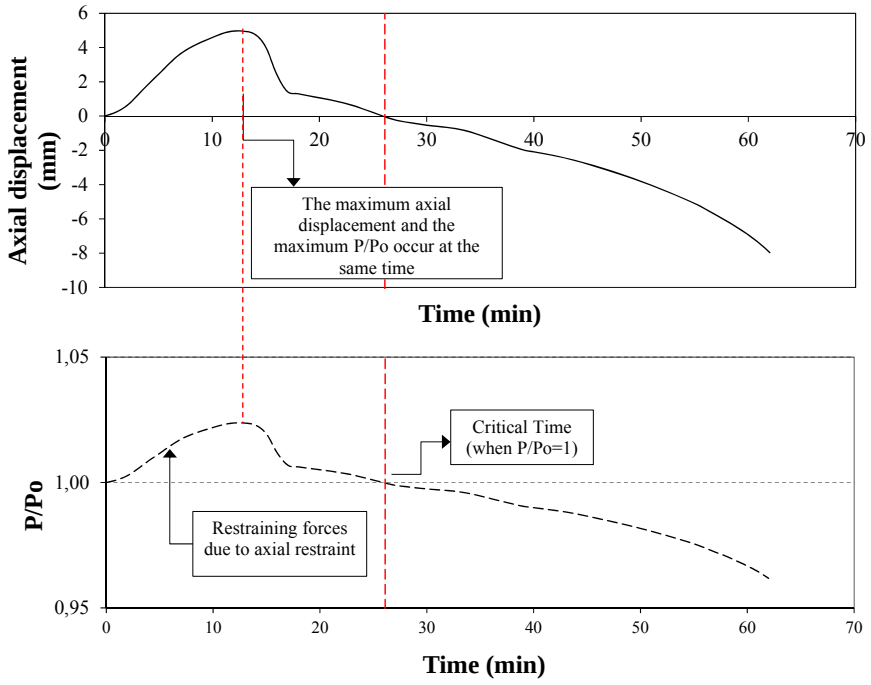

Figure 7.5. Typical behaviour of a CFT column within a frame

The evolution of the restraining forces is similar to the one already observed for the axial displacement since these forces are originated by the restriction that the

surrounding structure shows when facing the thermal elongation of the column. These forces increase up to a maximum value and then decrease due to the loss of strength of the steel tube until they recover the initial value of the applied load.

On the one hand, results in form of single values are also registered. Two of these results are the column force at failure which corresponds to the column axial buckling resistance obtained by the numerical model ($N_{fi,Rd,MODEL}$); and the time of fire resistance (FRR).

Another meaningful point obtained from the parametric analysis is the time at which the restraining force reach the initial value of the applied load and that will be hereafter denominated as critical time according to Pires et al. (2012) who gave this denomination to this instant of time after analyzing the results of an experimental program on CFT columns with restrained thermal elongation.

Before fully covering the analysis of the results, it is important to mention that in order to perform an accurate study of the generated data, a brief statistical analysis was executed in first place with the aim of detecting the outliers present in the sample as shown in Figure 7.6. In a preliminary examination of the columns responses it was detected that some cases showed excessively high FRR values or that even the failure of the column never occurred so that the FRR registered corresponded to the maximum calculation time assigned to the numerical analysis.

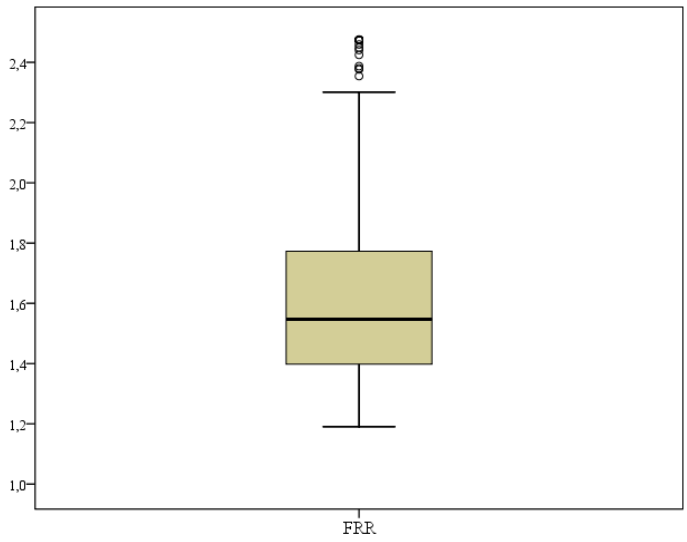

Figure 7.6. Detection of outliers in a boxplot.

The detection of outliers is an indispensable task to accomplish since they are not representative of the population and, therefore, in order to prevent the distortion of the statistical analysis results, these anomalous cases have to be rejected from the study.

Therefore, a univariate approach was applied to detect the outliers using the recorded FRR as a variable. Data were studied through a transformation to a normal distribution and those points more than 1.5 interquartile ranges below the first quartile or above the third quartile (or 3 times the standard deviation from the mean) were identified as outliers and excluded from the investigation.

An analysis of the outliers revealed that, in this occasion, these points coincided with those cases previously recognized as unusual whose FRR were higher than 180 minutes. As a consequence, only the cases with fire resistance times less than 180 minutes were employed in the analysis which subtly reduced the number of cases to 328.

As exposed before, the effect of the surrounding structure on the fire response of a CFT column can be separated into a beneficial effect given by the rotational restraint and a detrimental effect generated by the axial restraint. However, the global effect of the action of the frame on the fire behavior of the columns can be visualized in terms of the axial force that the column in supporting at failure with respect to the initial applied load.

In general it can be observed in Figure 7.7 that for specimens with relative slenderness up to 1.5 the axial force of the column at failure is less than the applied load which represents a global positive effect. At final stages of the fire when the column degradation state is advanced, the transference of load from the column to the surrounding frame becomes enhanced which reliefs the stress state of the column and increases its FRR. This effect is more noticeable in specimens with low slenderness and it growths with the increment in the stiffness ratio.

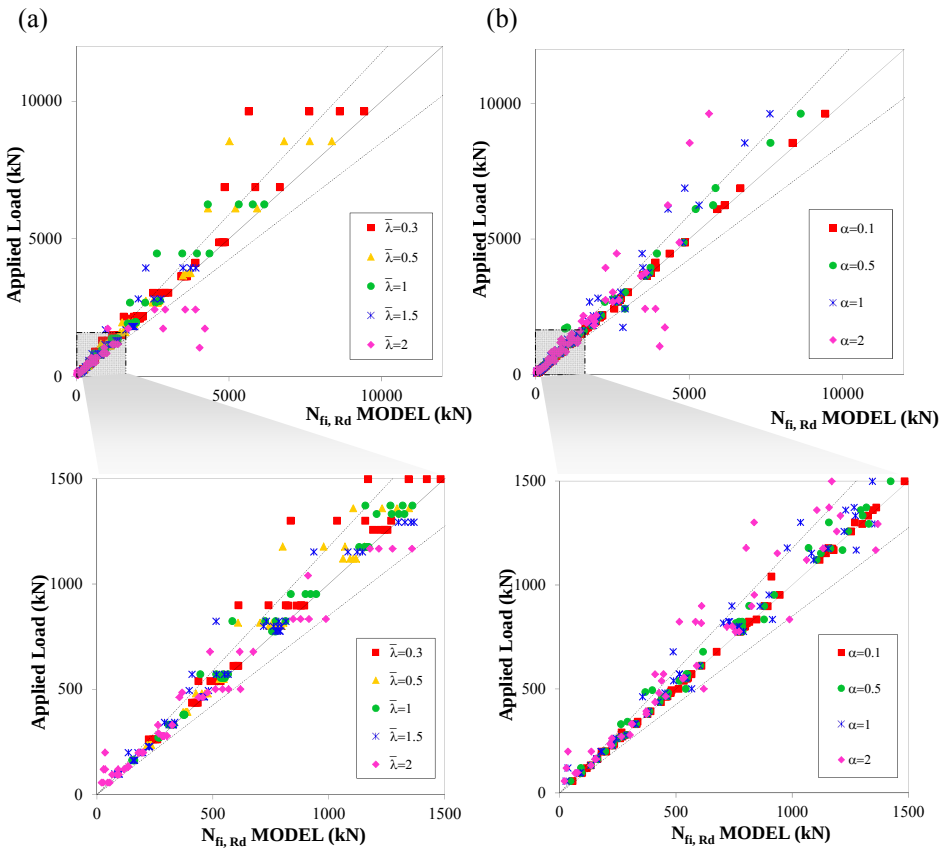

Figure 7.7. Comparison of the applied load and the buckling fire resistance of the columns within frames: (a) by relative slenderness; (b) by stiffness ratio.

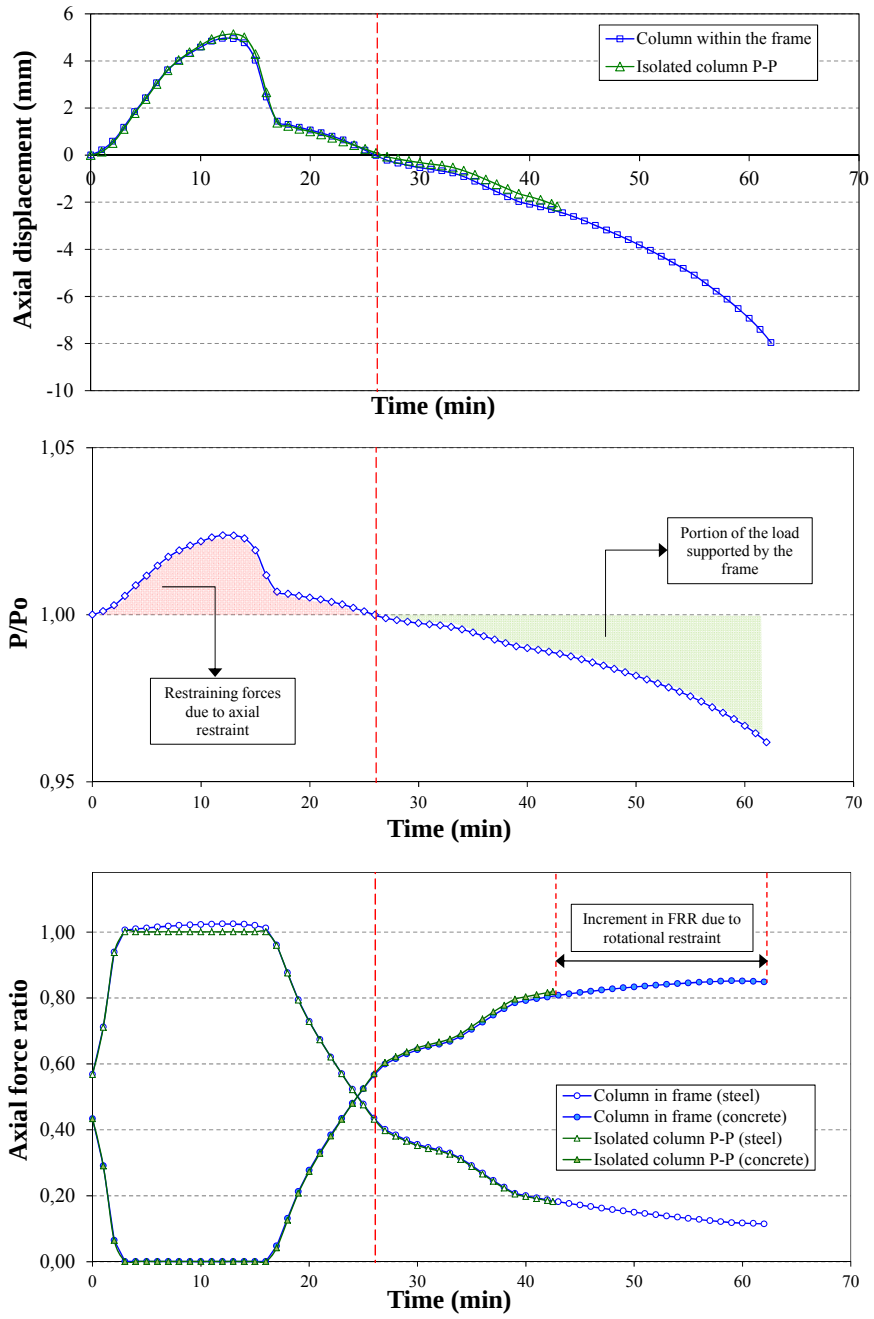

Figure 7.8. Fire response of specimen C193-5-1351-0.3 μ=0.3 α=0.5.

In those CFT columns with low slenderness, the role of the concrete core is very important and the fire response is highly influenced by this material which is protected by the steel tube and degrades slowly. Besides, the concrete core contributes to resisting the load and, during this period, the behavior becomes more ductile. Thus, the action of the frame is enhanced and the load is gradually transferred to the surrounding members as the concrete degrades and losses its mechanical properties due to elevated temperatures.

This typical behavior can be observed for the low slenderness specimen whose fire response along time in terms of axial displacement, restraining forces (P/Po) and axial force ratio is shown in Figure 7.8. The column represented is identified as C193-5-1351-0.3, with an external diameter of 193.7 mm, a steel tube thickness of 5 mm, a total length of 1351 mm and a relative slenderness of the column of 0.3. These results correspond to the simulation of the column within a frame with a moderate stiffness ratio α=0.5 and under a load level μ= 0.3.

Jointly with the response of the column in the frame it is plotted the fire response of the same column simulated as pinned-pinned in order to have a reference of the effects generated by the action of the surrounded structure.

With regard to the restraining forces (P/Po), it can be observed that given the short length of the column and the moderate rigidity of the frame, the increment in the supported axial load is quite low with a relative maximum value of P/Po=1.024 (2.4% of increment). As it has been exposed before, the evolution of the restraining forces follows the same path that the axial displacement, reaching a maximum value and subsequently decreasing due to the reduction of the column stiffness which makes the column attain less load.

The effect of the restraining forces is also noted in the axial displacement evolution figure where it is seen that the maximum axial displacement achieved by the isolated P-P column is slightly bigger than that reached by the assembled column due to the axial restraint. In this figure, it can be identified a deviation between the paths described by the two columns. This subtle change in the slope starts in the moment in which P/Po is less than 1 which means that the load is redistributed within the frame and the CFT column is released from a percentage of the axial load. This effect compensates the negative effect created by the axial restraint resulting in a considerable increment in the FRR. This observation confirms that assembling a CFT column to other structural members not only modifies the boundary conditions but also the loading conditions.

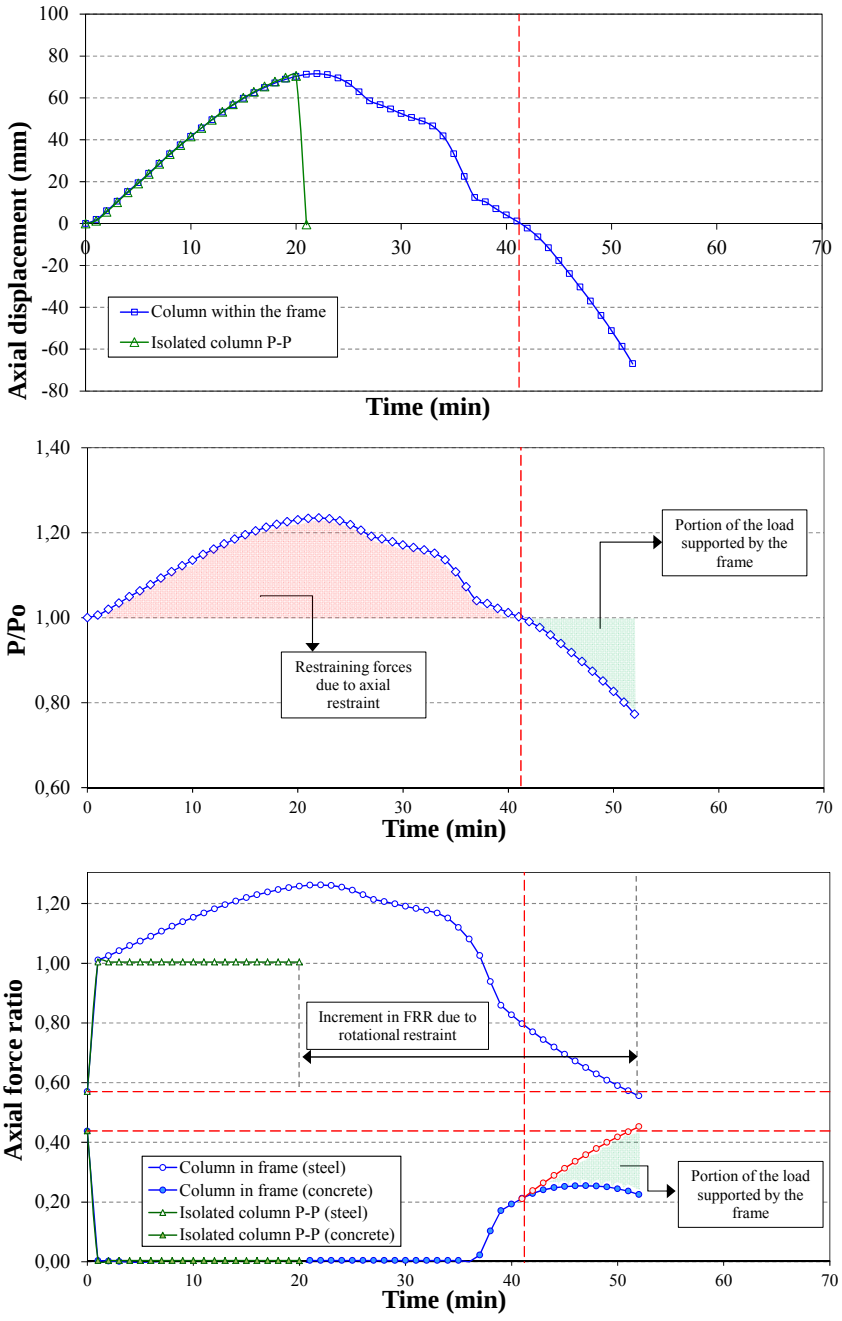

Figure 7.9. Fire response of specimen C193-5-9010-2 μ=0.3 α=0.5.

The described behavior becomes more obvious for the specimen showed in Figure 7.9. This specimen has the same sectional properties than the one previously studied but with a length of 9010 mm and, therefore, a relative slenderness of 2. Again, the fire behavior showed by a pinned-pinned column of the same characteristics is plotted. The first difference found between this specimen and the column in Figure 7.8 is the contribution of the frame in preventing the premature failure of the column due to buckling. In the first graph it can be noticed how the response of the column within the frame gets over the point where the isolated P-P column failed thus allowing the column to work during a longer period of time.

The explanation to this behavior may reside in the fact that, although during this stage the column is negatively affected by the restraining forces, the boundary conditions are changing due to the increment in the relative rigidity between the heated CFT column and the surrounding unheated members which modifies the buckling behavior. The action of the rotational restraint retains the column and prevents it from buckling.

In addition, the beneficial effect of the rotational restraint can be also observed from the point where the load supported by the composite column is less than the initially applied ($P/Po<1$). Again, from this point on, the redistribution of the load within the frame becomes relevant but, contrarily to the previous case, in this slender column the effect is more perceptible. In the third figure, where the axial force ratio along time is plotted, appears traced in red the theoretical evolution of the axial force ratio of the concrete core if the surrounding cold frame was not acting. This evolution has the same shape but inverse slope than the one described by the steel tube which is the commonly observed behavior on isolated columns so that the sum of the both components contribution is the total amount of applied load. However, for this specimen, it is noticed how the obtained evolution of the concrete core axial force ratio differs substantially from the theoretical one. The area enclosed by the two curves (shaded in green) corresponds to the percentage of load transferred from the CFT column to the frame.

A third type of response of CFT columns within frames is the one shown in Figure 7.10, very different from that described above for a column with the same relative slenderness. In this occasion, the cross-sectional size of the circular column is 273 mm and the steel tube is 16 mm thick. The stiffness ratio and the load level applied are the same than in the two preceding columns. The column has a length of 8402 mm and a relative slenderness of 2. As it can be observed in Figure 7.10, the mode in which this column fails differs from the one observed until the moment and it occurs during the stage in which the CFT column is supporting more load than

that initially applied, i.e. P/Po>1. The columns associated to this behavior can be identified in Figure 7.7 at the bottom part of the graph. Although this behavior is more likely to occur within very rigid frames, it is also detected under other values of stiffness ratio.

Analyzing the mentioned specimens, it has been noticed that this response occurs in slender columns subjected to elevated load levels. In particular, this response occurs in those slender columns whose steel tube is relatively thick and present medium to high outer diameters (C273-16, C508-16). Given the thickness of the steel tube, it attracts initially more load than in other CFT column where the tube is thinner. This phenomenon can be observed in the third graph of Figure 7.10 where the axial force ratio is plotted. At initial time, the force distribution between the two components of the column C273-16 is approximately 80%-20% for steel and concrete respectively whereas for the same specimen with size C273-5, which was also studied, the initial axial force ratio is 50%-50%.

Hence, even though the frame acts preventing the premature failure observed for the corresponding isolated pinned-pinned column it cannot avoid the occurrence of global buckling before the concrete core starts to work. The explanation to this response may reside in the fact that when the steel tube contracts, the concrete core still possesses an elevated level of stiffness due to the combined action of its outer size and thicker steel tube which delays its heating and degradation. Thus, at this point, the increment in the stiffness ratio between the unheated adjacent beams and the heated CFT column is not as significant so as to lead to an important modification of the boundary conditions of the member which would result in an increment in the FRR.

Therefore, although in this case the location of the CFT column within a frame increases the FRR with respect to the one registered for the isolated P-P column, the sudden type of failure is maintained. For these columns, the beneficial effect of the frame creating new paths to sustain the applied load and thus extending the duration of the column and assuring a soft failure does not occur.

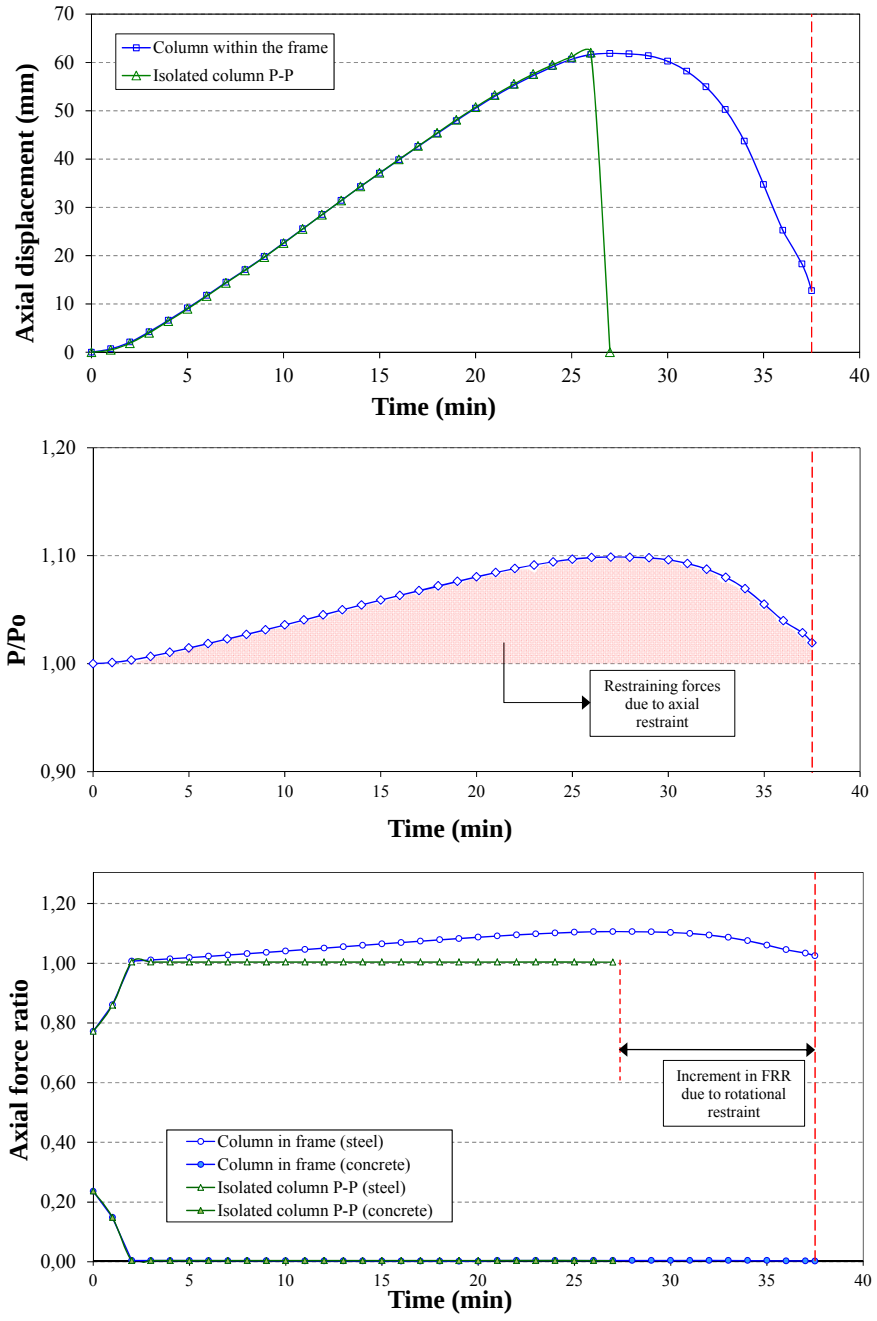

Figure 7.10. Fire response of specimen C273-16-8402-2 μ=0.3 α=0.5.

7.4.3. Influence of the parameters studied

7.4.3.1. Influence of the load level

As exposed before, for each combination of stiffness ratio and column type, three load levels were applied. In Figure 7.11, the evolution of the axial displacement along time is shown for two of the specimens studied. It is observed that for both columns the increment in the load level leads logically to a reduction in the FRR.

(a)

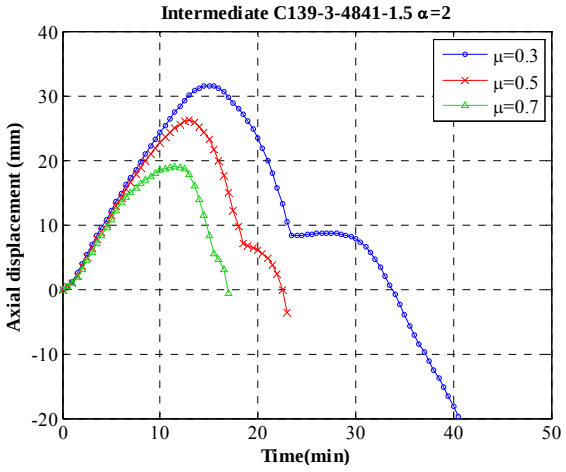

(b)

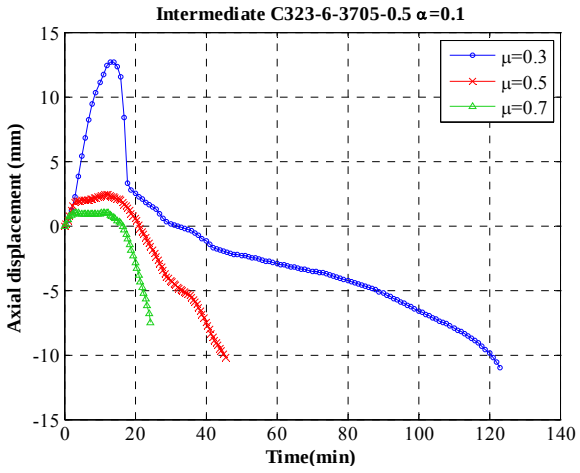

Figure 7.11. Influence of the load level on the axial displacement.

In Figure 7.11 and Figure 7.12, it can be detected that the influence of this parameter is the same for the axial displacement and for the restraining forces. Thus, a low load level allows for higher values of the maximum axial displacement and P/Po since the columns are supporting much less load and have more capacity to expand thus generating more restraining forces.

(a)

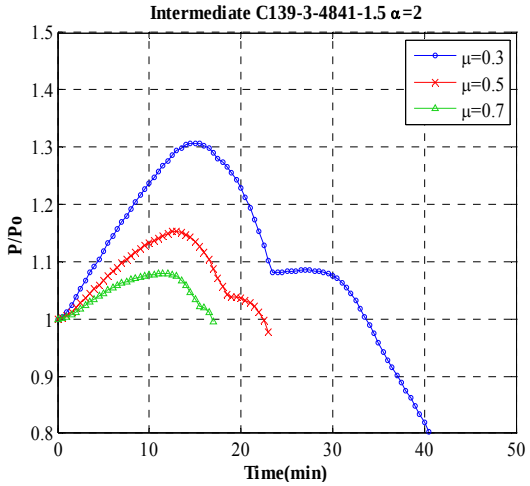

(b)

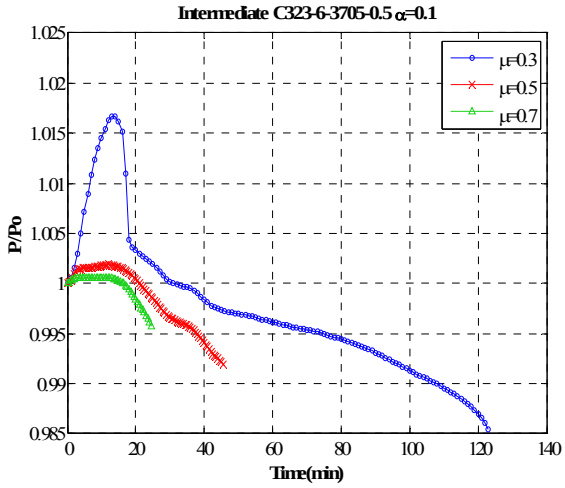

Figure 7.12. Influence of the load level on the restraining forces.

Thus, in the case of specimen C139-3-4841-1.5 within a frame characterized by a stiffness ratio of α=2 (Figure 7.12a), the maximum value of the restraining

forces is 1.31 for a load level μ=0.3, whereas the maximum value of P/Po for μ=0.7 is 1.08 which means that the increment in the load supported by the column with respect to the initial applied load varies from 31% to 8%. However, for the column C323-6-3705-0.5 within a frame with a low stiffness ratio α=0.1 (Figure 7.12b), the maximum increment in the supported load is 0.1% (P/Po=1.001) for an elevated load level μ=0.7 and 1.7% (P/Po=1.017) for the case with μ=0.3. Although both are marginal values due to the low rigidity of the frame, the trend is the same observed in the previous case.

The beneficial action of the frame is enhanced under lower load levels since in those cases the steel tube is not likely to fail prematurely and contacts back the concrete core. As seen in the figures analyzed above, it is from this point on when the redistribution of the forces within the frame takes more relevance. The lower the load level, the more notable the beneficial effect of the rotational restraint.

With regard to the critical time that was previously defined as the time when the axial force supported by the column reaches its initial value, it can be noticed that it decreases with an increment in the load level. Under an elevated load level, the steel tube is supporting much more load when expands and separates from the concrete core. The tube reaches before its maximum axial displacement, which in turn is smaller, and starts its contraction before giving lower critical time values. Note that in those cases where the steel tube fails before contacting back the concrete core, as observed for the column in Figure 7.10, the critical time does not even exist. In the corresponding annex, the fire response of all the analyzed specimens can be consulted.

7.4.3.2. Influence of the stiffness ratio

The fire response of the studied columns was simulated under four different levels of stiffness ratio which was defined as the relation between the stiffness of the adjacent beams and that of the CFT column at room temperature.

The next figures, Figure 7.13 and Figure 7.14, show the evolution of the axial displacement and the restraining forces along time. As it can be observed in both figures, an increment in the stiffness ratio leads to lower values of the maximum axial displacement as a consequence of the restraining forces generated by the axial restraint which, oppositely, are higher.

With respect to the fire resistance rating, it is higher for those columns within very rigid frames, since the beneficial effects of the rotational restraint are enhanced as the stiffness of the frame grows. For those specimens in which the critical time is

achieved and the frame starts to absorb part of the load supported by the column until that moment, it is observed that, for higher stiffness ratio values, this effect is more noticeable since, as expected, the percentage of load redistributed is more elevated.

(a)

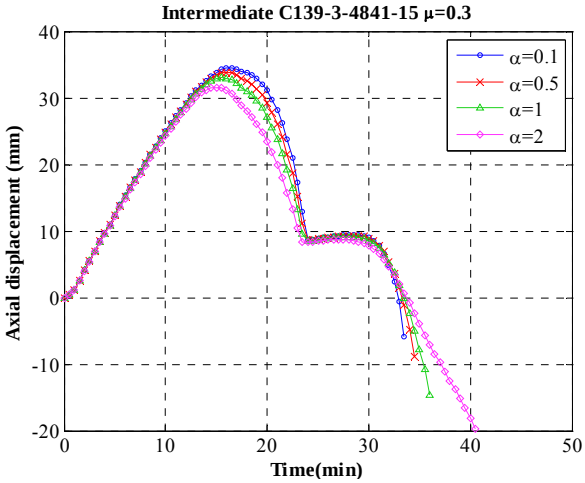

(b)

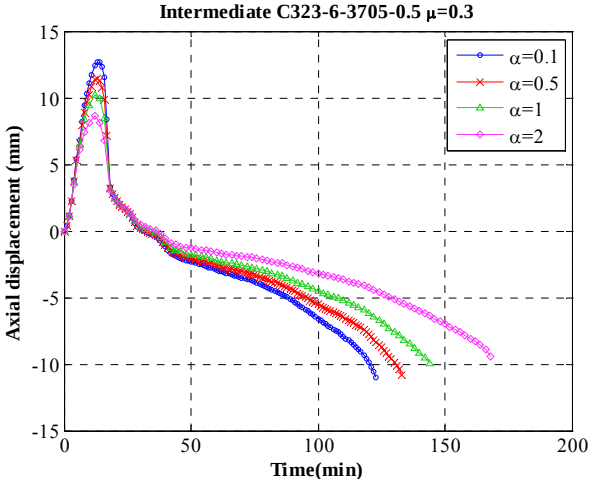

Figure 7.13. Influence of the stiffness ratio on the axial displacement.

It is worthy to mention that the increment in the FRR for higher values of the stiffness ratio is an effect which is more perceptible for specimens with low slenderness as can be observed between specimens (a) and (b) in Figure 7.13 and Figure 7.14.

Finally, regarding the critical time, it can be noticed that it does not vary with the stiffness ratio for one particular column under the same load level. This may be explained by the fact that until this point the beneficial and detrimental effects of the restraining frames compensate each other.

(a)

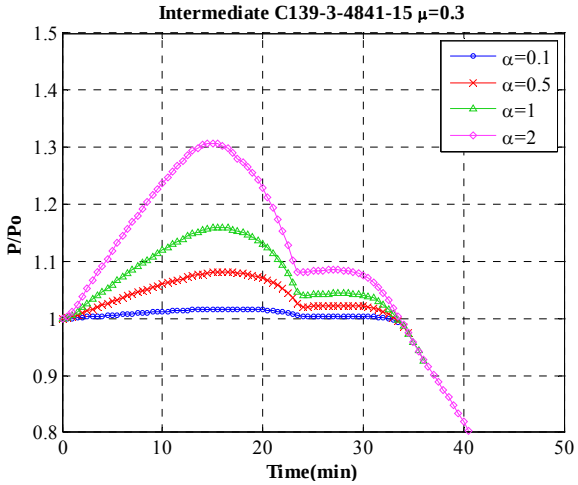

(b)

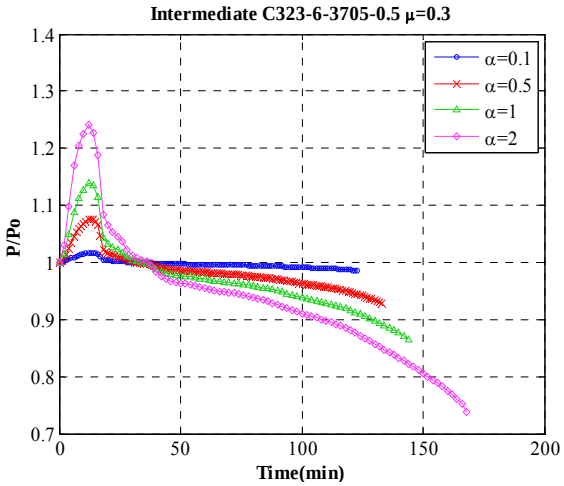

Figure 7.14. Influence of the stiffness ratio on the restraining forces

Note that in Annex I, the corresponding graphs for the specimens analyzed in the parametric studies are included.

7.4.4. Evaluation of the effective length

As it has been observed, the boundary conditions of a CFT column exposed to fire within a frame change due to the relative stiffness existing between the heated column and the non-exposed structural members. This phenomenon affects the column behavior and its buckling axial load under fire condition.

Since the design of a column for the fire situation is a task usually accomplished for isolated columns, the way in which the change in the boundary conditions could be incorporated in the design process has been, in the last decade, an aspect of study in the field of CFT columns. In the previous revision of the guidelines given by Eurocode 4 Part 1.2 (CEN 2005c) regarding this effect, it was described that for intermediate columns (which are the type of columns covered in this work), the effective length recommended to account for this phenomenon is 0.5L. Also it was pointed out that the UK National Annex recommended a value of 0.7L in order to be more conservative.

Several authors have investigated the effective length of CFT columns in fire with different results. Authors like Wang (1999) corroborated the recommendation made by the Eurocode 4 whereas other authors like Bailey (2000) pointed out that unsafe results were obtained if an effective length of 0.5L was employed and after a study on square CFT columns proposed higher values of the effective length for CFT columns placed at different stories.

Given that there is no a unified criterion regarding the effective length in fire, a new comparison is presented in this section with the data generated in the previous parametric analysis. The FRR obtained when the different columns were simulated within the frame is compared with the FRR obtained by the corresponding isolated P-P columns but assuming different effective lengths. The effective length ratio coefficients used for comparison were 1, 0.7 and 0.5. The value of unity is used for reference and the other two values are employed since they are the ones currently considered by practitioners.

In Figure 7.15, the comparison is shown for the different values of stiffness ratio considered in the parametric analysis. For each one, the comparison for each value of the effective length is presented separated by slenderness. As it can be observed, the numerical simulations of isolated pinned-pinned columns with an effective length of 1L, used for reference, give considerable safe results.

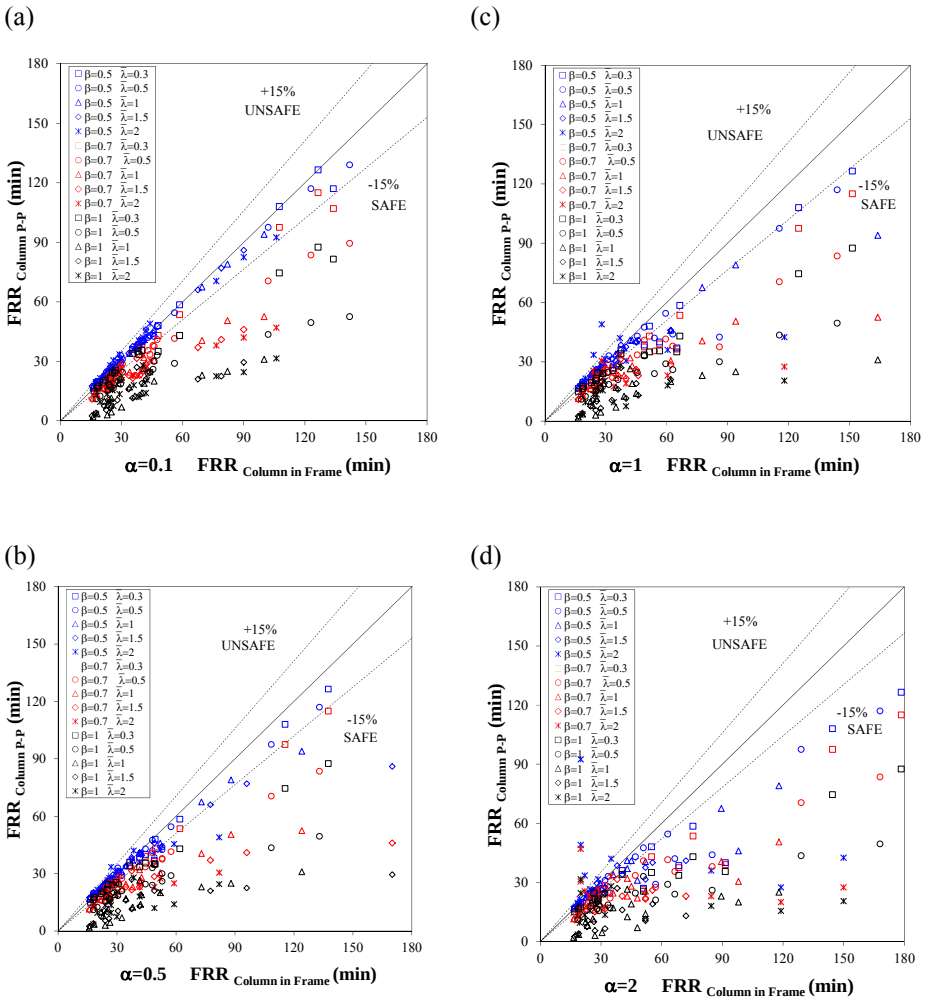

Figure 7.15. Comparison of the FRR obtained by the column within the frame with the FRR of isolated P-P columns under different effective lengths.

For the specimens with low slenderness which are those which usually present higher values of the FRR, the assumption of 0.5 or 0.7 gives in general safe results. In the case of low and moderate stiffness ratio (α=0.1 and α=0.5) the coefficient which gives results more similar to those obtained by the columns within the frame is 0.5. In the case of restraining frames with elevated rigidity (α=1 and α=2), this value also provides safe results. Under these frames the effect of the rotational restraint is significant and more in stub columns where, as it has been exposed previously, a great percentage of the load is redistributed in the frame.

However, since the simulation of the isolated P-P columns does not account for the variation in the supported axial load (P/Po), the obtained results tend to be safe.

Given that most of the FRR registered for the slender specimens studied in the parametric analysis lie between 30-60 minutes, Figure 7.16 is presented in which an enlarged view of this area is shown just for columns with a relative slenderness from 1 to 2.

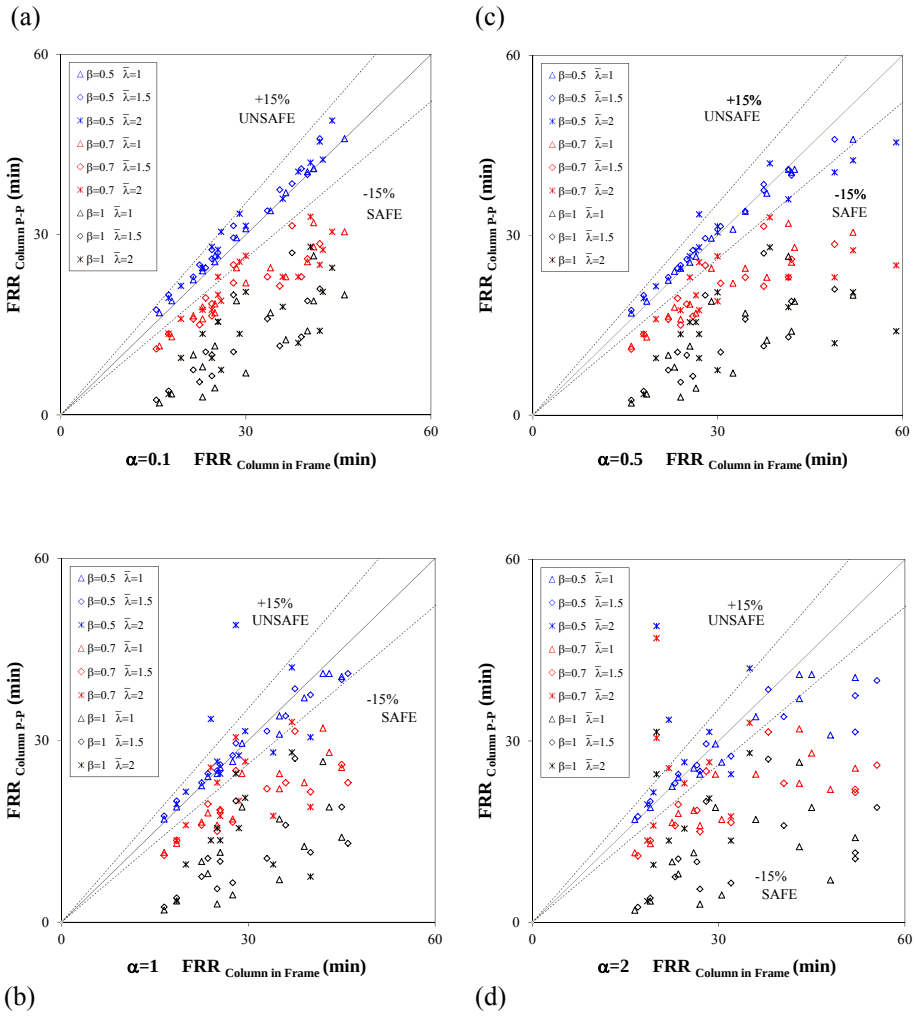

Figure 7.16. Slender specimens. Comparison of the FRR given by the column within the frame with the FRR of isolated P-P columns under different effective lengths.

As it can be noticed in Figure 7.16, generally the results are slightly different for slender columns. For an effective length of 0.5L, the results obtained for the isolated P-P columns in the numerical analysis are analogous to those registered for the FRR when the corresponding columns were simulated within the frame and although they lie inside the 15% limit, most of the points are unsafe predictions. This occurs mainly for the restraining frames with low stiffness ratio, α=0.1 and α=0.5. Therefore, in this situation, the employment of an effective length of 0.7L would be more appropriate to avoid obtaining unsafe predictions.

In the cases of restraining frames with high rigidity (α=1 and α=2), not very usual in the daily practice, the predictions given by the numerical simulation assuming an effective length of 0.5L are still unsafe for some specimens. Again, the employment of a value of 0.7L for the effective length is safer. However, as exposed above, the restrained CFT columns are simulated as isolated P-P columns with an specific effective length and, therefore, they account for an inherent safety factor since the diminution of the supported load due to its redistribution within the frame (which is significant for high rigidity frames, α=1 and α=2) is not modeled.

7.5. ANALYSIS OF CURRENT EUROCODE 4 GUIDELINES

The buckling fire resistance of the columns within frames included in the parametric analysis was computed by means of the general method of Eurocode 4 Part 1.2 Clause 4.3.5.1 (CEN 2005c) under two different assumptions for the effective length of CFT columns in fire. First, an effective length ratio of 0.5 was analyzed since it is the one given in Eurocode 4 for the fire design of columns at intermediate stories. After, the results produced by the effective length of 0.7L recommended in the UK National Annex to Eurocode 4 were analyzed.

In a previous section, a review of the general method of Eurocode 4 Part1-2 was presented. The work of several authors (Renaud et al. 2004, Aribert et al. 2008) on the definition of the flexural stiffness reduction coefficients employed in the method was mentioned, since they observed that using flexural stiffness reduction coefficients equal to unity led to unsafe results, as also corroborated researchers like Espinos et al. (2012). However, in this study, a value of 1 is adopted to carry out the comparison. Given the lack of agreement on the specific values for the coefficients, this is the value commonly adopted in daily practice by designers (Lennon et al. 2007).

7.5.1. Comparison with effective length considerations in Eurocode 4

In Figure 7.17, the values given by Eurocode 4 assuming an effective length of 0.5L are compared with model predictions for different relative slenderness.

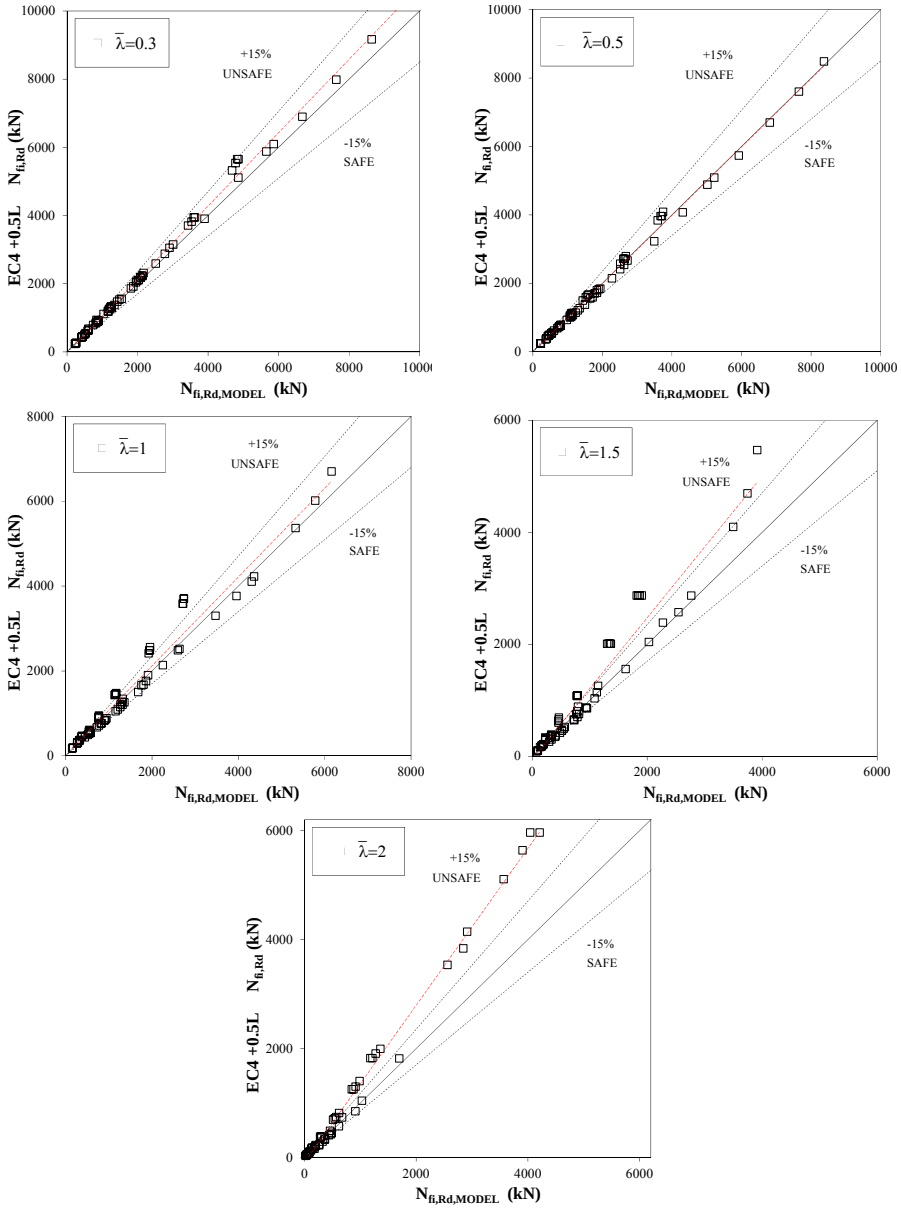

Figure 7.17. Comparison of predictions by EC4 method with 0.5L with fiber model results.

As it can be observed in Figure 7.17, the results obtained by Eurocode 4 show reasonable accuracy for specimens with low slenderness ($\bar{\lambda}$=0.3 and $\bar{\lambda}$=0.5). In these cases, all the points lie in the ±15% limits and the mean is bigger or equal to 1. However, as the relative slenderness of the columns increases, the number of unsafe cases also augments and some results lie beyond the 15% boundary placed at the unsafe side.

The analysis of all the cases can be done by means of Figure 7.18 where all the predictions for an effective length of 0.5L are plotted against fiber model results. This contrast shows that Eurocode 4 general method applied together with the assumption of an effective length of 0.5L leads generally to unsafe results and that this effect is even more visible for specimens with high slenderness for which, in addition, the method produces more disperse values of the error as it can be noticed in Figure 7.19 where the relative error is displayed. For this comparison, the mean obtained is unsafe and has a value of 0.91 (standard deviation σ=0.17).

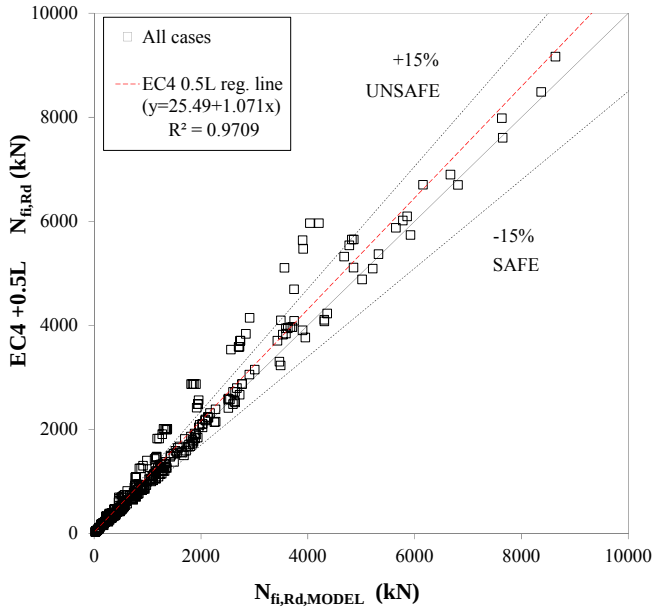

Figure 7.18. All cases. Comparison of predictions given by EC4 method with 0.5L with fiber model results.

As in the previous chapter, the error is calculated by:

$$\xi_{N,fi} = 1 - \frac{N_{fi,Rd,PREDICTED} - N_{fi,Rd,MODEL}}{N_{fi,Rd,MODEL}} \quad (7.2)$$

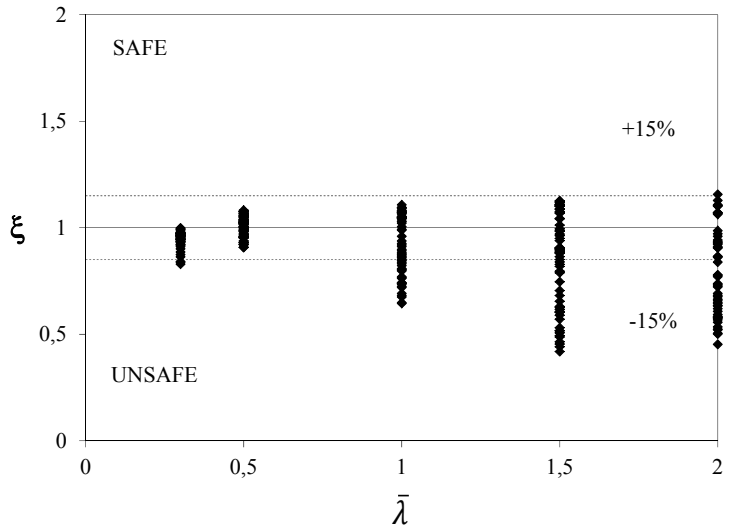

Figure 7.19. Relative error. Comparison between predictions given by EC4 with 0.5L and fiber model simulations.

7.5.2. Comparison with effective length considerations in UK National Annex to Eurocode 4

As it has been exposed before, the UK National Annex suggests the use of an effective length of 0.7L for fire design in the case of specimens continuous at their both ends (Hicks & Newman 2002).

Therefore, the fire buckling resistance for the columns included in the parametric analysis was calculated by following the Eurocode 4 Part 1.2 general method (CEN 2005c) and using stiffness flexural reduction coefficients equal to 1 but assuming an effective length of 0.7L.

The comparison of the calculated values with the fire buckling resistance obtained by means of the frame model is plotted in Figure 7.20 separated in function of the value of the relative slenderness.

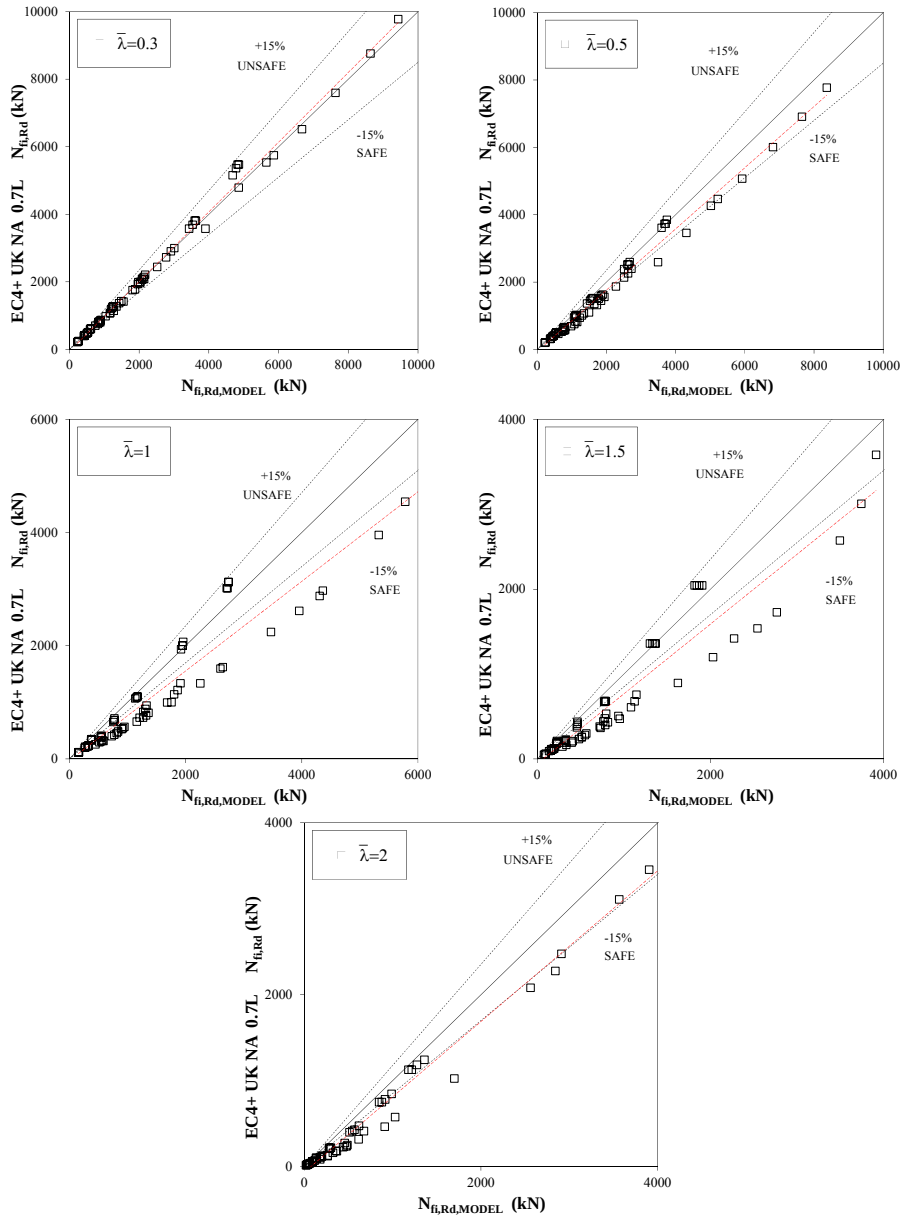

Figure 7.20. Comparison between the prediction given by EC4+ UK NA with 0.7L and numerical simulations

In contrast to what was observed in the previous comparison for 0.5L, the value of 0.7L produces safer results for all the cases and there are no points located outside the 15% limit on the unsafe side. All cases are shown together in Figure 7.21

where the regression line is also included according to the recommendations of CEN-Horizontal Group Fire (CEN 1999b) and where it can be seen that the mean lies on the safe side.

In this case, the improvement in the predictions may be explained by the fact that the tendency of the Eurocode 4 Part 1.2 Clause 4.3.5.1 general method of producing unsafe results when stiffness flexural reduction coefficients equal to 1 are employed, it is compensated by the use of a more conservative effective length for fire design.

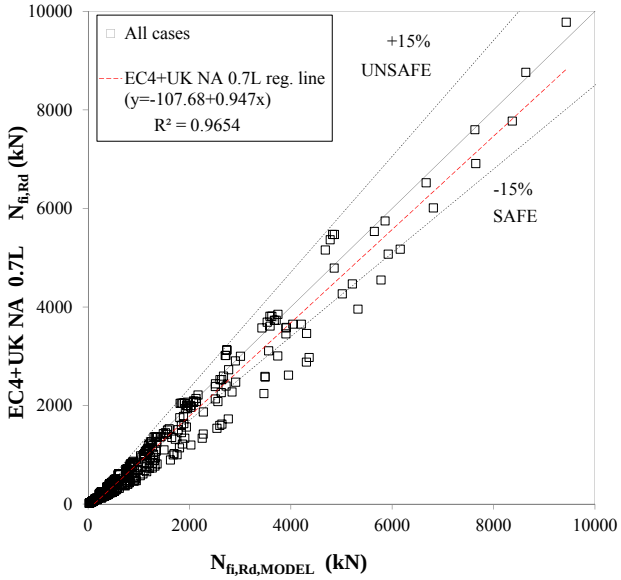

Figure 7.21. All cases. Comparison between the EC4+UK NA with 0.7L and numerical simulations.

The conservative character of the predictions calculated with 0.7L can also be checked in Figure 7.22 where the error is plotted. For this comparison, the mean is clearly safe, with a value of 1.20 (standard deviation σ=0.17).

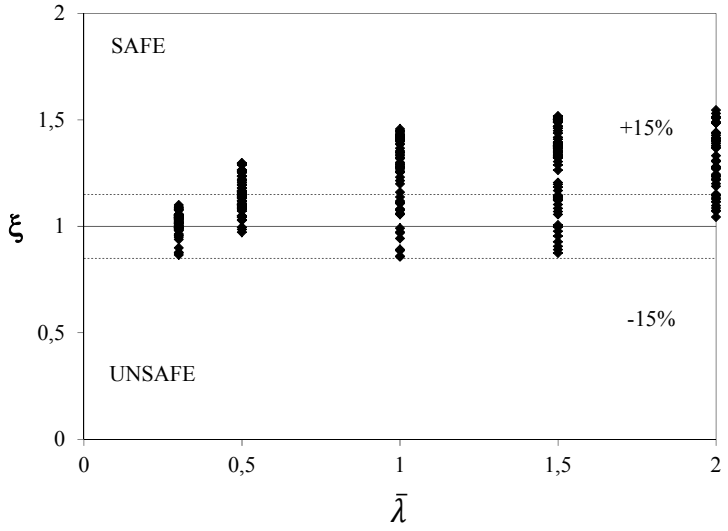

Figure 7.22. Relative error. Comparison between the results of the general method of EC4+UKNA with 0.7L and the numerical simulations.

7.6. ASSESSMENT OF THE PROPOSED METHOD

As a last step, the assessment of the proposed method for predicting the fire buckling resistance of CFT columns within frames was accomplished. In this case, three different alternatives for the effective length were examined. As in the previous case, the effective lengths of 0.5L and 0.7L were used in comparison. Nevertheless, as a novelty, a third option was incorporated in this study which consists of obtaining the effective length of the CFT column as a function of the thermal state of the column $\beta = \beta(T)$.

7.6.1. Proposed method predictions with 0.5L

Predictions of the buckling fire resistance given by the method proposed adopting an effective length of 0.5L according to Eurocode 4 Part 1.2 (CEN 2005c) were compared with numerical simulations. In Figure 7.23 this comparisons is

shown again for the different values of the relative slenderness analyzed in the parametric studies.

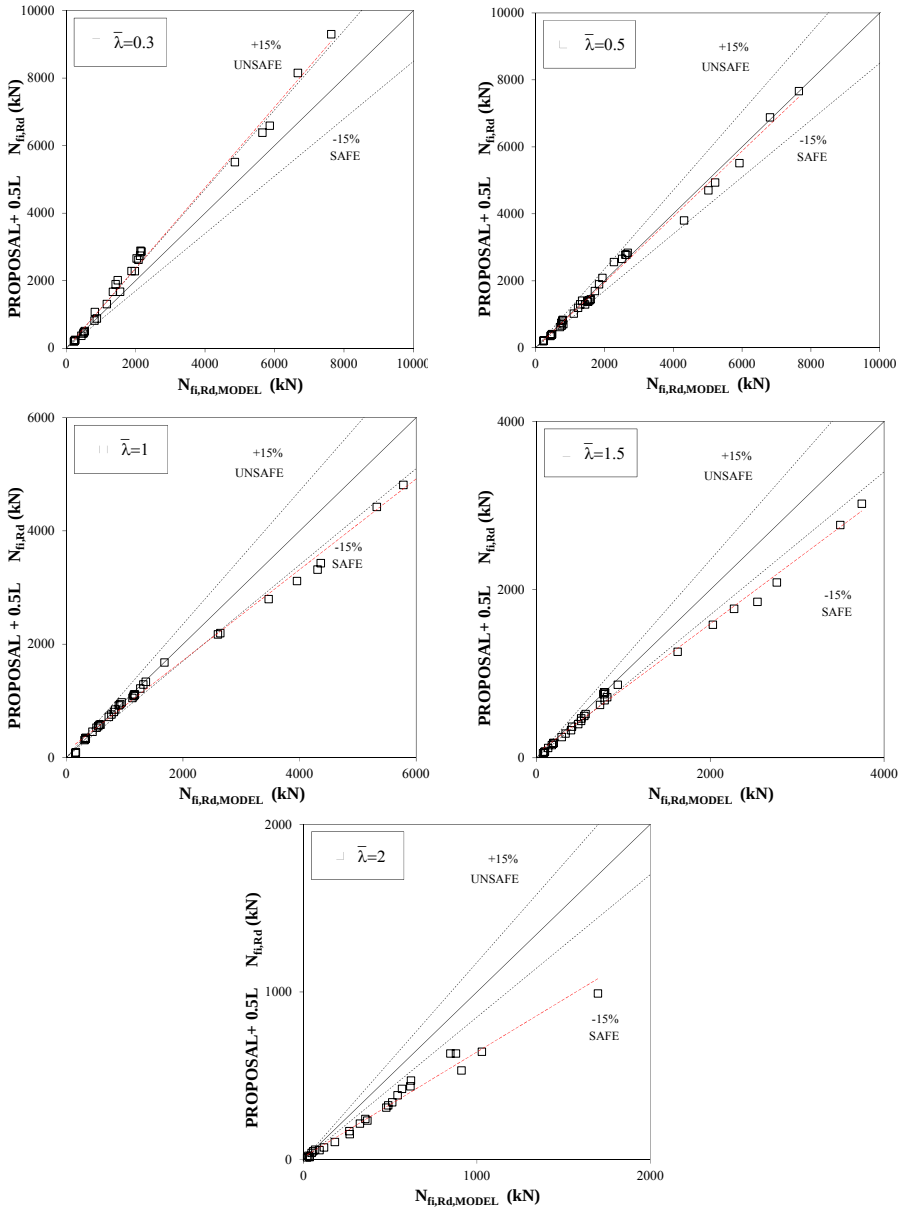

Figure 7.23. Comparison between the proposed method with 0.5L and model results.

When comparison results are analyzed it is detected that adopting a value of the effective length of 0.5L together with the proposed method leads to unsafe results for stub specimens whereas the predictions are considerably safe when the columns have higher slenderness.

If all cases are considered in comparison as it is shown in Figure 7.24, it can be seen that the mean has a value close to unity, μ=1.10 (σ=0.18), since the opposite tendencies observed compensate each other.

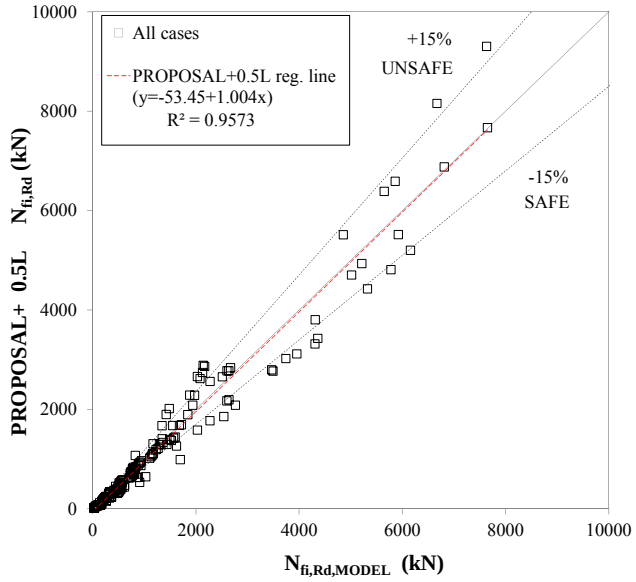

Figure 7.24. All cases. Comparison between the proposed method with 0.5L and numerical simulations.

The change in the character of the predictions is clearly observed in Figure 7.25 where the relative errors are plotted for the different values of the relative slenderness. It is worthy to mention that, since the proposed method is based on a set of equations which is function of the relative slenderness at room temperature, the influence of this aspect is now detected in these results.

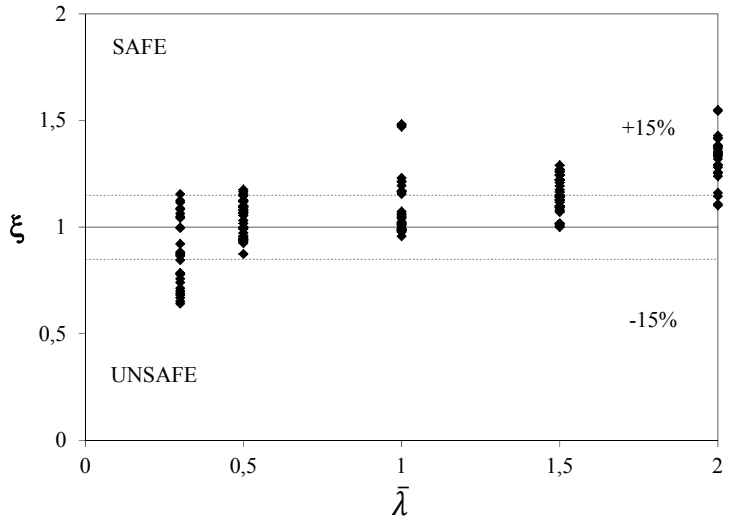

Figure 7.25. Relative error. Comparison between the results of the proposed method with 0.5L and the numerical simulations.

7.6.2. Proposed method predictions with 0.7L

The same procedure was followed to assess the accuracy of the proposed method when an effective length of 0.7L was assumed. Again, a comparison of the results produced by the proposed method with the values given by the numerical simulations for the buckling fire resistance is shown in Figure 7.26. As it can be observed, the predictions show reasonable accuracy for specimens with low slenderness. For those specimens with high values of the relative slenderness taking 0.7L for the effective length in fire is considerably safe.

In Figure 7.27, where all the cases are plotted, it can be observed that assuming 0.7L leads to safe results. These observations can be corroborated in Figure 7.28 where the relative errors are shown. In this case, the mean value is 1.42, clearly safe (standard deviation σ=0.26).

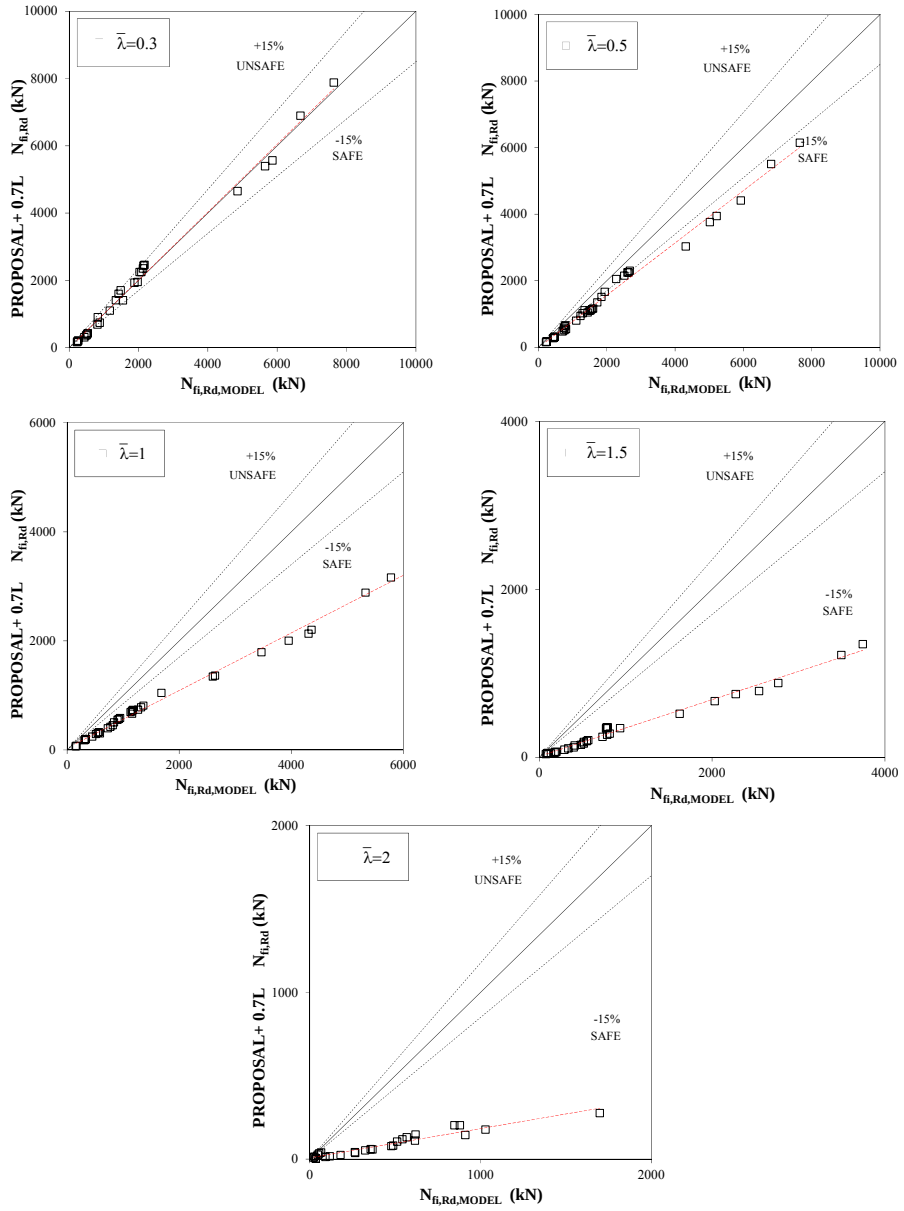

Figure 7.26. Comparison between the proposed method with 0.7L and model results.

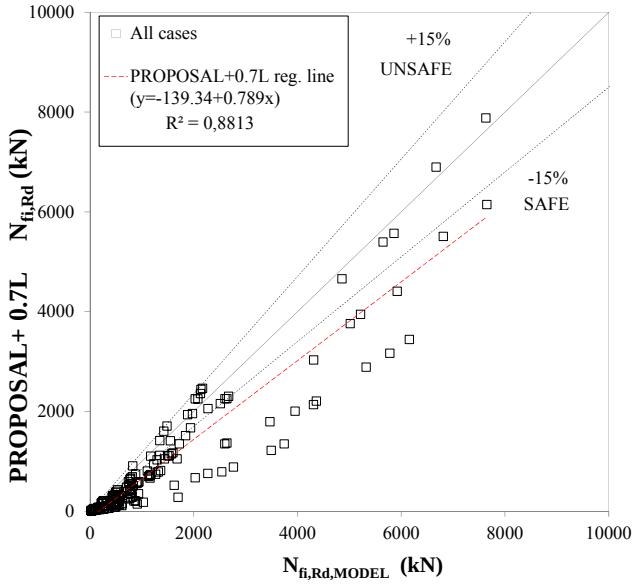

Figure 7.27. All cases. Comparison between the proposed method with 0.7L and numerical simulations.

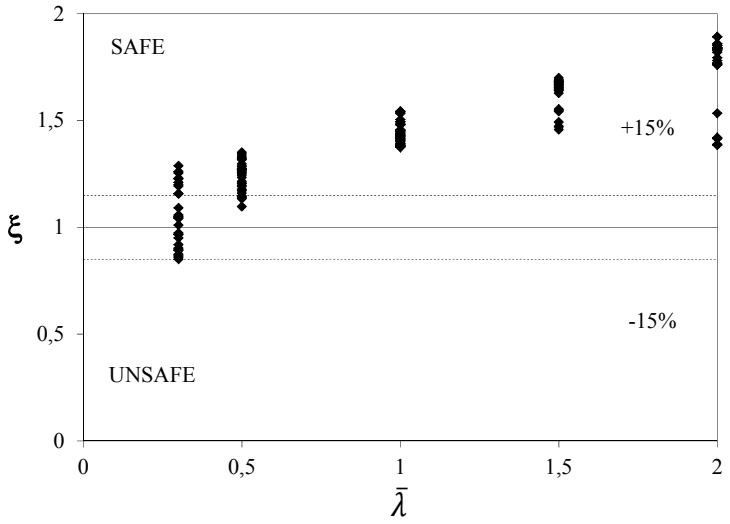

Figure 7.28. Relative error. Comparison between the results of the proposed method with 0.7L and the numerical simulations.

7.6.3. Proposed method predictions with $\beta = \beta(T)$

In order to calculate the temperature dependent effective length, the approach proposed by Wood (1974) for the effective length of columns in multi-story buildings at room temperature is extended to elevated temperatures.

Note that the Wood method (1974) was considered in the Annex E of the draft version of Eurocode 3 dating from 1992 but not included in the last version. Thus, according to Wood (1974), two distribution factors η_1 and η_2 are defined at the top and bottom ends of the column as shown in Figure 7.29 and are calculated by:

$$\eta_1 = \eta_2 = \frac{K_{heated\_column} + K_{column}}{K_{heated\_column} + K_{column} + 2K_{beam}} \tag{7.3}$$

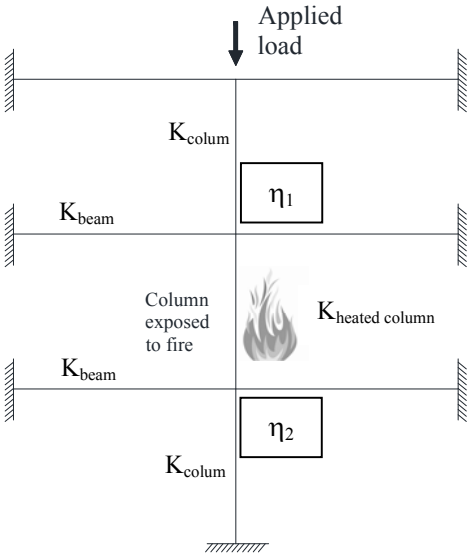

Figure 7.29. Distribution coefficients in Wood method for an intermediate column.

Once the factors are obtained, the effective length ratio is computed by means of the next expression in the case of columns in non-sway frames:

$$\beta = \frac{1 + 0.145(\eta_1 + \eta_2) - 0.265\eta_1\eta_2}{2 - 0.364(\eta_1 + \eta_2) - 0.247\eta_1\eta_2} \tag{7.4}$$

Authors like Gomes et al. (2007) had already employed this approach in the study of the buckling length of steel columns under fire in order to compute the effective length ratio at elevated temperatures by performing stability analysis of a frame.

In this work, the Wood method (1974) is applied to evaluate the predictions in terms of buckling fire resistance when the variation of the effective length in function of the temperature is taking into account. Therefore, in this case the factors η_1 and η_2 become dependent on the thermal state of the CFT columns for a given time of fire exposure.

Therefore, the buckling fire resistance of the analyzed columns was calculated by means of the proposed method considering the variation along time of the effective length ratio. The same comparisons as before were made, and the results obtained showed a higher dispersion of the predictions than those for the two previous options, although the tendency observed in the results is similar to the presented by the effective length of 0.7L (μ=1.41, σ=0.30). However, in this case, some unsafe points were detected for the lowest slenderness studied. In Figure 7.30 the proposed method predictions assuming the variation of the effective ratio along time are compared with the numerical predictions.

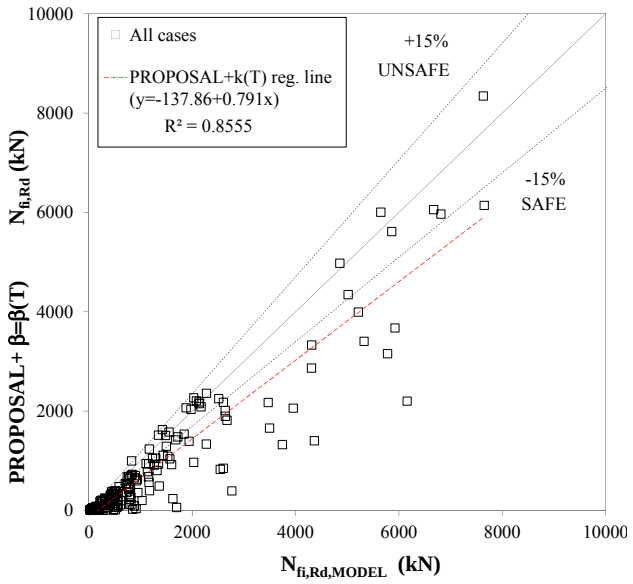

Figure 7.30. All cases. Comparison between the proposed method with β=β(T) and numerical simulations.

In order to observe clearly the accuracy of this combination in function of the relative slenderness, once more the contrast of the predictions with the numerical values are made separately in Figure 7.31.

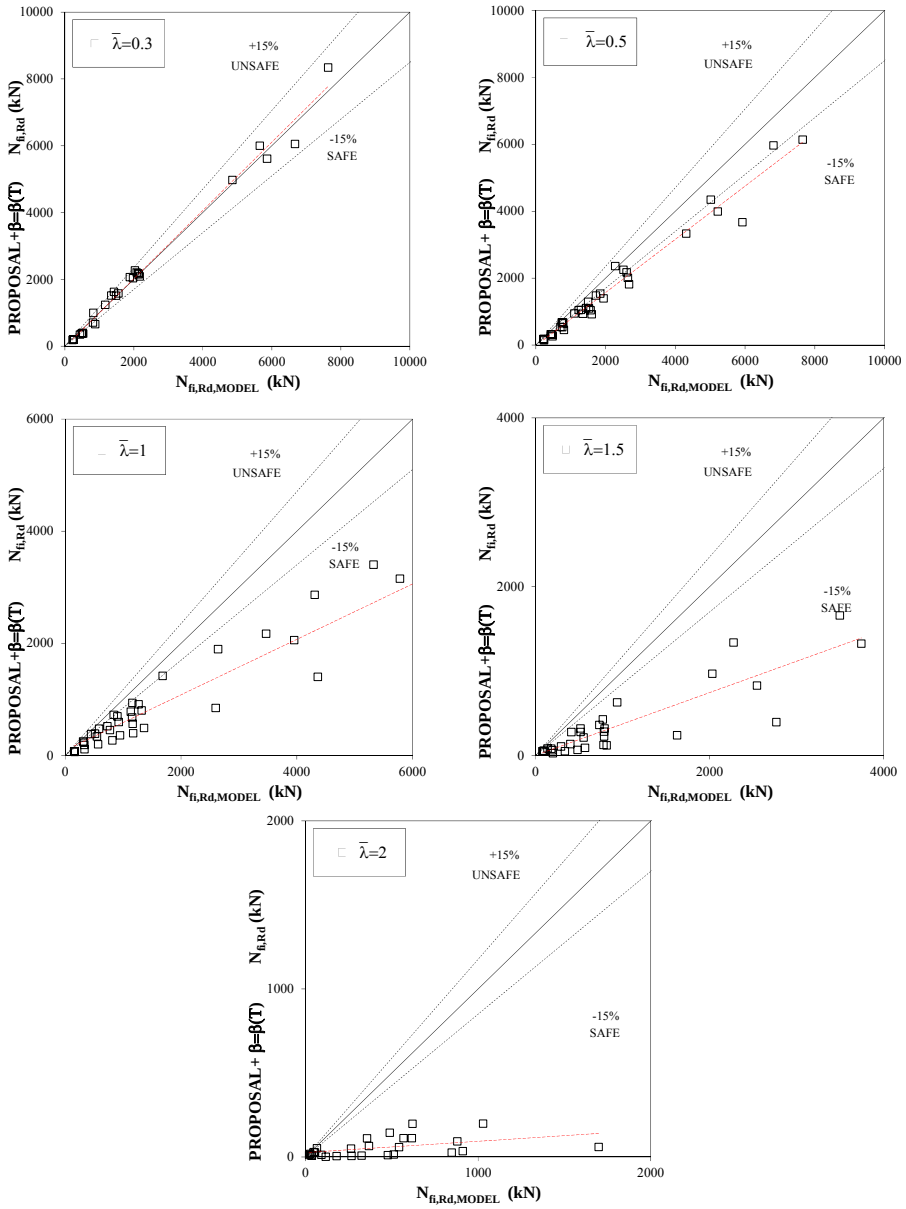

Figure 7.31. Comparison between the proposed method with β=β(T) and model results.

It can be observed that considering the variation of the stiffness ratio together with the method proposed produce very conservative results for columns with a relative slenderness at room temperature equal or higher than 1. This can be observed in Figure 7.32 in terms of the relative error.

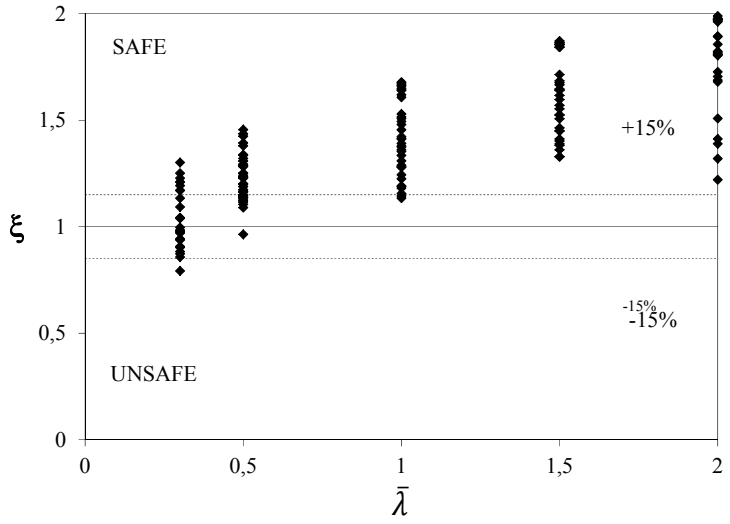

Figure 7.32. Relative error. Comparison between the results of the proposed method with β=β(T) and the numerical simulations.

7.6.4. Proposal for the effective length in fire

After a deep analysis of the results, it was considered that given that the expressions of the buckling correction factor proposed are function of the relative slenderness at room temperature, it would be convenient to adopt the same criteria in this case and recommend the employment of a certain value of the effective length ratio depending on the relative slenderness of the column at room temperature.

Therefore, if the proposed method is used for computing the buckling fire resistance of a CFT column within a frame located at an intermediate floor, the next values for the effective length are suggested to be adopted:

- For $\bar{\lambda}\leq 0.5$, a value of 0.7L
- For $\bar{\lambda}>0.5$, a value of 0.5L

With these combinations of values, the error given by the proposed model when compared to numerical simulations is shown in Figure 7.35. As it can be

observed, the results obtained are more equilibrated that in the previous observations, with a mean value of 1.17 (σ=0.15) lying on the safe side. It is important to note that, once more, the provisions given by the CEN-Horizontal Group Fire (CEN 1999b) have been contrasted and successful results have been obtained.

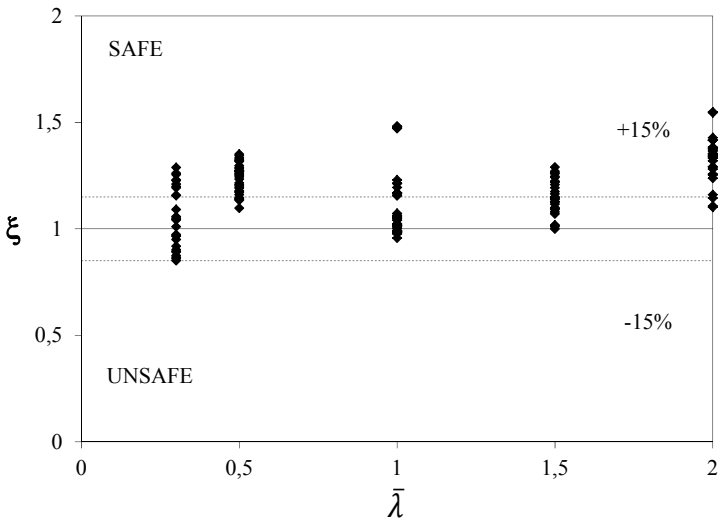

Figure 7.33. Relative error. Comparison between the results of the proposed method with the recommended effective lengths and the numerical simulations.

In Figure 7.34, the comparison between the predicted values of the buckling fire resistance and the values given by the fiber beam model is shown. This graph complements the information about the accuracy of the final proposal since it includes the regression line and its coefficient of determination R^2 for the prediction as recommended by CEN- Horizontal Group Fire (CEN 1999b).

With regard to the range of application of the proposed method, it is important to take into account that it was developed for standard fire periods ranging from R30 to R120. Therefore, for this analysis and comparison only those specimens of the parametric study which presented a value of FRR between these limits were considered.

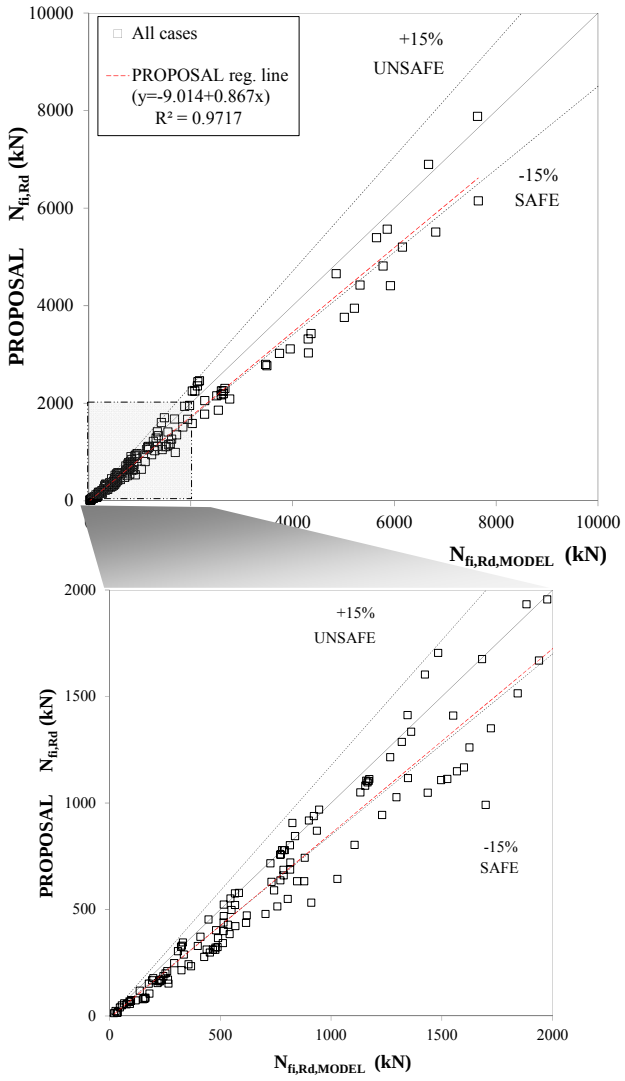

Figure 7.34. Comparison between the proposed method and numerical simulations.

In order to complete the assessment of the simple calculation model developed in this work, the values of the relative error obtained during the development of the method with isolated pinned-pinned columns were plotted jointly with the error calculated for the specimens studied within frames in Figure 7.35. In addition, the corresponding frequency histogram is presented in Figure 7.36. It can be noticed that the calculated errors clearly follow the shape of a normal

distribution with a mean value located in the safe side, according to the criteria proposed by CEN-Horizontal Group Fire (CEN 1999b).

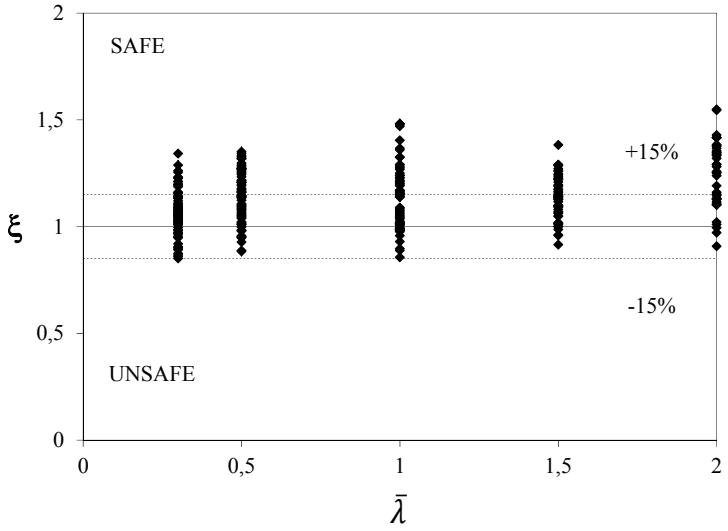

Figure 7.35. Relative error for all the columns studied with respect to numerical simulations.

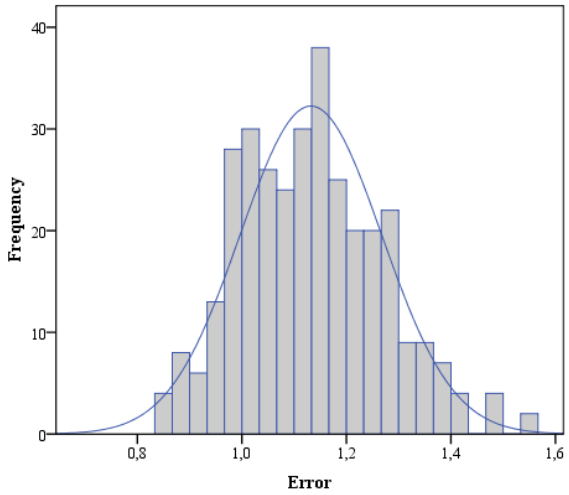

Figure 7.36. Frequency histogram for the prediction error of the proposed method.

Finally, once the predictions given by all the methods considered have been calculated, a comparison can be done for each of the specimens studied as shown in Figure 7.37. Besides, the values of the column force at failure predicted by the numerical model and the actual applied load are also plotted for comparison. In Figure 7.37, this multiple contrast is represented for two of the columns analyzed.

(a)

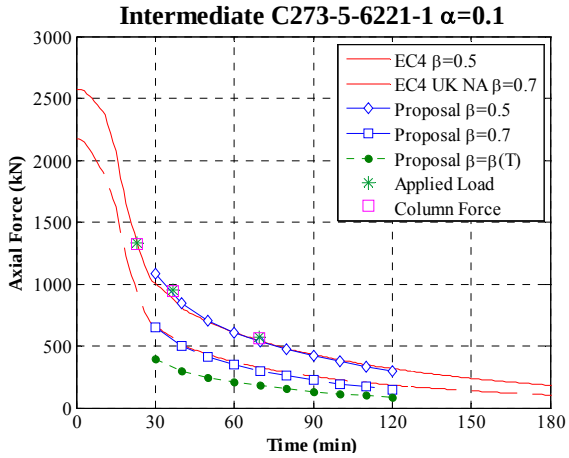

(b)

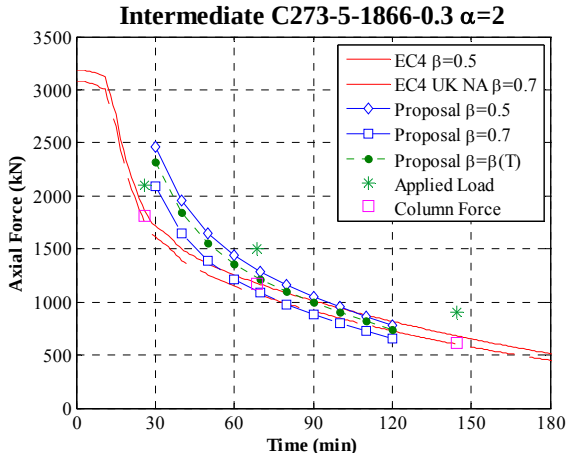

Figure 7.37. Comparison of the numerical simulation with the predictions given by the methods studied.

In this case, two columns with the same cross-section but with different slenderness are shown. It can be observed that for the columns with a relative slenderness of 1 (Figure 7.37a), the proposed method using 0.5L predicts the buckling force with accuracy. On the other hand, for the specimen with low

slenderness (Figure 7.37b), the method proposed combined with an effective length of 0.7L is the best option. Note that the curve defined for the prediction of the proposed method ranges from R30 to R120 since these are its limits of application.

In the same way, in this graph it can be checked that for the specimen within a very rigid frame (Figure 7.37b), the value of the applied load differs considerably from the value of the column force at failure since the surrounding frame is supporting part of this load and thus helping to the CFT column to achieve higher FRR. On the contrary, for the case with a stiffness ratio of 0.1(Figure 7.37a), the values of the applied load and the column force at failure are the same, since the redistribution of the load is not significant in these cases.

These observations corroborate the results of the analysis performed in this chapter and the conclusions extracted about the fire response of CFT columns within frames.

For all the columns studied, these graphs have been elaborated and they are in Annex I available for consultation.

8. CONCLUSIONS

This chapter includes the main conclusions drawn from the work in this thesis. Moreover, proposals for future work are given at the end of the chapter.

8.1. GENERAL CONCLUSIONS

In this work, the fire behavior of axially loaded circular concrete filled tubular columns was investigated through numerical modelling. A realistic thermal model was elaborated and then integrated in the fiber beam model developed. The accuracy of the numerical model was verified by contrasting its predictions with experimental results from own tests and tests available in the literature as well as against the predictions given by a consolidated advanced three-dimensional model. Satisfactory and realistic results in both the fire resistance times and the overall fire response where obtained for axially loaded circular CFT columns with any type of infill: plain, bar-reinforced or fiber reinforced concrete of normal and high strength. The validated model was employed for performing a parametric analysis and, based on the obtained results, developing a set of expressions for computing the cross-sectional temperature of CFT columns and a simple calculation method for CFT columns filled with normal strength concrete. Finally, provided the reduced computational cost of the fiber model presented, it was employed to carry out parametric studies with the aim to investigate the fire behavior of a CFT column within a frame. Comparison of the results produced by the numerical simulations with those obtained by means of the code provisions showed that the current recommendations lead to unsafe results. A new proposal is made by means of the simple calculation model providing accurate results which tend to be conservative. Therefore, it can be concluded that the general aim of this thesis and its corresponding specific objectives have been adequately accomplished in this dissertation.

8.2. SPECIFIC CONCLUSIONS

From the elaboration of the thermal model and the study of the thermal behavior of circular CFT columns the next conclusions were obtained:

- The thermal model is adequately validated against experimental results from different programs and is able to predict the cross-sectional temperatures of unprotected circular CFT columns with any type of infill: plain or fiber reinforced concrete of normal or high strength.
- The existence of a gap between the steel tube and the concrete core when a CFT column is exposed to fire is modeled as a layer of thickness zero in the finite differences thermal model developed. Assuming perfect contact between the two components produces inaccurate results. The adoption of a

constant value of 200 W/m^{2}K for the gap thermal conductance provides satisfactory results.

- The steel temperature evolution follows accurately the tests results. Regarding the internal temperatures of the concrete core, they match the experimental data with the exception of the range of temperatures between 100 and 200 ºC, where the evaporation of moisture occurs.
- For protected circular CFT columns the thermal model has proved to give accurate results of the steel tube temperature, although the number of cases used in validation was limited.
- The beneficial effect of the concrete infill on the thermal response of CFT columns is corroborated. This effect is more noticeable in protected profiles since the external protection delays the heating and prolongs the action of the concrete core acting as a heat sink.
- In CFT columns the fire protection thickness can be reduced in comparison with the needed for hollow steel sections due to the improvement in their thermal behavior.

Some conclusions were drawn from the numerical investigation on the fire behavior of CFT columns:

- The sliding occurring between the two components of the CFT column in fire situation leads to a load transfer process that can be divided in four stages.
- The clear differentiation of stages in the fire response of a CFT column is successfully taken as a basis for the development of a fiber beam model which considers the two components-the steel tube and the concrete core- in parallel connected by links.
- The general behavior characterized by four phases is observed in specimens submitted to moderate load levels. However, the type of failure changes for specimens under high load levels.
- The fiber beam model developed is sufficiently validated against test data from several sources and its capacity to predict the whole fire response of circular CFT columns with any type of infill was proved. Good agreement with the experimental responses was obtained both in terms of axial displacement and fire resistance time.
- The evolution of the fire response given by the fiber beam model is compared with the results of a consolidated advanced three-dimensional model and it is

observed a great agreement between the predictions of both models. However, the computational cost of the fiber beam model is significantly lower.

After the calibration of the thermo-mechanical model the next recommendations are obtained:

- The use of four fiber beam elements with co-rotational formulation, distributed plasticity and a mixed interpolation iterative scheme is the combination that best works with a satisfactory accuracy to computing time ratio.
- For a CFT column under fire, it can be considered that no friction exists between the steel tube and the concrete core. The inner links connecting the elements longitudinally in the model can be assumed to have a stiffness value ranging from 0 to 10 kN/m.
- The recommended value of L/1000 for the initial imperfection of the columns provides precise results.
- Although the preferred option is to introduce in the model the actual concrete content of moisture of the specimens reported in literature, a value of 3% and a value of 10% are assumed with good results for specimens with siliceous and calcareous aggregates respectively.
- For steel, the Eurocode 3 Part 1.2 (CEN 2005b) mechanical model gives an accurate response. For concrete, the model presented by Lie (1984) is the one which best reproduces the whole fire response of CFT columns when compared to the model from Eurocode 2 Part 1.2 (CEN 2004a) which gives conservative results.
- The recommendation made by authors like Hong & Varma (2009) or Espinos et al. (2010) of adopting the value of $\alpha_c = 6x10^{-6}$ $ºC^{-1}$ for the thermal expansion of concrete gives accurate predictions. In the case of steel, the Eurocode 3 Part 1.2 (CEN 2005b) thermal expansion model produces very precise results.

From the parametric studies and the development process of the simple calculation method, the main conclusions extracted are the following:

- The necessity of a simple procedure for the daily practice to compute the temperature field of CFT sections is detected.

- A set of expressions to calculate the cross-sectional temperature distribution of unprotected CFT columns filled with normal strength concrete is proposed. The method is successfully validated against numerical simulations and against real tests data. Since the expressions are elaborated under the guidelines of the CEN-Horizontal Group Fire (CEN 1999b) the predictions tend to be safe.
- An equivalent concrete core cross-section at room temperature can be used to represent the whole concrete core so as to obtain the same fire resistance of the column as by using the real non uniform temperature distribution. A expression for the radius of the equivalent concrete core cross-section is proposed given accurate results.
- With the adoption of the equivalent concrete core cross-section, the general method from Eurocode 4 Part 1-1 (CEN 2004b) for composite members at room temperature can be employed as a reference for the elaboration of a simple calculation model for CFT columns by the inclusion of a buckling correction factor.
- The analysis of the results of the parametric studies shows a change in the tendency of the data around a relative slenderness of 0.5 so that the expressions proposed in the calculation method for obtaining the buckling correction factor reflects this division.
- Good agreement is shown between the proposed calculation method and the numerical simulations. When compared to real fire tests on CFT columns, the proposed method estimates satisfactorily the buckling fire resistance of the columns, providing in most cases safe predictions according to the guidelines of the CEN-Horizontal Group Fire (CEN 1999b).

Given the reduced computational cost of the fiber beam model developed, it allows for its application to model the fire response of CFT columns within frames in order to study their integration with the surrounding structure though a parametric analysis. From this task, the next conclusions were drawn:

- The different effect of the axial and the rotational restraint described by authors like Wang (199) is corroborated.
- The rotational restraint affects positively the fire response of CFT columns by changing its boundary conditions. On the contrary, the axial restraint changes the load conditions of the column since restraining forces appear when the columns try to elongate.

- The subframe model employed in the parametric study allows for the creation of new loading paths which, in turn, permit a redistribution of the applied load which is enhanced as the heated CFT column losses its mechanical properties. The load is gradually transferred from the CFT column to the unheated surrounding structure and the moment of failure is considerably delayed. This effect is more notable for higher values of the stiffness ratio.
- The critical time is a reference time defined as the moment when the restraining forces become zero. For a specific column under a certain load level, the critical time does not vary with the rigidity of the frame.
- When the numerical results for the columns simulated in restraining frames are compared with the fire resistance times obtained for the corresponding isolated columns simulated as pinned-pinned, a generalized increment in the fire resistance times is observed.
- In general, when the buckling fire resistances of the assembled columns are compared to those given by the numerical simulations of isolated pinned-pinned columns analyzed under different effective length values, the results obtained for 0.5L tend to be unsafe and the adoption of 0.7L produce safer results. If more realistic predictions are desirable, the variation in the loading condition of a CFT column within a frame has to be considered.

The values of the buckling fire resistance obtained by the general method of Eurocode 4 Part 1.2 in its Clause 4.3.5.1(CEN 2005c) were compared with the numerical simulations of CFT columns within frames. Also, an assessment of the proposed simple method was accomplished. The next was concluded:

- If the Eurocode 4 Part 1.2 value of 0.5L for the effective length is employed, unsafe results are generally obtained. On the contrary, if the value of 0.7L suggested in the UK National Annex (Hicks & Newman 2002) is adopted, conservative predictions are produced.
- Predictions of the buckling fire resistance given by the proposed simple method show reasonable agreement with the results given by numerical simulation of the assembled columns. Due to the division of the method in function of the relative slenderness, the effective length value recommended also varies with this parameter. For $\overline{\lambda} \leq 0.5$ a value of 0.7L produces best results; for $\overline{\lambda} > 0.5$, an effective length of 0.5L is suggested.

8.3. FUTURE WORK

Once the results of this research work have been analyzed, some recommendations on future work can be proposed since by a single dissertation it is not possible to cover the extension of the problem studied if all the different scenarios for isolated and columns within frames want to be examined.

Firstly, the numerical model could be extended to protected columns provided that the thermal model for protected CFT sections is already developed and can be integrated in the thermo-mechanical model. Also, the thermal model should be extended to cover other types of protection materials. This would permit to perform an extensive study on the effects of the fire protection in the behavior of CFT columns with different types of infill and boundary conditions.

Since this thesis was limited to axially loaded columns, the analysis of the fire response of eccentrically loaded columns is a task to be addressed as future work. Thus, following the same methodology as in this work, the fiber beam model should be validated against experimental results from fire tests on CFT columns subjected to eccentric loads with the aim to perform the subsequent parametric analysis covering the list of parameters already considered in this thesis.

With respect to the set of expressions for computing the cross-sectional temperature of CFT sections, its application was restricted to circular CFT columns of normal strength so its extension to high strength concrete specimens and to columns filled with fiber reinforced concrete would be interesting in order to facilitate their design procedure.

In other to complete the fire design method proposed, it should be considered the possibility to extend it to bar-reinforced CFT columns. Parametric analyses should be carried out with the aim of accounting for all the parameters affecting the fire behavior and their usual range of values. Currently, the applicability of the method is restricted to fire resistance times ranging from the standard fire period of R30 to R120, but it is not validated beyond these. Thus, it should be extended to below and above the current limits to be able to cover any time of fire resistance, especially to higher fire periods since reinforcing bars increase considerably the FRR of CFT columns.

Regarding the study of the effect of axial and rotational restraints on the fire response of a CFT column within a frame, the analysis in this thesis was limited to unreinforced CFT columns located at an intermediate story. Therefore, to complete the conclusions drawn in this thesis, the pertinent study on CFT columns placed at

the top floor of frames should be carried out. An extensive parametric analysis should be executed with the aim of extracting solid conclusions and developing a new proposal which should be added to the one made in this work regarding the effective length in fire.

In relation to this issue, in the restraining frame model employed in this thesis, the beams adjacent to the heated column were assumed to be perfectly linear elastic which may constitute a limitation of the subframe model. Once the behavior of a CFT column in fire within a frame has been studied in depth and clear conclusions have been extracted, the behavior of the adjacent cold beams can be modified in order to consider the possible plastic behavior of the beams.

As a final point, it should be also recommendable the future expansion of the studies carried out in this work to other cross-section shapes and also to new configurations such as double-tube or double-skin tubular columns whose applicability in the building industry has increased recently concurrently with the investigations on their behavior at room and elevated temperature.

REFERENCES

ABAQUS. 2010. *ABAQUS/Standard Version 6.10 User's Manual: Volumes I-III*. Pawtucket, Rhode Island: Hibbitt, Karlsson & Sorensen, Inc.

Arcelor Mittal (AM). 2004. Case Studies: Car park of the Carrefour Hypermarket Aix. www.constructalia.com

Arcelor Mittal (AM). 2005. Case Studies: Montevideo. www.constructalia.com

Arcelor Mittal (AM). 2008. Case Studies: Caal ArcelorMittal Steel Centre. www.constructalia.com

Arcelor Mittal (AM). 2010. Case Studies: Rehabilitating two student accommodation sets in Toulouse. www.constructalia.com

ACI. 2007. *ACI 216.1M-07: Standard Method for Determining Fire Resistance of Concrete and Masonry Construction Assemblies*. Detroit, USA: American Concrete Institute.

AFNOR. 2007. *Calcul simplifié de la résistance au feu des profils creux remplis de béton exposés aux conditions d'incendie normalisé. Annexe PCRB*, pp. 9-16, NF-EN 1994-1-2/NA. Paris, France: Association Française de Normalisation.

Al-Khaleefi AM, Terro MJ, Alex AP, Wang Y. 2002. Prediction of fire resistance of concrete filled tubular steel columns using neural networks. *Fire Safety Journal* 37(4):339-352.

Ali F, O'Connor D. 2001. Structural performance of rotationally restrained steel columns in fire. *Fire Safety Journal.* 36: 679-691.

Anderberg Y, Thelandersson S. 1976. *Stress and deformation characteristics of concrete, 2-experimental investigation and material behaviour model. Bulletin 54*. Lund, Sweden: Lund Institute of Technology.

Aribert JM, Renaud C, Zhao B. 2008. Simple fire design for composite hollow-section columns. *Structures & Buildings* 161:325-336.

ASCE. 1999. *ASCE/SFPE 29-99: Standard Calculation Method for Structural Fire Protection*. Reston, USA: American Society of Civil Engineers.

Associated Factory Mutual Fire Insurance Companies (AFMFIC). 1917. *Fire tests of building columns*. Chicago, Illinois: Underwriters' Laboratories.

Association of New Urban Housing Technology (ANUHT). 2004. *Fire resistance design of non-insulated CFT columns – Guidelines, technical explanations and design examples* (in Japanese).

Ayoub A, Filippou FC. 2000. *Mixed formulation of nonlinear steel-concrete composite beam element*. Journal of Structural Engineering (ASCE). 126: 371-381.

ASTM. 1990. *Standard ASTM E119-88: Standard methods of fire test of building construction and materials*. Philadelphia, Pa: American Society for Testing and Materials.

Bailey C. 2000. Effective lengths of concrete-filled steel square hollow sections in fire. *Structures and Buildings* 140(2):169-178.

Beneš M, Štefan R. 2015. Hygro-thermo-mechanical analysis of spalling in concrete walls at high temperatures as a moving boundary problem. *International Journal of Heat and Mass Transfer* 8: 110–134.

Bergmann R, Matsui C, Meinsma C, Dutta D. 1995. *Design guide for concrete filled hollow section columns under static and seismic loading*. Köln, Germany: Comité International pour le Développement et l'Etude de la Construction Tubulaire (CIDECT).

Bianco M, Bilardi G, Pesavento F, Pucci G, Schrefler BA. 2003. A frontal solver tuned for fully coupled non-linear hygro-thermo-mechanical problems. *International Journal for Numerical Methods in Engineering* 57:1801-1818.

Buchanan AH. 2001. *Structural design for fire safety*. Chichester, England: John Wiley & Sons Ltd.

Canadian Commission on Building and Fire Codes. 2005. *NBCC, National Building Code of Canada.* National Research Council of Canada, Ottawa, Canada.

CEN. 1999a. *EN 1363-1: Fire resistance tests. Part 1: General requirements*. Brussels, Belgium: Comité Européen de Normalisation.

CEN 1999b *Document 99/130. Euroccodes-Fire Parts. Proposal for a methodology to check the accuracy of assessment methods.* TC-250-Horizontal Group Fire. Comité Européen de Normalisation.

CEN. 2002. *EN 1991-1-2, Eurocode 1: Actions on structures, Part 1.2: General actions - Actions on structures exposed to fire*. Brussels, Belgium: Comité Européen de Normalisation.

CEN. 2004a. *EN 1992-1-2, Eurocode 2: Design of concrete structures, Part 1.2: General rules – Structural fire design*. Brussels, Belgium: Comité Européen de Normalisation.

CEN. 2004b. *EN 1994-1-1, Eurocode 4: Design of composite steel and concrete structures. Part 1-1: General rules and rules for buildings*. Brussels, Belgium: Comité Européen de Normalisation.

CEN. 2005a. *EN 1993-1-1, Eurocode 3: Design of steel structures. Part 1-1: General rules and rules for buildings*. Brussels, Belgium: Comité Européen de Normalisation.

CEN. 2005b. *EN 1993-1-2, Eurocode 3: Design of steel structures, Part 1.2: General rules – Structural fire design*. Brussels, Belgium: Comité Européen de Normalisation.

CEN. 2005c. *EN 1994-1-2, Eurocode 4: Design of composite steel and concrete structures, Part 1.2: General rules* - Structural fire design. Brussels, Belgium: Comité Européen de Normalisation.

CEN. 2006. *EN 10210-2. Hot finished structural hollow sections of non-alloy and fine grain steels. Part 2: Tolerances, dimensions and sectional properties*. Brussels, Belgium: Comité Européen de Normalisation.

Chabot M, Lie TT. 1992. *Experimental studies on the fire resistance of hollow steel columns filled with bar-reinforced concrete. Internal report No. 628*. Ottawa, Canada: Institute for Research in Construction, National Research Council of Canada (NRCC).

Chen WF. 1982. *Plasticity in reinforced concrete*. McGraw-Hill.

Chung K, Park S, Choi S. 2008. Material effect for predicting the fire resistance of concrete-filled square steel tube column under constant axial load. *Journal of Constructional Steel Research* 64:1505-1515.

Chung K, Park S, Choi S. 2009. Fire resistance of concrete filled square steel tube columns subjected to eccentric axial load. *Steel Structures* 9(1):69-76.

CIDECT. 1970. *Monograph No. 1: Concrete filled hollow section steel columns*. Design manual, British edition.

CIDECT. 1979. *Monographie No. 5: Calcul des poteaux en prolils creux remplis de beton.*

COMETUBE. 1976. *Fire resistance of structural hollow sections. Cometube research. CIDECT programme 15A. Final report.*

Correia AM, Rodrigues JP. 2012. Fire resistance of steel columns with restrained thermal elongation. *Fire Safety Journal* 50: 1-11.

Correia AM, Rodrigues JP, Gomes F. 2013. A simplified calculation method for fire design of steel columns with restrained thermal elongations. *Computers and Structures* 116: 20-34.

Corus. 2007. *Celsius 355 Ovals - Sizes and Capacities, EC3 Version*. Corus Tubes - Structural & conveyance business.

Couto C, Vila Real P, Lopes N, Rodrigues JP. 2013. Buckling analysis of braced and unbraced steel frames exposed to fire. *Engineering Structures* 49: 541-559.

Crisfield MA. 1991. *Non-linear finite element analysis of solids and structures.* Vol. 1, Wiley, New York.

CSA. 1994. *CAN/CSA-S16.1-94. Limit States Design of Steel Structures*. Toronto, Canada: Canadian Standards Association.

Dai XH, Lam D. 2012. Shape effect on the behaviour of axially loaded concrete filled steel tubular stub columns at elevated temperature. *Journal of Constructional Steel Research* 73:117-127.

DBJ. 2003. *DBJ13-51-2003: Technical specification for concrete-filled steel tubular structures* (in Chinese). Fuzhou: The Construction Department of Fujian Province.

Denavit MD, Hajjar JF. 2010. *Nonlinear seismic analysis of circular concrete-filled steel tube members and frames*. Report No. NSEL-023. Department of Civil and Environmental Engineering. University of Illinois at Urbana-Champaign.

Diederichs U. 1987. *Modelle zur beschreibung der betonverformung bei instantionaren temperaturen.* In abschluβkolloquium bauwerke unter brandeinwirkung. Technische Universität Braunschweig.

Ding J, Wang YC. 2008. Realistic modelling of thermal and structural behaviour of unprotected concrete filled tubular columns in fire. *Journal of Constructional Steel Research* 64:1086-1102.

Drucker DC, Prager W. 1952. Soil mechanics and plastic analysis or limit design. *Quarterly of Applied Mathematics* 10:157–165.

Dusinberre GM. 1961. *Heat transfer calculations by finite differences*. Scranton, Pa: International Textbook Company.

ECCS. 1988. *Calculation of the fire resistance of centrally loaded composite steel-concrete columns exposed to the standard fire*. Technical note. ECCS

Technical Committee 3 – Fire Safety of Steel Structures. Brussels, Belgium: European Convention for Constructional Steelwork (ECCS).

Ellobody E, Young B. 2010. Investigation of concrete encased steel composite columns at elevated temperatures. *Thin-Walled Structures* 48:597-608.

Ellobody E, Young B, Lam D. 2006. Behaviour of normal and high strength concrete-filled compact steel tube circular stub columns. *Journal of Constructional Steel Research* 62:706-715.

Espinos A, Gardner L, Romero M, Hospitaler A. 2011. Fire behaviour of concrete filled elliptical steel columns. *Thin-Walled Structures* 49(2):239-255.

Espinos A, Romero ML, Hospitaler A. 2010. Advanced model for predicting the fire response of concrete filled tubular columns. *Journal of Constructional Steel Research* 66(8-9):1030-1046.

Espinos A, Romero ML, Hospitaler A. 2012. Simple calculation model for evaluating the fire resistance of unreinforced concrete filled tubular columns. *Engineering Structures* 42:231-244.

Espinos A, Romero ML, Hospitaler A. 2013. Fire design method for bar-reinforced circular and elliptical concrete filled tubular columns. *Engineering Structures* 56:384-395.

Espinos A, Romero ML, Portolés JM, Hospitaler A. 2014. Ambient and fire behavior of eccentrically loaded elliptical slender concrete-filled tubular columns. *Journal of Constructional Steel Research* 100: 97:107.

Espinos A, Romero ML, Serra E, Hospitaler A. 2015a. Experimental investigation on the fire behaviour of rectangular and elliptical slender concrete-filled tubular columns. *Thin-Walled Structures* 93:137–148.

Espinos A, Romero ML, Serra E, Hospitaler A. 2015b. Circular and square slender concrete-filled tubular columns under large eccentricities and fire. *Journal of Constructional Steel Research* 110: 90–100.

FIB. 2010. *Model Code 2010*. Lausanne, Switzerland: Fédération Internationale du Béton.

Filippou FC. 2011. Lecture notes from *CE221 Nonlinear Structural Analysis*. University of California at Berkeley.

Filippou FC, Constantinides M. 2004. *FEDEASLab. Getting started guide and simulation examples.* Technical report NEESgrid-2004-22. Department of Civil and Enviromental Engineering. University of California at Berkeley.

Filippou FC, Fenves GL. 2004. "*Methods of analysis for earthquake-resistant structures".* Earthquake Engineering: Form engineering seismology to performance-based engineering, Y. Bozorgnia and VV. Bertero, eds., CRC, Boca triton, Fla., Chapter 6.

Franssen JM. 2003. *SAFIR - A thermal/structural program modeling structures under fire*. Proceedings of the NASCC Conference. American Institute for Steel Construction, Baltimore.

Galambos TV. 1998. *Guide to stability design criteria for metal structures*. Fifth edition. New York: John Wiley and Sons Inc.

Gawin D, Majorana CE, Schrefler BA. 1999. Numerical analysis of hygro-thermal behaviour and damage of concrete at high temperature. *Mechanics of Cohesive-Frictional Materials* 4: 37-74.

Gawin D, Pesavento F, Schrefler BA. 2003. Modelling of hygro-thermal behaviour of concrete at high temperature with thermo-chemical and mechanical material degradation. *Computers Methods in Applied Mechanics and Engineering* 192: 1731–1771.

Ghojel J. 2004. Experimental and analytical technique for estimating interface thermal conductance in composite structural elements under simulated fire conditions. *Experimental Thermal and Fluid Science* 28:347-354.

Gomes F, Providencia e Costa P, Rodrigues JP, Neves I. 2007. Buckling length of a steel column for fire design. *Engineering Structures* 29: 2497-2502.

Grandjean G, Grimault JP, Petit L. 1980. *Determination de la duree au feu des profils creux remplis de* beton. CIDECT Research Project 15B–80/10. Cologne, Germany: Comité International pour le Développement et l'Etude de la Construction Tubulaire.

Guiaux P, Janns J. 1970. *Comportement au flambement des colonnes constituées de tubes en acier remplis de béton*. CRIF, MT 65.

Hajjar JF, Gourley BC. 1997. *A cyclic nonlinear model for concrete-filled tubes. 1. Formulation.* Journal of Structural Engineering (ASCE) 123: 736-744.

Hajjar JF, Gourley BC. 1997. *A cyclic nonlinear model for concrete-filled tubes. 1. Formulation.* Journal of Structural Engineering (ASCE) 123: 736-744.

Hajjar JF, Molodan A, Schiller PH. 1998a. *A distributed plasticity model for cyclic analysis of concrete-filled steel tube beam-columns and composite frames.* Engineering Structures. 20: 398-412.

Hajjar JF, Schiller PH, Molodan A. 1998b. *A distributed plasticity model for concrete-filled steel tube beam-columns with interlayer slip.* Engineering Structures. 20: 663-676.

Han LH. 1998. Fire resistance of concrete filled steel tubular columns. *Advances in Structural Engineering* 2(1):35-39.

Han LH. 2000. *Concrete filled steel tubular structures*. Peking: Science Press.

Han LH. 2001. Fire performance of concrete filled steel tubular beam-columns. *Journal of Constructional Steel Research* 57(6):697-711.

Han LH, Chen F, Liao FY, Tao Z, Uy B. 2013. Fire performance of concrete filled stainless steel tubular column. *Engineering Structures* 36: 165-181.

Han LH, Huo JS. 2003. Concrete-filled hollow structural steel columns after exposure to ISO-834 fire standard. *Journal of Structural Engineering (ASCE)* 129(1):68-78.

Han LH, Huo JS, Wang YC. 2005. Compressive and flexural behaviour of concrete filled steel tubes after exposure to standard fire. *Journal of Constructional Steel Research* 61:882-901.

Han LH, Li W, Bjorhovde R. 2014. Developments and advanced applications of concrete-filled steel tubular (CFST) structures: Members. *Journal of Constructional Steel Research* 100: 211-228.

Han LH, Lin XK. 2004. Tests on cyclic behaviour of concrete-filled hollow structural steel columns after exposure to the ISO-834 standard fire. *Journal of Structural Engineering (ASCE)* 130(11):1807-1819.

Han LH, Wang WH, Yu HX. 2010. Experimental behaviour of reinforced concrete (RC) beam to concrete-filled steel tubular (CFST) column frames subjected to ISO-834 standard fire. *Engineering Structures* 32: 3130-3144.

Han LH, Wang WH, Yu HX. 2012. Analytical behaviour of RC beam to CFST column frames subjected to fire. *Engineering Structures* 36: 394-410.

Han LH, Zhao XL, Yang YF, Feng JB. 2003a. Experimental study and calculation of fire resistance of concrete-filled hollow steel columns. *Journal of Structural Engineering (ASCE)* 129(3):346-356.

Han LH, Yang YF, Xu L. 2003b. An experimental study and calculation on the fire resistance of concrete filled SHS and RHS columns. *Journal of Constructional Steel Research* 59(4):427-452.

Harada K. 2004. Actual state of the codes on fire design in Japan. *Proceedings of the Workshop "Fire Design of Concrete Structures: What now? What next?"*. Milan, Italy, December 2-3, 2004. Brescia, Italy: Starrylink Editrice.

Hass R, Ameler J, Zies H. 2000. *Fire Resistance of Hollow Section Composite Columns with High Strength Concrete Filling. CIDECT Research Project 15P-12/00*. Brunswick, Germany: Comité International pour le Développement et l'Etude de la Construction Tubulaire.

Hicks SJ, Newman GM. 2002. *Design guide for SHS concrete filled columns.* Corus Tubes.

Hirakawa K, Saburi K, Kushima S, Kojima K. 2014. Performance-based design of a 300 m vertical city "ABENO HARUKAS". *International Journal of High-Rise Buildings* 3(1): 35-48.

Hognestad E. 1951. A study of combined bending and axial load in reinforced concrete members. *University of Illinois Engineering Experiment Station Bulletin* No. 399. Urbana, Illinois.

Hong S. 2007. *Fundamental behaviour and stability of CFT columns under fire loading*. PhD thesis. West Lafayette, Indiana: Purdue University.

Hong S, Varma AH. 2009. Analytical modeling of the standard fire behavior of loaded CFT columns. *Journal of Constructional Steel Research* 65:54-69.

Hu HT, Huang CS, Wu MH, Wu YM. 2003. Nonlinear analysis of axially loaded concrete-filled tube columns with confinement effect. *Journal of Structural Engineering (ASCE)* 129(10):1322-1329.

Hu X, Guo H, Yao Y. 2015. Interaction approach for concrete filled steel tube columns under fire conditions. *Journal of Building Engineering* 3:144-154.

Ibañez C, Romero ML, Hospitaler A. 2013. Fiber beam model for fire response simulation of axially loaded concrete filled tubular columns. *Engineering Structures.* 56: 182-193.

Ibañez C, Aguado JV, Romero ML, Espinos A, Hospitaler A. 2015. Fire design method for concrete filled tubular columns based on equivalent concrete core cross-section. *Fire Safety Journal.* 78: 10-23.

Iding RH, Bresler B, Nizamuddin Z. 1977. FIRES-T3. *A computer program for the fires response of structures – Thermal. Report No. UCB-FRG 77-15*. University of California, Berkeley.

Ikeda K, Ohmiya Y. 2009. Fire safety engineering of concrete-filled steel tubular column without fire protection. *Fire Science and Technology* 28(3):106-131.

Imani R, Bruneau M, Mosqueda G. 2015.Simplified analytical solution for axial load capacity of concrete-filled suble-skin tube (CFDST) columns subjected to fire. *Engineering Structures.*102: 156-175.

Ingberg SH, Sale PD. 1926. *Proceedings of the American Society for Testing and Materials* 26, II.

Ishikawa I, Fuchita Y, Endo F, Hirata T. 2010.Design and construction of new main office of OBAYASHI CORPORATION Technical Research Institute. *Concrete Journal* 48(10): 28-33.

ISO. 1980. *ISO 834: Fire resistance tests, elements of building construction*. Switzerland: International Standards Organisation.

Jeffers AE, Sotelino ED. 2009. Fiber heat transfer element for modelling the thermal response of structures in fire. *Journal of Structural Engineering*. 135(10):1191-2000

Khoury GA, Anderberg Y, Both K, Fellinger J, Høj NP, Majorana C. 2007. *Fire design of concrete structures – materials, structures and modelling.* Lausanne, Switzerland: FIB (Fédération Internationale du Béton).

Khoury GA, Dias WPS, Sullivan PJES. 1986. Deformation of concrete and cement paste loaded at constant temperatures from 140 to 720 ºC. *Materials and Structures* 19(110):97-104.

Khoury GA, Grainger BN, Sullivan PJE. 1985. Transient thermal strain of concrete: literature review, conditions within specimen and behaviour of individual constituents. *Magazine of Concrete Research* 37(132):131-144.

Kim DK, Choi SM, Kim JH, Chung KS, Park SH. 2005. Experimental study on fire resistance of concrete-filled steel tube column under constant axial loads. *International Journal of Steel Structures* 5(4):305-313.

Kimura M, Ohta H, Kaneki H, Kodaira A. 1990. Fire resistance of concrete filled square steel tubular columns subjected to combined load. *Journal of Structural and Construction Engineering.* 417: 63-70. (in Japanese).

Kodur VKR. 1998a. Performance of high strength concrete filled steel columns exposed to fire. *Journal of Structural Engineering (ASCE)* 25:975-981.

Kodur VKR. 1998b. Design equations for evaluating fire resistance of SFRC-filled HSS columns. *Journal of Structural Engineering (ASCE)* 124(6):671-677.

Kodur VKR. 1999. Performance-based fire resistance design of concrete-filled steel columns. *Journal of Constructional Steel Research* 51(1):21-36.

Kodur VKR. 2007. Guidelines for fire resistant design of concrete-filled steel HSS columns – State-of-the-art and research needs. *Steel Structures* 7:173-182.

Kodur VKR, Latour JC. 2005. *Experimental studies on the fire resistance of hollow steel columns filled with high-strength concrete*. Institute for Research in Construction, National Research Council of Canada (NRCC), Ottawa, Canada.

Kodur VKR, Lie TT. 1995. *Experimental studies on the fire resistance of circular hollow steel columns filled with steel fibre-reinforced concrete. Internal report No. 691*. Ottawa, Canada: Institute for Research in Construction, National Research Council of Canada.

Kodur VKR, Lie TT. 1996. Fire resistance of circular steel columns filled with fiber-reinforced concrete. *Journal of Structural Engineering* 122(7):776-782.

Kodur VKR, MacKinnon DH. 2000. Design of concrete-filled hollow structural steel columns for fire endurance. *Engineering Journal-AISC* 37(1):13-24.

Kodur VKR, Sultan MA. 2003. Effect of temperature on thermal properties of high-strength concrete. *Journal of Materials in Civil Engineering* 15(2):101-107.

Kodur VKR, Wang TC, Cheng FR. 2004. Predicting the fire resistance behavior of high strength concrete columns. *Cement and Concrete Composites*. 26: 141-153

Kordina K, Klingsch W. 1983. *Fire resistance of composite columns of concrete filled hollow sections. CIDECT Research Project 15C1/C2–83/27*. Cologne, Germany: Comité International pour le Développement et l'Etude de la Construction Tubulaire.

Lacuesta C, Romero ML, Ivorra S, Portoles JM. 2006. A three-dimensional numerical model of circular concrete filled columns. In: *Proceedings of the*

Eighth International Conference on Computational Structures Technology. Stirlingshire, UK: B.H.V. Topping, G. Montero, R. Montenegro (Editors). Paper 22, doi:10.4203/ccp.83.22.

Leite G, Gomide K, Moreno A, Silva V. 2010. Fire resistance of axially loaded slender concrete filled steel tubular columns. In: *Structures in fire: proceedings of the 6th international conference*, pp. 433-440. Lancaster: Destech publications, inc.

Lennon T, Moore DB, Wang YC, Bailey CG. 2007. *Designers´ guide to EN 1991-1-2, EN 1992-1-2, EN 1993-1-2 and EN 1994-1-2.* Thomas Telford Limited.

Leskela MV. 2009. Inconsistencies in the fire design rules of composite columns to EN 1994-1-2. *Steel Concrete Composite and Hybrid Structures*, pp. 489-494. Leeds, England.

Li GQ, Wang P, Wang Y.2010. Behavior and design of restrained steel column in fire.Part 1: Fire test. *Journal of Constructional Steel Research.* 66: 1138-1147.

Li LY, Purkiss J. 2005. Stress-strain constitutive equations of concrete material at elevated temperatures. *Fire Safety Journal* 40(7):669-686.

Lie TT. 1984. A procedure to calculate fire resistance of structural members. *Fire and materials* 8(1):40-48.

Lie TT. 1994. Fire resistance of circular steel columns filled with bar-reinforced concrete. *Journal of Structural Engineering (ASCE)* 120(5):1489-1509.

Lie TT, Caron SE. 1988a. *Fire resistance of circular hollow steel columns filled with siliceous aggregate concrete: Test results. Internal report No. 570*. Ottawa, Canada: Institute for Research in Construction, National Research Council of Canada (NRCC).

Lie TT, Caron SE. 1988b. *Fire resistance of circular hollow steel columns filled with carbonate aggregate concrete: Test results. Internal report No. 573*. Ottawa, Canada: Institute for Research in Construction, National Research Council of Canada (NRCC).

Lie TT, Chabot M. 1990. A method to predict the fire resistance of circular concrete filled hollow steel columns. *Journal of Fire Protection Engineering* 2(4):111-126.

Lie TT, Chabot M. 1992. *Experimental studies on the fire resistance of hollow steel columns filled with plain concrete. Internal report No. 611*. Ottawa, Canada:

Institute for Research in Construction, National Research Council of Canada (NRCC).

Lie TT, Irwin RJ. 1995. Fire resistance of rectangular steel columns filled with bar-reinforced concrete. *Journal of Structural Engineering (ASCE)* 121(5):797-805.

Lie TT, Kodur VKR. 1995a. *Fire resistance of steel hollow structural section columns filled with bar-reinforced concrete. Internal report No. 678*. Ottawa, Canada: Institute for Research in Construction, National Research Council of Canada.

Lie TT, Kodur VKR. 1995b. *Effect of temperature on thermal and mechanical properties of steel fibre-reinforced concrete. Internal report No. 695*. Ottawa, Canada: Institute for Research in Construction, National Research Council of Canada.

Lie TT, Kodur VKR. 1996. Fire resistance of steel columns filled with bar-reinforced concrete. *Journal of Structural Engineering (ASCE)* 122(1):30-36.

Lie TT, Stringer DC. 1994. Calculation of fire resistance of steel hollow structural steel columns filled with plain concrete. *Canadian Journal of Civil Engineering* 21(3):382-385.

Liew JYR, Xiong MX, Xiong DX. 2014. Design of high strength concrete filled tubular columns for tall buildings. *International Journal of High-Rise Buildings* 3(3): 215-221.

Liu P, Ho G, Lee A, Yin C, Lee K, Liu GL, Huang XY. 2012. The structural design of Tianjin Goldin Finance 117 Tower. *International Journal of High-Rise Buildings* 1(4): 271-281.

Lu H, Zhao X, Han L. 2009. Fire behaviour of high strength self-consolidating concrete filled steel tubular stub columns. *Journal of Constructional Steel Research* 65(10-11):1995-2010.

Lu H, Zhao X, Han L. 2011. FE modelling and fire resistance design of concrete filled double skin tubular columns. *Journal of Constructional Steel Research* 67: 1733-1748.

Mazzoni S. McKenna F, Scott MH, Fenves GL. 2009. *Open system for earthquake engineering simulation. User cmmand-language manual.* Pacific Earthquake Engineering Research Center. University of California at Berkeley.

Mander JB, Priestley MJN, Park R. 1988. Theoretical stress-strain model for confined concrete. *Journal of Structural Engineering (ASCE)* 114(8):1804-1826.

Matsumoto S, Hosozawa O, Narihara H, Komuro T, Kawamoto. 2014. Structural design of an ultra high-rise building using concrete filled tubular column with 780 N/mm^2 class high-strength steel and fc150 N/mm^2 high-strength concrete. *International Journal of Hig-Rise Buildings* 3(1): 73-79.

Moliner V, Espinos A, Romero ML, Hospitaler A. 2013. Fire behavior of eccentrically loaded slender high strength concrete-filled tubular columns. J*ournal of Constructional Steel Research* 83: 137–146.

Moura Correia AJP, Rodrigues JPC. 2011. Fire resistance of partially encased steel columns with restrained thermal elongation. *Journal of Constructional Steel Research* 67:593-601.

OneSteel Solutions (OSS). 2007. Big developers combine in steel to connect Flinders Link. *OneSteel Solutions* 8: 21-23.

Park S, Choi S, Chung K. 2008. A study on the fire-resistance of concrete-filled steel square tube columns without fire protection under constant central axial loads. *Steel and Composite Structures* 8(6):491-510.

Park S, Chung K, Choi S. 2007. A study on failure prediction and design equation of concrete filled square steel tube columns under fire condition. *Steel Structures* 7(3):183-191.

Phan LT. 1996. *Fire performance of high-strength concrete: a report of the state-of-the-art.* Gaithersburg, Maryland: Building and Fire Research Laboratory, National Institute of Standards and Technology.

Pi YL, Bradford MA, Uy B. 2006. *Second order nonlinear inelastic analysis of composite steel-concrete members. I: Theory.* Journal of Structural Engineering (ASCE). 132(5): 751-761.

Pires T, Rodrigues JP, Silva JJ. 2012. Fire resistance of concrete filled circular hollow columns with restrained thermal elongation. *Journal of Constructional Steel Research.* 77: 82-94.

Poh KW. 2001. Stress-strain-temperature relationships for structural steel. *Journal of Materials in Civil Engineering* 13(5):371-379.

Poon DCK, Shieh SS, Joseph LM, Chang CC. 2002. The sky's the limit. *Modern Steel Construction.* December 2002.

Portolés JM, Romero ML, Filippou FC, Bonet JL. 2011. Simulation and design recommendations of eccentrically loaded slender concrete-filled tubular columns. *Engineering Structures* 33(5):1576-1593.

Purkiss JA. 2007. *Fire Safety Engineering. Design of Structures* (Second Edition). Oxford, UK: Butterworth-Heinemann – Elsevier Ltd.

Renaud C. 2003. *Modelisation numerique, experimentation et dimensionnement practique des poteaux mixtes avec profil creux exposes a l'incendie*. PhD thesis. Institut National des Sciences Appliquees de Rennes, France.

Renaud C, Aribert JM, Zhao B. 2003. Advanced numerical model for the fire behaviour of composite columns with hollow steel section. *Steel and Composite Structures* 3(2):75-95.

Renaud C, Joyeux D, Kruppa J. 2004. *Improvement and extension of the simple calculation method for fire resistance of unprotected concrete filled hollow columns. CIDECT Research Project 15Q-12/03*. Saint-Rémy-lès-Chevreuse, France: Centre Technique Industriel de la Construction Métallique (CTICM).

Renaud C, Kruppa J. 2004. *Unprotected concrete filled columns fire tests – Verification of 15Q. CIDECT Research Project 15R*. Saint-Rémy-lès-Chevreuse, France: Centre Technique Industriel de la Construction Métallique (CTICM).

Ribeiro JCL, Fakury RH, de Las Casas EB. 2008. Eurocode structural fire design and its application for composite circular hollow section columns. *Journal of the Brazilian Society of Mechanical Science and Engineering* 30(1):39-46.

Richart FE, Brantzaeg A, Brown RL. 1928. *A study of failure of concrete under combined compressive stresses.* Bulletin nº 185. Engineering Experiment Station, University of Illinois, Urbana, IL.

Ritter W. 1899. Die bauweise hennebique. *Schweizerische Bauzeitung* 33.

Romero ML, Moliner V, Espinos A, Ibañez C, Hospitaler A. 2011. Fire behavior of axially loaded slender high strength concrete-filled tubular columns. *Journal of Constructional Steel Research* 67(12):1953-1965.

Romero ML, Espinos A, Portolés JM, Hospitaler A, Ibañez C. 2015.Slender double-tube ultra-high strength concrete-filled tubular columns under ambient temperature and fire. *Engineering Structures.* 99: 536-545.

Ruddy JL, Marlo JP, Ioannides SA, Alfawakhiri F. 2003. *Fire Resistance of Structural Steel Framing. Steel Design Guide 19*. Chicago, USA: American Institute of Steel Construction.

Rush D, Bisby L, Jowsey A, Lane B. 2015. Residual capacity of fire-exposed concrete-filled steel hollow section columns. *Engineering Structures.* 100:550–563

Saenz LP. 1964. Discussion of 'Equation for the stress-strain curve of concrete' by P. Desayi, and S. Krishnan. *Journal of the American Concrete Institute* 61:1229-1235.

Sakumoto Y, Okada T, Yoshida M, Taska S. 1994. Fire resistance of concrete filled fire resistant steel tube columns. *Journal of Materials in Civil Engineering* 6(2):169-184.

Schaumann P, Kodur V, Bahr O. 2009. Fire behaviour of hollow structural section steel columns filled with high strength concrete. *Journal of Constructional Steel Research* 65:1794-1802.

Schneider U. 1986. Modelling of concrete behaviour at high temperatures. Anchor RD, Malhotra HL, Purkiss JA, editors. *Proceedings of the international conference of design of structures against fire*, pp. 53-69. New York: Elsevier.

Schneider U. 1988. Concrete at high temperatures – A general review. *Fire Safety Journal* 13:55-68.

Schneider U, Haksever A. 1976. Bestimmung der aquialenten branddauer vor statisch bestimmt gelagerten stahlbetonbalken bei naturlichen branden. Bericht des Instituts fur Baustoffkunde und Stahlbetonbau der Technischen Universität Braunschweig. Braunschweig, Germany.

Shepherd PG, Burgess IW. 2011. On the buckling of axially restrained steel columns in fire. *Engineering Structures* 33: 2832-2838.

Song TY, Han LH, Yu HX. 2010. Concrete filled steel tube stub columns under combined temperature and loading. *Journal of Constructional Steel Research* 66:369-384.

Spacone E, Ciampi V, Filippou FC. 1996. *Mixed formulation of nonlinear beam finite-element.* Computers and Structures. 58(1): 71-83.

Sterner E, Wickström U. 1990. *TASEF – Temperature Analysis of Structures Exposed to Fire. SP Report 1990:05*. Borås, Sweden: Swedish National Testing and Research Institute.

Surorov, SA, Skurikhin VV. 2002. High-temperature heat insulating materials based on vermiculite. *Refractories and Industrial Ceramics* 43 (11-12): 383-389.

Tan KH, Tang CY. 2004. Interaction model for unprotected concrete filled steel columns under standard fire conditions. *Journal of Structural Engineering (ASCE)* 130(9):1405-1413.

Tan KH, Toh WS, Huang ZF, Phng GH. 2007. Structural responses of restrained steel columns at elevated temperatures. Part 1: Experiments. *Engineering Structures*. 29:1641-1652.

Tao Z, Han LH, Uy B, Chen X. 2011. Post-fire bond between the steel tube and concrete in concrete-filled steel tubular columns. *Journal of Constructional Steel Research* 67:484-496.

Taylor R, Filippou FC, Saritas A, Auricchio F. 2003. *Mixed finite element method for beam and frame roblems.* Computational Mechanics. 31: 192-203.

Terro MJ. 1998. Numerical modelling of the behaviour of concrete structures. *ACI Structural Journal* 95(2):183-193.

The Steel Construction Institute (SCI). 2008. *Best Practices in Steel Construction – Commercial Buildings*. Guidance for Architects, Designers & Constructors.

Tondini N, Hoang VL, Demonceau JF, Franssen JM. 2013. Experimental and numerical investigation of high strength steel circular columns subjected to fire. *Journal of Constructional Steel Research* 80: 57-81.

Twilt L, Hass R, Klingsch W, Edwards M, Dutta D. 1996. *Design guide for structural hollow section columns exposed to fire.* Cologne, Germany: Comité International pour le Développement et l'Etude de la Construction Tubulaire (CIDECT).

Varma AH, Ricles JM, Sause R, Lu LW. 2002. *Seismic behavior and modeling of high-strength composite concrete-filled steel tube (CFT) beam-columns.* Journal of Constructional Steel Research 58: 725:758.

Wainman DE, Toner RP. 1992. *BS476: Part 21 Fire Resistance Tests. The construction and testing of three loaded CHS columns filled with concrete.* Moorgate, Rotherham (UK): Swinden Laboratories. British Steel Technical.

Wang HB. 1995. *Heat transfer analysis of components of construction exposed to fire. PhD Thesis*. Dept. of Civil Engineering and Construction, University of Salford, UK.

Wang K, Young B. 2013. Fire resistance of concrete-filled high strength steel tubular columns. *Thin-Walled Structures* 71:46-56.

Wang YC. 1997a Effects of structural continuity on the fire resistance design of steel columns in non-sway multi-storey frames. *Fire Safety Journal* 28: 101-116.

Wang YC. 1997b. Some considerations in the design of unprotected concrete-filled steel tubular columns under fire conditions. *Journal of Constructional Steel Research* 44(3):203-223.

Wang YC. 1999. The effects of structural continuity on the fire resistance of concrete filled columns in non-sway frames. *Journal of Constructional Steel Research* 50:177-197.

Wang YC. 2000. A simple method for calculating the fire resistance of concrete-filled CHS columns. *Journal of Constructional Steel Research* 54(3):365-386.

Wang YC. 2005. Performance of steel-concrete composite structures in fire. *Progress in Structural Engineering and Materials* 7(2):86-102.

Wang YC, Burgess I, Wald F, Gillie M. 2013. *Performance-based fire engineering of structures*. CRC Press, Taylor & Francis Group.

Wang YC, Davies JM. 2003a. Fire tests of non-sway loaded and rotationally restrained steel column assemblies. *Journal of Constructional Steel Research.* 59: 359-383.

Wang YC, Davies JM. 2003b. An experimental study of the fire performance of non-sway loaded concrete-filled steel tubular column assemblies with extended end plate connections. *Journal of Constructional Steel Research.* 59: 819-838.

Wang YC, Kodur VKR. 1999. An approach for calculating the failure loads of unprotected concrete-filled steel columns exposed to fire. *Structural Engineering and Mechanics* 7(2):127–45.

Wang Y, Kodur V. 2000. Research toward use of unprotected steel structures. *Journal of Structural Engineering* 126(12):1442-1450.

Wang YC, Lennon T, Moore DB. 1995. The behavior of steel frames subject to fire. *Journal of Constructional Steel Research* 35: 291-322.

Wang YC, Orton AH. 2008. Fire resistant design of concrete filled tubular steel columns. *The Structural Engineer* 7:40-45.

Wang ZH, Tan KH. 2006. Green's function solution for transient heat conduction in concrete-filled CHS subjected to fire. *Engineering Structures* 28(11):1574-1585.

Wardenier, J. 2001. *Hollow Sections In Structural Applications.* CIDECT (Comité International pour le Développement et l'Etude de la Construction Tubulaire).

Wickström U. 1986. A very simple method for estimating tempertayre in fire exposed concrete estructures. *Swedish National Testing Institute-Fire Technology Technical Report SP-RAPP* 46: 186-194..

Wimer R, Baker W, Nagis M, Mazeika A. 2012. Case Study: Greendland's Suzhou Center, Wujiang. *International Journal on Tall Buildings and Urban Habitat* Issue III: 12-19.

Witteveen J, Twilt L, Bylaard FSK. 1977. The stability of braced and unbraced frames at elevated temperatures. *Second International Colloquium on Column Strength.* Liège, Belgium.

Wood RH, 1974. Effective lengths of columns in multi-storey buildings. *The Structural Engineer* 7(52): 235-244.

Yang H, Han LH, Wang YC. 2008a. Effects of heating and loading histories on post fire cooling behaviour of concrete filled steel tubular columns. *Journal of Constructional Steel Research* 64(5):556-570.

Yang H, Liu F, Gardner L.2015. Post-fire behaviour of slender reinforced concrete columns confined by circular steel tubes. *Thin-Walled Structures* 87: 12-29.

Yang H, Liu F, Gardner L.2013a. Performance of concrete-filled RHS columns exposed to fire on 3 sides. *Engineering Structures.* 56: 1986-2004.

Yang H, Liu F, Zhang S, Lv X. 2013b. Experimental investigation of concrete-filled square hollow section columns subjected to non-uniform exposure. *Engineering Structures.* 48: 292–312.

Yang H, Liu F, Zhang S, Lv X. 2013a. Experimental investigation of concrete-filled square hollow section columns subjected to non-uniform exposure. *Engineering Structures.* 48: 292–312.

Yao Y, Hu XX. 2015. Cooling behavior and residual strength of post-fire concrete filled steel tubular columns. *Journal of Constructional Steel Research* 112:282-292.

Yaw LL, Sukumar N, Kunnath SK. 2008. *Meshfree co-rotational formulation for two-dimensional continua.* International Journal for Numerical Methods in Engineering. 00: 1-38.

Yin J, Zha XX, Li LY. 2006. Fire resistance of axially loaded concrete filled steel tube columns. *Journal of Constructional Steel Research* 62(7):723-729.

Youssef MA, Moftah M. 2007. General stress-strain relationship for concrete at elevated temperatures. *Engineering Structures* 29:2618-2634.

Yu M, Zha X, Ye J, Li Y. 2010. Fire responses and resistance of concrete-filled steel tubular frame structures. *International Journal of Structural Stability and Dynamics* 10 (2): 253-271.

Yu M, Zha X, Ye J, Wang B. 2014. A unified method for calculating fire resistance of solid and hollow concrete-filled steel tube columns based on average temperature. *Engineering Structures* 71: 12-22.

Zha XX. 2003. FE analysis of fire resistance of concrete filled CHS columns. *Journal of Constructional Steel Research* 59:769-779.

Zhao XL, Han LH, Lu H. 2010. *Concrete-filled tubular members and connections*. Abingdon, Oxon: Spon Press.

ANNEX I.

PARAMETRIC ANALYSIS ON STRUCTURAL CONTINUITY

This Annex includes the results obtained from the parametric analysis on structural continuity in form of a series of figures in which the influence of the parameters studied is shown.

1. INFLUENCE OF APPLIED LOAD LEVEL

1.1. Influence of applied load level in the axial displacement

Stiffness ratio α=0.1

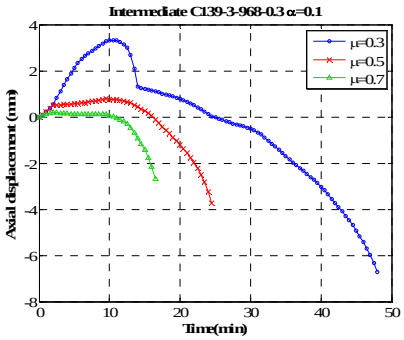

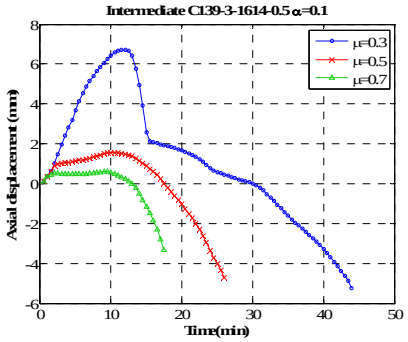

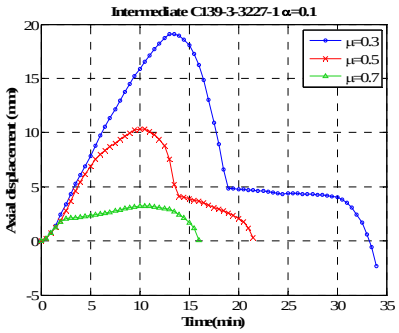

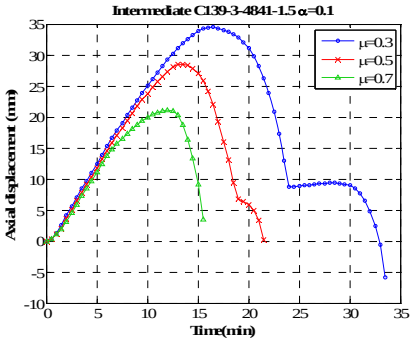

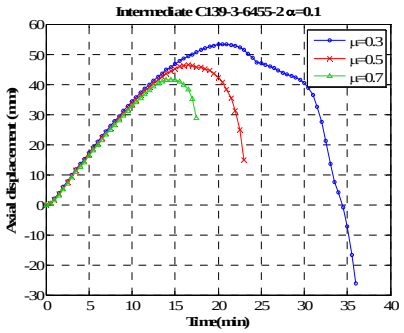

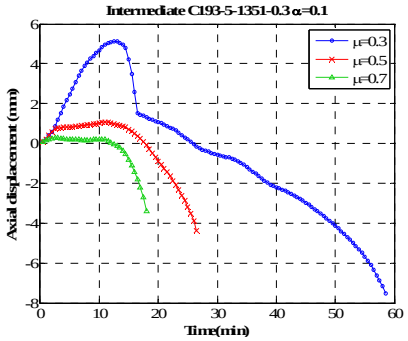

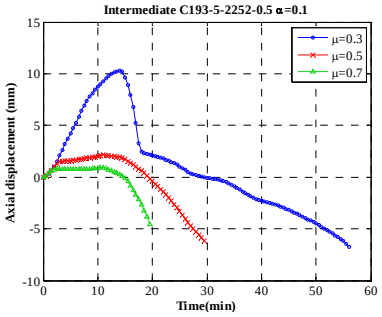
Intermediate C193-5-2252-0.5 α=0.1
Axial displacement (mm)
Time(min)
μ=0.3
μ=0.5
μ=0.7

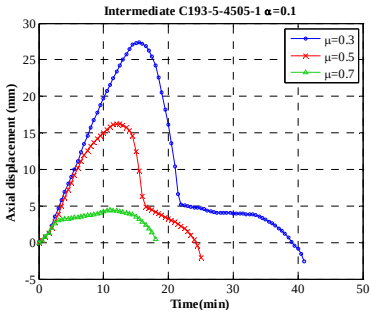
Intermediate C193-5-4505-1 α=0.1
Axial displacement (mm)
Time(min)
μ=0.3
μ=0.5
μ=0.7

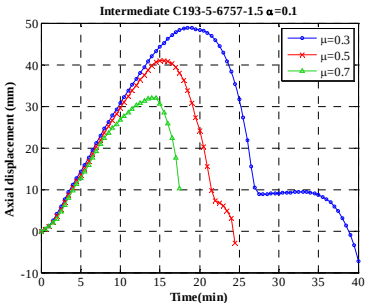
Intermediate C193-5-6757-1.5 α=0.1
Axial displacement (mm)
Time(min)
μ=0.3
μ=0.5
μ=0.7

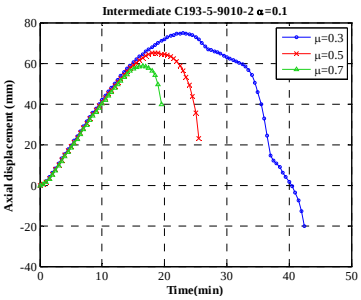
Intermediate C193-5-9010-2 α=0.1
Axial displacement (mm)
Time(min)
μ=0.3
μ=0.5
μ=0.7

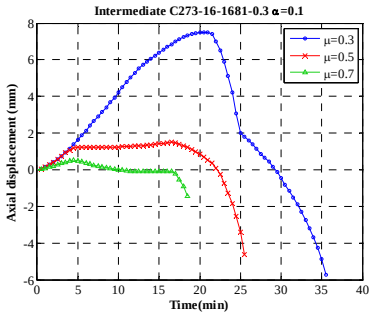
Intermediate C273-16-1681-0.3 α=0.1
Axial displacement (mm)
Time(min)
μ=0.3
μ=0.5
μ=0.7

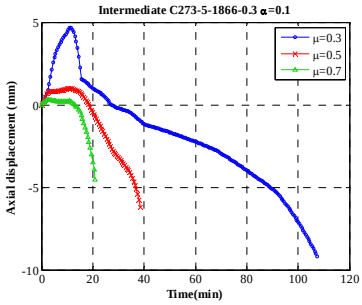
Intermediate C273-5-1866-0.3 α=0.1
Axial displacement (mm)
Time(min)
μ=0.3
μ=0.5
μ=0.7

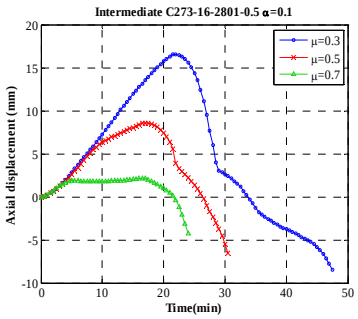
Intermediate C273-16-2801-0.5 α=0.1
Axial displacement (mm)
Time(min)
μ=0.3
μ=0.5
μ=0.7

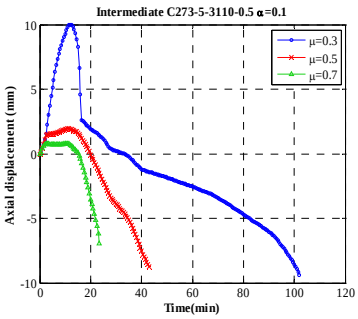
Intermediate C273-5-3110-0.5 α=0.1
Axial displacement (mm)
Time(min)
μ=0.3
μ=0.5
μ=0.7

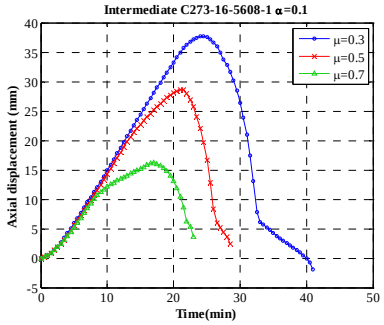
Intermediate C273-16-5608-1 α=0.1
Axial displacement (mm)
Time(min)
μ=0.3
μ=0.5
μ=0.7

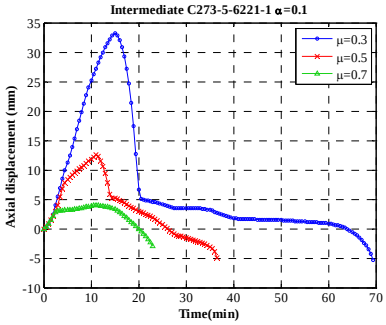
Intermediate C273-5-6221-1 α=0.1
Axial displacement (mm)
Time(min)
μ=0.3
μ=0.5
μ=0.7

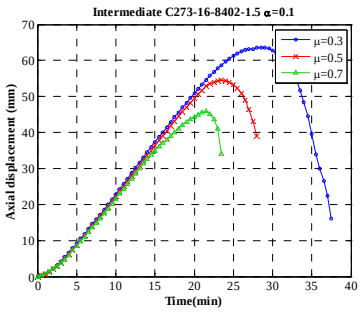
Intermediate C273-16-8402-1.5 α=0.1
Axial displacement (mm)
Time(min)
μ=0.3
μ=0.5
μ=0.7

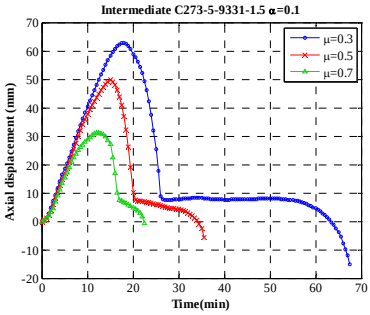
Intermediate C273-5-9331-1.5 α=0.1
Axial displacement (mm)
Time(min)
μ=0.3
μ=0.5
μ=0.7

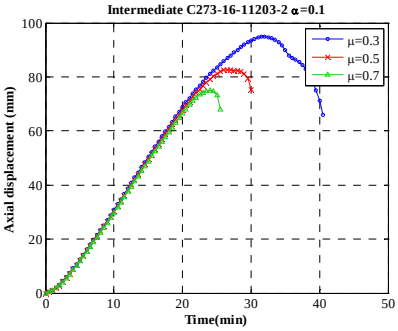
Intermediate C273-16-11203-2 α=0.1
Axial displacement (mm)
Time(min)
μ=0.3
μ=0.5
μ=0.7

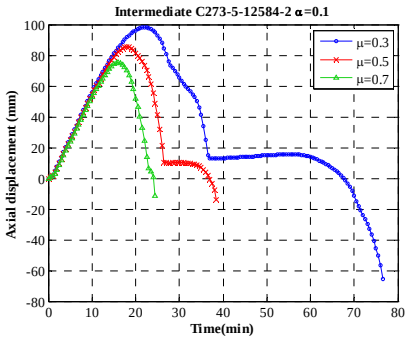
Intermediate C273-5-12584-2 α=0.1
Axial displacement (mm)
Time(min)
μ=0.3
μ=0.5
μ=0.7

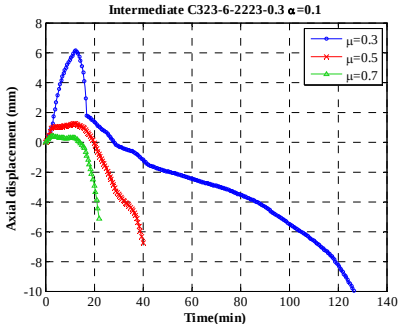
Intermediate C323-6-2223-0.3 α=0.1
Axial displacement (mm)
Time(min)
μ=0.3
μ=0.5
μ=0.7

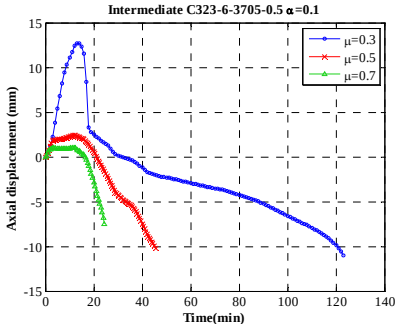
Intermediate C323-6-3705-0.5 α=0.1
Axial displacement (mm)
Time(min)
μ=0.3
μ=0.5
μ=0.7

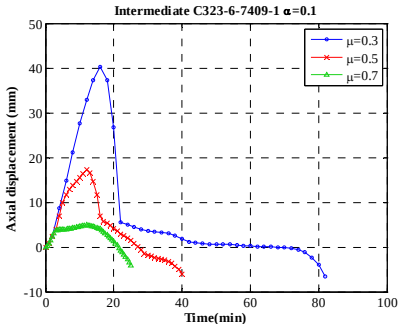
Intermediate C323-6-7409-1 α=0.1
Axial displacement (mm)
Time(min)
μ=0.3
μ=0.5
μ=0.7

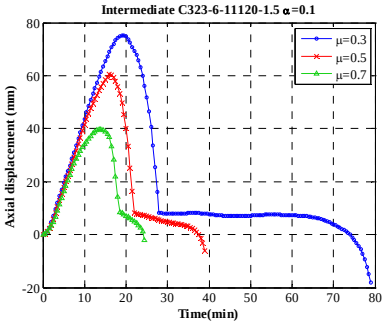
Intermediate C323-6-11120-1.5 α=0.1
Axial displacement (mm)
Time(min)
μ=0.3
μ=0.5
μ=0.7

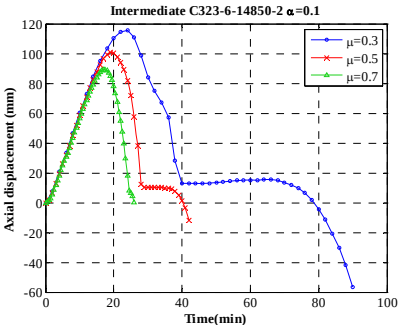
Intermediate C323-6-14850-2 α=0.1
Axial displacement (mm)
Time(min)
μ=0.3
μ=0.5
μ=0.7

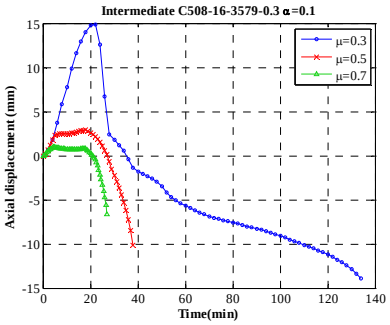
Intermediate C508-16-3579-0.3 α=0.1
Axial displacement (mm)
Time(min)
μ=0.3
μ=0.5
μ=0.7

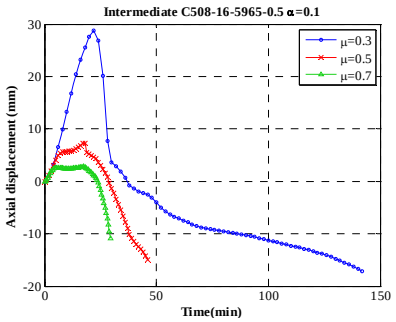
Intermediate C508-16-5965-0.5 α=0.1
Axial displacement (mm)
Time(min)
μ=0.3
μ=0.5
μ=0.7

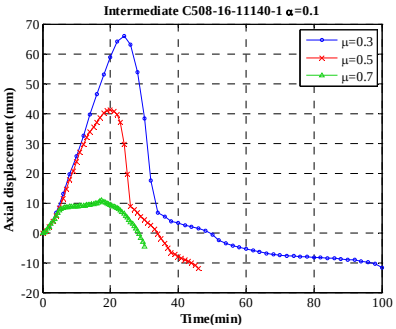
Intermediate C508-16-11140-1 α=0.1
Axial displacement (mm)
Time(min)
μ=0.3
μ=0.5
μ=0.7

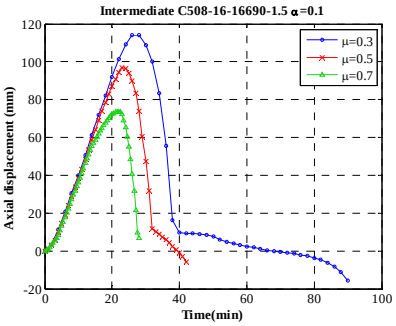
Intermediate C508-16-16690-1.5 α=0.1
Axial displacement (mm)
Time(min)
μ=0.3
μ=0.5
μ=0.7

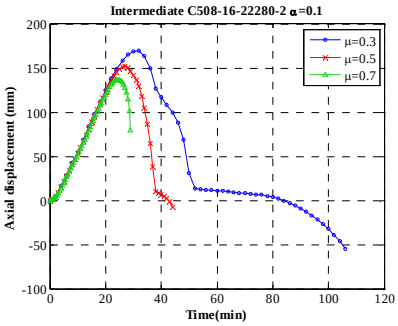
Intermediate C508-16-22280-2 α=0.1
Axial displacement (mm)
Time(min)
μ=0.3
μ=0.5
μ=0.7

Stiffness ratio α=0.5

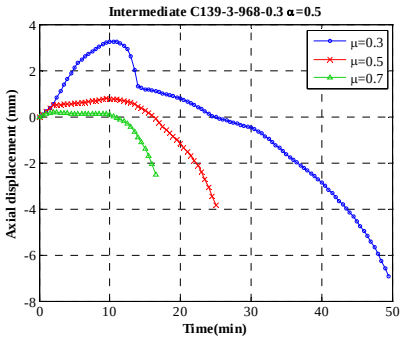

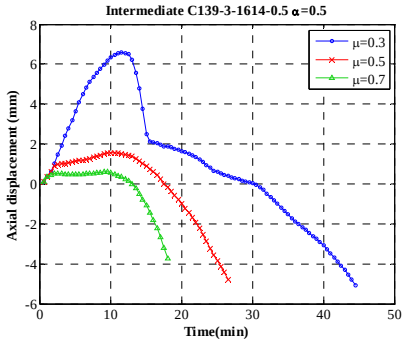

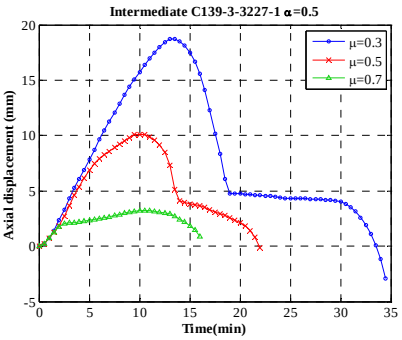

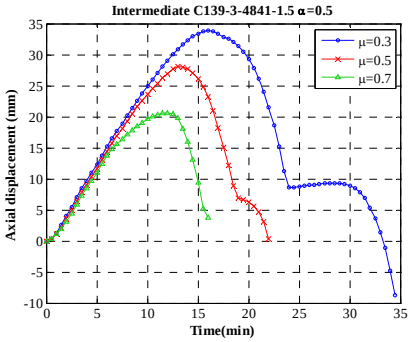

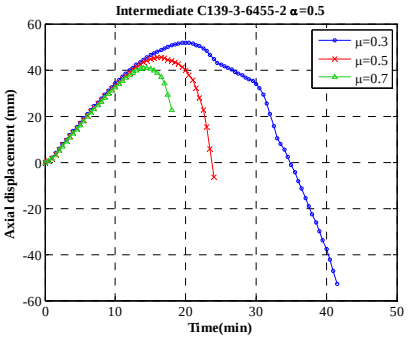

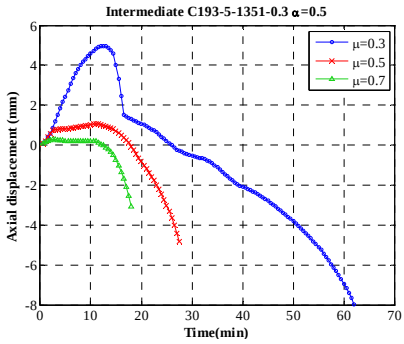

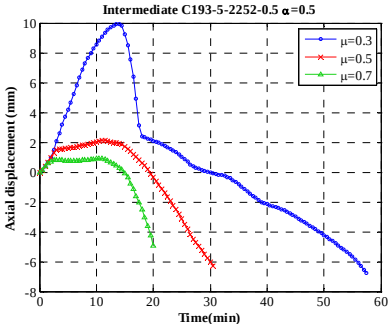
Intermediate C193-5-2252-0.5 α=0.5
μ=0.3
μ=0.5
μ=0.7
Axial displacement (mm)
Time(min)

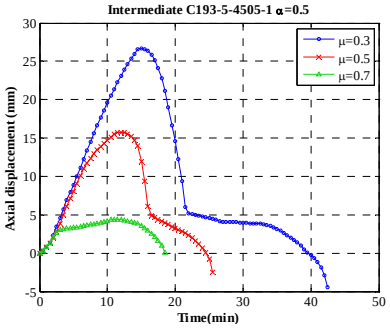
Intermediate C193-5-4505-1 α=0.5
μ=0.3
μ=0.5
μ=0.7
Axial displacement (mm)
Time(min)

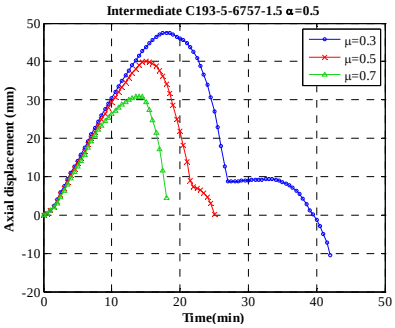
Intermediate C193-5-6757-1.5 α=0.5
μ=0.3
μ=0.5
μ=0.7
Axial displacement (mm)
Time(min)

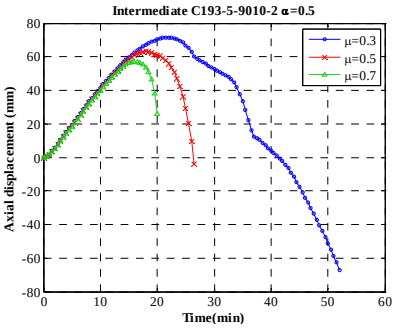
Intermediate C193-5-9010-2 α=0.5
μ=0.3
μ=0.5
μ=0.7
Axial displacement (mm)
Time(min)

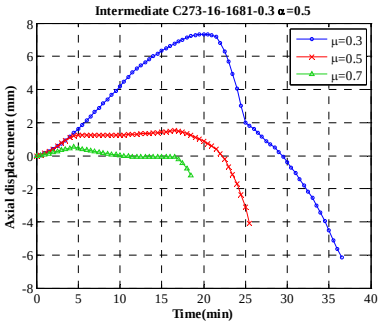
Intermediate C273-16-1681-0.3 α=0.5
μ=0.3
μ=0.5
μ=0.7
Axial displacement (mm)
Time(min)

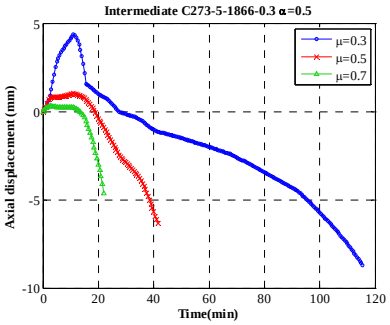
Intermediate C273-5-1866-0.3 α=0.5
μ=0.3
μ=0.5
μ=0.7
Axial displacement (mm)
Time(min)

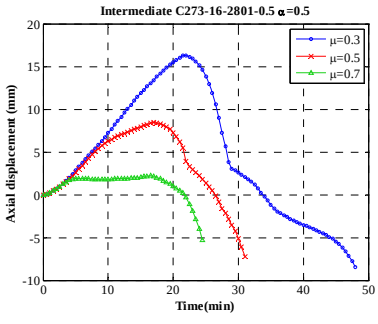
Intermediate C273-16-2801-0.5 α=0.5
μ=0.3
μ=0.5
μ=0.7
Axial displacement (mm)
Time(min)

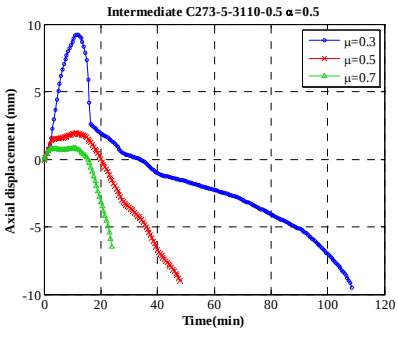
Intermediate C273-5-3110-0.5 α=0.5
μ=0.3
μ=0.5
μ=0.7
Axial displacement (mm)
Time(min)

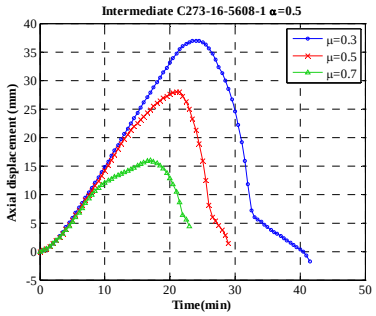
Intermediate C273-16-5608-1 α=0.5
Axial displacement (mm)
Time(min)
μ=0.3
μ=0.5
μ=0.7

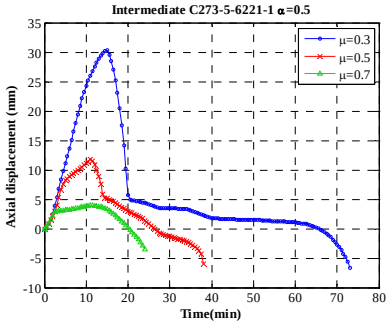
Intermediate C273-5-6221-1 α=0.5
Axial displacement (mm)
Time(min)
μ=0.3
μ=0.5
μ=0.7

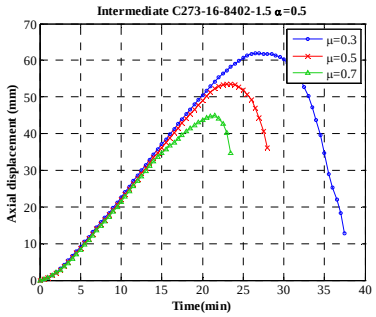
Intermediate C273-16-8402-1.5 α=0.5
Axial displacement (mm)
Time(min)
μ=0.3
μ=0.5
μ=0.7

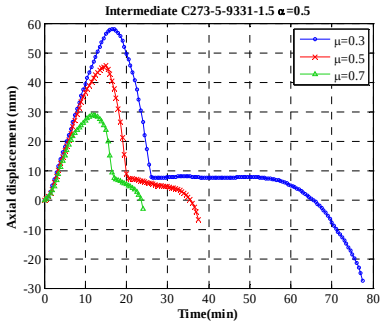
Intermediate C273-5-9331-1.5 α=0.5
Axial displacement (mm)
Time(min)
μ=0.3
μ=0.5
μ=0.7

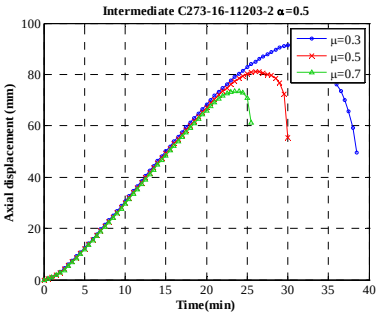
Intermediate C273-16-11203-2 α=0.5
Axial displacement (mm)
Time(min)
μ=0.3
μ=0.5
μ=0.7

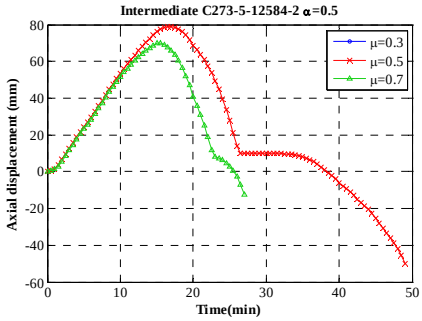
Intermediate C273-5-12584-2 α=0.5
Axial displacement (mm)
Time(min)
μ=0.3
μ=0.5
μ=0.7

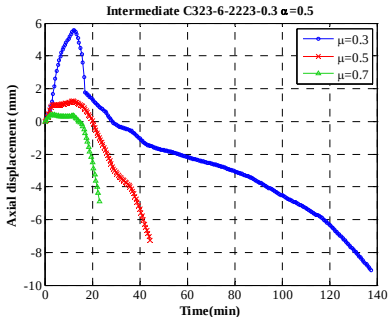
Intermediate C323-6-2223-0.3 α=0.5
Axial displacement (mm)
Time(min)
μ=0.3
μ=0.5
μ=0.7

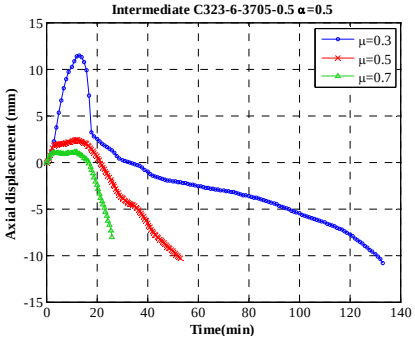
Intermediate C323-6-3705-0.5 α=0.5
Axial displacement (mm)
Time(min)
μ=0.3
μ=0.5
μ=0.7

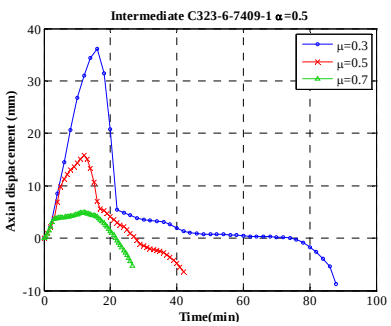
Intermediate C323-6-7409-1 α=0.5
Axial displacement (mm)
Time(min)
μ=0.3
μ=0.5
μ=0.7

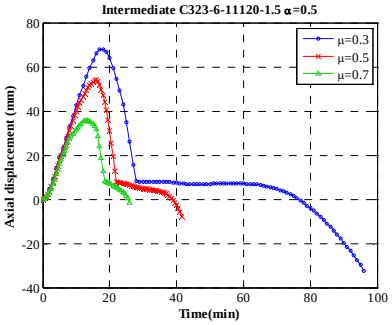
Intermediate C323-6-11120-1.5 α=0.5
Axial displacement (mm)
Time(min)
μ=0.3
μ=0.5
μ=0.7

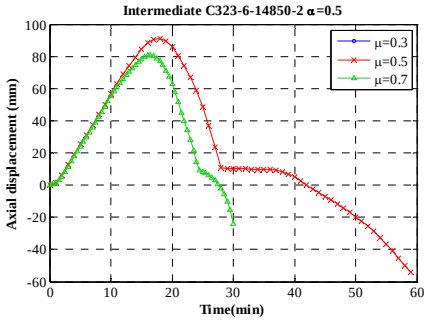
Intermediate C323-6-14850-2 α=0.5
Axial displacement (mm)
Time(min)
μ=0.3
μ=0.5
μ=0.7

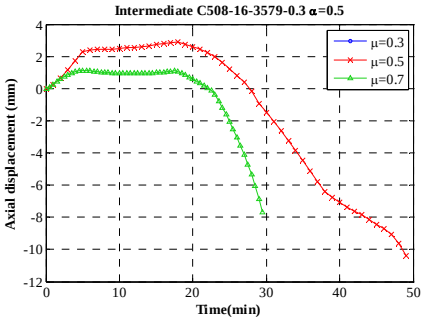
Intermediate C508-16-3579-0.3 α=0.5
Axial displacement (mm)
Time(min)
μ=0.3
μ=0.5
μ=0.7

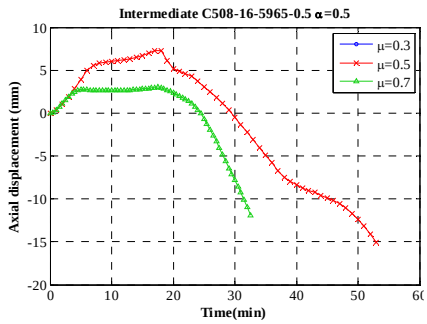
Intermediate C508-16-5965-0.5 α=0.5
Axial displacement (mm)
Time(min)
μ=0.3
μ=0.5
μ=0.7

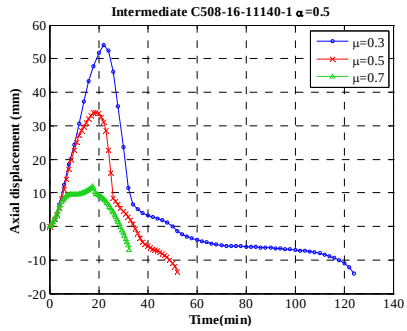
Intermediate C508-16-11140-1 α=0.5
Axial displacement (mm)
Time(min)
μ=0.3
μ=0.5
μ=0.7

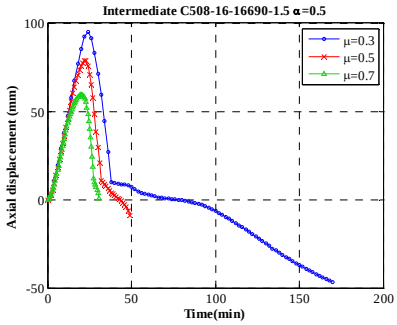
Intermediate C508-16-16690-1.5 α=0.5
Axial displacement (mm)
Time(min)
μ=0.3
μ=0.5
μ=0.7

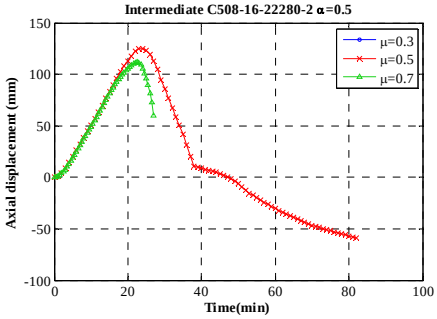
Intermediate C508-16-22280-2 α=0.5
Axial displacement (mm)
Time(min)
μ=0.3
μ=0.5
μ=0.7

Stiffness ratio α=1

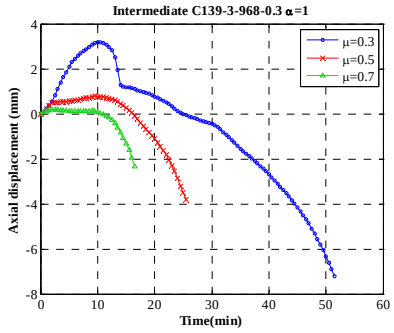

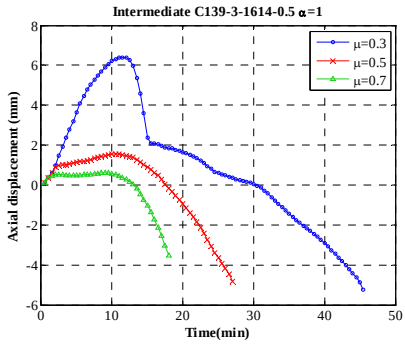

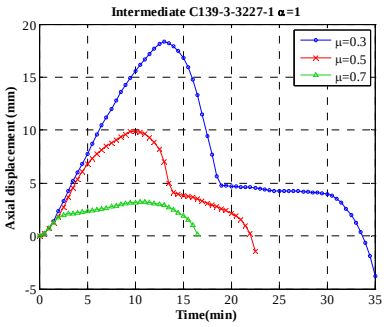

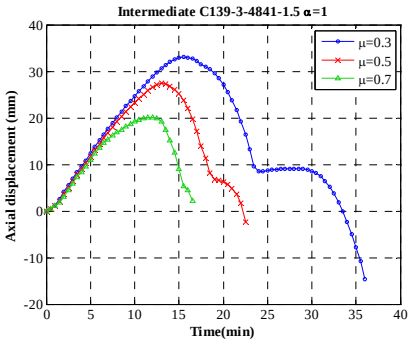

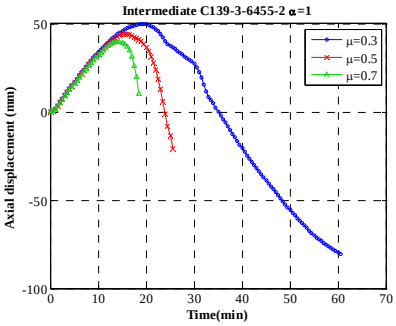

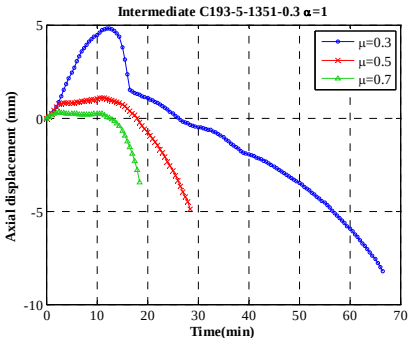

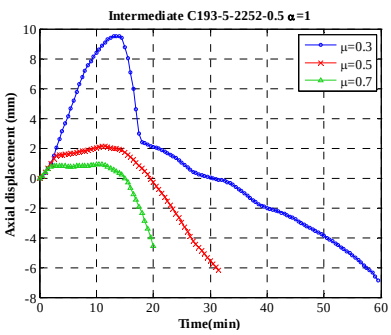
Intermediate C193-5-2252-0.5 α=1
Axial displacement (mm)
Time(min)
μ=0.3
μ=0.5
μ=0.7

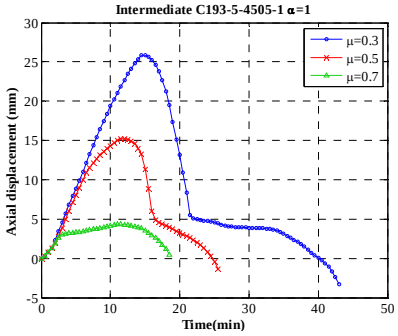
Intermediate C193-5-4505-1 α=1
Axial displacement (mm)
Time(min)
μ=0.3
μ=0.5
μ=0.7

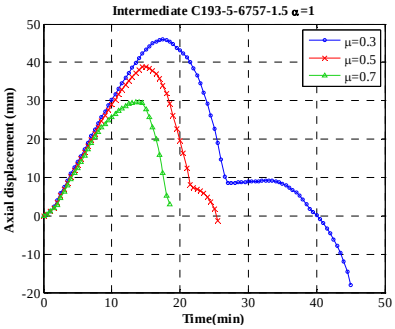
Intermediate C193-5-6757-1.5 α=1
Axial displacement (mm)
Time(min)
μ=0.3
μ=0.5
μ=0.7

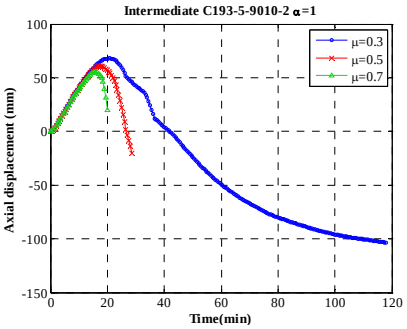
Intermediate C193-5-9010-2 α=1
Axial displacement (mm)
Time(min)
μ=0.3
μ=0.5
μ=0.7

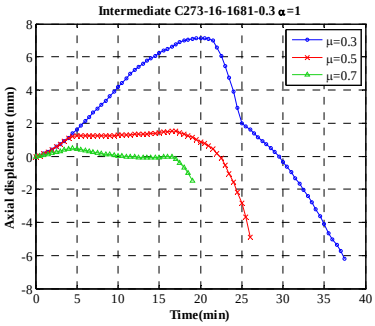
Intermediate C273-16-1681-0.3 α=1
Axial displacement (mm)
Time(min)
μ=0.3
μ=0.5
μ=0.7

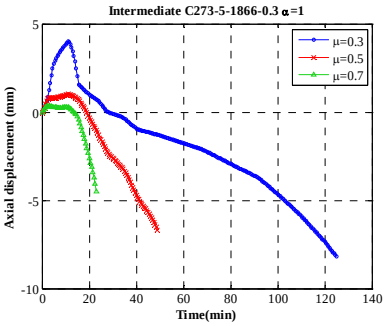
Intermediate C273-5-1866-0.3 α=1
Axial displacement (mm)
Time(min)
μ=0.3
μ=0.5
μ=0.7

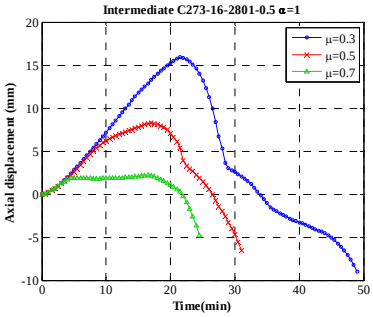
Intermediate C273-16-2801-0.5 α=1
Axial displacement (mm)
Time(min)
μ=0.3
μ=0.5
μ=0.7

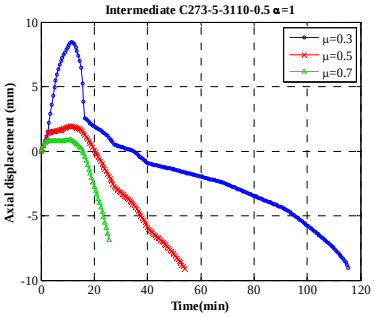
Intermediate C273-5-3110-0.5 α=1
Axial displacement (mm)
Time(min)
μ=0.3
μ=0.5
μ=0.7

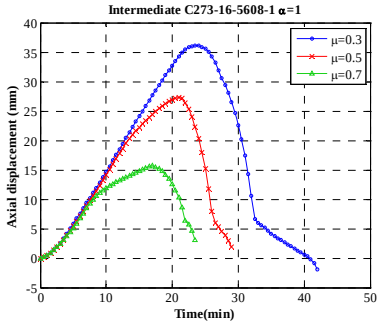
Intermediate C273-16-5608-1 α=1
Axial displacement (mm)
Time(min)
μ=0.3
μ=0.5
μ=0.7

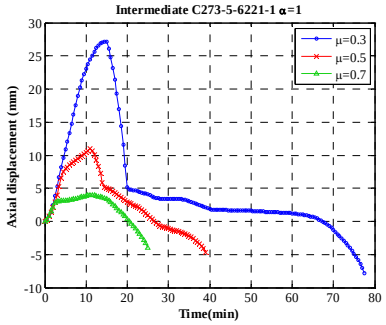
Intermediate C273-5-6221-1 α=1
Axial displacement (mm)
Time(min)
μ=0.3
μ=0.5
μ=0.7

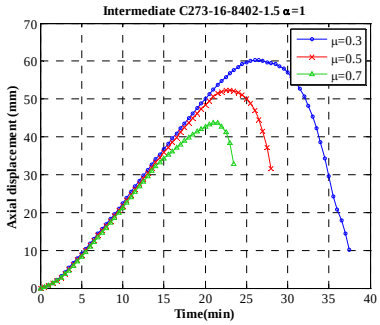
Intermediate C273-16-8402-1.5 α=1
Axial displacement (mm)
Time(min)
μ=0.3
μ=0.5
μ=0.7

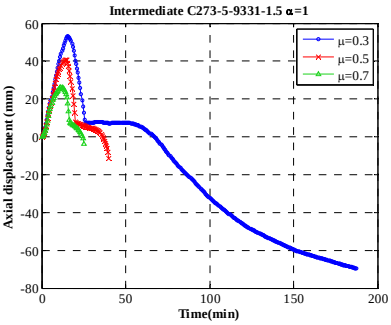
Intermediate C273-5-9331-1.5 α=1
Axial displacement (mm)
Time(min)
μ=0.3
μ=0.5
μ=0.7

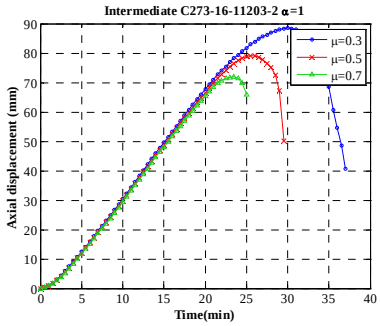
Intermediate C273-16-11203-2 α=1
Axial displacement (mm)
Time(min)
μ=0.3
μ=0.5
μ=0.7

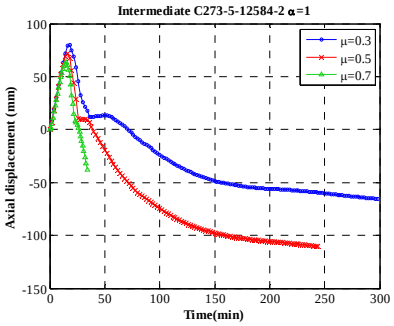
Intermediate C273-5-12584-2 α=1
Axial displacement (mm)
Time(min)
μ=0.3
μ=0.5
μ=0.7

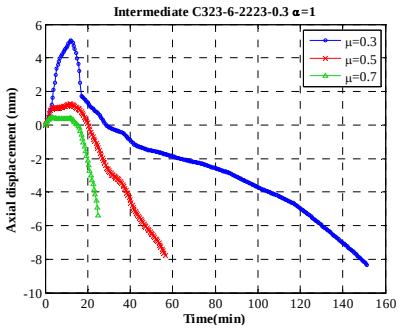
Intermediate C323-6-2223-0.3 α=1
Axial displacement (mm)
Time(min)
μ=0.3
μ=0.5
μ=0.7

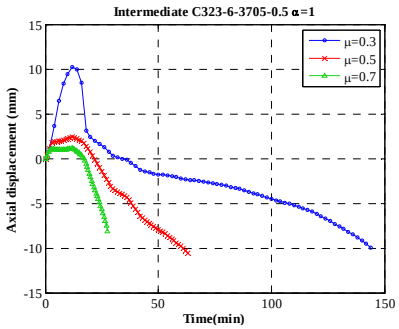
Intermediate C323-6-3705-0.5 α=1
Axial displacement (mm)
Time(min)
μ=0.3
μ=0.5
μ=0.7

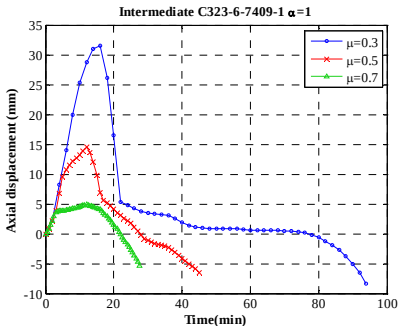
Intermediate C323-6-7409-1 α=1
Axial displacement (mm)
Time(min)
μ=0.3
μ=0.5
μ=0.7

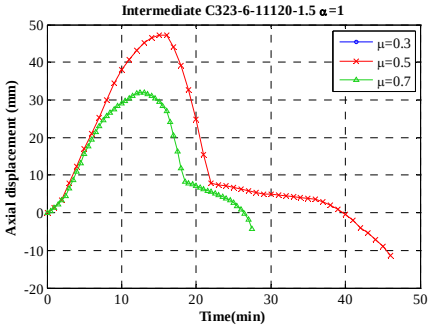
Intermediate C323-6-11120-1.5 α=1
Axial displacement (mm)
Time(min)
μ=0.3
μ=0.5
μ=0.7

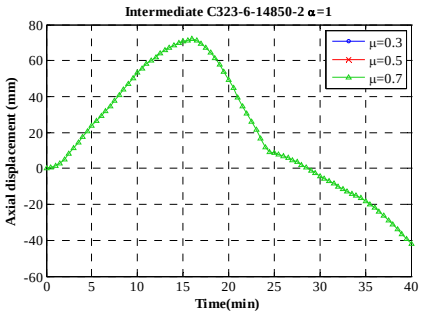
Intermediate C323-6-14850-2 α=1
Axial displacement (mm)
Time(min)
μ=0.3
μ=0.5
μ=0.7

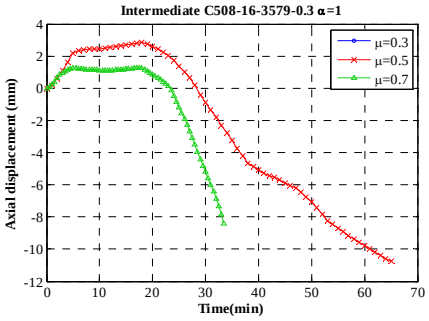
Intermediate C508-16-3579-0.3 α=1
Axial displacement (mm)
Time(min)
μ=0.3
μ=0.5
μ=0.7

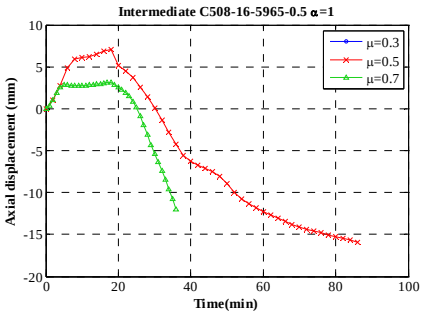
Intermediate C508-16-5965-0.5 α=1
Axial displacement (mm)
Time(min)
μ=0.3
μ=0.5
μ=0.7

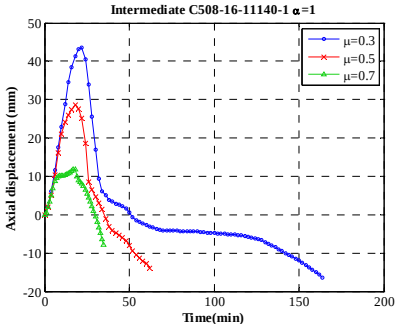
Intermediate C508-16-11140-1 α=1
Axial displacement (mm)
Time(min)
μ=0.3
μ=0.5
μ=0.7

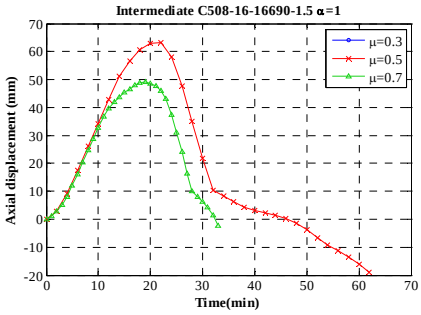
Intermediate C508-16-16690-1.5 α=1
Axial displacement (mm)
Time(min)
μ=0.3
μ=0.5
μ=0.7

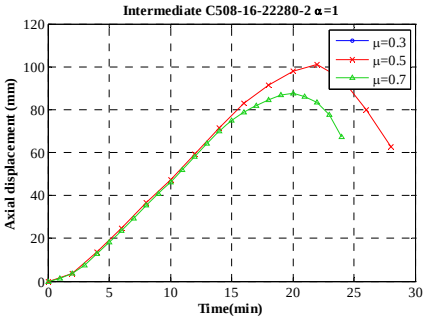
Intermediate C508-16-22280-2 α=1
Axial displacement (mm)
Time(min)
μ=0.3
μ=0.5
μ=0.7

Stiffness ratio α=2

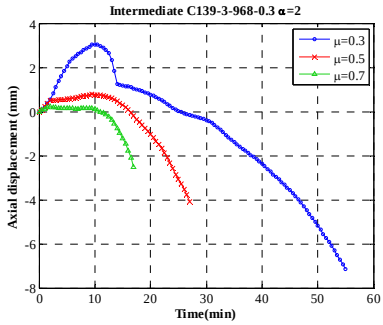

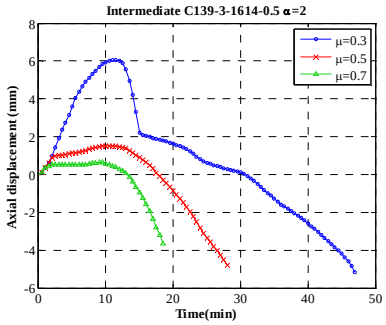

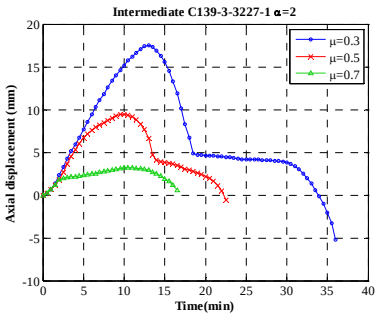

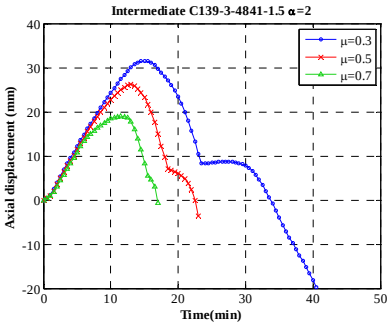

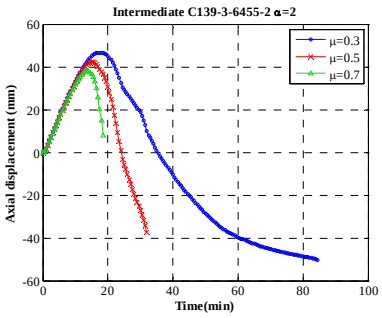

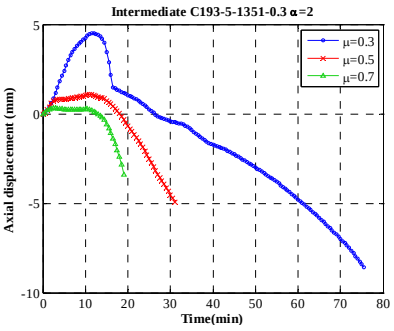

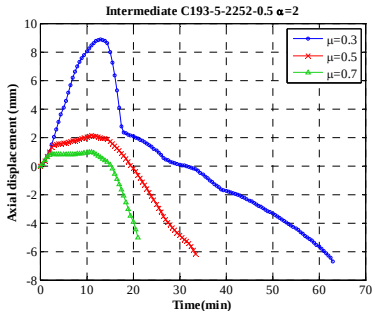
Intermediate C193-5-2252-0.5 α=2
Axial displacement (mm)
Time(min)
μ=0.3
μ=0.5
μ=0.7

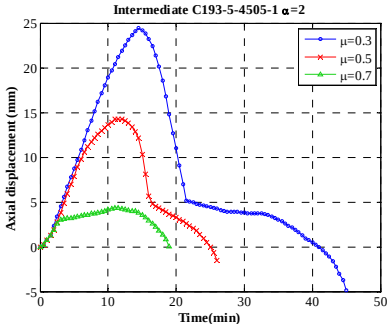
Intermediate C193-5-4505-1 α=2
Axial displacement (mm)
Time(min)
μ=0.3
μ=0.5
μ=0.7

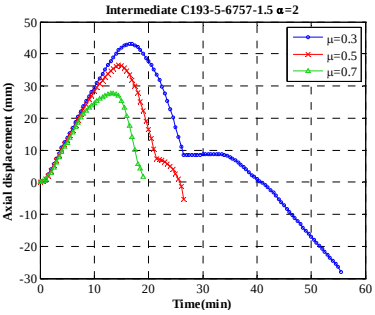
Intermediate C193-5-6757-1.5 α=2
Axial displacement (mm)
Time(min)
μ=0.3
μ=0.5
μ=0.7

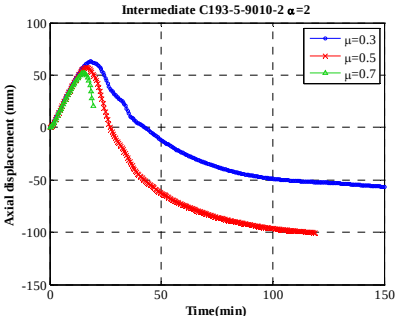
Intermediate C193-5-9010-2 α=2
Axial displacement (mm)
Time(min)
μ=0.3
μ=0.5
μ=0.7

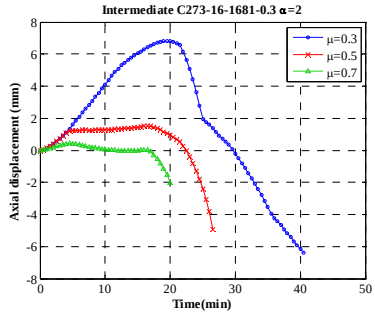
Intermediate C273-16-1681-0.3 α=2
Axial displacement (mm)
Time(min)
μ=0.3
μ=0.5
μ=0.7

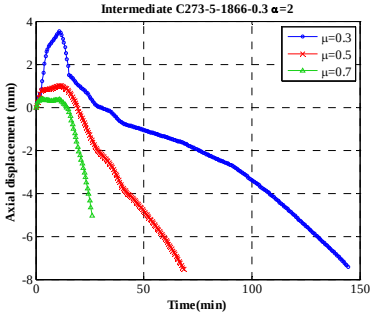
Intermediate C273-5-1866-0.3 α=2
Axial displacement (mm)
Time(min)
μ=0.3
μ=0.5
μ=0.7

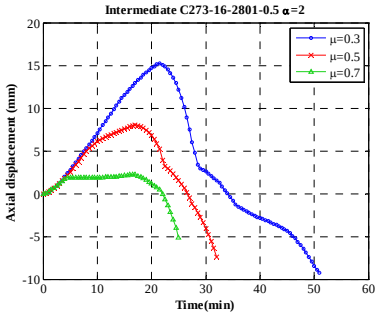
Intermediate C273-16-2801-0.5 α=2
Axial displacement (mm)
Time(min)
μ=0.3
μ=0.5
μ=0.7

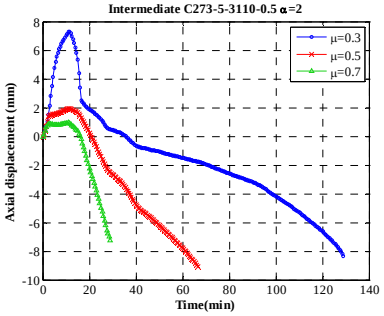
Intermediate C273-5-3110-0.5 α=2
Axial displacement (mm)
Time(min)
μ=0.3
μ=0.5
μ=0.7

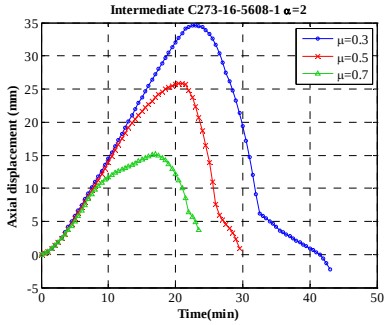
Intermediate C273-16-5608-1 α=2
Axial displacement (mm)
Time(min)
μ=0.3
μ=0.5
μ=0.7

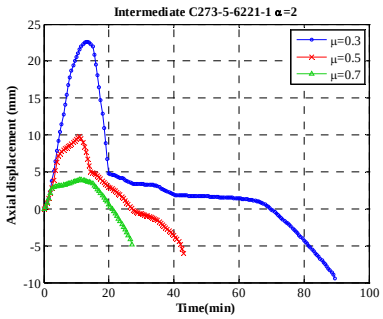
Intermediate C273-5-6221-1 α=2
Axial displacement (mm)
Time(min)
μ=0.3
μ=0.5
μ=0.7

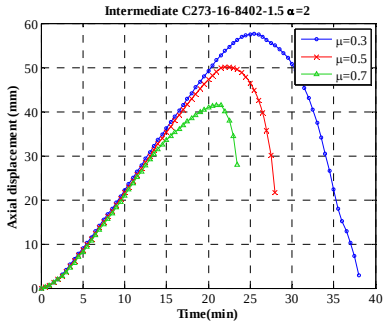
Intermediate C273-16-8402-1.5 α=2
Axial displacement (mm)
Time(min)
μ=0.3
μ=0.5
μ=0.7

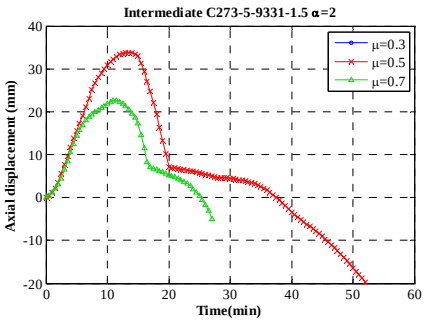
Intermediate C273-5-9331-1.5 α=2
Axial displacement (mm)
Time(min)
μ=0.3
μ=0.5
μ=0.7

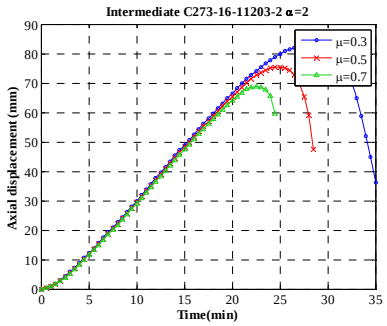
Intermediate C273-16-11203-2 α=2
Axial displacement (mm)
Time(min)
μ=0.3
μ=0.5
μ=0.7

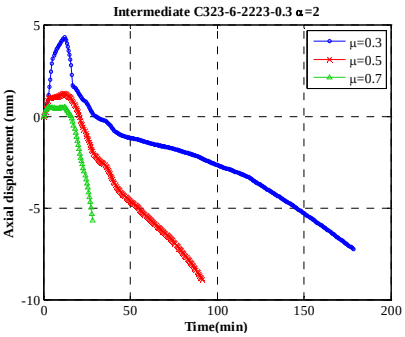
Intermediate C323-6-2223-0.3 α=2
Axial displacement (mm)
Time(min)
μ=0.3
μ=0.5
μ=0.7

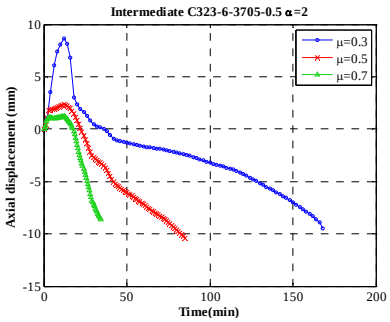
Intermediate C323-6-3705-0.5 α=2
Axial displacement (mm)
Time(min)
μ=0.3
μ=0.5
μ=0.7

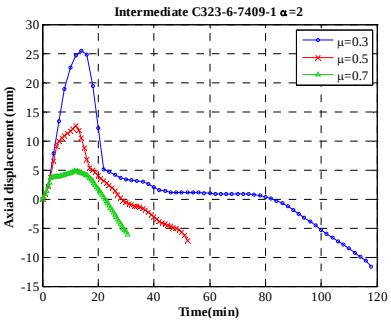
Intermediate C323-6-7409-1 α=2
Axial displacement (mm)
Time(min)
μ=0.3
μ=0.5
μ=0.7

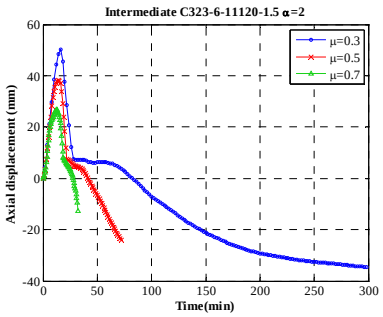
Intermediate C323-6-11120-1.5 α=2
Axial displacement (mm)
Time(min)
μ=0.3
μ=0.5
μ=0.7

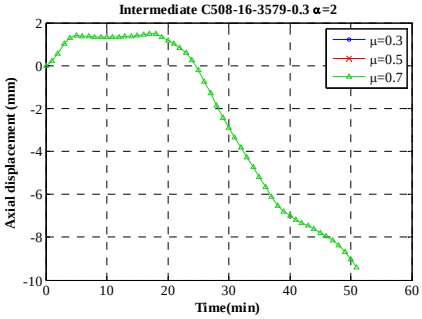
Intermediate C508-16-3579-0.3 α=2
Axial displacement (mm)
Time(min)
μ=0.3
μ=0.5
μ=0.7

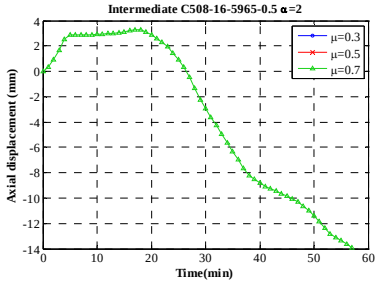
Intermediate C508-16-5965-0.5 α=2
Axial displacement (mm)
Time(min)
μ=0.3
μ=0.5
μ=0.7

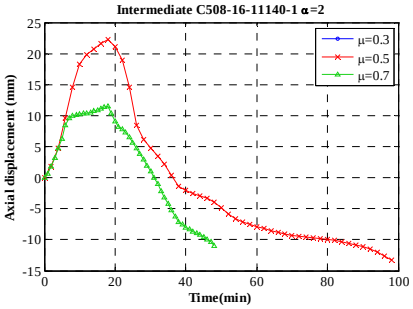
Intermediate C508-16-11140-1 α=2
Axial displacement (mm)
Time(min)
μ=0.3
μ=0.5
μ=0.7

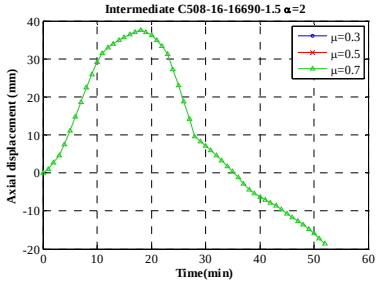
Intermediate C508-16-16690-1.5 α=2
Axial displacement (mm)
Time(min)
μ=0.3
μ=0.5
μ=0.7

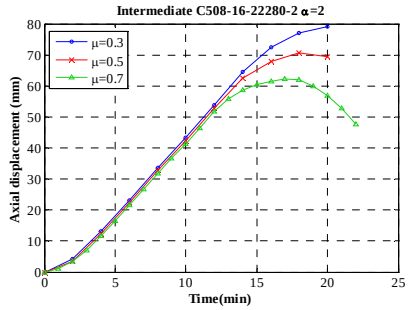
Intermediate C508-16-22280-2 α=2
Axial displacement (mm)
Time(min)
μ=0.3
μ=0.5
μ=0.7

1.2. Influence of applied load level in the restraining forces

Stiffness ratio α=0.1

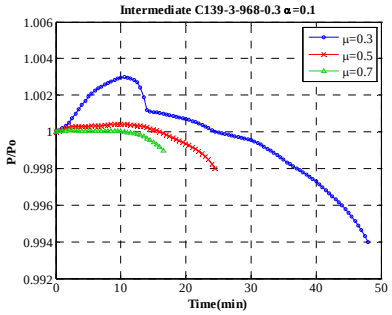

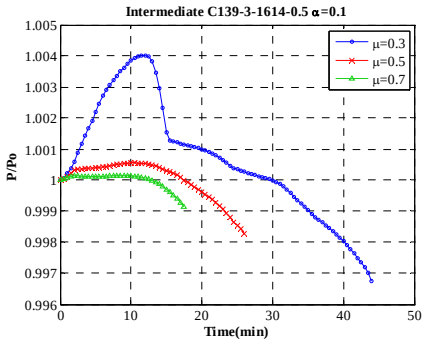

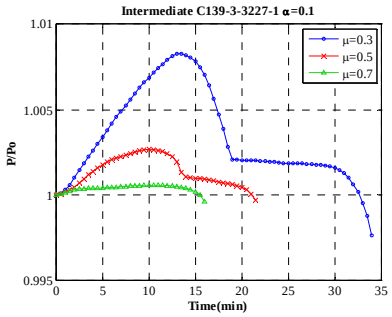

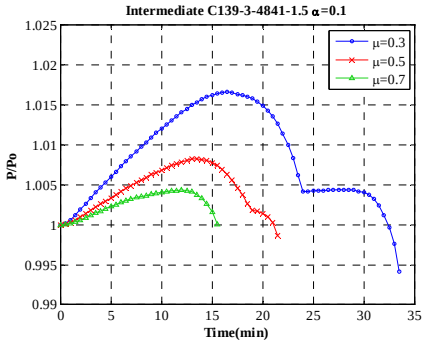

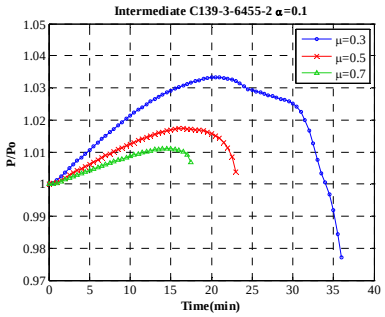

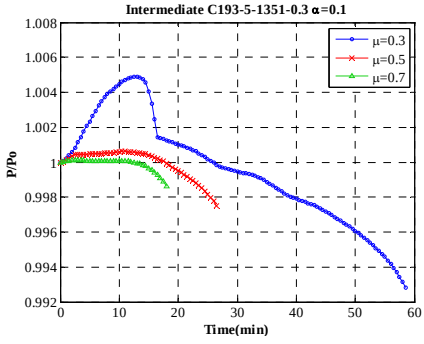

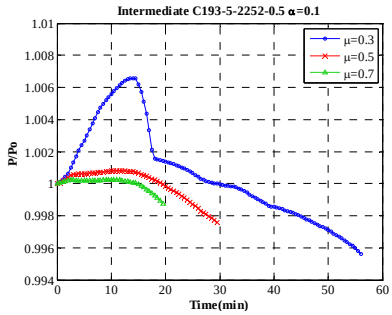
Intermediate C193-5-2252-0.5 α=0.1
μ=0.3
μ=0.5
μ=0.7
P/Po
Time(min)

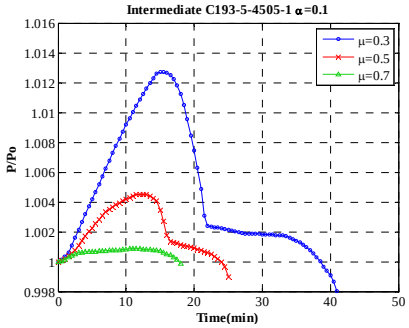
Intermediate C193-5-4505-1 α=0.1
μ=0.3
μ=0.5
μ=0.7
P/Po
Time(min)

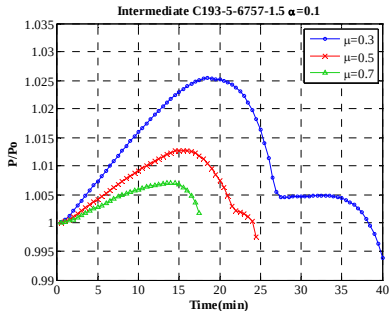
Intermediate C193-5-6757-1.5 α=0.1
μ=0.3
μ=0.5
μ=0.7
P/Po
Time(min)

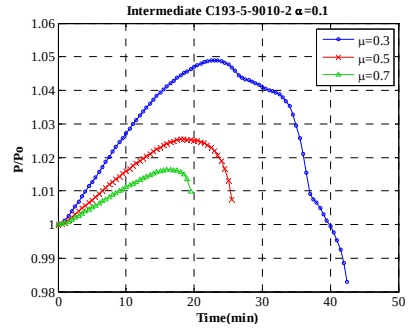
Intermediate C193-5-9010-2 α=0.1
μ=0.3
μ=0.5
μ=0.7
P/Po
Time(min)

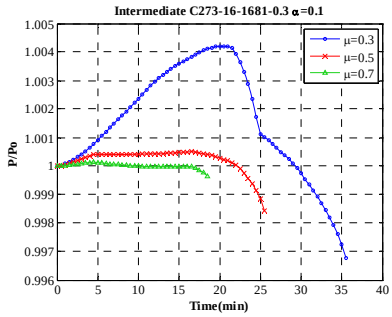
Intermediate C273-16-1681-0.3 α=0.1
μ=0.3
μ=0.5
μ=0.7
P/Po
Time(min)

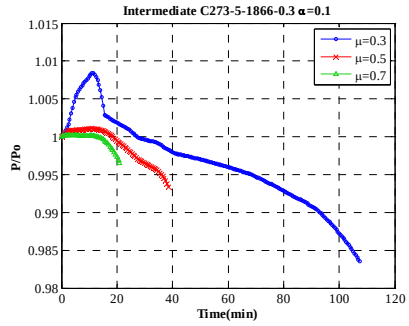
Intermediate C273-5-1866-0.3 α=0.1
μ=0.3
μ=0.5
μ=0.7
P/Po
Time(min)

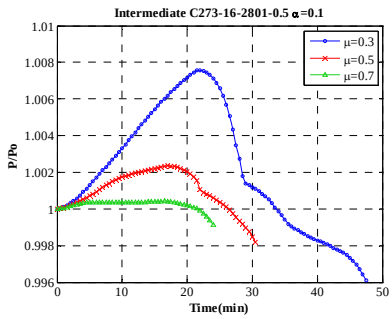
Intermediate C273-16-2801-0.5 α=0.1
μ=0.3
μ=0.5
μ=0.7
P/Po
Time(min)

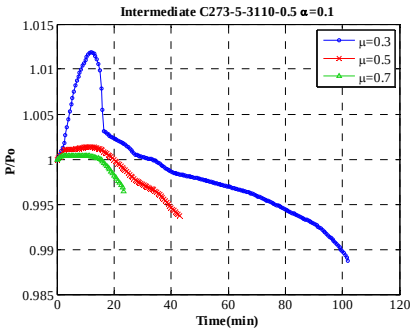
Intermediate C273-5-3110-0.5 α=0.1
μ=0.3
μ=0.5
μ=0.7
P/Po
Time(min)

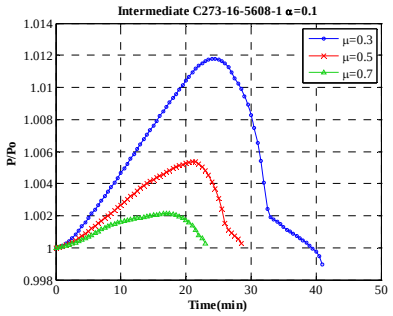
Intermediate C273-16-5608-1 α=0.1
μ=0.3
μ=0.5
μ=0.7
P/Po
Time(min)

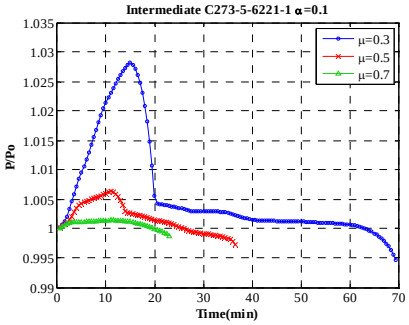
Intermediate C273-5-6221-1 α=0.1
μ=0.3
μ=0.5
μ=0.7
P/Po
Time(min)

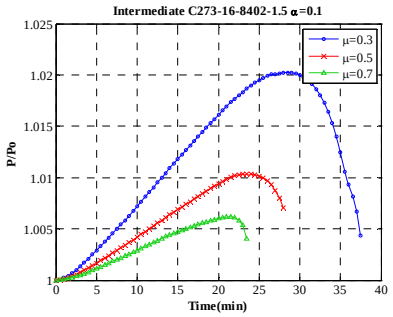
Intermediate C273-16-8402-1.5 α=0.1
μ=0.3
μ=0.5
μ=0.7
P/Po
Time(min)

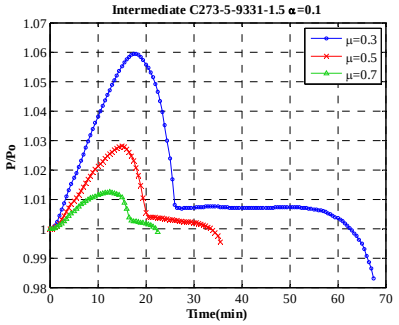
Intermediate C273-5-9331-1.5 α=0.1
μ=0.3
μ=0.5
μ=0.7
P/Po
Time(min)

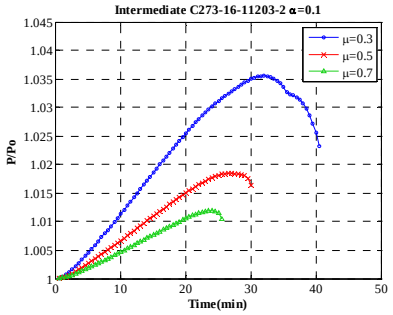
Intermediate C273-16-11203-2 α=0.1
μ=0.3
μ=0.5
μ=0.7
P/Po
Time(min)

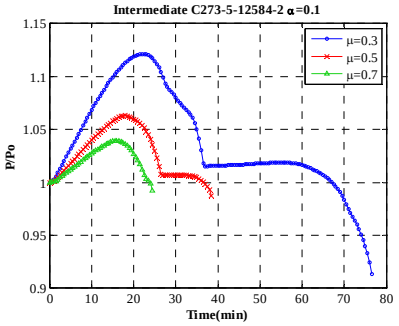
Intermediate C273-5-12584-2 α=0.1
μ=0.3
μ=0.5
μ=0.7
P/Po
Time(min)

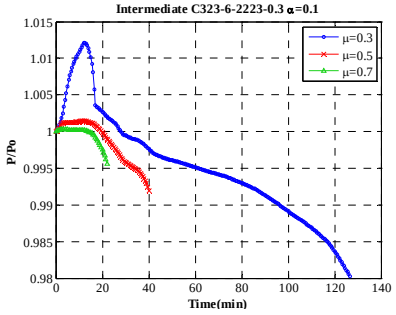
Intermediate C323-6-2223-0.3 α=0.1
μ=0.3
μ=0.5
μ=0.7
P/Po
Time(min)

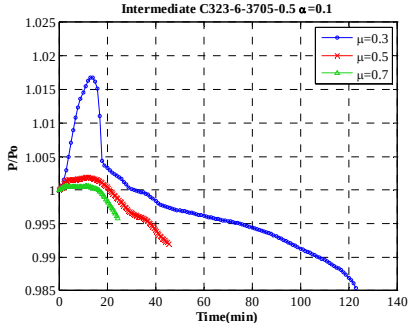
Intermediate C323-6-3705-0.5 α=0.1
μ=0.3
μ=0.5
μ=0.7
P/Po
Time(min)

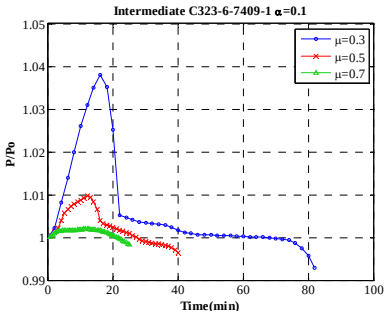
Intermediate C323-6-7409-1 α=0.1
μ=0.3
μ=0.5
μ=0.7
P/Po
Time(min)

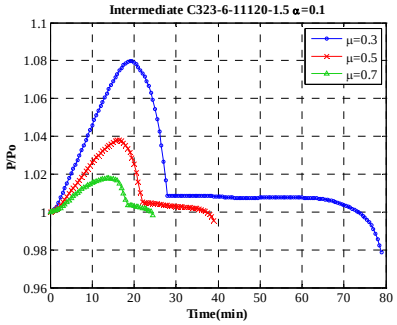
Intermediate C323-6-11120-1.5 α=0.1
μ=0.3
μ=0.5
μ=0.7
P/Po
Time(min)

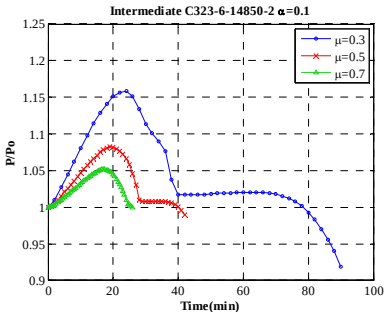
Intermediate C323-6-14850-2 α=0.1
μ=0.3
μ=0.5
μ=0.7
P/Po
Time(min)

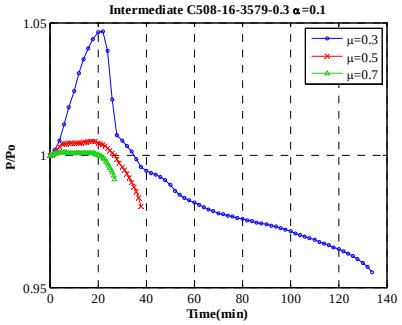
Intermediate C508-16-3579-0.3 α=0.1
μ=0.3
μ=0.5
μ=0.7
P/Po
Time(min)

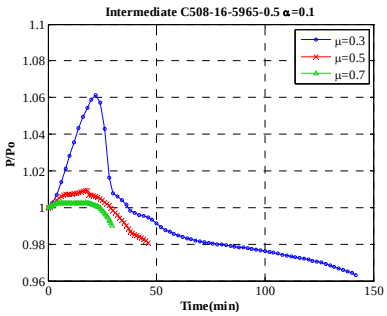
Intermediate C508-16-5965-0.5 α=0.1
μ=0.3
μ=0.5
μ=0.7
P/Po
Time(min)

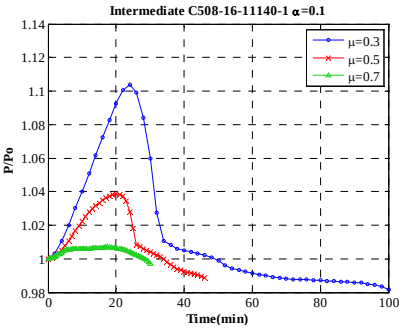
Intermediate C508-16-11140-1 α=0.1
μ=0.3
μ=0.5
μ=0.7
P/Po
Time(min)

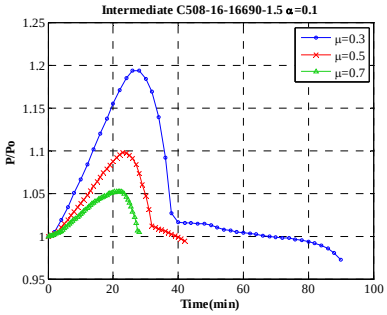
Intermediate C508-16-16690-1.5 α=0.1
μ=0.3
μ=0.5
μ=0.7
P/Po
Time(min)

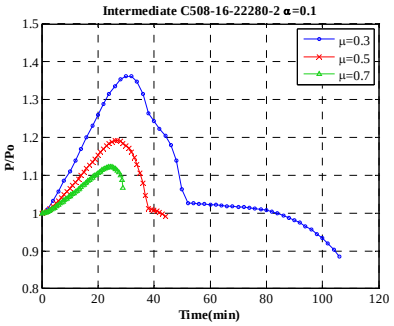
Intermediate C508-16-22280-2 α=0.1
μ=0.3
μ=0.5
μ=0.7
P/Po
Time(min)

Stiffness ratio α=0.5

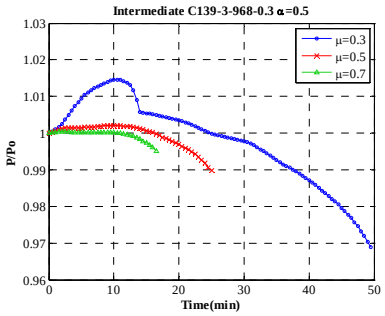

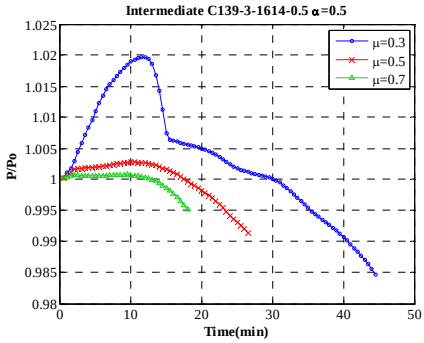

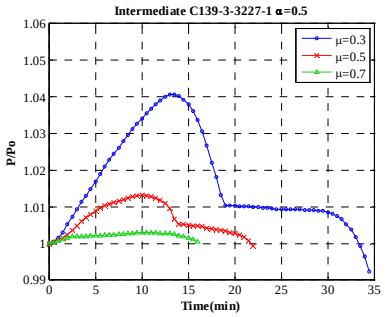

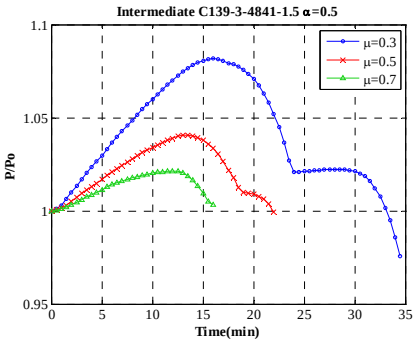

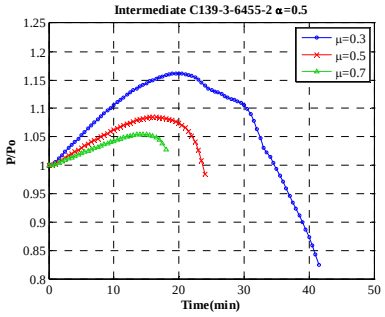

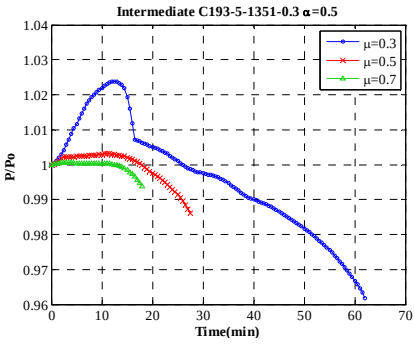

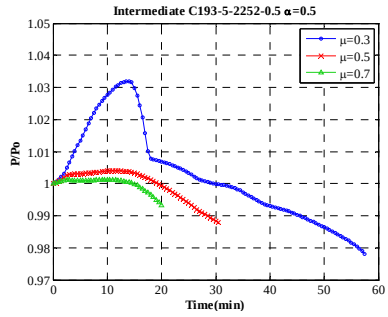
Intermediate C193-5-2252-0.5 α=0.5
μ=0.3
μ=0.5
μ=0.7
P/Po
Time(min)

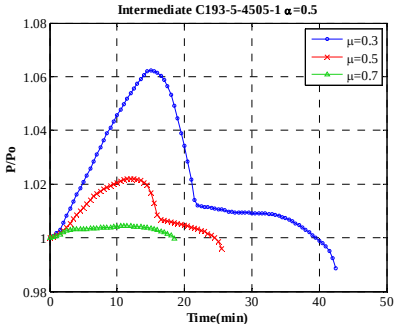
Intermediate C193-5-4505-1 α=0.5
μ=0.3
μ=0.5
μ=0.7
P/Po
Time(min)

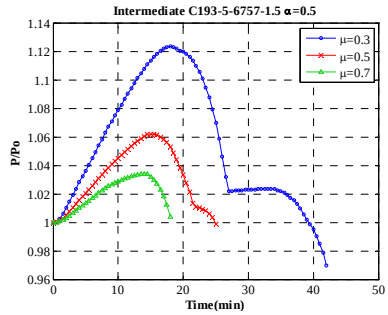
Intermediate C193-5-6757-1.5 α=0.5
μ=0.3
μ=0.5
μ=0.7
P/Po
Time(min)

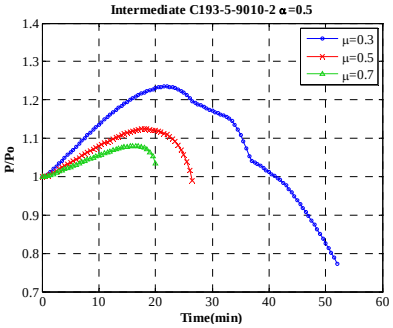
Intermediate C193-5-9010-2 α=0.5
μ=0.3
μ=0.5
μ=0.7
P/Po
Time(min)

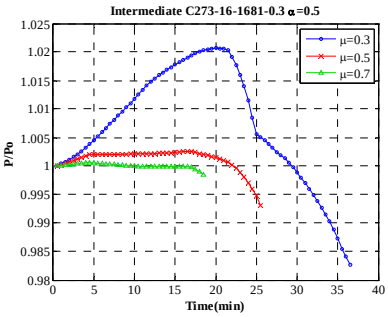
Intermediate C273-16-1681-0.3 α=0.5
μ=0.3
μ=0.5
μ=0.7
P/Po
Time(min)

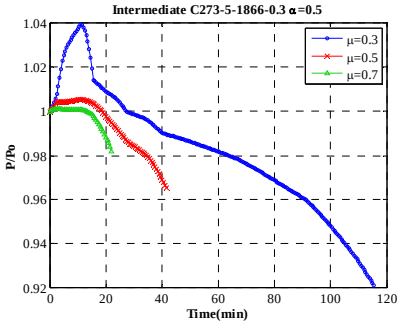
Intermediate C273-5-1866-0.3 α=0.5
μ=0.3
μ=0.5
μ=0.7
P/Po
Time(min)

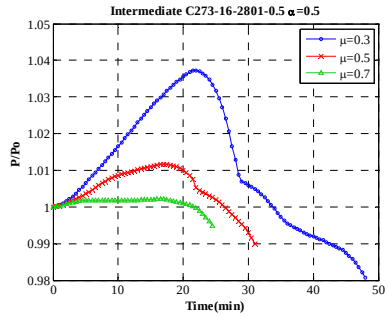
Intermediate C273-16-2801-0.5 α=0.5
μ=0.3
μ=0.5
μ=0.7
P/Po
Time(min)

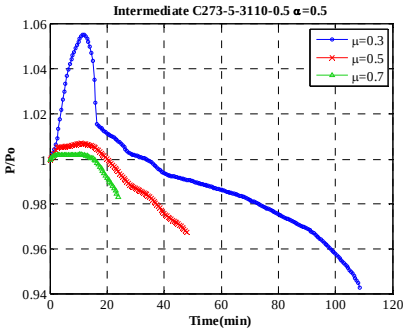
Intermediate C273-5-3110-0.5 α=0.5
μ=0.3
μ=0.5
μ=0.7
P/Po
Time(min)

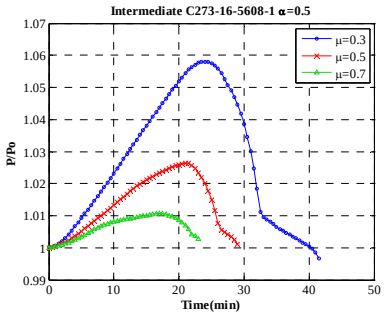
Intermediate C273-16-5608-1 α=0.5
P/Po
Time(min)
μ=0.3
μ=0.5
μ=0.7

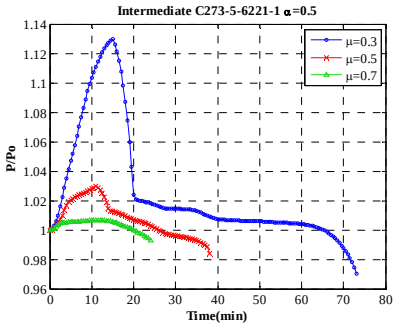
Intermediate C273-5-6221-1 α=0.5
P/Po
Time(min)
μ=0.3
μ=0.5
μ=0.7

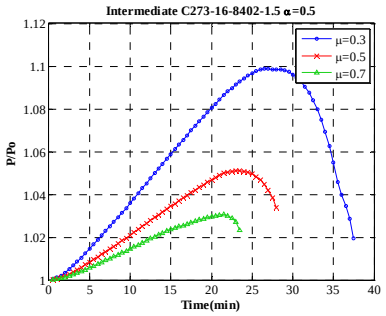
Intermediate C273-16-8402-1.5 α=0.5
P/Po
Time(min)
μ=0.3
μ=0.5
μ=0.7

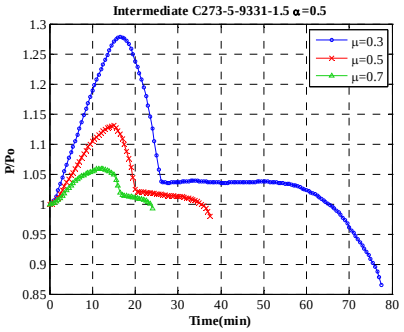
Intermediate C273-5-9331-1.5 α=0.5
P/Po
Time(min)
μ=0.3
μ=0.5
μ=0.7

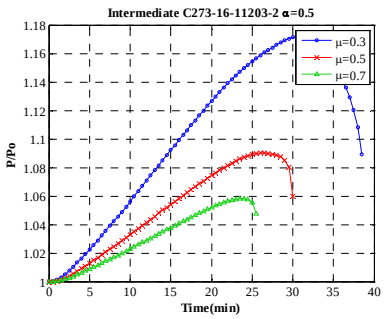
Intermediate C273-16-11203-2 α=0.5
P/Po
Time(min)
μ=0.3
μ=0.5
μ=0.7

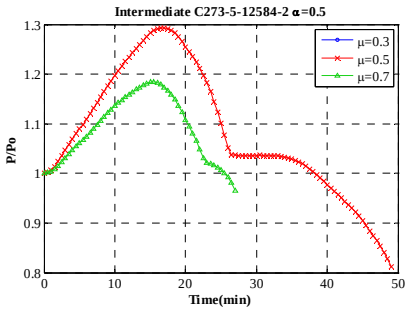
Intermediate C273-5-12584-2 α=0.5
P/Po
Time(min)
μ=0.3
μ=0.5
μ=0.7

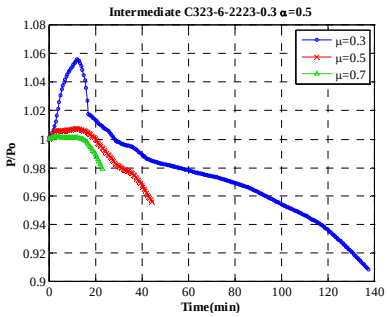
Intermediate C323-6-2223-0.3 α=0.5
P/Po
Time(min)
μ=0.3
μ=0.5
μ=0.7

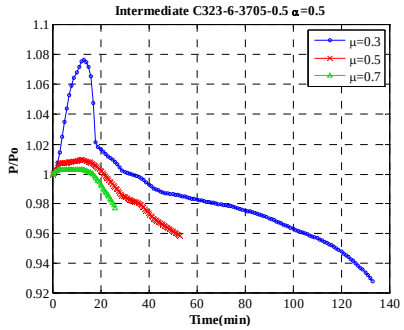
Intermediate C323-6-3705-0.5 α=0.5
P/Po
Time(min)
μ=0.3
μ=0.5
μ=0.7

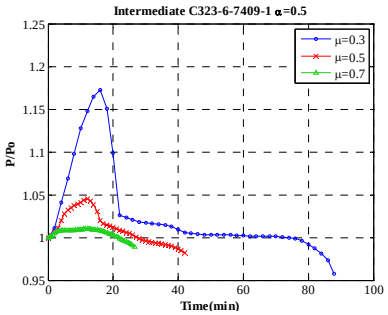
Intermediate C323-6-7409-1 α=0.5
μ=0.3
μ=0.5
μ=0.7
P/Po
Time(min)

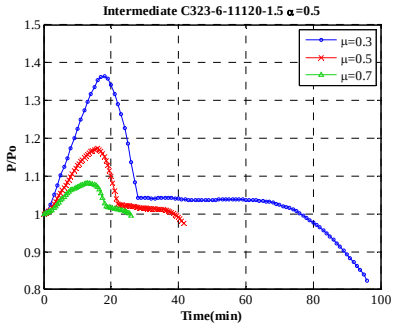
Intermediate C323-6-11120-1.5 α=0.5
μ=0.3
μ=0.5
μ=0.7
P/Po
Time(min)

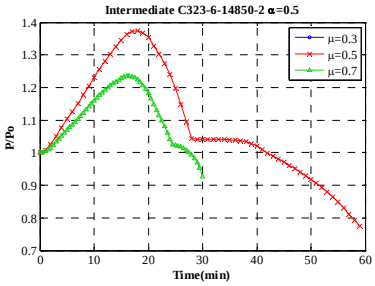
Intermediate C323-6-14850-2 α=0.5
μ=0.3
μ=0.5
μ=0.7
P/Po
Time(min)

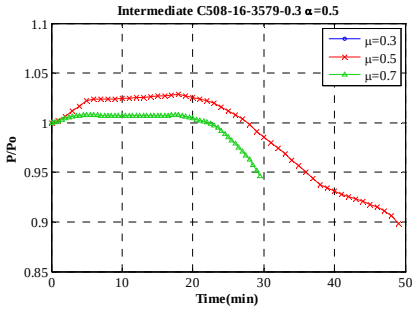
Intermediate C508-16-3579-0.3 α=0.5
μ=0.3
μ=0.5
μ=0.7
P/Po
Time(min)

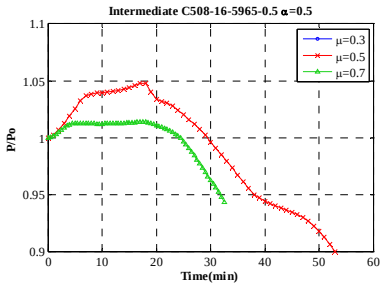
Intermediate C508-16-5965-0.5 α=0.5
μ=0.3
μ=0.5
μ=0.7
P/Po
Time(min)

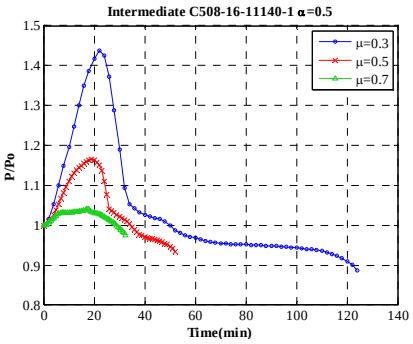
Intermediate C508-16-11140-1 α=0.5
μ=0.3
μ=0.5
μ=0.7
P/Po
Time(min)

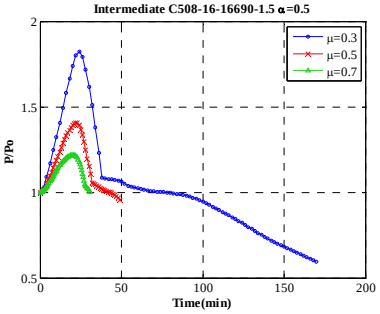
Intermediate C508-16-16690-1.5 α=0.5
μ=0.3
μ=0.5
μ=0.7
P/Po
Time(min)

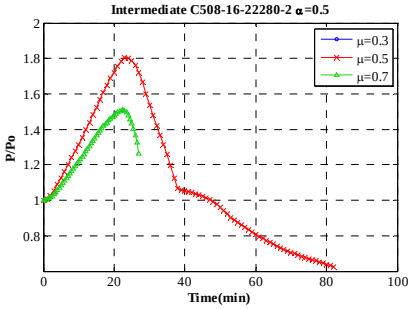
Intermediate C508-16-22280-2 α=0.5
μ=0.3
μ=0.5
μ=0.7
P/Po
Time(min)

Stiffness α=1

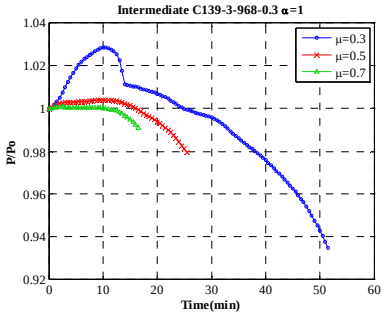

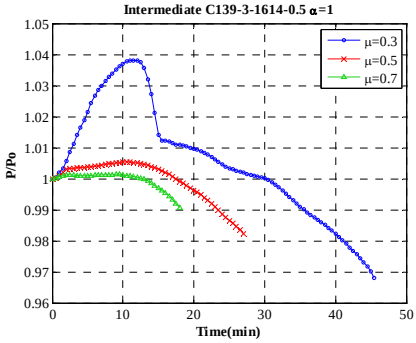

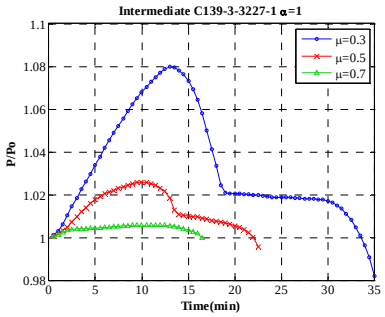

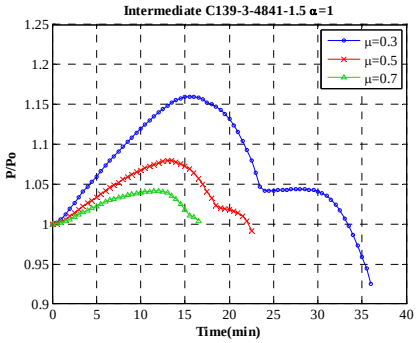

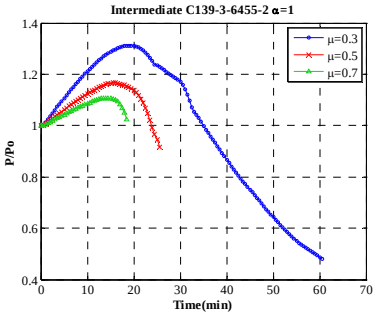

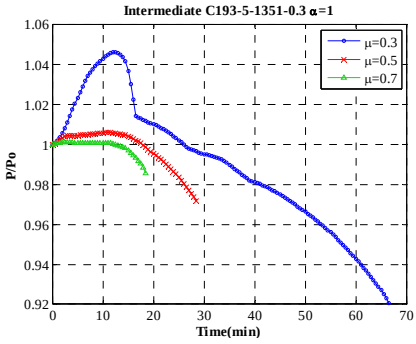

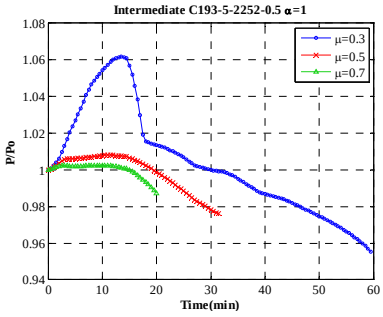
Intermediate C193-5-2252-0.5 α=1
μ=0.3
μ=0.5
μ=0.7
P/Po
Time(min)

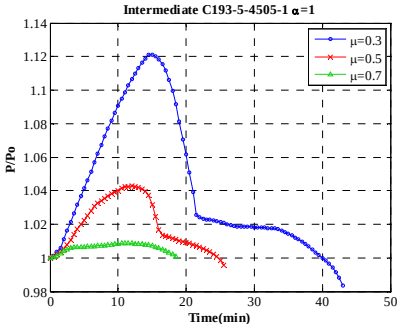
Intermediate C193-5-4505-1 α=1
μ=0.3
μ=0.5
μ=0.7
P/Po
Time(min)

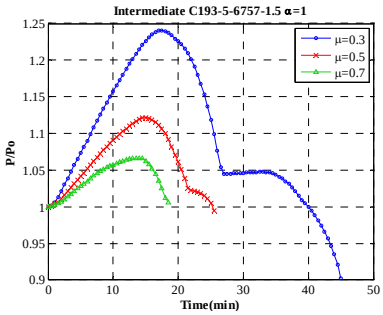
Intermediate C193-5-6757-1.5 α=1
μ=0.3
μ=0.5
μ=0.7
P/Po
Time(min)

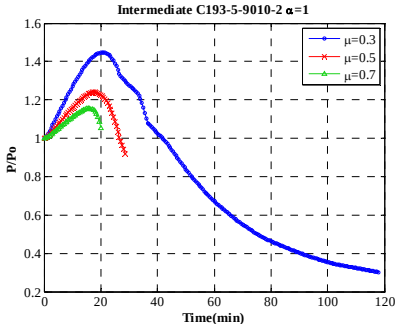
Intermediate C193-5-9010-2 α=1
μ=0.3
μ=0.5
μ=0.7
P/Po
Time(min)

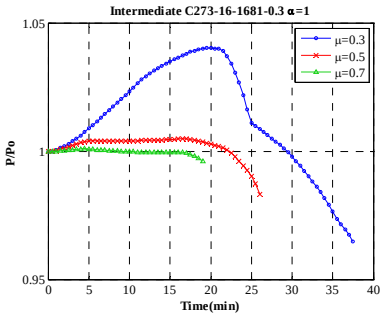
Intermediate C273-16-1681-0.3 α=1
μ=0.3
μ=0.5
μ=0.7
P/Po
Time(min)

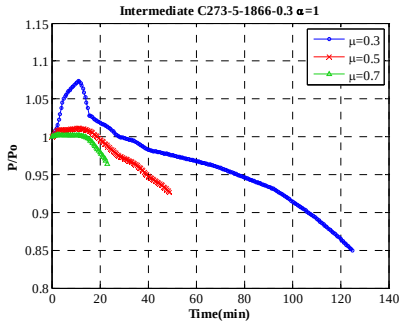
Intermediate C273-5-1866-0.3 α=1
μ=0.3
μ=0.5
μ=0.7
P/Po
Time(min)

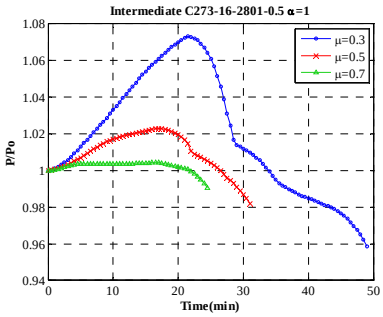
Intermediate C273-16-2801-0.5 α=1
μ=0.3
μ=0.5
μ=0.7
P/Po
Time(min)

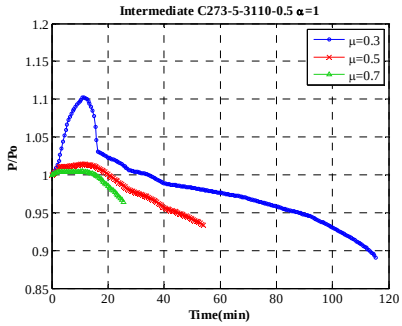
Intermediate C273-5-3110-0.5 α=1
μ=0.3
μ=0.5
μ=0.7
P/Po
Time(min)

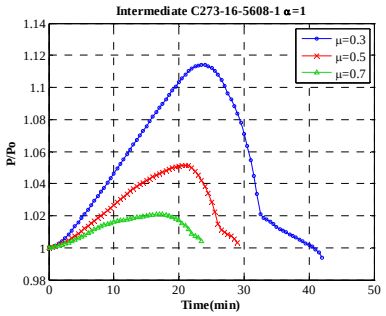
Intermediate C273-16-5608-1 α=1
μ=0.3
μ=0.5
μ=0.7
P/Po
Time(min)

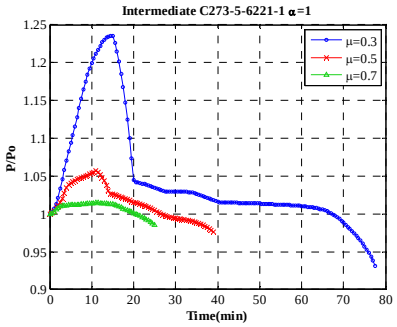
Intermediate C273-5-6221-1 α=1
μ=0.3
μ=0.5
μ=0.7
P/Po
Time(min)

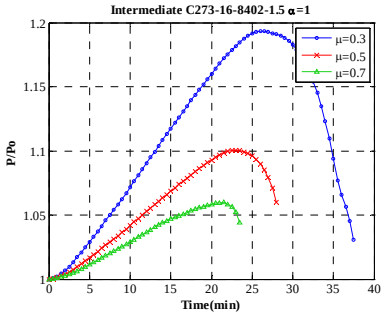
Intermediate C273-16-8402-1.5 α=1
μ=0.3
μ=0.5
μ=0.7
P/Po
Time(min)

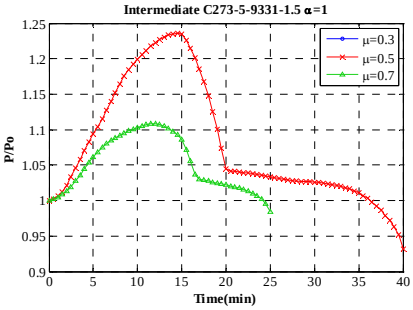
Intermediate C273-5-9331-1.5 α=1
μ=0.3
μ=0.5
μ=0.7
P/Po
Time(min)

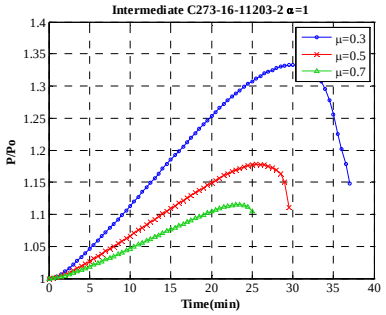
Intermediate C273-16-11203-2 α=1
μ=0.3
μ=0.5
μ=0.7
P/Po
Time(min)

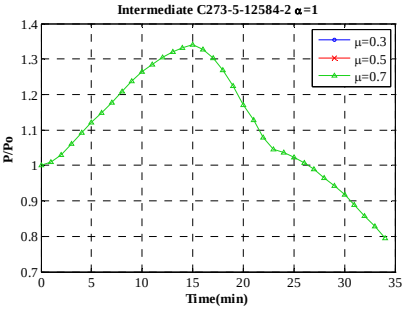
Intermediate C273-5-12584-2 α=1
μ=0.3
μ=0.5
μ=0.7
P/Po
Time(min)

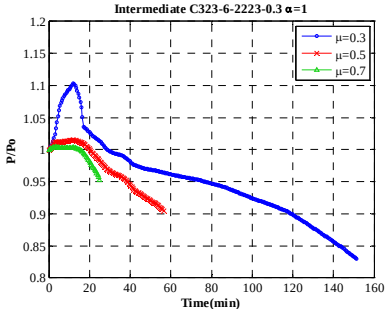
Intermediate C323-6-2223-0.3 α=1
μ=0.3
μ=0.5
μ=0.7
P/Po
Time(min)

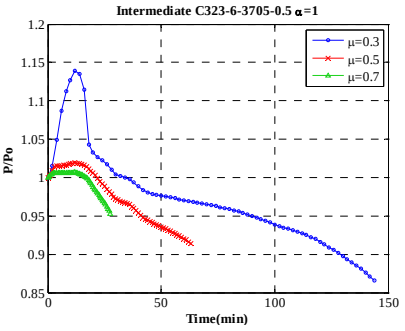
Intermediate C323-6-3705-0.5 α=1
μ=0.3
μ=0.5
μ=0.7
P/Po
Time(min)

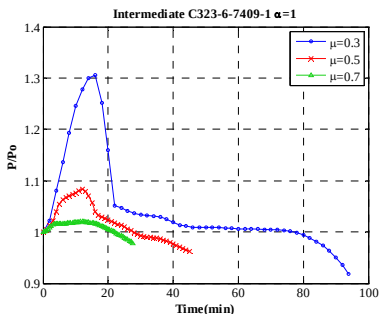
Intermediate C323-6-7409-1 α=1
μ=0.3
μ=0.5
μ=0.7
P/Po
Time(min)

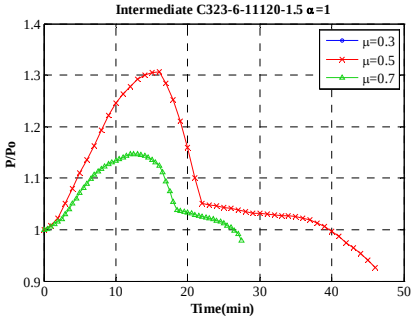
Intermediate C323-6-11120-1.5 α=1
μ=0.3
μ=0.5
μ=0.7
P/Po
Time(min)

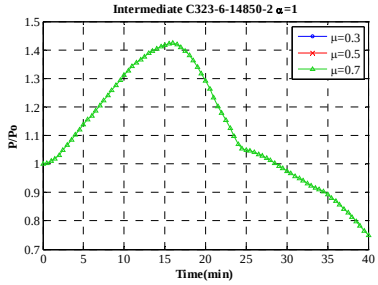
Intermediate C323-6-14850-2 α=1
μ=0.3
μ=0.5
μ=0.7
P/Po
Time(min)

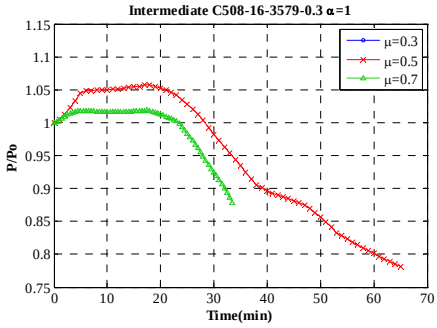
Intermediate C508-16-3579-0.3 α=1
μ=0.3
μ=0.5
μ=0.7
P/Po
Time(min)

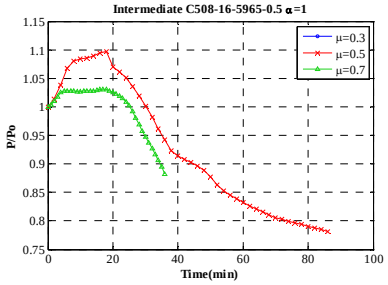
Intermediate C508-16-5965-0.5 α=1
μ=0.3
μ=0.5
μ=0.7
P/Po
Time(min)

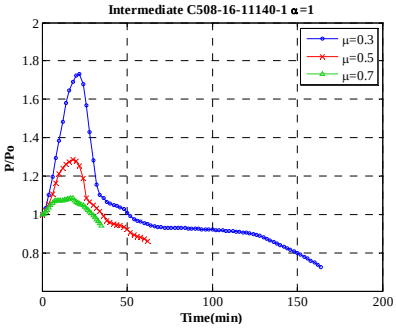
Intermediate C508-16-11140-1 α=1
μ=0.3
μ=0.5
μ=0.7
P/Po
Time(min)

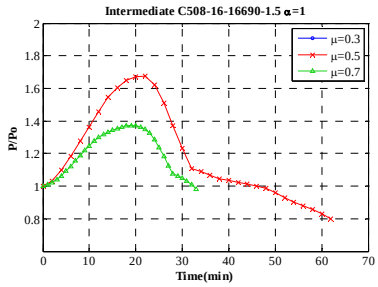
Intermediate C508-16-16690-1.5 α=1
μ=0.3
μ=0.5
μ=0.7
P/Po
Time(min)

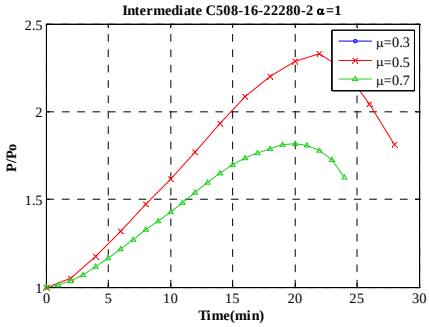
Intermediate C508-16-22280-2 α=1
μ=0.3
μ=0.5
μ=0.7
P/Po
Time(min)

Stiffness α=2

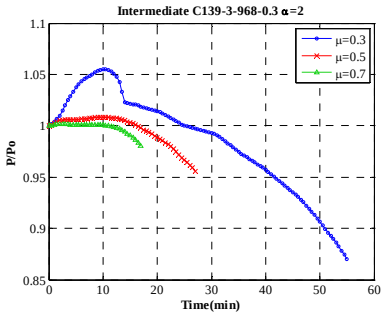

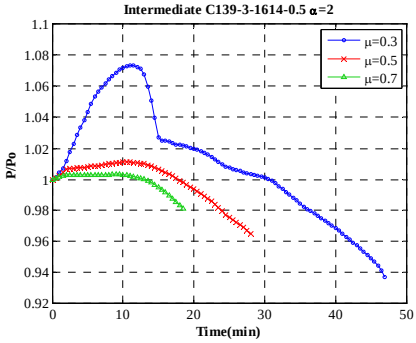

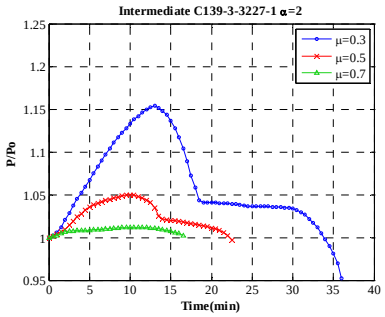

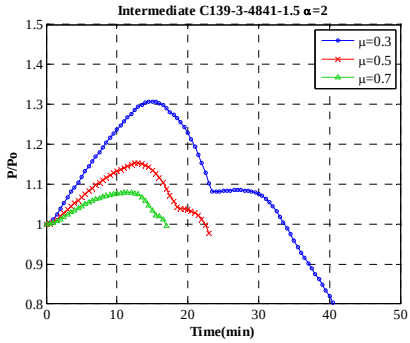

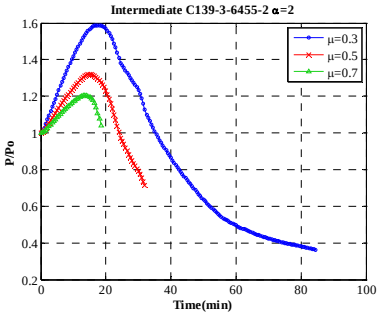

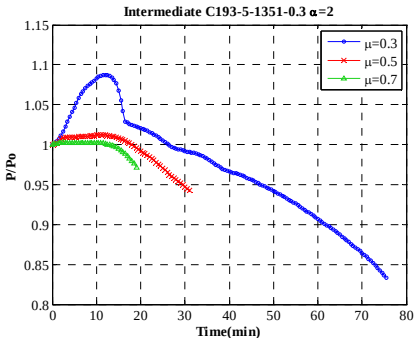

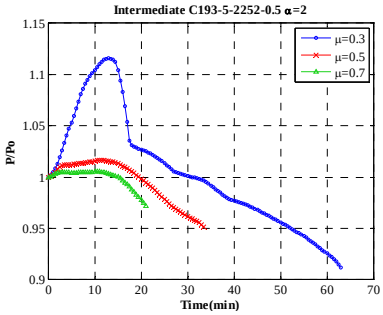
Intermediate C193-5-2252-0.5 α=2
μ=0.3
μ=0.5
μ=0.7
P/Po
Time(min)

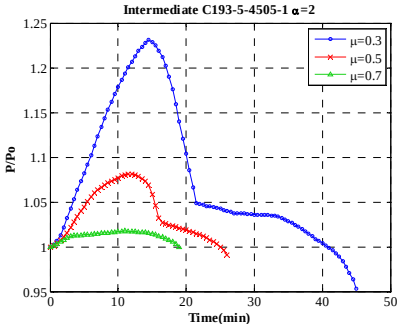
Intermediate C193-5-4505-1 α=2
μ=0.3
μ=0.5
μ=0.7
P/Po
Time(min)

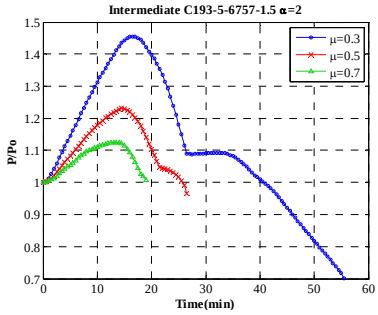
Intermediate C193-5-6757-1.5 α=2
μ=0.3
μ=0.5
μ=0.7
P/Po
Time(min)

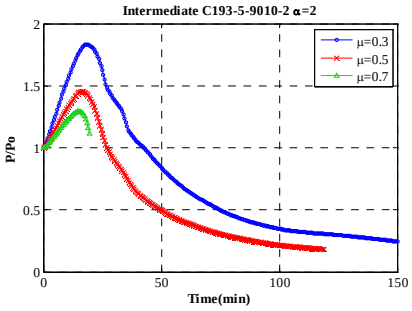
Intermediate C193-5-9010-2 α=2
μ=0.3
μ=0.5
μ=0.7
P/Po
Time(min)

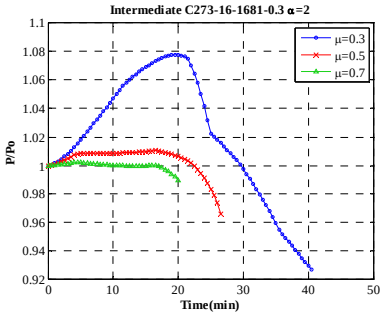
Intermediate C273-16-1681-0.3 α=2
μ=0.3
μ=0.5
μ=0.7
P/Po
Time(min)

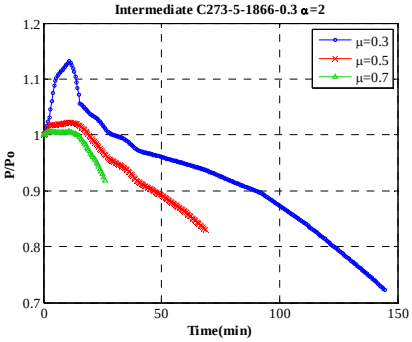
Intermediate C273-5-1866-0.3 α=2
μ=0.3
μ=0.5
μ=0.7
P/Po
Time(min)

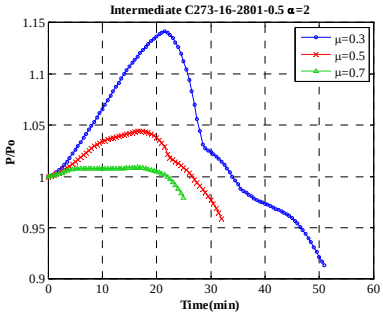
Intermediate C273-16-2801-0.5 α=2
μ=0.3
μ=0.5
μ=0.7
P/Po
Time(min)

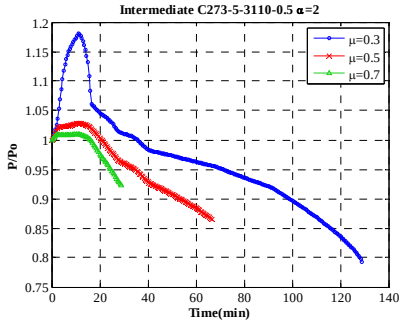
Intermediate C273-5-3110-0.5 α=2
μ=0.3
μ=0.5
μ=0.7
P/Po
Time(min)

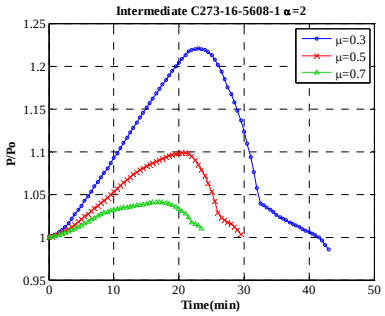
Intermediate C273-16-5608-1 α=2
μ=0.3
μ=0.5
μ=0.7
P/Po
Time(min)

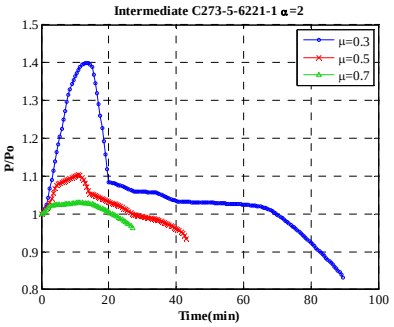
Intermediate C273-5-6221-1 α=2
μ=0.3
μ=0.5
μ=0.7
P/Po
Time(min)

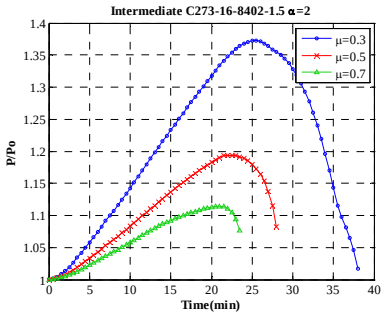
Intermediate C273-16-8402-1.5 α=2
μ=0.3
μ=0.5
μ=0.7
P/Po
Time(min)

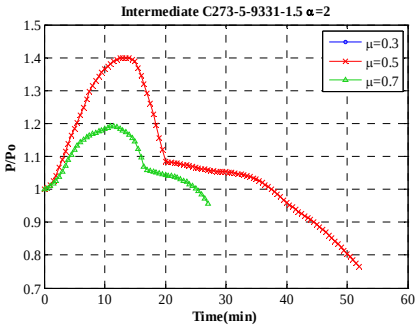
Intermediate C273-5-9331-1.5 α=2
μ=0.3
μ=0.5
μ=0.7
P/Po
Time(min)

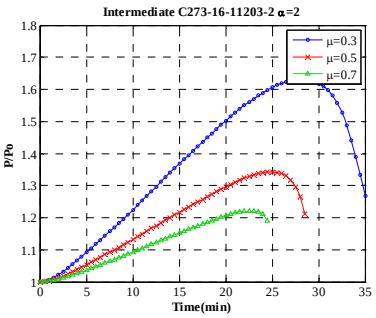
Intermediate C273-16-11203-2 α=2
μ=0.3
μ=0.5
μ=0.7
P/Po
Time(min)

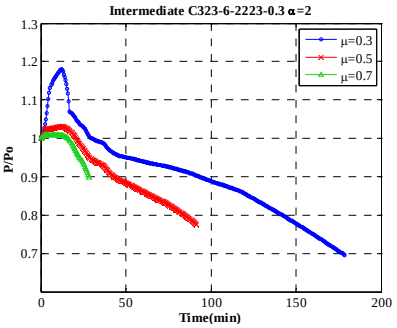
Intermediate C323-6-2223-0.3 α=2
μ=0.3
μ=0.5
μ=0.7
P/Po
Time(min)

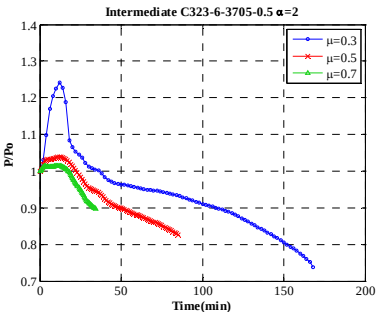
Intermediate C323-6-3705-0.5 α=2
μ=0.3
μ=0.5
μ=0.7
P/Po
Time(min)

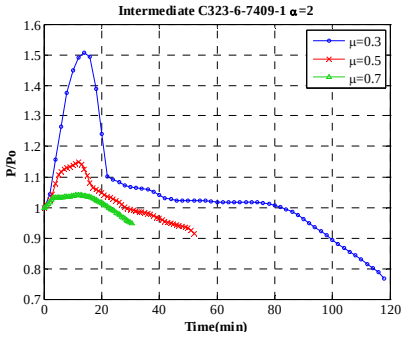
Intermediate C323-6-7409-1 α=2
μ=0.3
μ=0.5
μ=0.7
P/Po
Time(min)

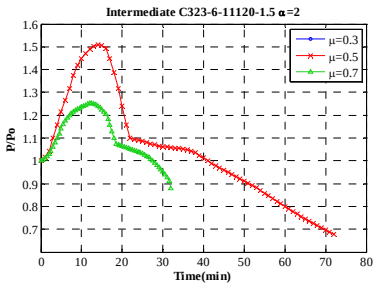
Intermediate C323-6-11120-1.5 α=2
μ=0.3
μ=0.5
μ=0.7
P/Po
Time(min)

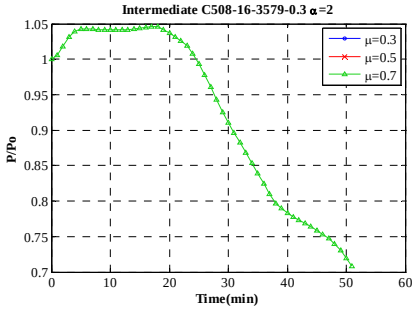
Intermediate C508-16-3579-0.3 α=2
μ=0.3
μ=0.5
μ=0.7
P/Po
Time(min)

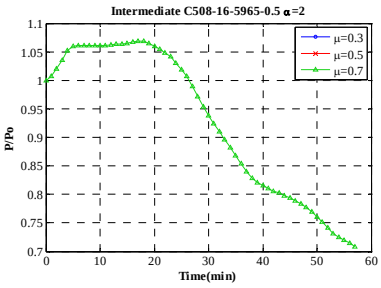
Intermediate C508-16-5965-0.5 α=2
μ=0.3
μ=0.5
μ=0.7
P/Po
Time(min)

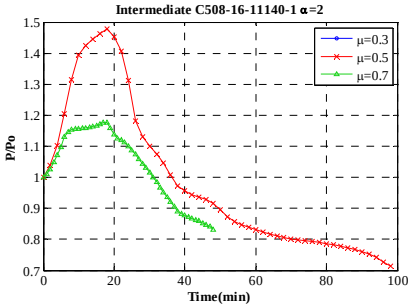
Intermediate C508-16-11140-1 α=2
μ=0.3
μ=0.5
μ=0.7
P/Po
Time(min)

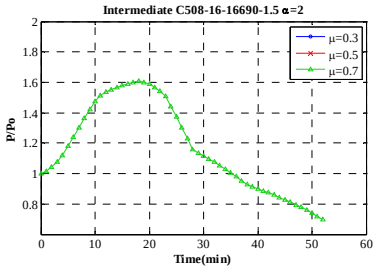
Intermediate C508-16-16690-1.5 α=2
μ=0.3
μ=0.5
μ=0.7
P/Po
Time(min)

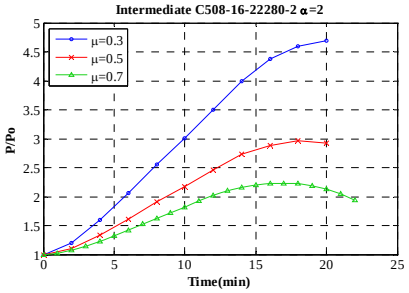
Intermediate C508-16-22280-2 α=2
μ=0.3
μ=0.5
μ=0.7
P/Po
Time(min)

2. INFLUENCE OF THE STIFFNESS RATIO

2.1. Influence of the stiffness ratio in the axial displacement

Load level μ=0.3

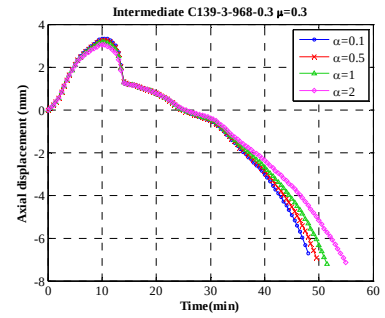

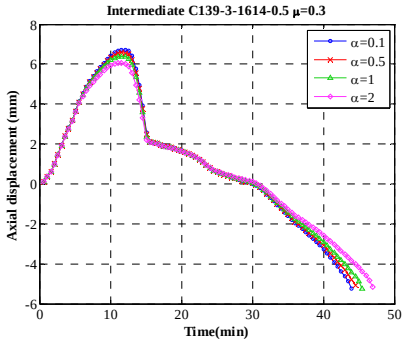

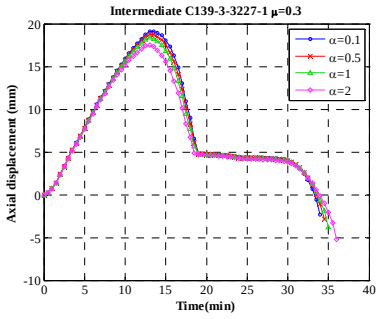

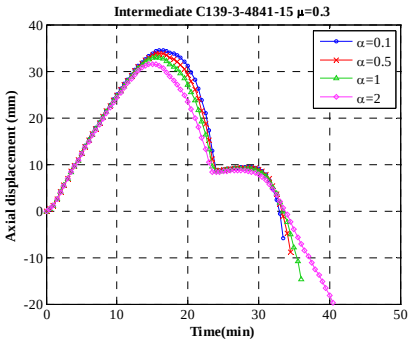

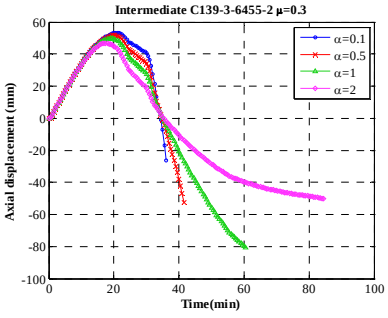

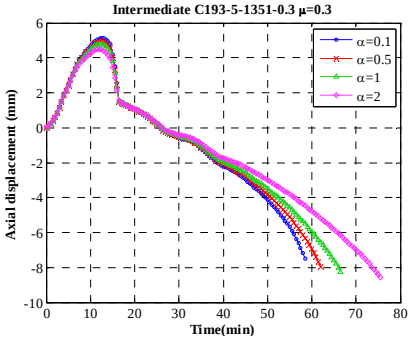

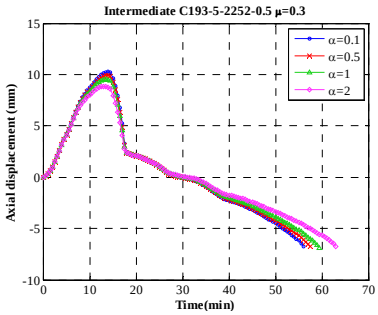
Intermediate C193-5-2252-0.5 μ=0.3
Axial displacement (mm)
Time(min)
α=0.1
α=0.5
α=1
α=2

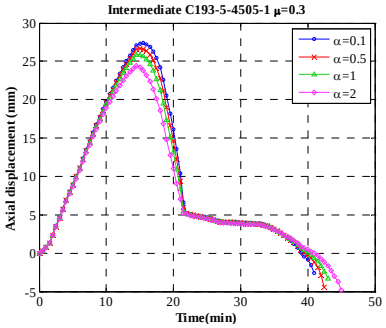
Intermediate C193-5-4505-1 μ=0.3
Axial displacement (mm)
Time(min)
α=0.1
α=0.5
α=1
α=2

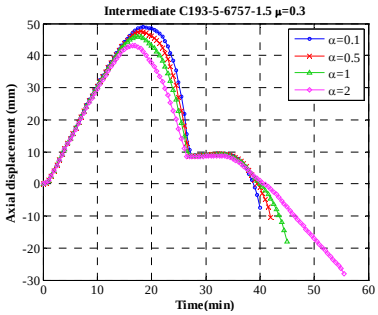
Intermediate C193-5-6757-1.5 μ=0.3
Axial displacement (mm)
Time(min)
α=0.1
α=0.5
α=1
α=2

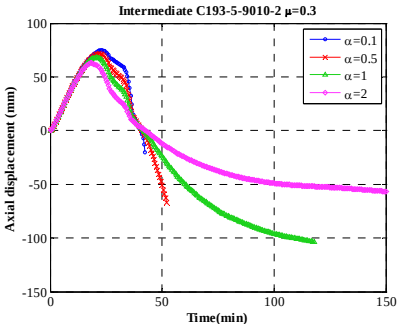
Intermediate C193-5-9010-2 μ=0.3
Axial displacement (mm)
Time(min)
α=0.1
α=0.5
α=1
α=2

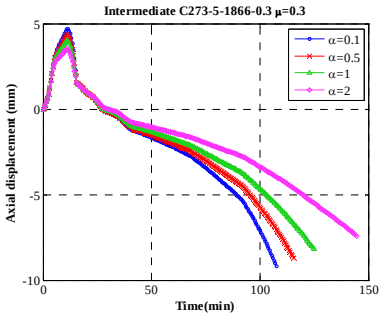
Intermediate C273-5-1866-0.3 μ=0.3
Axial displacement (mm)
Time(min)
α=0.1
α=0.5
α=1
α=2

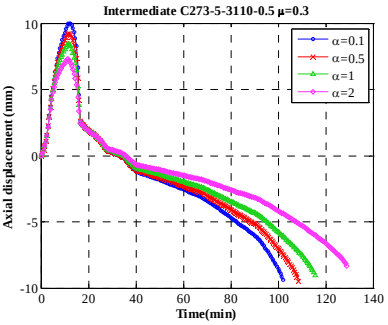
Intermediate C273-5-3110-0.5 μ=0.3
Axial displacement (mm)
Time(min)
α=0.1
α=0.5
α=1
α=2

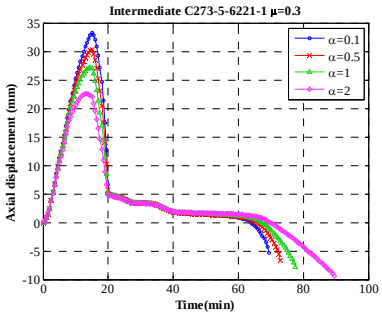
Intermediate C273-5-6221-1 μ=0.3
Axial displacement (mm)
Time(min)
α=0.1
α=0.5
α=1
α=2

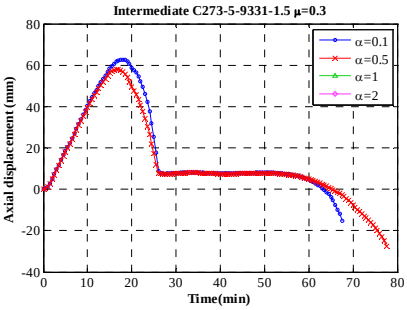
Intermediate C273-5-9331-1.5 μ=0.3
Axial displacement (mm)
Time(min)
α=0.1
α=0.5
α=1
α=2

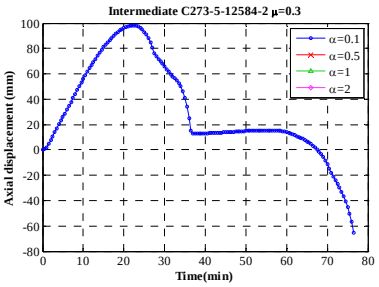
Intermediate C273-5-12584-2 μ=0.3
Axial displacement (mm)
Time(min)
α=0.1
α=0.5
α=1
α=2

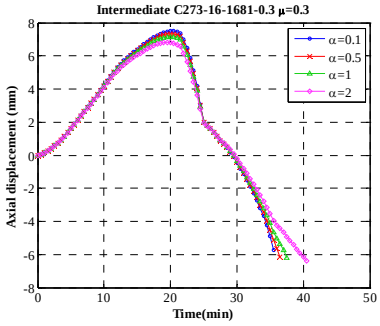
Intermediate C273-16-1681-0.3 μ=0.3
Axial displacement (mm)
Time(min)
α=0.1
α=0.5
α=1
α=2

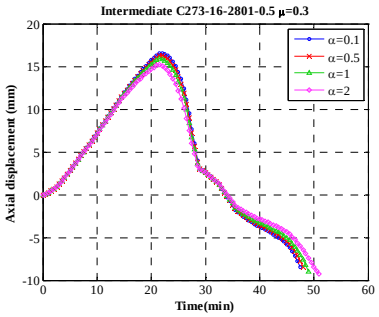
Intermediate C273-16-2801-0.5 μ=0.3
Axial displacement (mm)
Time(min)
α=0.1
α=0.5
α=1
α=2

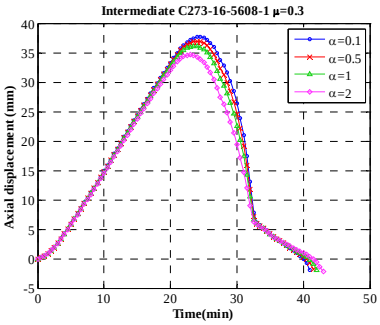
Intermediate C273-16-5608-1 μ=0.3
Axial displacement (mm)
Time(min)
α=0.1
α=0.5
α=1
α=2

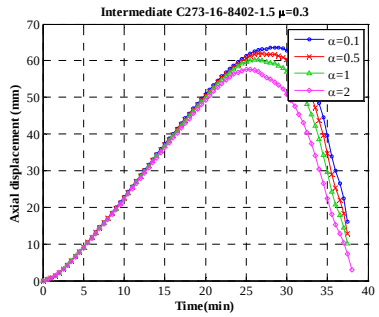
Intermediate C273-16-8402-1.5 μ=0.3
Axial displacement (mm)
Time(min)
α=0.1
α=0.5
α=1
α=2

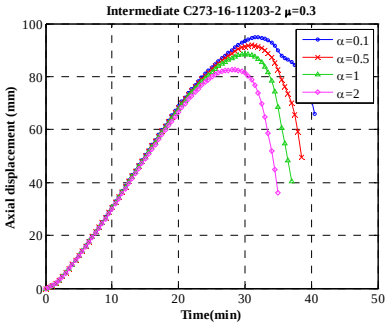
Intermediate C273-16-11203-2 μ=0.3
Axial displacement (mm)
Time(min)
α=0.1
α=0.5
α=1
α=2

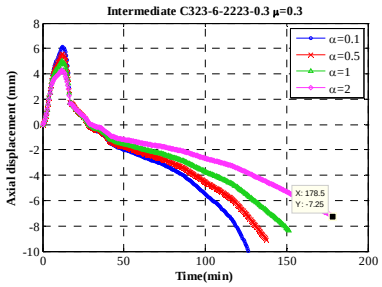
Intermediate C323-6-2223-0.3 μ=0.3
Axial displacement (mm)
Time(min)
α=0.1
α=0.5
α=1
α=2
X: 178.5
Y: -7.25

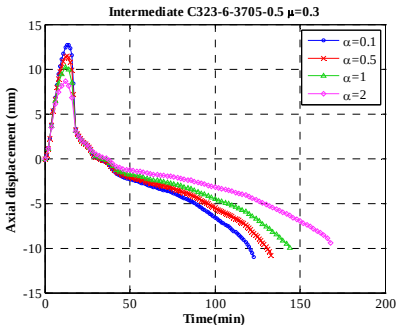
Intermediate C323-6-3705-0.5 μ=0.3
Axial displacement (mm)
Time(min)
α=0.1
α=0.5
α=1
α=2

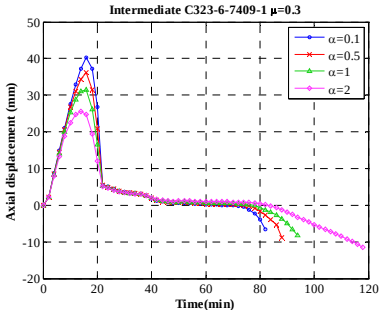
Intermediate C323-6-7409-1 μ=0.3
Axial displacement (mm)
Time(min)
α=0.1
α=0.5
α=1
α=2

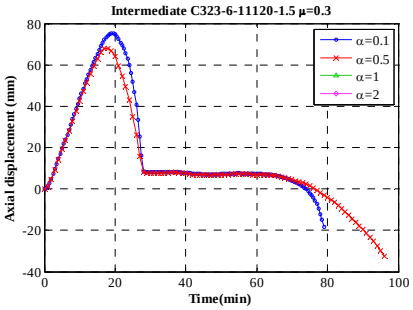
Intermediate C323-6-11120-1.5 μ=0.3
Axial displacement (mm)
Time(min)
α=0.1
α=0.5
α=1
α=2

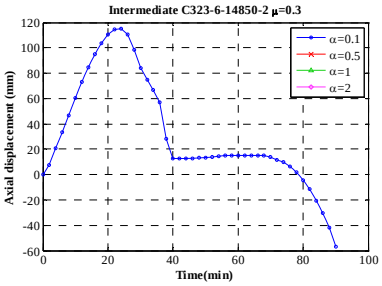
Intermediate C323-6-14850-2 μ=0.3
Axial displacement (mm)
Time(min)
α=0.1
α=0.5
α=1
α=2

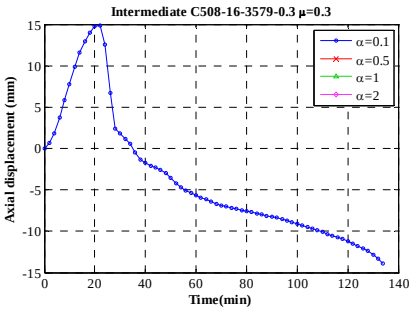
Intermediate C508-16-3579-0.3 μ=0.3
Axial displacement (mm)
Time(min)
α=0.1
α=0.5
α=1
α=2

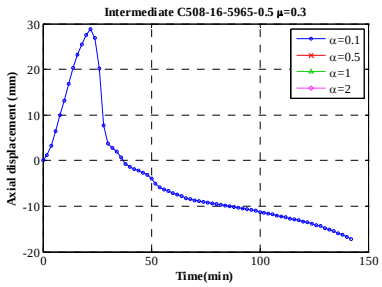
Intermediate C508-16-5965-0.5 μ=0.3
Axial displacement (mm)
Time(min)
α=0.1
α=0.5
α=1
α=2

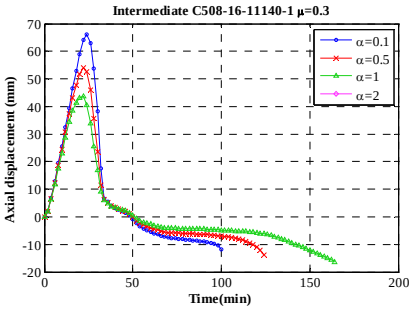
Intermediate C508-16-11140-1 μ=0.3
Axial displacement (mm)
Time(min)
α=0.1
α=0.5
α=1
α=2

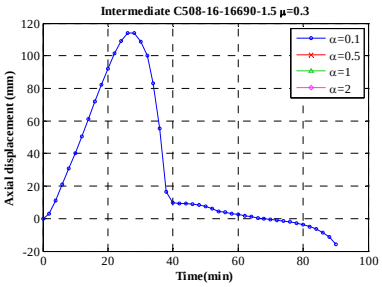
Intermediate C508-16-16690-1.5 μ=0.3
Axial displacement (mm)
Time(min)
α=0.1
α=0.5
α=1
α=2

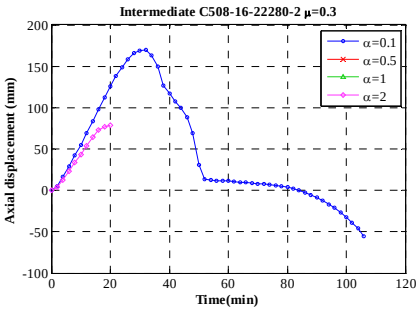
Intermediate C508-16-22280-2 μ=0.3
Axial displacement (mm)
Time(min)
α=0.1
α=0.5
α=1
α=2

Load level μ=0.5

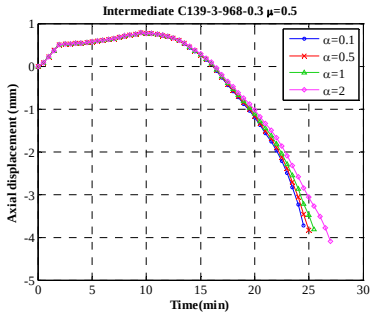

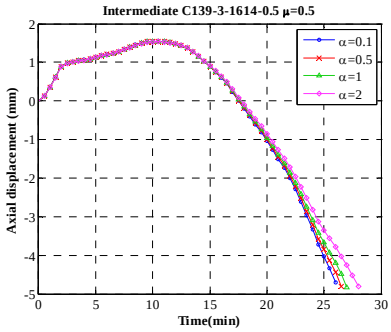

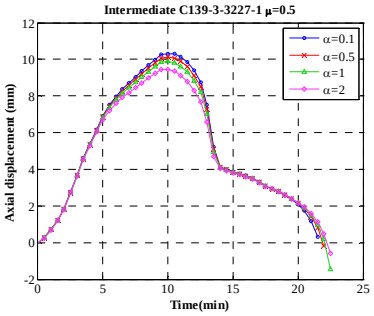

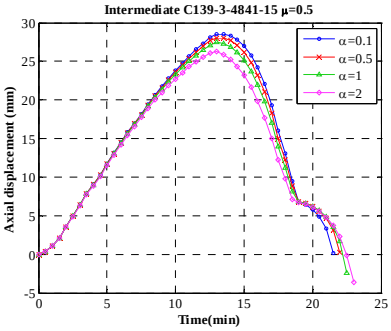

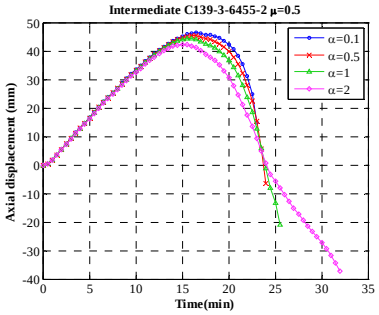

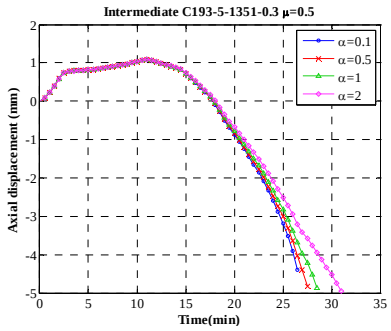

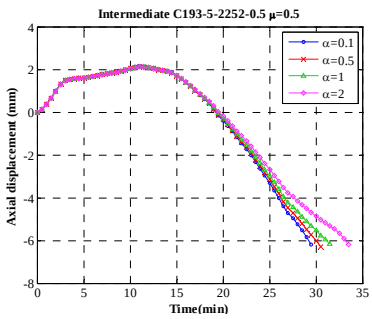
Intermediate C193-5-2252-0.5 μ=0.5
Axial displacement (mm)
Time(min)
α=0.1
α=0.5
α=1
α=2

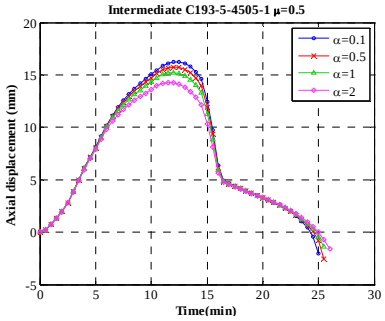
Intermediate C193-5-4505-1 μ=0.5
Axial displacement (mm)
Time(min)
α=0.1
α=0.5
α=1
α=2

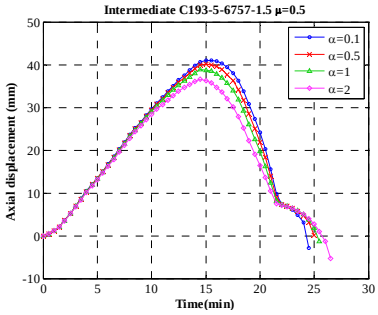
Intermediate C193-5-6757-1.5 μ=0.5
Axial displacement (mm)
Time(min)
α=0.1
α=0.5
α=1
α=2

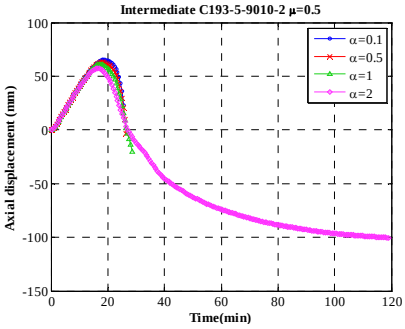
Intermediate C193-5-9010-2 μ=0.5
Axial displacement (mm)
Time(min)
α=0.1
α=0.5
α=1
α=2

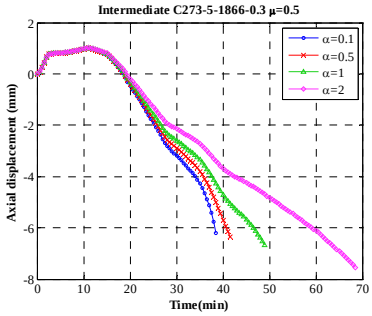
Intermediate C273-5-1866-0.3 μ=0.5
Axial displacement (mm)
Time(min)
α=0.1
α=0.5
α=1
α=2

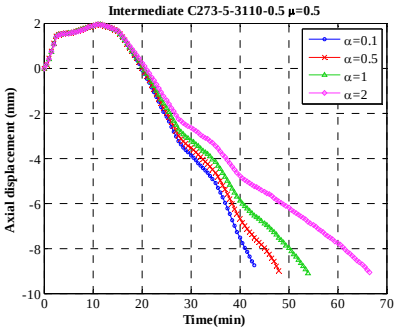
Intermediate C273-5-3110-0.5 μ=0.5
Axial displacement (mm)
Time(min)
α=0.1
α=0.5
α=1
α=2

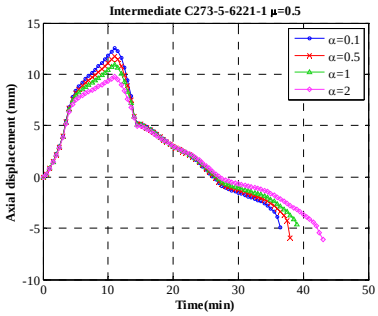
Intermediate C273-5-6221-1 μ=0.5
Axial displacement (mm)
Time(min)
α=0.1
α=0.5
α=1
α=2

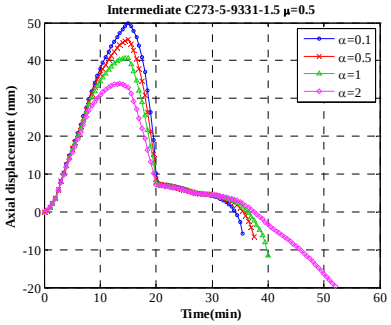
Intermediate C273-5-9331-1.5 μ=0.5
Axial displacement (mm)
Time(min)
α=0.1
α=0.5
α=1
α=2

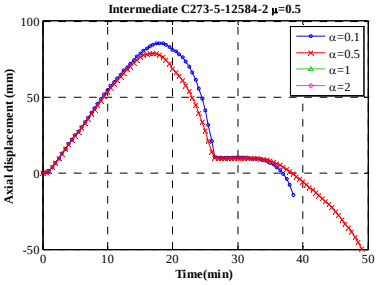
Intermediate C273-5-12584-2 μ=0.5
Axial displacement (mm)
Time(min)
α=0.1
α=0.5
α=1
α=2

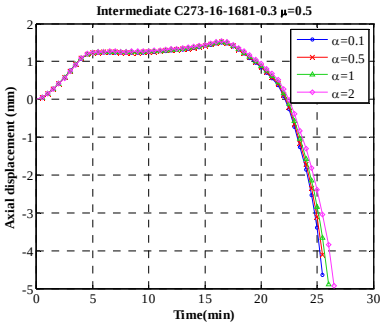
Intermediate C273-16-1681-0.3 μ=0.5
Axial displacement (mm)
Time(min)
α=0.1
α=0.5
α=1
α=2

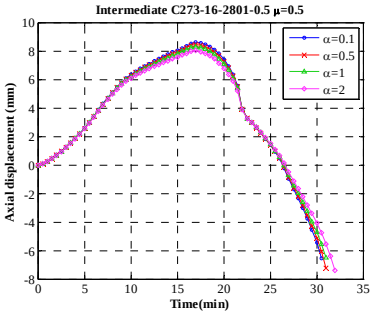
Intermediate C273-16-2801-0.5 μ=0.5
Axial displacement (mm)
Time(min)
α=0.1
α=0.5
α=1
α=2

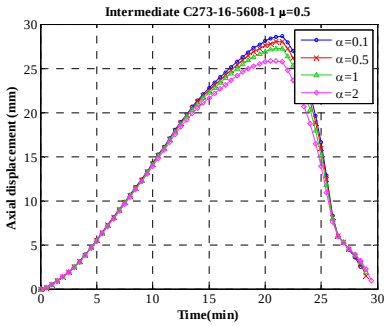
Intermediate C273-16-5608-1 μ=0.5
Axial displacement (mm)
Time(min)
α=0.1
α=0.5
α=1
α=2

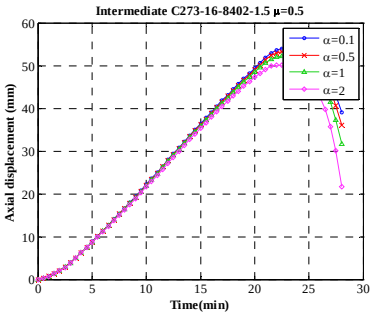
Intermediate C273-16-8402-1.5 μ=0.5
Axial displacement (mm)
Time(min)
α=0.1
α=0.5
α=1
α=2

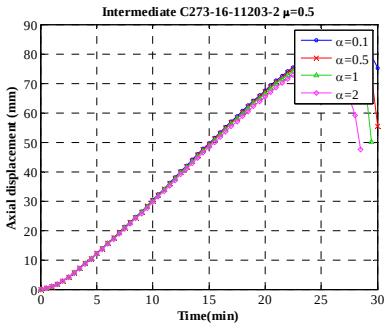
Intermediate C273-16-11203-2 μ=0.5
Axial displacement (mm)
Time(min)
α=0.1
α=0.5
α=1
α=2

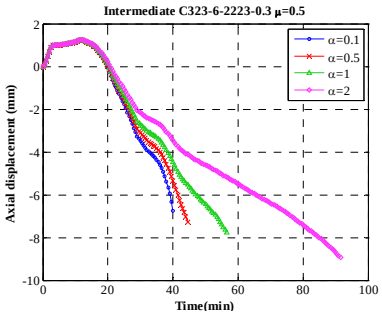
Intermediate C323-6-2223-0.3 μ=0.5
Axial displacement (mm)
Time(min)
α=0.1
α=0.5
α=1
α=2

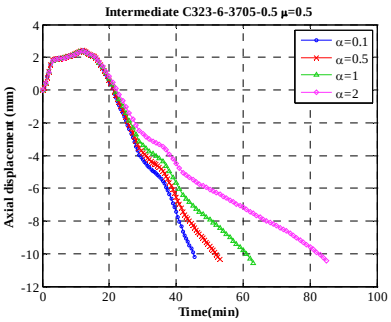
Intermediate C323-6-3705-0.5 μ=0.5
Axial displacement (mm)
Time(min)
α=0.1
α=0.5
α=1
α=2

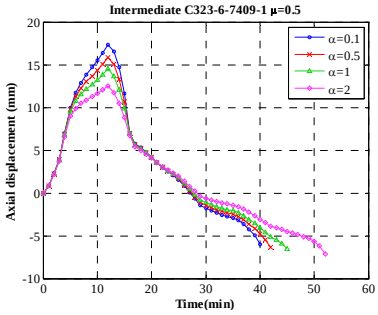
Intermediate C323-6-7409-1 μ=0.5
Axial displacement (mm)
Time(min)
α=0.1
α=0.5
α=1
α=2

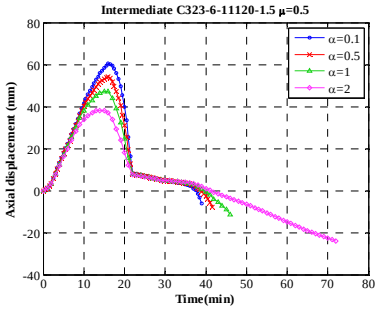
Intermediate C323-6-11120-1.5 μ=0.5
Axial displacement (mm)
Time(min)
α=0.1
α=0.5
α=1
α=2

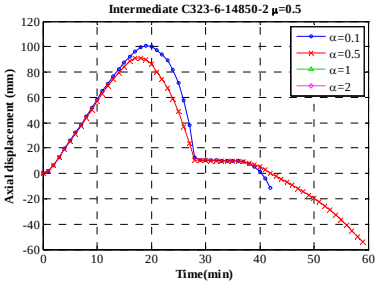
Intermediate C323-6-14850-2 μ=0.5
Axial displacement (mm)
Time(min)
α=0.1
α=0.5
α=1
α=2

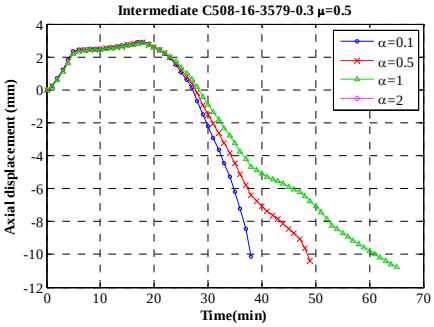
Intermediate C508-16-3579-0.3 μ=0.5
Axial displacement (mm)
Time(min)
α=0.1
α=0.5
α=1
α=2

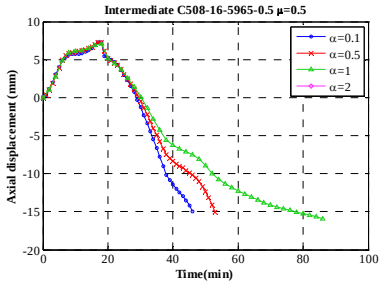
Intermediate C508-16-5965-0.5 μ=0.5
Axial displacement (mm)
Time(min)
α=0.1
α=0.5
α=1
α=2

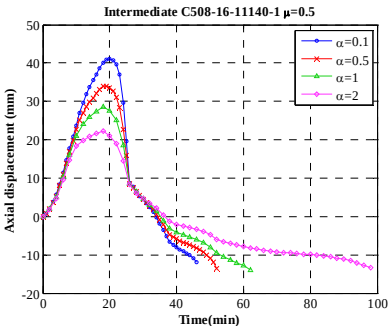
Intermediate C508-16-11140-1 μ=0.5
Axial displacement (mm)
Time(min)
α=0.1
α=0.5
α=1
α=2

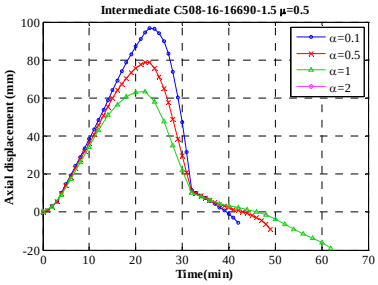
Intermediate C508-16-16690-1.5 μ=0.5
Axial displacement (mm)
Time(min)
α=0.1
α=0.5
α=1
α=2

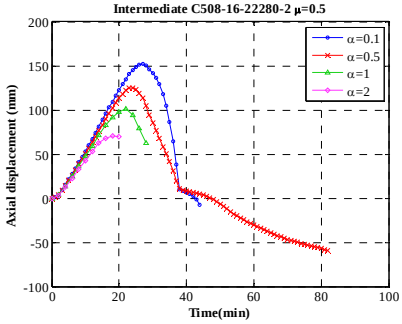
Intermediate C508-16-22280-2 μ=0.5
Axial displacement (mm)
Time(min)
α=0.1
α=0.5
α=1
α=2

Load level μ=0.7

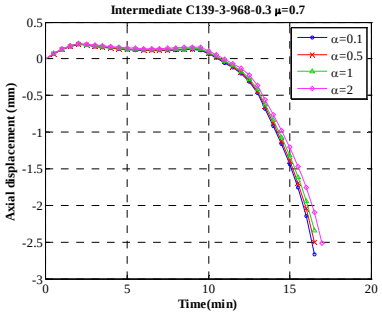

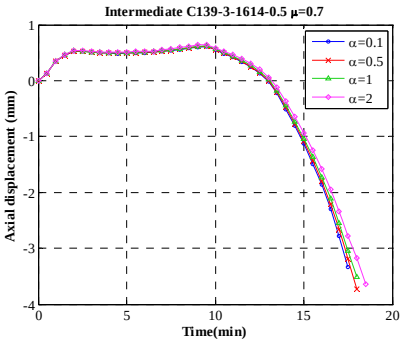

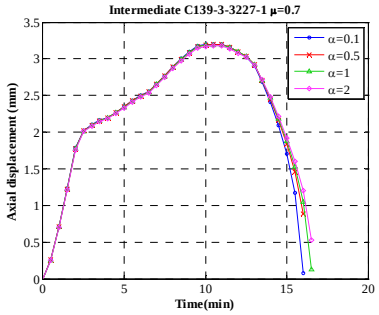

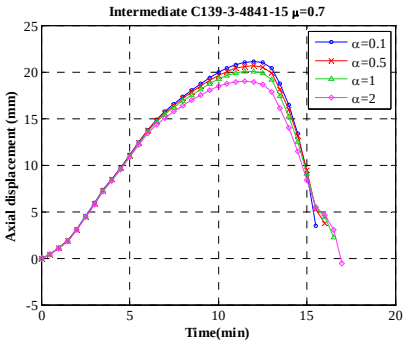

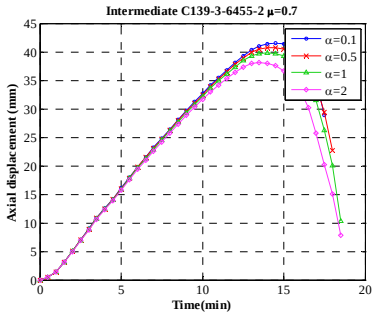

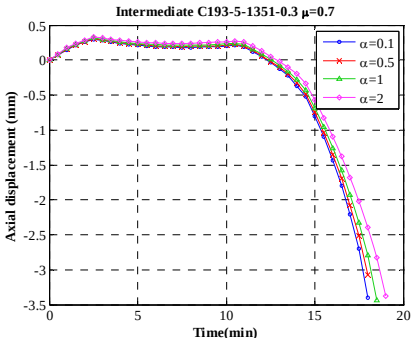

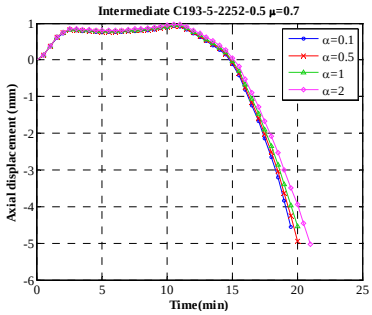
Intermediate C193-5-2252-0.5 μ=0.7
Axial displacement (mm)
Time(min)
α=0.1
α=0.5
α=1
α=2

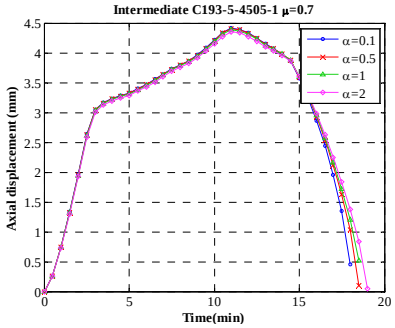
Intermediate C193-5-4505-1 μ=0.7
Axial displacement (mm)
Time(min)
α=0.1
α=0.5
α=1
α=2

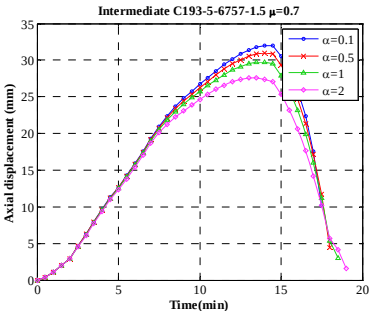
Intermediate C193-5-6757-1.5 μ=0.7
Axial displacement (mm)
Time(min)
α=0.1
α=0.5
α=1
α=2

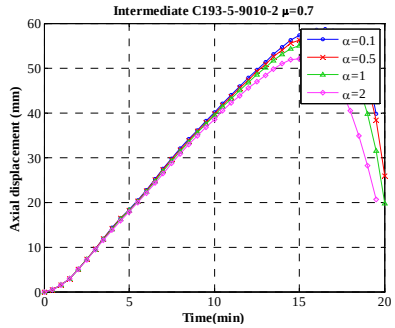
Intermediate C193-5-9010-2 μ=0.7
Axial displacement (mm)
Time(min)
α=0.1
α=0.5
α=1
α=2

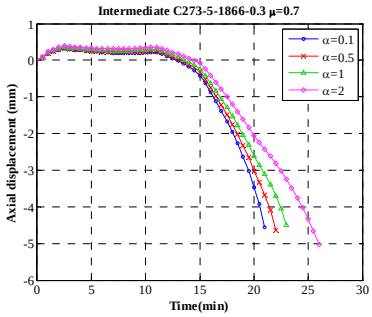
Intermediate C273-5-1866-0.3 μ=0.7
Axial displacement (mm)
Time(min)
α=0.1
α=0.5
α=1
α=2

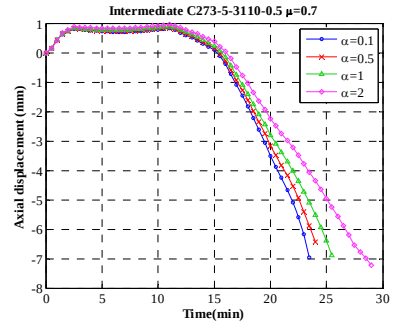
Intermediate C273-5-3110-0.5 μ=0.7
Axial displacement (mm)
Time(min)
α=0.1
α=0.5
α=1
α=2

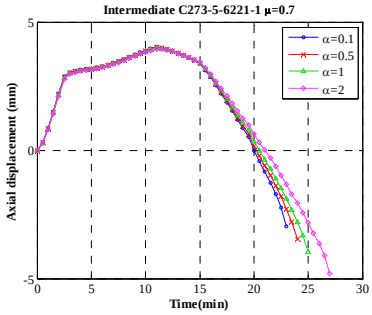
Intermediate C273-5-6221-1 μ=0.7
Axial displacement (mm)
Time(min)
α=0.1
α=0.5
α=1
α=2

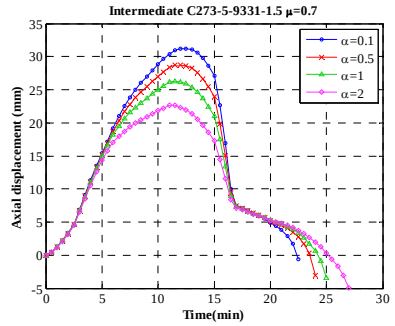
Intermediate C273-5-9331-1.5 μ=0.7
Axial displacement (mm)
Time(min)
α=0.1
α=0.5
α=1
α=2

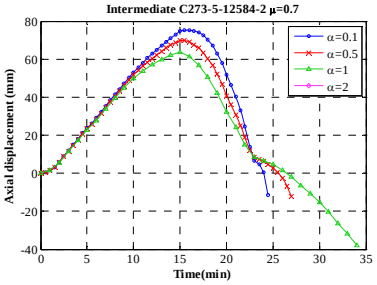
Intermediate C273-5-12584-2 μ=0.7
Axial displacement (mm)
Time(min)
α=0.1
α=0.5
α=1
α=2

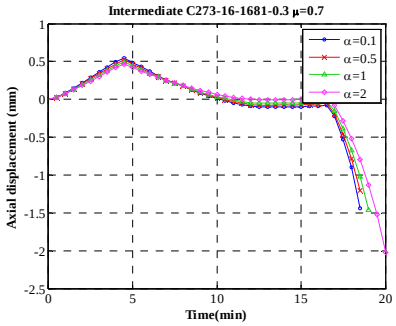
Intermediate C273-16-1681-0.3 μ=0.7
Axial displacement (mm)
Time(min)
α=0.1
α=0.5
α=1
α=2

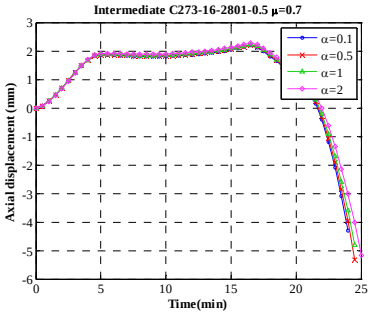
Intermediate C273-16-2801-0.5 μ=0.7
Axial displacement (mm)
Time(min)
α=0.1
α=0.5
α=1
α=2

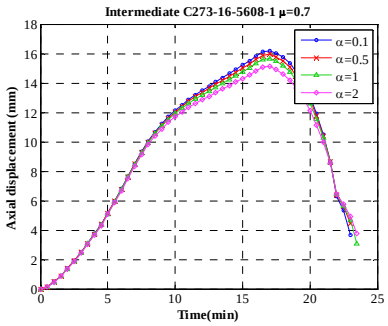
Intermediate C273-16-5608-1 μ=0.7
Axial displacement (mm)
Time(min)
α=0.1
α=0.5
α=1
α=2

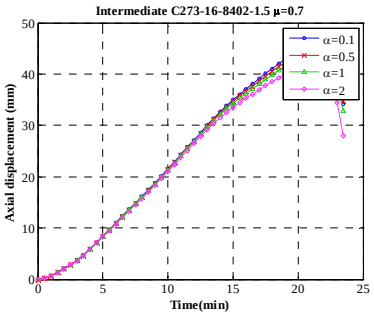
Intermediate C273-16-8402-1.5 μ=0.7
Axial displacement (mm)
Time(min)
α=0.1
α=0.5
α=1
α=2

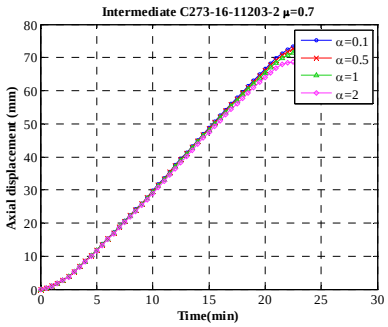
Intermediate C273-16-11203-2 μ=0.7
Axial displacement (mm)
Time(min)
α=0.1
α=0.5
α=1
α=2

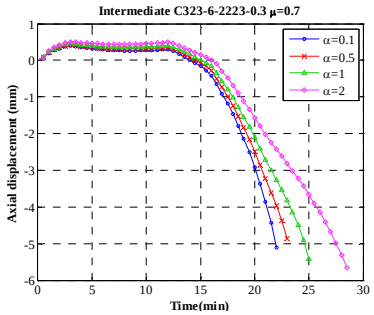
Intermediate C323-6-2223-0.3 μ=0.7
Axial displacement (mm)
Time(min)
α=0.1
α=0.5
α=1
α=2

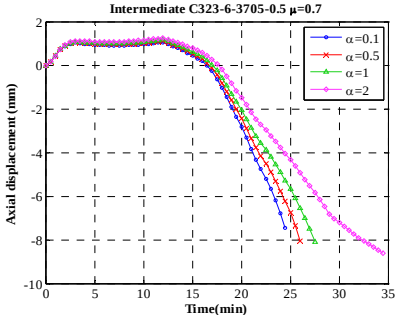
Intermediate C323-6-3705-0.5 μ=0.7
Axial displacement (mm)
Time(min)
α=0.1
α=0.5
α=1
α=2

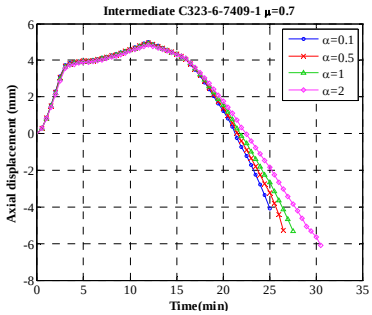
Intermediate C323-6-7409-1 μ=0.7
Axial displacement (mm)
Time(min)
α=0.1
α=0.5
α=1
α=2

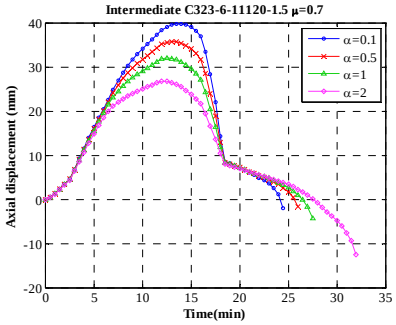
Intermediate C323-6-11120-1.5 μ=0.7
Axial displacement (mm)
Time(min)
α=0.1
α=0.5
α=1
α=2

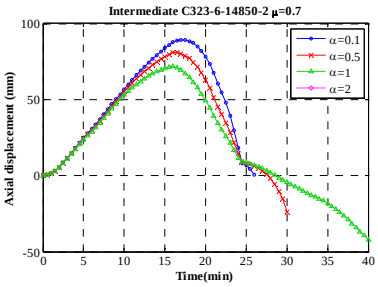
Intermediate C323-6-14850-2 μ=0.7
Axial displacement (mm)
Time(min)
α=0.1
α=0.5
α=1
α=2

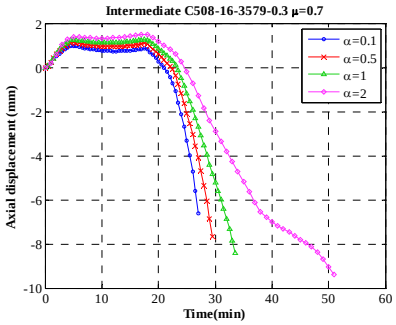
Intermediate C508-16-3579-0.3 μ=0.7
Axial displacement (mm)
Time(min)
α=0.1
α=0.5
α=1
α=2

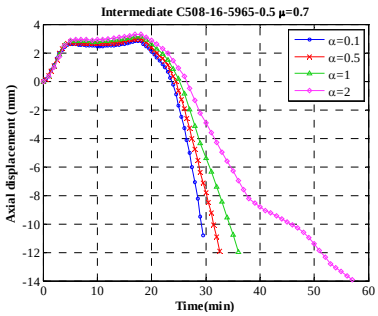
Intermediate C508-16-5965-0.5 μ=0.7
Axial displacement (mm)
Time(min)
α=0.1
α=0.5
α=1
α=2

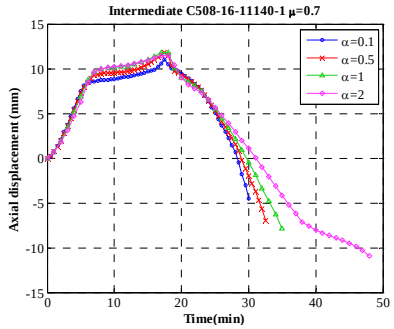
Intermediate C508-16-11140-1 μ=0.7
Axial displacement (mm)
Time(min)
α=0.1
α=0.5
α=1
α=2

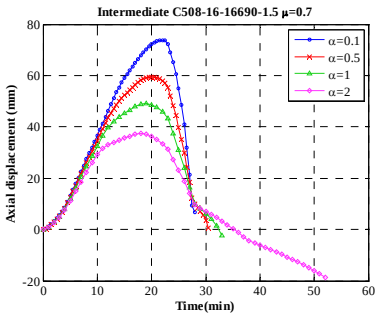
Intermediate C508-16-16690-1.5 μ=0.7
Axial displacement (mm)
Time(min)
α=0.1
α=0.5
α=1
α=2

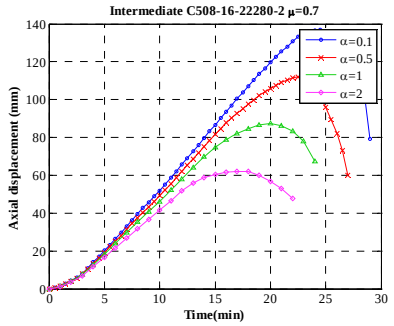
Intermediate C508-16-22280-2 μ=0.7
Axial displacement (mm)
Time(min)
α=0.1
α=0.5
α=1
α=2

2.2. Influence of the stiffness ratio in the restraining forces

Load level μ=0.3

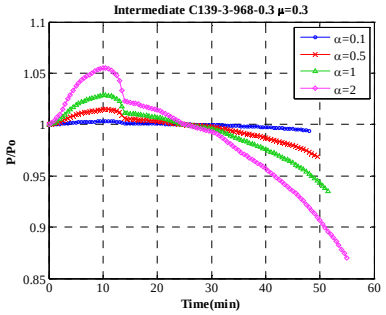

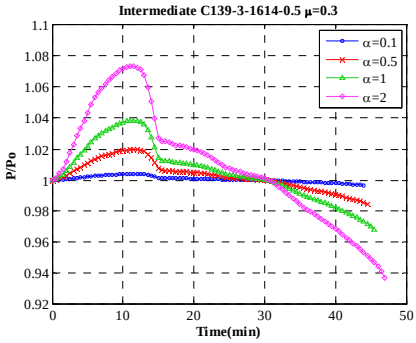

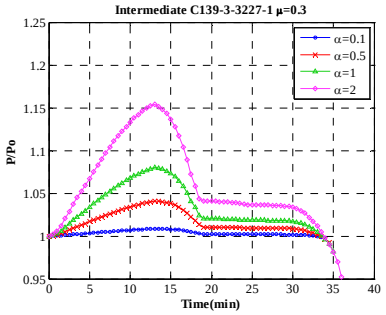

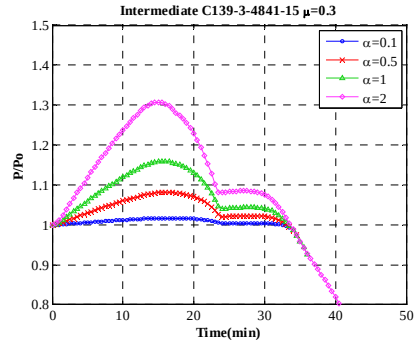

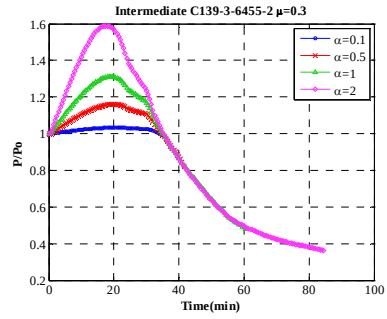

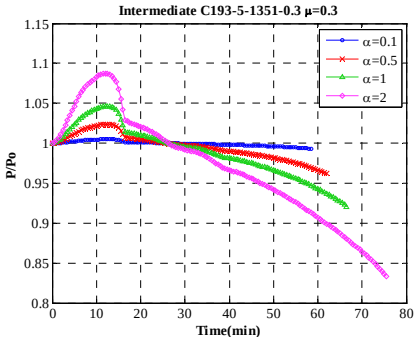

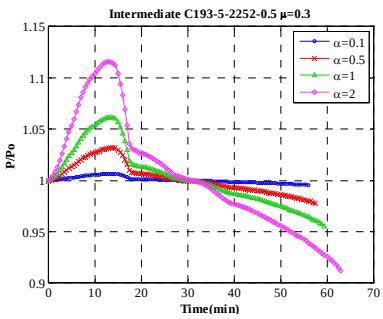
Intermediate C193-5-2252-0.5 μ=0.3
P/Po
Time(min)
α=0.1
α=0.5
α=1
α=2

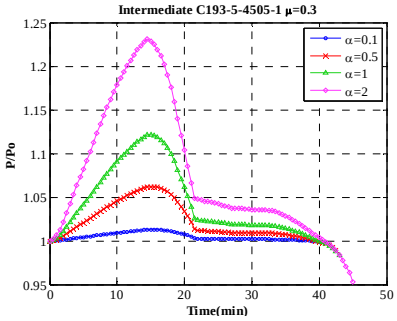
Intermediate C193-5-4505-1 μ=0.3
P/Po
Time(min)
α=0.1
α=0.5
α=1
α=2

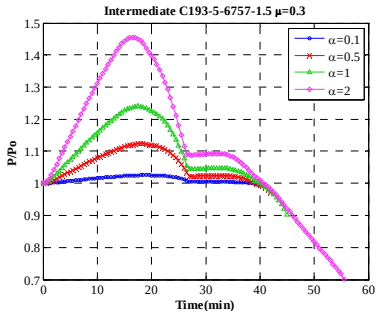
Intermediate C193-5-6757-1.5 μ=0.3
P/Po
Time(min)
α=0.1
α=0.5
α=1
α=2

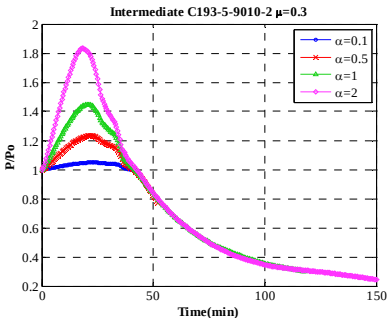
Intermediate C193-5-9010-2 μ=0.3
P/Po
Time(min)
α=0.1
α=0.5
α=1
α=2

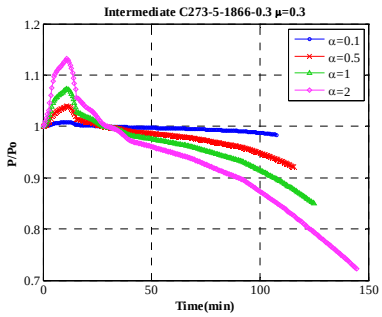
Intermediate C273-5-1866-0.3 μ=0.3
P/Po
Time(min)
α=0.1
α=0.5
α=1
α=2

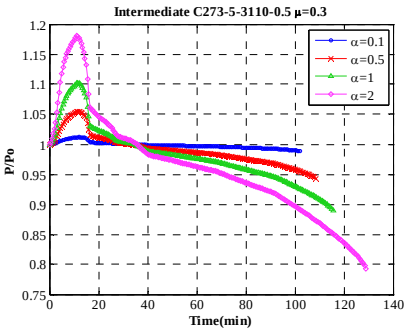
Intermediate C273-5-3110-0.5 μ=0.3
P/Po
Time(min)
α=0.1
α=0.5
α=1
α=2

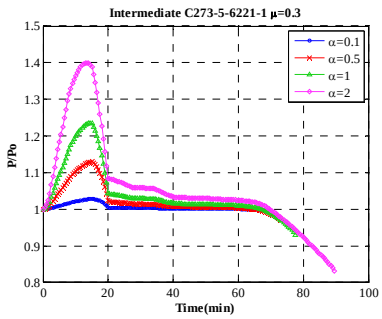
Intermediate C273-5-6221-1 μ=0.3
P/Po
Time(min)
α=0.1
α=0.5
α=1
α=2

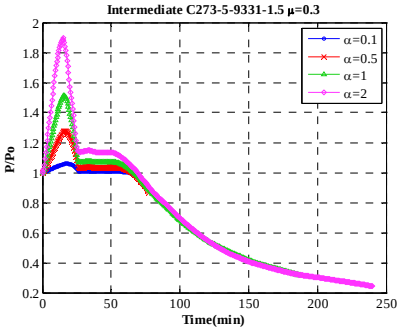
Intermediate C273-5-9331-1.5 μ=0.3
P/Po
Time(min)
α=0.1
α=0.5
α=1
α=2

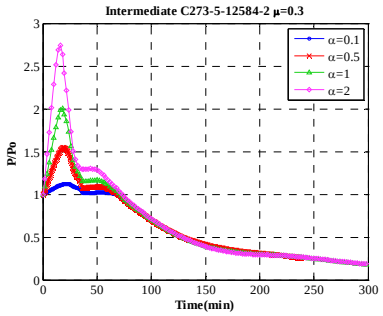
Intermediate C273-5-12584-2 μ=0.3
α=0.1
α=0.5
α=1
α=2
P/Po
Time(min)

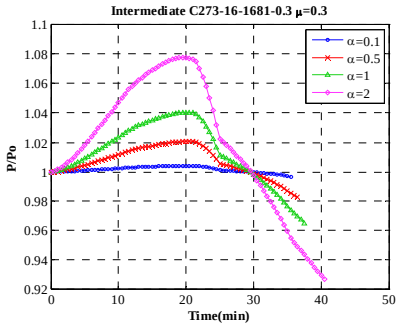
Intermediate C273-16-1681-0.3 μ=0.3
α=0.1
α=0.5
α=1
α=2
P/Po
Time(min)

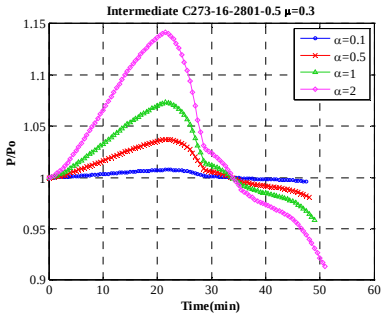
Intermediate C273-16-2801-0.5 μ=0.3
α=0.1
α=0.5
α=1
α=2
P/Po
Time(min)

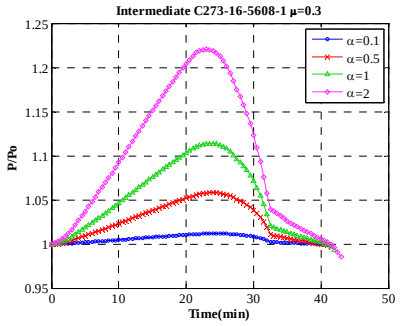
Intermediate C273-16-5608-1 μ=0.3
α=0.1
α=0.5
α=1
α=2
P/Po
Time(min)

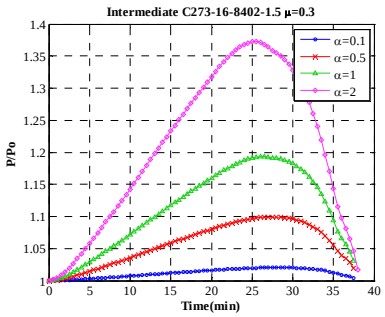
Intermediate C273-16-8402-1.5 μ=0.3
α=0.1
α=0.5
α=1
α=2
P/Po
Time(min)

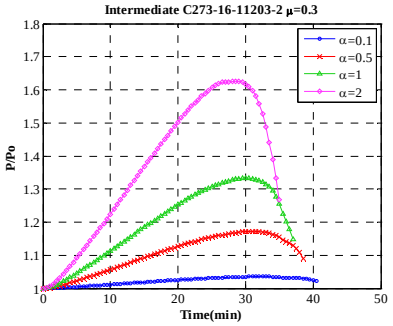
Intermediate C273-16-11203-2 μ=0.3
α=0.1
α=0.5
α=1
α=2
P/Po
Time(min)

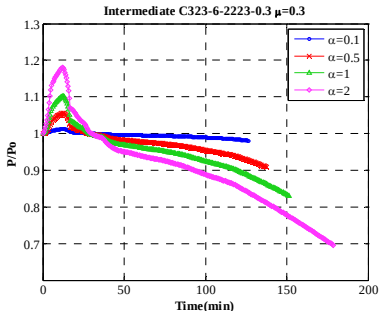
Intermediate C323-6-2223-0.3 μ=0.3
α=0.1
α=0.5
α=1
α=2
P/Po
Time(min)

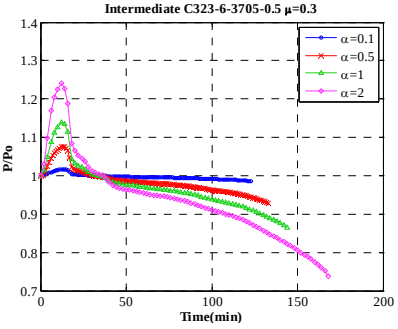
Intermediate C323-6-3705-0.5 μ=0.3
α=0.1
α=0.5
α=1
α=2
P/Po
Time(min)

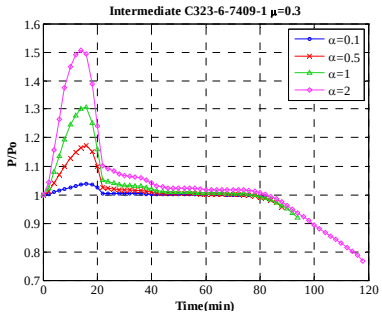
Intermediate C323-6-7409-1 μ=0.3
P/Po
Time(min)
α=0.1
α=0.5
α=1
α=2

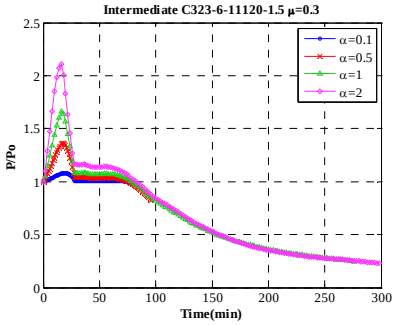
Intermediate C323-6-11120-1.5 μ=0.3
P/Po
Time(min)
α=0.1
α=0.5
α=1
α=2

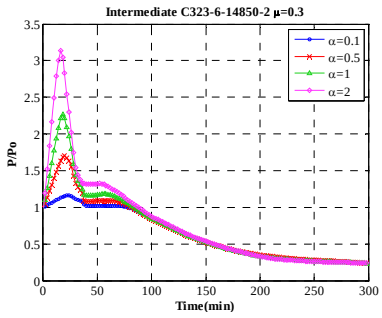
Intermediate C323-6-14850-2 μ=0.3
P/Po
Time(min)
α=0.1
α=0.5
α=1
α=2

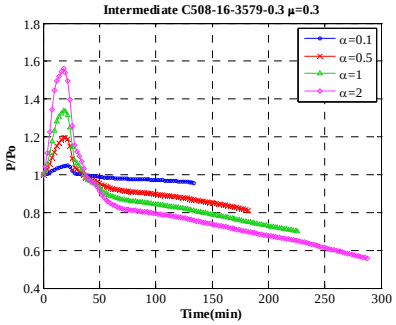
Intermediate C508-16-3579-0.3 μ=0.3
P/Po
Time(min)
α=0.1
α=0.5
α=1
α=2

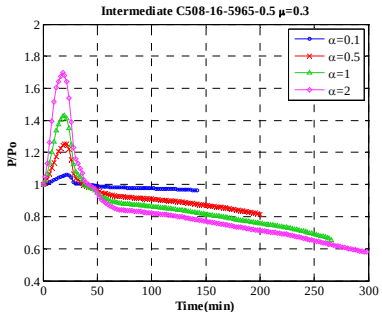
Intermediate C508-16-5965-0.5 μ=0.3
P/Po
Time(min)
α=0.1
α=0.5
α=1
α=2

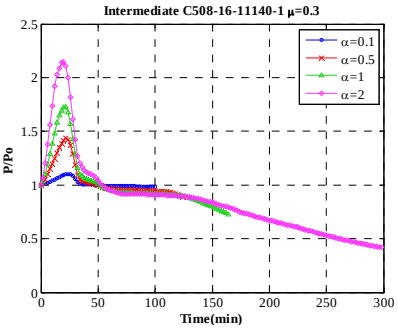
Intermediate C508-16-11140-1 μ=0.3
P/Po
Time(min)
α=0.1
α=0.5
α=1
α=2

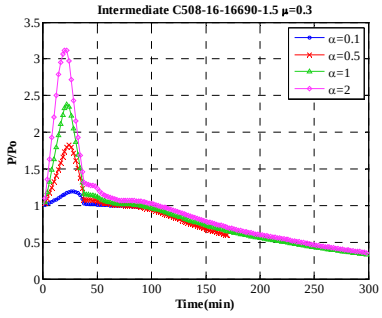
Intermediate C508-16-16690-1.5 μ=0.3
P/Po
Time(min)
α=0.1
α=0.5
α=1
α=2

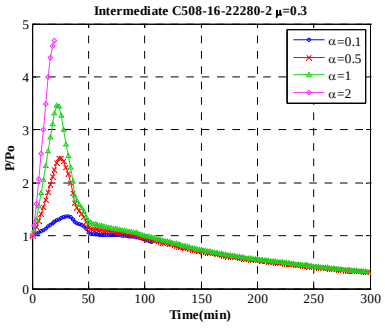
Intermediate C508-16-22280-2 μ=0.3
P/Po
Time(min)
α=0.1
α=0.5
α=1
α=2

Load level μ=0.5

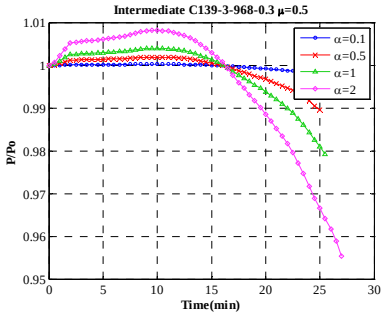

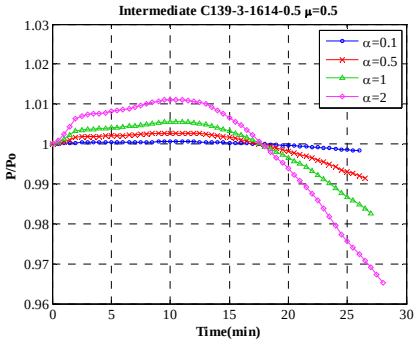

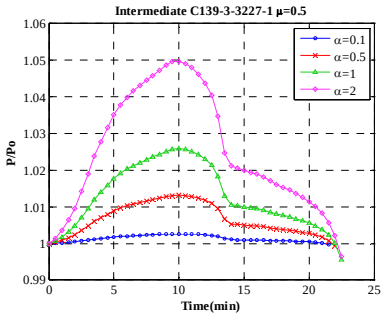

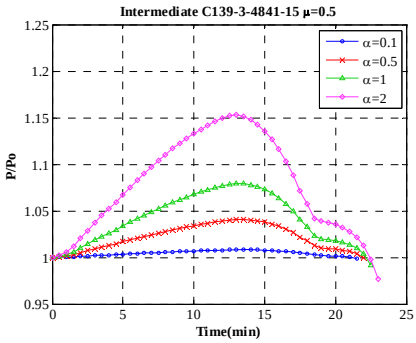

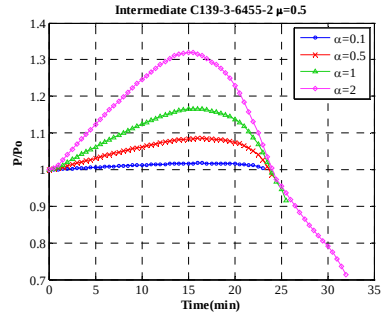

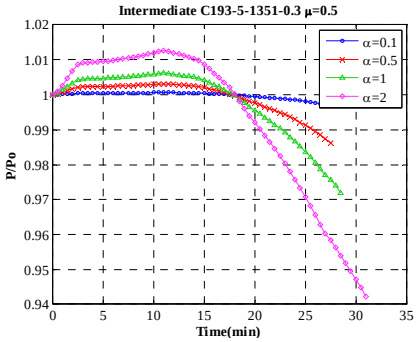

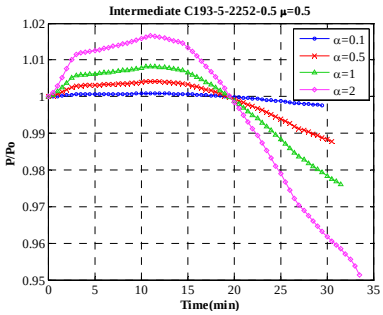
Intermediate C193-5-2252-0.5 μ=0.5
α=0.1
α=0.5
α=1
α=2
P/Po
Time(min)

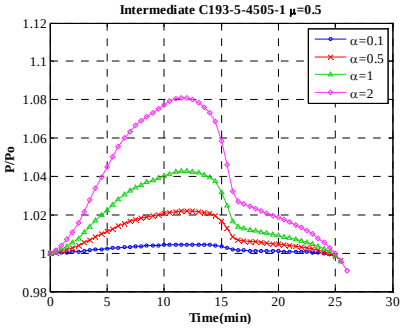
Intermediate C193-5-4505-1 μ=0.5
α=0.1
α=0.5
α=1
α=2
P/Po
Time(min)

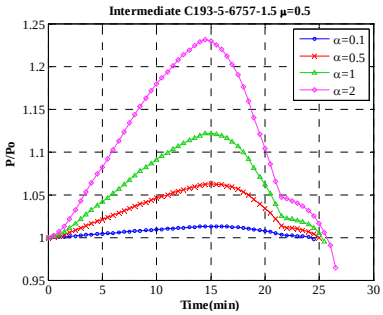
Intermediate C193-5-6757-1.5 μ=0.5
α=0.1
α=0.5
α=1
α=2
P/Po
Time(min)

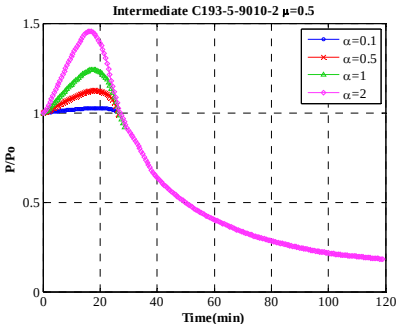
Intermediate C193-5-9010-2 μ=0.5
α=0.1
α=0.5
α=1
α=2
P/Po
Time(min)

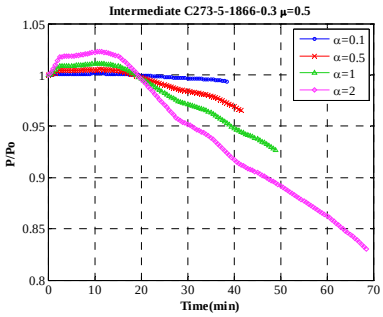
Intermediate C273-5-1866-0.3 μ=0.5
α=0.1
α=0.5
α=1
α=2
P/Po
Time(min)

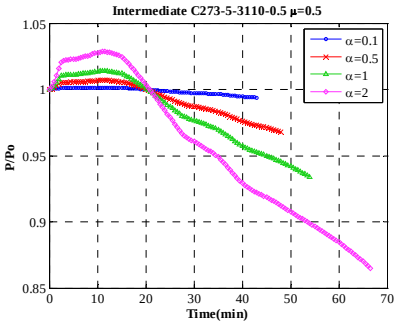
Intermediate C273-5-3110-0.5 μ=0.5
α=0.1
α=0.5
α=1
α=2
P/Po
Time(min)

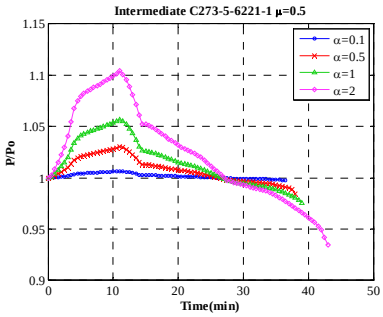
Intermediate C273-5-6221-1 μ=0.5
α=0.1
α=0.5
α=1
α=2
P/Po
Time(min)

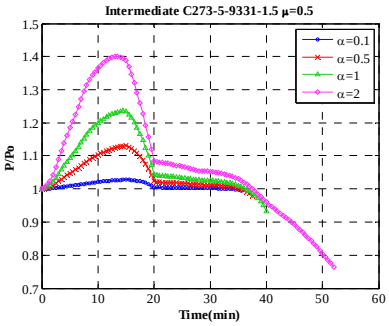
Intermediate C273-5-9331-1.5 μ=0.5
α=0.1
α=0.5
α=1
α=2
P/Po
Time(min)

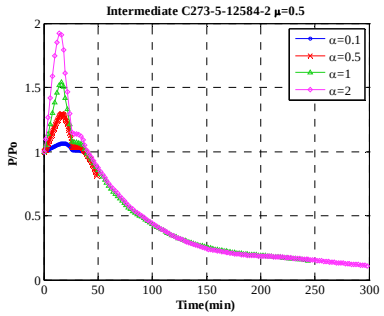
Intermediate C273-5-12584-2 μ=0.5
α=0.1
α=0.5
α=1
α=2
P/Po
Time(min)

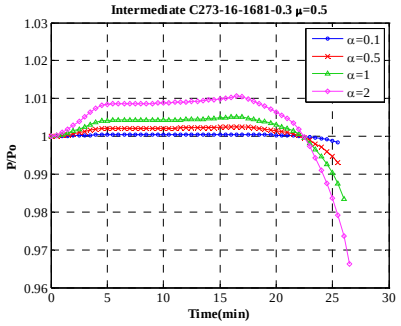
Intermediate C273-16-1681-0.3 μ=0.5
α=0.1
α=0.5
α=1
α=2
P/Po
Time(min)

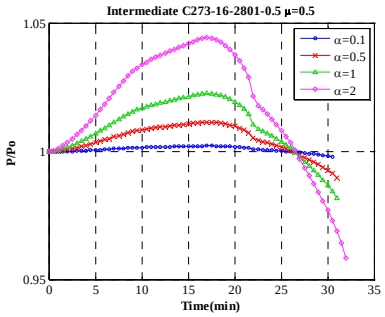
Intermediate C273-16-2801-0.5 μ=0.5
α=0.1
α=0.5
α=1
α=2
P/Po
Time(min)

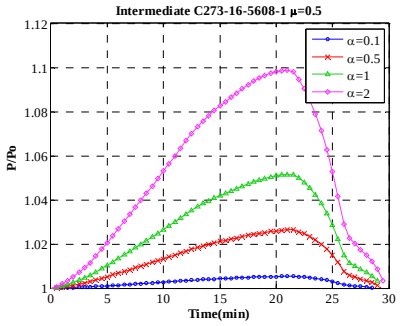
Intermediate C273-16-5608-1 μ=0.5
α=0.1
α=0.5
α=1
α=2
P/Po
Time(min)

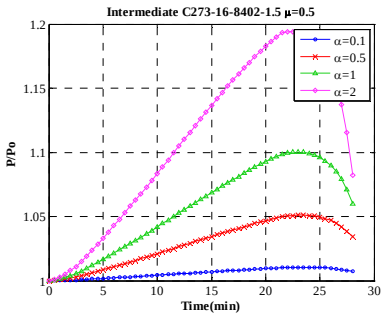
Intermediate C273-16-8402-1.5 μ=0.5
α=0.1
α=0.5
α=1
α=2
P/Po
Time(min)

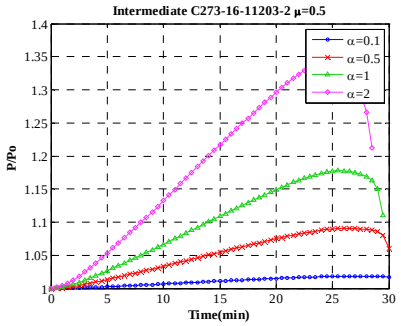
Intermediate C273-16-11203-2 μ=0.5
α=0.1
α=0.5
α=1
α=2
P/Po
Time(min)

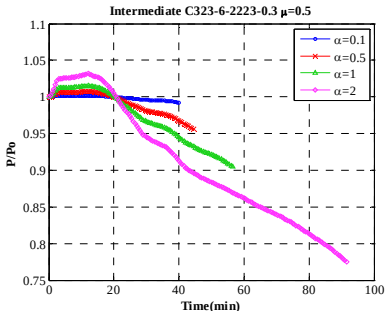
Intermediate C323-6-2223-0.3 μ=0.5
α=0.1
α=0.5
α=1
α=2
P/Po
Time(min)

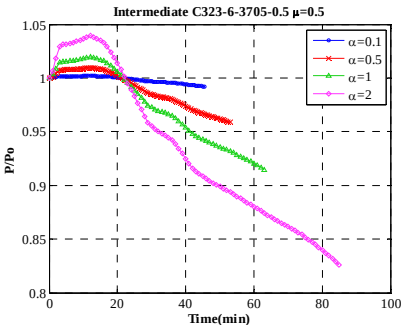
Intermediate C323-6-3705-0.5 μ=0.5
α=0.1
α=0.5
α=1
α=2
P/Po
Time(min)

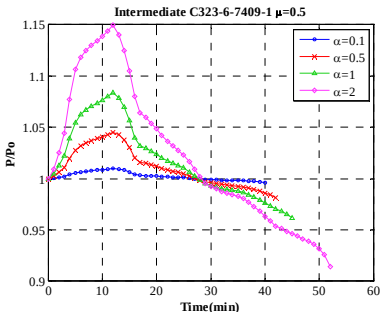
Intermediate C323-6-7409-1 μ=0.5
α=0.1
α=0.5
α=1
α=2
P/Po
Time(min)

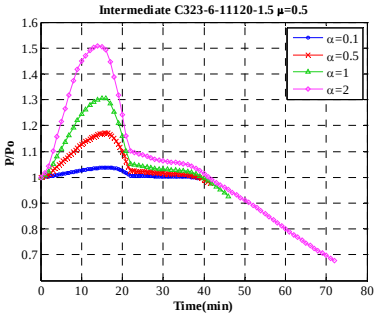
Intermediate C323-6-11120-1.5 μ=0.5
α=0.1
α=0.5
α=1
α=2
P/Po
Time(min)

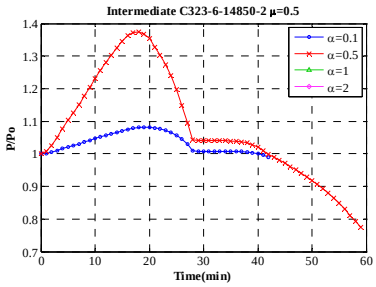
Intermediate C323-6-14850-2 μ=0.5
α=0.1
α=0.5
α=1
α=2
P/Po
Time(min)

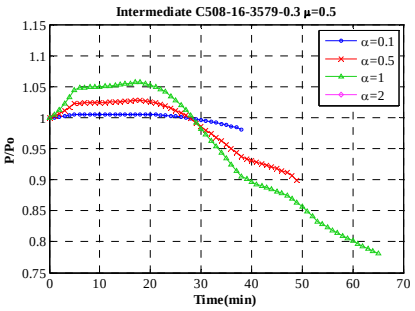
Intermediate C508-16-3579-0.3 μ=0.5
α=0.1
α=0.5
α=1
α=2
P/Po
Time(min)

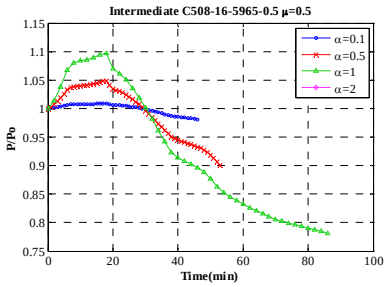
Intermediate C508-16-5965-0.5 μ=0.5
α=0.1
α=0.5
α=1
α=2
P/Po
Time(min)

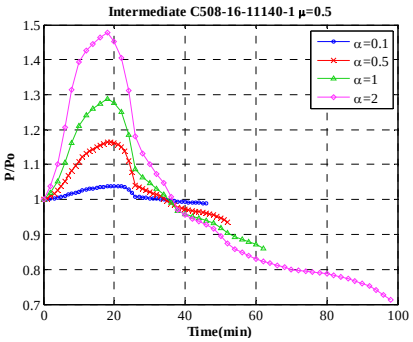
Intermediate C508-16-11140-1 μ=0.5
α=0.1
α=0.5
α=1
α=2
P/Po
Time(min)

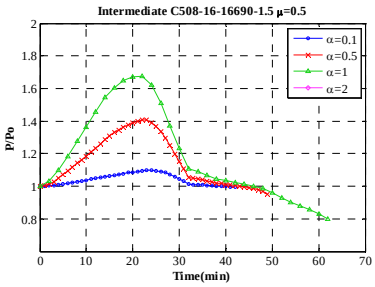
Intermediate C508-16-16690-1.5 μ=0.5
α=0.1
α=0.5
α=1
α=2
P/Po
Time(min)

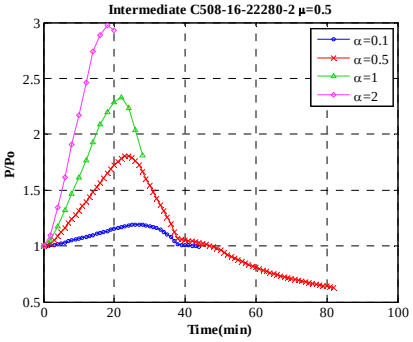
Intermediate C508-16-22280-2 μ=0.5
α=0.1
α=0.5
α=1
α=2
P/Po
Time(min)

Load level μ=0.7

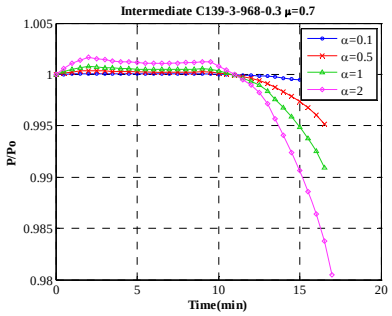

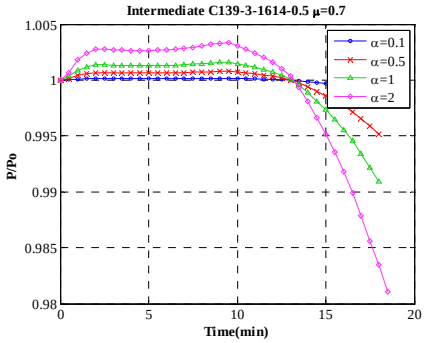

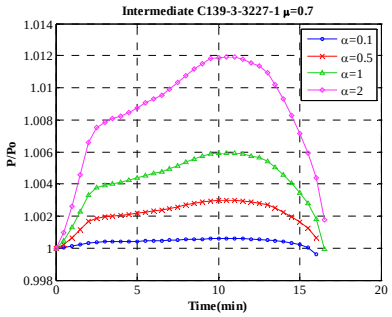

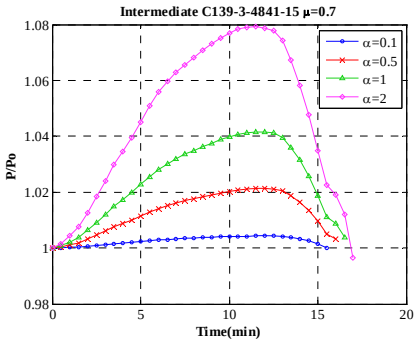

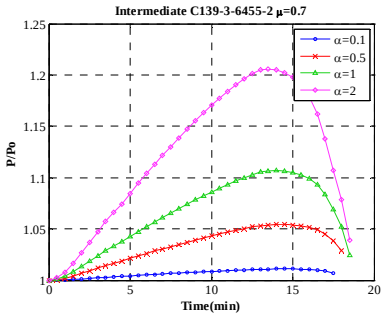

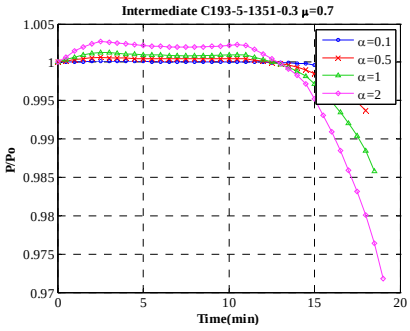

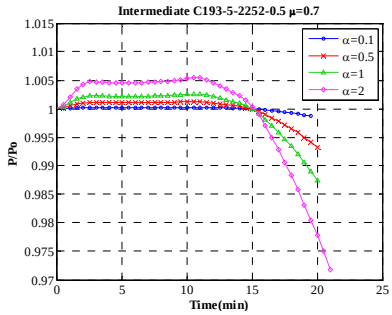
Intermediate C193-5-2252-0.5 μ=0.7
P/Po
Time(min)
α=0.1
α=0.5
α=1
α=2

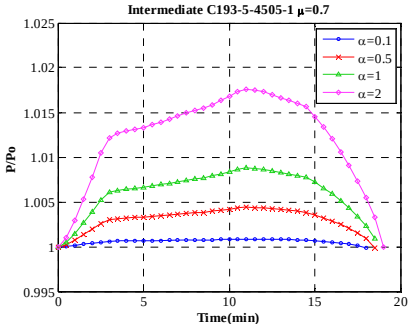
Intermediate C193-5-4505-1 μ=0.7
P/Po
Time(min)
α=0.1
α=0.5
α=1
α=2

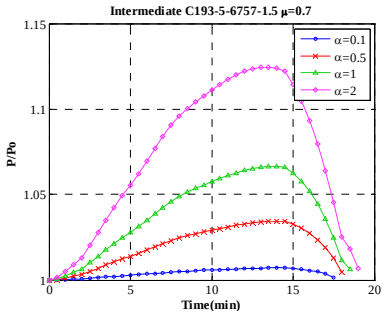
Intermediate C193-5-6757-1.5 μ=0.7
P/Po
Time(min)
α=0.1
α=0.5
α=1
α=2

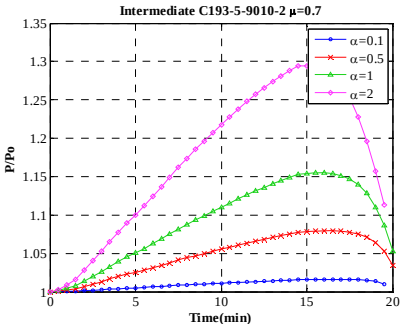
Intermediate C193-5-9010-2 μ=0.7
P/Po
Time(min)
α=0.1
α=0.5
α=1
α=2

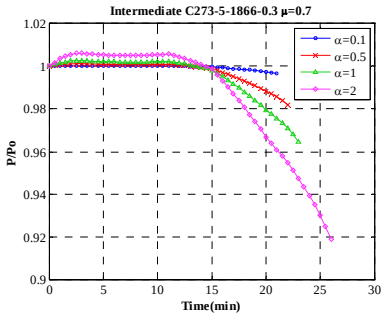
Intermediate C273-5-1866-0.3 μ=0.7
P/Po
Time(min)
α=0.1
α=0.5
α=1
α=2

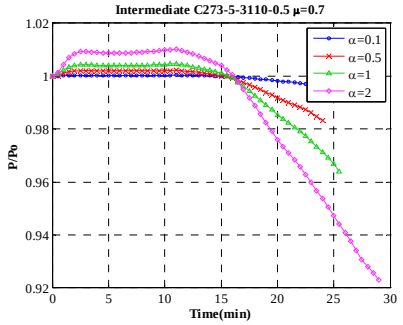
Intermediate C273-5-3110-0.5 μ=0.7
P/Po
Time(min)
α=0.1
α=0.5
α=1
α=2

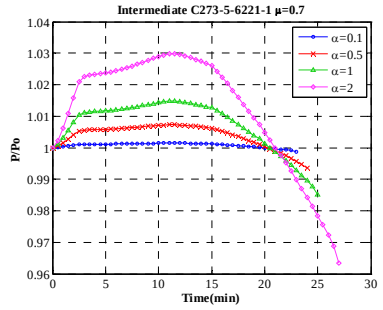
Intermediate C273-5-6221-1 μ=0.7
P/Po
Time(min)
α=0.1
α=0.5
α=1
α=2

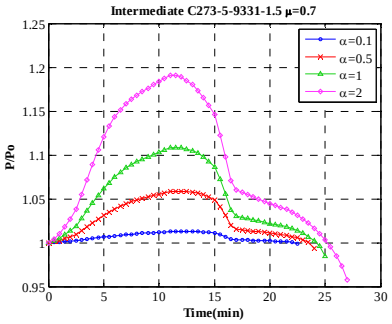
Intermediate C273-5-9331-1.5 μ=0.7
P/Po
Time(min)
α=0.1
α=0.5
α=1
α=2

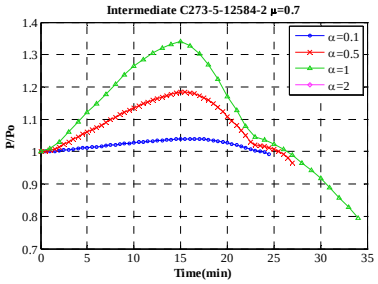
Intermediate C273-5-12584-2 μ=0.7
α=0.1
α=0.5
α=1
α=2
P/Po
Time(min)

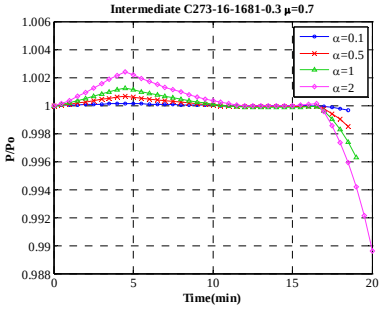
Intermediate C273-16-1681-0.3 μ=0.7
α=0.1
α=0.5
α=1
α=2
P/Po
Time(min)

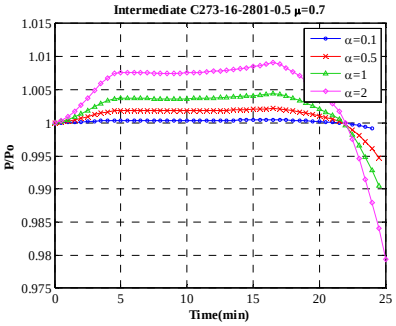
Intermediate C273-16-2801-0.5 μ=0.7
α=0.1
α=0.5
α=1
α=2
P/Po
Time(min)

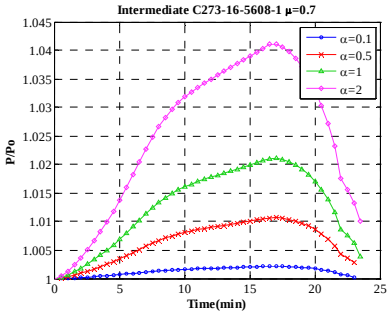
Intermediate C273-16-5608-1 μ=0.7
α=0.1
α=0.5
α=1
α=2
P/Po
Time(min)

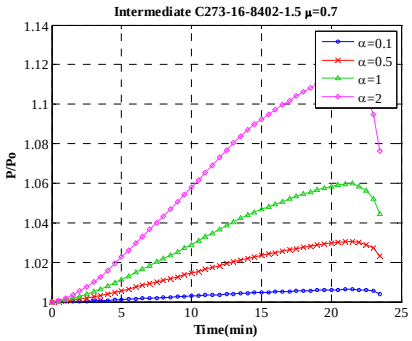
Intermediate C273-16-8402-1.5 μ=0.7
α=0.1
α=0.5
α=1
α=2
P/Po
Time(min)

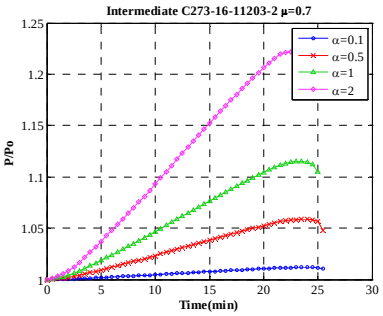
Intermediate C273-16-11203-2 μ=0.7
α=0.1
α=0.5
α=1
α=2
P/Po
Time(min)

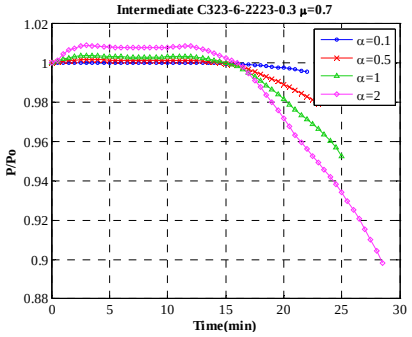
Intermediate C323-6-2223-0.3 μ=0.7
α=0.1
α=0.5
α=1
α=2
P/Po
Time(min)

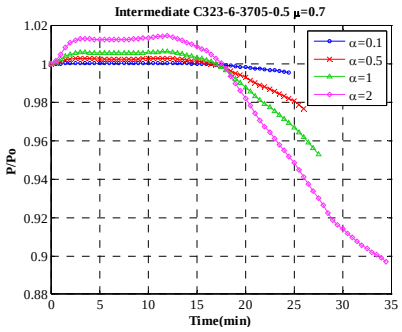
Intermediate C323-6-3705-0.5 μ=0.7
α=0.1
α=0.5
α=1
α=2
P/Po
Time(min)

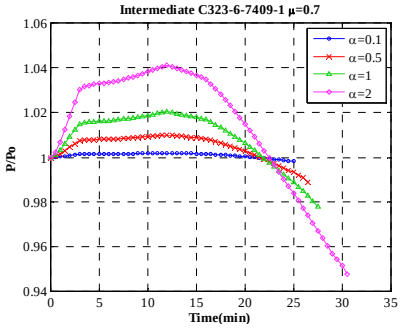
Intermediate C323-6-7409-1 μ=0.7
α=0.1
α=0.5
α=1
α=2
P/Po
Time(min)

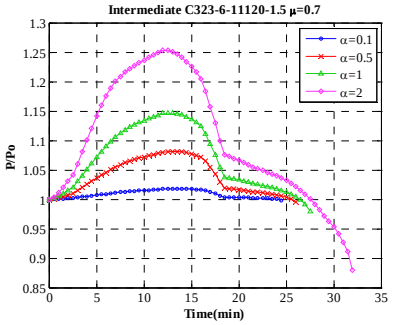
Intermediate C323-6-11120-1.5 μ=0.7
α=0.1
α=0.5
α=1
α=2
P/Po
Time(min)

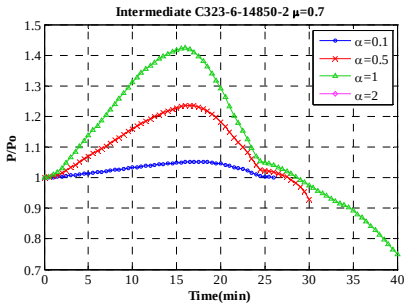
Intermediate C323-6-14850-2 μ=0.7
α=0.1
α=0.5
α=1
α=2
P/Po
Time(min)

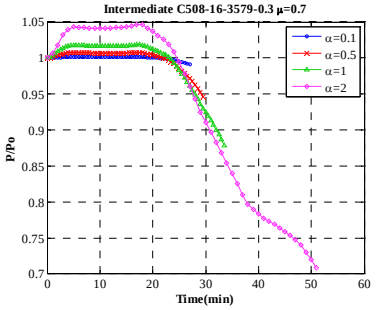
Intermediate C508-16-3579-0.3 μ=0.7
α=0.1
α=0.5
α=1
α=2
P/Po
Time(min)

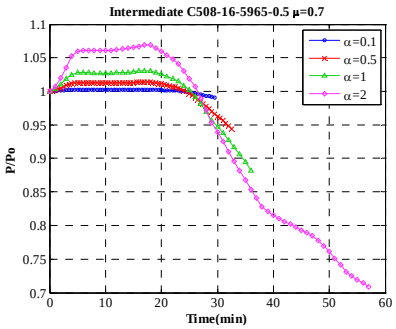
Intermediate C508-16-5965-0.5 μ=0.7
α=0.1
α=0.5
α=1
α=2
P/Po
Time(min)

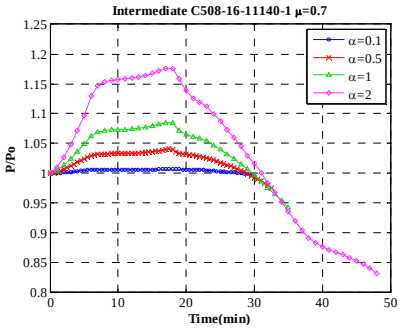
Intermediate C508-16-11140-1 μ=0.7
α=0.1
α=0.5
α=1
α=2
P/Po
Time(min)

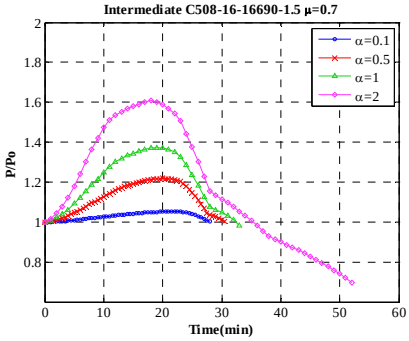
Intermediate C508-16-16690-1.5 μ=0.7
α=0.1
α=0.5
α=1
α=2
P/Po
Time(min)

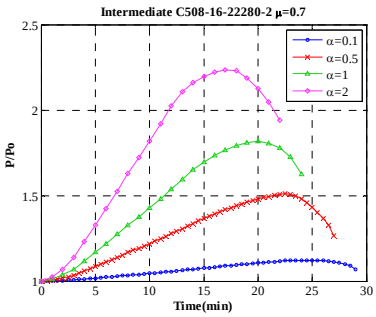
Intermediate C508-16-22280-2 μ=0.7
α=0.1
α=0.5
α=1
α=2
P/Po
Time(min)

3. COMPARISON OF THE MODEL RESULTS WITH PREDICTIONS GIVEN BY CURRENT CODE AND PROPOSED METHOD

Stiffness ratio α=0.1

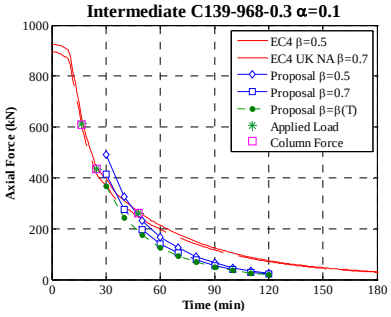

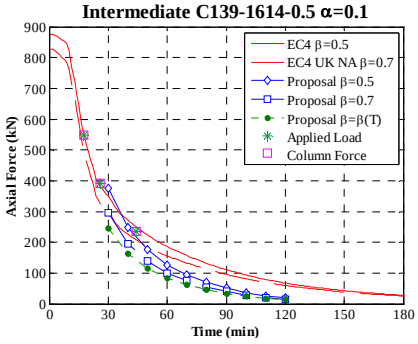

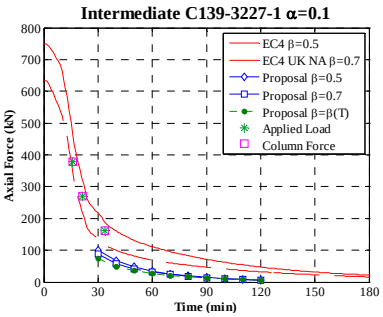

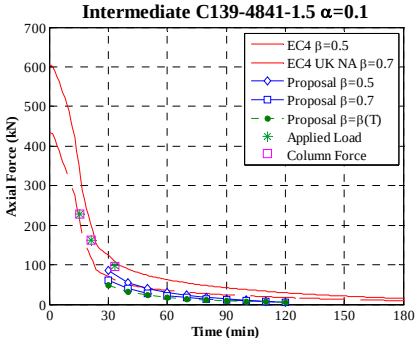

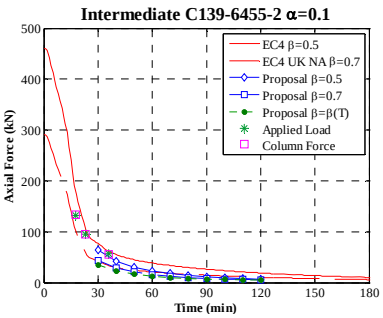

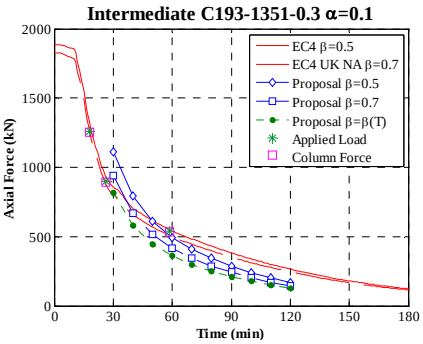

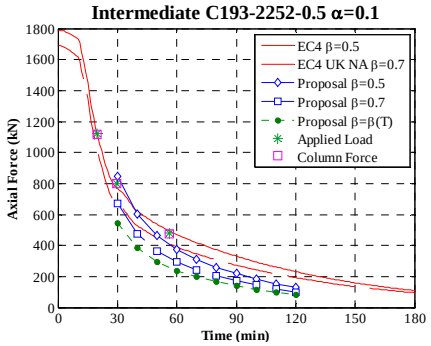
Intermediate C193-2252-0.5 α=0.1
Axial Force (kN)
Time (min)
EC4 β=0.5
EC4 UK NA β=0.7
Proposal β=0.5
Proposal β=0.7
Proposal β=β(T)
Applied Load
Column Force

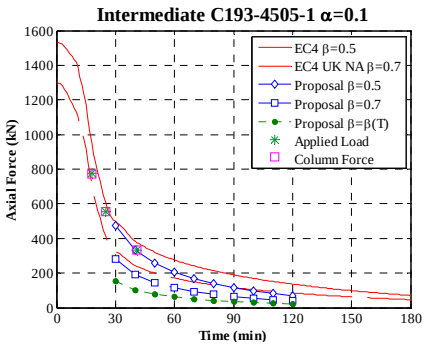
Intermediate C193-4505-1 α=0.1
Axial Force (kN)
Time (min)
EC4 β=0.5
EC4 UK NA β=0.7
Proposal β=0.5
Proposal β=0.7
Proposal β=β(T)
Applied Load
Column Force

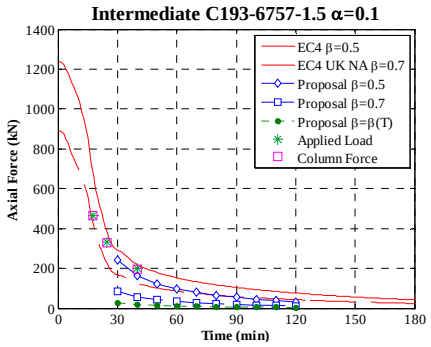
Intermediate C193-6757-1.5 α=0.1
Axial Force (kN)
Time (min)
EC4 β=0.5
EC4 UK NA β=0.7
Proposal β=0.5
Proposal β=0.7
Proposal β=β(T)
Applied Load
Column Force

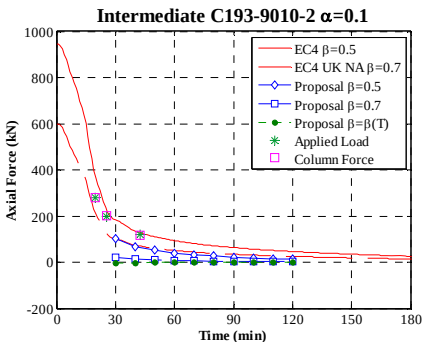
Intermediate C193-9010-2 α=0.1
Axial Force (kN)
Time (min)
EC4 β=0.5
EC4 UK NA β=0.7
Proposal β=0.5
Proposal β=0.7
Proposal β=β(T)
Applied Load
Column Force

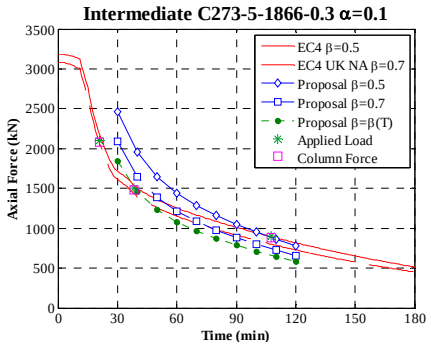
Intermediate C273-5-1866-0.3 α=0.1
Axial Force (kN)
Time (min)
EC4 β=0.5
EC4 UK NA β=0.7
Proposal β=0.5
Proposal β=0.7
Proposal β=β(T)
Applied Load
Column Force

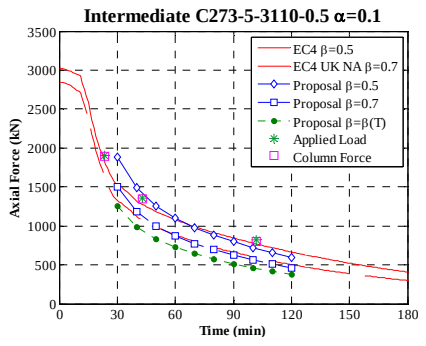
Intermediate C273-5-3110-0.5 α=0.1
Axial Force (kN)
Time (min)
EC4 β=0.5
EC4 UK NA β=0.7
Proposal β=0.5
Proposal β=0.7
Proposal β=β(T)
Applied Load
Column Force

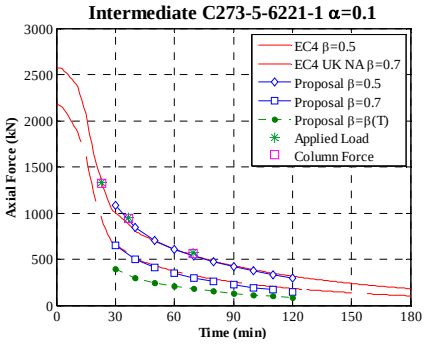
Intermediate C273-5-6221-1 α=0.1
Axial Force (kN)
Time (min)
EC4 β=0.5
EC4 UK NA β=0.7
Proposal β=0.5
Proposal β=0.7
Proposal β=β(T)
Applied Load
Column Force

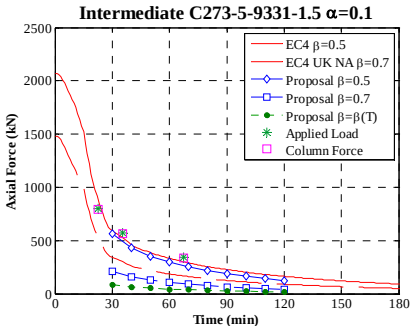
Intermediate C273-5-9331-1.5 α=0.1
Axial Force (kN)
Time (min)
EC4 β=0.5
EC4 UK NA β=0.7
Proposal β=0.5
Proposal β=0.7
Proposal β=β(T)
Applied Load
Column Force

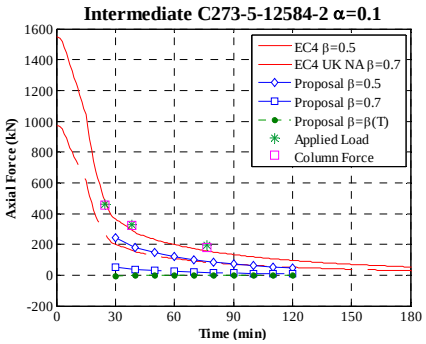
Intermediate C273-5-12584-2 α=0.1
Axial Force (kN)
Time (min)
EC4 β=0.5
EC4 UK NA β=0.7
Proposal β=0.5
Proposal β=0.7
Proposal β=β(T)
Applied Load
Column Force

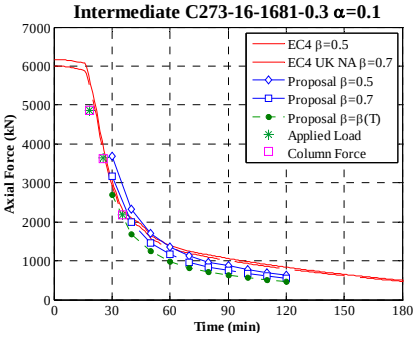
Intermediate C273-16-1681-0.3 α=0.1
Axial Force (kN)
Time (min)
EC4 β=0.5
EC4 UK NA β=0.7
Proposal β=0.5
Proposal β=0.7
Proposal β=β(T)
Applied Load
Column Force

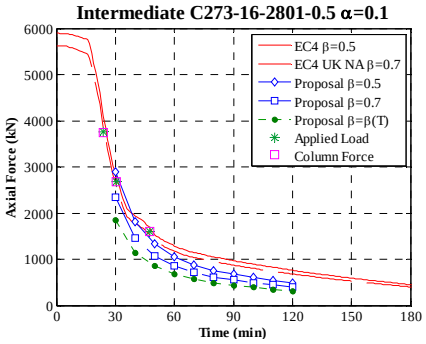
Intermediate C273-16-2801-0.5 α=0.1
Axial Force (kN)
Time (min)
EC4 β=0.5
EC4 UK NA β=0.7
Proposal β=0.5
Proposal β=0.7
Proposal β=β(T)
Applied Load
Column Force

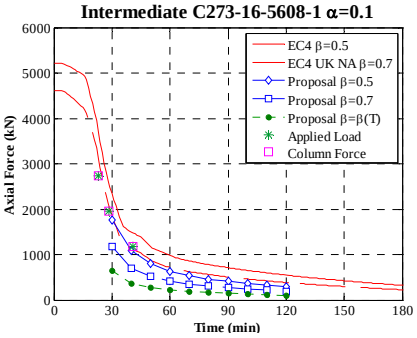
Intermediate C273-16-5608-1 α=0.1
Axial Force (kN)
Time (min)
EC4 β=0.5
EC4 UK NA β=0.7
Proposal β=0.5
Proposal β=0.7
Proposal β=β(T)
Applied Load
Column Force

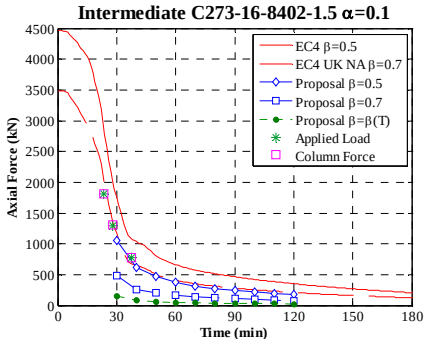
Intermediate C273-16-8402-1.5 α=0.1
EC4 β=0.5
EC4 UK NA β=0.7
Proposal β=0.5
Proposal β=0.7
Proposal β=β(T)
Applied Load
Column Force
Axial Force (kN)
Time (min)

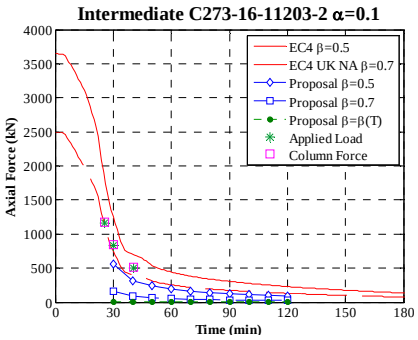
Intermediate C273-16-11203-2 α=0.1
EC4 β=0.5
EC4 UK NA β=0.7
Proposal β=0.5
Proposal β=0.7
Proposal β=β(T)
Applied Load
Column Force
Axial Force (kN)
Time (min)

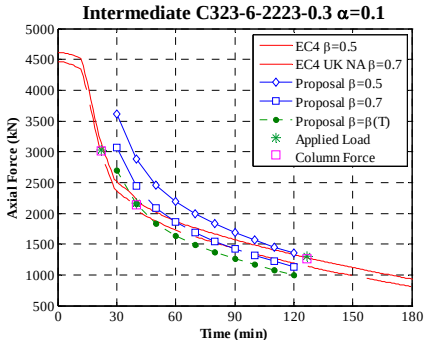
Intermediate C323-6-2223-0.3 α=0.1
EC4 β=0.5
EC4 UK NA β=0.7
Proposal β=0.5
Proposal β=0.7
Proposal β=β(T)
Applied Load
Column Force
Axial Force (kN)
Time (min)

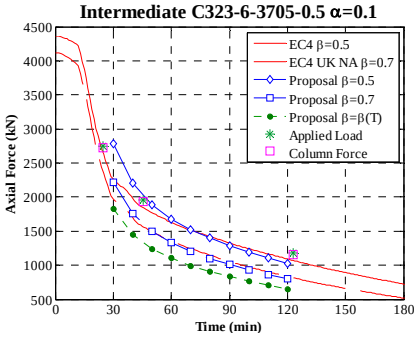
Intermediate C323-6-3705-0.5 α=0.1
EC4 β=0.5
EC4 UK NA β=0.7
Proposal β=0.5
Proposal β=0.7
Proposal β=β(T)
Applied Load
Column Force
Axial Force (kN)
Time (min)

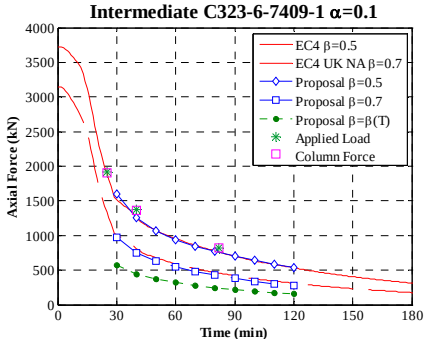
Intermediate C323-6-7409-1 α=0.1
EC4 β=0.5
EC4 UK NA β=0.7
Proposal β=0.5
Proposal β=0.7
Proposal β=β(T)
Applied Load
Column Force
Axial Force (kN)
Time (min)

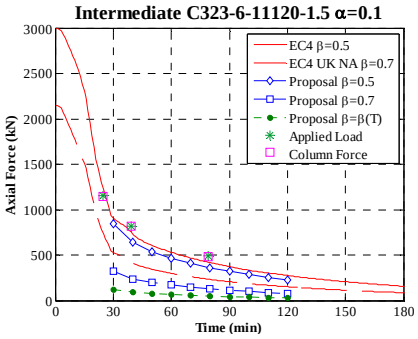
Intermediate C323-6-11120-1.5 α=0.1
EC4 β=0.5
EC4 UK NA β=0.7
Proposal β=0.5
Proposal β=0.7
Proposal β=β(T)
Applied Load
Column Force
Axial Force (kN)
Time (min)

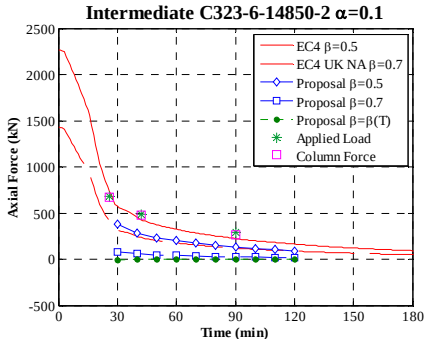
Intermediate C323-6-14850-2 α=0.1
Axial Force (kN)
Time (min)
EC4 β=0.5
EC4 UK NA β=0.7
Proposal β=0.5
Proposal β=0.7
Proposal β=β(T)
Applied Load
Column Force

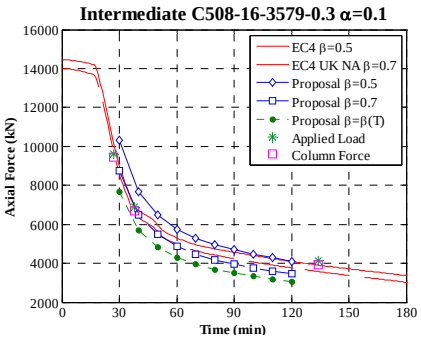
Intermediate C508-16-3579-0.3 α=0.1
Axial Force (kN)
Time (min)
EC4 β=0.5
EC4 UK NA β=0.7
Proposal β=0.5
Proposal β=0.7
Proposal β=β(T)
Applied Load
Column Force

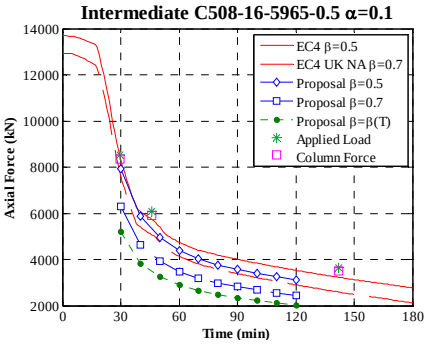
Intermediate C508-16-5965-0.5 α=0.1
Axial Force (kN)
Time (min)
EC4 β=0.5
EC4 UK NA β=0.7
Proposal β=0.5
Proposal β=0.7
Proposal β=β(T)
Applied Load
Column Force

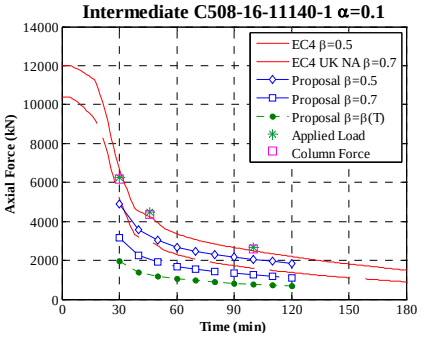
Intermediate C508-16-11140-1 α=0.1
Axial Force (kN)
Time (min)
EC4 β=0.5
EC4 UK NA β=0.7
Proposal β=0.5
Proposal β=0.7
Proposal β=β(T)
Applied Load
Column Force

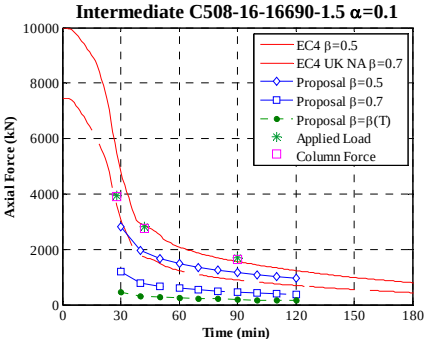
Intermediate C508-16-16690-1.5 α=0.1
Axial Force (kN)
Time (min)
EC4 β=0.5
EC4 UK NA β=0.7
Proposal β=0.5
Proposal β=0.7
Proposal β=β(T)
Applied Load
Column Force

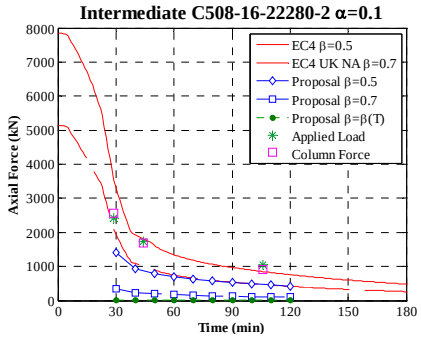
Intermediate C508-16-22280-2 α=0.1
Axial Force (kN)
Time (min)
EC4 β=0.5
EC4 UK NA β=0.7
Proposal β=0.5
Proposal β=0.7
Proposal β=β(T)
Applied Load
Column Force

Stiffness ratio α=0.5

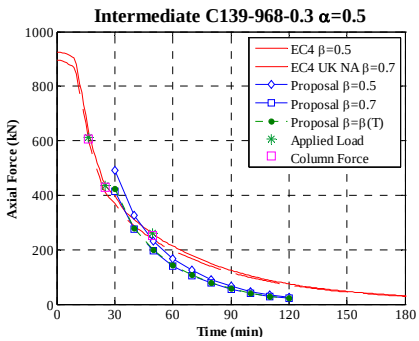

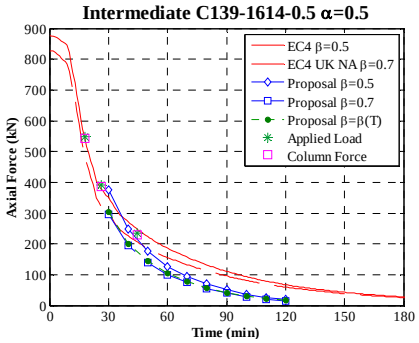

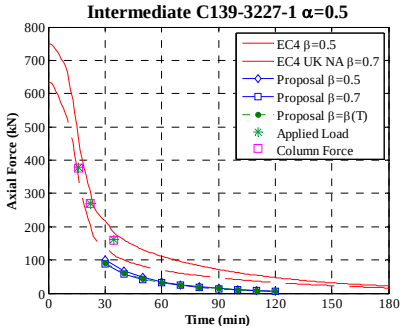

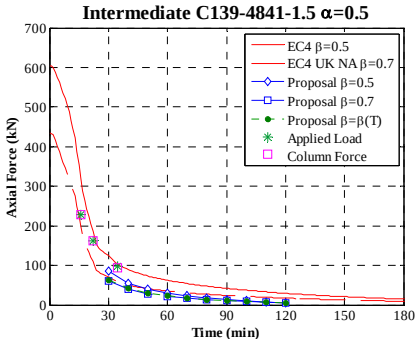

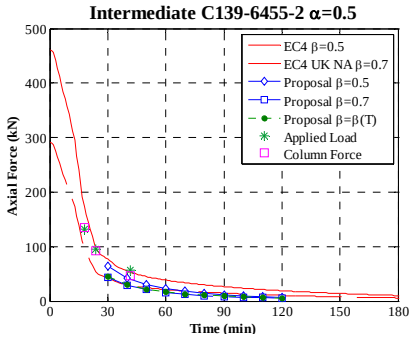

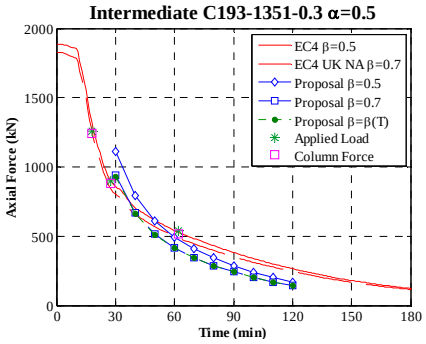

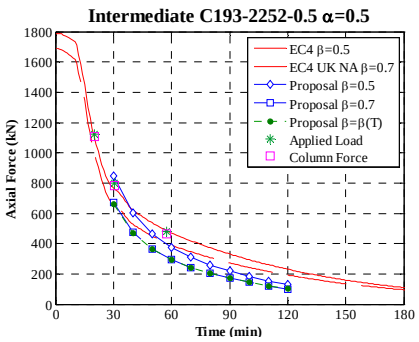
Intermediate C193-2252-0.5 α=0.5
Axial Force (kN)
Time (min)
EC4 β=0.5
EC4 UK NA β=0.7
Proposal β=0.5
Proposal β=0.7
Proposal β=β(T)
Applied Load
Column Force

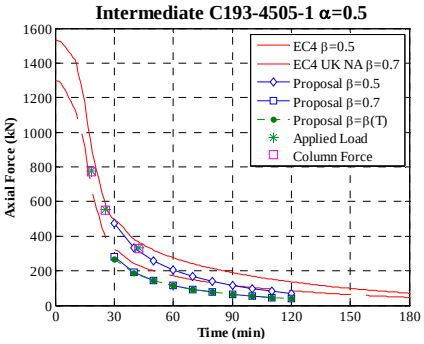
Intermediate C193-4505-1 α=0.5
Axial Force (kN)
Time (min)
EC4 β=0.5
EC4 UK NA β=0.7
Proposal β=0.5
Proposal β=0.7
Proposal β=β(T)
Applied Load
Column Force

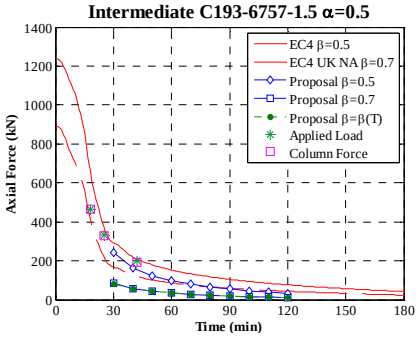
Intermediate C193-6757-1.5 α=0.5
Axial Force (kN)
Time (min)
EC4 β=0.5
EC4 UK NA β=0.7
Proposal β=0.5
Proposal β=0.7
Proposal β=β(T)
Applied Load
Column Force

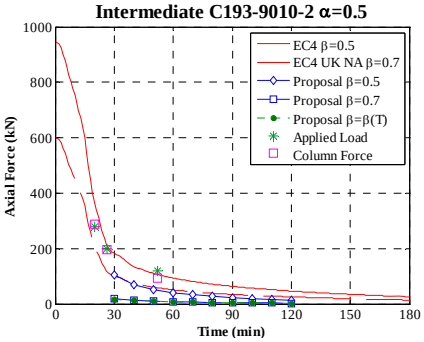
Intermediate C193-9010-2 α=0.5
Axial Force (kN)
Time (min)
EC4 β=0.5
EC4 UK NA β=0.7
Proposal β=0.5
Proposal β=0.7
Proposal β=β(T)
Applied Load
Column Force

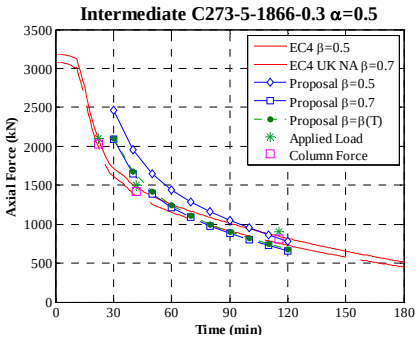
Intermediate C273-5-1866-0.3 α=0.5
Axial Force (kN)
Time (min)
EC4 β=0.5
EC4 UK NA β=0.7
Proposal β=0.5
Proposal β=0.7
Proposal β=β(T)
Applied Load
Column Force

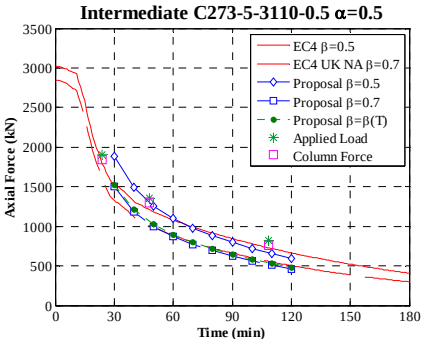
Intermediate C273-5-3110-0.5 α=0.5
Axial Force (kN)
Time (min)
EC4 β=0.5
EC4 UK NA β=0.7
Proposal β=0.5
Proposal β=0.7
Proposal β=β(T)
Applied Load
Column Force

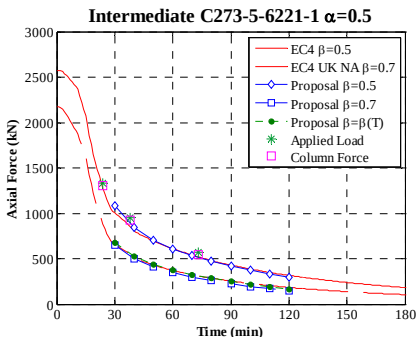
Intermediate C273-5-6221-1 α=0.5
Axial Force (kN)
Time (min)
EC4 β=0.5
EC4 UK NA β=0.7
Proposal β=0.5
Proposal β=0.7
Proposal β=β(T)
Applied Load
Column Force

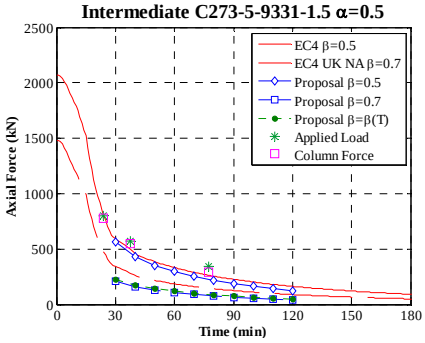
Intermediate C273-5-9331-1.5 α=0.5
Axial Force (kN)
Time (min)
EC4 β=0.5
EC4 UK NA β=0.7
Proposal β=0.5
Proposal β=0.7
Proposal β=β(T)
Applied Load
Column Force

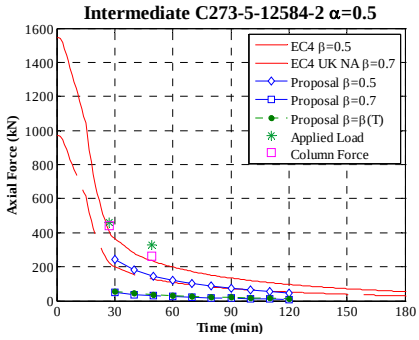
Intermediate C273-5-12584-2 α=0.5
Axial Force (kN)
Time (min)
EC4 β=0.5
EC4 UK NA β=0.7
Proposal β=0.5
Proposal β=0.7
Proposal β=β(T)
Applied Load
Column Force

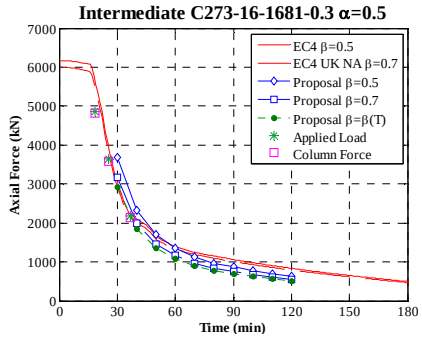
Intermediate C273-16-1681-0.3 α=0.5
Axial Force (kN)
Time (min)
EC4 β=0.5
EC4 UK NA β=0.7
Proposal β=0.5
Proposal β=0.7
Proposal β=β(T)
Applied Load
Column Force

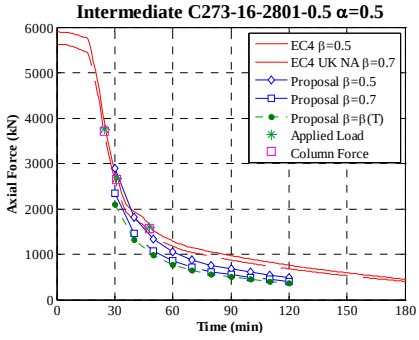
Intermediate C273-16-2801-0.5 α=0.5
Axial Force (kN)
Time (min)
EC4 β=0.5
EC4 UK NA β=0.7
Proposal β=0.5
Proposal β=0.7
Proposal β=β(T)
Applied Load
Column Force

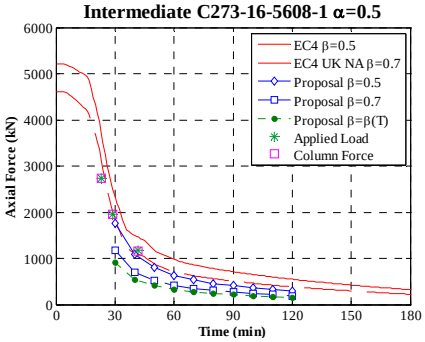
Intermediate C273-16-5608-1 α=0.5
Axial Force (kN)
Time (min)
EC4 β=0.5
EC4 UK NA β=0.7
Proposal β=0.5
Proposal β=0.7
Proposal β=β(T)
Applied Load
Column Force

Intermediate C273-16-8402-1.5 α=0.5

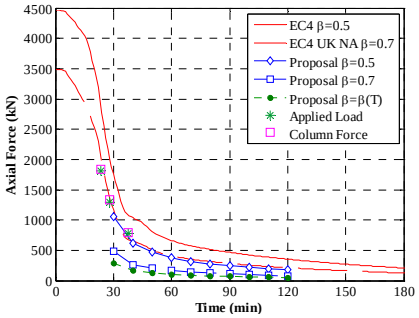

Intermediate C273-16-11203-2 α=0.5

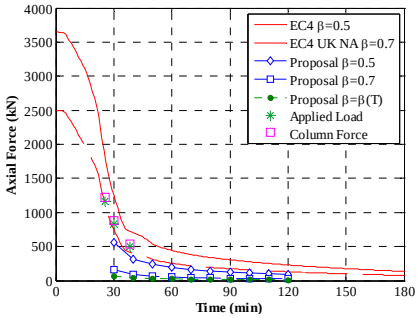

Intermediate C323-6-2223-0.3 α=0.5

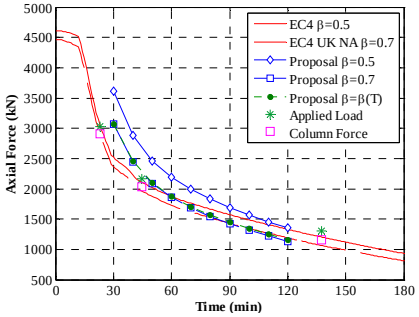

Intermediate C323-6-3705-0.5 α=0.5

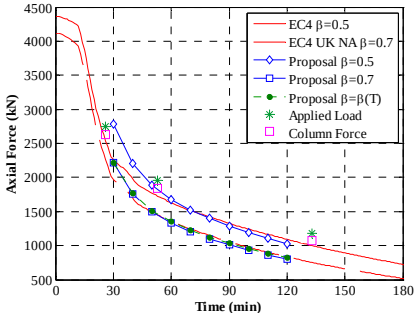

Intermediate C323-6-7409-1 α=0.5

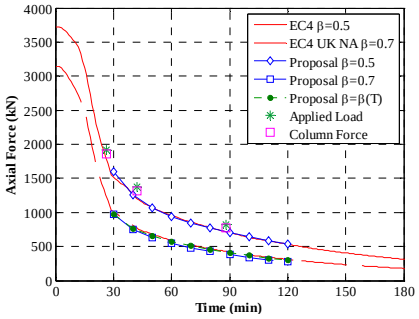

Intermediate C323-6-11120-1.5 α=0.5

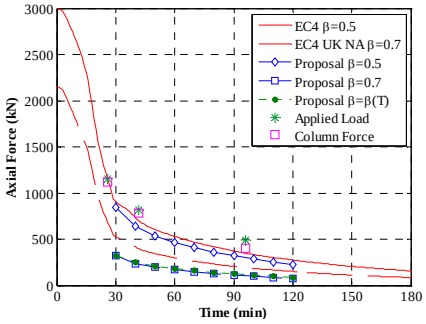

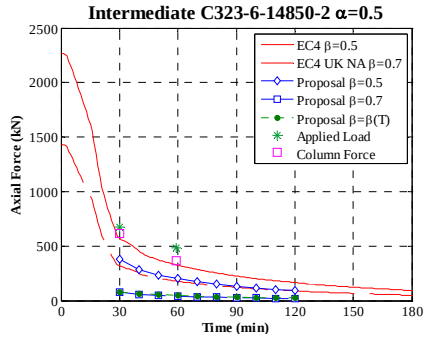
Intermediate C323-6-14850-2 α=0.5
Axial Force (kN)
Time (min)
EC4 β=0.5
EC4 UK NA β=0.7
Proposal β=0.5
Proposal β=0.7
Proposal β=β(T)
Applied Load
Column Force

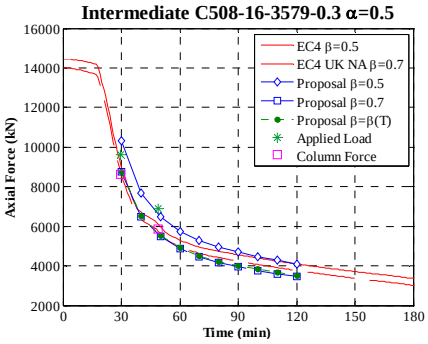
Intermediate C508-16-3579-0.3 α=0.5
Axial Force (kN)
Time (min)
EC4 β=0.5
EC4 UK NA β=0.7
Proposal β=0.5
Proposal β=0.7
Proposal β=β(T)
Applied Load
Column Force

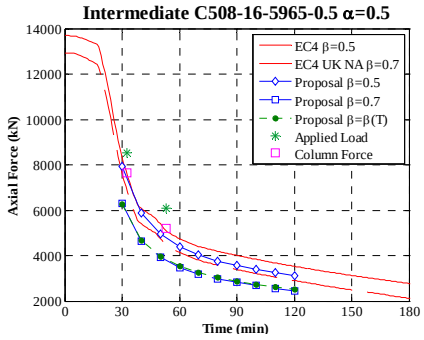
Intermediate C508-16-5965-0.5 α=0.5
Axial Force (kN)
Time (min)
EC4 β=0.5
EC4 UK NA β=0.7
Proposal β=0.5
Proposal β=0.7
Proposal β=β(T)
Applied Load
Column Force

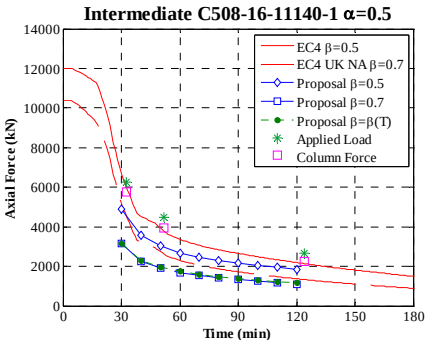
Intermediate C508-16-11140-1 α=0.5
Axial Force (kN)
Time (min)
EC4 β=0.5
EC4 UK NA β=0.7
Proposal β=0.5
Proposal β=0.7
Proposal β=β(T)
Applied Load
Column Force

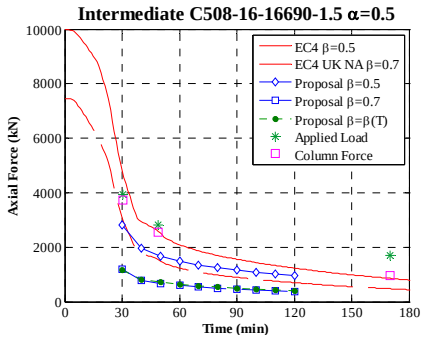
Intermediate C508-16-16690-1.5 α=0.5
Axial Force (kN)
Time (min)
EC4 β=0.5
EC4 UK NA β=0.7
Proposal β=0.5
Proposal β=0.7
Proposal β=β(T)
Applied Load
Column Force

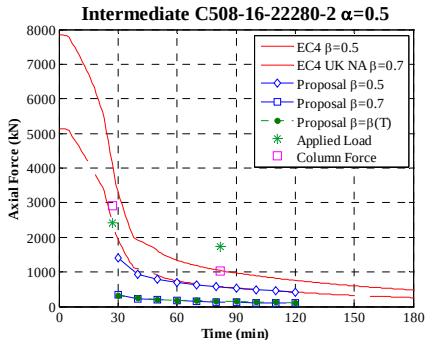
Intermediate C508-16-22280-2 α=0.5
Axial Force (kN)
Time (min)
EC4 β=0.5
EC4 UK NA β=0.7
Proposal β=0.5
Proposal β=0.7
Proposal β=β(T)
Applied Load
Column Force

Stiffness ratio α=1

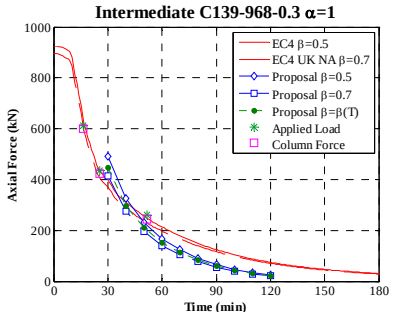

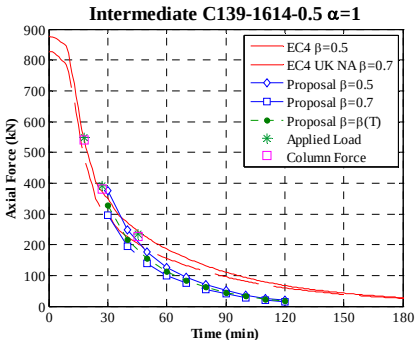

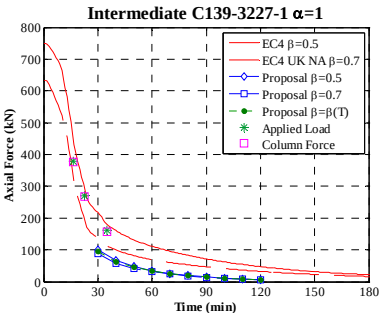

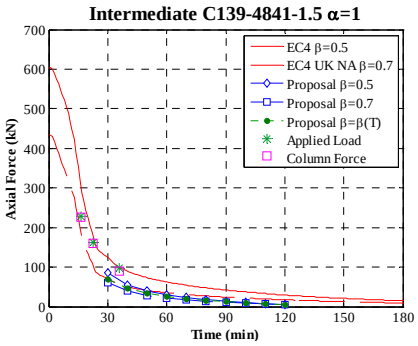

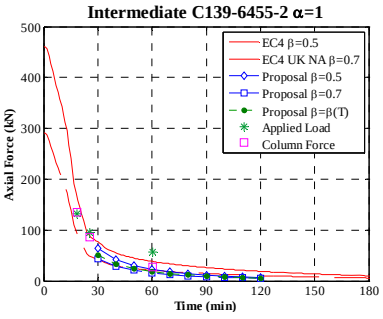

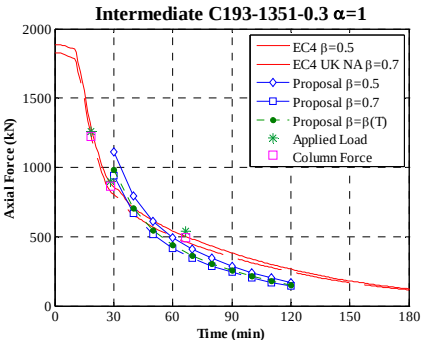

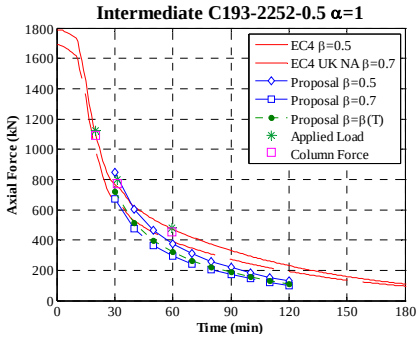
Intermediate C193-2252-0.5 α=1
EC4 β=0.5
EC4 UK NA β=0.7
Proposal β=0.5
Proposal β=0.7
Proposal β=β(T)
Applied Load
Column Force
Axial Force (kN)
Time (min)

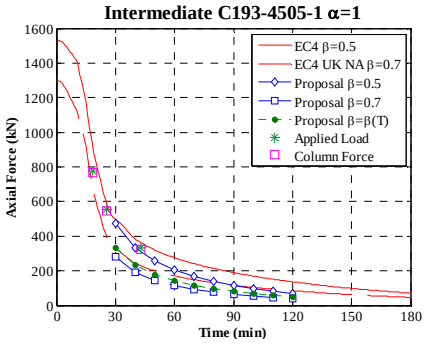
Intermediate C193-4505-1 α=1
EC4 β=0.5
EC4 UK NA β=0.7
Proposal β=0.5
Proposal β=0.7
Proposal β=β(T)
Applied Load
Column Force
Axial Force (kN)
Time (min)

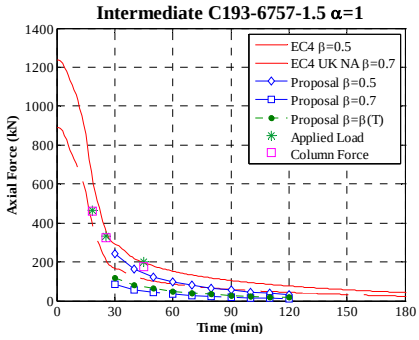
Intermediate C193-6757-1.5 α=1
EC4 β=0.5
EC4 UK NA β=0.7
Proposal β=0.5
Proposal β=0.7
Proposal β=β(T)
Applied Load
Column Force
Axial Force (kN)
Time (min)

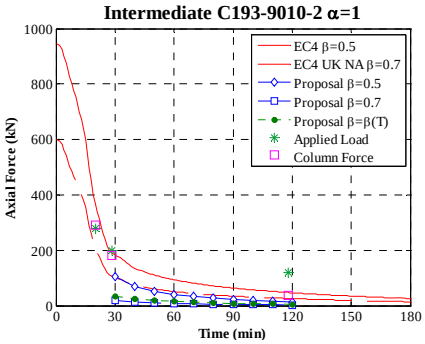
Intermediate C193-9010-2 α=1
EC4 β=0.5
EC4 UK NA β=0.7
Proposal β=0.5
Proposal β=0.7
Proposal β=β(T)
Applied Load
Column Force
Axial Force (kN)
Time (min)

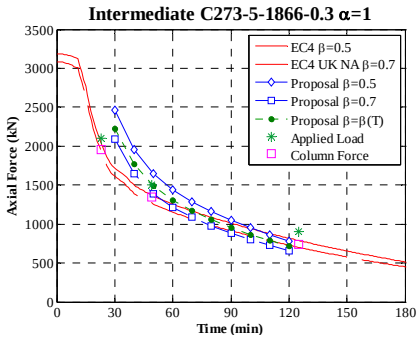
Intermediate C273-5-1866-0.3 α=1
EC4 β=0.5
EC4 UK NA β=0.7
Proposal β=0.5
Proposal β=0.7
Proposal β=β(T)
Applied Load
Column Force
Axial Force (kN)
Time (min)

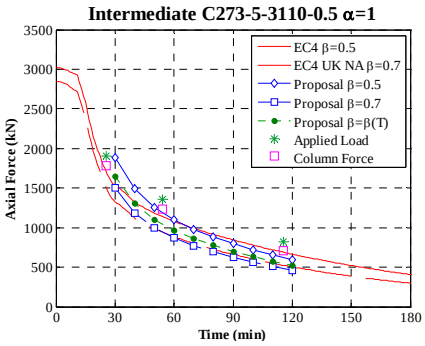
Intermediate C273-5-3110-0.5 α=1
EC4 β=0.5
EC4 UK NA β=0.7
Proposal β=0.5
Proposal β=0.7
Proposal β=β(T)
Applied Load
Column Force
Axial Force (kN)
Time (min)

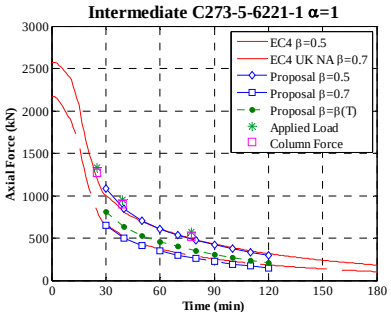
Intermediate C273-5-6221-1 α=1
Axial Force (kN)
Time (min)
EC4 β=0.5
EC4 UK NA β=0.7
Proposal β=0.5
Proposal β=0.7
Proposal β=β(T)
Applied Load
Column Force

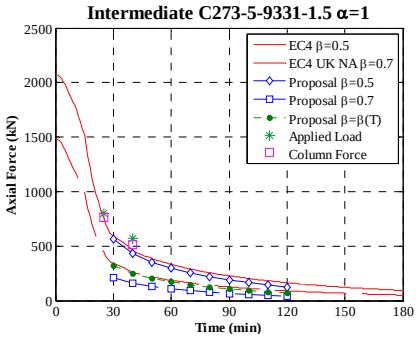
Intermediate C273-5-9331-1.5 α=1
Axial Force (kN)
Time (min)
EC4 β=0.5
EC4 UK NA β=0.7
Proposal β=0.5
Proposal β=0.7
Proposal β=β(T)
Applied Load
Column Force

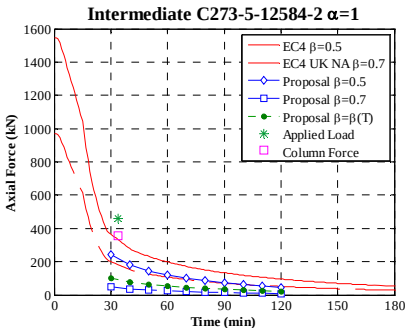
Intermediate C273-5-12584-2 α=1
Axial Force (kN)
Time (min)
EC4 β=0.5
EC4 UK NA β=0.7
Proposal β=0.5
Proposal β=0.7
Proposal β=β(T)
Applied Load
Column Force

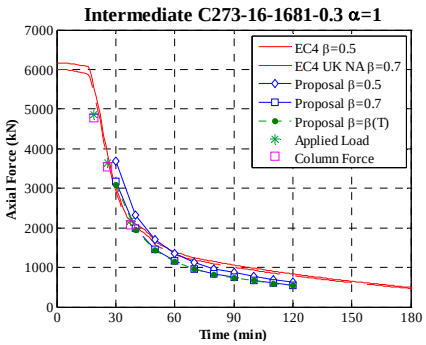
Intermediate C273-16-1681-0.3 α=1
Axial Force (kN)
Time (min)
EC4 β=0.5
EC4 UK NA β=0.7
Proposal β=0.5
Proposal β=0.7
Proposal β=β(T)
Applied Load
Column Force

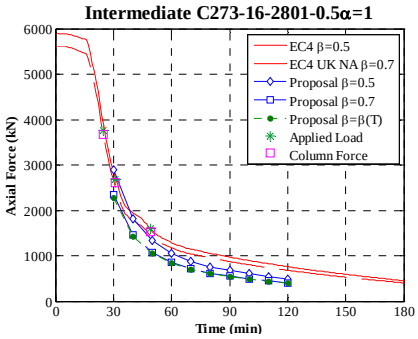
Intermediate C273-16-2801-0.5α=1
Axial Force (kN)
Time (min)
EC4 β=0.5
EC4 UK NA β=0.7
Proposal β=0.5
Proposal β=0.7
Proposal β=β(T)
Applied Load
Column Force

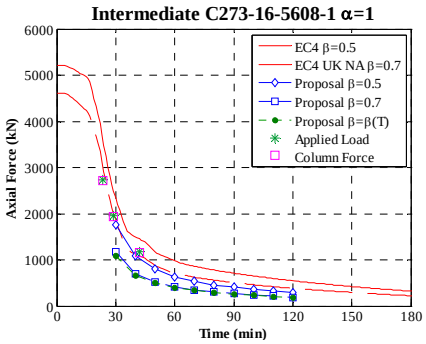
Intermediate C273-16-5608-1 α=1
Axial Force (kN)
Time (min)
EC4 β=0.5
EC4 UK NA β=0.7
Proposal β=0.5
Proposal β=0.7
Proposal β=β(T)
Applied Load
Column Force

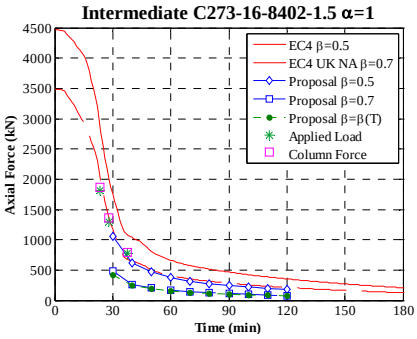
Intermediate C273-16-8402-1.5 α=1
Axial Force (kN)
Time (min)
EC4 β=0.5
EC4 UK NA β=0.7
Proposal β=0.5
Proposal β=0.7
Proposal β=β(T)
Applied Load
Column Force

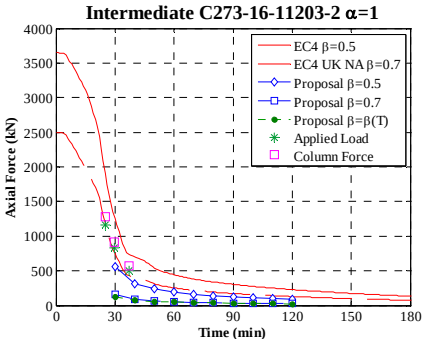
Intermediate C273-16-11203-2 α=1
Axial Force (kN)
Time (min)
EC4 β=0.5
EC4 UK NA β=0.7
Proposal β=0.5
Proposal β=0.7
Proposal β=β(T)
Applied Load
Column Force

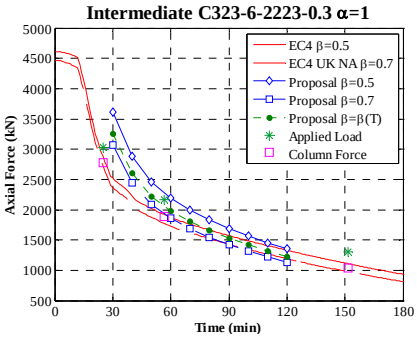
Intermediate C323-6-2223-0.3 α=1
Axial Force (kN)
Time (min)
EC4 β=0.5
EC4 UK NA β=0.7
Proposal β=0.5
Proposal β=0.7
Proposal β=β(T)
Applied Load
Column Force

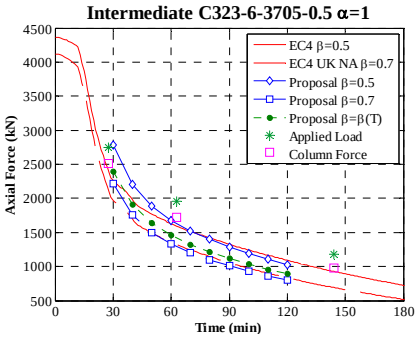
Intermediate C323-6-3705-0.5 α=1
Axial Force (kN)
Time (min)
EC4 β=0.5
EC4 UK NA β=0.7
Proposal β=0.5
Proposal β=0.7
Proposal β=β(T)
Applied Load
Column Force

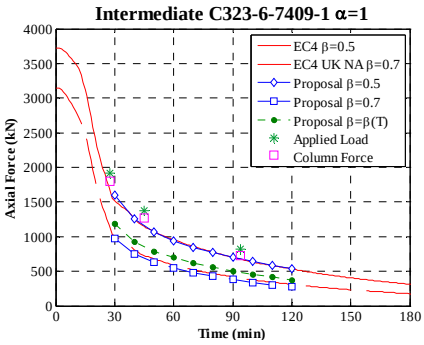
Intermediate C323-6-7409-1 α=1
Axial Force (kN)
Time (min)
EC4 β=0.5
EC4 UK NA β=0.7
Proposal β=0.5
Proposal β=0.7
Proposal β=β(T)
Applied Load
Column Force

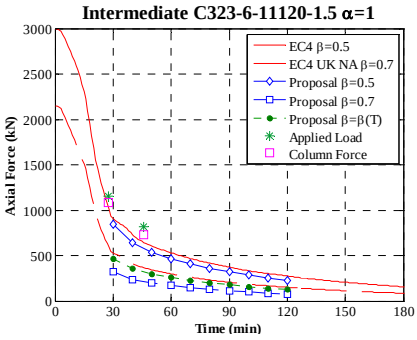
Intermediate C323-6-11120-1.5 α=1
Axial Force (kN)
Time (min)
EC4 β=0.5
EC4 UK NA β=0.7
Proposal β=0.5
Proposal β=0.7
Proposal β=β(T)
Applied Load
Column Force

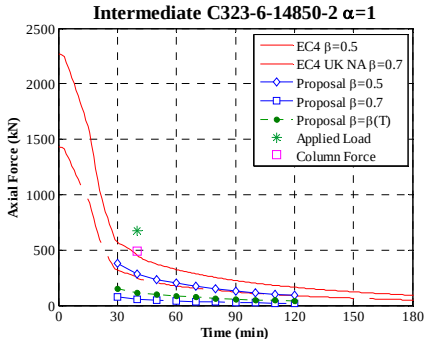
Intermediate C323-6-14850-2 α=1
Axial Force (kN)
Time (min)
EC4 β=0.5
EC4 UK NA β=0.7
Proposal β=0.5
Proposal β=0.7
Proposal β=β(T)
Applied Load
Column Force

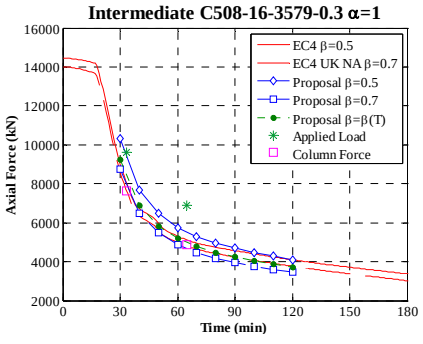
Intermediate C508-16-3579-0.3 α=1
Axial Force (kN)
Time (min)
EC4 β=0.5
EC4 UK NA β=0.7
Proposal β=0.5
Proposal β=0.7
Proposal β=β(T)
Applied Load
Column Force

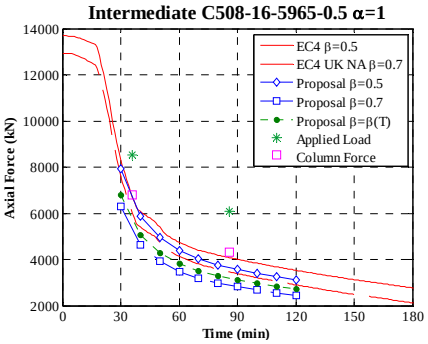
Intermediate C508-16-5965-0.5 α=1
Axial Force (kN)
Time (min)
EC4 β=0.5
EC4 UK NA β=0.7
Proposal β=0.5
Proposal β=0.7
Proposal β=β(T)
Applied Load
Column Force

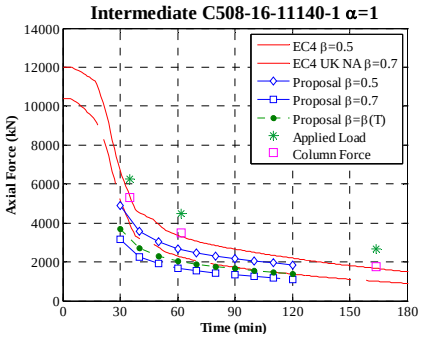
Intermediate C508-16-11140-1 α=1
Axial Force (kN)
Time (min)
EC4 β=0.5
EC4 UK NA β=0.7
Proposal β=0.5
Proposal β=0.7
Proposal β=β(T)
Applied Load
Column Force

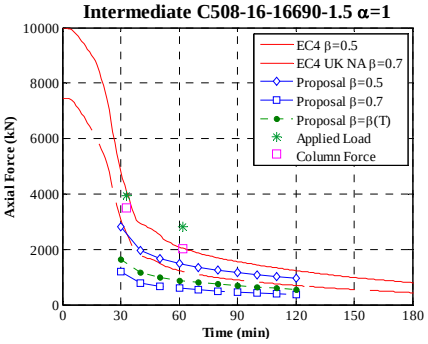
Intermediate C508-16-16690-1.5 α=1
Axial Force (kN)
Time (min)
EC4 β=0.5
EC4 UK NA β=0.7
Proposal β=0.5
Proposal β=0.7
Proposal β=β(T)
Applied Load
Column Force

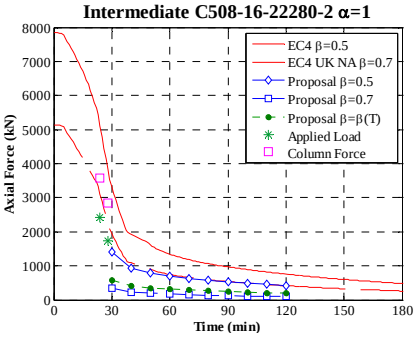
Intermediate C508-16-22280-2 α=1
Axial Force (kN)
Time (min)
EC4 β=0.5
EC4 UK NA β=0.7
Proposal β=0.5
Proposal β=0.7
Proposal β=β(T)
Applied Load
Column Force

Stiffness ratio α=2

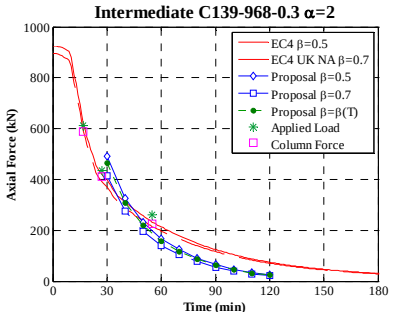

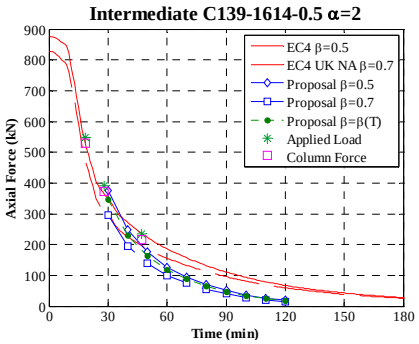

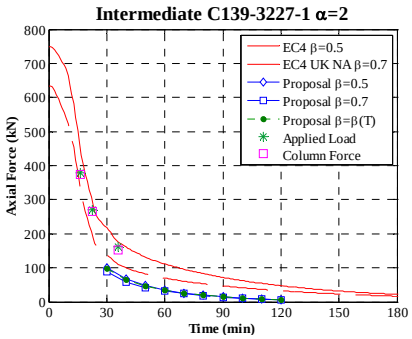

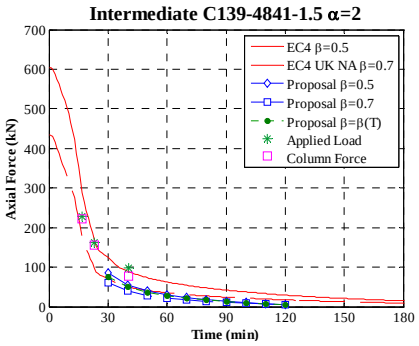

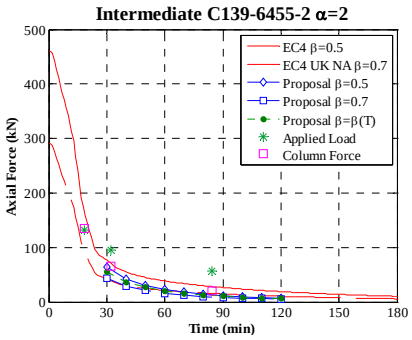

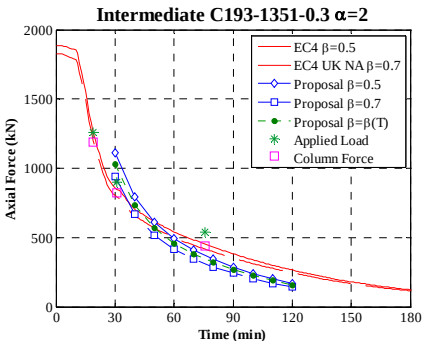

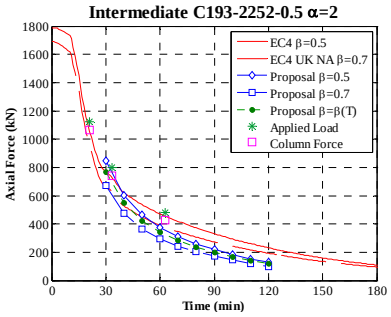
Intermediate C193-2252-0.5 α=2
EC4 β=0.5
EC4 UK NA β=0.7
Proposal β=0.5
Proposal β=0.7
Proposal β=β(T)
Applied Load
Column Force
Axial Force (kN)
Time (min)

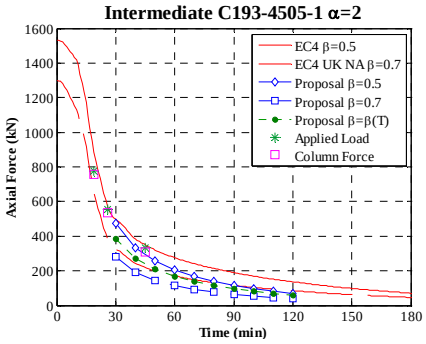
Intermediate C193-4505-1 α=2
EC4 β=0.5
EC4 UK NA β=0.7
Proposal β=0.5
Proposal β=0.7
Proposal β=β(T)
Applied Load
Column Force
Axial Force (kN)
Time (min)

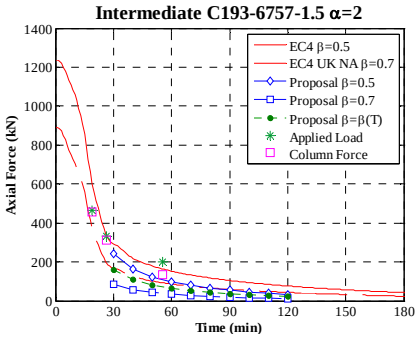
Intermediate C193-6757-1.5 α=2
EC4 β=0.5
EC4 UK NA β=0.7
Proposal β=0.5
Proposal β=0.7
Proposal β=β(T)
Applied Load
Column Force
Axial Force (kN)
Time (min)

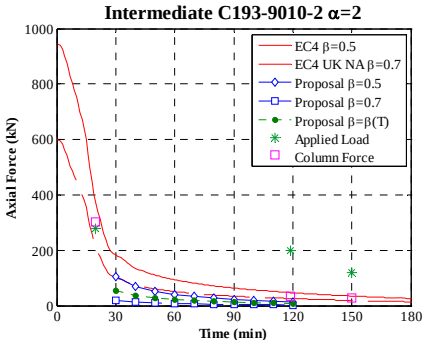
Intermediate C193-9010-2 α=2
EC4 β=0.5
EC4 UK NA β=0.7
Proposal β=0.5
Proposal β=0.7
Proposal β=β(T)
Applied Load
Column Force
Axial Force (kN)
Time (min)

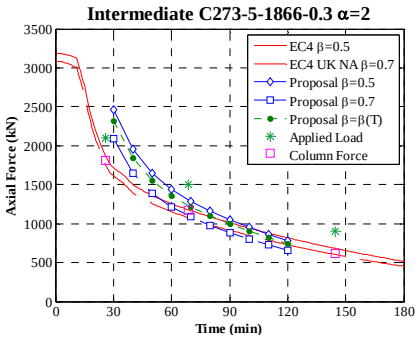
Intermediate C273-5-1866-0.3 α=2
EC4 β=0.5
EC4 UK NA β=0.7
Proposal β=0.5
Proposal β=0.7
Proposal β=β(T)
Applied Load
Column Force
Axial Force (kN)
Time (min)

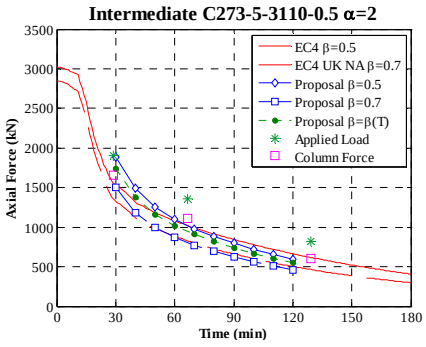
Intermediate C273-5-3110-0.5 α=2
EC4 β=0.5
EC4 UK NA β=0.7
Proposal β=0.5
Proposal β=0.7
Proposal β=β(T)
Applied Load
Column Force
Axial Force (kN)
Time (min)

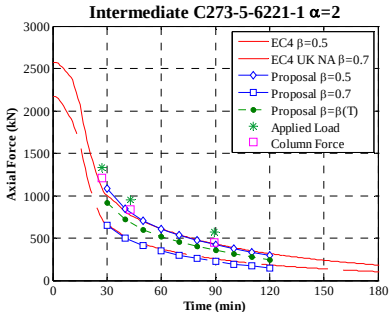
Intermediate C273-5-6221-1 α=2
EC4 β=0.5
EC4 UK NA β=0.7
Proposal β=0.5
Proposal β=0.7
Proposal β=β(T)
Applied Load
Column Force
Axial Force (kN)
Time (min)

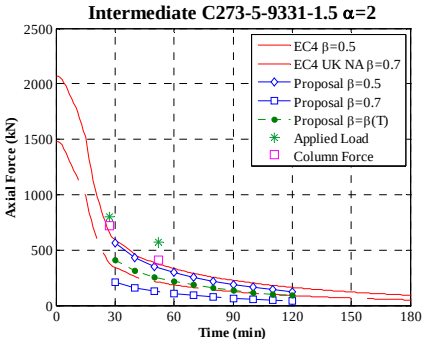
Intermediate C273-5-9331-1.5 α=2
EC4 β=0.5
EC4 UK NA β=0.7
Proposal β=0.5
Proposal β=0.7
Proposal β=β(T)
Applied Load
Column Force
Axial Force (kN)
Time (min)

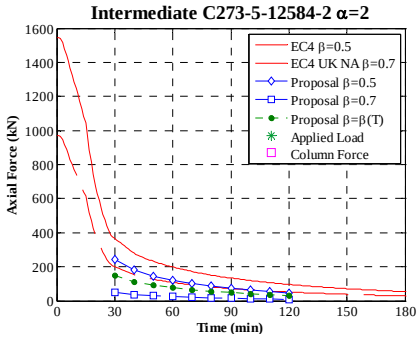
Intermediate C273-5-12584-2 α=2
EC4 β=0.5
EC4 UK NA β=0.7
Proposal β=0.5
Proposal β=0.7
Proposal β=β(T)
Applied Load
Column Force
Axial Force (kN)
Time (min)

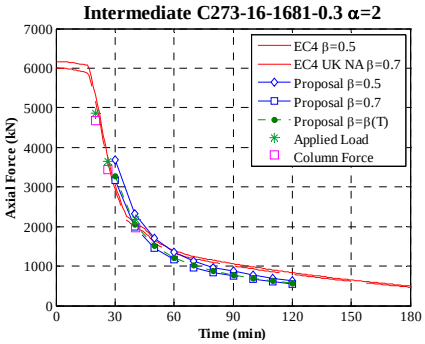
Intermediate C273-16-1681-0.3 α=2
EC4 β=0.5
EC4 UK NA β=0.7
Proposal β=0.5
Proposal β=0.7
Proposal β=β(T)
Applied Load
Column Force
Axial Force (kN)
Time (min)

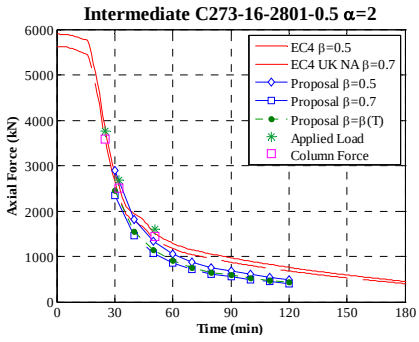
Intermediate C273-16-2801-0.5 α=2
EC4 β=0.5
EC4 UK NA β=0.7
Proposal β=0.5
Proposal β=0.7
Proposal β=β(T)
Applied Load
Column Force
Axial Force (kN)
Time (min)

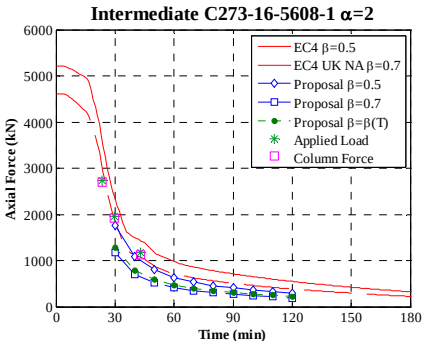
Intermediate C273-16-5608-1 α=2
EC4 β=0.5
EC4 UK NA β=0.7
Proposal β=0.5
Proposal β=0.7
Proposal β=β(T)
Applied Load
Column Force
Axial Force (kN)
Time (min)

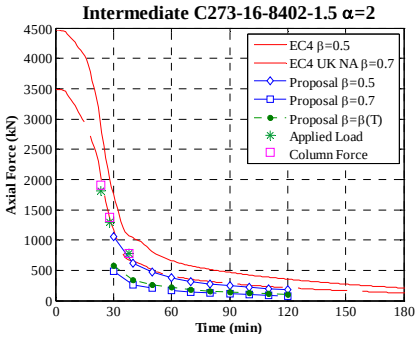
Intermediate C273-16-8402-1.5 α=2
Axial Force (kN)
Time (min)
EC4 β=0.5
EC4 UK NA β=0.7
Proposal β=0.5
Proposal β=0.7
Proposal β=β(T)
Applied Load
Column Force

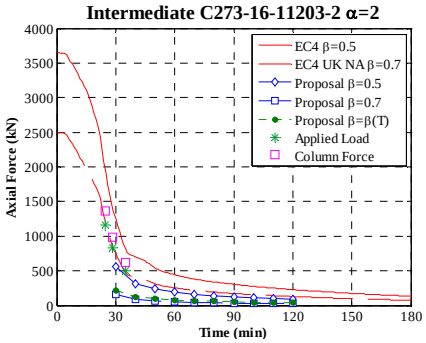
Intermediate C273-16-11203-2 α=2
Axial Force (kN)
Time (min)
EC4 β=0.5
EC4 UK NA β=0.7
Proposal β=0.5
Proposal β=0.7
Proposal β=β(T)
Applied Load
Column Force

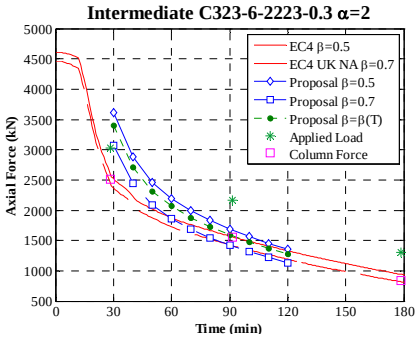
Intermediate C323-6-2223-0.3 α=2
Axial Force (kN)
Time (min)
EC4 β=0.5
EC4 UK NA β=0.7
Proposal β=0.5
Proposal β=0.7
Proposal β=β(T)
Applied Load
Column Force

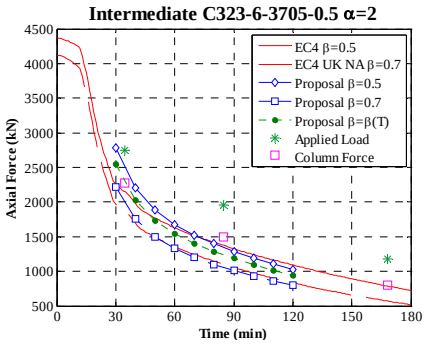
Intermediate C323-6-3705-0.5 α=2
Axial Force (kN)
Time (min)
EC4 β=0.5
EC4 UK NA β=0.7
Proposal β=0.5
Proposal β=0.7
Proposal β=β(T)
Applied Load
Column Force

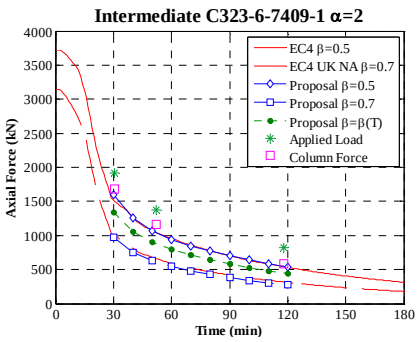
Intermediate C323-6-7409-1 α=2
Axial Force (kN)
Time (min)
EC4 β=0.5
EC4 UK NA β=0.7
Proposal β=0.5
Proposal β=0.7
Proposal β=β(T)
Applied Load
Column Force

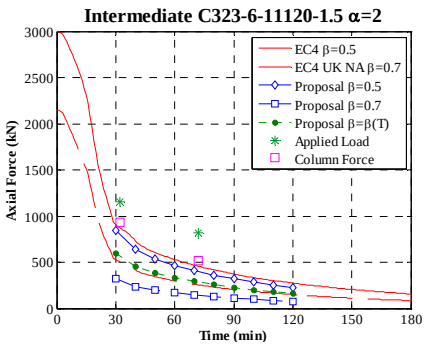
Intermediate C323-6-11120-1.5 α=2
Axial Force (kN)
Time (min)
EC4 β=0.5
EC4 UK NA β=0.7
Proposal β=0.5
Proposal β=0.7
Proposal β=β(T)
Applied Load
Column Force

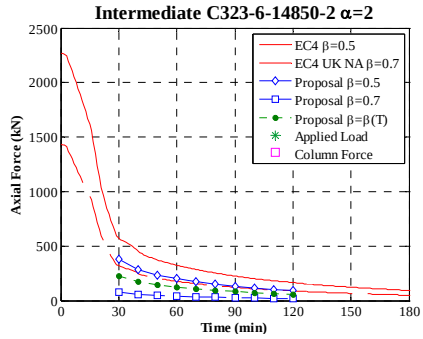
Intermediate C323-6-14850-2 α=2
Axial Force (kN)
Time (min)
EC4 β=0.5
EC4 UK NA β=0.7
Proposal β=0.5
Proposal β=0.7
Proposal β=β(T)
Applied Load
Column Force

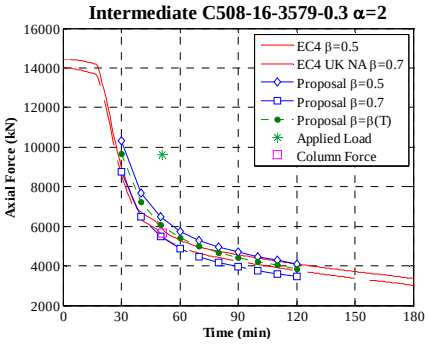
Intermediate C508-16-3579-0.3 α=2
Axial Force (kN)
Time (min)
EC4 β=0.5
EC4 UK NA β=0.7
Proposal β=0.5
Proposal β=0.7
Proposal β=β(T)
Applied Load
Column Force

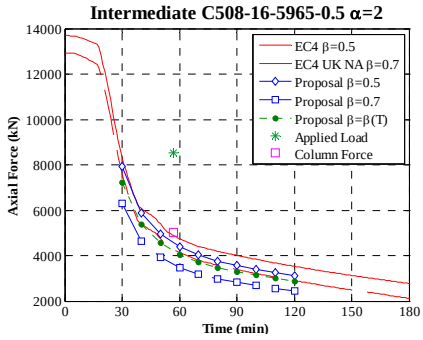
Intermediate C508-16-5965-0.5 α=2
Axial Force (kN)
Time (min)
EC4 β=0.5
EC4 UK NA β=0.7
Proposal β=0.5
Proposal β=0.7
Proposal β=β(T)
Applied Load
Column Force

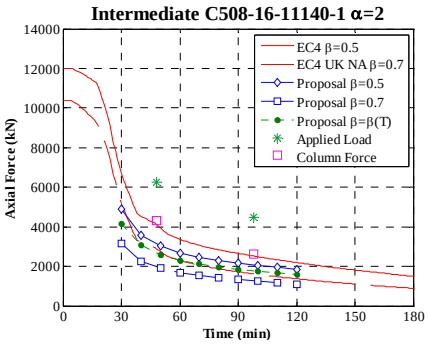
Intermediate C508-16-11140-1 α=2
Axial Force (kN)
Time (min)
EC4 β=0.5
EC4 UK NA β=0.7
Proposal β=0.5
Proposal β=0.7
Proposal β=β(T)
Applied Load
Column Force

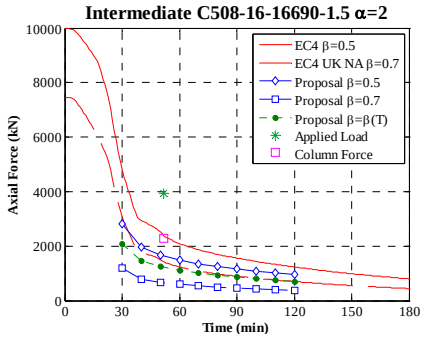
Intermediate C508-16-16690-1.5 α=2
Axial Force (kN)
Time (min)
EC4 β=0.5
EC4 UK NA β=0.7
Proposal β=0.5
Proposal β=0.7
Proposal β=β(T)
Applied Load
Column Force

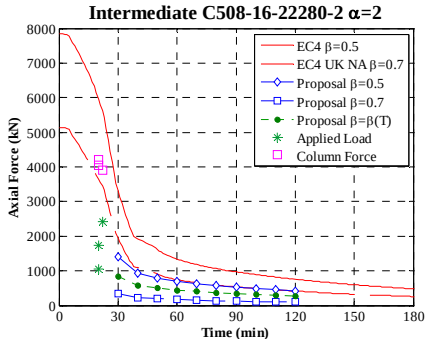
Intermediate C508-16-22280-2 α=2
Axial Force (kN)
Time (min)
EC4 β=0.5
EC4 UK NA β=0.7
Proposal β=0.5
Proposal β=0.7
Proposal β=β(T)
Applied Load
Column Force

ANNEX II.

MATERIAL CONSTITUTIVE MODELLING

This Annex includes the formulation of the different material models which have been used in the several studies accomplished during this thesis. The thermal properties and constitutive laws of steel and concrete at elevated temperatures of the models employed are presented.

1. CONCRETE AT ELEVATED TEMPERATURES

1.1. Thermal properties of concrete at elevated temperatures

1.1.1. Formulation from Eurocode 2

Eurocode 2 Part 1.2 (CEN 2004a) Section 3.3 comprises the definition of the thermal properties of concrete at elevated temperatures, for both concrete with siliceous and calcareous aggregates. Eurocode 4 Part 1-2 (CEN 2005c) has incorporated the same properties with some little changes.

Thermal elongation

The thermal elongation of concrete $(\Delta l/l)_c$ may be obtained from the following equations, which are referred to the length of the member at ambient temperature (20ºC):

Siliceous aggregates:

$$(\Delta l / l)_c = -1.8 \cdot 10^{-4} + 9 \cdot 10^{-6} \cdot \theta_c + 2.3 \cdot 10^{-11} \cdot \theta_c^{\,3} \quad \text{for } 20^{\circ}\text{C} \le \theta_c \le 700^{\circ}\text{C}$$

$$(\Delta l / l)_c = 14 \cdot 10^{-3} \quad \text{for } 700^{\circ}\text{C} \le \theta_c \le 1200^{\circ}\text{C}$$

Calcareous aggregates:

$$(\Delta l / l)_c = -1.2 \cdot 10^{-4} + 6 \cdot 10^{-6} \cdot \theta_c + 1.4 \cdot 10^{-11} \cdot \theta_c^{\,3} \quad \text{for } 20^{\circ}\text{C} \le \theta_c \le 805^{\circ}\text{C}$$

$$(\Delta l / l)_c = 12 \cdot 10^{-3} \quad \text{for } 805^{\circ}\text{C} \le \theta_c \le 1200^{\circ}\text{C}$$

where θ_c is the temperature of concrete, in ºC.

According to EC4 Part 1-2 Section 3.3.2(3), in simple calculation models, the relationship between the thermal elongation $(\Delta l/l)_c$ and concrete temperature may be considered to be linear, through the following expression:

$$(\Delta l / l)_c = 18 \cdot 10^{-6} \cdot (\theta_c - 20)$$

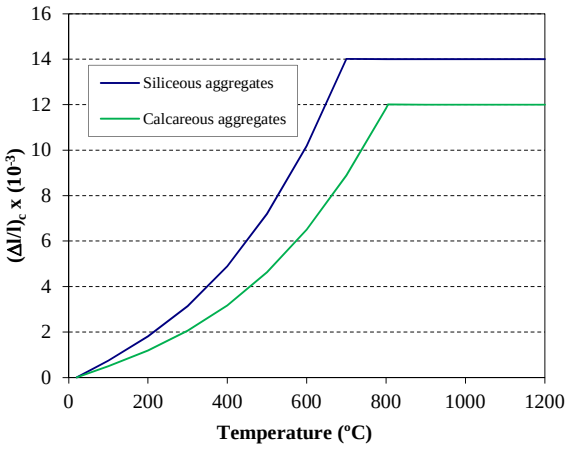

Figure 1. Thermal elongation of concrete at elevated temperatures according to EC2 (CEN 2004a).

Specific heat

For dry concrete (moisture content of 0%), with calcareous or siliceous aggregates, the specific heat may be determined from the following equations:

$c_c = 900$ (J/kgK) for $20^\circ\text{C} \le \theta_c \le 100^\circ\text{C}$

$c_c = 900 + (\theta_c - 100)$ (J/kgK) for $100^\circ\text{C} \le \theta_c \le 200^\circ\text{C}$

$c_c = 1000 + (\theta_c - 200)/2$ (J/kgK) for $200^\circ\text{C} \le \theta_c \le 400^\circ\text{C}$

$c_c = 1100$ (J/kgK) for $400^\circ\text{C} \le \theta_c \le 1200^\circ\text{C}$

where θ_c is the temperature of concrete, in ºC.

If the moisture content is not considered explicitly in the calculation method, the previous formulae needs to be modified by adding a constant peak value $c_{c,peak}$ between 100 ºC and 115 ºC, with a linear decrease between 115 ºC and 200 ºC, which permits to model implicitly the heat consumption which occurs due to water evaporation in this range of temperatures. This peak value is equal to:

$c_{c.peak} = 900$ J/kgK for a moisture content of 0% of concrete weight

$c_{c.peak} = 1470$ J/kgK for a moisture content of 1.5% of concrete weight

$c_{c.peak} = 2020$ J/kgK for a moisture content of 3% of concrete weight

It is worth noting that, according to EC4 Part 1-2 Section 3.3.2(8), in hollow sections filled with concrete, a moisture content of a 10% may be found, and in that case a value $c_{c.peak}$ = 5600 J/kgK should be used.

In simple calculation models, EC4 Part 1-2 3.3.2(6) allows for the use of a constant value for the specific heat equal to 1000 J/kgK.

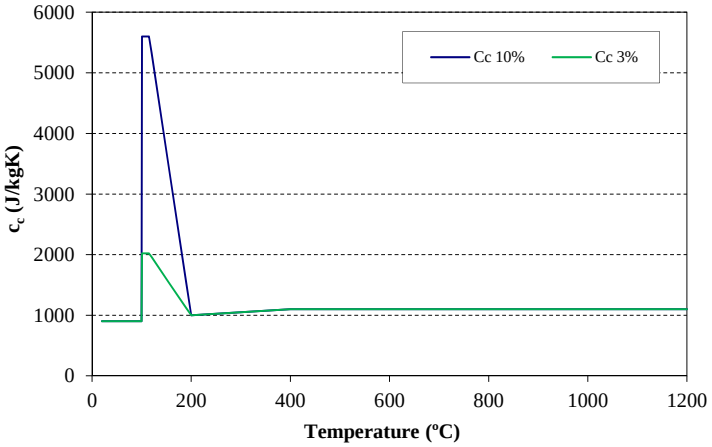

Figure 2. Specific heat of concrete at elevated temperatures, according to EC2 (CEN 2004a).

Density

EC4 Part 1-2 3.4(3) allows for the use of a constant density value for unreinforced normal weight concrete equal to 2300 kg/m^3.

Thermal conductivity

The thermal conductivity of concrete λ_c can adopt values comprised between the following lower and upper limits.

Upper limit:

$$\lambda_c = 2 - 0.2451\cdot(\theta_c/100) + 0.0107\cdot(\theta_c/100)^2 \text{ (W/mK) for } 20^o\text{C} \le \theta_c \le 1200^o\text{C}$$

Lower limit:

$$\lambda_c = 1{,}36 - 0.136\cdot(\theta_c/100) + 0.0057\cdot(\theta_c/100)^2 \text{ (W/mK) for } 20^o\text{C} \le \theta_c \le 1200^o\text{C}$$

where θ_c is the temperature of concrete, in ºC.

EC4 Part 1-2 3.3.2(9) recommends the use of the upper limit for steel-concrete composite members.

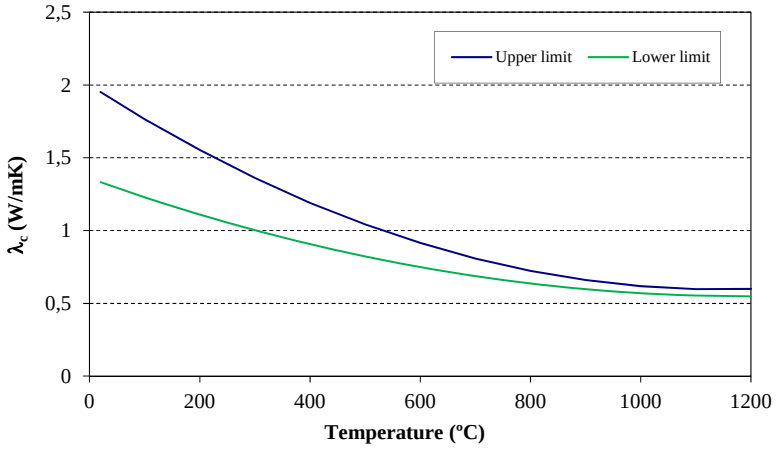

Figure 3. Specific heat of concrete at elevated temperatures, according to EC2 (CEN 2004a).

In simple calculation models, EC4 Part 1-2 3.3.2(12) establishes that a constant value of 1.60 W/mK may be adopted for the thermal conductivity of concrete.

1.1.2. Formulation by Kodur & Sultan

Kodur & Sultan (2003) determined the relevant thermal properties of high-strength concrete (HSC) as a function of temperature for their use in fire resistance calculations. The authors observed that the thermal properties, at elevated temperatures, exhibited by steel fiber-reinforced HSC are similar to those of plain HSC.

For high strength concrete:

Thermal capacity

For concrete with calcareous aggregates, the thermal capacity of concrete can be obtained by means of:

$$\rho_c c_c = 2.45 \cdot 10^6 (J/m^3{}^oC) \qquad 0^oC \le \theta_c \le 400^oC$$
$$\rho_c c_c = (0.0260 \cdot \theta_c - 12.850) \cdot 10^6 (J/m^3{}^oC) \qquad 400^oC \le \theta_c \le 475^oC$$
$$\rho_c c_c = (0.0143 \cdot \theta_c - 6.295) \cdot 10^6 (J/m^3{}^oC) \qquad 475^oC \le \theta_c \le 650^oC$$
$$\rho_c c_c = (0.1894 \cdot \theta_c - 120.11) \cdot 10^6 (J/m^3{}^oC) \qquad 650^oC \le \theta_c \le 735^oC$$
$$\rho_c c_c = (-0.2630 \cdot \theta_c + 212.40) \cdot 10^6 (J/m^3{}^oC) \qquad 735^oC \le \theta_c \le 800^oC$$
$$\rho_c c_c = 2.00 \cdot 10^6 (J/m^3{}^oC) \qquad 800^oC \le \theta_c \le 1000^oC$$

For concrete with siliceous aggregates it can be computed as follows:

$$\rho_c c_c = (0.005 \cdot \theta_c + 1.7) \cdot 10^6 (J/m^3{}^oC) \qquad 0^oC \le \theta_c \le 200^oC$$
$$\rho_c c_c = (2.70 \cdot 10^6 (J/m^3{}^oC) \qquad 200^oC \le \theta_c \le 400^oC$$
$$\rho_c c_c = (0.013 \cdot \theta_c - 2.50) \cdot 10^6 (J/m^3{}^oC) \qquad 400^oC \le \theta_c \le 500^oC$$
$$\rho_c c_c = (-0.013 \cdot \theta_c - 10.50) \cdot 10^6 (J/m^3{}^oC) \qquad 500^oC \le \theta_c \le 600^oC$$
$$\rho_c c_c = 2.00 \cdot 10^6 (J/m^3{}^oC) \qquad 600^oC \le \theta_c \le 1000^oC$$

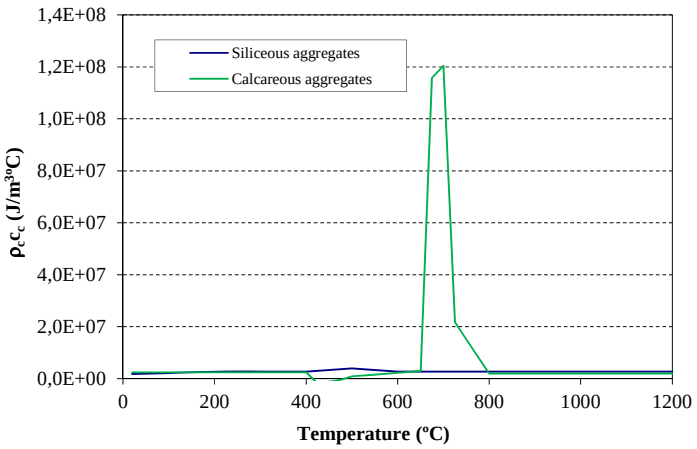

Figure 4. Thermal capacity of high strength concrete at elevated temperatures, according to Kodur & Sultan (2003)

Thermal conductivity

The thermal conductivity of concrete with calcareous aggregates can be obtained as follows:

$$\lambda_c = 2.00 - 0.0013\theta_c \,(\mathrm{W/m^oC}) \qquad 0^oC \le \theta_c \le 300^oC$$
$$\lambda_c = 2.21 - 0.0020\theta_c \,(\mathrm{W/m^oC}) \qquad 300^oC \le \theta_c \le 1000^oC$$

In the case of concrete with siliceous aggregates it is computed by means of:

$$\lambda_c = 2.00 - 0.0011\theta_c \,(\mathrm{W/m^oC}) \qquad 0^oC \le \theta_c \le 1000^oC$$

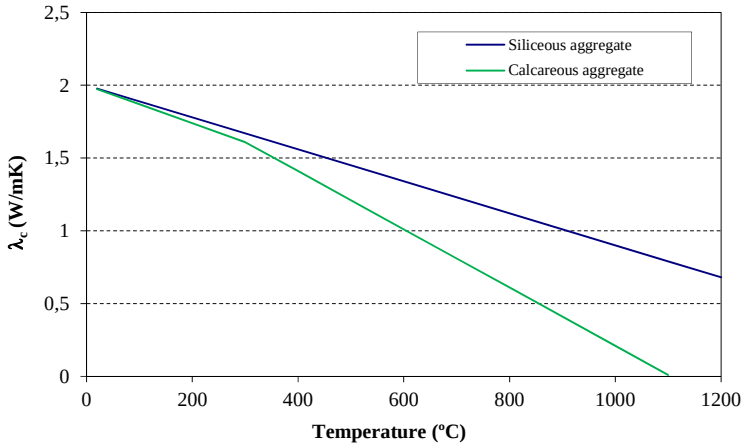

Figure 5. Thermal conductivity of high strength concrete at elevated temperatures, according to Kodur & Sultan (2003)

For steel fiber reinforced high strength concrete:

Thermal capacity

For concrete with calcareous aggregates, the thermal capacity of concrete can be obtained by means of:

$$\rho_c c_c = 3.81 \cdot 10^6 (J/m^3{}^oC) \qquad 0^oC \le \theta_c \le 400^oC$$
$$\rho_c c_c = (-0.0165 \cdot \theta_c + 10.41) \cdot 10^6 (J/m^3{}^oC) \qquad 400^oC \le \theta_c \le 475^oC$$
$$\rho_c c_c = (0.0079 \cdot \theta_c - 1.182) \cdot 10^6 (J/m^3{}^oC) \qquad 475^oC \le \theta_c \le 625^oC$$
$$\rho_c c_c = (0.2333 \cdot \theta_c - 142.06) \cdot 10^6 (J/m^3{}^oC) \qquad 625^oC \le \theta_c \le 700^oC$$
$$\rho_c c_c = (-0.1800 \cdot \theta_c + 147.25) \cdot 10^6 (J/m^3{}^oC) \qquad 700^oC \le \theta_c \le 800^oC$$
$$\rho_c c_c = 3.25 \cdot 10^6 (J/m^3{}^oC) \qquad 800^oC \le \theta_c \le 1000^oC$$

The thermal capacity of concrete with siliceous aggregates can be obtained by means of:

$$\rho_c c_c = (0.006 \cdot \theta_c + 1.60) \cdot 10^6 (J/m^3{}^oC) \qquad 0^oC \le \theta_c \le 100^oC$$
$$\rho_c c_c = (2.20 \cdot 10^6 (J/m^3{}^oC) \qquad 100^oC \le \theta_c \le 400^oC$$
$$\rho_c c_c = (0.011 \cdot \theta_c - 2.20) \cdot 10^6 (J/m^3{}^oC) \qquad 400^oC \le \theta_c \le 500^oC$$
$$\rho_c c_c = (-0.011 \cdot \theta_c + 8.80) \cdot 10^6 (J/m^3{}^oC) \qquad 500^oC \le \theta_c \le 600^oC$$
$$\rho_c c_c = 2.20 \cdot 10^6 (J/m^3{}^oC) \qquad 600^oC \le \theta_c \le 1000^oC$$

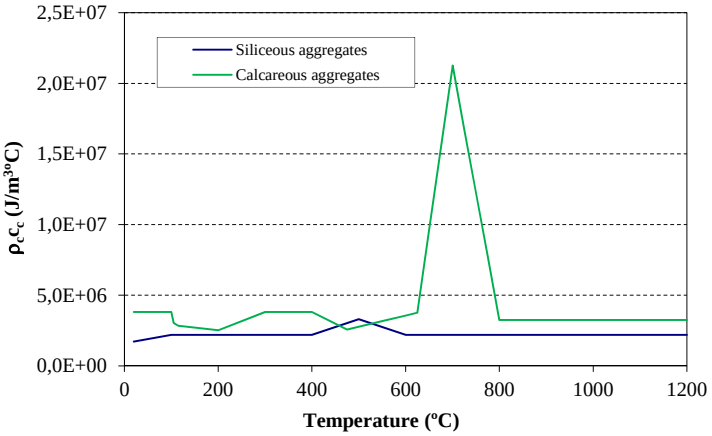

Figure 6. Thermal capacity of steel fiber reinforced HSC at elevated temperatures, according to Kodur & Sultan (2003)

Thermal conductivity

The thermal conductivity of concrete with calcareous aggregates can be obtained as follows:

$$\lambda_c = 1.80 - 0.0016 \cdot \theta_c \,(\mathrm{W/m^oC}) \qquad 0^oC \le \theta_c \le 500^oC$$
$$\lambda_c = 1.20 - 0.0004 \cdot \theta_c \,(\mathrm{W/m^oC}) \qquad 500^oC \le \theta_c \le 1000^oC$$

In the case of concrete with siliceous aggregates:

$$\lambda_c = 2.50 - 0.0034 \cdot \theta_c \,(\mathrm{W/m^oC}) \qquad 0^oC \le \theta_c \le 200^oC$$
$$\lambda_c = 2.24 - 0.0021 \cdot \theta_c \,(\mathrm{W/m^oC}) \qquad 200^oC \le \theta_c \le 400^oC$$
$$\lambda_c = 1.40 (\mathrm{W/m^oC}) \qquad 400^oC \le \theta_c \le 1000^oC$$

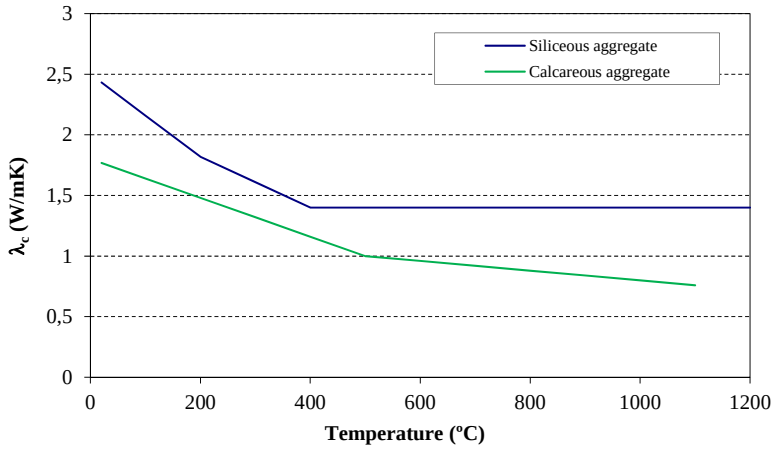

Figure 7. Thermal conductivity of steel fiber reinforced HSC at elevated temperatures, according to Kodur & Sultan (2003)

1.1.3. Formulation by Lie & Kodur

In order to be applied in fire design, Lie & Kodur (1996) determined the relevant properties for steel fiber reinforced concrete of normal strength.

Thermal capacity

For concrete with calcareous aggregates, the thermal capacity of concrete is calculated by:

$$\rho_c c_c = 2.566 \cdot 10^6 (J/m^3 {}^oC) \qquad 0^oC \le \theta_c \le 400^oC$$
$$\rho_c c_c = (0.1765 \cdot \theta_c - 68.034) \cdot 10^6 (J/m^3 {}^oC) \qquad 400^oC \le \theta_c \le 410^oC$$
$$\rho_c c_c = (-0.05043 \cdot \theta_c + 25.00671) \cdot 10^6 (J/m^3 {}^oC) \qquad 410^oC \le \theta_c \le 445^oC$$
$$\rho_c c_c = 2.566 \cdot 10^6 (J/m^3 {}^oC) \qquad 445^oC \le \theta_c \le 500^oC$$
$$\rho_c c_c = (0.01603 \cdot \theta_c - 5.44881) \cdot 10^6 (J/m^3 {}^oC) \qquad 500^oC \le \theta_c \le 635^oC$$
$$\rho_c c_c = (0.16635 \cdot \theta_c + 100.90225) \cdot 10^6 (J/m^3 {}^oC) \qquad 635^oC \le \theta_c \le 715^oC$$
$$\rho_c c_c = (-0.22103 \cdot \theta_c + 176.07343) \cdot 10^6 (J/m^3 {}^oC) \qquad 715^oC \le \theta_c \le 785^oC$$
$$\rho_c c_c = 2.566 \cdot 10^6 (J/m^3 {}^oC) \qquad \theta_c > 785^oC$$

For concrete with siliceous aggregates, the thermal capacity can be computed as follows:

$$\rho_c c_c = (0.005 \cdot \theta_c + 1.7) \cdot 10^6 (J/m^3 {}^oC) \qquad 0^oC \le \theta_c \le 200^oC$$
$$\rho_c c_c = (2.7 \cdot 10^6 (J/m^3 {}^oC) \qquad 200^oC \le \theta_c \le 400^oC$$
$$\rho_c c_c = (0.013 \cdot \theta_c - 2.5) \cdot 10^6 (J/m^3 {}^oC) \qquad 400^oC \le \theta_c \le 500^oC$$
$$\rho_c c_c = (-0.013 \cdot \theta_c - +10.5) \cdot 10^6 (J/m^3 {}^oC) \qquad 500^oC \le \theta_c \le 600^oC$$
$$\rho_c c_c = (2.7 \cdot 10^6 (J/m^3 {}^oC) \qquad \theta_c > 600^oC$$

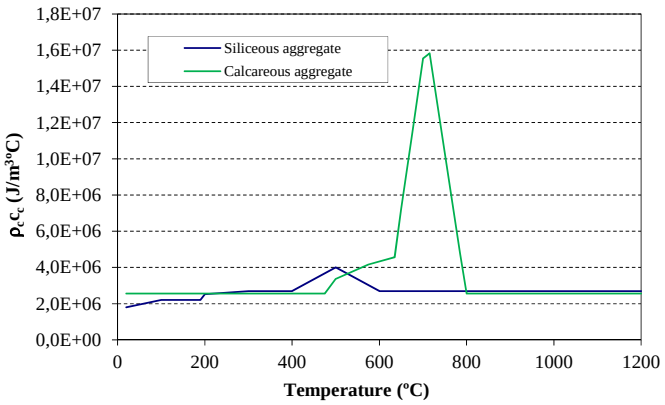

Figure 8. Thermal capacity of steel fiber reinforced NSC at elevated temperatures, according to Lie & Kodur (1996)

Thermal conductivity

The thermal conductivity of steel –fiber reinforced concrete with calcareous aggregates can be obtained as follows:

$\lambda_c = 2.00 - 0.001775\theta_c$ (W/m°C) $\quad 0°C \le \theta_c \le 500°C$

$\lambda_c = 1.402 - 0.000579\theta_c$ (W/m°C) $\quad 500°C \le \theta_c \le 1000°C$

For steel –fiber reinforced concrete with siliceous aggregates, the thermal conductivity is calculated by:

$\lambda_c = 3.22 - 0.007\theta_c$ (W/m°C) $\quad 0°C \le \theta_c \le 200°C$

$\lambda_c = 2.24 - 0.0021\theta_c$ (W/m°C) $\quad 200°C \le \theta_c \le 400°C$

$\lambda_c = 1.40_c$ (W/m°C) $\quad 400°C \le \theta_c \le 1000°C$

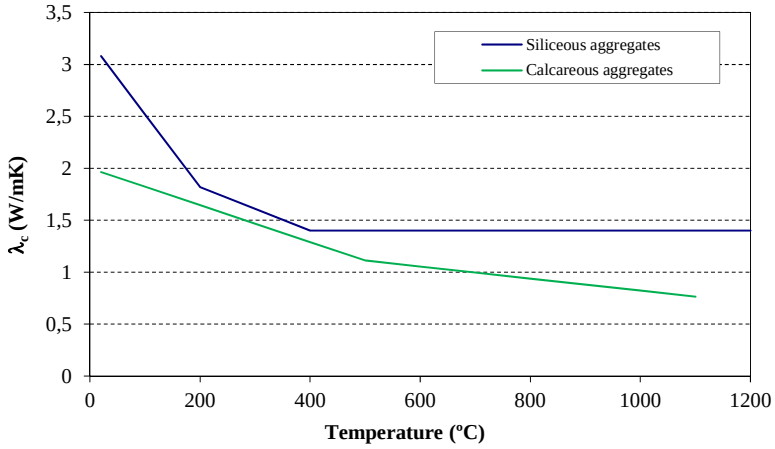

Figure 9. Thermal conductivity of steel fiber reinforced NSC at elevated temperatures, according to Lie & Kodur (1996)

1.2. Mechanical properties of concrete at elevated temperatures

1.2.1. Lie's model

The formulation of the stress-strain relations at elevated temperatures proposed by Lie (1984) is as follows:

For $\varepsilon_c \le \varepsilon_{\max}$: $f_c = f_c^{'} \cdot \left[1 - \left(\frac{\varepsilon_{\max} - \varepsilon_c}{\varepsilon_{\max}} \right)^2 \right]$

For $\varepsilon_c > \varepsilon_{\max}$: $f_c = f_c^{'} \cdot \left[1 - \left(\frac{\varepsilon_c - \varepsilon_{\max}}{\varepsilon_{\max}} \right)^2 \right]$

where:

- $\varepsilon_{\max} = 0.0025 + (6.0 \cdot \theta_c + 0.04 \cdot \theta_c^{\,2}) \cdot 10^{-6}$
- $f_c^{'} = f_{c0}^{'}$ for $0^o C \le \theta_c \le 450^o C$

  $f_c^{'} = f_{c0}^{'} \cdot \left[2.011 - 2.353 \cdot \left(\frac{\theta_c - 20}{1000} \right) \right]$ for $450^o C \le \theta_c \le 874^o C$

  $f_c^{'} = 0$ for $\theta_c > 874^o C$

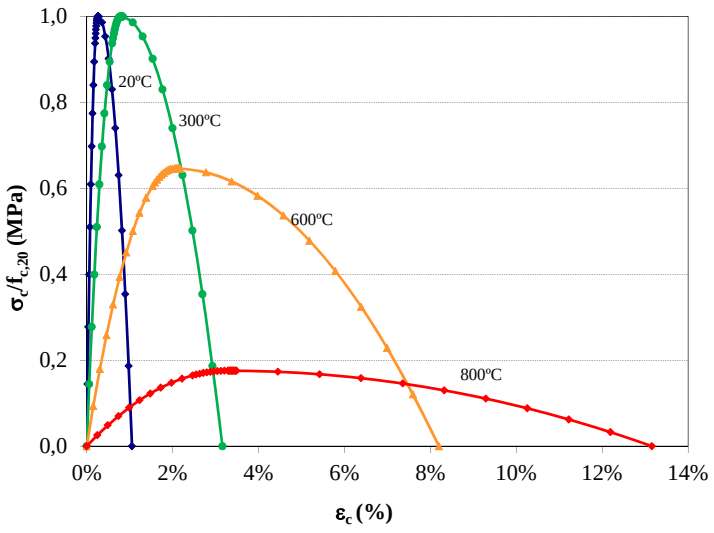

Figure 10. Lie's model (1984) for NSC at different temperatures.

1.2.2. Eurocode 2 model

The mechanical properties of concrete at elevated temperatures are given in Section 3.2.2 of Eurocode 2 Part 1.2 (CEN 2004a). For uniaxially stressed concrete under compression, the general stress-strain curve is used, which can be obtained from the following expressions:

Strain range	Stress
$\varepsilon_{c,\theta} \leq \varepsilon_{c1,\theta}$	$\sigma_{c,\theta} = \dfrac{3 \cdot \varepsilon_{c,\theta} \cdot f_{c,\theta}}{\varepsilon_{c1,\theta}\left[2 + \left(\dfrac{\varepsilon_{c,\theta}}{\varepsilon_{c1,\theta}}\right)^3\right]}$
$\varepsilon_{c1,\theta} \leq \varepsilon_{c,\theta} \leq \varepsilon_{cu1,\theta}$	For numerical purposes, a descending branch should be adopted. Linear or non-linear models are permitted.

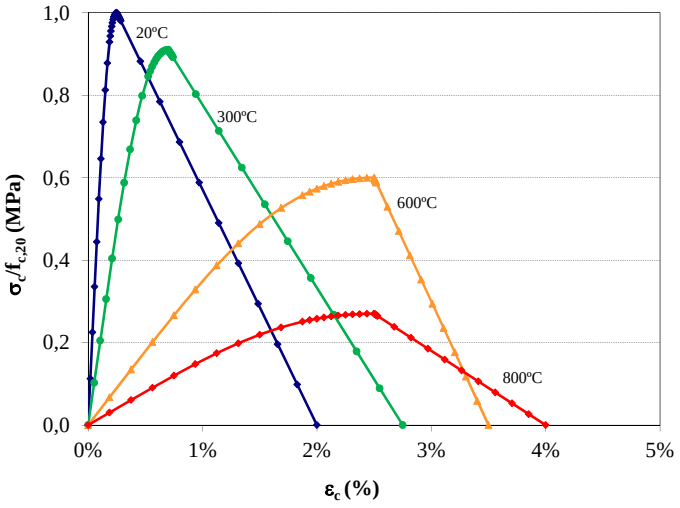

Figure 11. Eurocode 2 model (CEN 2004a) for NSC at different temperatures (calcareous aggregates).

This mathematical model is defined by means of two parameters: the compressive strength ($f_{c,\theta}$) for a given temperature, and the strain corresponding to the peak stress ($\varepsilon_{c1,\theta}$). The values of these parameters are obtained for each temperature by means of applying the reduction factors in Table 3.1 of EC2 Part 1-2 Section 3.2.2.1, where the value of the ultimate strain $\varepsilon_{cu1,\theta}$ which defines the extension of the descending branch is also included.

1.2.3. Model by Kodur et al.

The formulation of the mechanical model for high strength concrete by Kodur et al. (2004) is also employed to simulate the behaviour of steel fiber reinforced concrete of high strength. The next relationships are used:

$$\text{For } \varepsilon_c \le \varepsilon_{\max}: \; f_c = f_c^{'} \cdot \left[1 - \left(\frac{\varepsilon_{\max} - \varepsilon_c}{\varepsilon_{\max}} \right)^H \right]$$

$$\text{For } \varepsilon_c > \varepsilon_{\max}: \; f_c = f_c^{'} \cdot \left[1 - \left(\frac{30(\varepsilon_c - \varepsilon_{\max})}{(130 - f_{co}^{'})\varepsilon_{\max}} \right)^2 \right]$$

where:

- $H = 2.28 - 0.012 f_{c0}^{'}$
- $\varepsilon_{\max} = 0.0018 + (6.7 \cdot f_{c0}^{'} + 6 \cdot \theta_c + 0.03 \cdot \theta_c^{\,2}) \cdot 10^{-6}$
- $f_c^{'} = f_{c0}^{'} \cdot [1.0625 - 0.003125 \cdot (\theta_c - 20)]$ for $\theta_c \le 100^o C$
- $f_c^{'} = 0.75 f_{c0}^{'}$ for $100^o C \le \theta_c \le 400^o C$
- $f_c^{'} = f_{c0}^{'}(1.33 - 0.00145 \cdot \theta_c)$ for $0^o C \le \theta_c \le 450^o C$

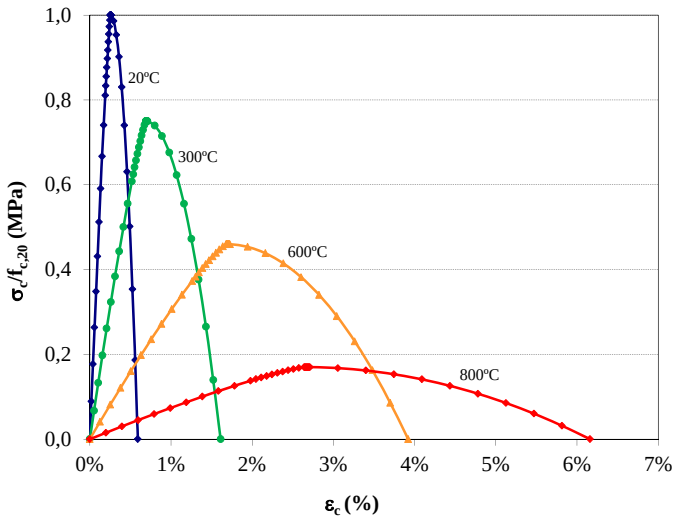

Figure 12. Model by Kodur et al. (2004) model at different temperatures. For plain and steel fiber reinforced HSC.

1.2.4. Model by Lie & Kodur

Together with the thermal properties of normal strength steel fiber concrete, Lie& Kodur (1995) also made a proposal of a mechanical model considering the effect of temperature. The stress-strain relationships for the case of carbonate aggregates concrete are the next:

$$\text{For } \varepsilon_c \le \varepsilon_{\max}: \; f_c = f_c^{'} \cdot \left[1 - \left(\frac{\varepsilon_{\max} - \varepsilon_c}{\varepsilon_{\max}} \right)^2 \right]$$

$$\text{For } \varepsilon_c > \varepsilon_{\max}: \; f_c = f_c^{'} \cdot \left[1 - \left(\frac{(\varepsilon_c - \varepsilon_{\max})}{3\varepsilon_{\max}} \right)^2 \right]$$

where:

- $\varepsilon_{\max} = 0.003 + (7 \cdot \theta_c + 0.05 \cdot \theta_c^{\,2}) \cdot 10^{-6}$
- $f_c^{'} = f_{c0}^{'} \cdot [1 + 0.000769 \cdot (\theta_c - 20)]$ for $\theta_c \le 150^{o} C$
- $f_c^{'} = 1.1 f_{c0}^{'}$ for $150^{o} C \le \theta_c \le 400^{o} C$

- $f_c^{'} = f_{c0}^{'}(2.011 - 2.353(\theta_c - 20/1000)$ for $\theta_c \geq 400^{o}C$

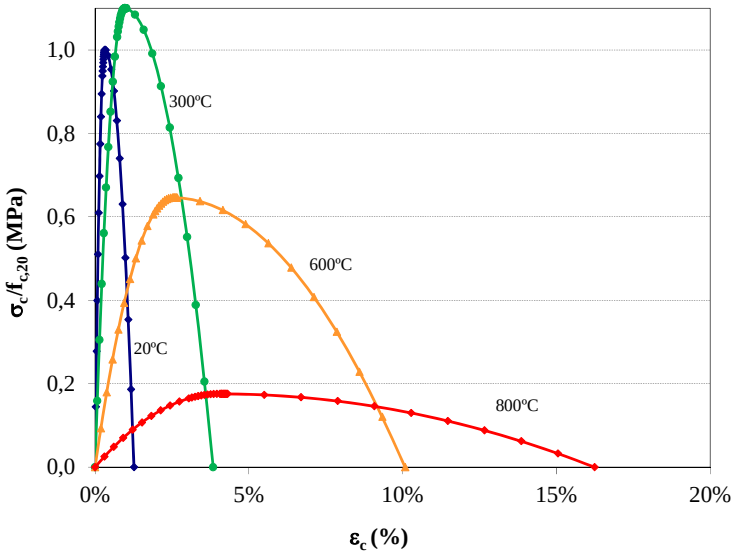

Figure 13. Model by Lie & Kodur (1995) for steel fiber reinforced NSC at different temperatures

2. STEEL AT ELEVATED TEMPERATURES

2.1. Thermal properties of steel at elevated temperatures

2.1.1. Formulation from Eurocode 3

The thermal properties of steel at elevated temperatures are described in Eurocode 3 Part 1.2 (CEN 2005b), Section 3.4. In EC4 Part 1.2 (CEN 2005c), the same definition of the thermal properties has been included, with some minor changes which will be specified below. The formulation of the thermal properties of steel, according to Eurocode 3 Part 1.2 is presented next.

Thermal elongation

The thermal elongation of steel $(\Delta l/l)_a$ may be determined from the following equations, referred to the length of the member at room temperature (20ºC):

$$(\Delta l/l)_a = 1.2\cdot10^{-5}\cdot\theta_a + 0.4\cdot10^{-8}\cdot\theta_a^{\,2} - 2.416\cdot10^{-4} \qquad \text{for } 20^{\circ}\text{C} \le \theta_a \le 750^{\circ}\text{C}$$

$$(\Delta l/l)_a = 1.1\cdot10^{-2} \qquad \text{for } 750^{\circ}\text{C} \le \theta_a \le 860^{\circ}\text{C}$$

$$(\Delta l/l)_a = 2\cdot10^{-5}\cdot\theta_a - 6.2\cdot10^{-3} \qquad \text{for } 860^{\circ}\text{C} \le \theta_a \le 1200^{\circ}\text{C}$$

where θ_a is the temperature of steel, in ºC.

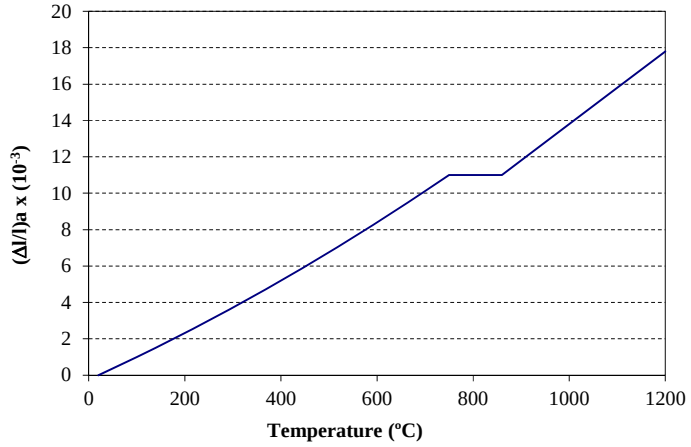

Figure 14. Thermal elongation of steel at elevated temperatures, according to EC3 (CEN 2005b)

In simple calculation models, the variation of the thermal elongation of steel $(\Delta l/l)_a$ with the temperature may be considered to be linear, according to EC4 Part1-2 Section 3.3.1(3), through the following equation:

$$(\Delta l / l)_a = 14 \cdot 10^{-6} \cdot (\theta_a - 20)$$

Specific heat

The specific heat of steel, c_a, is given by the following expressions:

$$c_a = 425 + 7.73 \cdot 10^{-1} \cdot \theta_a - 1.69 \cdot 10^{-3} \cdot \theta_a^{\,2} + 2.22 \cdot 10^{-6} \cdot \theta_a^{\,3} \text{ (J/kgK)} \quad \text{for } 20^{\circ}\text{C} \le \theta_a \le 600^{\circ}\text{C}$$

$$c_a = 666 + \frac{13002}{738 - \theta_a} \text{ (J/kgK)} \quad \text{for } 600^{\circ}\text{C} \le \theta_a \le 735^{\circ}\text{C}$$

$$c_a = 545 + \frac{17820}{\theta_a - 731} \text{ (J/kgK)} \quad \text{for } 735^{\circ}\text{C} \le \theta_a \le 900^{\circ}\text{C}$$

$$c_a = 650 \text{ (J/kgK)} \quad \text{for } 900^{\circ}\text{C} \le \theta_a \le 1200^{\circ}\text{C}$$

where θ_a is the temperature of steel, in ºC.

According to EC4 Part 1-2 Section 3.3.1(6), in simple calculation models the specific heat of steel may be considered to be independent of the temperature, adopting a value of 600 J/kgK.

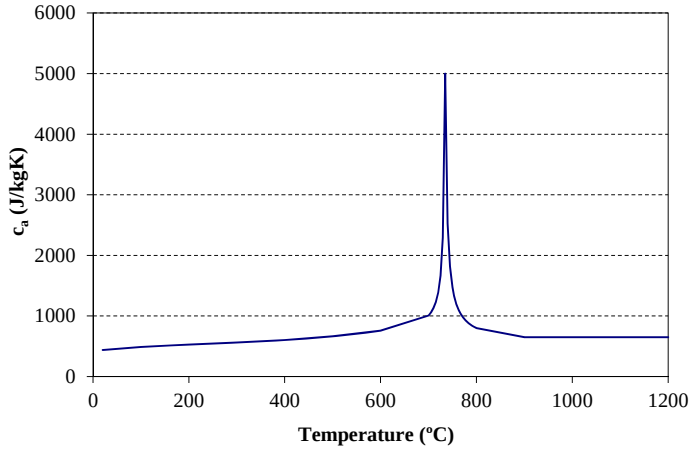

Figure 15. Specific heat of steel at elevated temperatures, according to EC3 (CEN 2005b).

Thermal conductivity

The thermal conductivity of steel, λ_a, should be determined from the following equations:

$$\lambda_a = 54 - 3.33 \cdot 10^{-2} \cdot \theta_a \ \text{(W/mK)} \qquad \text{for } 20^{\circ}\text{C} \le \theta_a \le 800^{\circ}\text{C}$$

$$\lambda_a = 27.3 \ \text{(W/mK)} \qquad \text{for } 800^{\circ}\text{C} \le \theta_a \le 1200^{\circ}\text{C}$$

where θ_a is the temperature of steel, in ºC.

According to EC4 Part 1-2 Section 3.3.1(9), in simple calculation models the thermal conductivity of steel may be considered to be independent of the temperature, adopting a value of 45 W/mK.

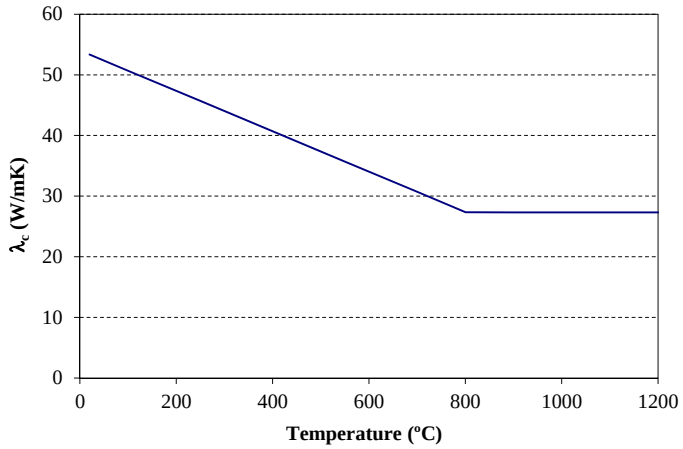

Figure 16. Thermal conductivity of steel at elevated temperatures, according to EC3 (CEN 2005b).

Density

The density of steel ρ_a shall be considered to be independent of the temperature, according to EC4 Part 1-2 Section 3.4(1), with a value ρ_a = 7850 kg/m^3.

2.1.2. Eurocode 3 model

The mechanical behaviour of structural steel at elevated temperatures can be reproduced by the following mathematical model:

Strain range	Stress	Tangent modulus
$\varepsilon_{a,\theta} \le \varepsilon_{p,\theta}$	$\sigma_{a,\theta} = E_{a,\theta} \cdot \varepsilon_{a,\theta}$	$E_{a,\theta}$
	$\sigma_{a,\theta} = f_{p,\theta} - c + \frac{b}{a} \cdot \sqrt{a^2 - (\varepsilon_{y,\theta} - \varepsilon_{a,\theta})^2}$	
	with:	
$\varepsilon_{p,\theta} \le \varepsilon_{a,\theta} \le \varepsilon_{y,\theta}$	$a^2 = (\varepsilon_{y,\theta} - \varepsilon_{p,\theta}) \cdot \frac{\varepsilon_{y,\theta} - \varepsilon_{p,\theta} + c}{E_{a,\theta}}$	$\frac{b \cdot (\varepsilon_{y,\theta} - \varepsilon_{a,\theta})}{a \cdot \sqrt{a^2 - (\varepsilon_{y,\theta} - \varepsilon_{a,\theta})^2}}$
	$b^2 = E_{a,\theta} \cdot (\varepsilon_{y,\theta} - \varepsilon_{p,\theta}) \cdot c + c^2$	
	$c = \frac{(f_{y,\theta} - f_{p,\theta})^2}{E_{a,\theta} \cdot (\varepsilon_{y,\theta} - \varepsilon_{p,\theta}) - 2 \cdot (f_{y,\theta} - f_{p,\theta})}$	
$\varepsilon_{y,\theta} \le \varepsilon_{a,\theta} \le \varepsilon_{t,\theta}$	$\sigma_{a,\theta} = f_{y,\theta}$	0
$\varepsilon_{t,\theta} \le \varepsilon_{a,\theta} \le \varepsilon_{u,\theta}$	$\sigma_{a,\theta} = f_{y,\theta} \cdot [1 - (\varepsilon_{a,\theta} - \varepsilon_{t,\theta}) / (\varepsilon_{u,\theta} - \varepsilon_{t,\theta})]$	-

where:

- $\varepsilon_{p,\theta} = f_{p,\theta} / E_{a,\theta}$ is the strain at the proportional limit
- $\varepsilon_{y,\theta}$ is the yield strain
- $\varepsilon_{t,\theta}$ is the limiting strain for yield strength
- $\varepsilon_{u,\theta}$ is the ultimate strain

The parameters $f_{y,\theta}$ (effective yield strength), $f_{p,\theta}$ (proportional limit) and $E_{a,\theta}$ (elastic modulus) for a certain temperature θ_a are obtained by applying the reduction factors $k_{y,\theta}$, $k_{p,\theta}$, $k_{E,\theta}$ in Table 3.1 of EC3 Part 1-2 3.2.1 to the corresponding values at room temperature f_y, E_a.

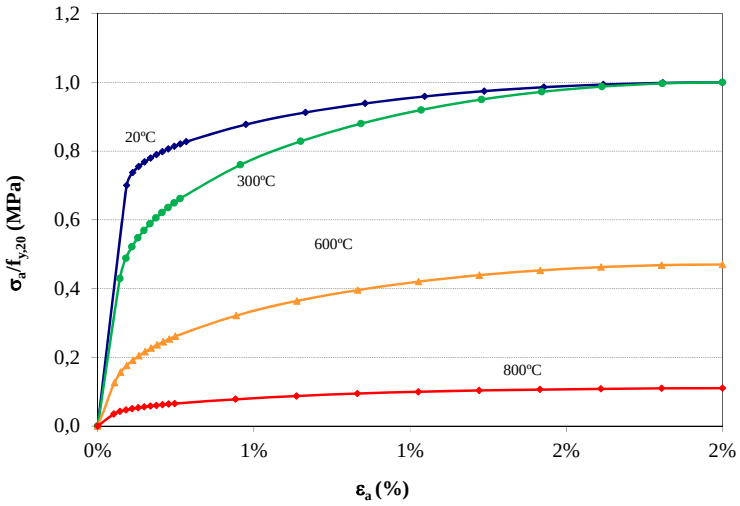

Figure 17. Eurocode 3 model (CEN 2005b) for structural steel at elevated temperatures.